# HEAT TRANSFER IN ECCENTRIC ANNULI

BY

**ESMAIL MOHAMED ALI MOKHEIMER**

A Dissertation Presented to the

FACULTY OF THE COLLEGE OF GRADUATE STUDIES

**KING FAHD UNIVERSITY OF PETROLEUM & MINERALS**

DHAHRAN, SAUDI ARABIA

In Partial Fulfillment of the
Requirements for the Degree of

**DOCTOR OF PHILOSOPHY**

**In**

**MECHANICAL ENGINEERING**

**NOVEMBER, 1995**

# KING FAHD UNIVERSITY OF PETROLEUM AND MINERALS

## DHAHRAN, SAUDI ARABIA

*This Dissertation, written by*

## ESMAIL MOHAMED ALI MOKHEIMER

*Under the direction of his dissertation committee, and approved by all the members, has been presented to and accepted by the Dean, College of Graduate Studies, in partial fulfillment of the requirements for the degree of*

## DOCTOR OF PHILOSOPHY IN MECHANICAL ENGINEERING

Dissertation Committee:

25/12/1995

Chairman ( Prof. M. A. I. El-Shaarawi )

Member ( Dr. Habib I. Abulahamayel )

Dr. M. O. Budair
Department Chairman

Member ( Prof. B. S. Yilbas )

Dr. Ala Al-Rabeh
Dean, College of Graduate Studies

Member ( Dr. F. D. Zaman )

Date : 26 12 95

*This work is dedicated*
*to*

*My great Mother and Father,*
*my brothers and sister,*
*my wife Sanaa,*
*my daughter Mentu-Allah*
*and*
*my son Yahya*

# Acknowledgment

All praise to almighty ALLAH, who gave me the chance, patience, ability and time to accomplish this work.

Acknowledgment is due to King Fahd University of Petroleum and Minerals(KFUPM) for the support of this research.

My deep thanks are offered to my main dissertation advisor Dr. Maged A. I. El-Shaarawi for his constant help and guidance throughout this work. Dr. El-Shaarawi was sincerely conveying his experience to me through his constructive criticism of each stage of this research. Dr. El-Shaarawi is actually a capable advisor and it was a real experience for me to be in contact with such a person to whom I owe a lot in my future academic career. Thanks are also due to Dr. Habib I. Abualhamayel (the Dean of College of Engineering) who, as a member of my dissertation committee, presented to me valuable advises and constructive suggestions during different stages of this research. Deep and sincere thanks go also to my dissertation committee members Dr. Bekir S. Yilbas and Dr. Fiazuddin Zaman for their interest, helpful suggestions and careful reading of the manuscript.

I would like to express my thanks to the Data Processing Center (DPC) staff and in particular the ACS group who facilitated the use of the main frame during this research. Thanks also are due to the central library staff who offered a lot of help through the library materials which made this work convenient.

I am also grateful to Dr. Ala Al-Rabeh (the Dean of the College of the Graduate Studies), Dr. Mohammad Budair (the Chairman of The Mechanical Engineering Dept.) and Dr. Abdulghany El-Fraaydhi (the Graduate Coordinator in M.E. Dept.) for their support in using the university facilities.

Thanks are due to my colleagues and my friends who made my stay here at KFUPM pleasant.

Last but not least, I owe my beloved family an expression of gratitude for their patience, encouragement and moral support which made this work possible.

# Contents

Appendices

# List of Tables

# List of Figures

# DISSERTATION ABSTRACT

**Name** : **Esmail M. A. Mokheimer**
**Title** : **Heat Transfer in Eccentric Annuli**
**Major Field** : **Mechanical Engineering**
**Date of Degree** : **November, 1995**

Various modes of heat transfer through eccentric annuli have been studied either analytically or numerically. These include transient conduction with uniform internal heat generation in eccentrically hollow cylinders, the fully developed free convection in open-ended vertical annuli, the developing forced convection in eccentric annuli and the developing free convection in open-ended vertical eccentric annuli. Four pairs of thermal boundary conditions have been investigated in which one of the boundaries is heated isothermally or with uniform heat flux while the other boundary is kept adiabatic or isothermal at the ambient temperature. The case under study is called case I when the heated wall is the inner wall while it is called case O when the heated wall is the outer wall.

The transient conduction has been solved numerically using a finite difference technique. The obtained steady-state numerical solutions have been compared with their corresponding available (if any)/derived analytical solutions. This comparison provided a means of validation of the present finite-difference scheme and its method of solution. The obtained numerical temperature profiles were used to obtain useful engineering parameters such as the maximum temperature within the annulus material and the time needed to reach steady-state conditions. The eccentricity and the boundary conditions were found to affect the heat transfer parameters greatly. The internal heat generation was found to affect the steady-state time slightly.

Fully developed free convection in vertical open-ended eccentric annuli has been solved numerically for boundary conditions of the first and fourth kind while an analytical solution was provided for boundary conditions of the third kind. Results for the heat transfer parameters such as the temperature distribution, mean bulk temperature, average velocity, induced volumetric flow rate, heat absorbed, the local Nusselt number and the circumferentially-averaged Nusselt number have been presented in a series of figures covering a wide range of eccentricities. It was found that the heat transfer rate and the induced volumetric flow rate increase with eccentricity.

A mathematical model based on the boundary layer theory has been developed to describe the flow and heat taransfer in the entry region of eccentric annuli. This model has been derived and formulated in a general manner to describe both free and forced convection. A finite-difference algorithm has been developed to numerically solve the relevant equations. The developing laminar forced convection in eccentric annuli has been solved using this algorithml and the results show good agreement with the work reported previously. Then the free convection problem has been solved for the four pairs of thermal boundary conditions.

DOCTOR OF PHILOSOPHY DEGREE

KING FAHD UNIVERSITY OF PETROLEUM AND MINERALS
Dhahran, Saudi Arabia

November, 1995

# ملخص الرسالة


الإسم : إسماعيل محمد على مخيمر

عنوان الرسالة : سريان الحرارة خلال الحيز الحلقي بين اسطوانتين غيرمتحدتى المركز

التخصص : الهندسة الميكانيكية

تاريخ الشهادة : نوفمبر ١٩٩٥م



فى هذه الرسالة تم دراسة صور مختلفة من سريان الحرارة خلال الحيز الحلقى بين اسطوانتين غير متحدتى المركز إما بالطرق التحليلية أو بالطرق العددية · و اشتملت الدراسة سريان الحرارة بالتوصيل الغير مستقر والمستقر مع وجود توليد حرارى منتظم داخل اسطوانات مفرغة لامركزيا · كما تم دراسة سريان الحرارة بالحمل الحر الكامل التطور فى الحيز الحلقى بين اسطوانتين رأسيتين غير متحدتى المركز ومفتوحتى الطرفين · وذلك بالإضافة إلى دراسة كل من الحمل القسرى المتطور بين إسطوانات لامتمركزة والحمل الحر بين الإسطوانات اللامتمركزة الرأسية المفتوحة · ولقد أجريت هذه الدراسات تحت اربعة ازواج من الظروف الحرارية المختلفة عند الجدران وفى هذه الظروف الحرارية يحفظ احد الجدران عند درجة حرارة ثابتة أو تنقل عبره الحرارة بمعدل ثابت بالنسبة لوحدة المساحات بينما يحفظ الجدار الآخر عند درجة حرارة ثابتة مساوية لدرجة حرارة الوسط الخارجى أو يعزل حراريا · ولقد تم تسمية الجدار الذى ينقل الحرارة أو المحفوظ عند درجة حرارة أعلى بالجدار النشط · وتسمى الحالة التى يتم دراستها الحالة ( ١ ) اذا كان الجدار الداخلى هو الجدار النشط وتسمى الحالة ( 0 ) اذا كان الجدار النشط هو الجدار الخارجى · وقد تم حل مسألة سريان الحرارة بالتوصيل الحرارى غير المستقر مع توليد حرارى داخلى منتظم عدديا باستخدام طريقة الفروق المحدودة بينما تم حل مسألة التوصيل الحرارى المستقر تحليليا وتمت مقارنة الحل المستقر الذى تم الحصول عليه بالطرق العددية عند زمن كبير مع الذى تم الحصول عليه تحليليا وأوضحت هذه المقارنة صلاحية طريقة الفروق المحدودة التى استخدمت · ومن منحنيات درجات الحرارة الناتج تم الحصول على بعض المعاملات الهندسية ذات التطبيق العملى مثل درجة الحرارة العظمى داخل الإسطوانة والوقت المطلوب للوصول إلى حالة الإستقرار الحرارى · وقد وجد أن الإختلاف المركزى ( البعد بين مركزى الإسطوانتين ) والظروف الحرارية عند الجدران لهما تأثير كبير على سريان الحرارة بينما لوحظ أن التوليد الحرارى الداخلى له تأثير طفيف على قيمة الوقت المطلوب للوصول إلى حالة الإستقرار الحرارى · كما تم دراسة انتقال الحرارة بالحمل الحر الكامل التطور خلال الحيز الحلقى بين الإسطوانات اللامتمركزة الرأسية المفتوحة باستخدام طريقة الفروق المحدودة تحت ظروف حرارية من النوع الأول والثالث والرابع وقد تم الحصول على نتائج لتوزيع درجات الحرارة ودرجة الحرارة المتوسطة ومعدل سريان المائع المسحوب طبيعيا ( نتيجة تسخين جدار الإسطوانة ) وكمية الحرارة التى اكتسبها هذا المائع والقيم العددية المحلية والمتوسطة لمعاملات انتقال الحرارة على الجدران · وقد وجد أن قيم هذه المعاملات وكمية الحرارة المكتسبة ومعدل سريان المائع تزداد بزيادة الإختلاف المركزى ( البعد بين مركزى الإسطوانتين ) · ولقد تم استنباط نموذج رياضى من معادلات بقاء المادة والطاقة وكمية الحركة وقائم على نظرية الطبقة المتاخمة فى مدخل الإسطوانات اللامتمركزة · ولقد تم استنتاج وكتابة هذا النموذج بطريقة عامة جعلته قادرا على حل كل من الحمل القسرى والحمل الحر فى منطقة المدخل غير كاملة التطور · ولقد استخدمت طريقة الفروق المحدودة لحل معادلات هذا النموذج عدديا · و أوضحت نتائج دراسة الحمل القسرى الغير كامل التطور باستخدام هذا النموذج الرياضى اتفاقا طيبا مع ماسبق نشره فى هذا المجال ، و بعد ذلك تم حل مسألة الحمل الحر الغير كامل التطور بين الإسطوانات اللامتمركزة الرأسية المفتوحة باستخدام هذا النموذج وذلك لأربعة ازواج من الظروف الحرارية المختلفة عند الجدران ·


درجة الدكتوراه في الفلسفة

جامعة الملك فهد للبترول والمعادن

الظهران - المملكة العربية السعودية

نوفمبر ١٩٩٥م

# Nomenclature

a location of the positive pole of the bipolar coordinate system on the x-axis of the Cartesian coordinate system ( constant in the bipolar transformation equations, equal to $r_i \, Sinh \, \eta_i$ or $r_o \, Sinh \, \eta_o$ )

$a^*$ heat transfer coefficient, $q'' / (T_w - T_m)$

A cross-sectional area of the annulus, $\pi ( r_o^2 - r_i^2 )$

$A^*$ constant of the integration in eq. (4.4), its value depends on the case under study

B constant of the integration in eq. (4.4), its value depends on the case under study

$c_p$ specific heat of the fluid at constant pressure

C constant of the integration in eq. (4.4), its value depends on the case under study

$C^*$ constant in eq. (4.4), its value depends on the case under study

$D_h$ hydraulic or equivalent diameter of annulus, $2 ( r_o - r_i ) = 2 a ( 1 - N ) \, csch \, \eta_o$

D constant of integration in eq.(4.4), its value depends on the case under study

e eccentricity (distance between the axes of the two cylinders forming the eccentric annulus), $a ( Coth \, \eta_o - Coth \, \eta_i)$

E dimensionless eccentricity, $e / ( r_o - r_i )$

f coefficient of friction , $( p_o - p ) D_h / ( \rho \bar{u}^2 z ) = \frac{P}{Z Re}$ for forced convection or

volumetric flow rate for free convection, $f = \pi\left(r_o^{\,2} - r_i^{\,2}\right)\bar{u} = 2\int_0^{\pi}\int_{\eta_o}^{\eta_i} u\,h^2\,d\eta\,d\xi$

F body force per unit volume or dimensionless volumetric flow rate,

$$f/\pi l\gamma Gr^* = 8(1-N)^2\int_0^{\pi}\int_{\eta_o}^{\eta_i} U\,H^2\,d\eta\,d\xi/\pi$$

g gravitational body force per unit mass(acceleration)

Gr Grashof number, $\mp\, g\,\beta\,(t_w - t_o)D^3/\gamma^2$ in cases with isothermal wall

Or, $\mp\, g\,\beta\,q\,D^4\,/\,2\gamma^2 k$ in cases with uniform heat flux at the wall, the plus and minus signs apply to upward (heating) and downward (cooling) flows, respectively. Thus Gr is always positive

$Gr^*$ modified Grashof number, $Gr^* = Gr\,D_h/l$

h coordinate transformation scale factor, $a/(Cosh\,\eta - Cos\,\xi)$

H dimensionless coordinate transformation scale factor,

$$h/D_h = \frac{0.5\,Sinh(\eta_o)}{(1-N)\left(Cosh(\eta) - Cos(\xi)\right)}$$

i index for the finite-difference grid in $\eta$-direction

j index for the finite-difference grid in $\xi$-direction

k thermal conductivity of fluid

$l$ height of annulus

L dimensionless height of annulus ( value of Z at annulus exit ), $l/Gr^*$ for free convection

m number of intervals in $\xi$-direction

n number of intervals in $\eta$-direction or infinite series summation index in the fully developed flow solution

$n^*$ direction normal to either boundary of the annulus and the positive direction of $q''$

N radius ratio, $r_i / r_o = Sinh\ \eta_o / Sinh\ \eta_i$

$Nu_y^{M,x}$ local Nusselt number at any point where $M$, $x$ and y are dummy variables; $M$ stands for the kind of the boundary conditions, $x$ stands for the case under consideration which may be $I$ or $O$ and y stands for the wall, thus $Nu_i^{I,O}$ indicates Nusselt number on the inner wall in case 1.O, $a^* D_h / k$

$Nu_{y,e}^{M,x}$ the value of $Nu_y^{M,x}$ at the channel exit

$\overline{Nu}_y^{M,x}$ Nusselt number averaged around the periphery of wall $y$.

$\overline{Nu}_{y,e}^{M,x}$ the value of $\overline{Nu}_y^{M,x}$ at the channel exit

p pressure of fluid inside the channel at any cross-section

$p'$ pressure defect at any point, $p - p_s$

$p_{fd}$ pressure at any cross-section if the flow were hydrodynamically fully-developed straight at the entrance, for forced convection

$p_o$ pressure of fluid at annulus entrance

$p_s$ hydrostatic pressure, $\mp \rho_o g z$ where the minus and plus signs are for upward (heating) and downward (cooling) flows, respectively

P dimensionless pressure defect at any point, $p' D_h^4 / \rho_o l^2 \gamma^2 Gr^2$ for free convection or $p - p_o / (\rho \bar{u}^2)$ for forced convection

$P_{fd}$ dimensionless value of $p_{fd}$, , for forced convection

Pr Prandtl number, $\mu c_p / k$

$q''$ local heat flux at either boundary which is defined to be positive when it heats the fluid, $-k\,\partial T/\partial n^* = \pm(k/h)(\partial T/\partial \eta)$ where the upper and lower signs stand for the inner and outer walls, respectively, in case of fluid heating and vice versa in case of fluid cooling

$q''_{iw}$ the value of $q''$ at the inner wall

$q''_{ow}$ the value of $q''$ at the outer wall

q heat gained or lost by fluid from the entrance up to a particular elevation in the annulus, $\rho_o f c_p (T_m - T_o)$

$\bar{q}$ heat gained or lost by fluid from the entrance up to the annulus exit, i.e., value of $q$ at $z = l$, $\rho_o f c_p (\bar{T}_m - T_o)$

$Q$ dimensionless heat absorbed from the entrance up to any particular elevation, $q/[\pi \rho_o c_p l \gamma Gr^* (T_w - T_o)] = F\theta_m$

$\bar{Q}$ dimensionless heat absorbed up to the annulus exit, i.e., value of $Q$ at $z = l$, $\bar{q}/[\pi \rho_o c_p l \gamma Gr^* (T_w - T_o)] = F\bar{\theta}_m$

$Q'''$ internal heat generation per unit volume (set equal to zero in all cases considred except in conduction problem)

$r_i$ inner radius of annulus

$r_o$ outer radius of annulus

Ra Rayleigh number, Gr Pr

$Ra^*$ modefied Rayleigh number, $Gr^* Pr = Ra\, D_h / l$

Re Reynolds number, $\rho \bar{u} D_h / \mu$

T temperature at any point

$T_m$ mixing-cup (mixed-mean) temperature over any cross section of the annulus at a given z, $\int_A T u\, d A / (A \bar{u}) = 2\int_0^{\pi}\int_{\eta_o}^{\eta_i} T u^2\, d\eta\, d\xi \;/\; [\pi\,(r_o^2 - r_i^2)]$

$\bar{T}_m$ mixing cup temperature at annulus exit, i.e. value of $T_m$ at $z = l$

$T_o$ ambient or entrance temperature

$T_w$ isothermal heated wall temperature

u axial (streamwise) velocity component at any point

$u_{fd}$ fully developed axial velocity component

$u_o$ entrance axial velocity, $\bar{u}$ (average velocity)

$\bar{u}$ average u (volume flow rate per unit area), $\int_A u dA / A$

$= 2\int_0^{\pi}\int_{\eta_o}^{\eta_i} u h^2\, d\eta\, d\xi / [\pi\,(r_o^2 - r_i^2)\bar{u}] = 2\int_0^{\pi}\int_{\eta_o}^{\eta_i} u h^2\, d\eta\, d\xi / [\pi a^2 (1 - N^2) Csch^2 \eta_o \bar{u}]$

U dimensionless axial velocity at any point, $\frac{u r_o^2}{l\gamma Gr^*}$ for free convection or $u / \bar{u}$ for forced convection

$U_{fd}$ dimensionless fully-developed axial velocity component, $\frac{u_{fd} r_o^2}{l\gamma Gr^*}$ for free convection or $u_{fd} / \bar{u}$ for forced convection

$\bar{U}$ dimensionless average axial velocity at any point , $\frac{\bar{u} r_o^2}{l\gamma Gr^*}$ or 1 for forced convection

$U_{max,fd}$ maximum local value of $U_{fd}$

$v$ $\eta$-direction velocity component

$V$ velocity vector or dimensionless $\eta$-velocity component, $vD_h / \gamma$

$w$ $\xi$-direction velocity component

$W$ dimensionless $\xi$-velocity component, $wD_h / \gamma$

x the first transverse direction in the Cartesian coordinate system

y the second transverse direction in the Cartesian coordinate system

z axial coordinate in both the Cartesian and bipolar coordinate systems (measured from the annulus entrance)

$z_{fd}$ value of z at which the flow reaches hydrodynamic full-development

Z dimensionless axial coordinate in both the Cartesian and bipolar coordinate systems, $z / (D_h Re)$ for forced convection or $z / l Gr^*$ for free convection

$Z_{fd}$ dimensionless value of $z_{fd}$ , $z_{fd} / (D_h Re)$

**Greek letters:**

$\alpha$ thermal diffusivity of fluid, $k / \rho c_p$

$\beta$ volumetric coefficient of thermal expansion

$\eta$ the first transverse bipolar coordinate

$\eta_i$ value of $\eta$ on the inner surface of the annulus,

$\eta_o$ value of $\eta$ on the outer surface of the annulus,

$\Delta\eta$ numerical grid mesh size in $\eta$-direction, $(\eta_i - \eta_o) / n$

$\Delta\eta$ numerical grid mesh size in $\eta$-direction, $(\eta_i - \eta_o) / n$

$\nabla$ the gradient operator or pressure drop increment at a given Z, $P - P_{fd}$

$\nabla_{fd}$ fully-developed pressure drop increment , $(P - P_{fd})_{fd}$

$\theta$ dimensionless temperature, $(T - T_o)/(T_w - T_o)$ for isothermal walls or

$\frac{T - T_o}{q'' D_h / K}$ for uniform heat flux

$\theta_m$ dimensionless mixed-mean temperature, $(T_m - T_o)/(T_w - T_o)$

$\bar{\theta}_m$ dimensionless mixed-mean temperature ($\theta$) at channel exit

$\theta_{fd}$ fully-developed value of $\theta$

$\mu$ dynamic viscosity of fluid

$\gamma$ kinematic viscosity of fluid, $\mu / \rho$

$\xi$ the second transverse bipolar coordinate

$\Delta\xi$ numerical grid mesh size in $\xi$-direction, $\pi / m$

$\rho$ density of fluid

$\tau$ dimensionless time, $\alpha t / D_h^2$

$\phi$ normalized value of $\eta$, $(\eta - \eta_o)/(\eta_i - \eta_o)$

$\Phi$ viscous dissipation

$\psi$ normalized value of $\xi$, $\xi / \pi$

# Chapter 1

# INTRODUCTION

Flow and heat transfer in eccentric annuli have proved to be a useful model for many applications. For example conduction and / or natural convection in eccentric annuli occur in many situations in the electrical, nuclear, solar and thermal storage fields. In the electrical field, cooling of underground electric transmission cables is affected by the position of the cable within its outer housing [1-2].

In the nuclear field, fuel element and the target tube assemblies following irradiation can be greatly influenced due to inner tubular eccentricities. Likewise natural convection cooling of casks containing nuclear waste can exceed thermal guidelines if positioning becomes overly eccentric [3]. A key problem in the storage of nuclear wastes is the determination of insulating effect of the annular air space surrounding a cylindrical nuclear waste canister embedded in a geologic repository . In this situation, heat will be transferred from the canister, through the insulating air space and into the surrounding rock. Heat may be transferred through the air space by conduction between the fluid layers or by natural convection. In the case of natural convection the thermal resistance

of the air gap will be much smaller than that in the case of pure conduction and the equilibrium temperature of the canister will be correspondingly lower. This temperature is critical because it is the primary factor which determines the life span of the metal containers [3].

In heat transfer equipment, such as tubular heat exchangers, the interest in the eccentric annulus arises because of the problem of tube misalignment which frequently occurs in a closebacked heat exchanger.

The conduction heat transfer and the fully developed laminar free convection in a vertical eccentric annulus are very important limiting cases for the more general problem of developing free convection in a vertical annulus. The fully developed natural convection is the limiting case if the vertical annulus is high enough. On the other hand, the conduction mode of heat transfer takes place before the onset of free convection when the temperature is low. Applications of conduction heat transfer in the eccentric annulus configuration are numerous. These include the prediction of the temperature distribution around an underground electric transmission cable and in eccentrically hollow shafts or eccentric insulations. Another important practical application is the conduction heat transfer in the eccentric shaft of the spark ignition Wankel rotary engine [4].

The present work aims at obtaining a solution for the developing laminar free convection in open-ended vertical eccentric annuli. To the best of our knowledge, such a solution has not been previously reported in the literature. Moreover, through an extensive literature review , it has been found that there is a lack of information

regarding the limiting cases of pure conduction in eccentric annuli especially under the transient conditions and fully developed laminar natural convection.

Conduction heat transfer in eccentric hollow cylinders has been treated only for the steady state case with two isothermal boundaries [5]. This motivated the present work to fill also this gab. Thus the present work deals with conduction as well as developing and fully developed free convection in eccentric annuli under variety of thermal boundary conditions.

For the developing free convection a model has been developed during the present work. The adequacy of this model and its code of solution has been checked using mainly the analytical results of the fully developed free convection studied during the present work. However, the validity of the present model and the code of solution has also been confirmed by using this model and its pertinent computer code in solving the developing laminar forced convection in the entrance region of an eccentric annulus. The latter case has already been solved by Feldman et al. [6,7] and the results obtained for this forced convection case are compared with the previously reported work.

The extensive literature review made during the present work is summarized in the following chapter. The objectives of the present work along with the general problem formulation is outlined in Chapter 3. Methods of solutions are outlined in Chapter 4. Results and discussions for the conduction and fully developed free convection are the material of Chapters 5 and 6, respectively. Chapters 7 and 8

include the results for the developing forced and free convection, respectively. Conclusions and recommendations are presented in Chapter 9.

# Chapter 2

# LITERATURE REVIEW

Special attention will be given in this chapter to previous work related to the three problems under investigation, namely, conduction heat transfer in eccentrically hollow cylinders, fully developed laminar free convection in vertical eccentric annuli, developing laminar forced convection in eccentric annuli and free convection in vertical open ended eccentric annuli. The literature review for each problem will be presented separately.

## 2.1 Conduction Heat Transfer in Eccentric Hollow Cylinders

Conduction heat transfer in eccentric annuli is useful in predicting the temperature distribution in the ground around a buried cable [8]. The current carrying capacity of underground cables is limited by the maximum allowable electrical insulation temperature that is required for long life and high reliability. This limiting temperature is about 85 $^{o}$C [2] and occurs at the inner surface of the insulation in contact

with the conductor. Eccentricity may be introduced during the manufacturing of an insulated cable. This eccentricity will result in a nonuniform circumferential temperature distribution on the inner surface of the insulation leading to a temperature concentration at some points above the allowable limit of temperature. So the temperature distribution should be carefully monitored or previously predicted in the cases where eccentricity is expected.

The problem of steady conduction heat transfer in an eccentrically hollow infinitely long cylinder with internal heat generation has been analyzed by El-Saden [5]. El-Saden presented a general analytical solution for the energy equation written in bipolar coordinates which were firstly used by Macdonald [9] to solve a torsion problem. The constants involved in this analytical solution were provided for a case with isothermal boundary conditions and no further trials were considered to evaluate those constants for other types of thermal boundary conditions.

Instead of using bipolar coordinates in their analysis for the problem of heat transfer from a buried cable, Eckert and Drake [8] superimposed the solution of a heat source and a heat sink(mirror-image system) to obtain expressions for the isotherms, the heat transfer rate and the thermal resistance.

Using the bicylindrical (bipolar) coordinate system, Bau and Sadhal [10] presented an analytical solution for heat losses from a buried pipe beneath an isothermal surface. They considered two cases, the first one involves a mixed (convective) boundary condition with a uniform heat transfer coefficient at the pipe surface. In the second case, a laminar flow with linear temperature variation along the pipe axis was considered.

Encouraged by the above results, DiFelice and Bau [11] used a similar method to analyze the conductive heat transfer in an eccentric annulus, between a buried pipe and the surface of a semi infinite medium, and between two pipes imbedded in an infinite medium. These complicated geometries were handled through the use of the bicylindrical (bipolar) coordinate system. With convective boundary conditions imposed on all surfaces, DeFelice and Bau obtained an exact solution for the foregoing cases and constructed an approximate formula for the shape factor. In their analysis for the thermal resistance of a buried cylinder with constant heat flux boundary conditions, Thiyagrajan and Yovanovich [12] solved the governing differential equation for the steady conduction heat transfer through a homogeneous and isotropic medium. They provided an analytical expression for the temperature distribution considering the boundary conditions of constant heat flux on the outer surface of the cylinder and an isothermal ground surface at a given temperature.

The present literature review reveals that there is no previous work reported for the problem of transient conduction heat transfer in eccentrically hollow cylinders with or without internal heat generation. Also, there are no results available for the case of steady conduction in eccentrically hollow cylinders with combinations of thermal boundary conditions other than the isothermal one. These latter results represent the limiting mode of heat transfer before the onset of natural convection which will be handled in the present work.

## 2.2 Fully Developed Laminar Convection

Considerable work has been carried out to study the problem of flow and heat transfer in annuli, both concentric and eccentric. The present survey includes both forced and free convection in vertical annuli. In the available literature there are two essential papers related to fully developed laminar flow in concentric annuli. The first of these, by Reynolds et al. [13], presented for the first time a general formulation of the fully developed forced convection problem in concentric annuli for arbitrarily prescribed wall temperatures or heat fluxes. Four fundamental thermal boundary conditions were introduced. Combinations of solutions corresponding to these boundary conditions may be used to obtain solutions corresponding to more complicated boundary conditions that may be practically found. The second paper, by EL-Shaarawi and Al-Nimr [14], presented a detailed analysis for the fully developed laminar free convection flow in vertical open-ended concentric annuli. Moreover, they presented analytical solutions corresponding to the four fundamental boundary conditions.

Convection heat transfer in concentric annuli has been extensively studied but relatively few studies have been reported for eccentric annuli. Using bipolar coordinates, Cladwell [15] and Piercy et al. [16] independently showed that Macdonald's equation [9] for the torsion moment is comparable to the equation for the volumetric flow rate of a fully developed forced laminar flow through an eccentric annulus.

Following another procedure, Heyda [17] determined the Green's function in bipolar coordinates for a potential flow in an eccentric annulus and used this potential solution to obtain a solution of the momentum equation. Heyda obtained the velocity profile analytically in the form of an infinite series but did not perform the integration necessary to arrive at the relationship between the volume flow rate and the pressure gradient.

Snyder [18] utilized the general solution obtained by El-Saden [5] to reach a solution for the differential equation describing the slug flow heat transfer in an eccentric annulus, but for different boundary conditions. Snyder obtained the temperature distribution for boundary condition of the second kind with the outer wall insulated while the inner wall heated with an axial uniform heat flux per unit length keeping its temperature uniform circumferentially. Using the same technique, Snyder and Goldstein [19] obtained the velocity distribution for the fully developed forced laminar flow through eccentric annuli.

Redberger and Charles [20] numerically solved the same problem using the bipolar coordinates. The differential equation was replaced by a finite difference representation and an iterative method was used to solve the resultant set of algebraic equations. Without using the transformation to the bipolar coordinates, Cheng and Hwang [21] obtained a solution for the energy equation in cylindrical coordinates for the fully developed laminar forced convection in eccentric annular ducts with heat sources and constant wall temperature gradient. Their boundary conditions can be considered

some sort of the second kind but they add the condition of having uniform circumferential temperature distribution on the active wall. They used the point matching method, the details of which were indicated in a previous paper by Cheng and Jamil [22]. Using the method introduced by Cheng and Hwang, Trombetta [23] introduced an approximate analytical solution for the energy equation in cylindrical coordinates describing the hydrodynamically and thermally fully developed forced convection in eccentric annuli. Using the velocity distribution reported previously for forced laminar flow in eccentric annuli, Trombetta solved the energy equation under the boundary conditions of first , second and fourth kind.

In his study for the flow of non-Newtonian fluids in an eccentric annulus, Guckes [24] calculated the volumetric flow rate for laminar fully developed forced flow of power law and Bingham-Plastic fluids. His finite difference representation of the axial momentum equation resulted in a set of algebraic equations that arose when this representation of the axial momentum equation is applied at each grid point in the domain of solution. The coefficients of this set of algebraic equations form a band matrix. The solution of this band matrix was accomplished by a forward-backward algorithm similar to that given in Rosenberg [25].

Feldman et al. [6,7] reported results for the fully developed forced convection in an eccentric annulus after solving the developing flow problem Ozgan and Tosun [26]

applied the geometric inversion to the eccentric annulus system to predict the maximum velocity locus and velocity contours in laminar and turbulent forced flows.

Recently the problem of fully developed forced convection in eccentric annuli has been treated numerically by Suzuki et al. [27]. The finite difference equivalents of the governing equations of velocity and temperature fields written in bipolar coordinate system were solved with an iterative procedure. Their study has been carried out for two cases of the second kind thermal boundary conditions.

Patankar et al. [28] presented a numerical study for laminar fully developed mixed convection in vertical eccentric annular ducts. They solved the equations governing the velocity and temperature on a body conforming grid by using a finite-volume technique.

The present literature review reveals that no work has been reported for the problem of fully developed laminar free convection in vertical eccentric annuli.

## 2.3 Developing Laminar Convection

The problem of developing free convection in channels and ducts has been widely studied for different geometries. The present work is aimed at obtaining a solution for the developing laminar free convection in a vertical eccentric annulus. However, for the sake of completeness and understanding of the physics of the

developing convection we will introduce a literature review for the developing convection in different geometries.

### 2.3.1 Developing Convection between Parallel Plates

The developing free convection between isothermal vertical parallel plates has been firstly studied by Elenbaas [29]. The average Nusselt number over a wide range of Rayleigh number was determined theoretically and experimentally. Elenbaas [30] extended the parallel-plate results to other geometries such as vertical tubes of different shapes of cross section.

The development of free convection between heated vertical plates has been studied by Bodoia and Osterle [31]. They solved the equations governing the free convection between two vertical isothermal plates kept at the same temperature. In their analysis they assumed that the pressure defect ( difference between the local pressure and ambient pressure at a specific elevation ) to be zero at both the inlet and outlet of the channel. They calculated the required height to suck a specific flow rate, using a noniterative method to solve the set of algebraic equations resulted from the finite-difference representation of the boundary-layer equations in the developing region. They also evaluated the velocity and temperature profiles along with the variation of the pressure defect through the developing region.

Dyer and Fowler [32], Aung, Fletcher and Sernas [33], Miyatake and Fujii [34,35] and Miyatake et al. [36] used the same boundary-layer model and the solution method of Bodoia and Osterle [31] for the vertical parallel plates to deal with other

various thermal boundary conditions. An analytical method based on a slug flow linearization of the governing boundary-layer-type equations has been used for this problem by Quintiere and Mueller [37].

Narang and Krishnamoorthy [38,39] pointed out that there was no explicit solution for the pressure and velocity field for flow between parallel plates at low Reynolds numbers. This was the motivation of their work through which they provided such a solution by linearizing the inertial terms in the Navier-Stokes equations, parallel and perpendicular to the flow. In their analysis the nonlinear inertia term $V.\nabla V$ was replaced by $< V >.\nabla V$ where $< V >$ represents the average velocity over the cross section of the parallel plates. Aung and Worku [40,41] presented a numerical study for the developing flow and flow reversal in a vertical parallel-plate channel with asymmetric wall temperature. They also assumed the pressure defect at the inlet and the outlet to be zero.

Utilizing the vorticity transport equation along with the stream function instead of the momentum equations and the primitive variables, Ingham et al. [42] conducted a numerical investigation of steady laminar combined convection flows in vertical parallel plate ducts with asymmetric constant wall temperatures. The streamwise diffusion terms in the governing equations were neglected and the resulting parabolic equations were expressed in an implicit finite-difference scheme and solved using a marching technique.

To illustrate the substantial influences of heating conditions, Chin-Hasiang et al. [43] presented a study with closed-form expressions for the thermal characteristics of free convection in the locally fully developed region with vertical parallel-plate channels. They conducted their study for three combinations of thermal boundary conditions which are namely (isothermal-isothermal, isoflux-isothermal, and isolflux-isoflux). The pressure defect in this analysis also was considered to be zero at both the inlet and outlet of the channel.

Rostami and Mortazavi [44] presented an analytical prediction of the Nusselt number in a simultaneously developing laminar flow between parallel plates. In their analysis they considered the wall temperatures to be uniform and equal.

### 2.3.2 Developing Convection through Cylindrical Ducts

By means of a linearization approximation, Langhaar et al. [45] solved the Navier-Stokes equations for the case of steady forced flow in the entrance length of a straight tube. Lundegren et al. [46] devised a means of determining the pressure drop due to the entrance region in ducts of arbitrary cross section. They linearized the inertia terms of the momentum equation, employed the mechanical energy equation, and applied an integral technique. Their resulting expressions neither require nor provide entrance region velocity distribution but are capable of providing the entrance region pressure loss from the knowledge of only inlet and fully developed velocity profiles.

Laminar forced flow in the entrance region of a circular pipe has been studied numerically by Hornbeck [47] who solved the boundary-layer equations, using a method similar to that introduced by Bodoia [48].

Giving attention to the incompressible laminar flow in entry of rectangular ducts, Han [49] solved the problem of determining the hydrodynamic entrance length in a rectangular channel by the method of linearization of Navier-Stokes equations.

Reviewing and discussing the previously introduced analytical work to study the laminar incompressible flow in the entrance region of ducts with different cross sections, Sparrow et al. [50] devised a method of analysis for determining the developing laminar flow velocities and the corresponding pressure drop in the entrance region of tubes and ducts. The method was formulated in a general manner which applies to ducts of any cross section. Specific application was made for flow in a circular tube and in a parallel-plate channel.

Kageyama and Izumi [51], Davis and Perona [52] and Dyer [53] extended the method of Bodoia and Osterle [31] to study the developing free convection in vertical circular tubes with both the constant heat flux and the isothermal conditions. Takhar [54] used the von Karman - Polhausen integral method to predict the flow and heat transfer due to free convection in the entry region of an isothermally cooled vertical open-ended pipe. Meric [55] applied a Laplace transform to the slug flow linearization technique, used by Quintiere and Mueller [37], to study this problem.

Studying the laminar entrance flow of an incompressible viscous fluid in a square duct, Carlson and Hornbeck [56] developed two approximate mathematical

hydrodynamic models, the more exact one of them includes the transverse momentum equations. The two models have been developed based on an order of magnitude analysis.

### 2.3.3 Developing Convection through Concentric Annular Ducts

Hatton and Quarmby [57] presented the solution of Graetz problem in an annulus with a heated core and an insulated outer wall with both uniform temperature and heat input on the inside wall. Using an approximate integral method Reynolds et al. [58] solved the governing equations for the heat transfer in annular passages with simultaneously developing velocity and temperature profiles in laminar forced flow. They reported that the flow remains laminar for a distance of 13 diameters downstream for Reynolds number of 27,000. Their results were presented for Pr = 0.7. Sparrow and Lin [59] applied a method similar to that introduced in [50] to provide the axial velocity distribution and the axial pressure drop for laminar forced flow in the entrance region of concentric annular ducts.

Based on a simple linearized finite-difference scheme, Coney and El-Shaarawi [60] presented a numerical solution for the boundary-layer equations describing a hydrodynamically developing laminar flow with constant physical properties in the entrance region of concentric annuli with rotating inner walls. In their analysis they extended the method of solution which was firstly introduced by Bodoia and Osterle [31].

Coney and El-Shaarawi [61] investigated laminar forced convection heat transfer in concentric annuli with simultaneously developing hydrodynamic and thermal boundary layers. They presented results for thermal boundary conditions of the third kind as defined by Reynolds et al. [13]. First they solved the hydrodynamic entry length problem to obtain the velocity profile. Then, they solved the energy equation to obtain the temperature profiles.

El-Shaarawi and Sarhan [62] extended the method of solution presented before [60 and 61] to solve the problem of developing laminar free convection in open-ended vertical concentric annuli with a rotating inner cylinder for which the energy and momentum equations are coupled through the buoyancy term. In their analysis, El-Shaarawi and Sarhan assumed that the pressure defect at the entrance of the annulus should equal to a negative value to be obtained by applying Bernoulli's equation at the entrance. Results were presented for boundary conditions of the third kind (i.e., one wall is kept isothermal while the other is kept adiabatic).

As a special case of the previous one, El-Shaarawi and Sarhan [63] presented the results for the developing laminar free convection in heated vertical open-ended concentric annuli with stationary walls for the boundary condition of the third kind. Al-Arabi et al. [64] conducted a numerical and experimental study for the natural convection through vertical annuli with one wall uniformly heated and the other is adiabatic, i.e. thermal boundary conditions of the second kind.

In a more general case, El-Shaarawi and Kodah [65] dealt with the developing natural convection in an open-ended vertical concentric annulus with two rotating

boundaries and a uniformly heated inner wall. The governing equations have been solved numerically. Rogers and Yao [66] discussed the physics involved in the natural convection and the buoyancy-driven motion of a viscous fluid enclosed in a tall heated vertical concentric annulus with inner wall heated at uniform heat flux while the outer is insulated.

### 2.3.4 Developing Flow through Eccentric Annular Ducts

Vilenski et al. [67] Pointed out that the solution of the problem of heat transfer in channels with annular cross section is usually restricted to the axial symmetrical cases. Moreover, it is difficult to obtain an analytical solution to the problem of heat transfer in the thermal input section in the absence of axial symmetry. So, they presented a numerical solution to the problem of laminar forced flow and heat transfer in an eccentric slit. In their study, they presented an analysis for the Graetz problem for boundary condition of the second kind with two different but uniform heat fluxes on the walls. They presented results for uniform heat flux at one wall while the other was insulated. Their solution was obtained by using the alternating direction implicit method in writing the finite difference representation of the governing equations.

Feldman et al. [6,7] analyzed the hydrodynamic and thermal entrance region for forced convection in straight eccentric ducts. Because of the absence of the axisymetry, the three velocity components are present in the entrance region. Based on the boundary-layer theory, they developed a model of two governing equations for the hydrodynamic problem, namely, the continuity and the streamwise momentum equation. The two

transverse momentum equations have been dropped through an order of magnitude analysis. To complete their hydrodynamic model, they used the integral form of the continuity equation and an additional relation between the two transverse velocity components.

The above extensive literature review shows that there is no available work pertaining to free convection in vertical eccentric annuli.

# Chapter 3

# OBJECTIVES OF THE PRESENT WORK AND PROBLEM FORMULATION

## 3.1 Objectives of the Present Work

The present work is aimed at obtaining a solution for the developing laminar free convection in open-ended vertical eccentric annuli. The lack of information regarding the limiting cases of conduction and fully developed free convection heat transfer in such a geometry, motivated the study of these limiting cases during the present work. It is worth mentioning that if a vertical annulus is sufficiently high, the developing free convection in such an annulus would reach its fully developed state. On the other hand, if the temperature difference is too small the conduction mode of heat transfer would prevail before the onset of free convection. Thus, it might be seen that the above cases of conduction and fully developed free convection are limiting cases for the more

general problem under investigation. So the objectives of the present work are to investigate the following.

1. Conduction heat transfer in infinitely long eccentric hollow cylinders with internal uniform heat generation per unit volume.
2. Fully developed laminar free convection in vertical eccentric annuli.
3. Developing laminar free convection in vertical eccentric annuli.
4. Developing laminar forced convection in eccentric annuli.

It is worth mentioning here that the fourth problem, developing laminar forced convection, has been treated by Feldman et al. [6,7]. However, it will be solved here to check the validity of the proposed model and the adequacy of the numerical scheme and the computer code developed to solve the proposed model.

## 3.2 Mathematical Model and Problem Formulation

### 3.2.1 Introduction

The first step in any analytical, or numerical, solution of fluid and heat flow problems is to choose an orthogonal coordinate system such that its coordinate surfaces coincide with the boundary surfaces of the region under consideration. For example the rectangular coordinate system is useful for rectangular regions, the cylindrical coordinate systems are used for regions having boundaries with cylindrical shapes, while the spherical coordinate system is used for bodies having spherical boundaries and so on.

The aim of the present work is to investigate the heat transfer in eccentric cylindrical annuli for which a two-dimensional cross section is given in Figure 3.1(a). Because of the asymmetry involved in the geometry under consideration the cylindrical coordinate will be difficult to use in expressing the governing equations. The most powerful orthogonal curvilinear coordinate system which could be used to express the partial differential equations describing the flow and heat transfer through eccentric annuli is the bipolar coordinate system shown in Fig. 3.1(b). The bipolar coordinate system is nothing but a set of orthogonal eccentric cylinders. So the boundary surfaces of an eccentric annulus may be taken as one of the coordinates and the other coordinate will be the set of the eccentric cylinders which orthogonally intersect the boundaries of the annulus.

### 3.2.2 Bipolar Coordinate System

The transformation of the governing equations into bipolar coordinate system is very tedious, however the details of transformation into a general orthogonal curvilinear coordinate were reported before [68-69]. Writing down the governing equations in a general orthogonal curvilinear coordinate system, one can easily rewrite them in the particular orthogonal coordinate system desired. In this study we have adopted the bipolar coordinate system *($\eta$, $\xi$ and z)* which has the following relations to the Cartesian coordinate system *(x, y and z)*.

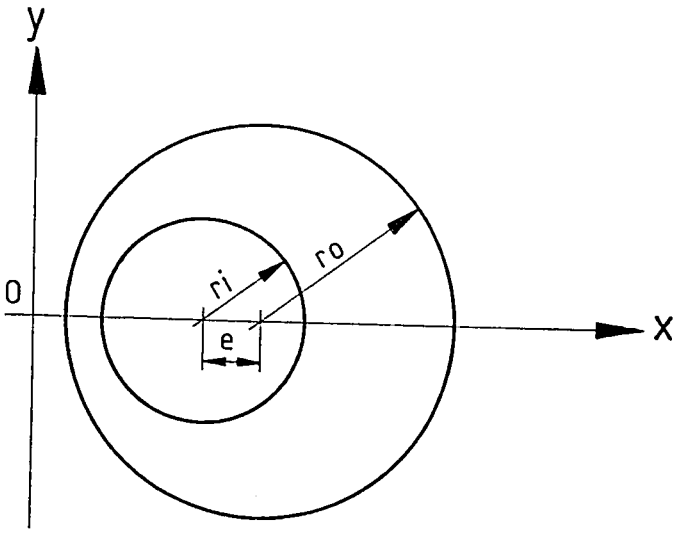


Fig. 3.1(a) Two-dimensional plane of the gometry under consideration.

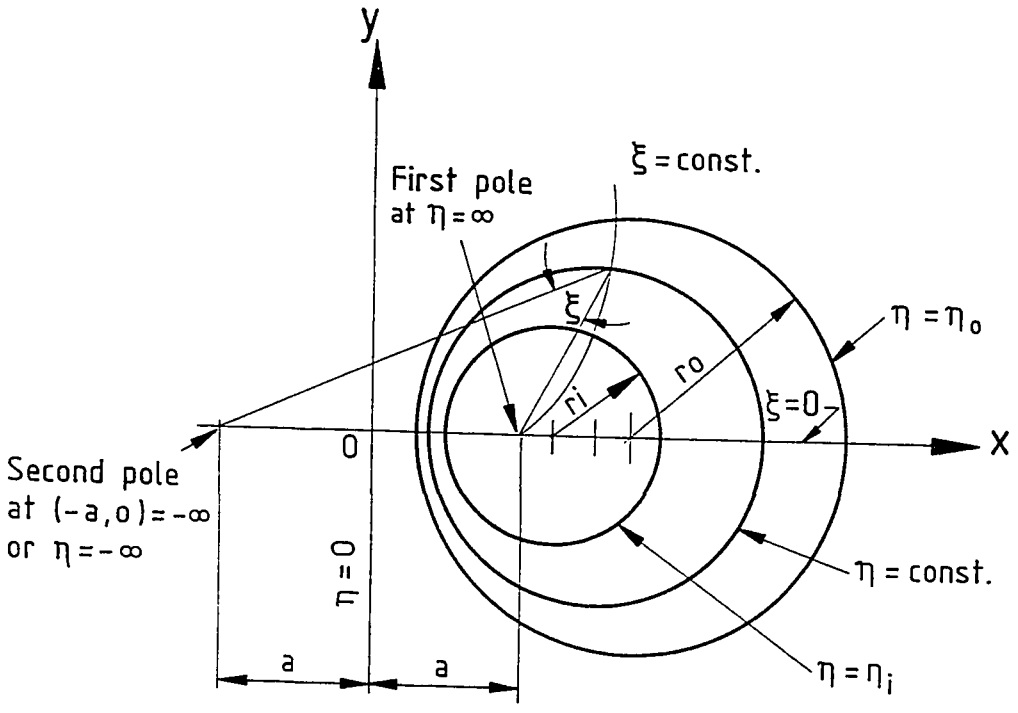


Fig. 3.1 (b) Bipolar coordinate system.

$$x=\frac{a\ Sinh(\eta)}{Cosh(\eta)-Cos(\xi)} \tag{3.1}$$

$$y=\frac{a\ Sin(\xi)}{Cosh(\eta)-Cos(\xi)} \tag{3.2}$$

$$z = z \tag{3.3}$$

In the above relations, $a = r_i\ Sinh(\eta_i) = r_o\ Sinh(\eta_o)$, where $r_i$ and $r_o$ are the radii of the inner and outer cylinders, respectively, while $\eta_i$ and $\eta_o$ denote inner and outer annulus surfaces defined by the following two equations in terms of the annulus radius ratio, $N = r_i/r_o$, and the dimensionless eccentricity, $E = e/(r_o - r_i)$,

$$\eta_i = Cosh^{-1}\left(\frac{N(1+E)^2+(1-E)^2}{2NE}\right) \tag{3.4}$$

$$\eta_o = Cosh^{-1}\left(\frac{N(1-E)^2+(1+E)^2}{2E}\right) \tag{3.5}$$

The details of the relations between the Cartesian coordinates *( x,y, and z )* and the bipolar Coordinates *(η, ξ and z)* are summarized in Appendix A. Appendix B includes the derivation of the relationships between the geometrical parameters, such as radius ratio N and relative eccentricity E, and the bipolar coordinates of the boundaries, $\eta_i$ and $\eta_o$.

### 3.2.3 General Form of The Governing Equations

The governing equations describing flow and heat transfer through an eccentric annulus are the conservation equations of mass (continuity equation), momentum

(Navier-Stokes equations) and energy. Assuming constant physical properties, one can write the full conservation equations in a vectorial form as follows.

**Continuity Equation**

$$\nabla . V = 0 \tag{3.6}$$

**Momentum Equation**

$$\rho \frac{DV}{Dt} = F - \nabla P + \mu \nabla^2 V \tag{3.7}$$

**Energy Equation**

$$\rho c_p \frac{DT}{Dt} = k \nabla^2 T + Q''' + \mu \Phi \tag{3.8}$$

These equations can be rewritten in any general orthogonal curvilinear coordinate system. However, in our case the bipolar coordinate system has been adopted to simplify the form of the governing equations and easily impose the boundary conditions. The above equations in this coordinate system will be as follows.

**The continuity equation**

$$\frac{\partial hw}{\partial \xi} + \frac{\partial hv}{\partial \eta} + \frac{\partial h^2 u}{\partial z} = 0 \tag{3.9}$$

## Momentum (Navier -Stokes) Equations

### 1 - Momentum equation in ξ- direction

$$\rho\left(\frac{\partial w}{\partial t}+\frac{w}{h}\frac{\partial w}{\partial \xi}+\frac{v}{h^2}\frac{\partial hw}{\partial \eta}+u\frac{\partial w}{\partial z}-\frac{v^2}{h^2}\frac{\partial h}{\partial \xi}\right)=F_\xi-\frac{1}{h}\frac{\partial P}{\partial \xi}$$
$$+\frac{\mu}{h}\left\{\frac{\partial^2}{\partial z^2}(hw)+\frac{1}{h^2}\frac{\partial^2(hw)}{\partial \eta^2}+\frac{1}{h^2}\frac{\partial^2(hw)}{\partial \xi^2}\right\} \qquad (3.10)$$
$$+\frac{\mu}{h}\left\{\frac{2}{h^3}\left(\frac{\partial(hv)}{\partial \xi}-\frac{\partial(hw)}{\partial \eta}\right)\frac{\partial h}{\partial \eta}+\frac{2}{h^2}\frac{\partial h}{\partial \xi}\frac{\partial(hu)}{\partial z}\right\}$$

### 2. Momentum Equation in η- direction

$$\rho\left(\frac{\partial v}{\partial t}+\frac{w}{h^2}\frac{\partial(hv)}{\partial \xi}+\frac{v}{h}\frac{\partial v}{\partial \eta}+u\frac{\partial v}{\partial z}-\frac{w^2}{h^2}\frac{\partial h}{\partial \eta}\right)=F_\eta-\frac{1}{h}\frac{\partial P}{\partial \eta}$$
$$+\frac{\mu}{h}\left\{\frac{\partial^2}{\partial z^2}(hv)+\frac{1}{h^2}\frac{\partial^2(hv)}{\partial \eta^2}+\frac{1}{h^2}\frac{\partial^2(hv)}{\partial \xi^2}\right\} \qquad (3.11)$$
$$+\frac{\mu}{h}\left\{-\frac{2}{h^3}\left(\frac{\partial(hv)}{\partial \xi}-\frac{\partial(hw)}{\partial \eta}\right)\frac{\partial h}{\partial \xi}+\frac{2}{h^2}\frac{\partial h}{\partial \eta}\frac{\partial(hu)}{\partial z}\right\}$$

### 3. Momentum Equation in Z - direction

$$\rho\left(\frac{\partial u}{\partial t}+\frac{w}{h}\frac{\partial u}{\partial \xi}+\frac{v}{h}\frac{\partial u}{\partial \eta}+u\frac{\partial u}{\partial z}\right)=F_z-\frac{\partial P}{\partial z}+\frac{\mu}{h^2}\left[\frac{\partial^2 u}{\partial \xi^2}+\frac{\partial^2 u}{\partial \eta^2}+h^2\frac{\partial^2 u}{\partial z^2}\right] \qquad (3.12)$$

### The Energy Equation

$$\rho C_p\left(\frac{\partial T}{\partial t}+\frac{w}{h}\frac{\partial T}{\partial \xi}+\frac{v}{h}\frac{\partial T}{\partial \eta}+u\frac{\partial T}{\partial z}\right)=\frac{K}{h^2}\left[\frac{\partial^2 T}{\partial \xi^2}+\frac{\partial^2 T}{\partial \eta^2}+h^2\frac{\partial^2 T}{\partial z^2}\right]+Q'''+\mu\,\Phi \qquad (3.13)$$

In the above equations $h$ is the coordinate transformation scale factor [$h = a/(\cosh \eta - \cos\xi)$]. The details of writing the above equations in a general curvilinear orthogonal coordinate system then in bipolar coordinates are presented in Appendix C. The foregoing equations along with the initial and/or the boundary conditions will be rewritten for each case under consideration separately. Thus, the above general equations will be reduced according to the case under consideration. Detailed analysis for each case will be introduced hereinafter.

## 3.3 Governing Equations for the Limiting Cases

### 3.3.1 Transient Conduction in Eccentrically Hollow Cylinders

Prior to the onset of free convection in an annular channel the conduction mode is the prevailing heat transfer mode particularly when the temperature is low and radiation is negligible. Heat conduction and heat storage capacity in eccentric configurations may also be important in cases of eccentrically drilled tubes or hollow shafts or eccentric insulations.

Since an annulus has two boundary surfaces on which thermal conditions may be independently imposed, there is a large number of conduction heat transfer problems of significant interest. However, with some common assumptions [70] the energy equation becomes linear and homogeneous and consequently the superposition technique can be utilized provided that the boundary conditions are also linear. With the application of such a mathematical technique, a solution (temperature field) satisfying arbitrary boundary conditions could be determined by simply adding multiples of solutions (temperature fields) satisfying certain simple boundary conditions. For example, on each of the two

boundary surfaces, one of the following three linear boundary conditions is usually employed. The temperature may be constant, or the temperature gradient (normal to the boundary) may be constant (i.e., constant heat flux when the thermal conductivity $k$ is constant), or there may be heat exchange by convection with an environment at a constant ambient temperature according to Newton's law of cooling (i.e., heat transfer is linearly proportional to the difference between the temperature of the boundary and that of the environment). These simple-linear boundary conditions are usually referred to as the boundary condition of the first kind, the second kind, and the third kind, respectively [70]. Thus, for an annulus, there are nine heat conduction problems corresponding to the possible nine combinations of the aforesaid thermal conditions on the two surface boundaries. Ozisik [70] presented exact solutions for these nine heat conduction problems in concentric hollow cylinders when the boundary conditions of the first, second, and third kind are homogeneous. However, since the two cylindrical boundaries of an annulus have unequal areas these nine combinations of the three simple-linear boundary conditions can indeed give 18 different physical situations when the asymmetric thermal conditions are interchanged on the inner and outer boundaries in each case.

The above discussion concerning superposition of solutions corresponding to simple boundary conditions is also applicable to fully developed forced or natural convection in annular passages. However, the boundary condition of the third kind is meaningless in such convection problems. Therefore, Reynolds et al. [13] completely solved the problem of heat transfer to fully developed laminar flow in concentric annuli by defining only four fundamental boundary conditions. These fundamental boundary

conditions are combinations of the aforesaid boundary conditions of the first and second kind when applied on each of the two boundaries of an annulus. The fundamental boundary conditions of the first type correspond to a prescribed isothermal temperature at one wall while the opposite wall is kept isothermal at the inlet fluid temperature. The second fundamental boundary conditions are when one wall is maintained at uniform heat flux (constant temperature gradient) and the opposite wall is adiabatic. The fundamental boundary conditions of the third kind are obtained by keeping one of the walls isothermal and the opposite wall adiabatic. The fourth fundamental boundary conditions correspond to one wall maintained at uniform heat flux while the opposite wall is kept isothermal at the inlet fluid temperature.

The geometry of the problem under consideration is an infinitely long as compared to the pipe diameter, eccentrically hollow cylinder for which a two-dimensional cross-section is shown in Fig. 3.1. The eccentric annular material is assumed to have constant physical properties and uniform internal heat generation per unit volume. For any prescribed thermal conditions on the two circular boundaries of this geometry and an initial condition, the unsteady heat conduction in the eccentric annulus is governed, in the bipolar ($\eta$-$\xi$) plane, by the energy equation, eq. (3.13), with the convective and the viscous dissipation terms dropped since $v = w = u = 0$ everywhere. Moreover, the axial diffusion of energy in the axial direction is also omitted since the cylinder considered is infinitely long. Hence, the following two-dimensional transient energy equation is the governing equation for the transient conduction in the eccentric annulus:

$$\frac{\partial^2 T}{\partial \eta^2} + \frac{\partial^2 T}{\partial \xi^2} + h^2 \frac{Q'''}{k} = \frac{h^2}{\alpha} \frac{\partial T}{\partial \tau} \tag{3.14}$$

It is to be noted that in each of the previously specified four fundamental boundary conditions there is one boundary maintained either adiabatic ($\partial T/\partial \eta = 0$) or at ambient temperature $T_o$. The boundary opposite to that maintained adiabatic or at $T_o$ is called the heat transfer boundary [14]. Thus, as the heat transfer boundary might be the inner or the outer surface, there are eight fundamental solutions that can be considered. For each of the previously mentioned four fundamental thermal boundary conditions there are two possible cases that can be considered, namely, case I, in which the heat transfer boundary is at the inner surface and case O, in which the heat transfer boundary is at the outer surface. Thus each of the eight cases that can be considered under the previously defined four fundamental boundary conditions may be designated by a number (1, 2, 3, or 4) and a letter (either I or O). The number would refer to the fundamental boundary conditions under consideration (e.g., 1 refers to fundamental boundary conditions of first type) and the letter refers to the heat transfer boundary. Thus, case (1.I) refers to a case under fundamental boundary conditions of the first type with the inner surface being the heat transfer boundary. Similarly, case (3.O) refers to a case under fundamental boundary conditions of the third kind with the outer surface being the heat transfer boundary, and so on. The following table summarizes the aforesaid eight fundamental thermal boundary conditions.

**Table 3.1 The Fundamental Thermal Boundary Conditions**

| Case | Inner Boundary, $\eta_i$ | Outer Boundary, $\eta_o$ |
|---|---|---|
| 1.I | $T = T_w$ | $T = T_o$ |
| 1.O | $T = T_o$ | $T = T_w$ |
| 2.I | $q_i'' = k(\frac{1}{h}\frac{\partial T}{\partial \eta})_{\eta_i}$ | $(\frac{\partial T}{\partial \eta})_{\eta_o} = 0$ |
| 2.O | $(\frac{\partial T}{\partial \eta})_{\eta_i} = 0$ | $q_o'' = -k(\frac{1}{h}\frac{\partial T}{\partial \eta})_{\eta_o}$ |
| 3.I | $T = T_w$ | $(\frac{\partial T}{\partial \eta})_{\eta_o} = 0$ |
| 3.O | $(\frac{\partial T}{\partial \eta})_{\eta_i} = 0$ | $T = T_w$ |
| 4.I | $q_i'' = \pm k(\frac{1}{h}\frac{\partial T}{\partial \eta})_{\eta_i}$ | $T = To$ |
| 4.O | $T = T_o$ | $q_o'' = \mp k(\frac{1}{h}\frac{\partial T}{\partial \eta})_{\eta_o}$ |

(3.15)

The equation (3.14) and the boundary conditions are linear in the dependent variable *(T)* and hence fundamental solutions can be utilized to obtain more general solutions. It is worth mentioning here that in the cases of uniform heat flux boundary conditions on the heat transfer wall (cases 2 and 4), the plus and minus signs in the conditions on the $\eta = \eta_i$ are applicable for heating and cooling respectively. However, the minus and plus signs in the boundary conditions on $\eta = \eta_o$ are for heating and cooling respectively. In the present investigation only cooling the heat transfer boundary will be considered during the analysis of the two cases 2.I and 2.O, while heating the heat transfer boundary will be considered in all other cases.

Using the dimensionless parameters given in the nomenclature the governing equation (3.14) can be written, for all the cases under consideration, in the following non-dimensional form:

$$\frac{\partial^2\theta}{\partial\eta^2}+\frac{\partial^2\theta}{\partial\xi^2}+H^2Q=H^2\frac{\partial\theta}{\partial t} \tag{3.16}$$

Due to symmetry, the following two boundary conditions with respect to $\xi$ are applicable:

$$\text{For } \xi=0 \text{ and } \xi=\pi : \partial\theta/\partial\xi = 0 \tag{3.17}$$

On the other hand, in all the cases considered the annular material is initially at ambient temperature, i.e.,

$$\text{For } t\le 0 : \theta = 0 \tag{3.18}$$

For $t>0$ the heat is internally generated in the annular material and simultaneously one of its surfaces is isothermally heated to $T_w$ (or with uniform heat flux) while the other surface is kept either at the initial ambient temperature $T_o$ or adiabatic. Thus the four pairs of the fundamental thermal boundary conditions with respect to $\eta$ can be written in dimensionless form as follows:

**Table 3.2 The Dimensionless Forms of the Fundamental Thermal Boundary Conditions**

| Case | Inner Boundary, $\eta_i$ | Outer Boundary, $\eta_o$ |
|---|---|---|
| 1.I | $\theta=1.0$ | $\theta=0$ |
| 1.O | $\theta=0$ | $\theta=1.0$ |
| 2.I | $\left.\frac{\partial\theta}{\partial\eta}\right\|_{\eta_i} = \pm H(\eta_i,\xi)$ | $\left.\frac{\partial\theta}{\partial\eta}\right\|_{\eta_o} = 0$ |
| 2.O | $\left.\frac{\partial\theta}{\partial\eta}\right\|_{\eta_i} = 0$ | $\left.\frac{\partial\theta}{\partial\eta}\right\|_{\eta_o} = \mp H(\eta_o,\xi)$ |
| 3.I | $\theta=1.0$ | $\left.\frac{\partial\theta}{\partial\eta}\right\|_{\eta_o} = 0$ |
| 3.O | $\left.\frac{\partial\theta}{\partial\eta}\right\|_{\eta_i} = 0$ | $\theta=1.0$ |
| 4.I | $\left.\frac{\partial\theta}{\partial\eta}\right\|_{\eta_i} = \pm H(\eta_i,\xi)$ | $\theta=0$ |
| 4.O | $\theta=0$ | $\left.\frac{\partial\theta}{\partial\eta}\right\|_{\eta_o} = \mp H(\eta_o,\xi)$ |

(3.19)

### 3.3.2 Steady Conduction in Eccentrically Hollow Cylinders

Under steady-state conditions equation (3.16) reduces to:

$$\frac{\partial^2\theta}{\partial\eta^2}+\frac{\partial^2\theta}{\partial\xi^2} = -H^2 Q = \frac{-C^*}{(\cosh\eta-\cos\xi)^2} \tag{3.20}$$

Such steady-state conditions are achieved at considerably large values of time, i.e., the solution to the transient problem should asymptotically approach its corresponding steady-state value. Thus, steady-state analytical solutions can provide a check on the adequacy of the present transient numerical results. At considerable large values of $t$, the transient solutions should asymptotically approach such steady-state results. It is worth mentioning

here that for the thermal boundary conditions of the second kind the steady state will be reached if and only if the heat generated within the annular material equals to the heat transfer at the active wall with opposite signs (i.e., if the heat generated is exothermic, the active wall should have a cooling effect). Thus a special relation between the heat transfer rate at the active wall and the rate of heat generation within the annular material will be developed and evaluated, hereunder, through a simple energy balance for the two cases considered , namely cases 2.I and 2.O.

### 3.3.2.1 Special Analysis for Boundary Conditions of the Second Kind

For this type of boundary conditions with the exothermic internal heat generation the steady state conditions can not be achieved for heating with uniform heat flux at one boundary while keeping the other boundary adiabatic. However, the steady state can be achieved for exothermic internal heat generation with uniformly cooling the heat transfer boundary while keeping the other boundary adiabatic. The physics of such problems state that at the steady state the heat generated within the annulus should be equal to the heat rejected at the heat transfer wall. So the following simple energy balance can be written

$$Q''' \pi (r_o^2 - r_i^2) L = q''_{iw} (2\pi r_i L) \quad for \quad case \quad 2.I. \quad or$$
$$= q''_{ow} (2\pi r_o L) \quad for \quad case \quad 2.O.$$

With some manipulation, one can write the following dimensionless relation between the internal heat generation and the cooling heat flux at the heat transfer boundary;

$$Q = \frac{4N}{1+N} \quad for\ \ case\ 2.I.\ or$$

$$= \frac{4}{1+N} \quad for\ \ case\ 2.O.$$

Where:

$$Q = \frac{Q''' D_h}{q''_{iw}} \quad for\ case\ \ 2.I.\ \ or$$

$$= \frac{Q''' D_h}{q''_{ow}} \quad for\ case\ \ 2.O.$$

Using the dimensionless parameters given in the nomenclature along with the above definitions of $Q$ the governing equation will be the same as for all cases considered.

### 3.3.3 Fully Developed Laminar Forced Convection

The fully developed laminar forced convection has been already solved by Trombetta [21] for different thermal boundary conditions. However, the analytical solution of this hydrodynamically fully developed steady forced flow will be provided here for the sake of completeness. This hydrodynamically fully developed flow, which occurs if the channel is sufficiently long, provides an analytical check on the numerical solution to be obtained for the developing laminar forced convection. For this problem the flow is assumed to be steady and the fluid is assumed to be a Newtonian with constant properties and hence the energy equation is uncoupled from the equations of motion. Body forces, viscous dissipation, internal heat generation and the radiation heat transfer are absent. In addition to the above assumptions, for hydrodynamic full development $v = w = 0$ and $\partial u / \partial z = 0$ everywhere. Hence the continuity equation (3.9)

and the inertia terms on the left hand side of eq. (3.12) vanishes while the $\xi$- and $\eta$-momentum equations (3.10 and 3.11) reduce to $\partial p / \partial \xi = 0$ and $\partial p / \partial \eta = 0$, respectively. Accordingly for hydrodynamically fully developed forced flow $\partial p / \partial z = [ (dp/dz)_{fd} ]$ = constant and the resulting axial momentum equation reduces to

$$\frac{\partial^2 u_{fd}}{\partial \xi^2}+\frac{\partial^2 u_{fd}}{\partial \eta^2}=h^2\left(\frac{d p}{d z}\right)_{fd} \tag{3.21}$$

Using the dimensionless parameters given in the nomenclature the equation above can be written in a dimensionless form as

$$\frac{\partial^2 U_{fd}}{\partial \xi^2}+\frac{\partial^2 U_{fd}}{\partial \eta^2}=H^2\left(\frac{d P}{d Z}\right)_{fd} \quad =\frac{-C^*}{(\cosh\eta - \cos\xi)^2} \tag{3.22 a}$$

This equation is identical to equation (3.20) of the steady-state heat conduction with internal heat generation.

For fluids having Prandtl number less than unity, the hydrodynamic development length is larger than the thermal entrance length. Consequently, a hydrodynamically fully developed forced flow of a fluid of $Pr \leq 1$ is also thermally fully developed. Under such full-development conditions $\partial \theta / \partial Z = 0$ (for boundary conditions of first, third and fourth kind), $V = W = 0$ and hence for these three kinds of boundary conditions eq. (3.13) in a dimensionless form reduces to

$$\frac{\partial^2 \theta_{fd}}{\partial \eta^2}+\frac{\partial^2 \theta_{fd}}{\partial \xi^2}=0, \tag{3.22 b}$$

which is typically the steady conduction equation with no heat generation.

On the other hand $\partial \theta / \partial Z$ is constant for boundary conditions of the second kind. A complete solution for the velocity and temperature at any section in the channel always depends on the solution of the preceeding section (i.e., to solve for the temperature and velocity profiles in the fully developed region, the velocity and temperature profiles as the flow exits from the developing region should be known). Therefore, the solution of the fully developed free convection under thermal boundary conditions of the second kind will be obtained via the solution of the developing region.

### 3.3.4 Fully Developed Laminar Free Convection in Vertical Open-Ended Eccentric Annuli

Free convection heat transfer in an eccentric annulus occurs in many industrial situations as mentioned before. The analysis of fully developed convection is very important in predicting the amount of heat transfer in heat transfer equipment. Fully developed natural convection in open-ended vertical annuli is the limiting case for the more general problem of developing free convection in such channels. In the latter case fully developed conditions can be achieved if the annulus is sufficiently high or, more general, if the Rayleigh number has a sufficiently low value.

The in-depth literature survey summarized in Chapter 2 has revealed that there is no previous work reported for the problem of the fully developed free convection in open-ended vertical eccentric annular channels. The lack of information regarding this fully developed convection motivated the present work.

Figure 3.2 shows a two-dimensional cross-sectional elevation and a plan for the channel under consideration. It comprises a vertical eccentric annulus of finite length,

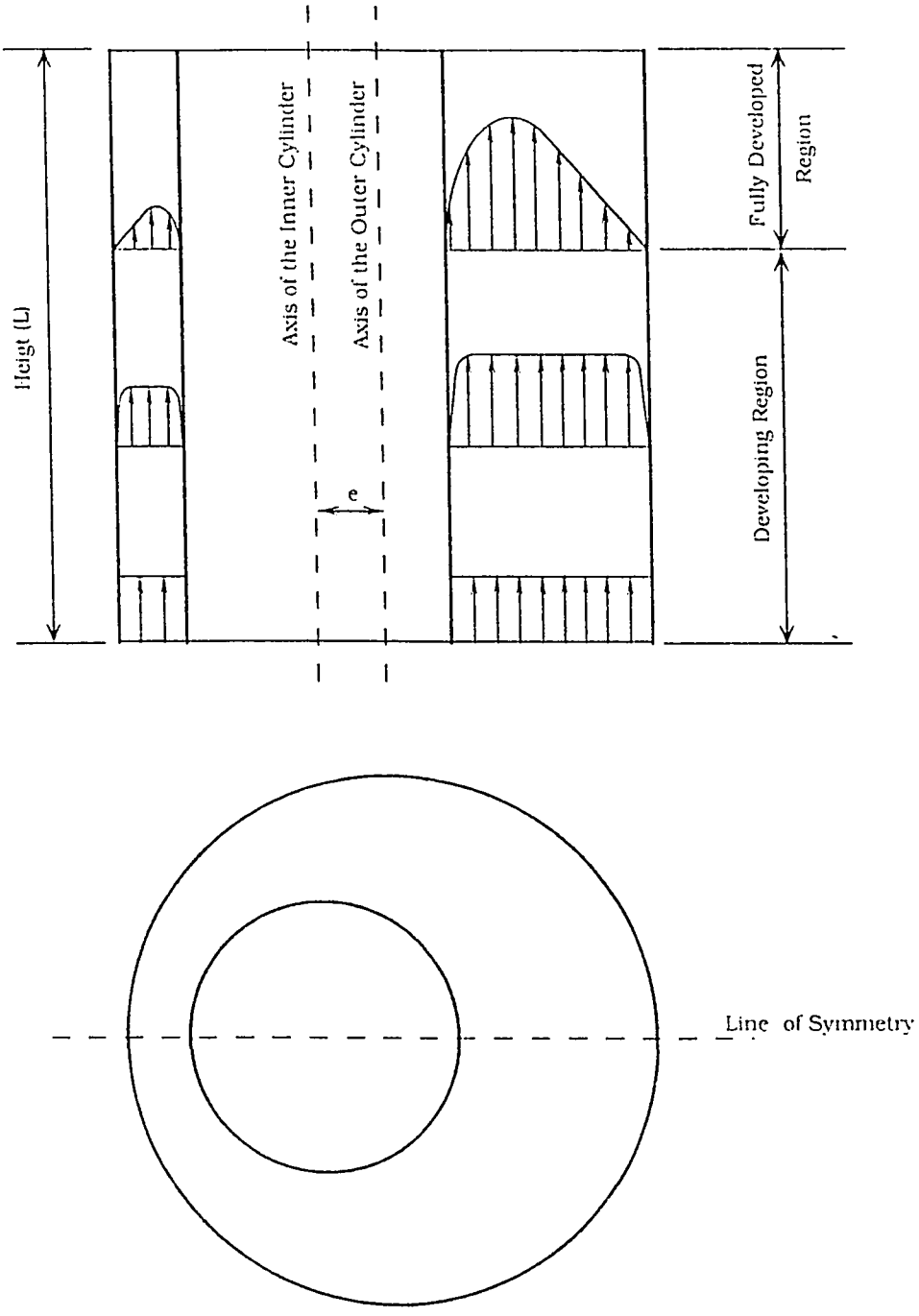


Fig. 3.2 Two dimensional elevation and plan for the geometry under consideration

open at both ends and immersed in a stagnant Newtonian fluid of infinite extent maintained at constant temperature $T_o$. Free convection flow is induced inside this annular channel as a result of heating or cooling one of the channel walls either isothermally or with a uniform heat flux while keeping the other wall either adiabatic or at ambient temperature. The fluid enters the channel at the ambient temperature $T_o$ and is assumed to have constant physical properties but obeys the Boussinesq approximation according to which its density is allowed to vary with temperature in only the gravitational body force term of the vertical (axial) momentum equation. Thus Boussinesq approximation neglects the compressibility effect everywhere except for the buoyancy-force term. Body forces in other than the vertical direction, viscous dissipation, internal heat generation, and radiation heat transfer are absent. If the channel is sufficiently high, fully-developed flow conditions can be achieved.

Fully developed free convection in the vertical annular channel means that the velocity components in $\eta$ and $\xi$ directions (namely v and w, respectively) vanish, the axial velocity component $u$ does not vary with the axial coordinate, i.e., $u = u(\eta,\xi)$ or $\partial u / \partial z = 0$, and the flow is also thermally fully developed [14], i.e., $\partial^2 T / \partial z^2 = 0$. Thus, the continuity equation automatically vanishes and the momentum equations in $\eta$ and $\xi$ directions reduce respectively to $\partial p / \partial \eta = 0$, i.e., p is independent of $\eta$, and $\partial p / \partial \xi = 0$, i.e., $p$ is also independent of $\xi$. Consequently, the pressure is a function of $z$ only (hence $\partial p / \partial z = dp/dz$) and the equations which govern the fully developed free convection in vertical eccentric annuli, in terms of the dimensionless parameters given in the nomenclature, are the following $z$-momentum and energy equations, respectively.

$$\frac{1}{H^2}\left(\frac{\partial^2 U}{\partial \eta^2}+\frac{\partial^2 U}{\partial \xi^2}\right)-\frac{1}{4(1-N)^2}\frac{dP}{dZ}=-\frac{\theta}{4(1-N)^2} \tag{3.23}$$

$$\frac{1}{H^2}\left(\frac{\partial^2 \theta}{\partial \eta^2}+\frac{\partial^2 \theta}{\partial \xi^2}\right)=4(1-N)^2.\mathrm{Pr}.U.\frac{\partial \theta}{\partial Z} \tag{3.24}$$

### 3.3.4.1 General Analysis

Differentiating eq. (3.23) with respect to $Z$, taking into consideration that $\partial U/\partial Z = 0$, gives

$$\frac{\partial \theta}{\partial Z}=\frac{\partial^2 P}{\partial Z^2} \tag{3.25}$$

Substituting for $\theta$ from (3.23) into (3.24), taking into consideration (3.24) and that, since $P = f(Z)$, $\partial^2/\partial\eta^2\,(dP/dZ) = \partial^2/\partial\xi^2\,(dP/dZ) = 0$, yields

$$\frac{1}{UH^2}\left(\frac{\partial^2}{\partial\eta^2}\left(\frac{1}{H^2}\left(\frac{\partial^2 U}{\partial\eta^2}+\frac{\partial^2 U}{\partial\xi^2}\right)\right)+\frac{\partial^2}{\partial\xi^2}\left(\frac{1}{H^2}\left(\frac{\partial^2 U}{\partial\eta^2}+\frac{\partial^2 U}{\partial\xi^2}\right)\right)\right)=\mathrm{Pr}.\frac{d^2 P}{dZ^2} \tag{3.26}$$

The left hand side of eq. (3.26) is a function of $\eta$ and $\xi$ only while its right hand side is a function of $Z$ only. Hence a solution of eq. (3.26) in the form $U = U(\eta,\xi)$ is possible only if

$$d^2 P/dZ^2=\alpha \tag{3.27}$$

where $\alpha$ is a constant. From eq. (3.25) and (3.27) we then have

$$\partial\theta/\partial Z=\alpha \tag{3.28}$$

which means that, in the fully developed flow region, $\partial \theta / \partial Z$ is also constant and hence $\theta$ varies linearly with Z. Thus, regardless of the value of *Pr*, a hydrodynamically fully developed free convection ($\partial U / \partial Z = 0$) necessarily means that the flow is also thermally fully developed.

Equation (3.28) implies that for a point of given $\eta$ and $\xi$ the dimensionless temperature ($\theta$) varies linearly with *Z* as the fluid moves axially from one cross-section to another. However, in some of the cases under consideration (boundary conditions of first, third and fourth kind) at least one of the annulus boundaries ($\eta_i$ or $\eta_o$) is kept isothermal and hence $\partial \theta / \partial Z = 0$ on such an isothermal boundary while $\partial \theta / \partial Z = \alpha$ = *constant* for boundary conditions of the second kind. The value of $\alpha$ will be dependent on the thermal conditions at the entrance of the channel, i.e., to determine the value of $\alpha$ for the fully developed free convection with boundary conditions of the second kind the entrance developing region should be solved first, otherwise many solutions may be obtained for the energy equation (3.24) by adding, to its solution if exist, any arbitrary constant that will automatically satisfy the Neuman boundary conditions (boundary conditions of the second kind). Thus the solution for the boundary conditions of the second kind can be obtained by solving the developing problem rather than solving equations (3.23) and (3.24). On the other hand, the combination of equation (3.28) with an isothermal boundary condition leads to the conclusion that $\alpha$, for such a fully-developed region, must equal zero ($\alpha = 0$). Consequently, the energy equation (3.24) reduces (under thermal boundary conditions of the first, third and fourth kinds) to the following.

$$\left(\frac{\partial^2\theta}{\partial\eta^2}+\frac{\partial^2\theta}{\partial\xi^2}\right)=0 \tag{3.29}$$

Equation (3.27) with $\alpha = 0$ means that the pressure gradient ($dP/dZ$) in the fully-developed region is constant (i.e. $P$ varies linearly with $Z$). However, if the channel is extremely high the fully-developed region could occupy a very large portion of the channel height, the developing length could be neglected in comparison with that of the fully-developed region and hence the assumption of fully-developed flow right from the channel entrance can be made. In this case, integrating eq. (3.27) twice and applying the boundary conditions that the pressure is atmospheric at both inlet and exit of the annulus, i.e. $P = 0$ at $Z = 0$ and L [14] leads to the following simplified form of equation (3.23).

$$\left(\frac{\partial^2 U}{\partial\eta^2}+\frac{\partial^2 U}{\partial\xi^2}\right)=-\frac{\theta}{4(1-N)^2}H^2 \tag{3.30}$$

Finally, the governing equations for the fully developed laminar free convection, subject to the thermal boundary conditions of the first, third and fourth kinds are equations (3.29) and (3.30) which are strongly coupled through the buoyancy term. Due to symmetry about the x-axis, the governing equations (3.29) and (3.30) need to be solved in only half of the channel, i.e. for $0 \le \xi \le \pi$. In all cases under consideration equation (3.30) is subject to the following hydrodynamic and symmetric boundary conditions, respectively.

$$\left.\begin{array}{l} For\ \eta=\eta_i\ or\ \eta=\eta_o\ ,\ U=0 \\ For\ \xi=0\ or\ \xi=\pi\ ,\ \partial U/\partial\xi=0 \end{array}\right\} \tag{3.31}$$

## 3.4 Developing Laminar Forced Convection in Eccentric Annuli and Free Convection in Vertical Open-Ended Eccentric Annuli

Fluid entering a duct or a channel from a reservoir undergoes a hydrodynamic and thermal development, whereby the relatively uniform inlet velocity (temperature) profile gradually transforms into a fully developed profile. This entrance region has been widely studied because the velocity development increases the pressure drop and enhances the heat transfer rate.

Laminar convection in the free regime with simultaneously developing hydrodynamic and thermal boundary layers in vertical eccentric annuli is of practical importance in many engineering situations. In atomic reactors, heat generated by atomic reactions is transferred to the coolant flowing through the annular gap between the fuel element and the coolant channel wall. Free convection is present during shut-down periods or following the coolant pump failure, and has significant effects when the coolant flow rate is reduced during periods of low operations.

The objective of this part of our study is to present an analysis for the laminar free convection in open-ended vertical eccentric annuli, for which, to the best of the author's knowledge, there is no work available in the literature.

A new model will be developed during the present work to analyze the laminar forced and free convection in eccentric annuli with simultaneously developing hydrodynamic and thermal boundary layers. The forced convection problem will be

solved here for the sake of validation of the proposed model by comparison with the previously published work of Feldman et al. [6,7].

### 3.4.1 The Governing Equations

In the entrance region the steady flow is three dimensional. Due to The absence of symmetry in the geometry under consideration the three velocity components exist. The governing equations for an incompressible fluid with constant properties and the same assumptions mentioned in Sections 3.3.3 and 3.3.4 will be eqs. (3.9) through (3.12). However, no practical means appears to be available to solve these partial differential equations in their entirety. Therefore, some simplifying assumptions, based on the boundary-layer theory (Schlichting [71] and El-Shaarawi [72] ), will be used hereinafter to develop a simpler model.

The differential continuity equation (3.9) subject to the no slip conditions on the two boundaries can be written in the following integral form.

$$\pi (r_o^2 - r_i^2)\bar{u} = 2\int_0^{\pi}\int_{\eta_o}^{\eta_i} h^2 u \, d\xi \, d\eta \tag{3.32}$$

Assuming the pressure to be a function of the axial coordinate only ($\partial p / \partial \eta = \partial p / \partial \xi = 0$ ), neglecting the axial diffusion of momentum and energy ($\partial^2 / \partial z^2 = 0$ ), dropping the $\eta$- momentum equation since the $\eta$- velocity component (v) is much smaller than the $\xi$- and z-velocity components (w and u ) and introducing the dimensionless parameters given in the nomenclature, the five equations (3.9) through (3.12) and (3.22) can be replaced by the following five dimensionless reduced equations.

**Continuity Equation**

$$\frac{\partial(HW)}{\partial\xi}+\frac{\partial(HV)}{\partial\eta}+k_1\frac{\partial(H^2U)}{\partial Z}=0 \tag{3.33}$$

**ξ- Momentum Equation**

$$\frac{W}{H}\frac{\partial W}{\partial\xi}+\frac{V}{H^2}\frac{\partial HW}{\partial\eta}+K_1U\frac{\partial W}{\partial Z}-\frac{V^2}{H^2}\frac{\partial H}{\partial\xi}$$
$$=\frac{1}{H^3}\left(\frac{\partial^2 HW}{\partial\eta^2}+\frac{\partial^2 HW}{\partial\xi^2}\right)-\frac{2}{H^4}\left(\frac{\partial HW}{\partial\eta}-\frac{\partial HV}{\partial\xi}\right)\frac{\partial H}{\partial\eta}+\frac{2K_1}{H^2}\frac{\partial H}{\partial\xi}\frac{\partial U}{\partial Z} \tag{3.34}$$

**Axial, Z- Momentum Equation**

$$\frac{W}{H}\frac{\partial U}{\partial\xi}+\frac{V}{H}\frac{\partial U}{\partial\eta}+K_1U\frac{\partial U}{\partial Z}=-K_2\frac{\partial P}{\partial Z}+K_3\theta+\frac{1}{H^2}\left(\frac{\partial^2U}{\partial\xi^2}+\frac{\partial^2U}{\partial\eta^2}\right) \tag{3.35}$$

**The Energy Equation**

$$\frac{W}{H}\frac{\partial\theta}{\partial\xi}+\frac{V}{H}\frac{\partial\theta}{\partial\eta}+K_1U\frac{\partial\theta}{\partial Z}=\frac{1}{\mathrm{Pr}.H^2}\left(\frac{\partial^2\theta}{\partial\xi^2}+\frac{\partial^2\theta}{\partial\eta^2}\right) \tag{3.36}$$

**Integral Form of the Continuity Equation**

$$\bar{U}=\frac{8(1-N)}{\pi(1+N)}\int_0^{\pi}\int_{\eta_w}^{\eta_e}U\,H^2\,d\eta\,d\xi \tag{3.37}$$

where;

$K_1=4(1-N)^2$ and $K_2=K_3=\dfrac{1}{4(1-N)^2}$ for free convection and

$K_1=K_2=1$ and $K_3=0$ for forced convection,

For the case of forced convection $\bar{U}=1.0$

In addition to the thermal boundary conditions (3.19), the above set of the governing equations are subjected to the following boundary conditions;

***at Z = 0,***

$$V = W = \theta = 0.0,\ U = U_o \tag{3.38}$$

($U_o$ equal unity for forced convection and unknown for free convection in a channel of a given height), for $\eta_o < \eta < \eta_i$

***for Z > 0;***

at $\xi = 0$ and $\xi = \pi$, the line of symmetry,

$$\frac{\partial V}{\partial \xi} = \frac{\partial W}{\partial \xi} = \frac{\partial U}{\partial \xi} = \frac{\partial \theta}{\partial \xi} = 0 \tag{3.39}$$

**Boundary conditions with respect to the pressure**

In some previous studies of developing free convection [31-36, 51-53] the pressure defect (the difference between the local pressure in the channel and the ambient pressure at the same elevation) was taken to be zero at the inlet, ignoring the acceleration of the fluid to the channel inlet. The correct initial condition, given by the application of Bernoulli's equation at the entrance has been taken into account by [37,55]. So the boundary conditions for the pressure will be

At $Z = 0$, $P = -U_o^2/2$ for free convection and

$P = 0$ for forced convection (3.40)

At $Z = L$ $P = 0$ for free convection only.

It is worth mentioning here that another model (called the second order model) based on an order of magnitude analysis (the details of which are presented in Appendix C) has also been developed and used to solve both of the free and forced convection in

an eccentric annulus. This latter model comprises five equations in five unknowns which are the reduced axial momentum equation, the integral form of the continuity, the $\eta$- and $\xi$- momentum equations in addition to the energy equation.

# Chapter 4

# METHODS OF SOLUTION

Methods of solution for the governing equations of each of the cases presented in the previous chapter will be summarized hereinafter. Most of these governing equations is very difficult to solve analytically. Hence, numerical methods have been basically used to provide solutions for most of these cases and analytical solutions could be obtained for some of the limiting cases whenever it is possible.

## 4.1. Steady Conduction in Eccentrically Hollow Cylinders

The general solution of the steady-state equation (3.20) is given by El-Saden [5], as

$$\theta_s(\eta,\xi) = \theta_c + \theta_p \,, \tag{4.1}$$

where the complementary part of the solution, after applying the boundary conditions (3.17), is

$$\theta_c = A^*\eta + B + \sum_{n=1}^{\infty}(C e^{n\eta} + D\ e^{-n\eta})\cos n\xi, \tag{4.2}$$

and the particular integral part of the solution, which is due to the internal heat generation, is

$$\theta_p = -\frac{C^*}{2}\frac{\cosh\eta}{\cosh\eta - \cos\xi} = -\frac{C^*}{2}\coth\eta - C^*\sum_{n=1}^{\infty}\coth\eta\, e^{-n\eta}\cos n\xi \tag{4.3}$$

The series part on the right-hand side of (4.2) or (4.3) is due to the eccentricity and the general solution (4.1) can now be written in the following form

$$\theta_s = A^*\eta + B - \frac{C^*}{2}\coth\eta + \sum_{n=1}^{\infty}\cos n\xi\,[C e^{n\eta} + (D - C^*\coth\eta)e^{-n\eta}] \tag{4.4}$$

It is worth mentioning that the right-hand side of equation (4.3) was given by El-Saden [5]; it can be obtained by finding a Fourier-cosine expansion of the even function [1/(coshη - cos ξ)] as shown in [73]. The details of this step is shown in Appendix E.

Applying the boundary conditions (3.19) the constants $A^*$, $B$, $C$, and $D$ in equation (4.4) are obtained for the cases considered as given in Table 4.1. It is worth noting that the values of these constants for cases (1.I) and (1.O) are given in Table 4.1 for the sake of completeness. These were obtained before by El-Saden, but in terms of two constant but different dimensional values of temperatures on the boundary surfaces.

Special analysis has been given for case 2 to evaluate the value of the constant $B$. The boundary conditions of this case are Neuman (derivative) boundary conditions as shown in Table 3.1. Therefore, many solutions can be found for the steady conduction

Table 4.1 Constants of the analytical solutions (eq. (4.4))

| Case | A | B | C | D |
|---|---|---|---|---|
| **1.I** | $\frac{\frac{C^*}{2}\left(Coth(\eta_i)-Coth(\eta_o)\right)+1}{\eta_i-\eta_o}$ | $\frac{\frac{C^*}{2}\left(\eta_i\,Coth(\eta_o)-\eta_o\,Coth(\eta_i)\right)-\eta_o}{\eta_i-\eta_o}$ | $\frac{C^*\left(Coth(\eta_o)-Coth(\eta_i)\right)}{\eta_i-\eta_o}$ | $\frac{\left(C^*\left[e^{2\eta_i}\,Coth(\eta_o)-e^{2\eta_o}\,Coth(\eta_i)\right]\right)}{e^{2\eta_i}-e^{2\eta_o}}$ |
| **1.O** | $\frac{\frac{C^*}{2}\left(Coth(\eta_i)-Coth(\eta_o)\right)-1}{\eta_i-\eta_o}$ | $\frac{\frac{C^*}{2}\left(\eta_i\,Coth(\eta_o)-\eta_o\,Coth(\eta_i)\right)+\eta_i}{\eta_i-\eta_o}$ | $\frac{C^*\left(Coth(\eta_o)-Coth(\eta_i)\right)}{\eta_i-\eta_o}$ | $\frac{\left(C^*\left[e^{2\eta_i}\,Coth(\eta_o)-e^{2\eta_o}\,Coth(\eta_i)\right]\right)}{e^{2\eta_i}-e^{2\eta_o}}$ |
| **2.I** | $\frac{-c^*}{2\,Sinh^2(\eta_o)} = \frac{-N}{2(1-N)^2(1+N)}$ | - | $\frac{\left(C^*\left[Coth(h_o)-Coth(h_i)+\frac{1}{n}\left(\frac{1}{Sinh^2(h_o)}-\frac{1}{Sinh^2(h_i)}\right)\right]-\frac{N}{\left[n(1-N)\right]}\right)}{e^{2nh_i}-e^{2nh_o}}$ | $\frac{\left(C^*\left[e^{2\eta_i}\,Coth(\eta_o)-e^{2\eta_o}\,Coth(\eta_i)+\frac{1}{n}\left(\frac{e^{2\eta_i}}{Sinh^2(\eta_o)}-\frac{e^{2\eta_o}}{Sinh^2(\eta_i)}\right)\right]-\frac{N\,e^{2\eta_o}}{\left[n(1-N)\right]}\right)}{e^{2\eta_i}-e^{2\eta_o}}$ |
| **2.O** | $\frac{-c^*}{2\,Sinh^2(\eta_i)} = \frac{-N^2}{2(1-N)^2(1+N)}$ | - | $\frac{\left(C^*\left[Coth(\eta_o)-Coth(\eta_i)+\frac{1}{n}\left(\frac{1}{Sinh^2(\eta_o)}-\frac{1}{Sinh^2(\eta_i)}\right)\right]-\frac{1}{\left[n(1-N)\right]}\right)}{e^{2\eta_i}-e^{2\eta_o}}$ | $\frac{\left(C^*\left[e^{2\eta_i}\,Coth(\eta_o)-e^{2\eta_o}\,Coth(\eta_i)+\frac{1}{n}\left(\frac{e^{2\eta_i}}{Sinh^2(\eta_o)}-\frac{e^{2\eta_o}}{Sinh^2(\eta_i)}\right)\right]-\frac{e^{2\eta_i}}{\left[n(1-N)\right]}\right)}{e^{2\eta_i}-e^{2\eta_o}}$ |
| **3.I** | $\frac{-C^*}{2\,Sinh^2(\eta_o)}$ | $1+\frac{C^*}{2}\,Coth(\eta_i)+\frac{C^*}{2}\,\frac{\eta_i}{Sinh^2(\eta_o)}$ | $\frac{\left(C^*\left[Coth(\eta_i)-Coth(\eta_o)-\frac{1}{n\,Sinh^2(\eta_o)}\right]\right)}{e^{2\eta_i}+e^{2\eta_o}}$ | $\frac{\left(C^*\left[e^{2\eta_o}\,Coth(\eta_i)+e^{2\eta_i}\,Coth(\eta_o)+\frac{e^{2\eta_i}}{n\,Sinh^2(\eta_o)}\right]\right)}{e^{2\eta_i}+e^{2\eta_o}}$ |
| **3.O** | $\frac{-C^*}{2\,Sinh^2(\eta_i)}$ | $1+\frac{C^*}{2}\,Coth(\eta_o)+\frac{C^*}{2}\,\frac{\eta_o}{Sinh^2(\eta_i)}$ | $\frac{\left(C^*\left[Coth(\eta_o)-Coth(\eta_i)-\frac{1}{n\,Sinh^2(\eta_i)}\right]\right)}{e^{2\eta_i}+e^{2\eta_o}}$ | $\frac{\left(C^*\left[e^{2\eta_o}\,Coth(\eta_o)+e^{2\eta_o}\,Coth(\eta_i)+\frac{e^{2\eta_o}}{n\,Sinh^2(\eta_i)}\right]\right)}{e^{2\eta_i}+e^{2\eta_o}}$ |
| **4.I** | $\frac{1}{2}\left(\pm\frac{N}{1-N}-\frac{-C^*}{Sinh^2(\eta_i)}\right)$ | $\frac{C^*}{2}\,Coth(\eta_o)-A\,\eta_o$ | $\frac{\left(C^*\left[Coth(\eta_o)-Coth(\eta_i)-\frac{1}{n\,Sinh^2(\eta_i)}\right]\pm\frac{N}{\left[n(1-N)\right]}\right)}{e^{2\eta_i}+e^{2\eta_o}}$ | $\frac{\left(C^*\left[e^{2\eta_i}\,Coth(\eta_o)+e^{2\eta_o}\,Coth(\eta_i)+\frac{e^{2\eta_o}}{n\,Sinh^2(\eta_i)}\right]\mp\frac{N\,e^{2\eta_o}}{\left[n(1-N)\right]}\right)}{e^{2\eta_i}+e^{2\eta_o}}$ |
| **4.O** | $\frac{1}{2}\left(\mp\frac{1}{1-N}-\frac{-C^*}{Sinh^2(\eta_o)}\right)$ | $\frac{C^*}{2}\,Coth(\eta_i)-A\,\eta_i$ | $\frac{\left(C^*\left[Coth(\eta_i)-Coth(\eta_o)-\frac{1}{n\,Sinh^2(\eta_o)}\right]\mp\frac{1}{\left[n(1-N)\right]}\right)}{e^{2\eta_i}+e^{2\eta_o}}$ | $\frac{\left(C^*\left[e^{2\eta_o}\,Coth(\eta_i)+e^{2\eta_i}\,Coth(\eta_o)+\frac{e^{2\eta_i}}{n\,Sinh^2(\eta_o)}\right]\pm\frac{e^{2\eta_i}}{\left[n(1-N)\right]}\right)}{e^{2\eta_i}+e^{2\eta_o}}$ |

equation (3.20) by adding arbitrary constant to any solution of this equation if any. However, a particular value of this constant depends on the initial conditions for the transient conduction. Hence, the constant $B$ can be evaluated for a particular initial condition by equating the expression of equation (4.4) and the steady-state solution obtained by solving the transient case, equation (3.16), for the same initial and boundary conditions as the time approaches infinity. The transient case has been solved numerically using the same code for all the cases under consideration (i.e., using the same finite difference equations and the same algorithm of solution for the resultant set of algebraic equations). The numerical solution will be presented hereunder.

## 4.2 Transient Conduction in Eccentrically Hollow Cylinders

Equation (3.16) is very difficult to solve analytically since $H$ is a function of $\eta$ and $\xi$; hence we resort to numerical solution. Due to symmetry equation (3.16) needs to be solved for $0 \leq \xi \leq \pi$, i.e., in only half the slab shown in Fig. 4.1 which shows the numerical grid in the $\eta$-$\xi$ plane. In this complex plane, the dependent variable $\theta$ is computed, for a given time $t$, at the intersections of the grid lines and $(i, j)$ is a typical mesh point. Mesh points are numbered consecutively; $i$ is progressing in the $\eta$-direction with $i = 1, 2, 3, ...,$ n+1 from the outer surface and $j$ is progressing in the $\xi$-direction with $j = 1, 2, 3, ...,$ m+1 from the wide side of the annulus (at $\xi = 0$).

Using the traditional alternating-direction implicit (ADI) finite-difference scheme, we faced difficulties in obtaining convergent numerical solutions. On the other hand, the

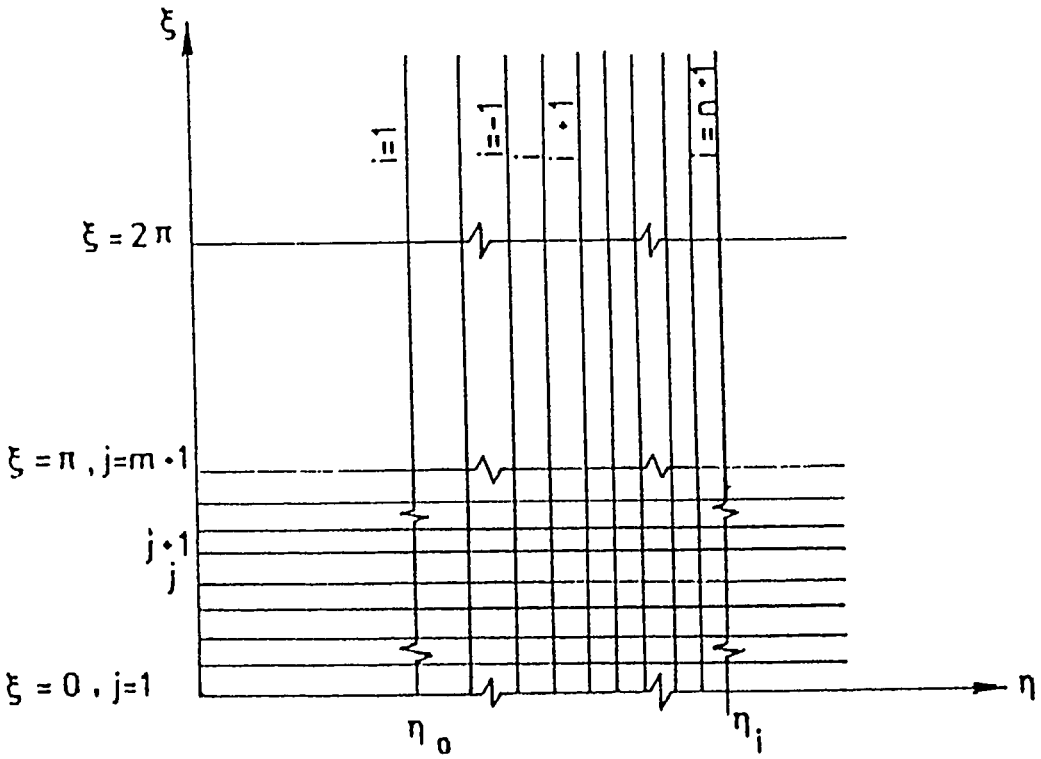


Fig. 4.1 The transformed geometry in η-ξ plane and the numerical mesh network.

following finite-difference scheme has proved to be successful for all values of the dimensionless eccentricity *(E)*.

$$\frac{\theta_{i-1,j} - 2\theta_{i,j} + \theta_{i+1,j}}{(\Delta\eta)^2} + \frac{\theta^*_{i,j-1} - 2\theta^*_{i,j} + \theta^*_{i,j+1}}{(\Delta\xi)^2} + H^2_{i,j} Q = H^2_{i,j} \frac{\theta_{i,j} - \theta^*_{i,j}}{\Delta t} \tag{4.5}$$

where the asterisk (*) superscript denotes at the previous time step and hence the superscripted $\theta^*$ are known.

The two boundary conditions given by equation (3.17) can be written, using central differences and fictitious points as

$$\theta_{i,0} = \theta_{i,2} \tag{4.6}$$

and

$$\theta_{i,m+2} = \theta_{i,m} \tag{4.7}$$

Similarly, the boundary conditions (3.19) on the outer and inner surfaces in cases having the outer or the inner wall insulated can be rewritten, respectively, as

$$\theta_{0,j} = \theta_{2,j} \tag{4.8}$$

and

$$\theta_{n+2,j} = \theta_{n,j} \tag{4.9}$$

In cases 2.I and 2.O which have uniform heat flux on the heat transfer boundary, the thermal condition at this boundary will be expressed using a central difference along with fictitious points. For case 4.I., a backward finite difference representation of the first derivative will be used to express the boundary condition on the inner wall, while a forward finite difference will be used to express the boundary condition on the outer wall for case 4.O. So, for these cases with uniform heat flux on the boundary we have

For case 2.I :

$$\frac{\theta_{n+2,j}-\theta_{n,j}}{2\Delta\eta} = -H(n+1,j) \tag{4.10}$$

For case 2.O :

$$\frac{\theta_{2,j}-\theta_{0,j}}{2\Delta\eta} = H(1,j) \tag{4.11}$$

For case 4.I :

$$\frac{\theta_{n+1,j}-\theta_{n,j}}{\Delta\eta} = H(n+1,j) \tag{4.12}$$

For case 4.O :

$$\frac{\theta_{2,j}-\theta_{1,j}}{\Delta\eta} = -H(1,j) \tag{4.13}$$

The problem under consideration is governed by three controlling parameters, namely, the annulus radius ratio *(N)*, the dimensionless eccentricity *(E)*, and the dimensionless internal heat generation *(Q)*. A numerical solution can be obtained by first selecting values of these controlling parameters. In the present work computations were carried out in an annulus of radius ratio 0.5 for various selected values of $E$ and $Q$. The radius ratio 0.5 was chosen since it represents a typical annular geometry with its value of $N$ far enough from unity ($N = 1$) which represents the case of a slab bound by two parallel-plate surfaces. Knowing the radius ratio *(N)* and the eccentricity *(E)*, the values of $\eta$ for the inner and outer surfaces are computed by the following two equations which are computer-usable forms of equations (3.4) and (3.5) respectively:

$$\eta_i = log_e\left[\frac{N(1+E^2)+(1-E^2)}{2NE}+\sqrt{\left(\frac{N(1+E^2)+(1-E^2)}{2NE}\right)^2-1}\right] \tag{4.14}$$

$$\eta_o = log_e\left[\frac{N(1-E^2)+(1+E^2)}{2E}+\sqrt{\left(\frac{N(1-E^2)+(1+E^2)}{2E}\right)^2-1}\right] \tag{4.15}$$

Having computed $\eta_i$ and $\eta_o$ the value of $\Delta\eta$ is obtained by dividing ($\eta_i$ - $\eta_o$) over $n$ (the number of steps in the $\eta$-direction).

For given $\Delta\xi$ and $\Delta t$ the numerical procedure continues as follows. For each value of $j$ (starting from $j$ = 1) equation (4.5) is applied with $i$ = 2, 3, ..., and $n$ to give ($n$ - 1) equations in ($n$ - 1) unknown values of $\theta$. It should be noted here that for cases 2.I and 2.O, where central differences have been used to express the boundary conditions at the two boundaries, equation (4.5) is applied with i = 1,2,3,....., (n+1) to give (n+1) equations in (n+1) unknowns. The matrix of coefficients of the resulting system of linear equations is a tridiagonal matrix and hence Thomas method is used to obtain numerical solution for the interior grid points (for each value of $j$). This procedure is repeated for all values of $j$ from $j$ = 1 until $j = m+1$ to scan the whole mesh network. Equations (4.6) and (4.7) are used to obtain expressions for the values of $\theta$ at the fictitious points resulting from applying equation (4.5) on the two $\xi$-boundaries. Moreover, equation (4.8) or equation (4.9) is used to do the same on the adiabatic boundary in cases 2.I. and 3.I or 2.O. and 3.O, respectively.

Equations 4.10 through 4.13 will be used to express the fictitious points involved when equation (4.5) is applied on the heat transfer boundary in cases 2.I, 2.O, 4.I and 4.O,

respectively. The obtained values of $\theta$ at the present time step will then be considered as old values (superscripted $\theta$) for the next time step and thus the whole process can be repeated until steady-state conditions are reached. Steady-state conditions mean that the obtained values of $\theta$ do not change with further increase in time. The criterion of achieving that in case 2 was to have the difference between the value of the temperature at any grid point at two successive time steps to be less than $10^{-7}$. For all other cases considered, none of the computer runs was allowed to stop before the obtained numerical results converge to corresponding analytical steady-state solution with a maximum tolerance of 1 %.

## 4.3 Fully Developed Laminar Forced Convection

For hydrodynamically fully developed forced convection, the governing equation (eq. 3.22a) is uncoupled from the energy equation (3.22b) for which solutions have been provided for different thermal boundary conditions by Trombetta [23]. Hence, the solution of the energy equation for this problem will not be provided here. However, the solution of the axial momentum equation (the governing equation of the hydrodynamic part of this problem) will be presented here since it provides an analytical check on the numerical solution for the developing forced convection which will be solved by the present proposed model. This equation is identical to the equation of steady-state heat conduction with internal heat generation. The solution of this equation ($U_{fd}$) is typically given by the right hand side of equation (4.4), noting that $C^*$ is the constant in eq. (3.22a) and its value is given by:

$$C^* = -(dP/dZ)_{fd} H^2(\text{Cosh}\,\eta - \text{Cos}\,\xi)^2 = -(\text{Sinh}^2\,\eta_o)\,(dP/dZ)_{fd} / \,[4(1-N)^2] \qquad (4.16a)$$

Applying the boundary conditions (3.31) the constants of integration $A^*$, $B$, $C$ and $D$ of eq. (4.4) can be determined as given hereinafter

$$A^* = C^*(\,Coth\,\eta_i - coth\,\eta_o\,)/[2\,(\eta_i - \eta_o)] \qquad (4.16b)$$

$$B = C^*(\eta_i\,Coth\,\eta_o - \eta_o\,coth\,\eta_i)/[2\,(\eta_i - \eta_o)] \qquad (4.16c)$$

$$C = C^*(\,Coth\,\eta_i - coth\,\eta_o\,)/(e^{2n\eta i} - e^{2n\eta o}) \qquad (4.16d)$$

$$D = C^*(e^{2n\eta i}\,coth\,\eta_o - e^{2n\eta o}\,Coth\,\eta_i\,)/(e^{2n\eta i} - e^{2n\eta o}) \qquad (4.16e)$$

## 4.4 Fully Developed Laminar Free Convection

### 4.4.1 Fundamental Solutions of the First and Fourth Kinds

For thermal boundary conditions of the first and fourth kinds the energy equation (3.29) will be solved analytically. The analytical solutions obtained for $\theta$ will be substituted in the momentum equation (3.30), which will then be solved numerically. Equation (3.30) can be replaced by the following finite-difference representation

$$\frac{U(i-1,j)-2U(i,j)+U(i+1,j)}{(\Delta\eta)^2}+\frac{U(i,j-1)-2U(i,j)+U(i,j+1)}{(\Delta\xi)^2}=\frac{-\theta(i,j)(H(i,j))^2}{4(1-N)^2} \qquad (4.17)$$

The above equation will be solved iteratively after rearranging its terms as follows.

$$U(i,j)=\frac{1}{2\left(\dfrac{1}{(\Delta\eta)^2+(\Delta\xi)^2}\right)}\left[\frac{U^*(i-1,j)+U^*(i+1,j)}{(\Delta\eta)^2}+\frac{U^*(i,j-1)+U^*(i,j+1)}{(\Delta\xi)^2}+\frac{\theta(i,j)\,H^2(i,j)}{4(1-N)^2}\right] \qquad (4.18)$$

in which the asterisk superscript means values from the previous iteration.

The problem under investigation is governed by three dimensionless parameters, namely, the radius ratio, $N$, the eccentricity, $E$, and the Prandtl number, $Pr$. For a fluid of a given $Pr$ in an annulus of given $N$ and $E$, the solution starts by calculating the corresponding values of $\eta_i$ and $\eta_o$ by means of eqs. (4.14) and (4.15), respectively. Selecting the numbers of increments in $\eta$ and $\xi$ directions ($n$ and $m$, respectively) the values of $\Delta\eta$ and $\Delta\xi$ can be computed.

The algorithm of solution is to assume a velocity field at all grid points, $U^*(i,j)$. Substitute these values of $U^*$ together with the known values of $\theta(i,j)$ and $H(i,j)$ on the right hand side of eq. (4.18) to obtain the new values of $U(i,j)$. If the relative error between $U$ and $U^*$ at all grid points ( $(U(i,j) - U^*(i,j))/ U(i,j)$ ) satisfies a prescribed solution criterion ( $\leq 10^{-4}$ in the present work) stop the iteration process, otherwise continue the iteration process after updating the values of $U^*$ according to the following relaxation equation.

$$U^*(i,j) = U^*_{old}(i,j) + w[U(i,j) - U^*_{old}(i,j)] \tag{4.19}$$

In the above equation $w$ is a relaxation factor which has been found through numerical experimentation to be 0.8.

### 4.4.2 Fundamental Solution of the Third Kind

For the thermal boundary conditions of the third kind, the wall opposite to the heat transfer surface is perfectly insulated. Hence, the fluid temperature in the annulus becomes ultimately uniform at the same temperature as the heated surface ($\theta = 1$

everywhere in the fully-developed region). Therefore, fully-developed free-convection flow under thermal conditions of the third kind is an isothermal flow having a temperature which equals that of the heat transfer boundary. Consequently, we have, in both cases 3.I and 3.O, $P = 0$, $\theta = 1$ and $\partial\theta/\partial\eta = \partial\theta/\partial\xi = \partial^2\theta/\partial\eta^2 = \partial^2\theta/\partial\xi^2 = 0$ everywhere. Hence, the energy equation (3.29) vanishes and the axial momentum equation (3.30) reduces to

$$\frac{\partial^2 U_{fd}}{\partial \eta^2}+\frac{\partial^2 U_{fd}}{\partial \xi^2}=-\frac{H^2}{4(1-N)^2}=-\frac{C^*}{(Cosh\eta-Cos\xi)^2} \tag{4.20}$$

Thus, the physics of the problem of fully-developed free convection does not distinguish between case I and case O under thermal boundary conditions of the third kind and we simply have only one fully-developed solution of the third kind. Equation (4.20) is similar in shape to the equation of steady-state heat conduction with internal heat generation. The solution of this equation ($U_{fd}$) is typically given by the right hand side of equation (4.4), noting that the value of $C^*$ is the constant in eq. (4.20) whic is given below as;

$$C^* = Sinh^2(\eta_o)/16(1-N)^4 \tag{4.21a}$$

$A^*$, $B$, $C$ and $D$ in the right hand side of eq. (4.4) are the constants of integration obtained after applying the boundary conditions (3.31) and have the following values.

$$A^* = \frac{C^*}{2}\frac{Coth(\eta_i)-Coth(\eta_o)}{\eta_i-\eta_o} \tag{4.21b}$$

$$B=\frac{C^*}{2}\frac{\eta_i Coth(\eta_o)-\eta_o Coth(\eta_i)}{\eta_i-\eta_o} \tag{4.21c}$$

$$C = C^* \frac{Coth(\eta_i) - Coth(\eta_o)}{e^{2n\eta_i} - e^{2n\eta_o}} \tag{4.21d}$$

$$D = C^* \frac{e^{2n\eta_i} Coth(\eta_o) - e^{2n\eta_o} Coth(\eta_i)}{e^{2n\eta_i} - e^{2n\eta_o}} \tag{4.21e}$$

### 4.4.3 Fundamental Solution of the Second Kind

This type of thermal boundary conditions is Nueman (derivative) boundary condition (i.e., any arbitrary constant in the solution of the energy equation (3.24) if it exists will satisfy this boundary condition). Moreover, the energy equation (3.24) is strongly coupled with the axial momentum equation (3.23). Hence, the solution of these two simultaneous equations is very difficult to obtain analytically. An iterative numerical method may be used to solve these two equations. This method can be summarized as follows; first assume a temperature profile and use it to solve equation (3.23) for the velocity U. The velocity profiles obtained from equation (3.23) can be used now to solve equation (3.24) for the temperature θ. This procedure will be repeated until the differences between the assumed temperature profiles to solve equation (3.23) and the temperature profiles obtained from the solution of equation (3.24) converge to a prescribed value. However the solutions obtained by this method were found to be affected by the assumed temperature profiles as a first iteration. Moreover, it was concluded that it is better to have the first iteration of the temperature profile as that coming out from the developing region. Therefore, it was decided that the solution of the fully developed free convection would be better obtained via the solution of the developing free convection which will be presented in Chapter 8.

## 4.5 Developing Laminar Forced Convection in Eccentric Annuli and Free Convection in Vertical Open-Ended Eccentric Annuli

### 4.5.1 Finite Difference Representation

The presently proposed model describing these two problems comprises equations (3.33) through (3.37). Until now there is no analytical means known to solve this set of equations. Hence, the governing equations have been numerically treated using a finite difference technique. Considering the mesh network of Fig 4.1, replacing the first and second order derivatives in $\eta$ and $\xi$ directions by central finite-differences, with the exception of using a backward representation for the first derivative of $(HV)$ with respect to $\eta$ in the continuity equation, and using backward finite-differences to express the first derivatives with respect to Z, equations (3.33) through (3.37) can be written in the following forms, respectively.

**Finite-Difference Representation of the Continuity Equation**

$$\frac{H(i,j+1)W(i,j+1)-H(i,j-1)W(i,j-1)}{2\Delta\xi}+\frac{H(i,j)V(i,j)-H(i-1,j)V(i-1,j)}{\Delta\eta}$$
$$+K_1 H^2(i,j)\frac{U(i,j)-U^*(i,j)}{\Delta Z}=0$$

rearranging

$$V(i,j)=\frac{\Delta\eta}{H(i,j)}\left(\frac{H(i-1,j)V(i-1,j)}{\Delta\eta}-\frac{H(i,j+1)W(i,j+1)-H(i,j-1)W(i,j-1)}{2\Delta\xi}\right.$$
$$\left.-K_1 H^2(i,j)\frac{U(i,j)-U^*(i,j)}{\Delta Z}\right) \qquad (4.22)$$

**Finite Difference Representation of the ξ Momentum Equation**

$$\frac{W^*(i,j)}{H(i,j)}\frac{W(i,j+1)-W(i,j-1)}{2\Delta\xi}+\frac{V^*(i,j)}{(H(i,j))^2}\frac{H(i+1,j)W(i+1,j)-H(i-1,j)W(i-1,j)}{2\Delta\eta}$$

$$+K_1U^*(i,j)\frac{W(i,j)-W^*(i,j)}{\Delta Z}-\frac{(V^*(i,j))^2}{(H(i,j))^2}\frac{H(i,j+1)-H(i,j-1)}{2\Delta\xi}$$

$$=\frac{1}{(H(i,j))^3}\left\{\begin{array}{l}\dfrac{H(i-1,j)W(i-1,j)-2H(i,j)W(i,j)+H(i+1,j)W(i+1,j)}{(\Delta\eta)^2}\\+\dfrac{H(i,j-1)W(i,j-1)-2H(i,j)W(i,j)+H(i,j+1)W(i,j+1)}{(\Delta\xi)^2}\end{array}\right\}$$

$$-\frac{2}{(H(i,j))^4}\left(\frac{H(i+1,j)-H(i-1,j)}{2\Delta\eta}\right)\left(\begin{array}{l}\dfrac{H(i+1,j)W(i+1,j)-H(i-1,j)W(i-1,j)}{2\Delta\eta}\\-\dfrac{H(i,j+1)V(i,j+1)-H(i,j-1)V(i,j-1)}{2\Delta\xi}\end{array}\right)$$

$$+\frac{2K_1}{(H(i,j))^2}\frac{H(i,j+1)-H(i,j-1)}{2\Delta\xi}\frac{U(i,j)-U^*(i,j)}{\Delta Z}$$

rearranging;

$$W(i,j)\left(K_1\frac{U^*(i,j)}{\Delta Z}+\frac{2}{(H(i,j))^2}\left(\frac{1}{(\Delta\eta)^2}+\frac{1}{(\Delta\xi)^2}\right)\right)=$$

$$-\frac{W^*(i,j)}{H(i,j)}\frac{W(i,j+1)-W(i,j-1)}{2\Delta\xi}-\frac{V^*(i,j)}{(H(i,j))^2}\frac{H(i+1,j)W(i+1,j)-H(i-1,j)W(i-1,j)}{2\Delta\eta}$$

$$+K_1U^*(i,j)\frac{W^*(i,j)}{\Delta Z}+\frac{H(i,j+1)-H(i,j-1)}{2\Delta\xi(H(i,j))^2}\left((V^*(i,j))^2+2K_1\frac{U(i,j)-U^*(i,j)}{\Delta Z}\right)$$

$$\frac{1}{(H(i,j))^3}\left\{\begin{array}{l}\dfrac{H(i-1,j)W(i-1,j)+H(i+1,j)W(i+1,j)}{(\Delta\eta)^2}\\+\dfrac{H(i,j-1)W(i,j-1)+H(i,j+1)W(i,j+1)}{(\Delta\xi)^2}\end{array}\right\}$$

$$-\frac{2}{(H(i,j))^4}\left(\frac{H(i+1,j)-H(i-1,j)}{2\Delta\eta}\right)\left(\begin{array}{l}\dfrac{H(i+1,j)W(i+1,j)-H(i-1,j)W(i-1,j)}{2\Delta\eta}\\-\dfrac{H(i,j+1)V(i,j+1)-H(i,j-1)V(i,j-1)}{2\Delta\xi}\end{array}\right)$$

(4.23)

**Finite Difference representation of the Axial Momentum Equation**

$$\left(\frac{1}{(\Delta\eta)^2}+\frac{V(i,j)H(i,j)}{2\Delta\eta}\right)U(i-1,j)-\left(\frac{2}{(\Delta\eta)^2}+\frac{2}{(\Delta\xi)^2}+K_1\frac{(H(i,j))^2U^*(i,j)}{\Delta Z}\right)U(i,j)$$
$$+\left(\frac{1}{(\Delta\eta)^2}-\frac{V(i,j)H(i,j)}{2\Delta\eta}\right)U(i+1,j)+\left(\frac{1}{(\Delta\xi)^2}+\frac{W(i,j)H(i,j)}{2\Delta\xi}\right)U(i,j-1)$$
$$+\left(\frac{1}{(\Delta\xi)^2}-\frac{W(i,j)H(i,j)}{2\Delta\xi}\right)U(i,j+1)-K_2\frac{(H(i,j))^2P}{\Delta Z}$$
$$=-K_2\frac{(H(i,j))^2P^*}{\Delta Z}-K_3(H(i,j))^2\theta(i,j)-K_1\frac{(H(i,j)U^*(i,j))^2}{\Delta Z}$$

rearranging

$$\left(\frac{1}{(\Delta\eta)^2}+\frac{V(i,j)H(i,j)}{2\Delta\eta}\right)U(i-1,j)-\left(\frac{2}{(\Delta\eta)^2}+\frac{2}{(\Delta\xi)^2}+K_1\frac{(H(i,j))^2U^*(i,j)}{\Delta Z}\right)U(i,j)$$
$$+\left(\frac{1}{(\Delta\eta)^2}-\frac{V(i,j)H(i,j)}{2\Delta\eta}\right)U(i+1,j)+\left(\frac{1}{(\Delta\xi)^2}+\frac{W(i,j)H(i,j)}{2\Delta\xi}\right)U(i,j-1)$$
$$+\left(\frac{1}{(\Delta\xi)^2}-\frac{W(i,j)H(i,j)}{2\Delta\xi}\right)U(i,j+1)-K_2\frac{(H(i,j))^2P}{\Delta Z}$$
$$=-K_2\frac{(H(i,j))^2P^*}{\Delta Z}-K_1\frac{(H(i,j)U^*(i,j))^2}{\Delta Z}-K_3(H(i,j))^2\theta(i,j)$$

(4.24)

**Finite Difference Representation of the Energy Equation**

$$\frac{W^*(i,j)}{H(i,j)}\frac{\theta(i,j+1)-\theta(i,j-1)}{2\Delta\xi}+\frac{V^*(i,j)}{H(i,j)}\frac{\theta(i+1,j)-\theta(i-1,j)}{2\Delta\eta}$$
$$+K_1U^*(i,j)\frac{\theta(i,j)-\theta^*(i,j)}{\Delta Z}$$
$$=\frac{1}{\mathrm{Pr.}\left(H(i,j)\right)^2}\left\{\frac{\theta(i-1,j)-2\theta(i,j)+\theta(i+1,j)}{(\Delta\eta)^2}+\frac{\theta(i,j-1)-2\theta(i,j)+\theta(i,j+1)}{(\Delta\xi)^2}\right\}$$

Rearranging;

$$\theta(i,j)\left(\frac{K_1U^*(i,j)}{\Delta Z}+\frac{2}{\mathrm{Pr.}\left(H(i,j)\right)^2}\left(\frac{1}{(\Delta\eta)^2}+\frac{1}{(\Delta\xi)^2}\right)\right)$$
$$=K_1\frac{U^*(i,j)\theta^*(i,j)}{\Delta Z}+\frac{1}{\mathrm{Pr.}\left(H(i,j)\right)^2}\left\{\frac{\theta(i-1,j)+\theta(i+1,j)}{(\Delta\eta)^2}+\frac{\theta(i,j-1)+\theta(i,j+1)}{(\Delta\xi)^2}\right\} \quad (4.25)$$
$$-\frac{V^*(i,j)}{H(i,j)}\frac{\theta(i+1,j)-\theta(i-1,j)}{2\Delta\eta}-\frac{W^*(i,j)}{H(i,j)}\frac{\theta(i,j+1)-\theta(i,j-1)}{2\Delta\xi}$$

**Integral Form of the Continuity Equation**

$$\bar{U}=\frac{8(1-N)}{\pi(1+N)}\left(\begin{array}{l}\sum_{j=2}^{M}\sum_{i=2}^{n}U(i,j)\left(H(i,j)\right)^2+\\ 0.5\sum_{i=2}^{n}U(i,1)\left(H(i,1)\right)^2+U(i,M+1)\left(H(i,M+1)\right)^2\end{array}\right)\Delta\eta\,\Delta\xi \quad (4.26)$$

It is worth mentioning that in the foregoing equations an asterisk superscript (*) means at the previous axial step. At each mesh point the number of equations is 5 and equals the number of unknowns which are namely $P$, $U$, $V$, $W$ and $\theta$

## 4.5.2 Method of Solution

1- In case of free convection assume a value for the uniform axial velocity profile at the entrance $U_o$. Since $W = V = 0$, the inlet pressure will be $P_o=-\frac{U_c^2}{2}$ for this free convection case. On the other hand, for forced convection $U_o = 1$ and $P_o = 0$.

2 - For the case of free convection, solve the energy equation iteratively to find the values of the temperature at the first plane after the inlet cross section ( $\theta_{i,j}$ ); Guass-Seidle iteration method has been used. For the case of forced convection go to the next step (# 3) directly after step 1 above and the energy equation will be solved after step 5 below (i.e., after obtaining the three velocity components *U*, *W* and *V*).

3 - Now to solve for the two unknowns P and U at the aforesaid plane the integral form of the continuity equation and the finite difference form of the axial momentum equation can be used. The set of algebraic equations result from the application of the axial momentum equation at each interior node of the solution grid along with that equation resulted from expressing the integral continuity equation using the trapezoidal rule will be put in a matrix form. The general format for this matrix corresponds to ***n*** segments in $\eta$-direction and ***m*** segments in $\xi$-direction. However, as a representative example, a grid of ***5*** segments in $\eta$-direction and ***3*** segments in $\xi$-direction will be used to develop such a matrix format as presented hereunder. The method of solving this matrix is an extension to the special form of the Guass-Jordan elimination scheme which was previously used by El-Shaarawi [74].

**The matrix form of step 3 is;**

$$\begin{bmatrix}
0.5H_{21}^2 & 0.5H_{31}^2 & 0.5H_{41}^2 & 0.5H_{51}^2 & H_{12}^2 & H_{22}^2 & H_{32}^2 & H_{42}^2 & H_{52}^2 & H_{13}^2 & H_{23}^2 & H_{33}^2 & 0.5H_{14}^2 & 0.5H_{24}^2 & 0.5H_{34}^2 & 0.5H_{44}^2 & 0 \\
a & b & 0 & 0 & C_1 & 0 & 0 & 0 & 0 & 0 & 0 & 0 & 0 & 0 & 0 & 0 & S_P \\
d & a & b & 0 & 0 & C_1 & 0 & 0 & 0 & 0 & 0 & 0 & 0 & 0 & 0 & 0 & S_P \\
0 & d & a & b & 0 & 0 & C_1 & 0 & 0 & 0 & 0 & 0 & 0 & 0 & 0 & 0 & S_P \\
0 & 0 & d & a & b & 0 & 0 & C_1 & 0 & 0 & 0 & 0 & 0 & 0 & 0 & 0 & S_P \\
E & 0 & 0 & d & a & b & 0 & 0 & F & 0 & 0 & 0 & 0 & 0 & 0 & 0 & S_P \\
0 & E & 0 & 0 & d & a & b & 0 & 0 & F & 0 & 0 & 0 & 0 & 0 & 0 & S_P \\
0 & 0 & E & 0 & 0 & d & a & b & 0 & 0 & F & 0 & 0 & 0 & 0 & 0 & S_P \\
0 & 0 & 0 & E & 0 & 0 & d & a & b & 0 & 0 & F & 0 & 0 & 0 & 0 & S_P \\
0 & 0 & 0 & 0 & E & 0 & 0 & d & a & b & 0 & 0 & F & 0 & 0 & 0 & S_P \\
0 & 0 & 0 & 0 & 0 & E & 0 & 0 & d & a & b & 0 & 0 & F & 0 & 0 & S_P \\
0 & 0 & 0 & 0 & 0 & 0 & E & 0 & 0 & d & a & b & 0 & 0 & F & 0 & S_P \\
0 & 0 & 0 & 0 & 0 & 0 & 0 & E & 0 & 0 & d & a & b & 0 & 0 & F & S_P \\
0 & 0 & 0 & 0 & 0 & 0 & 0 & 0 & C_{M+1} & 0 & 0 & d & a & b & 0 & 0 & S_P \\
0 & 0 & 0 & 0 & 0 & 0 & 0 & 0 & 0 & C_{M+1} & 0 & 0 & d & a & b & 0 & S_P \\
0 & 0 & 0 & 0 & 0 & 0 & 0 & 0 & 0 & 0 & C_{M+1} & 0 & 0 & d & a & b & S_P \\
0 & 0 & 0 & 0 & 0 & 0 & 0 & 0 & 0 & 0 & 0 & C_{M+1} & 0 & 0 & d & a & S_P
\end{bmatrix}
\begin{bmatrix} U_{21} \\ U_{31} \\ U_{41} \\ U_{51} \\ U_{22} \\ U_{32} \\ U_{42} \\ U_{52} \\ U_{23} \\ U_{33} \\ U_{43} \\ U_{53} \\ U_{24} \\ U_{34} \\ U_{44} \\ U_{54} \\ P \end{bmatrix}
=
\begin{bmatrix} R_{conv} \\ R_{conv} \\ R_{conv} \\ R_{conv} \\ R_{conv} \\ R_{conv} \\ R_{conv} \\ R_{conv} \\ R_{conv} \\ R_{conv} \\ R_{conv} \\ R_{conv} \\ R_{conv} \\ R_{conv} \\ R_{conv} \\ R_{conv} \end{bmatrix}$$

Where:

$$a=-\left(\frac{2}{(\Delta\eta)^2}+\frac{2}{(\Delta\xi)^2}+K_1\frac{(H(i,j))^2U^*(i,j)}{\Delta Z}\right),$$

$$b=\frac{1}{(\Delta\eta)^2}-\frac{H(i,j)V^*(i,j)}{2\Delta\eta},$$

$$d=\frac{1}{(\Delta\eta)^2}+\frac{H(i,j)V^*(i,j)}{2\Delta\eta},$$

$$C_1=2\left(\frac{1}{(\Delta\xi)^2}-\frac{H(i,1)W^*(i,1)}{2\Delta\xi}\right),$$

$$C_{M+1}=2\left(\frac{1}{(\Delta\xi)^2}+\frac{H(i,M+1)W^*(i,M+1)}{2\Delta\xi}\right),$$

$$E=\left(\frac{1}{(\Delta\xi)^2}+\frac{H(i,j)W^*(i,j)}{2\Delta\xi}\right),$$

$$F=\left(\frac{1}{(\Delta\xi)^2}-\frac{H(i,j)W^*(i,j)}{2\Delta\xi}\right),$$

$$S_p = -K_2 \frac{(H(i,j))^2}{\Delta Z} ,$$

$$R_{cont} = 0.5 \sum_{i=2}^{n} U^*(i,1)(H(i,1))^2 + U^*(i,M+1)(H(i,M+1))^2 + \sum_{j=2}^{M} \sum_{i=2}^{n} U^*(i,j)(H(i,j))^2 ,$$

$$R_{ame} = -K_1 \frac{(H(i,j)U^*(i,j))^2}{\Delta Z} - K_2 \frac{(H(i,j))^2}{\Delta Z} P^* - K_3 (H(i,j))^2 \theta$$

4 - Solve ξ-momentum equations for *W*, following the same method used to solve the energy equation (step # 2 above).

5 - Use the continuity equation to evaluate V at all the interior grid points

6 - Repeat steps 2-5 to advance axially until the pressure defect *P* becomes zero for the free convection. For forced convection solve the energy equation using Guass-Seidle iteration method and then repeat steps 2-5 to advance axially; the execution of the program will be stopped when the maximum developing velocity becomes equal to 99 % of the corresponding maximum fully developed velocity.

# Chapter 5

# RESULTS AND DISCUSSION FOR CONDUCTION IN ECCENTRIC ANNULI

## 5.1 Introduction

Prior to the onset of free convection in an annular channel the conduction mode is the prevailing heat transfer mode particularly when the temperature is low and radiation is negligible. Heat conduction and heat storage capacity in eccentric configurations may also be important in cases of eccentrically drilled tubes or hollow shafts or eccentric insulations.

The problem of transient and steady conduction in eccentric annuli has been investigated during the present work for four pairs of fundamental thermal boundary

conditions. The problem formulation and the method of solution have been presented in Chapters 3 and 4, respectively. Results and discussions for the different cases will be presented hereunder.

The steady state conduction through an eccentric annulus (eq. 3.20) has been readily solved during the present work for all cases under consideration using the general solution given by El-Saden [5] (eq. 4.4 and Table 4.1). However, for case 2 which has Neuman boundary conditions the value of the constant $B$ has not been given in Table 4.1. Moreover, for particular initial conditions, the value of $B$ has been evaluated for different values of eccentricity using the corresponding steady-state solutions obtained numerically by solving the transient conduction problem (eq. 3.16). For cases 1, 3, and 4, the steady-state analytical solutions obtained provide a check on the adequacy of the present computer code and consequently on the transient numerical results. The numerical transient solutions were found to asymptotically approach (at considerably large values of the time $t$) the steady-state solutions available given by equation (4.4) and Table 4.1. None of the computer runs was allowed to stop before the transient numerical results converge to the corresponding steady-state analytical solution with a maximum tolerance less than 1% (in the value of the local dimensionless temperature $\theta$ at any mesh point). A thorough study has been conducted to investigate the influence of the number of series-terms (in eq. (4.4)) on the analytical solution. It has been found that there are lower and upper limits for the number of series-terms the values of which depend on the geometry under consideration ( N and E). With small number of series terms (i.e., lower limit) the solution looses accuracy. With large number of terms

above the upper limit divergence of the solution occurs due to having very high value exponential terms ( see Table 4.1). Number of series terms ranging between 10 and 100 has been investigated. The solution obtained using 15 series terms compared with that obtained using 10 series terms and a considerable difference has been noticed. Then a solution obtained using 20 series terms compared with that for 15-term solutions and the difference decreases than that between the 10 and 15-term solution. The 25-term solution was compared with that of 20 terms and the difference was negligible and so was the case for higher number of series terms (e.g., the 30-term solution when compared to 25-term solution and so on ) until the upper limit of each case was reached. Out of such study a series of 20 terms has been used for all cases under consideration.

On the other hand, a thorough numerical experimentation has been conducted to investigate the effect of mesh sizes on the numerical results obtained and the computer CPU time. For example, the steady-state times obtained for case 1.O with $N = 0.5$, $Q = 5$, $E = 0.5$ and $\Delta t = 10^{-3}$ corresponding to mesh sizes $m$ x $n$ = 20 x 20, 25 x 25, 30 x 30, 20 x 40, 35 x 35, and 35 x 40 are, respectively, 0.512, 0.511, 0.511, 0.507, 0.509, and 0.509. The corresponding computer CPU times (using WF 77 Sys D) are, respectively, 63.35, 98.90, 142.52, 128.07, and more than 180 (CPU secs) in the last two cases. Similarly, the steady-state times for the same values of $N$, $Q$, $E$, and $\Delta t$ in case 1.I for mesh sizes $m$ x $n$ = 20 x 15, 20 x 20, 20 x 25, 20 x 30, 20 x 35, 25 x 25, 40 x 20, 30 x 30, and 40 x 35 are, respectively, 0.514, 0.507, 0.504, 0.501, 0.500, 0.505, 0.500, 0.503, and 0.501. It might be worth mentioning that time steps as low as $10^{-5}$ were used in some cases (at the expense of the computer execution time). However, for the sake of unification in

comparisons all the results presented in the present work have been obtained using $m$ x $n$ = 20 x 20 and $\Delta t = 10^{-3}$. Results for each case will be presented separately hereinafter.

## 5.2 Temperature Results for Cases 1.I and 1.O

For case 1.I and a given $E$ ($E = 0.8$) in an annulus of $N = 0.5$, Fig. 5.1(a) shows the variation with time of the dimensionless temperature on an intermediate surface having $\eta = \eta^* = (\eta_i + \eta_o)/2$ for two values of $Q$, namely, $Q = 0$ and 5. For either value of $Q$ and a given $\xi$, the temperature of this surface increases with time until it reaches the steady-state value (at $t_s = 0.749$ and 0.658 for $Q = 0$ and 5, respectively). The figure shows that, for any value of $Q$, the narrow side of the annulus ( $\xi \rightarrow \pi$) reaches the steady-state conditions much faster than the wide side ( $\xi \rightarrow 0$). This is attributed to the larger heat storage capacity of the wide side compared to that of the narrow side. On the other hand, for given time and $\xi$ the temperature value with internal heat generation is, as expected, larger than its corresponding value without internal heat generation ($Q = 0$).

The effect of eccentricity on the transient response of the temperature of the system is clarified in Fig. 5.1(b). For case 1.I and a given $Q$ ($Q = 5$) in an annulus of $N = 0.5$, this figure gives the variation with time of the dimensionless temperature on the intermediate surface of $\eta = \eta^* = (\eta_i + \eta_o)/2$ for two values of $E$, namely, $E = 0.1$ and $E = 0.8$. As can be seen from this figure, the eccentricity has a prominent effect on the transient temperature distribution. For a given time *(t)*, as the value of $E$ increases the temperature distribution on the surface of a given $\eta$ becomes more dependent on $\xi$. In a concentric annulus ($E = 0$) in both cases 1.I and 1.O, the isothermal lines, without or with

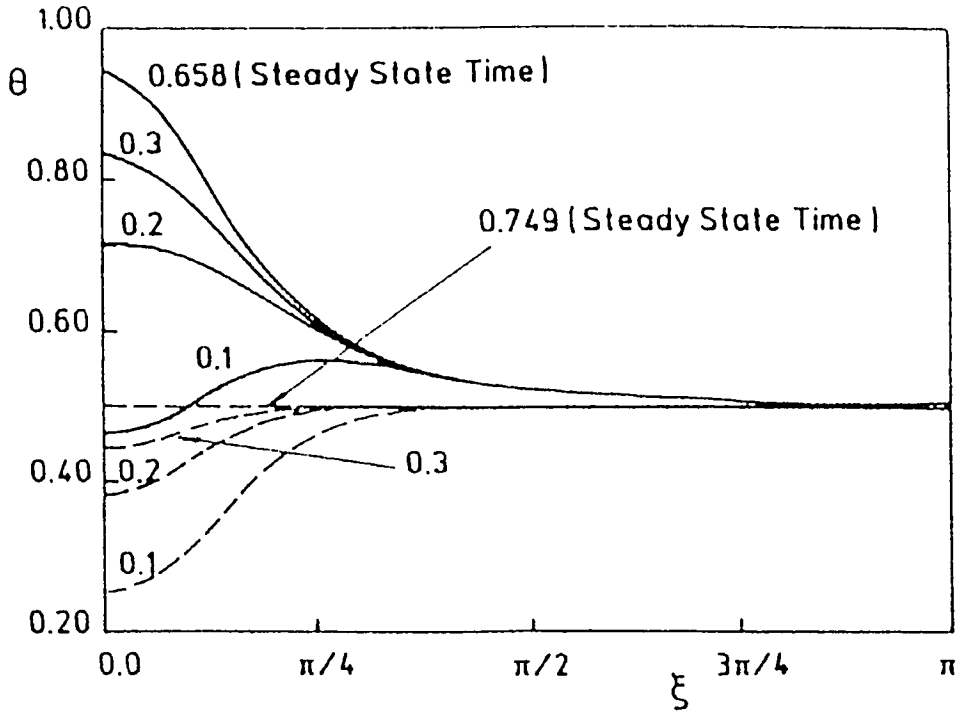


Fig. 5.1(a) Effect of $Q$ on transient temperature distribution at $\eta = \eta^*$ in case I.I, $N = 0.5$, $E = 0.8$, ---- $Q = 0$, —— $Q = 5$.

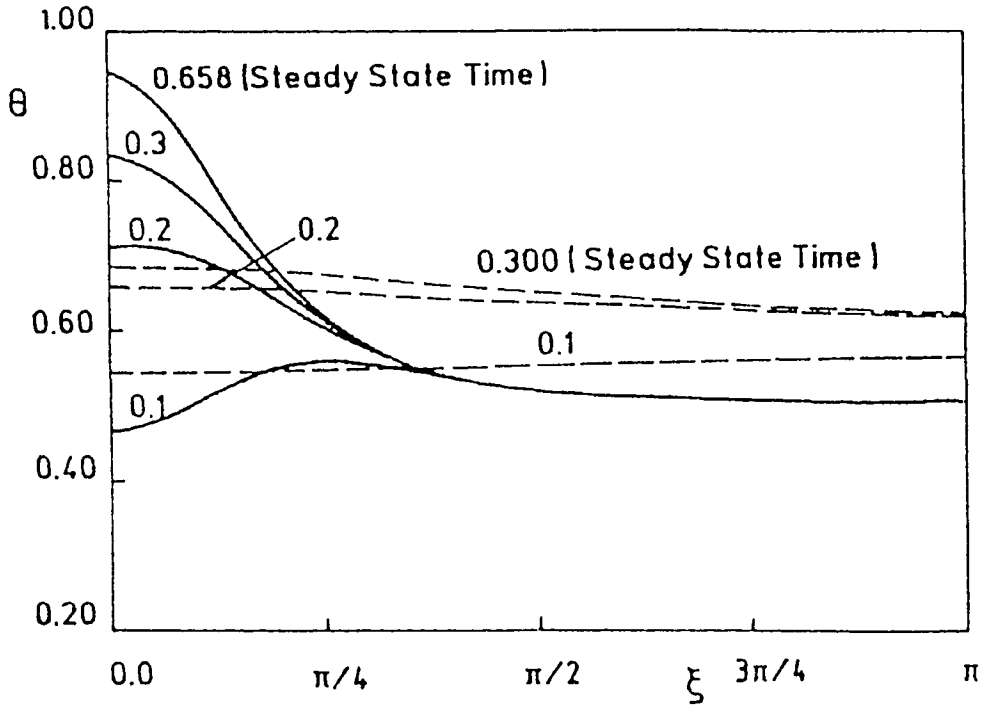


Fig. 5.1(b) Effect of eccentricity on transient temperature distribution at $\eta = \eta^*$ in case I.I, $N = 0.5$, $Q = 5$, ---- $E = 0.1$, —— $E = 0.8$.

internal heat generation, are concentric circles, i.e., the temperature is independent of the angular coordinate. However, as the annulus deviates from the concentric situation the temperature in the wide side ( $\xi \rightarrow 0$) becomes higher than that in the narrow side ($\xi \rightarrow \pi$). This is due to the larger internal heat generated in the wide side of the annulus since this side has more material per unit length than the narrow side. It is worth mentioning here that for boundary conditions of the first kind without internal heat generation the temperature distribution become linear in the ($\eta$-$\xi$) plane (conduction through a flat wall) for which the isothermal lines can be presented by eccentric circles in the physical (x-y) plane (i.e., at a given $\eta$ the temperature is independent of the angular position $\xi$). The dependence on the angular position $\xi$ becomes more pronounced with the increase in eccentricity $E$ and the heat generation Q.

## 5.3 Temperature Results for Cases 2.I and 2.O

In the present case and according to the physics of the problem presented in Chapter 3, at $t > 0$ the heat is internally generated uniformly within the annulus material and cooling with uniform heat flux will simultaneously take place at one of its surfaces while the other surface is kept insulated. As was given in section 3.3.2.1, the energy balance in this situation shows that, in order to achieve steady state conditions, the ratio between the possible rate of heat generation and the heat flux on the heat transfer wall( the heat ratio $Q$) in case 2.I is N-times that in case 2.O. This is mainly attributed to difference

in the area of heat transfer in the two cases. For N = 0.5 the heat ratio $Q$ in case 2.O is twice that in case 2.I in order that steady state conditions can be reached.

For case 2.I, Fig. 5.2(a) shows the temperature response at the point of intersection of the inner cooled wall with the line of symmetry at the widest and narrowest sides of the annulus (i.e., $\xi = 0$ and $\xi = \pi$, respectively) for different values of the eccentricity E. The temperature response at intersection points of the line of symmetry with the outer insulated wall are indicated in Fig. 5.2(b). Figures 5.3(a) and 5.3(b) show similar temperature responses corresponding to case 2.O. These four figures show that the temperature of the annulus material in the widest side increases with time approaching asymptotically its constant steady-state value while that of the annulus material in the narrow side decreases approaching its steady-state constant value.

The difference between the level of temperature in the widest side and that in the narrowest side increases with eccentricity. This is attributed to the fact that the increase in eccentricity decreases the distance between the insulated and cooled walls in the narrowest side (i.e., reduces the local resistance to the conduction heat transfer on this side) which makes the cooling more effective. In addition to this, the increase in eccentricity results in a reduction in the volume of the solid material in the narrowest side which means a reduction in the amount of heat generated on this side compared to that generated on the widest side while keeping the same uniform heat flux in the adjacent cooling surface.

For a relatively small eccentricity (E = 0.1), Figures 5.4(a) and 5.4(b) show the transient variation of temperature with $\xi$ around half the periphery of the inner cooled wall and the outer insulated wall, respectively, for case 2.I. The corresponding variations for E

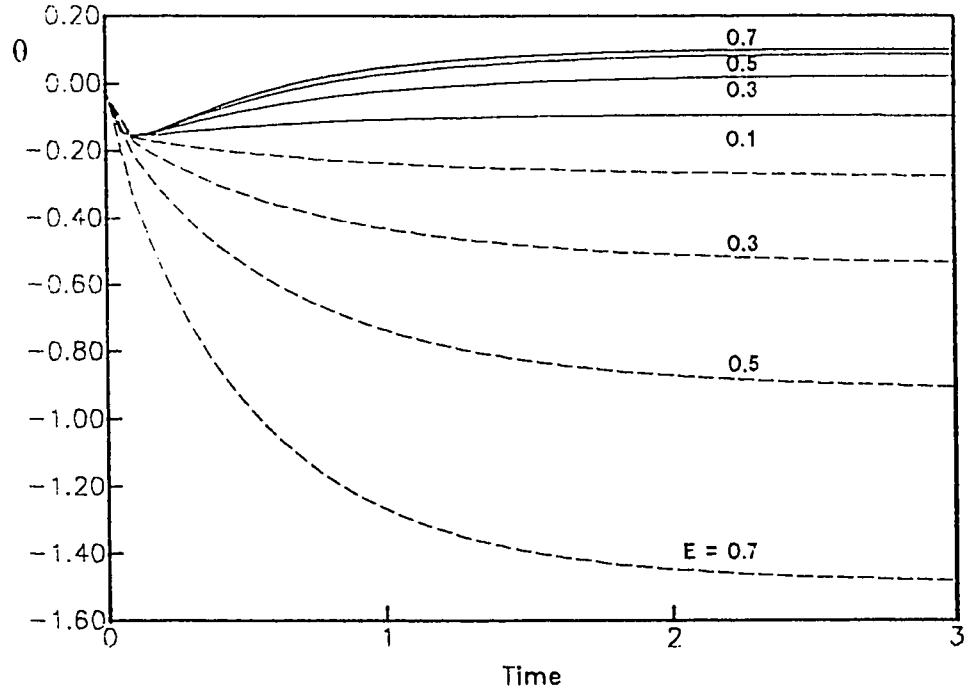


Fig. 5.2(a) Effect of eccentricity on the temperature response at the inner cooled wall in case 2.I, N = 0.5, —— $\xi = 0.0$, – – – $\xi = \pi$ .

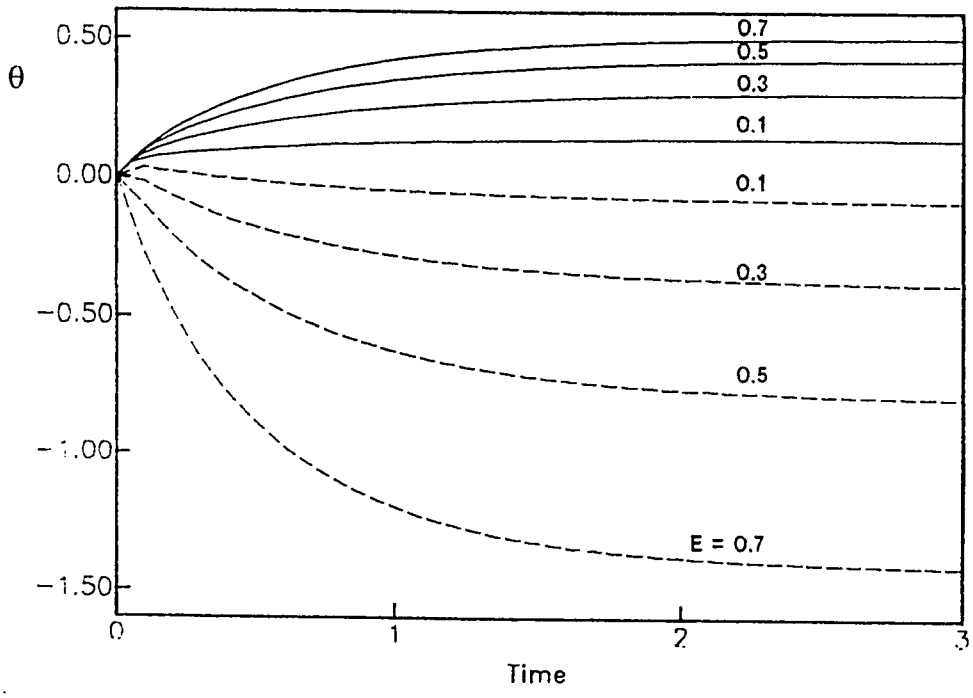


Fig. 5.2(b) : Effect of eccentricity on the temperature response at the outer insulated wall in case 2.I, N = 0.5, —— $\xi = 0.0$, – – – $\xi = \pi$.

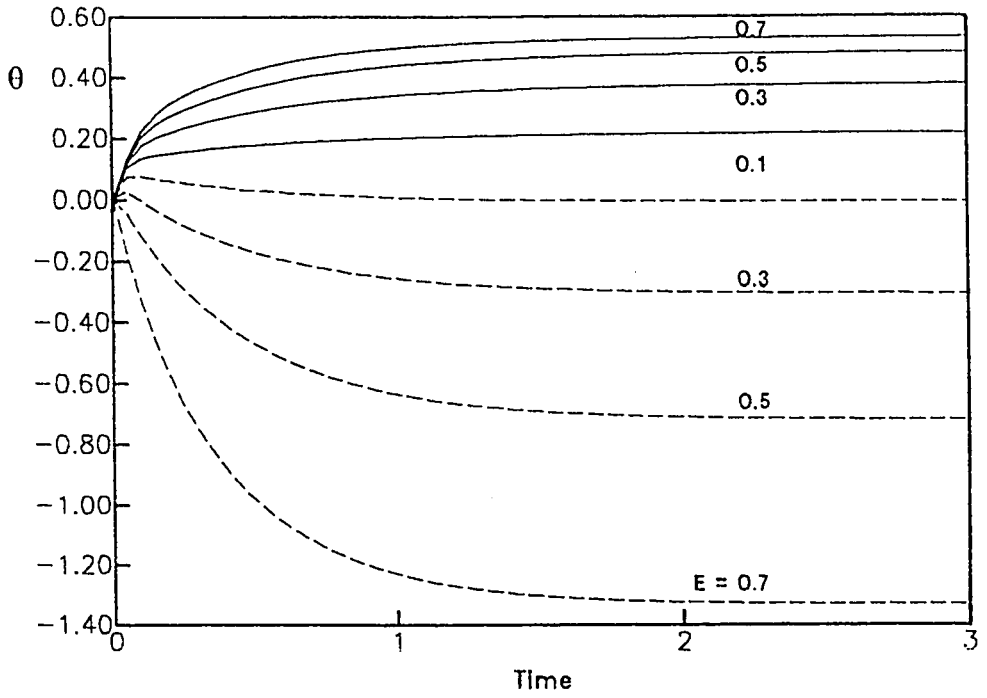


Fig. 5.3(a) : Effect of eccentricity on the temperature response at the inner insulated wall in case 2.O, N = 0.5, —— $\xi = 0.0$, – – – $\xi = \pi$.

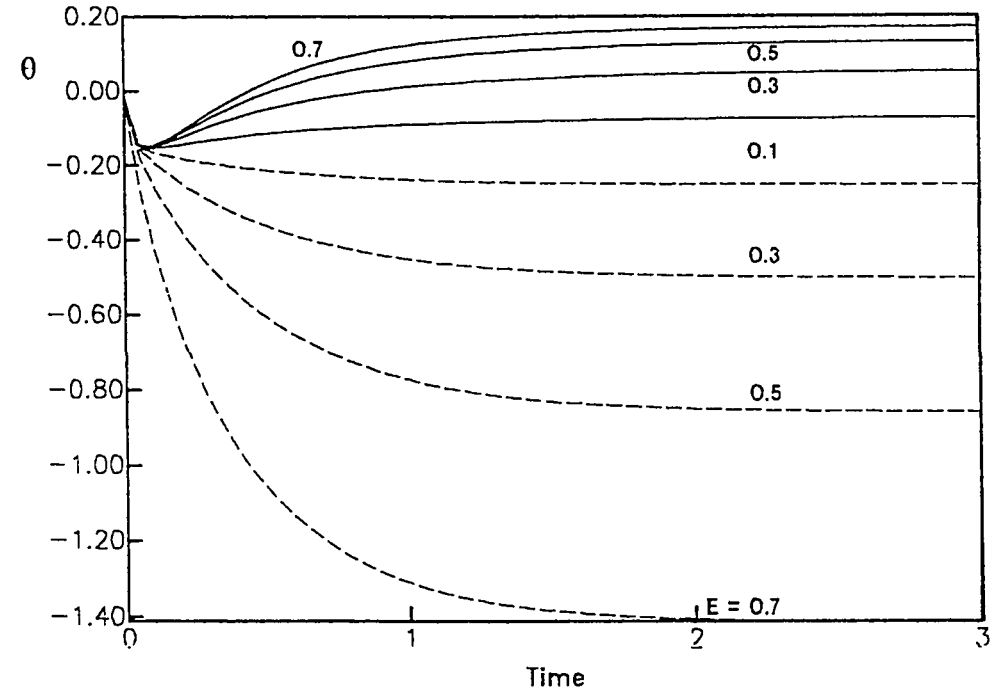


Fig. 5.3(b) : Effect of eccentricity on the temperature response at the outer cooled wall in case 2.O, N = 0.5, —— $\xi = 0.0$, – – – $\xi = \pi$.

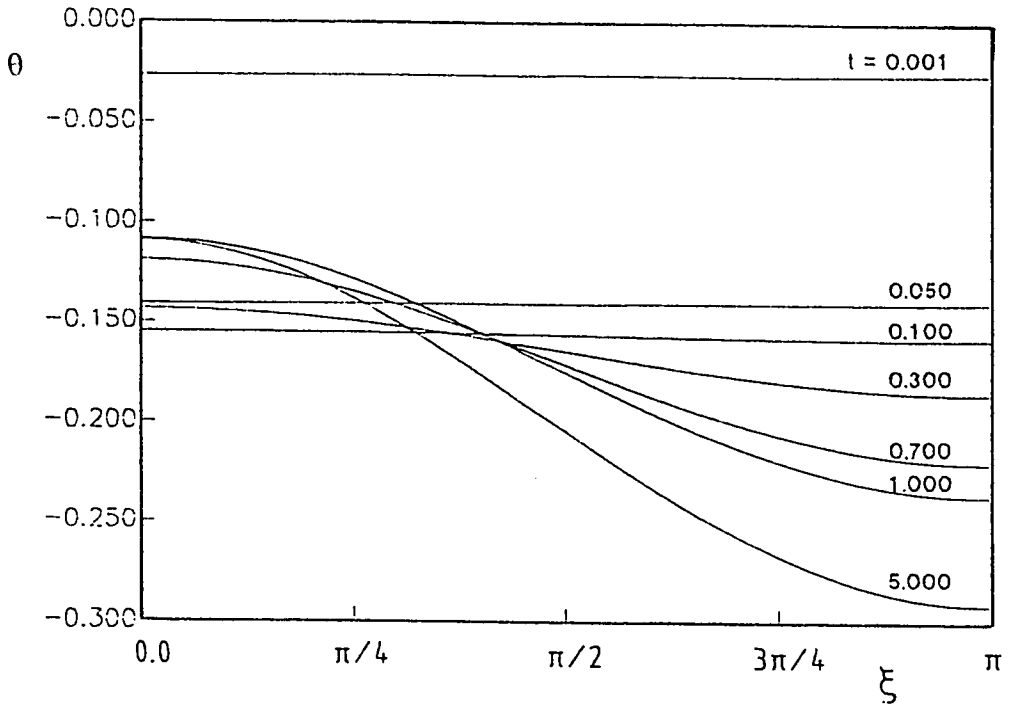


Fig. 5.4(a) : Transient temperature distribution on the inner cooled wall in case 2.I,

N = 0.5, E = 0.1.

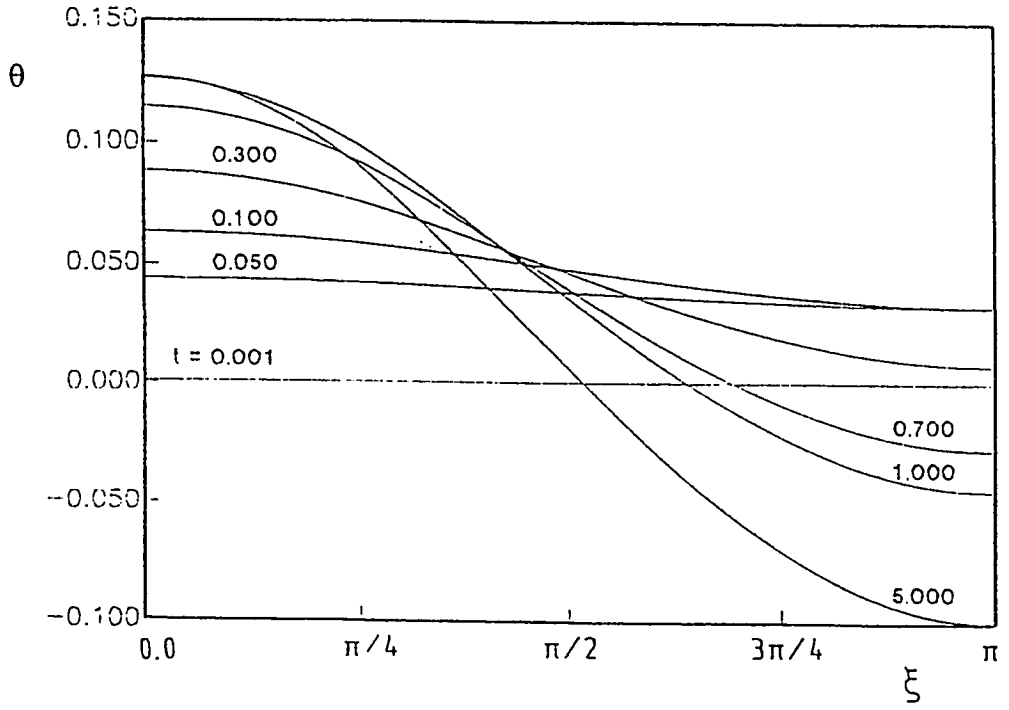


Fig. 5.4(b) : Transient temperature distribution on the outer insulated wall in case 2.I,

N = 0.5, E = 0.1.

= 0.7 are presented in Figs. 5.5(a) and 5.5(b). For case 2.O, Figures 5.6(a) through 5.7(b) show the transient variation of temperature with $\xi$ on the inner insulated wall and the outer cooled wall for E = 0.1 and E = 0.7, respectively.

Inspection of this set of figures show that the annulus material is subject to two contradictory effects. One is the reduction of temperature due to the cooling effect on the heat transfer wall and the other is the raising of temperature due to the heat generation within the annulus material. For a relatively large eccentricity (e.g., E = 0.7), as the time elapses the temperature of the insulated wall increases near the widest side and decreases near the narrowest side. For a relatively small eccentricity (e.g., E = 0.1) the insulated-wall temperature firstly increases everywhere then as time elapses it continues increasing near the widest side but decreases near the narrowest side. This increase in temperature near the widest side and its decrease near the narrowest side continue until the steady-state conditions are reached. On the other hand, the temperature of the heat transfer (cooled) wall firstly decreases everywhere and then as time elapses it increases near the widest side and continues decreasing near the narrowest side until the steady-state conditions are reached. From the above set of figures, one can conclude that the cooling effect of the heat transfer wall will be pronounced near the narrowest side and the reduction in the temperature due to this cooling effect increases with time on both the insulated and cooled walls near that side of the annulus. However, the heat generation will be prominent in the widest side and hence the temperature of both walls increases near that side. This is attributed to the decrease/increase of the resistance and the heat generated per unit length in the narrow/wide side of the annulus.

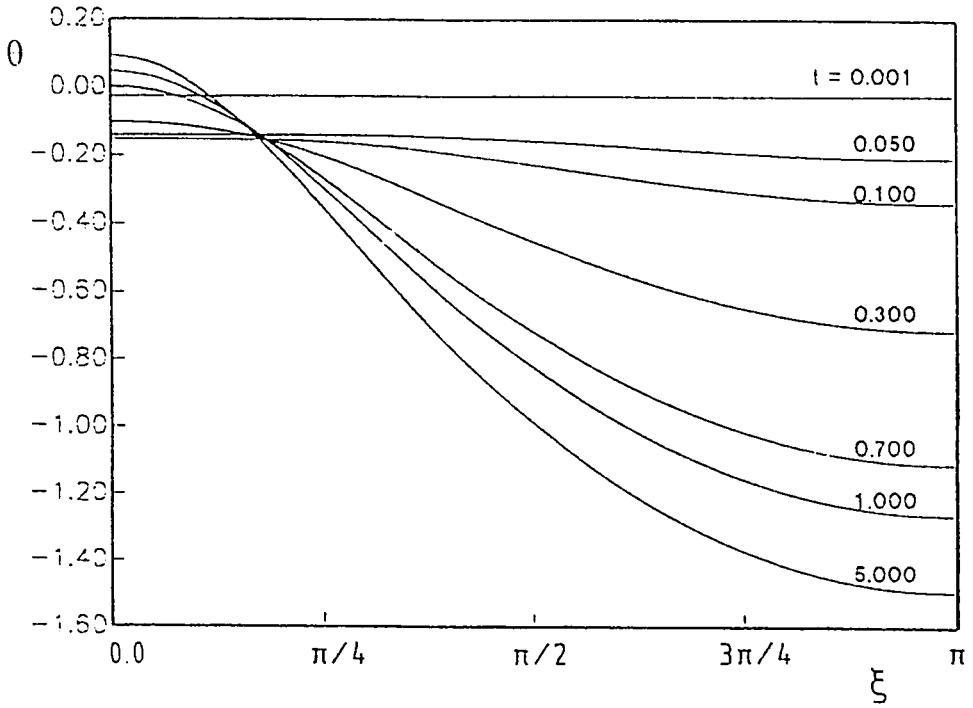


Fig. 5.5(a) : Transient temperature distribution on the inner cooled wall in case 2.I,

N = 0.5, E = 0.7.

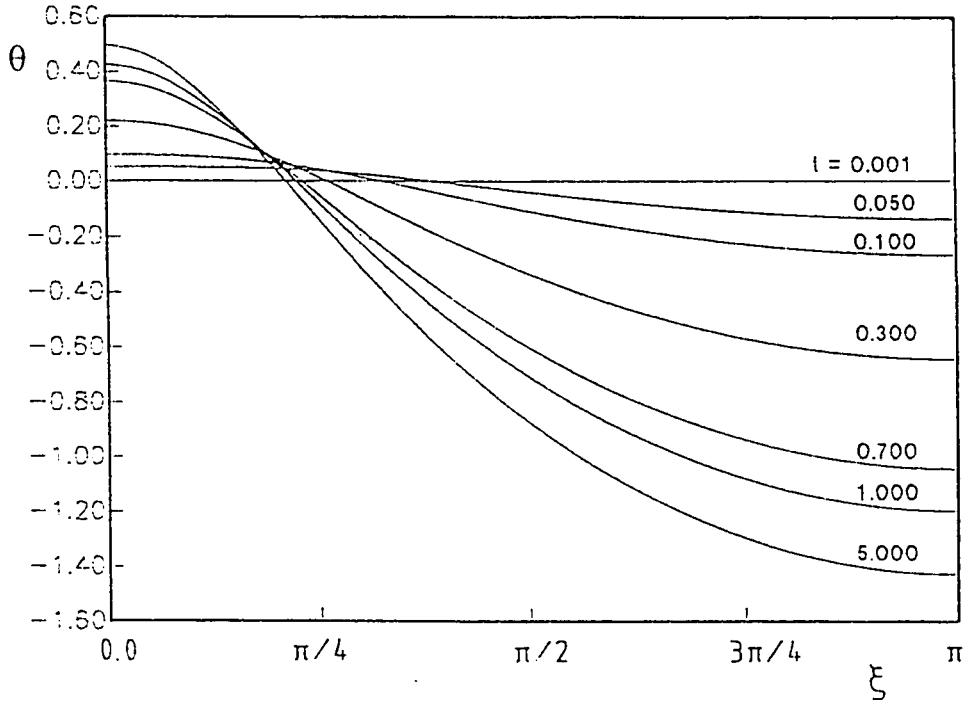


Fig. 5.5(b) : Transient temperature distribution on the outer insulated wall in case 2.I,

N = 0.5, E = 0.7.

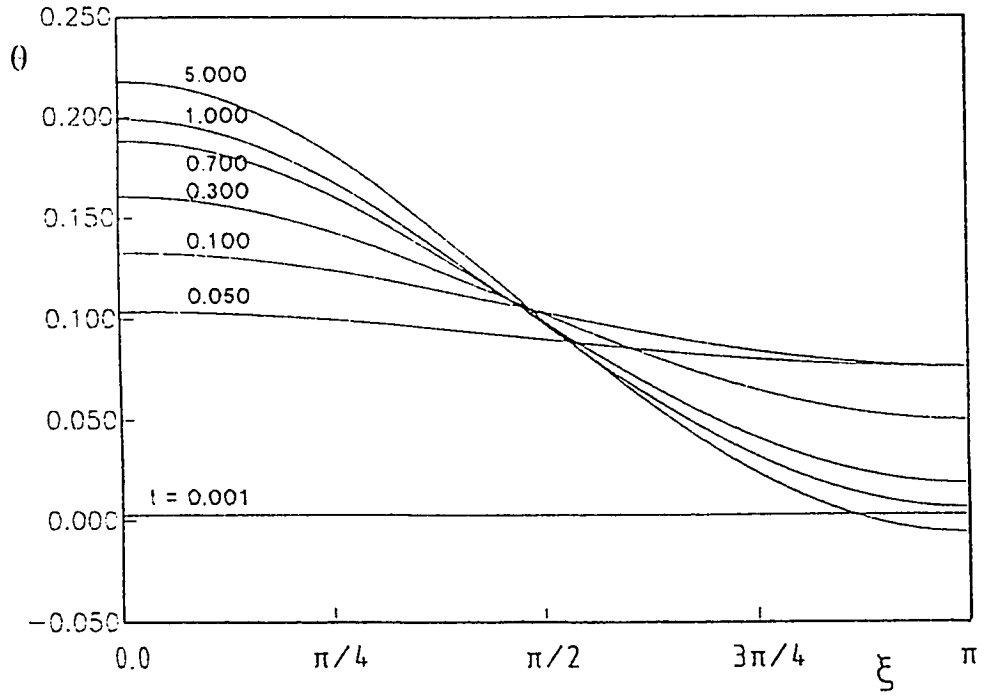


Fig. 5.6(a) : Transient temperature distribution on the inner insulated wall in case 2.O, N = 0.5, E = 0.1.

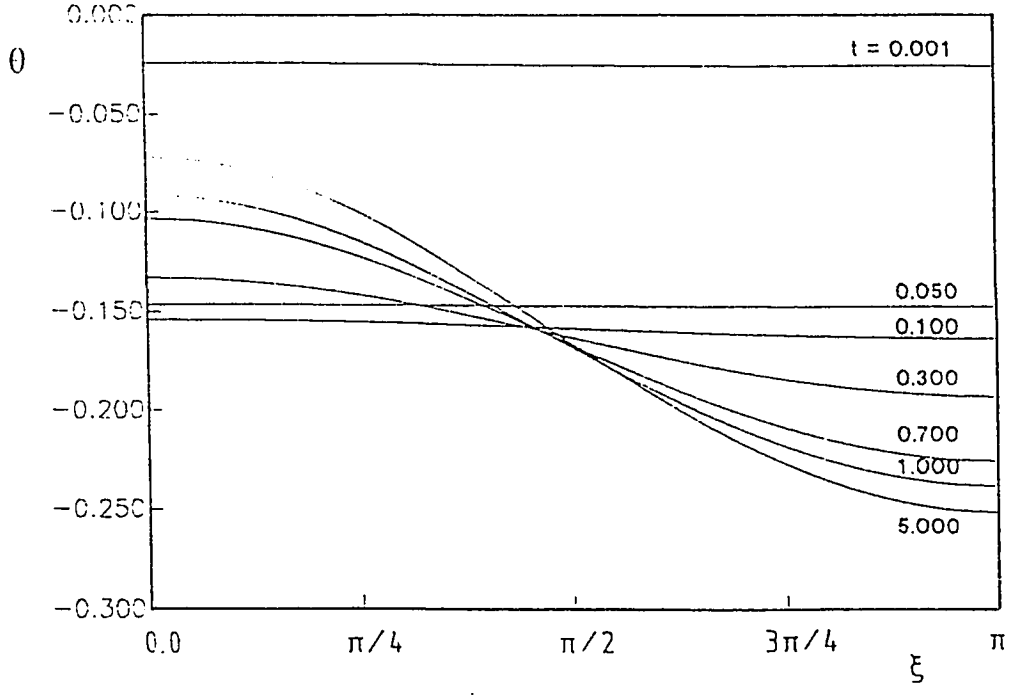


Fig. 5.6(b) : Transient temperature distribution on the outer cooled wall in case 2.O, N = 0.5, E = 0.1.

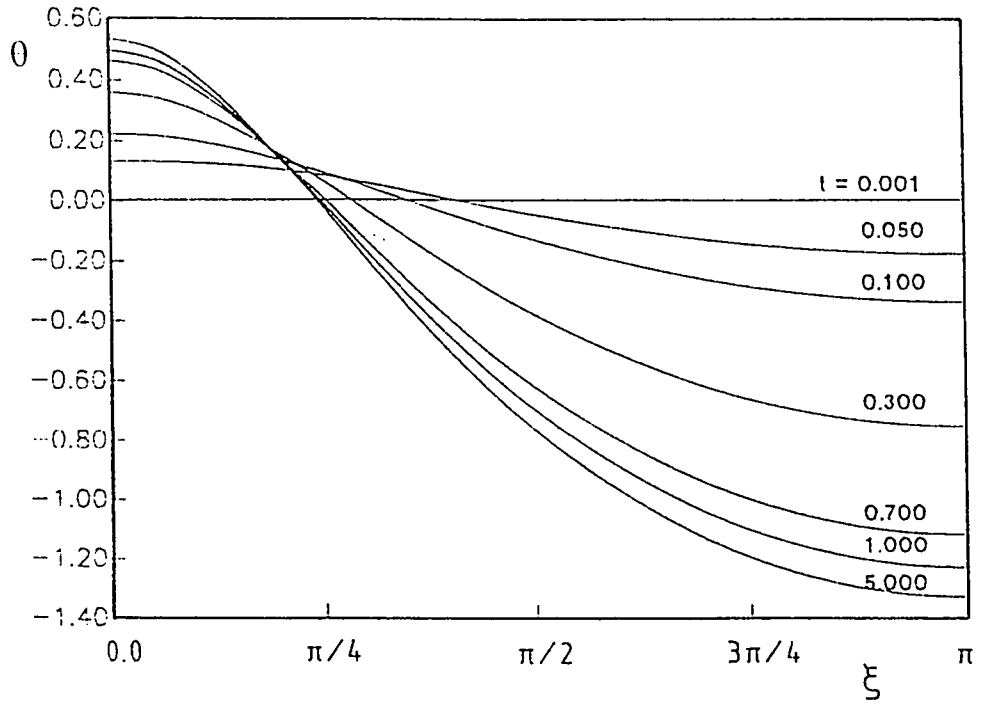


Fig. 5.7(a) : Transient temperature distribution on the inner insulated wall in case 2.O, N = 0.5, E = 0.7.

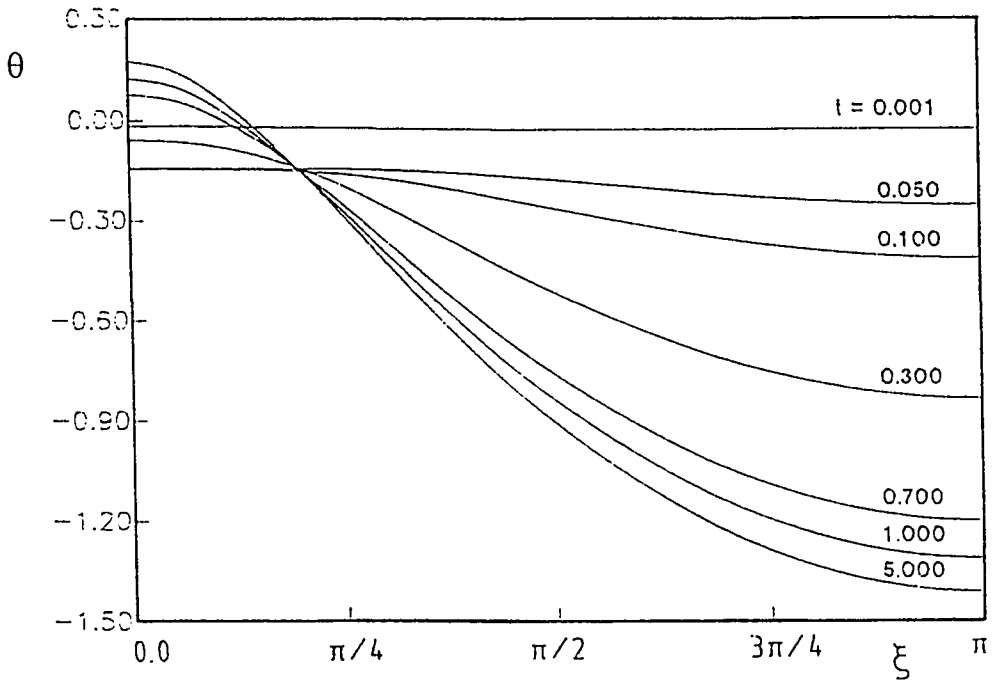


Fig. 5.7(b) : Transient temperature distribution on the outer cooled wall in case 2.O, N = 0.5, E = 0.7.

Figures 5.8(a) through 5.11(b) show the transient variation of temperature with $\eta$ (i.e., across the annulus material between the inner and outer boundaries) in the widest side and the narrowest sides for E = 0.1 and 0.7. This set of figures show that the temperature profiles of the annulus material which is initially uniform at a zero value (ambient temperature) decreases near the heat transfer wall due to the cooling effect of that boundary and it increases near the insulated wall due to the heat generation. As time elapses the temperature of the annulus material continues decreasing near the narrowest side and increasing near the widest side until the steady-state conditions are reached at relatively large values of time. At the steady-sate conditions, the maximum temperature is attained on the insulated wall on the widest side ($\xi = 0$) while the minimum temperature is attained on the heat transfer wall on the narrowest side ($\xi = \pi$).

Comparing the set of figures corresponding to the relatively small eccentricity (E = 0.1) with those for E = 0.7, it can be seen that for this small eccentricity the temperature profiles in the widest and narrowest sides of the annulus have almost the same shape with values not very much different for each side. This is attributed to the nearly uniform distribution of the annulus material and consequently the conduction resistance and the heat generated per unit length in both sides of the annulus. However, for the larger eccentricities (e.g., E = 0.7), the temperature profiles on the narrowest side tend to be flat. This may be attributed to the fact that the conduction resistance decreases in the narrowest side with the increase in eccentricity and for this type of boundary conditions (uniform cooling at one boundary while the other boundary is insulated) the decrease in the

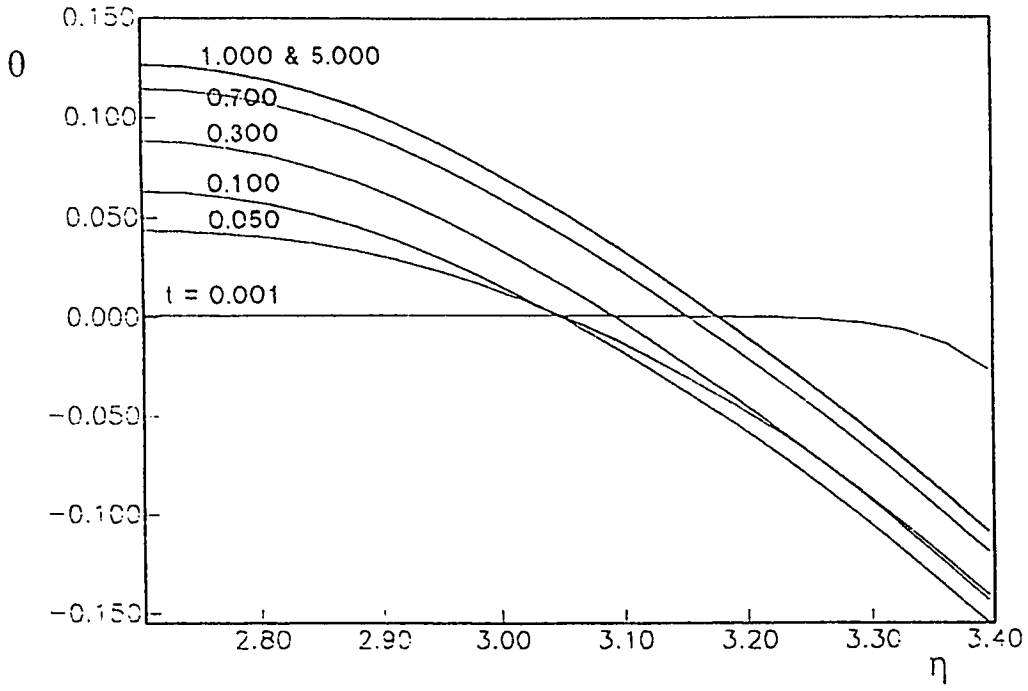


Fig. 5.8(a) : Temperature profiles at $\xi = 0.0$ in case 2.I, N = 0.5, E = 0.1.

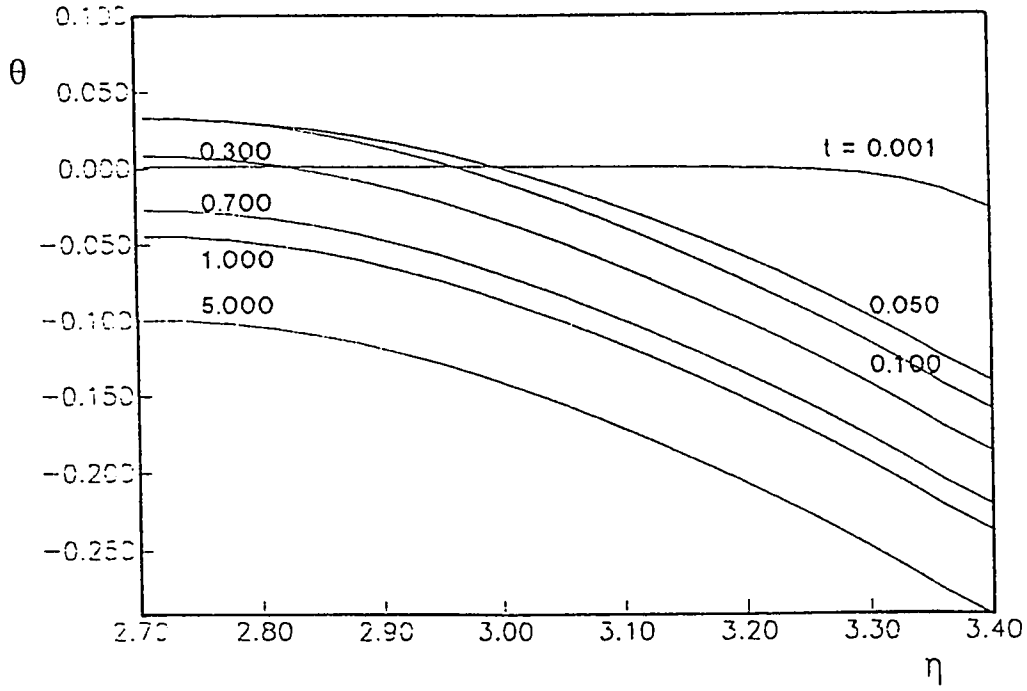


Fig. 5.8(b) : Temperature profiles at $\xi = \pi$ in case 2.I, N = 0.5, E = 0.1.

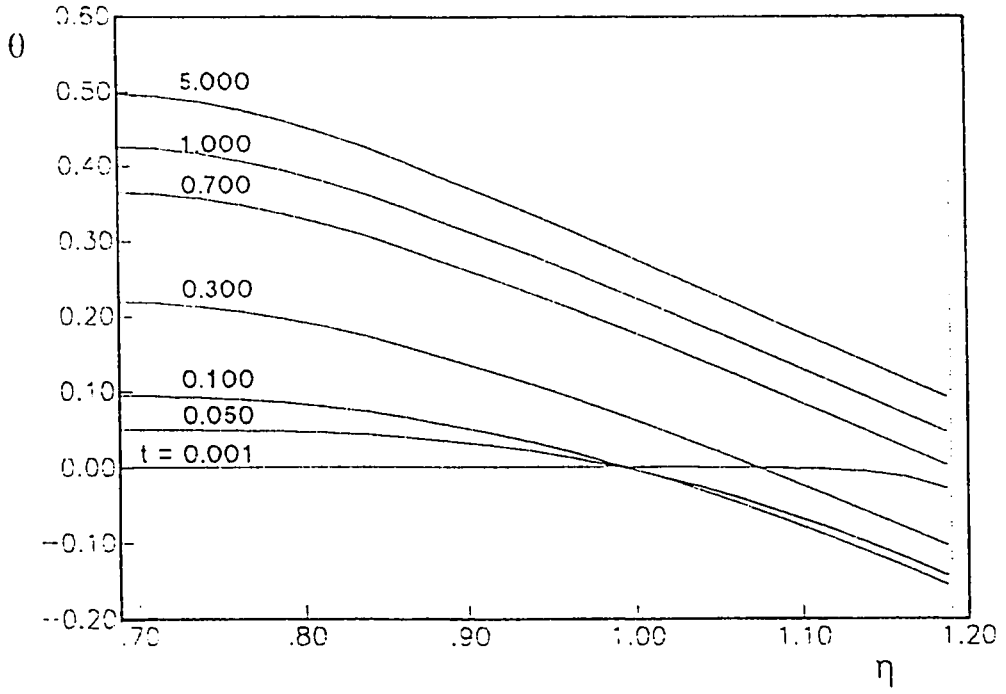


Fig. 5.9(a) : Temperature profiles at $\xi = 0.0$ in case 2.I, N = 0.5, E = 0.7.

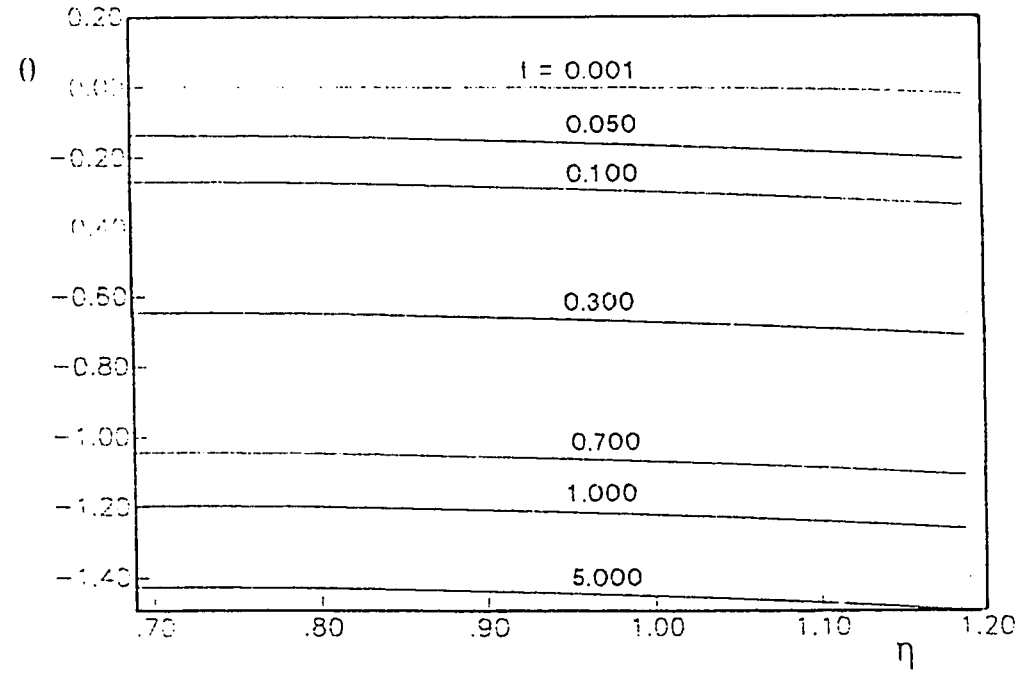


Fig. 5.9(b) : Temperature profiles at $\xi = \pi$ in case 2.I, N = 0.5, E = 0.7.

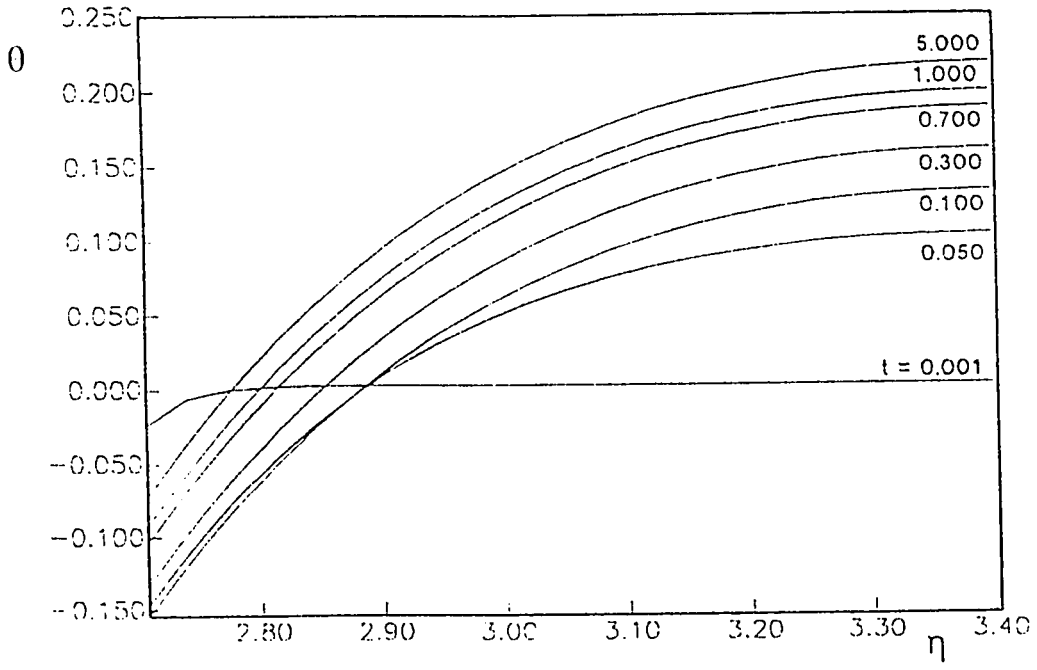


Fig. 5.10(a) : Temperature profiles at $\xi = 0.0$ in case 2.O, N = 0.5, E = 0.1.

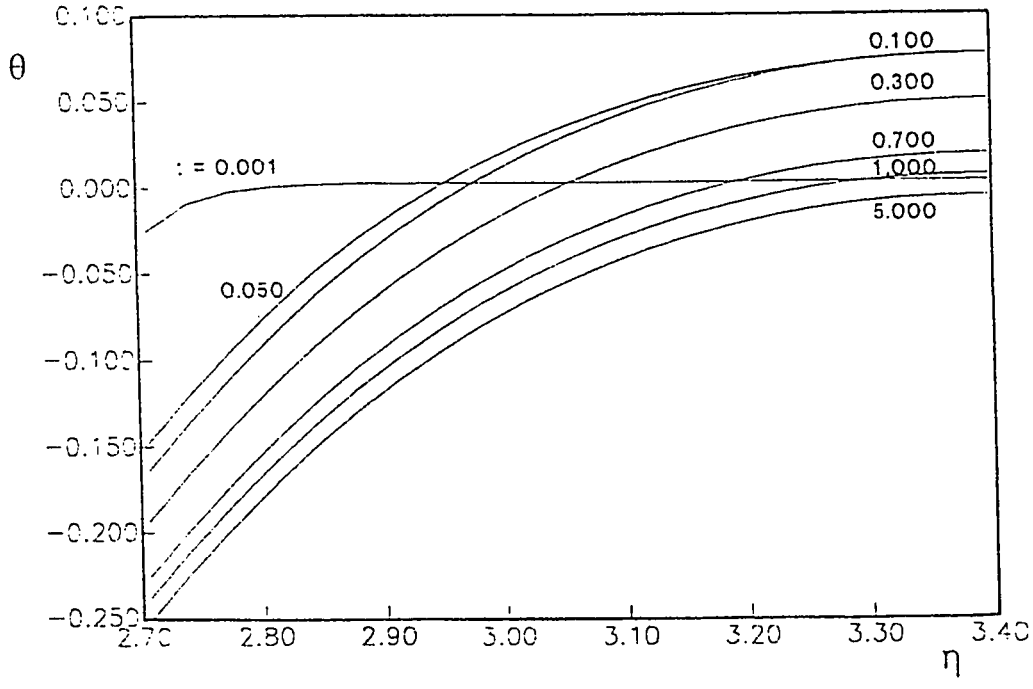


Fig. 5.10(b) : Temperature profiles at $\xi = \pi$ in case 2.O, N = 0.5, E = 0.1.

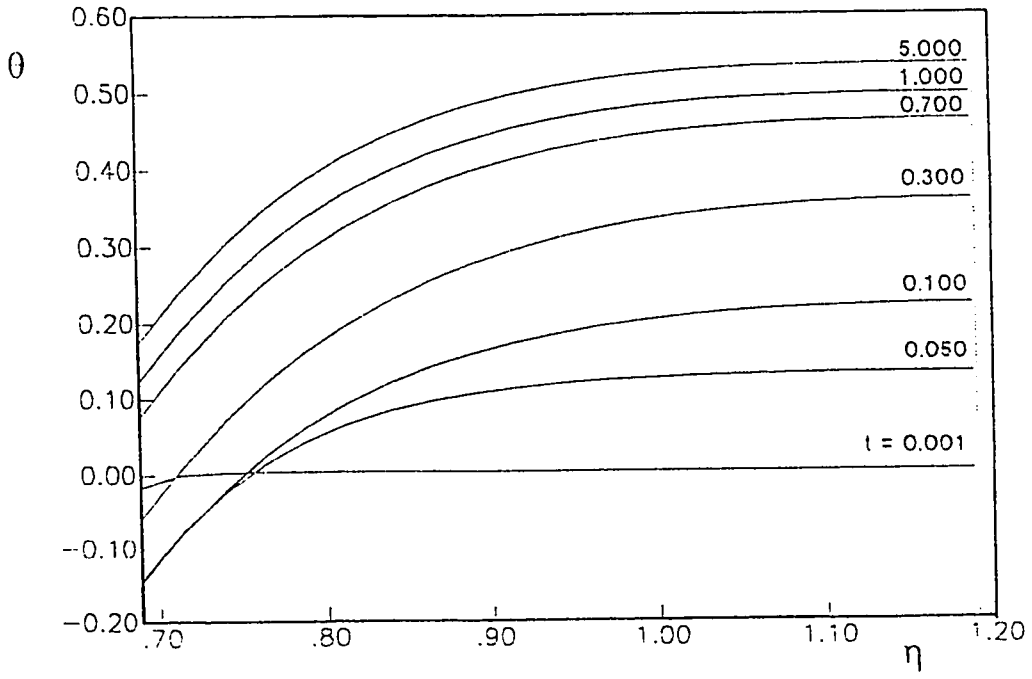


Fig. 5.11(a) : Temperature profiles at $\xi = 0.0$ in case 2.O, N = 0.5, E = 0.7.

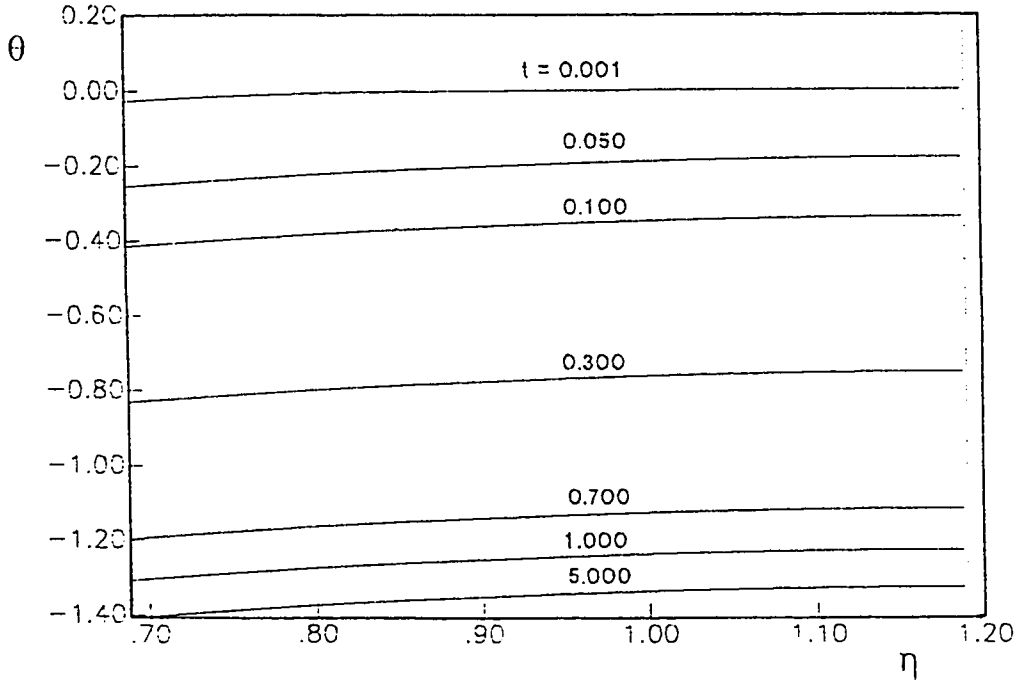


Fig. 5.11(b) : Temperature profiles at $\xi = \pi$ in case 2.O, N = 0.5, E = 0.7.

conduction resistance results in a reduction in the temperature difference across this resistance(i.e., flattening the temperature profiles near the narrowest side).

Figures 5.12(a) through 5.13(b) present the numerically obtained steady-state temperature variation with $\xi$ on the insulated and cooled walls for cases 2.I and 2.O. Having these numerically obtained steady-state solutions (as a result of numerically solving the transient problem at very large values of time) make it is possible to evaluate the numerical value of the constant $B$ in the steady-state analytical solution for the particular initial conditions under consideration. This can be done by putting the numerically obtained steady-state solutions on the left hand side of eq.(4.4) ( the steady-state analytical solution) to find the undetermined value of $B$ which appears on its right hand side. This constant ( $B$ ) was found to be dependent on the case under study ( case 2.I or case 2.O) and on the eccentricity. The variation of this constant with E is plotted in Figure 5.14 for cases 2.I and 2.O.

## 5.4 Temperature Results for Cases 3.I and 3.O

Figure 5.15(a) shows the transient temperature distribution on the insulated boundary of an annulus of radius ratio 0.5 and dimensionless eccentricity 0.7 under thermal boundary conditions 3.I and 3.O without internal heat generation ( $Q = 0$ ). Due to the presence of an insulated boundary, steady-state can only be achieved under these conditions when the annulus material temperature becomes uniform and equals the temperature of the heated boundary (i.e., dimensionless temperature $\theta_s = 1$ everywhere). As can be seen from Figure 5.15(a) as the time elapses the temperature of the insulated

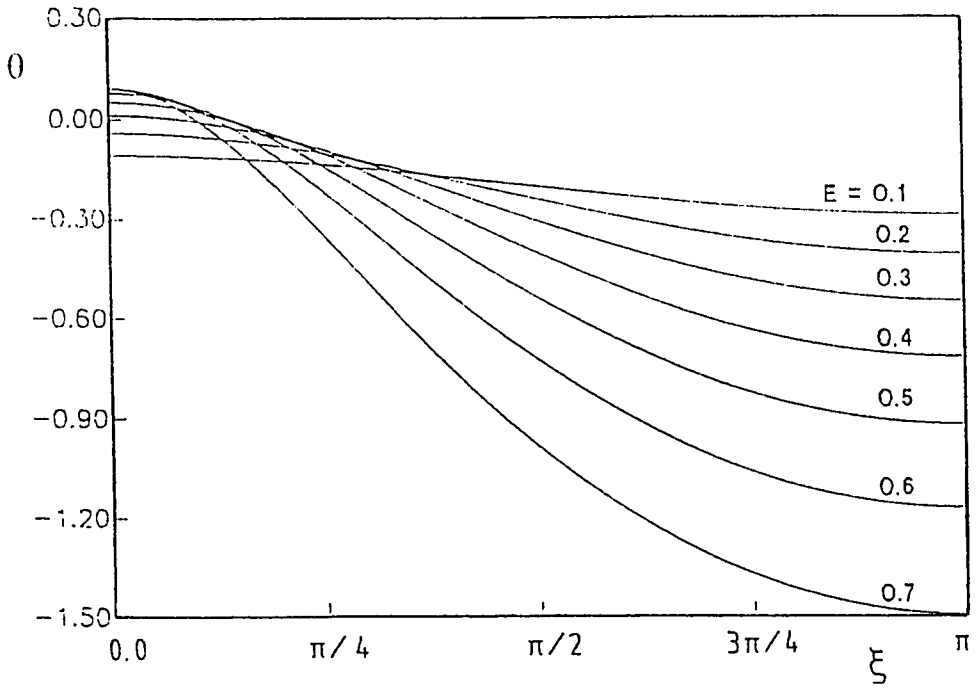


Fig. 5.12(a) : Variation of the steady state temperature with ξ, at the inner cooled wall for different values of E in case 2.I, N = 0.5.

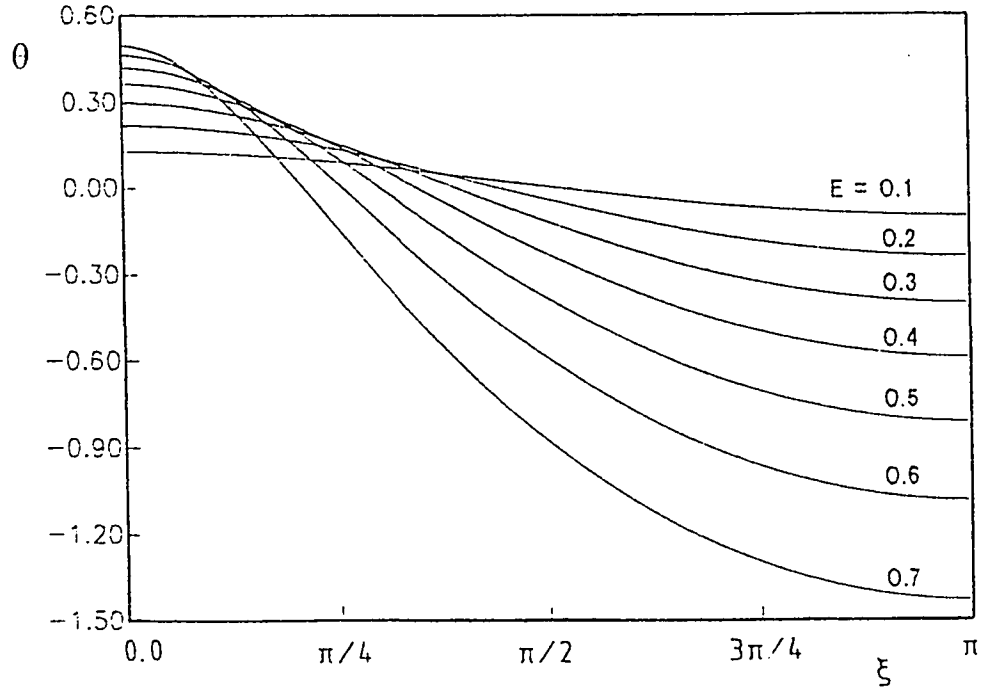


Fig. 5.12(b) : Variation of the steady state temperature with ξ, at the outer insulated wall for different values of E in case 2.I, N = 0.5.

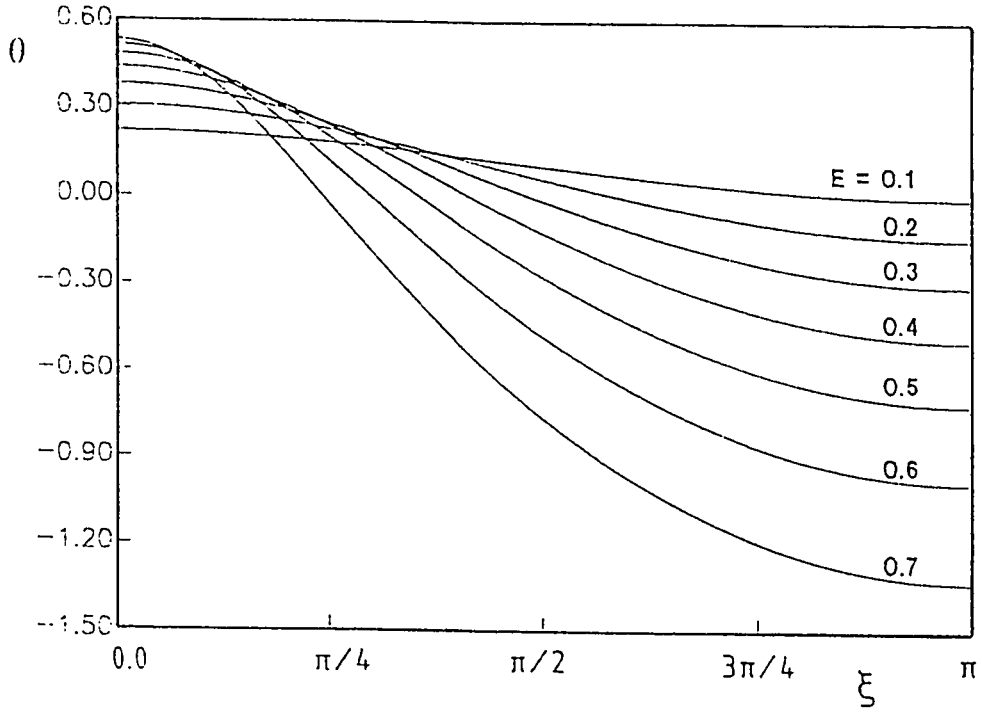


Fig. 5.13(a) : Variation of the steady state temperature with ξ, at the inner insulated wall for different values of E in case 2.O, N = 0.5.

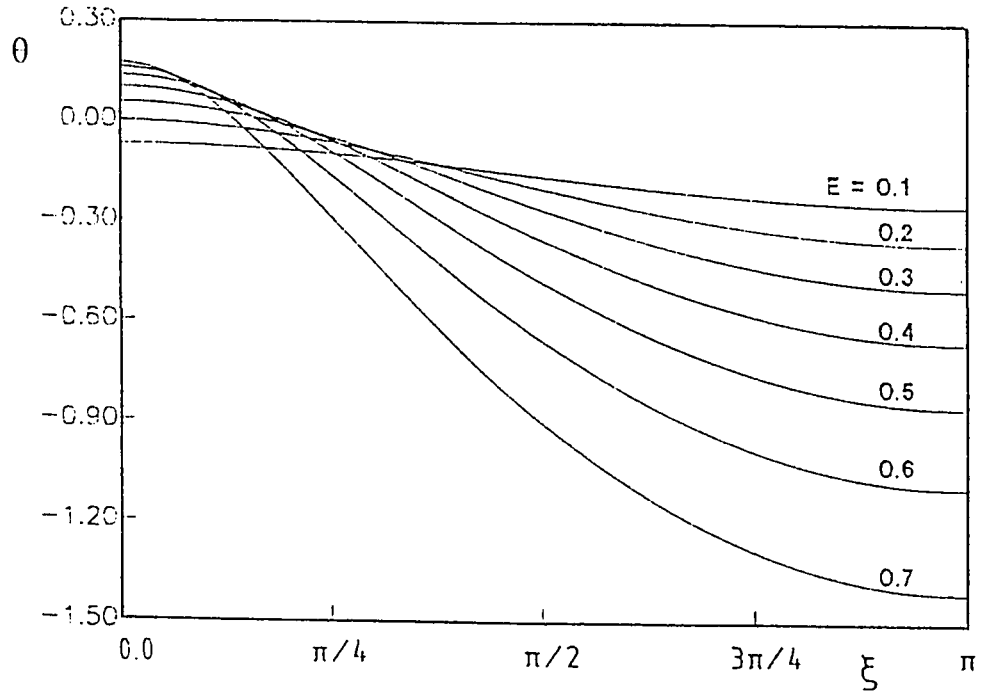


Fig. 5.13(b) : Variation of the steady state temperature with ξ, at the outer cooled wall for different values of E in case 2.O, N = 0.5.

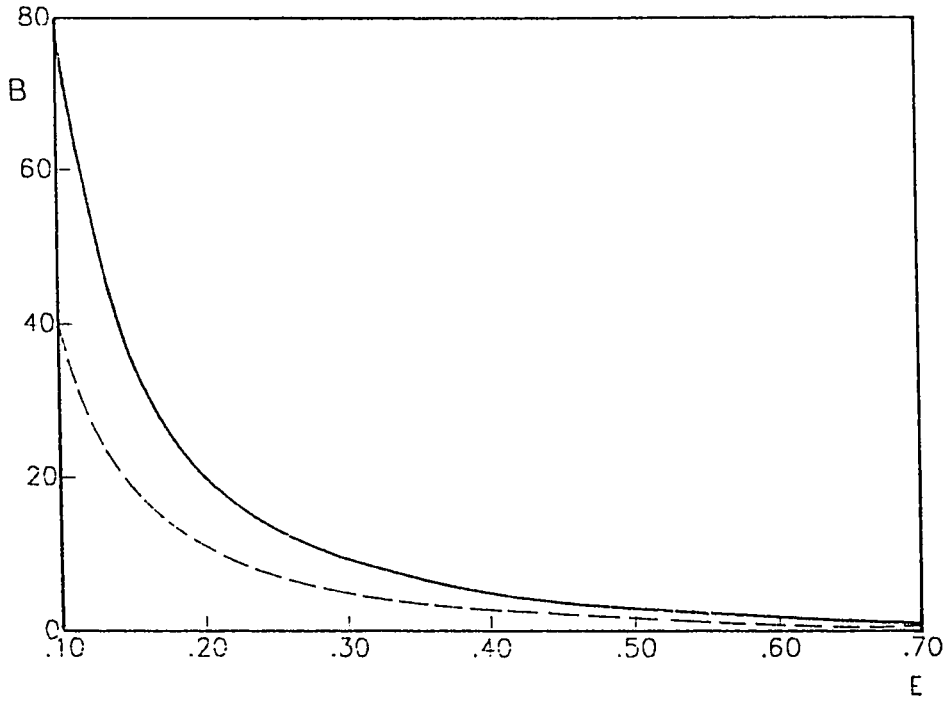


Fig. 5.14 : Effect of eccentricity on the value of the constant B in the analytical solution for zero initial conditions, —— Case 2.I., – – – Case 2.O, N = 0.5

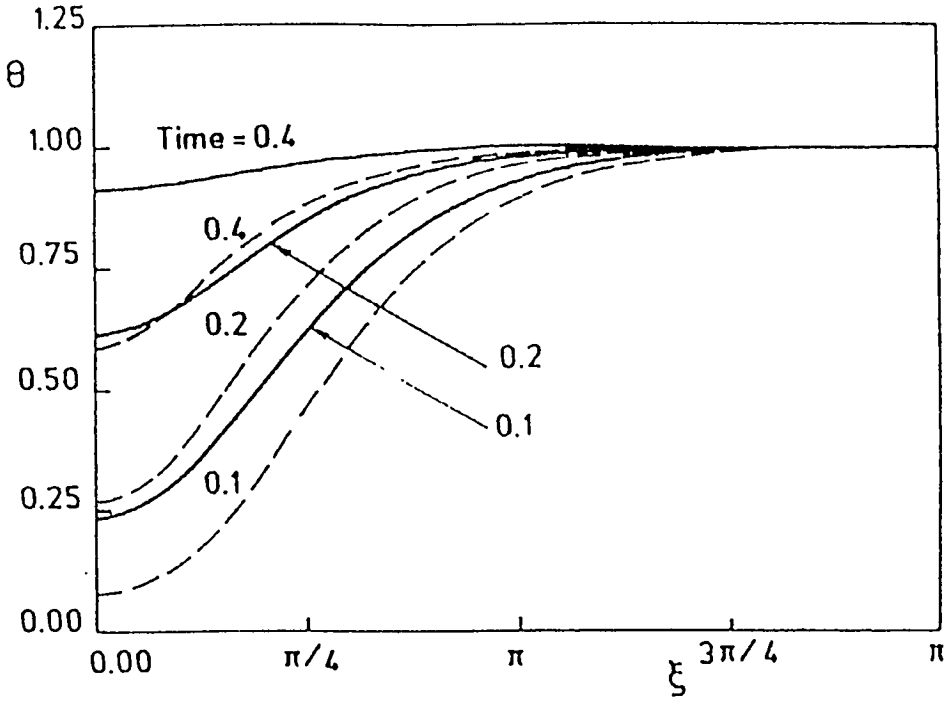


Fig. 5.15(a) : Effect of boundary conditions on temperature distribution on insulated wall,

$N = 0.5$, $E = 0.7$, $Q = 0$, - - - - case 3.1, —— case 3.O.

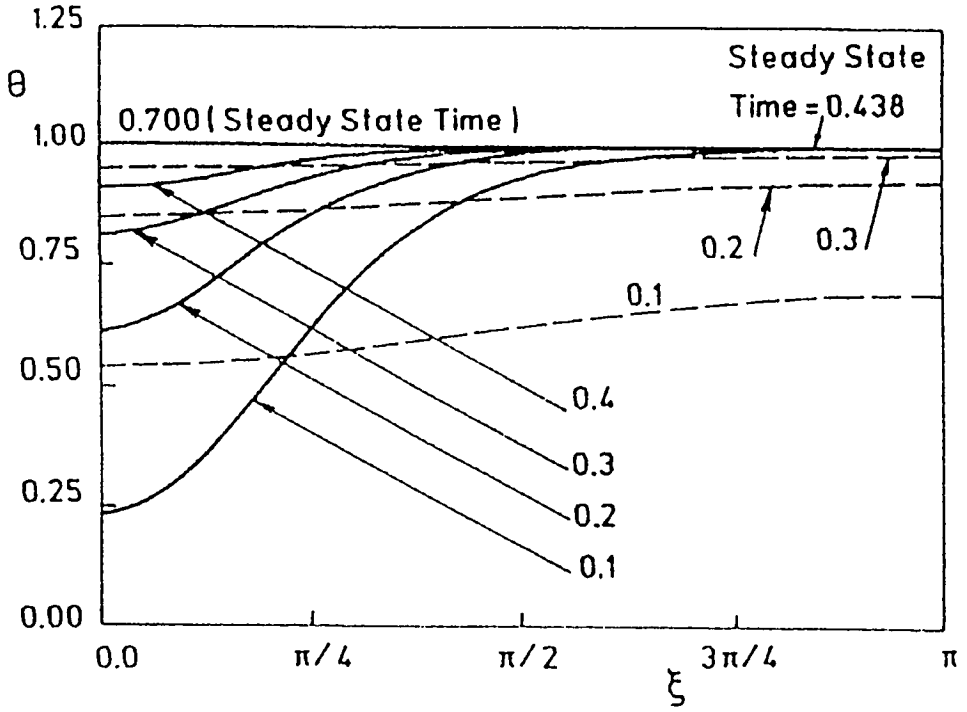


Fig. 5.15 (b) : Transient temperature distribution on the inner insulated wall

temperature in case 3.O, $N = 0.5$, $Q = 0$, - - - - $E = 0.1$, —— $E = 0.7$.

surface (and similarly that of the internal annulus material) increases and approaches asymptotically the aforesaid unity value. However, the narrow-side of the annulus reaches such steady-state conditions faster than the wide-side. Therefore, the process of increasing the temperature towards equalization at steady-state conditions occurs not only by diffusion of heat in the radial-like ($\eta$) direction (from the heat transfer boundary to the insulated surface) but also in the circumferential $\xi$-direction (from the narrow-side to the wide-side of the annulus). This latter mechanism of conduction heat transfer has a longer path than the former (which is the only mechanism in a concentric case) and hence it can be anticipated that eccentricity, as will be shown later, would increase the time needed to reach steady-state conditions. For given time and $\xi$, Fig. 5.15(a) shows that the temperature under thermal boundary conditions 3.O is higher than that under thermal boundary conditions 3.I. Moreover, the system reaches steady-state conditions in case 3.O faster than in case 3.I. These are attributed to the larger heat transfer surface area in case 3.O than in case 3.I. Moreover, reaching steady-state more quickly for case 3.O is also likely due to the surface over which the temperature is kept constant at the steady-state value $\theta = 1$ (i.e., there is much more material at $\theta = 1$).

To clarify the effect of eccentricity, Figs. 5.15(b) and 5.16(a) give the time-variation of the insulated (inner) wall temperature for two values of eccentricity, namely, $E = 0.1$ and $E = 0.7$, in an annulus of $N = 0.5$ under thermal conditions 3.O without and with internal heat generation, respectively. Both figures show that increasing the value of $E$ makes the temperature more dependent on the $\xi$-coordinate. Without internal heat generation ($Q = 0$), the $\xi$-direction diffusion of heat is always from the narrow

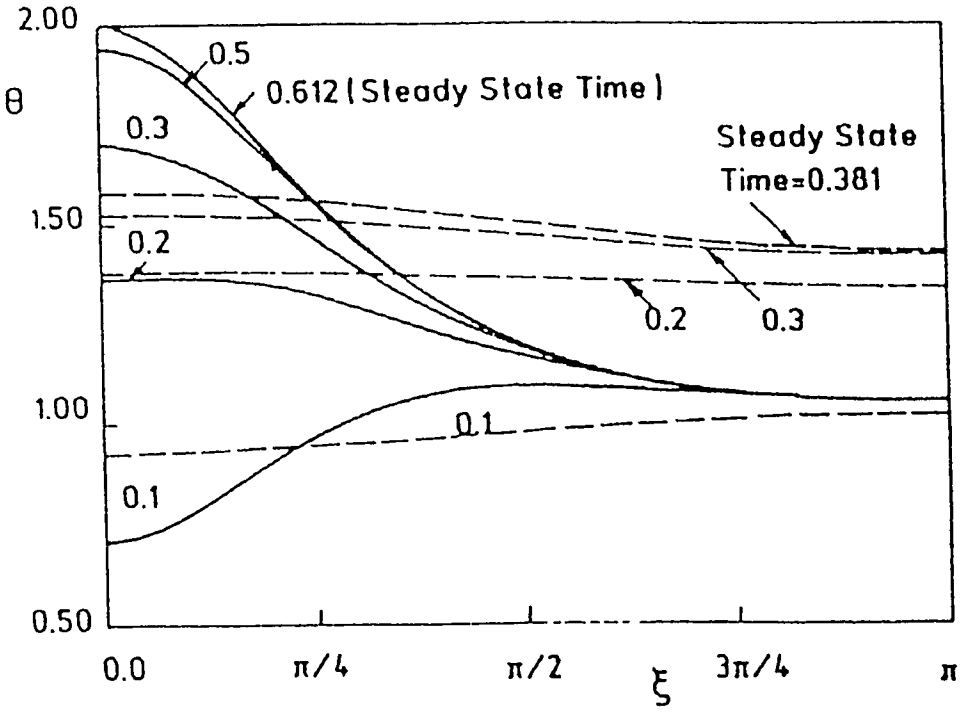


Fig. 5.16(a) : Transient temperature distribution on the inner insulated wall in case 3.O,

$N = 0.5, Q = 5$, - - - - $E = 0.1$, —— $E = 0.7$.

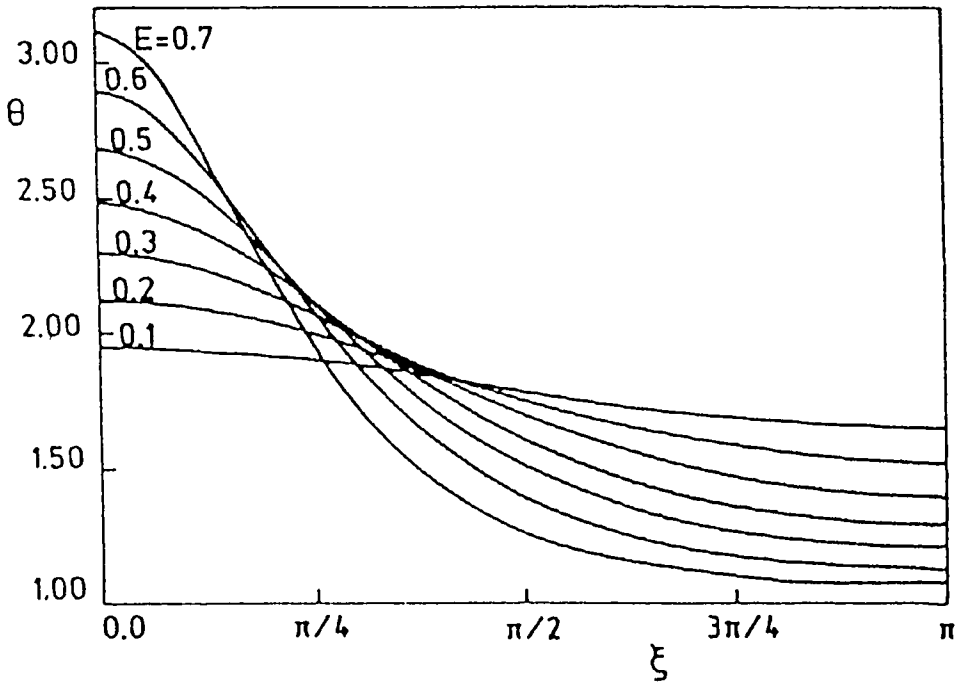


Fig. 5.16(b) : Steady-state temperature distribution on the outer insulated wall in case 3.1

for various eccentricities, $N = 0.5$, $Q = 5$.

side ($\xi \rightarrow \pi$) to the wide side ($\xi \rightarrow 0$), as can be seen from Fig. 5.15(b). However, with internal heat generation ($Q \neq 0$) Fig.5.16(a) shows that at large values of time the $\xi$-direction diffusion of heat reverses its direction and becomes from the large side to the narrow side of the annulus. This is attributed to the more material per unit length on this side and hence the increase in the temperature of the solid in the wide side as a result of internal heat generation. Figure 5.16(b) focuses on the pronounced effect of eccentricity on the insulated wall temperature. This figure gives the steady-state temperature distribution on the outer wall of an annulus of $N = 0.5$ under thermal conditions 3.I for a value of $Q = 5$. The figure clearly shows that increasing the value of $E$ causes an increase in the wall temperature on the wide side and a decrease in this temperature on the narrow side.

Engineers are not frequently concerned with the details of the temperature field but only with maximum temperature and the time required to reach steady-state conditions. From the previous presented results it is clear that for given time, $E$ and $Q$, the maximum solid temperature in both cases 3.I and 3.O would occur on the insulated wall at $\xi = 0$. Figures 5.17(a) and 5.17(b) give for cases 3.I and 3.O, respectively, the variation of such maximum temperature with time at two different eccentricity values in an annulus of $N = 0.5$ for various values of $Q$.

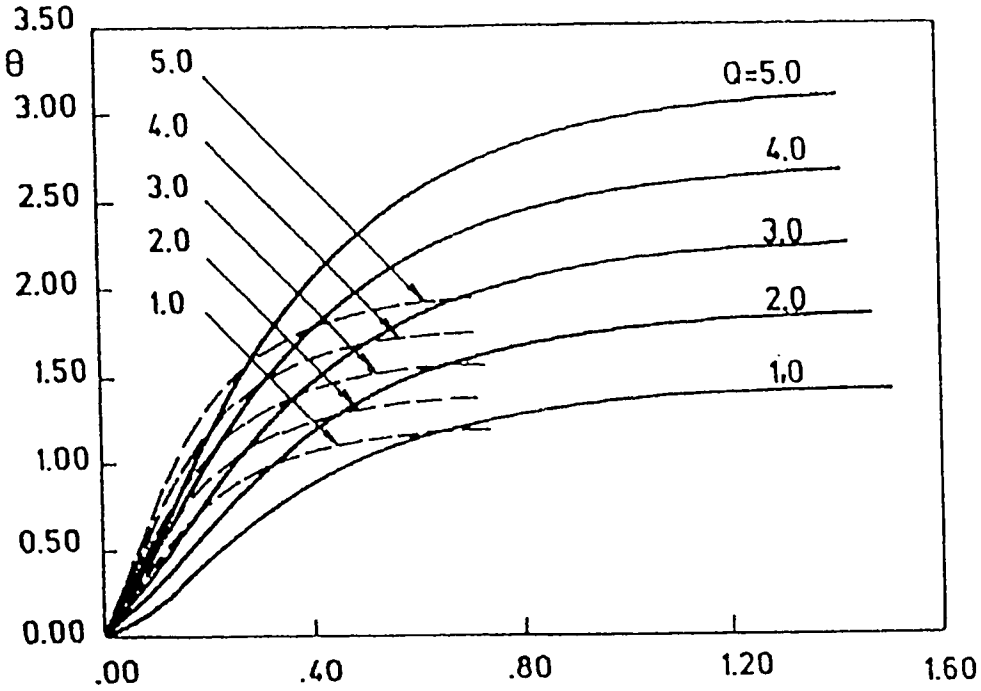


Fig. 5.17(a) : Variation of maximum temperature on the outer insulated wall in case 3.1,

$\xi = 0, N = 0.5$, - - - - $E = 0.1$, —— $E = 0.7$.

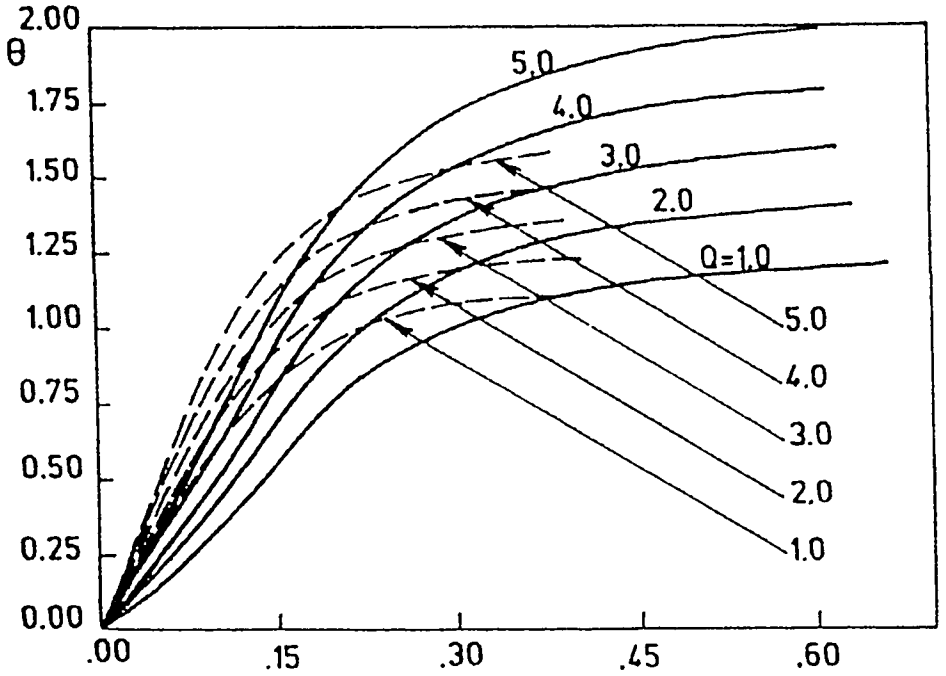


Fig. 5.17(b) : Variation of maximum temperature on the inner insulated wall in case 3.0,

$\xi = 0, N = 0.5$, - - - - $E = 0.1$, —— $E = 0.7$.

## 5.5 Temperature Results for Cases 4.I and 4.O

The variation with time of the temperature profiles against $\eta$ (i.e., across the solid between the inner and outer boundaries) at $\xi = 0.0$ (i.e., the widest side of the annulus) are shown in Fig. 5.18(a) for case 4.O for a relatively small value of eccentricity (E = 0.1) at two values of the heat ratio Q, namely, Q = 0.0 (i.e., case with no internal heat generation) and Q = 5.0. The same profiles are shown fig. 5.18(b) but for a large value of the eccentricity, namely, E = 0.7. As can be seen from these two figures, for a given time *t*, the dimensionless temperature is zero (ambient temperature) at the inner wall (i.e., the largest value of $\eta$) and increases monotonically as one moves from the inner cooled surface to the outer heated surface (having the smallest value of $\eta$). Also, for given Q and location inside the annulus (i.e., a given $\eta$) the temperature increases with time due to internal heat generation (if any) and the heat added through the outer wall until the steady-state temperature profile is reached. Moreover, the temperature for given $\eta$ and time is larger in the case with internal heat generation ( $Q > 0$ ) than in the case without internal heat generation ( $Q = 0$ ).

A comparison between Fig. 5.18(a) and Fig. 5.18(b) reveals that increasing the eccentricity results in a general increase in the value of the annulus material temperature on this side of the annulus. This is attributed to the increase in the quantity of heat generated per unit length on this wide side of the annulus as a result of having more solid material (on this side) when the eccentricity increases. The comparison between the two figures indicates also that, within the investigated range of Q and E, the eccentricity is the prominent factor that influences the time required to reach steady-state conditions. The

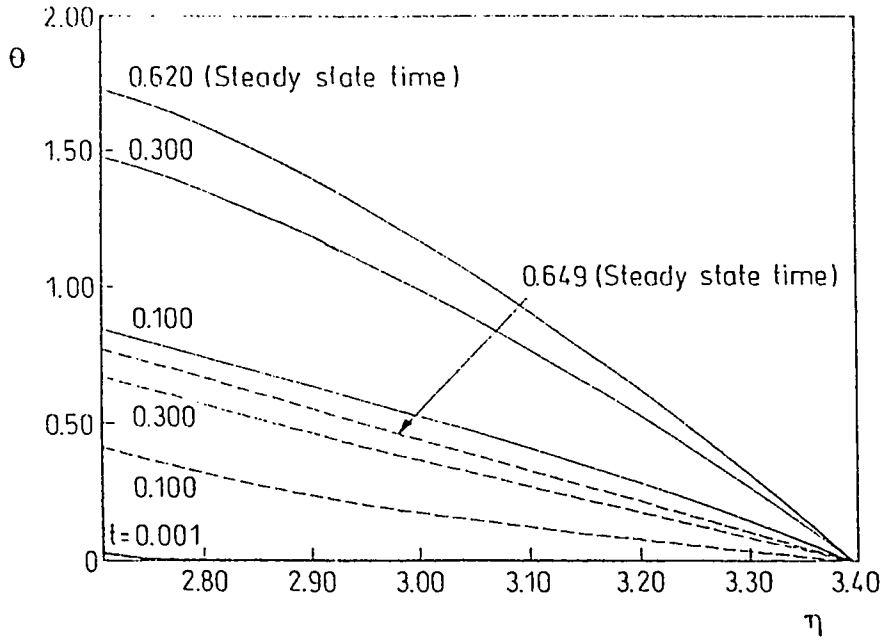


Fig. 5.18(a) : Temperature profiles at $\xi = 0$ in case 4.O, N = 0.5, E = 0.1,

---- $Q = 0$, —— $Q = 5$.

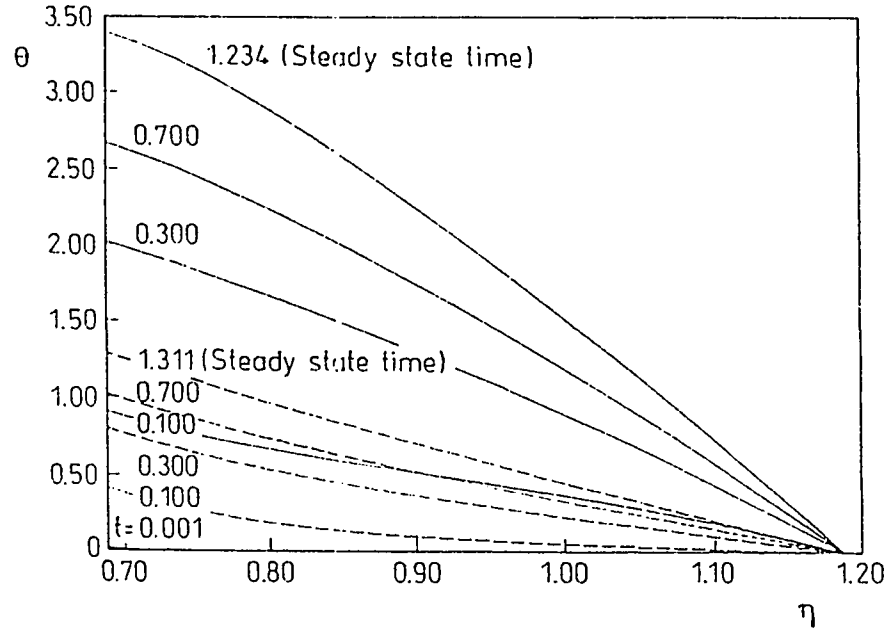


Fig. 5.18(b) : Temperature profiles at $\xi = 0$ in case 4.O, N = 0.5, E = 0.7,

---- $Q = 0$, —— $Q = 5$.

values of the steady-state time $t_s$ for E = 0.1 are 0.620 and 0.649 for $Q$ = 5 and 0, respectively, while the corresponding values of E = 0.7 are 1.234 and 1.311. Thus the steady state-time ($t_s$) increases considerably with the eccentricity E and decreases slightly with the heat ratio $Q$.

For E = 0.1 and 0.7 Figs. 5.19(a) and 5.19(b) respectively show, for $\xi = \pi$ (i.e., the narrowest side of the annulus), temperature profiles corresponding to the same time values given in Figs. 5.18(a) and 5.18(b). The general trends of these temperature profiles are similar to those profiles of Figs. 5.18(a) and 5.18(b). However, it is noticeable that the values of the temperature in the narrow side of the annulus (Figs. 5.19(a) and 5.19(b)) are generally lower than those in the wide side (Figs. 5.18(a) and 5.18(b)). This is because the cooling effect through the boundary maintained at the ambient temperature is more pronounced on the narrow side of the annulus due to its smaller heat storage capacity when compared with the wide side which has more material per unit length. The difference between the temperature values on the wide and the narrow sides is more remarkable for the larger value of the eccentricity $E$. Indeed, as $E$ tends to zero (concentric annulus) the azimuthal variation of temperature would vanish (i.e., axisymmetric temperature profile for $E = 0$).

The transient temperature profiles corresponding to $Q = 0$ and $Q = 5$ across the wide side of the annulus ($\xi = 0$) under thermal boundary conditions 4.I are shown in Figs. 5.20(a) and 5.20(b) for E = 0.1 and 0.7, respectively. The corresponding profiles across the narrow side of the annulus ($\xi = \pi$) are shown in Figs. 5.21(a) and 5.21(b). In this case (4.I), the dimensionless outer wall temperature is zero (ambient) and the temperature increases as

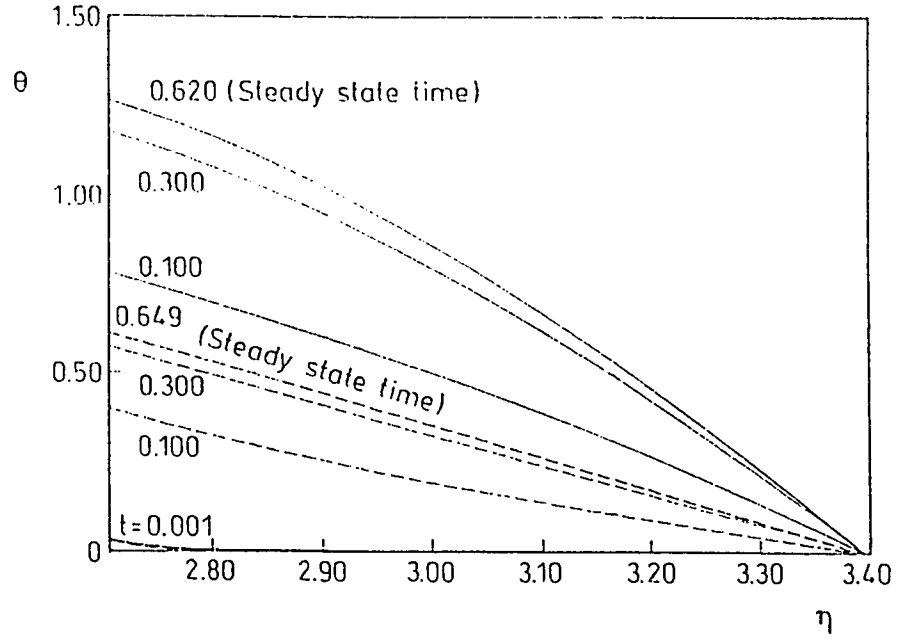


Fig. 5.19(a) : Temperature profiles at $\xi = \pi$ in case 4.O, N = 0.5, E = 0.1,

- - - - $Q = 0$, —— $Q = 5$.

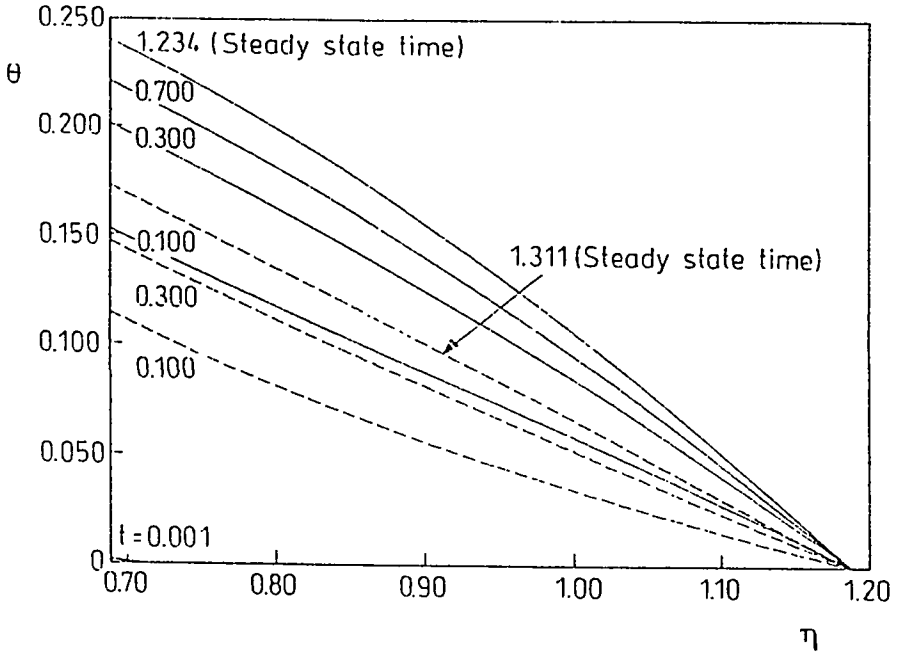


Fig. 5.19(b) : Temperature profiles at $\xi = \pi$ in case 4.O, N = 0.5, E = 0.7,

- - - - $Q = 0$, —— $Q = 5$.

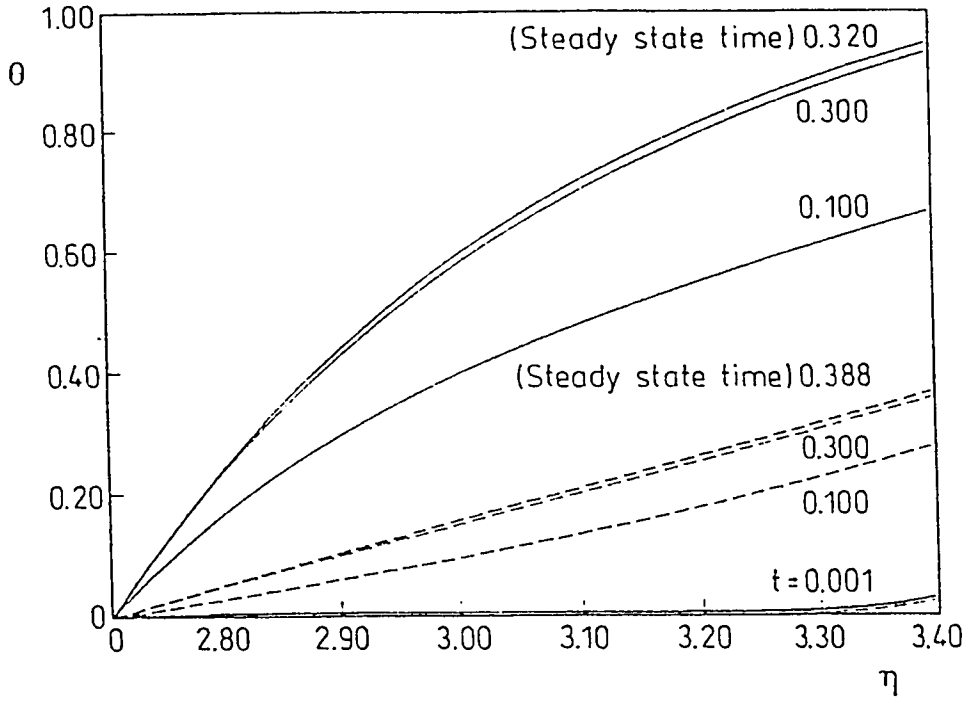


Fig. 5.20(a) : Temperature profiles at $\xi = 0$ in case 4.I, N = 0.5, E = 0.1,

- - - - $Q = 0$, —— $Q = 5$.

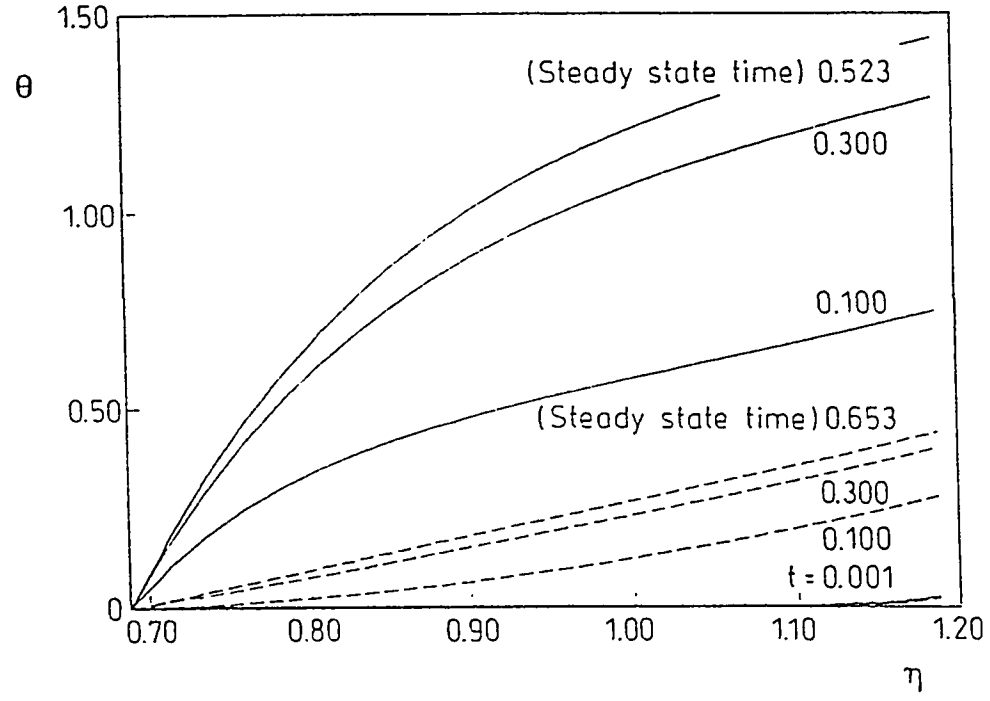


Fig. 5.20(b) : Temperature profiles at $\xi = 0$ in case 4.I, N = 0.5, E = 0.7,

- - - - $Q = 0$, —— $Q = 5$.

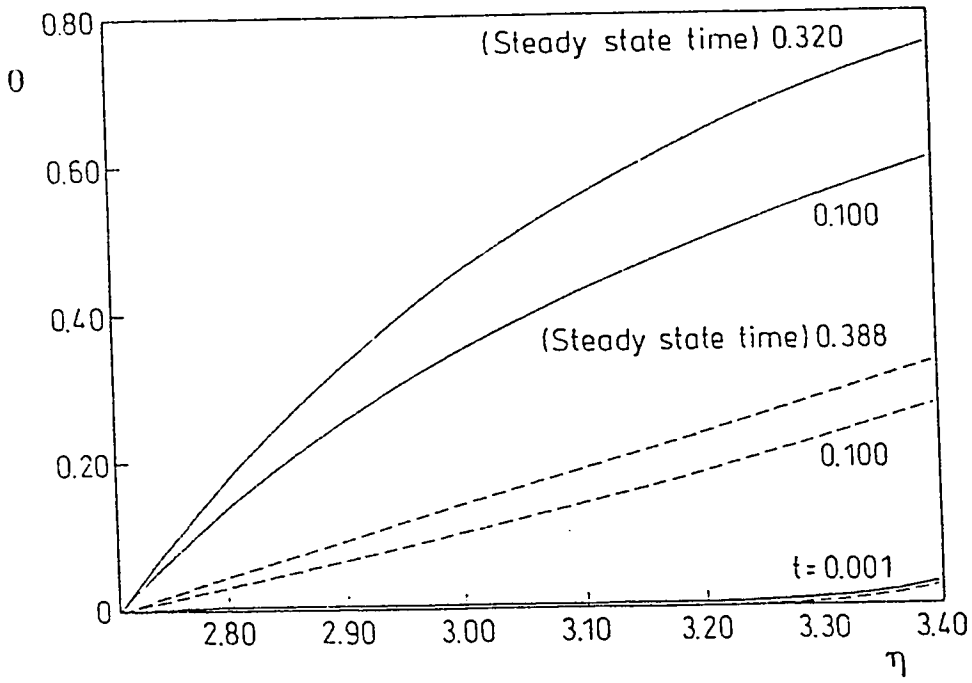


Fig. 5.21(a) : Temperature profiles at $\xi = \pi$ in case 4.1, N = 0.5, E = 0.1,

- - - - $Q = 0$, —— $Q = 5$.

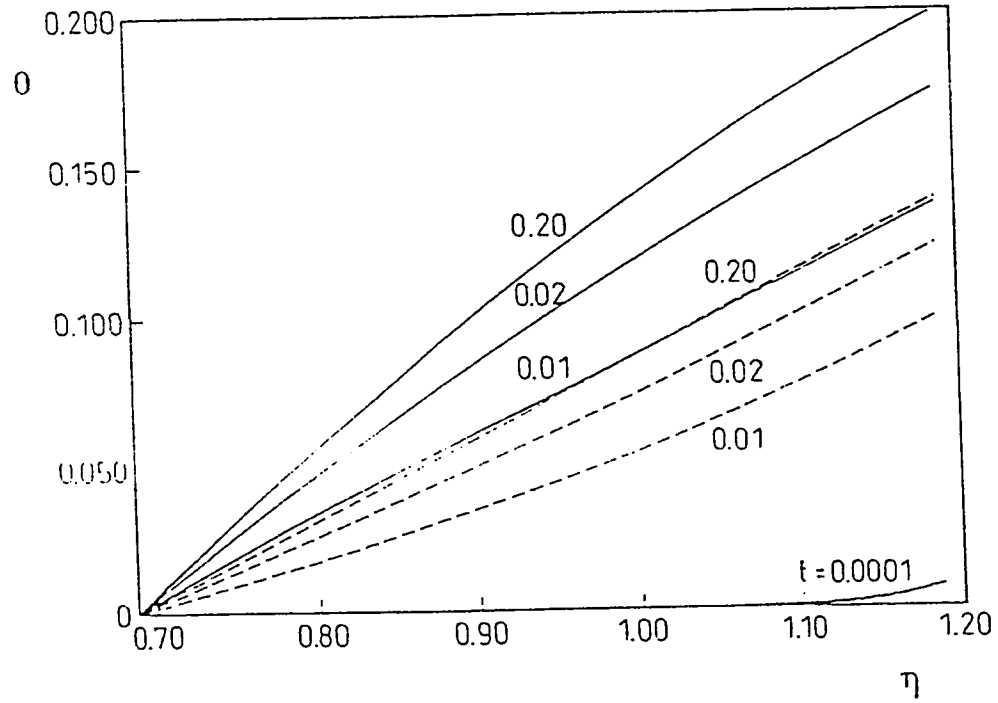


Fig. 5.21(b) : Temperature profiles at $\xi = \pi$ in case 4.1, N = 0.5, E = 0.7,

- - - - $Q = 0$, —— $Q = 5$.

one moves from the smallest value of $\eta$ to its largest value (at the inner wall). Similar to case 4.O, increasing the value of eccentricity causes a general increase in the values of the temperature on the wide side of the annulus. Also, within the investigated ranges of $Q$ and $E$, the effect of $E$ is more pronounced than the effect of $Q$ on the time required to reach the steady-state conditions ($t_s$).

Comparing Figs. 5.18(a) through 5.19(b) on one side with Figs. 5.20(a) through 5.21(b) on the other side reveals the following. The temperature levels attained in case 4.O are higher than those attained in case 4.I. This is because the heat transfer boundary in the former case has a larger area per unit length than that in the latter. Consequently, the heat added per unit length through the heat transfer boundary is more in case 4.O than in case 4.I. The comparison between the aforesaid figures indicates also that the steady-state conditions are generally achieved faster in case 4.I than in case 4.O.

## 5.6 Maximum Material Temperature and Steady-State Time

The detailed transient temperature profiles presented in the previous sections are useful in exploring the physics of the problem under consideration and understanding its pertinent mechanism of heat transfer. However, thermal, control, and materials engineers are not frequently concerned with such detailed temperature profiles but only with the maximum attainable annulus material temperature, the time history of this maximum temperature, and the time needed to reach the steady-state conditions ($t_s$). The maximum

attainable annulus material temperature in the two cases (4.I and 4.O) occurs on the heat transfer boundary when steady-state conditions are achieved.

For some selected values of the dimensionless eccentricity $E$ and two values of Q, Figs. 5.22(a) and 5.22(b) give the variation of this maximum steady-state temperature around half the periphery ($0 \leq \xi \geq \pi$) of the outer and inner heated surfaces of the annulus (i.e., on $\eta = \eta_o$ and $\eta_i$) in case 4.O and 4.I, respectively. The results presented in these two figures can be obtained by means of the analytical steady-state equation (4.4) or from the numerical solution at considerably large values of time, i.e., $t \geq t_s$. Each of these two figures clarifies also the effect of the eccentricity on the temperature distribution around the periphery of the heated wall. The larger the value of the eccentricity E, the more deviation of the heated-wall-temperature distribution from axisymmetry (i.e., the temperature becomes more dependent on the angular or azimuthal $\xi$-direction). Moreover, the larger the eccentricity the higher the maximum attainable heated-wall temperature on the wide side of the annulus ($\xi = 0$) and the lower the minimum attainable heated-wall temperature on its narrow side ($\xi = \pi$). Also, Figs. 5.22(a) and 5.22(b) show that the increase in the value of the heat ratio $Q$ makes the deviation from axisymmetry more pronounced. This is because as the value of $Q$ increases the heat generated per unit length on the wide side of the annulus becomes more than that generated on the narrow side due to the asymmetry distribution of the solid material.

Examples of the time history of the heated-wall-temperature distribution will be presented for cases 4.I and 4.O. For two values of $Q$, namely 0 and 5, Figs. 5.23(a) and 5.23(b) show such transient distribution around half the periphery of the inner surface for E

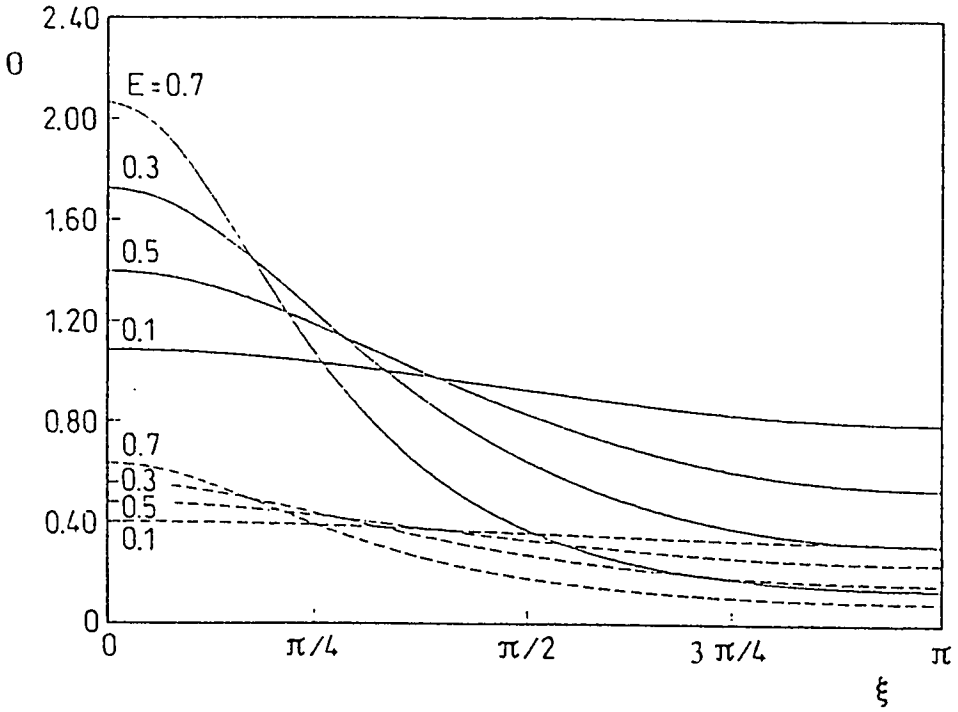


Fig. 5.22(a) : Steady-state temperature on the outer heated wall in case 4.O, N = 0.5,

- - - - $Q = 0$, —— $Q = 5$.

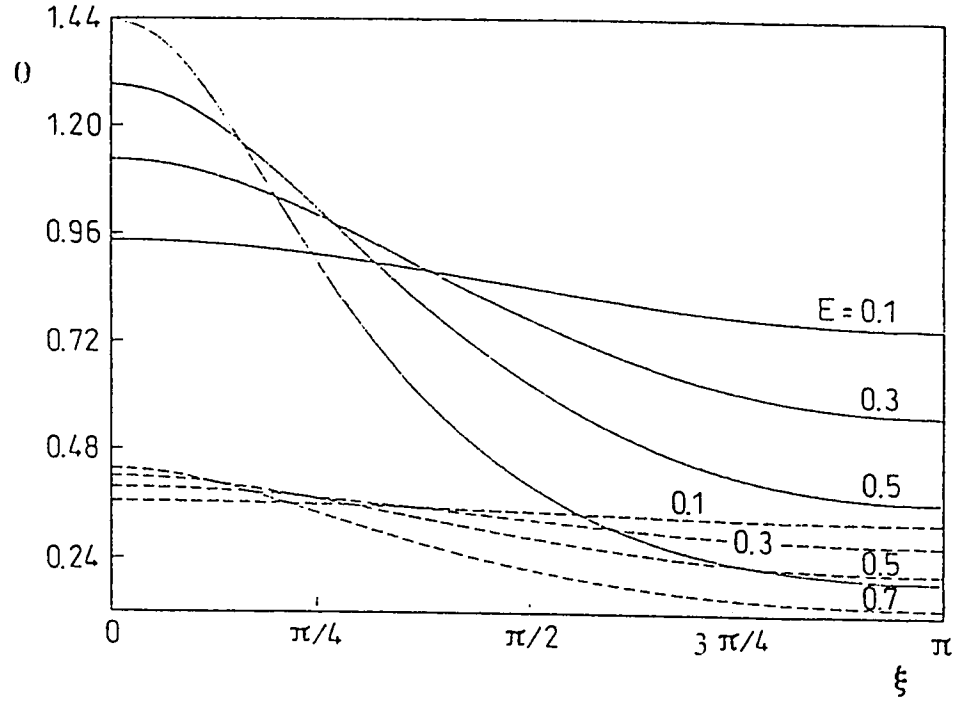


Fig. 5.22(b) : Steady-state temperature on the inner heated wall in case 4.I, N = 0.5,

- - - - $Q = 0$, —— $Q = 5$.

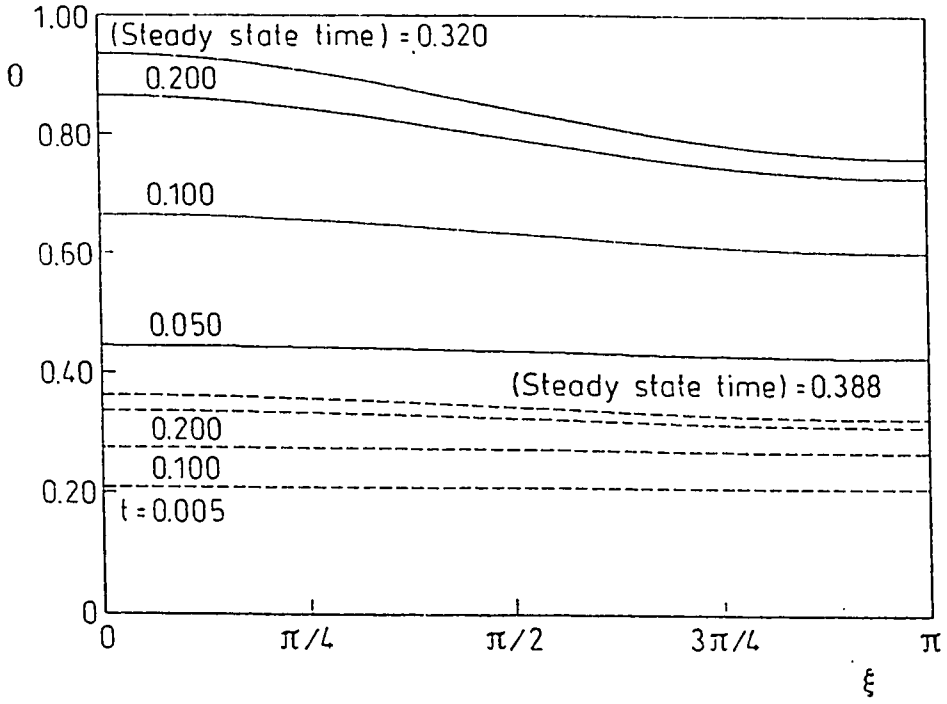


Fig. 5.23(a) : Transient temperature on the inner heated wall in case 4.I, N = 0.5,

E = 0.1, ---- $Q = 0$, —— $Q = 5$.

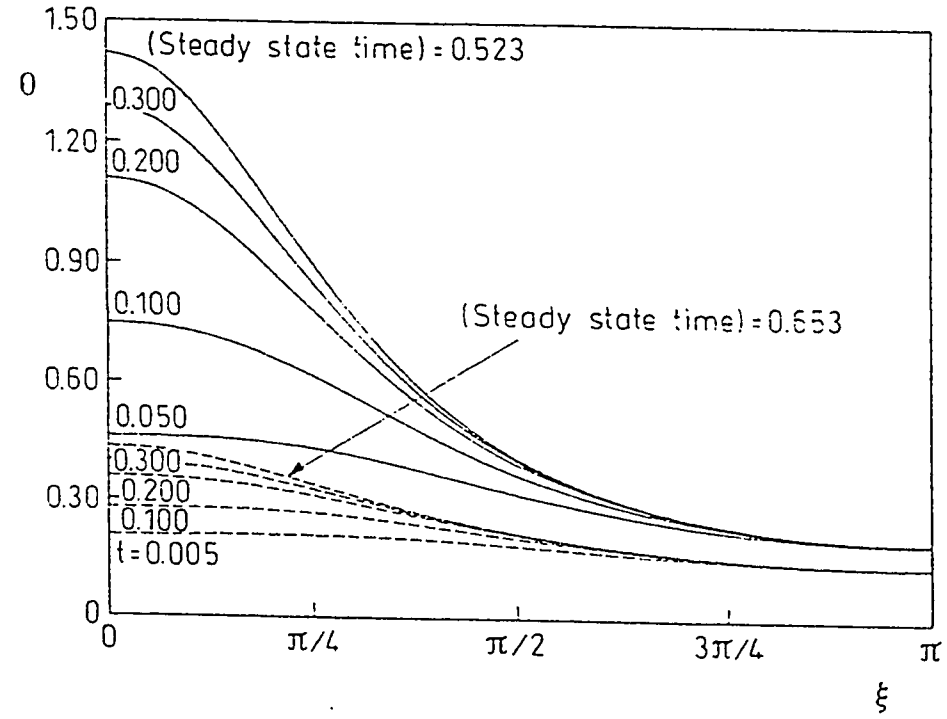


Fig. 5.23(b) : Transient temperature on the inner heated wall in case 4.I, N = 0.5,

E = 0.7, ---- $Q = 0$, —— $Q = 5$.

= 0.1 and 0.7, respectively. As can be seen from these two figures, at small values of the non-dimensional time $t$ (e.g., $t \leq 0.1$ in Fig.5.23(a) and $t \leq 0.005$ in Fig. 5.23(b)) the surface temperature is almost uniform, having a value near enough to the initial temperature (zero). As time elapses the heated-surface temperature at any $\xi$-location increases. As the value of eccentricity E increases the heated-surface temperature at $\xi = 0$ (the wide side) becomes much higher than its value at $\xi = \pi$. Again this is anticipated since the dependence of temperature on $\xi$ vanishes as E tends to zero. Figures 5.23(c) and 5.23 (d) present the corresponding results for case 4.O.

To best clarify the effect of the eccentricity E on $\xi$-variation of the heated-wall temperature with time, Figs. 5.24(a) and 5.24(b) give, for $Q = 0$ and $5$, respectively, this temperature in case 4.I versus the non-dimensional time $t$ at the two locations $\xi = 0$ and $\pi$ for various chosen values of the eccentricity E. The corresponding results for case 4.O are presented in Figs. 5.24(c) and 5.24(d). In other words these four figures show the variation of the maximum and minimum wall temperature with time. As can be seen from these two figures, the higher the value of the eccentricity E or the heat ratio $Q$, the larger the difference between the maximum and minimum wall temperatures (at $\xi = 0$ and $\pi$, respectively).

The parameter of special importance to thermal and control engineers is the time needed to reach the steady-state conditions ($t_s$). Due to such importance, the detailed results of this particular parameter are given in Figs. 5.25(a), 5.25(b), 5.25(c) and 5.25(d) for cases 1.I and 1.O, 3.I and 3.O, 4.O and 4.I, respectively. In this set of figures, the dimensionless steady-state time is drawn against the non-dimensional heat ratio (or heat

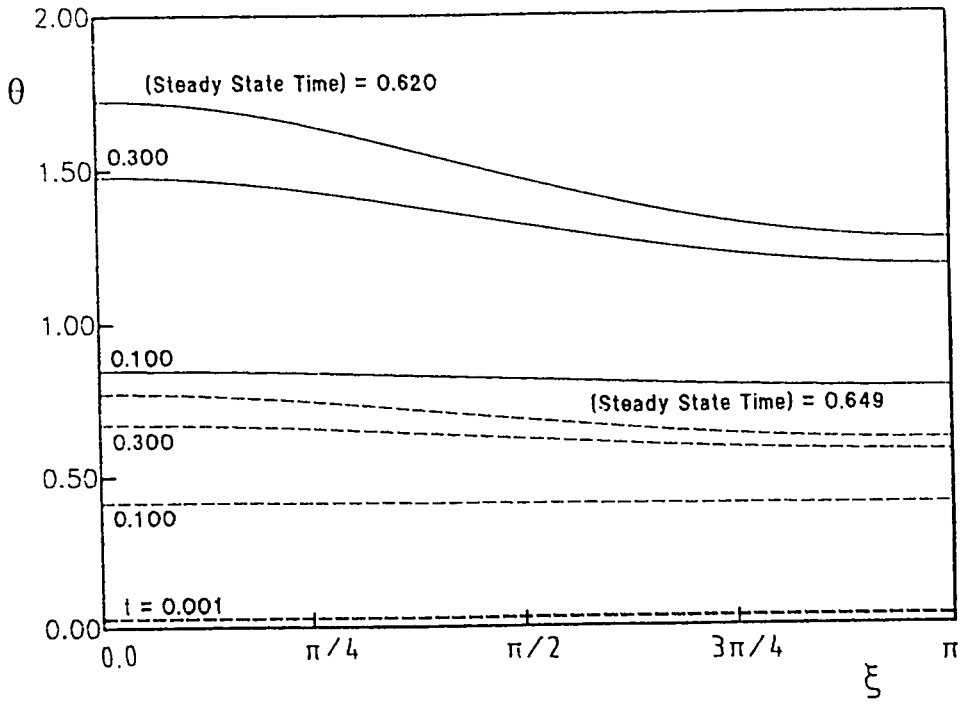


Fig. 5.23(c) : Transient temperature on the inner heated wall in case 4.O, N = 0.5, E = 0.1, - - - - $Q = 0$, —— $Q = 5$.

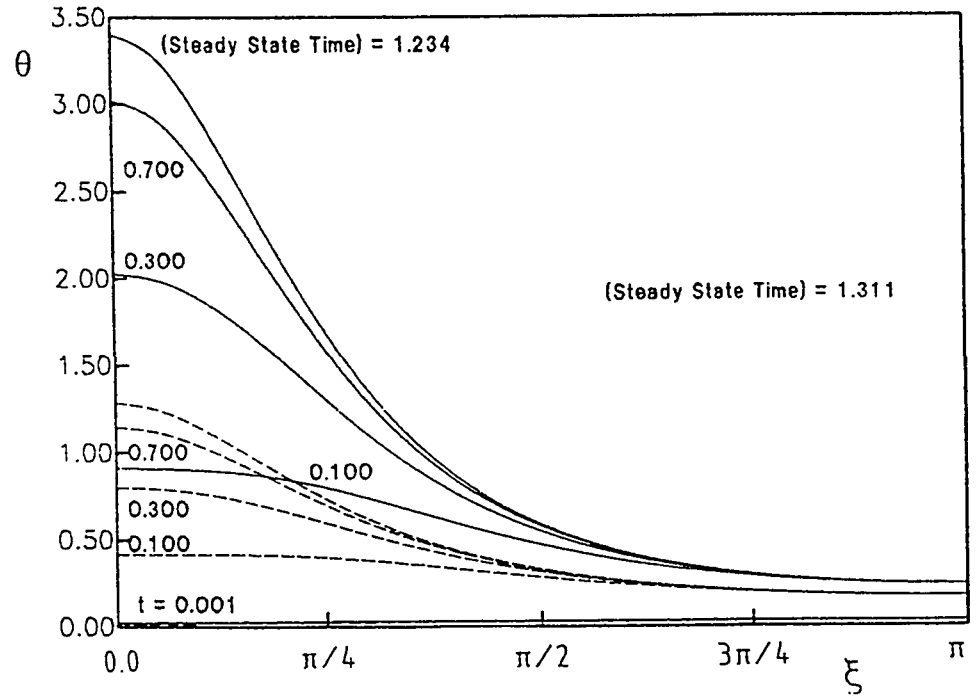


Fig. 5.23(d) : Transient temperature on the inner heated wall in case 4.O, N = 0.5, E = 0.7, - - - - $Q = 0$, —— $Q = 5$.

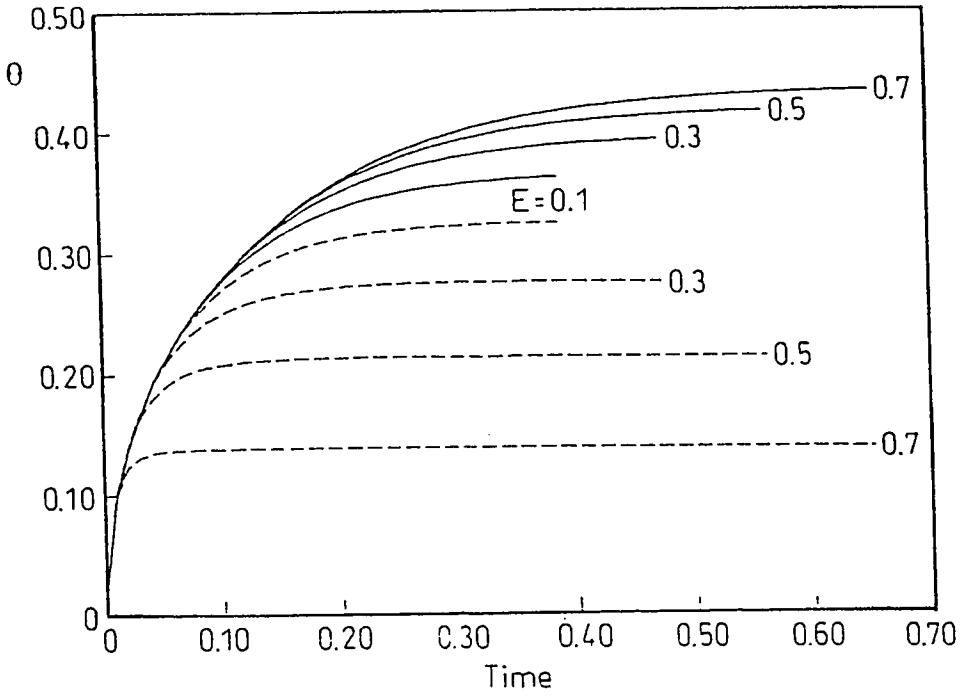


Fig. 5.24(a) : Inner wall transient temperature in case 4.I, N = 0.5,$Q$ = 0,

—— $\xi = 0.0$, – – – $\xi = \pi$.

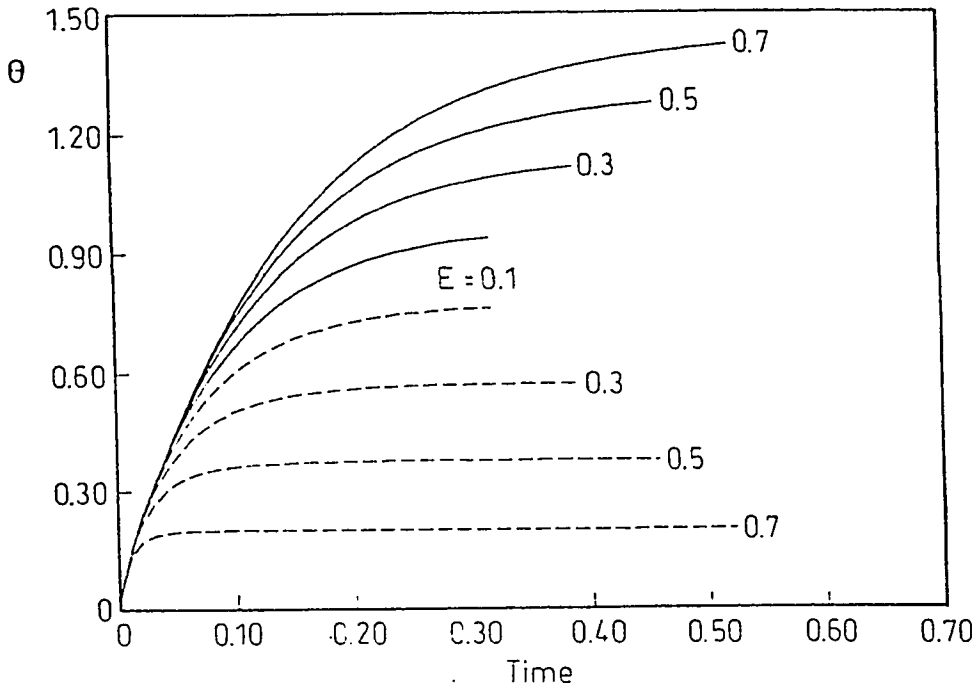


Fig. 5.24(b) : Inner wall transient temperature in case 4.I, N = 0.5,$Q$ = 5,

—— $\xi = 0.0$, – – – $\xi = \pi$.

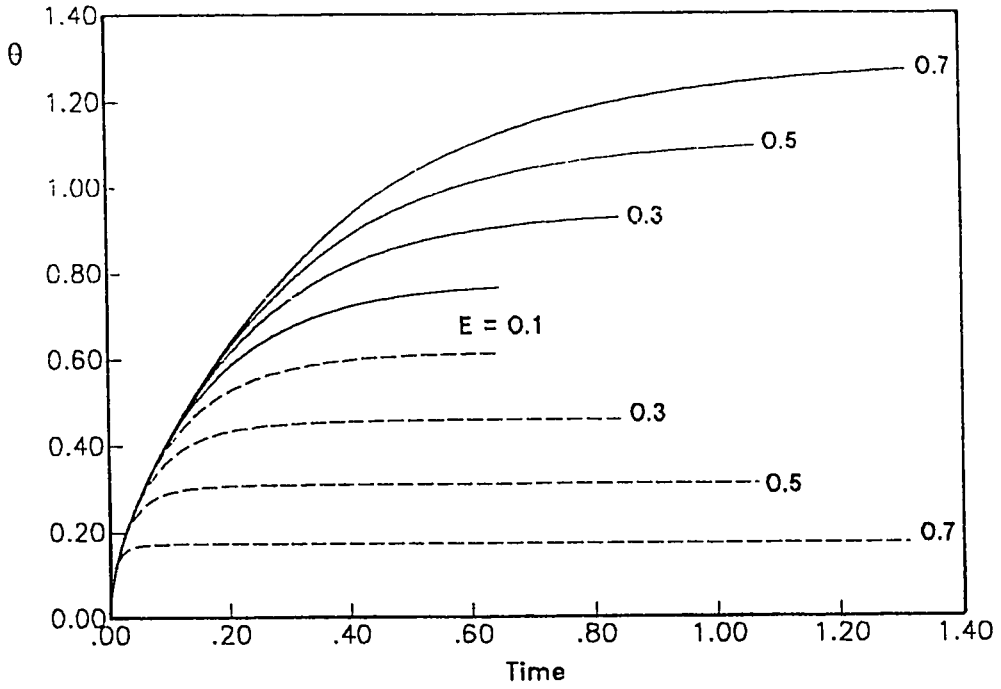


Fig. 5.24(c) : Inner wall transient temperature in case 4.O, N = 0.5,$Q$ = 0, —— $\xi$ = 0.0, – – – $\xi = \pi$.

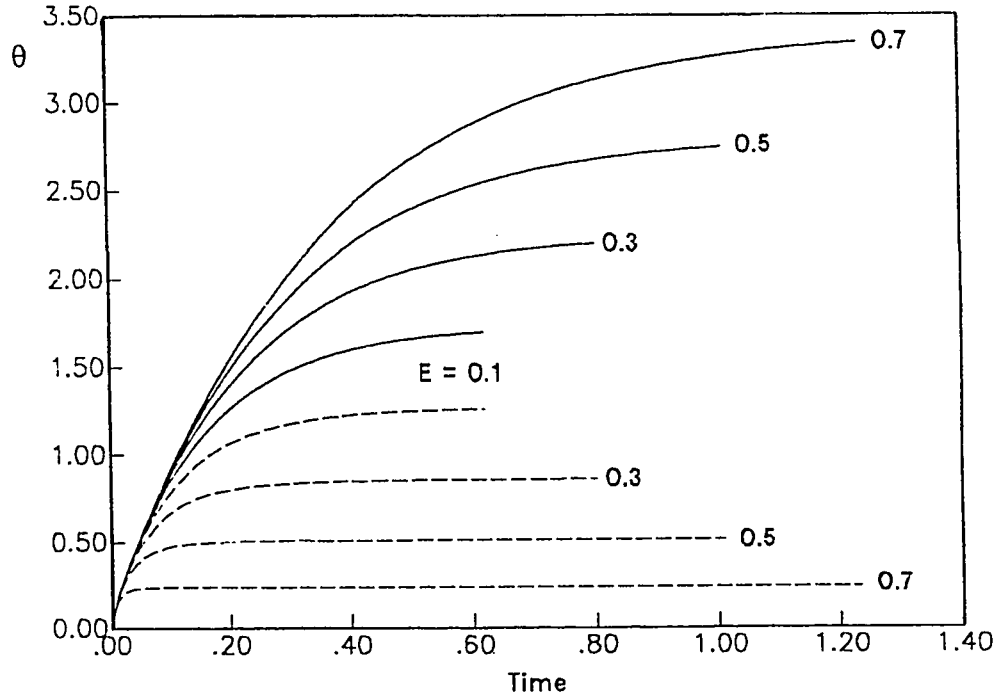


Fig. 5.24(d) : Inner wall transient temperature in case 4.O, N = 0.5,$Q$ = 5, —— $\xi$ = 0.0, – – – $\xi = \pi$.

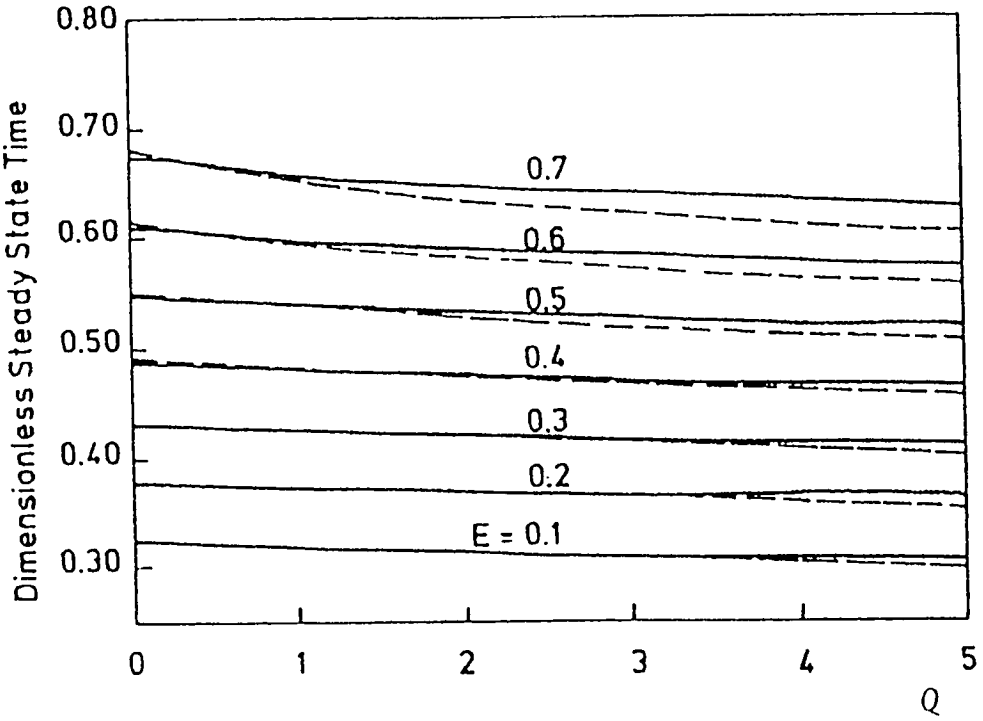


Fig. 5.25(a) : Steady-state time against heat generation for various eccentricities,$N$ = 0.5,

- - - - case 1.I, —— case 1.O.

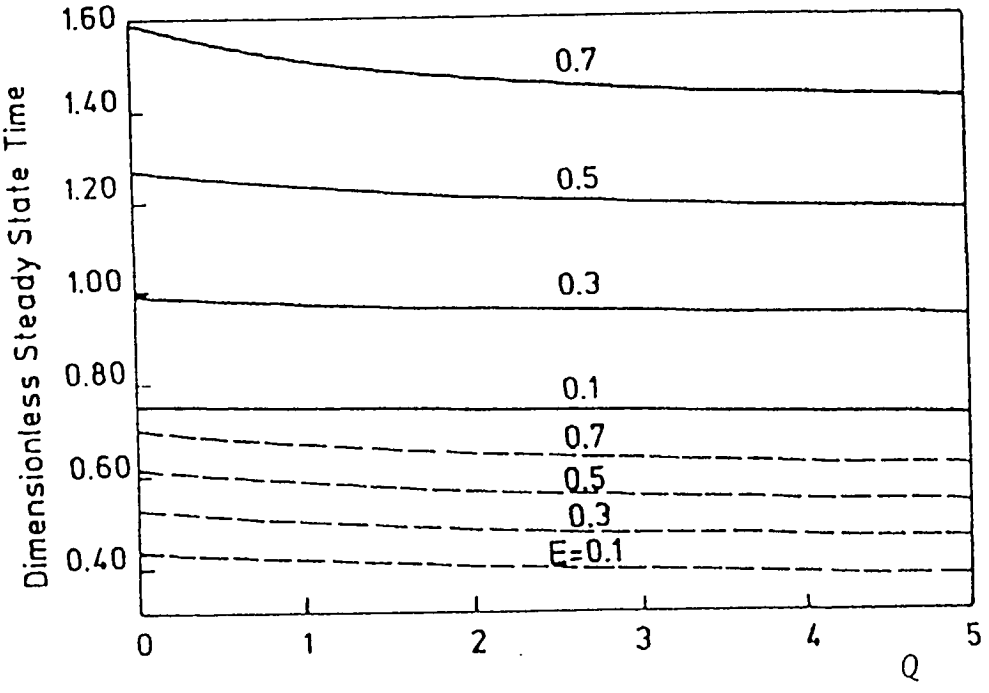


Fig. 5.25(b) : Steady-state time against heat generation for various eccentricities,$N$ = 0.5,

- - - - case 3.I, —— case 3.O.

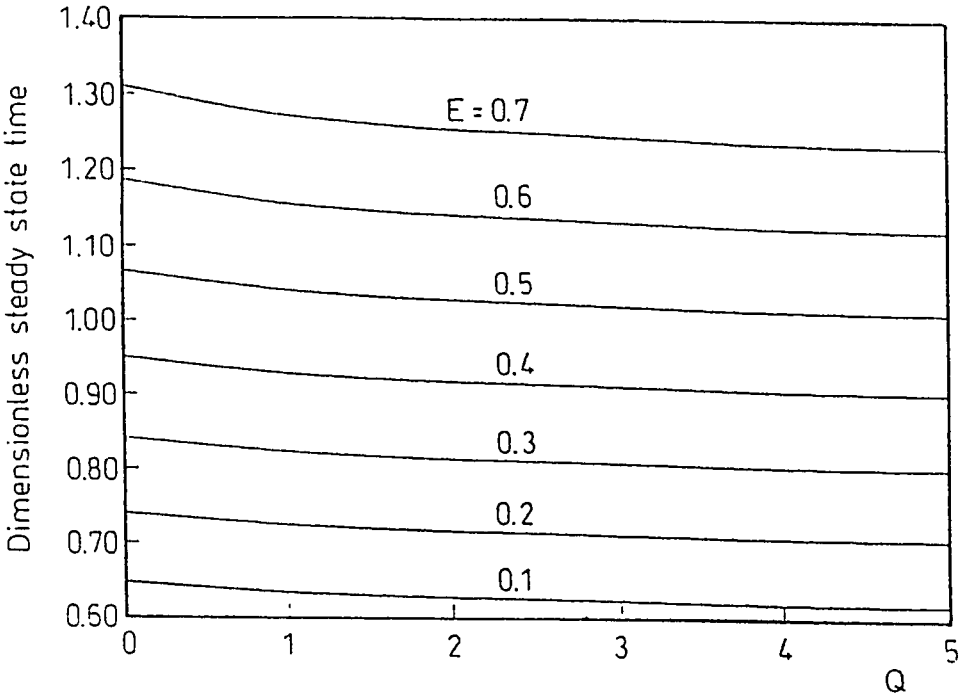


Fig. 5.25(c) : Variation of the Steady-state time with the heat ratio for various eccentricities, $N = 0.5$, case 4.O.

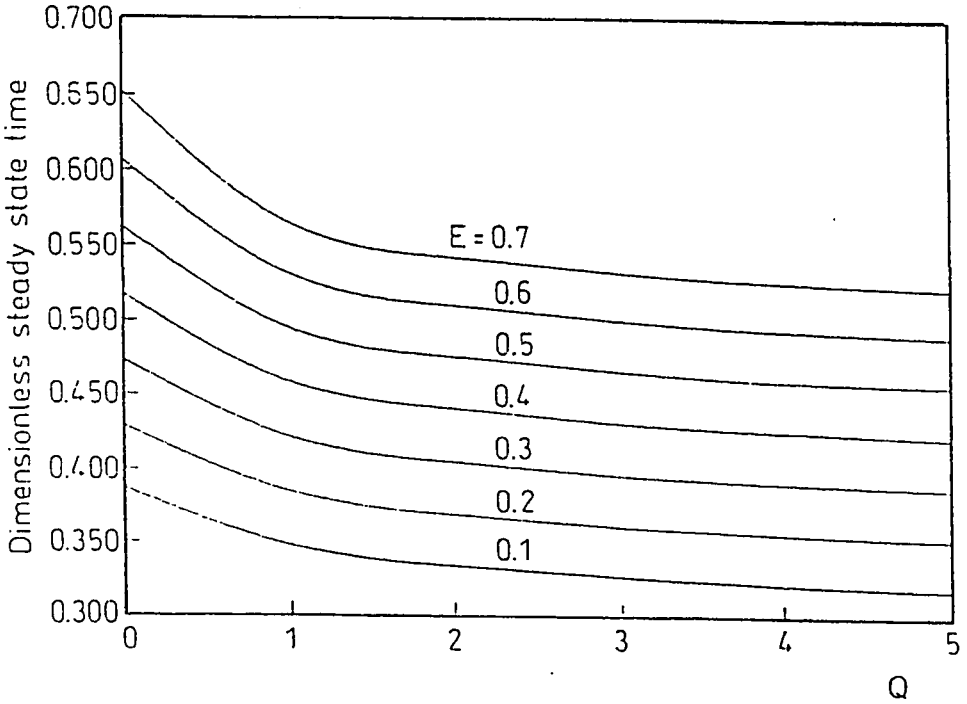


Fig. 5.25(d) : Variation of the Steady-state time with the heat ratio for various eccentricities, $N = 0.5$, case 4.I.

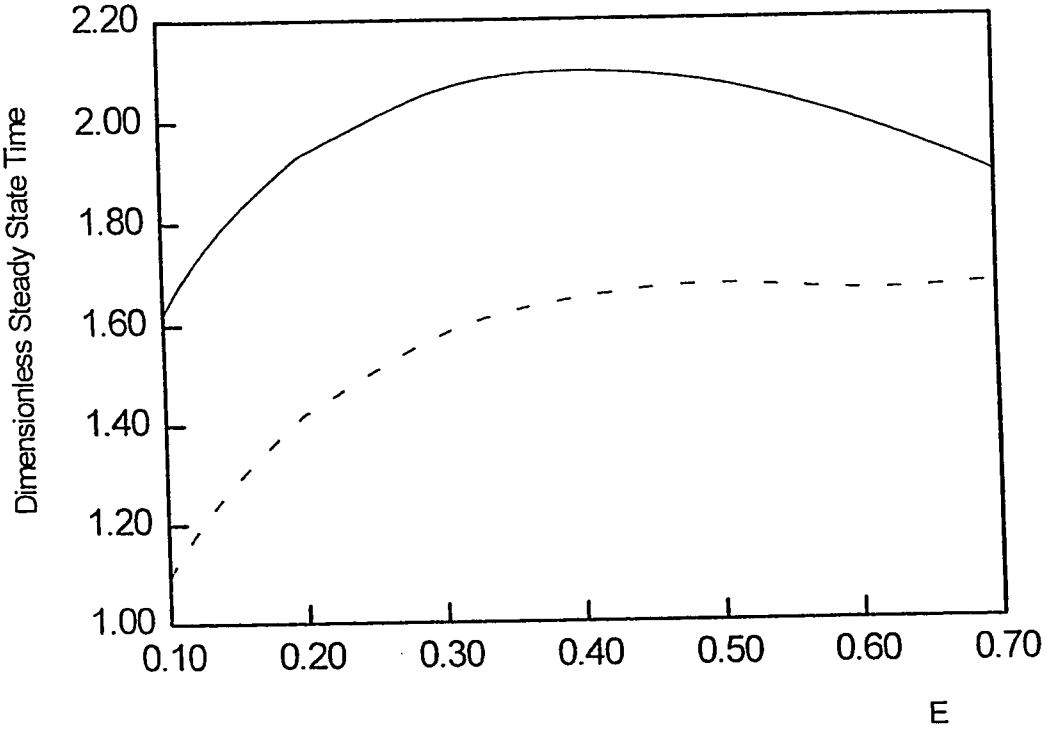


Fig. 5.25(e) : Variation of the Steady-state time with eccentricity, $N = 0.5$,

—— case 2.O , – – – case 2.I.

generation) $Q$ for various values of the eccentricity E. This set of figures shows that, within the investigated ranges of $Q$ and E, the eccentricity is the dominant factor on $t_s$. The higher the value of eccentricity the more time needed to reach steady-state conditions. For a given eccentricity (E), the effect of $Q$ on $t_s$ is more pronounced in case I then in case O. For given eccentricity (E) and heat ratio (heat generation) ($Q$), the time needed to reach steady-state conditions in case O is more than that needed in case I.

It is worth mentioning that the computer runs for any of the curves shown in these set of figures (i.e., a given $E$) were made using the same $\eta$and $\xi$ mesh sizes so that the order of numerical error magnitude would be the same for all values of $Q$.

Finally the results of $t_s$ for cases 2.I and 2.O is presented Fig. 5.25(e). The criterion to reach the stead-state conditions in these two particular cases was arbitrarily chosen as indicated before in section 4.2. Recalling that for all other cases which have been investigated (cases 1.I, 1.O, 3.I, 3.O, 4.I and 4.O) the constant $B$ of the analytical steady-state solution(eq. 4.4) is readily available prior the corresponding numerical solution is obtained from the transient problem at considerably large values of $t$. Thus, it was possible in these cases to compare the numerical solution obtained at considerably large values of $t$ (i.e., the steady-state solution obtained numerically) with the corresponding analytical steady-state solution (eq. 4.4).

# Chapter 6

# RESULTS AND DISCUSSION FOR FULLY-DEVELOPED LAMINAR FREE CONVECTION IN OPEN-ENDED ECCENTRIC VERTICAL ANNULI

## 6.1 Introduction

Fully developed free convection in open-ended vertical annuli is the limiting case of the more general problem of developing free convection in such channels. The in-depth literature survey reported in Chapter 2 has revealed that there is no previous work reported for the problem of fully-developed free convection in vertical open-ended

eccentric channels. In this chapter, a study has been carried out to analyze the fully developed free convection in a vertical eccentric annulus of N = 0.5 for three pairs of the fundamental thermal boundary conditions(first, third and fourth kinds). The governing equations and the boundary conditions of this problem have been derived and presented in Chapter 3. The method of solution for the three cases under consideration has been outlined in Chapter 4. In this study, we have utilized the available analytical solutions, [75,76], for the energy equation under the thermal conditions of the first, third and fourth kinds to solve the axial momentum equation which is coupled to the energy equation through the buoyancy term. An analytical solution for the energy equation under the thermal conditions of the second kind is not readily available and hence the fully developed free convection problem was not considered in this case. The validity of the proposed method of solution for the three pairs of thermal conditions has been checked using a simple energy balance. This simple energy balance sates that for fully developed flow in an annulus with one isothermal wall the heat crossing this wall should pass across the other wall. This makes the temperature of the fluid flowing through the annular space in case 3, in which we have one wall perfectly insulated, ultimately equal to the temperature of the isothermal wall; this greatly simplified the analysis as was indicated before (in Chapter 4). For the other cases, namely, case 1.I, 1.O, 4.I, and 4.O, the ratio of the average heat flux at the outer wall to that at the inner wall should equal always to the radius ratio N; this has been confirmed in all the cases studied.

During the present work, we have investigated the effect of eccentricity on the flow and heat transfer parameters, such as temperature and velocity distributions,

average velocity, induced flow rate, the mean bulk temperature, and the local and average Nusselt number. The definitions of the dimensionless heat transfer parameters and their pertinent equations will be presented hereinafter

### 6.1.1 Average Velocity

The dimensionless average velocity can be expressed as a function of the local dimensionless velocity as

$$\bar{U} = \frac{8}{\pi}\frac{1-N}{1+N}\int_{0}^{\pi}\int_{\eta_o}^{\eta_i} U H^2 \, d\eta \, d\xi \tag{6.1}$$

This integration has been evaluated numerically using the trapezoidal rule as

$$\bar{U} = \frac{8}{\pi}\frac{1-N}{1+N}\left(\begin{array}{l}\sum_{j=2}^{m}\sum_{i=2}^{n} U(i,j)(H(i,j))^2 \\ +0.5\sum_{i=2}^{n}\left(U(i,1)(H(i,1))^2 + U(i,m+1)(H(i,m+1))^2\right)\end{array}\right)\Delta\eta\,\Delta\xi \tag{6.2}$$

### 6.1.2 Average Flow Rate

The induced flow rate due to the heating of one of the annulus boundaries can be calculated from the following dimensional equation

$f = 2\int_{0}^{\pi}\int_{\eta_o}^{\eta_i} u h^2 \, d\eta \, d\xi$ and in dimensionless form it can be written as;

$$F = (1-N^2)\bar{U} \quad \text{and for } N = 0.5,\ F = \frac{3}{4}\bar{U} \tag{6.3}$$

### 6.1.3 Average Temperature ( Mixing-Cup Temperature )

$$T_m = \frac{\int_A T u \, dA}{f} = \frac{\iint_{XY} T u \, dx \, dy}{f} \tag{6.4}$$

Using the dimensionless temperature and substituting for T one can write

$$\theta_m = \frac{8}{\pi}\frac{1-N}{1+N}\frac{\int_0^{\pi}\int_{\eta_o}^{\eta_i}\theta U H^2 d\eta d\xi}{\bar{U}} \tag{6.5}$$

This integration has been evaluated numerically using the trapezoidal rule as follows;

$$\theta_m = \frac{8}{\pi}\frac{(1-N)}{(1+N)\bar{U}}\left(\begin{array}{l}\sum_{j=2}^{m}\sum_{i=2}^{n}\theta(i,j)U(i,j)(H(i,j))^2 \\ +0.5\sum_{i=2}^{n}\left(\begin{array}{l}\theta(i,1)U(i,1)(H(i,1))^2 \\ +\theta(i,m+1)U(i,m+1)(H(i,m+1))^2\end{array}\right)\end{array}\right)\Delta\eta\,\Delta\xi \tag{6.6}$$

## 6.1.4 Local Nusselt Number

The local Nusselt number has been calculated based on the local dimensionless heat flux on the boundaries and the final derived formulae are tabulated below

**Table 6.1 Local Nusselt number on the inner and outer walls for case 1 and 4**

| Case | Inner Wall | Outer Wall |
|---|---|---|
| 1.I | $Nu_i^{1.I} = \frac{1}{1-\theta_m}\left(\frac{1}{H}\frac{\partial\theta}{\partial\eta}\right)\Big\|_{\eta_i}$ | $Nu_o^{1.I} = \frac{1}{\theta_m}\left(\frac{1}{H}\frac{\partial\theta}{\partial\eta}\right)\Big\|_{\eta_o}$ |
| 1.O | $Nu_i^{1.O} = -\frac{1}{\theta_m}\left(\frac{1}{H}\frac{\partial\theta}{\partial\eta}\right)\Big\|_{\eta_i}$ | $Nu_o^{1.O} = -\frac{1}{1-\theta_m}\left(\frac{1}{H}\frac{\partial\theta}{\partial\eta}\right)\Big\|_{\eta_o}$ |
| 4.I | $Nu_i^{4.I} = \frac{1}{\theta_{iw}-\theta_m}$ | $Nu_o^{4.I} = \frac{1}{\theta_m}\left(\frac{1}{H}\frac{\partial\theta}{\partial\eta}\right)\Big\|_{\eta_o}$ |
| 4.O | $Nu_i^{4.O} = -\frac{1}{\theta_m}\left(\frac{1}{H}\frac{\partial\theta}{\partial\eta}\right)\Big\|_{\eta_i}$ | $Nu_o^{4.O} = \frac{1}{\theta_{ow}-\theta_m}$ |

(6.7)

## 6.1.5 Average Nusselt Number

An analytical expression has been obtained for the circumferentially-averaged Nusselt number and the results are tabulated below (the method of obtaining these expressions will be detailed for each case under study)

**Table 6.2 Circumferentially averaged Nusselt number on the inner and outer walls for cases 1 and 4**

| Case | Inner Wall | Outer Wall |
|---|---|---|
| 1.I | $\overline{Nu_i^{1.I}} = \dfrac{2(1-N)}{N(1-\theta_m)(\eta_i-\eta_o)}$ | $\overline{Nu_o^{1.I}} = \dfrac{2(1-N)}{\theta_m(\eta_i-\eta_o)}$ |
| 1.O | $\overline{Nu_i^{1.O}} = \dfrac{2(1-N)}{N\theta_m(\eta_i-\eta_o)}$ | $\overline{Nu_o^{1.O}} = \dfrac{2(1-N)}{(1-\theta_m)(\eta_i-\eta_o)}$ |
| 4.I | $\overline{Nu_i^{4.I}} = \dfrac{1}{\overline{(\theta_{iw})}_c-\theta_m}$ | $\overline{Nu_o^{4.I}} = \dfrac{N}{\theta_m}$ |
| 4.O | $\overline{Nu_i^{4.O}} = \dfrac{1}{N\theta_m}$ | $\overline{Nu_o^{4.O}} = \dfrac{1}{\overline{(\theta_{ow})}_c-\theta_m}$ |

(6.8)

All the values of the circumferentially- averaged Nusselt number can be calculated by numerically integrating the local Nusselt Number using the following formulas.

**1 - On the inner wall**

$$\overline{Nu_y^{x.I}} = \frac{2(1-N)}{N\pi}\int_0^{\pi} (Nu_y^{x.I})H(\eta_i,\xi)d\xi \tag{6.9}$$

**2 - On the outer wall**

$$\overline{Nu_y^{x.O}} = \frac{2(1-N)}{\pi}\int_0^{\pi} (Nu_y^{x.O})H(\eta_i,\xi)d\xi \tag{6.10}$$

where $x$ may be 1 or 4 (denoting the case under consideration) and $y$ may be $i$ or $o$ denoting the wall on which the Nusselt number is to be calculated.

## 6.2 Fundamental Solution of the First Kind

In this case, the two boundaries of the annulus are kept isothermal, one of which is at the inlet ambient fluid temperature, $T_o$, while the opposite boundary is at a higher or a lower temperature, $T_w$. Equation (3.29) subject to the boundary conditions (3.17) and (3.19) (for cases 1.I and 1.O) has the following closed-form solution (El-Saden [5] ).

$$\frac{\theta-\theta_o}{\theta_i-\theta_o}=\frac{\eta-\eta_o}{\eta_i-\eta_o} \tag{6.14}$$

Using the above linear relationship between $\theta$ and $\eta$ the differentiation of the temperature with respect to $\eta$, $\partial\theta/\partial\eta = (\theta_i - \theta_o) / (\eta_i - \eta_o)$, can now be used to obtain the following closed-form equations for the local Nusselt number which varies circumferentially on the inner and outer walls of the annulus.

$$Nu_i^{1.I} = \frac{1}{(1-\theta_m)(\eta_i-\eta_o)H_i} \tag{6.15}$$

$$Nu_o^{1.I} = \frac{1}{\theta_m(\eta_i-\eta_o)H_o} \tag{6.16}$$

$$Nu_i^{1.O} = \frac{1}{\theta_m(\eta_i-\eta_o)H_i} \tag{6.17}$$

$$Nu_o^{1.O} = \frac{1}{(1-\theta_m)(\eta_i-\eta_o)H_o} \tag{6.18}$$

Closed-form expressions for the circumferentially averaged Nusselt number on the inner and outer walls of the annulus (tabulated before) can be obtained by integrating the above expressions around either wall from $\xi = 0$ to $\xi = \pi$ and then divide by the pertinent arc length, i.e.,

$$\overline{Nu_i^{1.I}} = \frac{1}{\pi r_i}\int_0^{\pi} h_i\, Nu_i^{1.I}\, d\xi = \frac{2(1-N)}{N\pi}\int_0^{\pi} H_i\, Nu_i^{1.I}\, d\xi = \frac{2(1-N)}{N(1-\theta_m)(\eta_i-\eta_o)} \tag{6.19}$$

$$\overline{Nu_o^{1.I}} = \frac{1}{\pi r_o}\int_0^{\pi} h_o\, Nu_o^{1.I}\, d\xi = \frac{2(1-N)}{\pi}\int_0^{\pi} H_o\, Nu_o^{1.I}\, d\xi = \frac{2(1-N)}{\theta_m(\eta_i-\eta_o)} \tag{6.20}$$

$$\overline{Nu_i^{1.O}} = \frac{1}{\pi r_i}\int_0^{\pi} h_i\, Nu_i^{1.O}\, d\xi = \frac{2(1-N)}{N\pi}\int_0^{\pi} H_i\, Nu_i^{1.O}\, d\xi = \frac{2(1-N)}{N\theta_m(\eta_i-\eta_o)} \tag{6.21}$$

$$\overline{Nu_o^{1.O}} = \frac{1}{\pi r_o}\int_0^{\pi} h_o\, Nu_o^{1.O}\, d\xi = \frac{2(1-N)}{\pi}\int_0^{\pi} H_o\, Nu_o^{1.O}\, d\xi = \frac{2(1-N)}{(1-\theta_m)(\eta_i-\eta_o)} \tag{6.22}$$

Moreover, eq. (6.14) can also be used to find values of $\theta\,(i,j)$ needed on the right hand side of eq. (4.18) to facilitate the numerical solution for the fully-developed velocity profiles $U$ and then $\bar{U}$, $F$ and $\theta_m$.

All results to be presented in this chapter are for a fluid of Pr = 0.7 in an annulus of N = 0.5. However, for the thermal boundary conditions of the third kind results showing the effect of the annulus radius ratio on the induced flow rate will also be given. The radius ratio 0.5 was chosen since it represents a typical annular geometry with a value of N far enough from unity (N = 1) which represents the case of parallel plate channels. Only a representative sample of the obtained results will be presented here. Figures 6.1(a) and 6.1(b) show the temperature profiles in the widest and narrowest sides of the annulus for different values of the eccentricity E for cases 1.I and 1.O, respectively.

For relatively small, moderate, and large eccentricities (E = 0.1, 0.5 and 0.9), Figs. 6.2(a), 6.2 (b-c) and 6.2 (d-f) respectively show, for case 1.I, examples of the computed fully-developed velocity profiles as one rotates around the annulus from its widest gap side ( $\psi = \xi/\pi = 0$ ) to its narrowest gap side ( $\psi = 1$, i.e., $\xi = \pi$ ). The corresponding set of results for case 1.O are shown in Figs. 6.3(a), 6.3(b-c) and 6.3(d-f), respectively. To have a complete insight into the effect of eccentricity on the fully-developed velocity profiles ( U ) in the annular gap, Figs. 6.4(a) and 6.4(b) present, for cases 1.I and 1.O respectively, the velocity profiles in the widest and narrowest sides of the annular gap (i.e. at the line of symmetry) for various values of the eccentricity E. The point of $x/r_o = 0.0$ on the abscissa of these figures represents the axis of the outer wall while points having zero values of U correspond to the inner and outer walls of the annulus. As can be seen from these figures, increasing the value of the eccentricity ( E ) makes the fully-developed velocity profiles deviate more and more from the axial symmetric profile which exists in the case of a concentric annulus. In other words, the eccentricity creates a circumferential variation in the axial velocity profiles; such a circumferential variation increases with the value of E. To clarify this circumferential variation in detail for case 1.I, Figs. 6.5(a) and 6.5(b) give the variation of U with $\xi$ for some selected values of the normalized $\eta$-coordinate ( $\phi$ ) in a slight eccentric annulus having E = 0.1. The corresponding results for E = 0.5 are shown in Figs. 6.5(c-d).

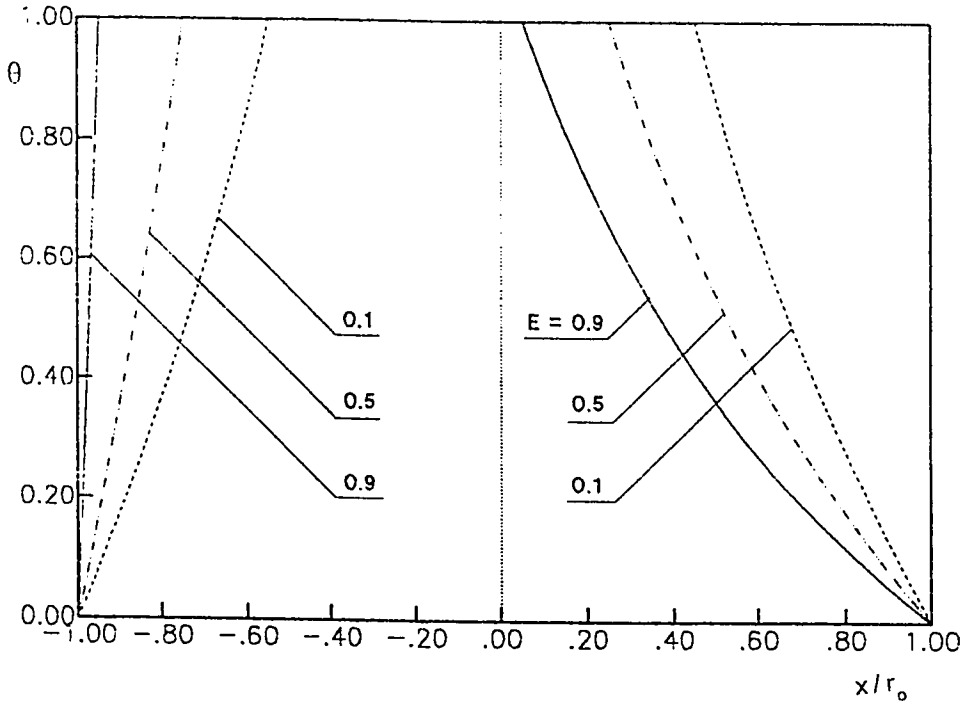


Fig. 6.1(a) : Fully-developed temperature profiles in the widest and narrowest sides of the gap in case 1.1.

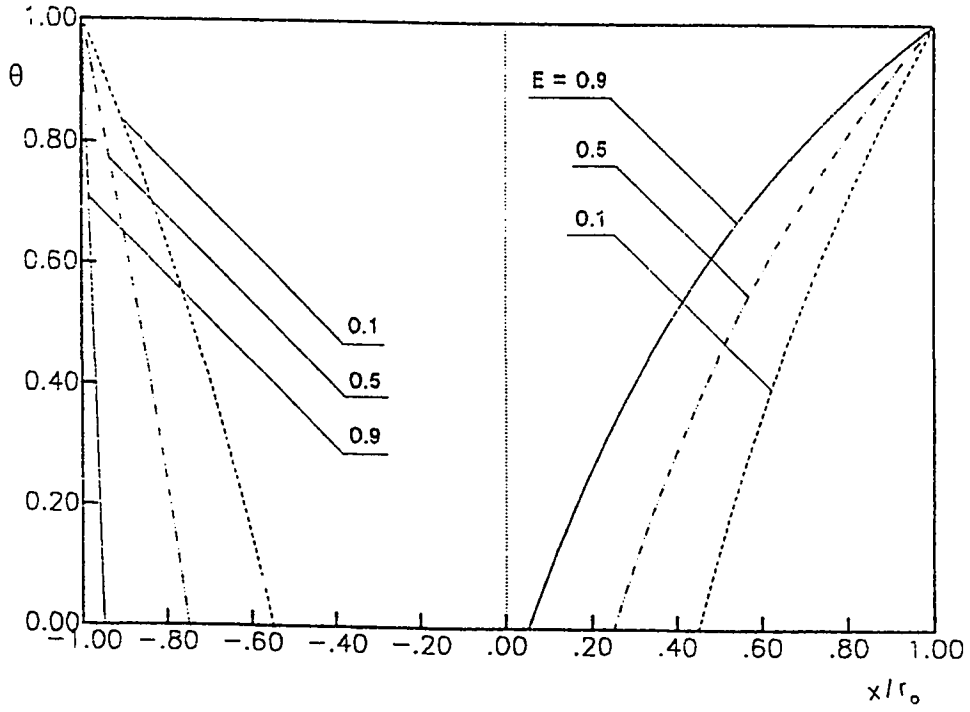


Fig. 6.1(b) : Fully-developed temperature profiles in the widest and narrowest sides of the gap in case 1.O.

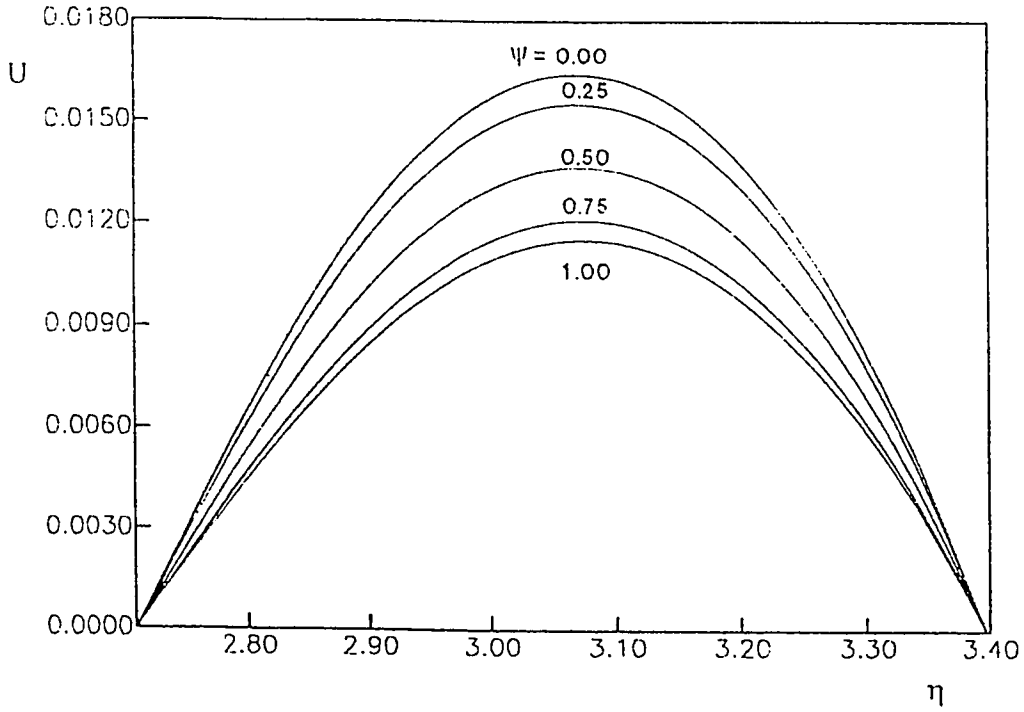


Fig. 6.2(a) : Variation of the fully developed axial velocity, U with η at different values of ψ ranges between 0.0 to 1.0, Case I.I., E = 0.1

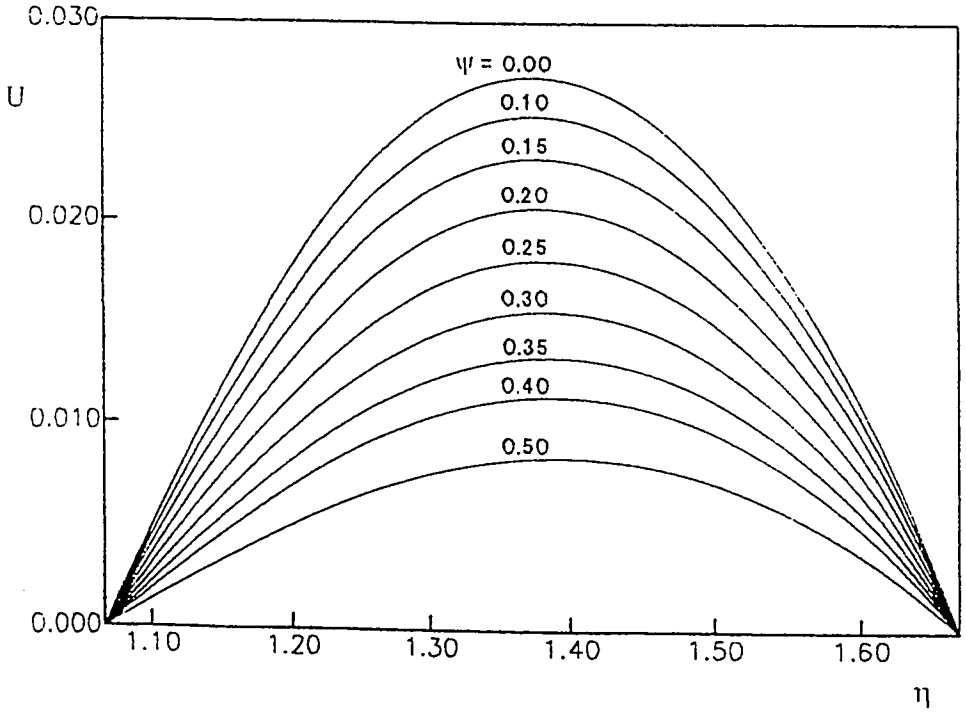


Fig. 6.2(b) : Variation of the fully developed axial velocity, U with η at different values of ψ ranges between 0.0 to 0.5, Case I.I., E = 0.5

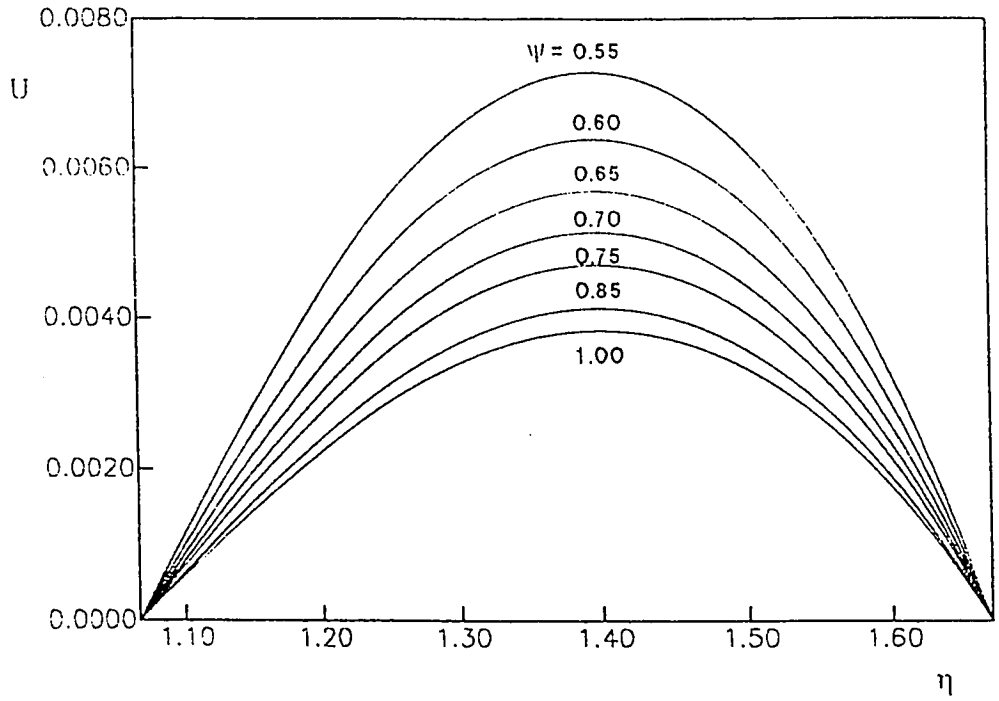


Fig. 6.2(c) : Variation of the fully developed axial velocity, U with η at different values of ψ ranges between 0.55 to 1.0, Case I.I., E = 0.5

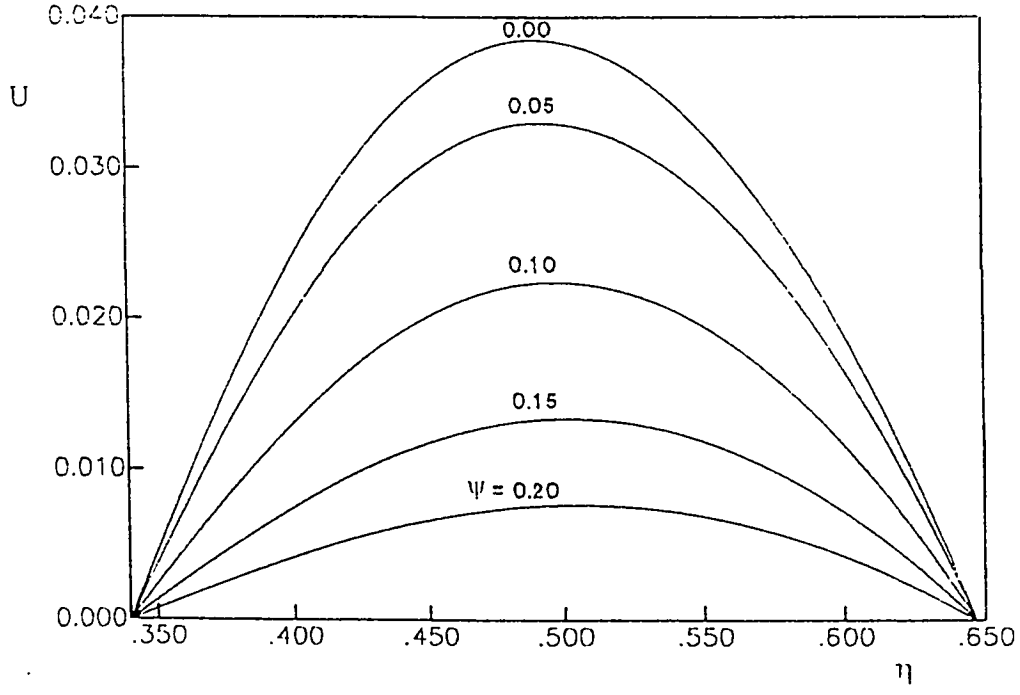


Fig. 6.2(d) : Variation of the fully developed axial velocity, U with η at different values of ψ ranges between 0.0 to 0.2, Case I.I., E = 0.9

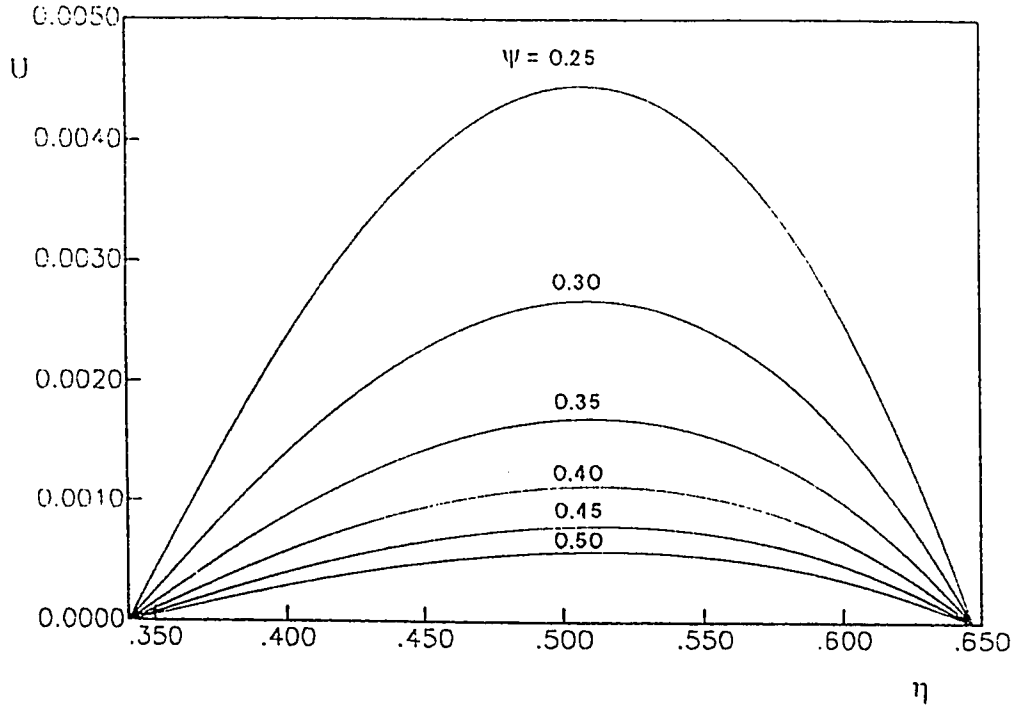


Fig. 6.2(e) : Variation of the fully developed axial velocity, U with η at different values of ψ ranges between 0.25 to 0.5, Case I.I., E = 0.9

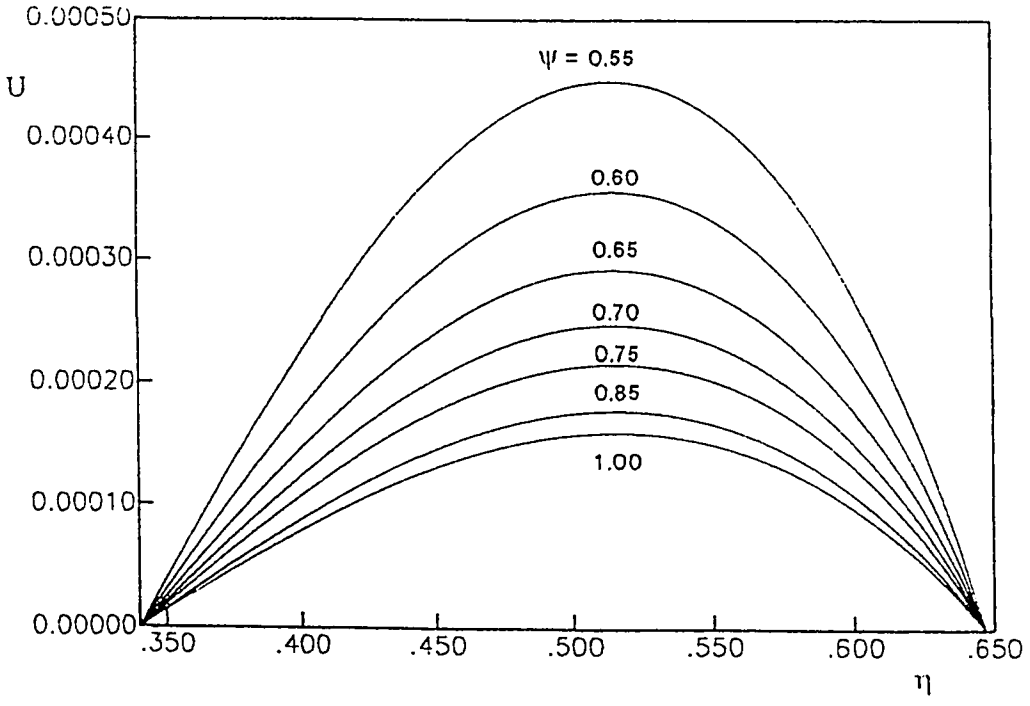


Fig. 6.2(f) : Variation of the fully developed axial velocity, U with η at different values of ψ ranges between 0.55 to 1.0, Case I.I., E = 0.9

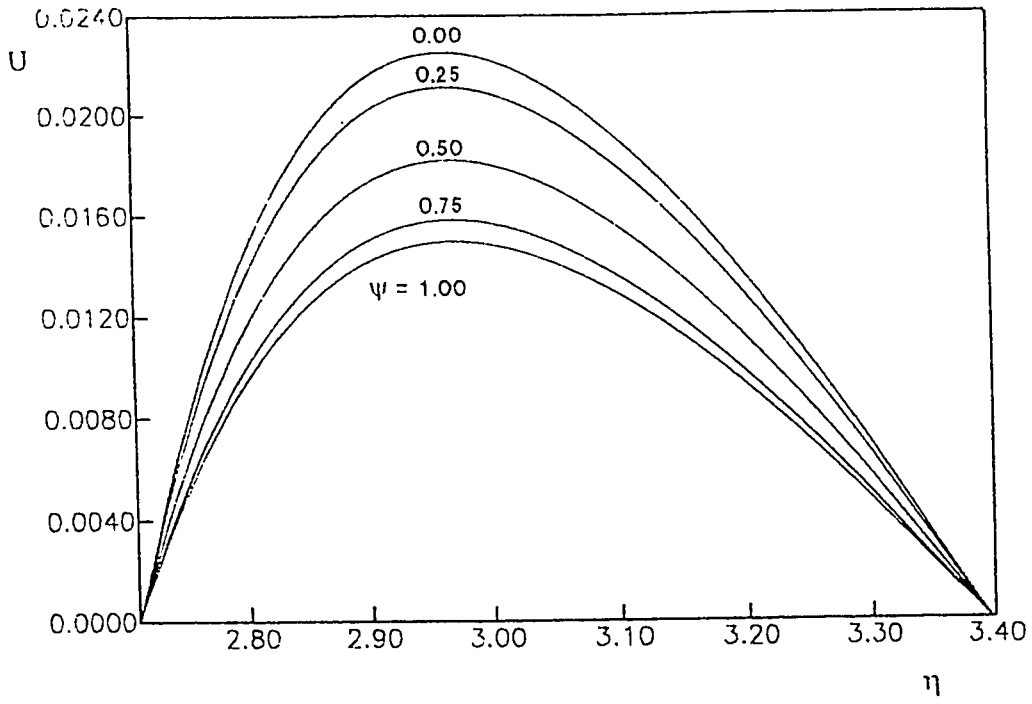


Fig. 6.3(a) : Variation of the fully developed axial velocity, U with η at different values of ψ ranges between 0.0 to 1.0, Case 1.O., E = 0.1

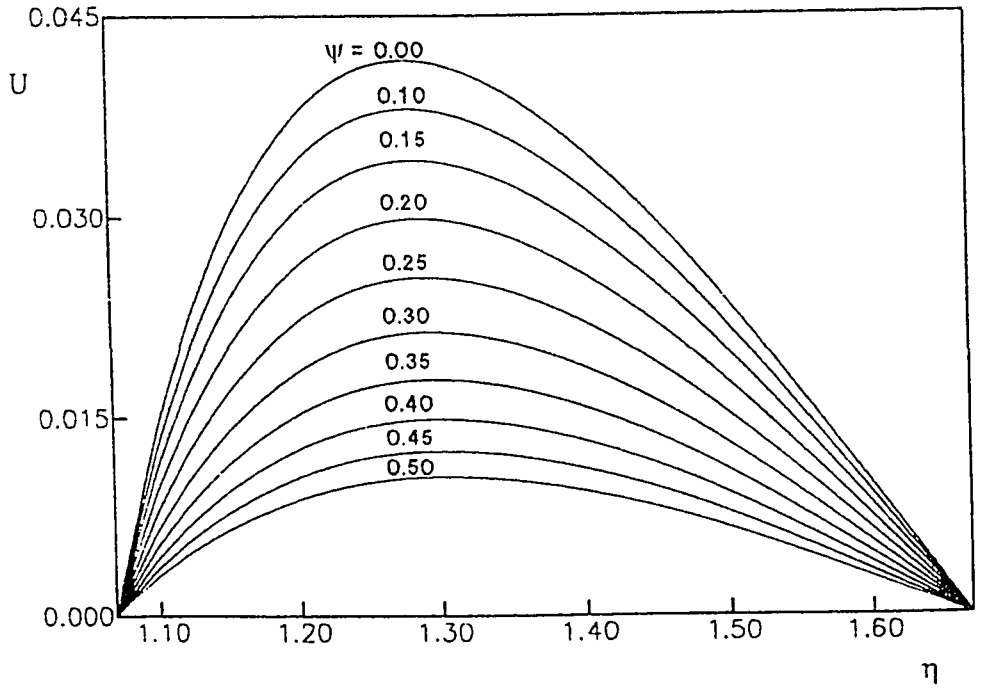


Fig. 6.3(b) : Variation of the fully developed axial velocity, U with η at different values of ψ ranges between 0.0 to 0.5, Case 1.O., E = 0.5

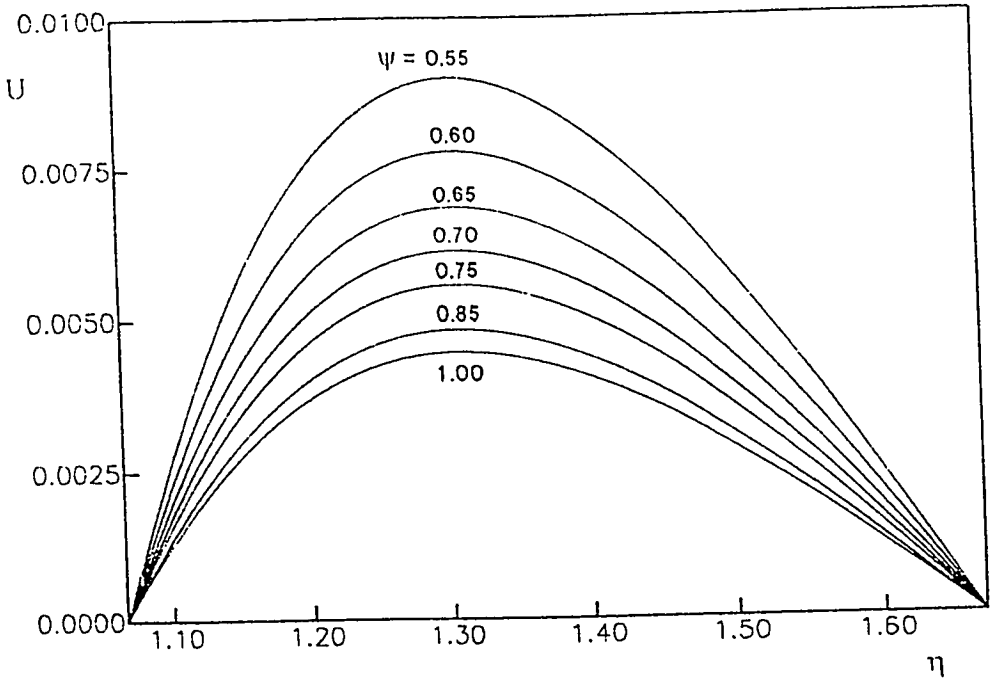


Fig. 6.3(c) : Variation of the fully developed axial velocity, U with η at different values of ψ ranges between 0.55 to 1.0, Case I.O., E = 0.5

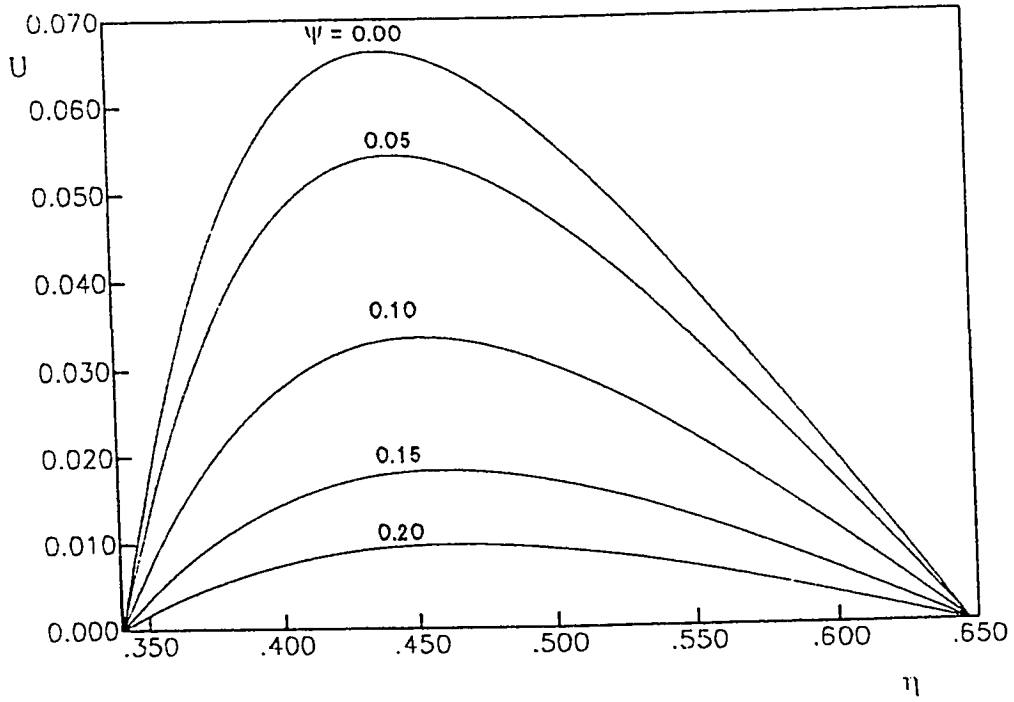


Fig. 6.3(d) : Variation of the fully developed axial velocity, U with η at different values of ψ ranges between 0.0 to 0.2, Case I.O., E = 0.9

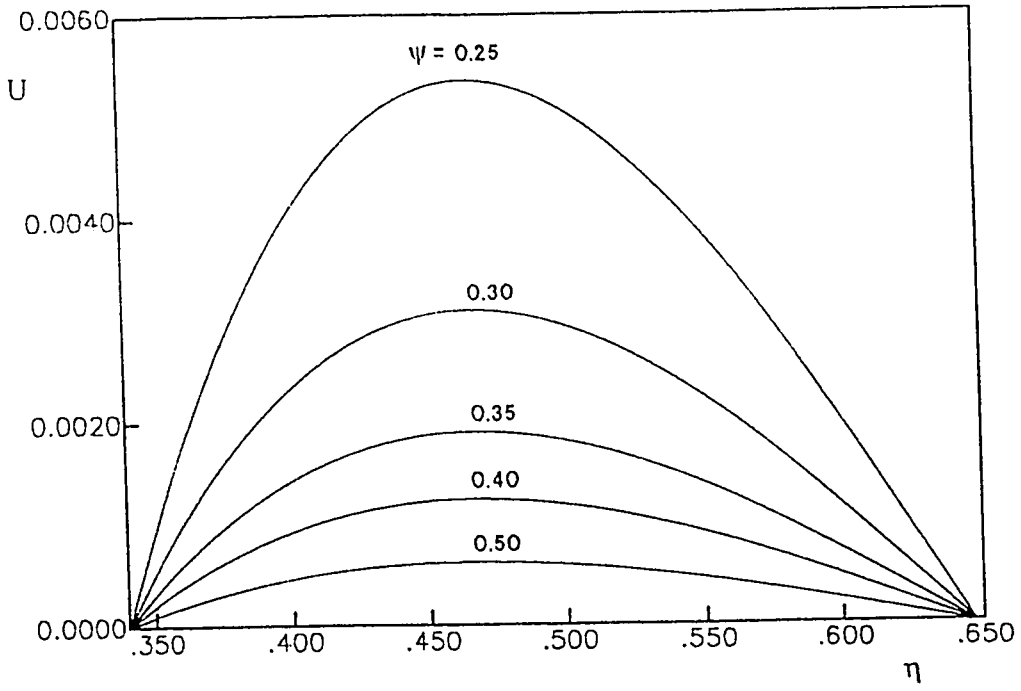


Fig. 6.3(e) : Variation of the fully developed axial velocity, U with η at different values of ψ ranges between 0.25 to 0.5, Case 1.O., E = 0.9

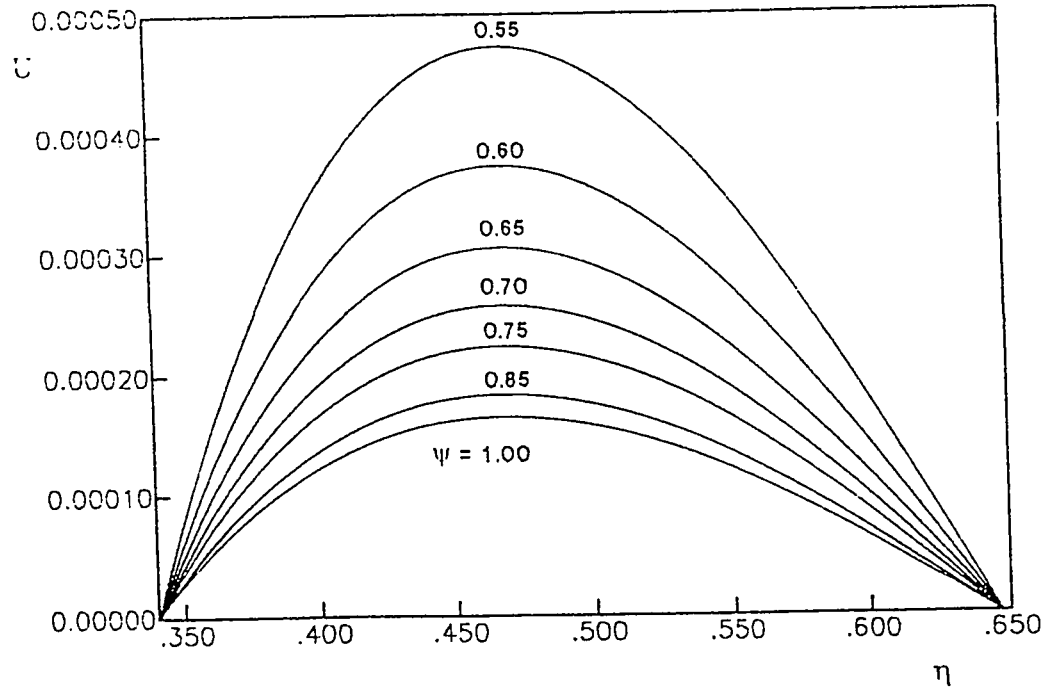


Fig. 6.3(f) : Variation of the fully developed axial velocity, U with η at different values of ψ ranges between 0.55 to 1.0, Case 1.O., E = 0.9

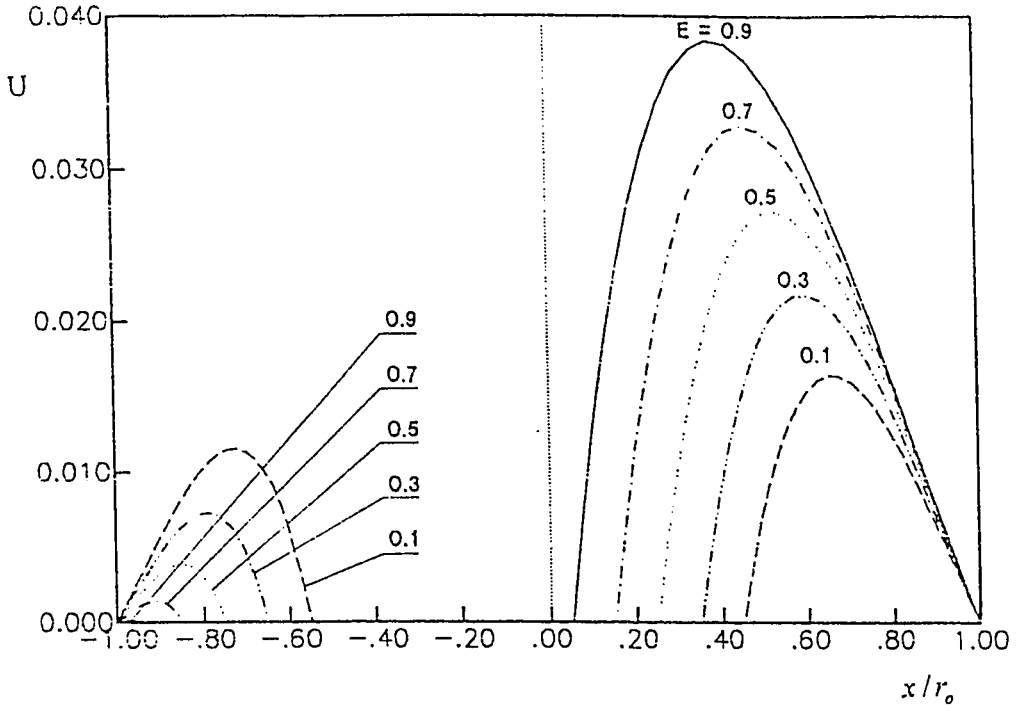


Fig. 6.4(a) : Fully-developed velocity profiles in the widest and narrowest sides of the gap in case 1.I.

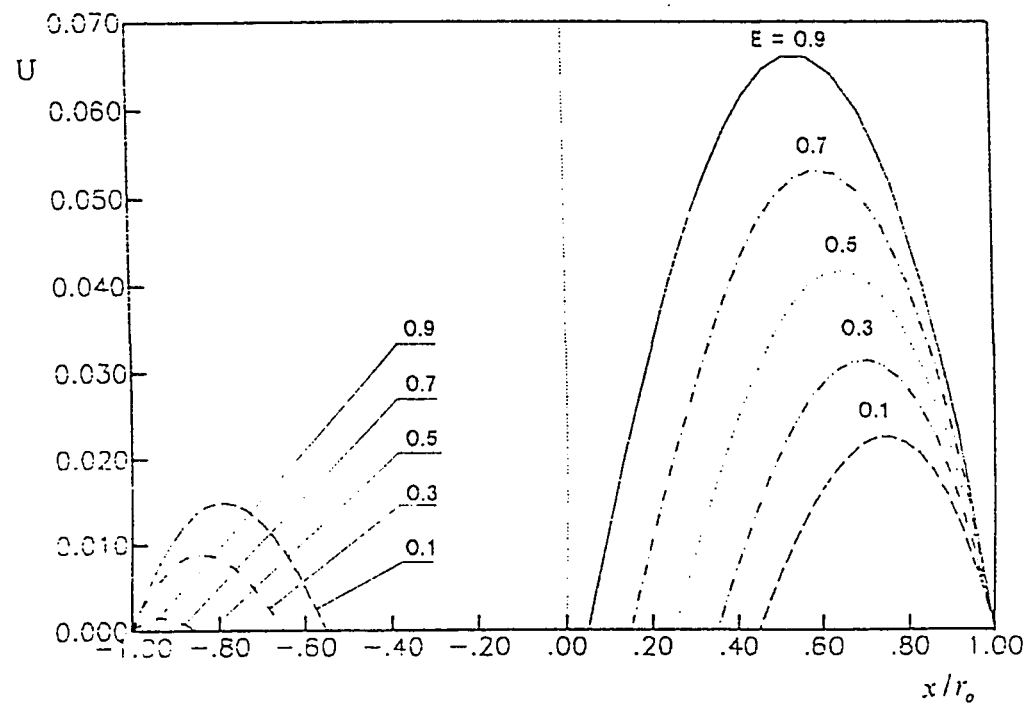


Fig. 6.4(b) : Fully-developed velocity profiles in the widest and narrowest sides of the gap in case 1.O.

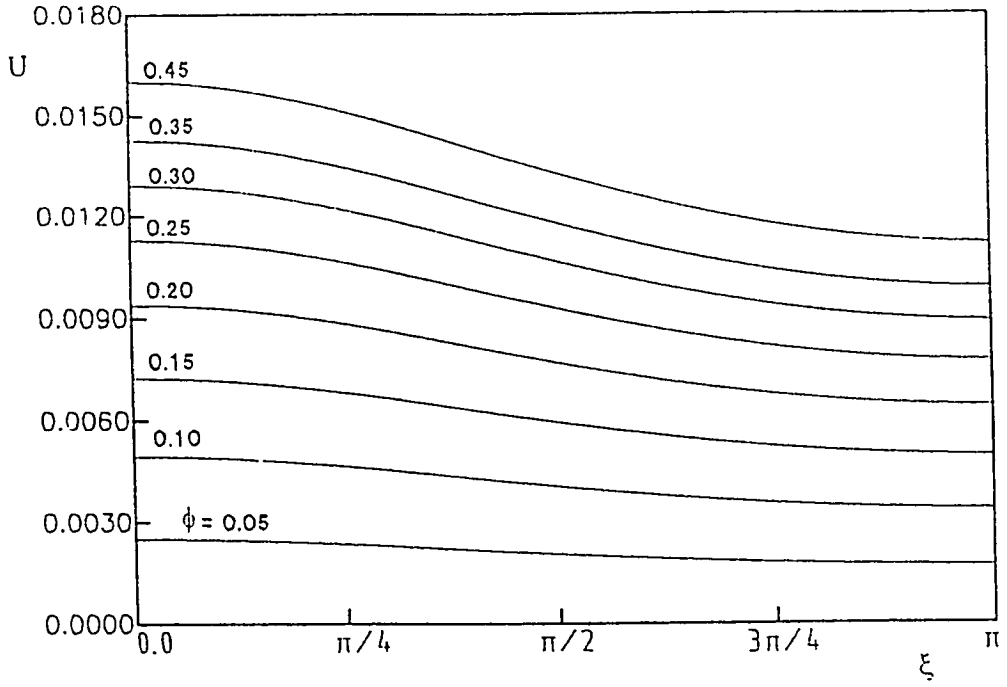


Fig. 6.5(a) : Variation of fully developed axial velocity with ξ at different values of ϕ ranges between 0.05 to 0.45, Case I.I., E = 0.1

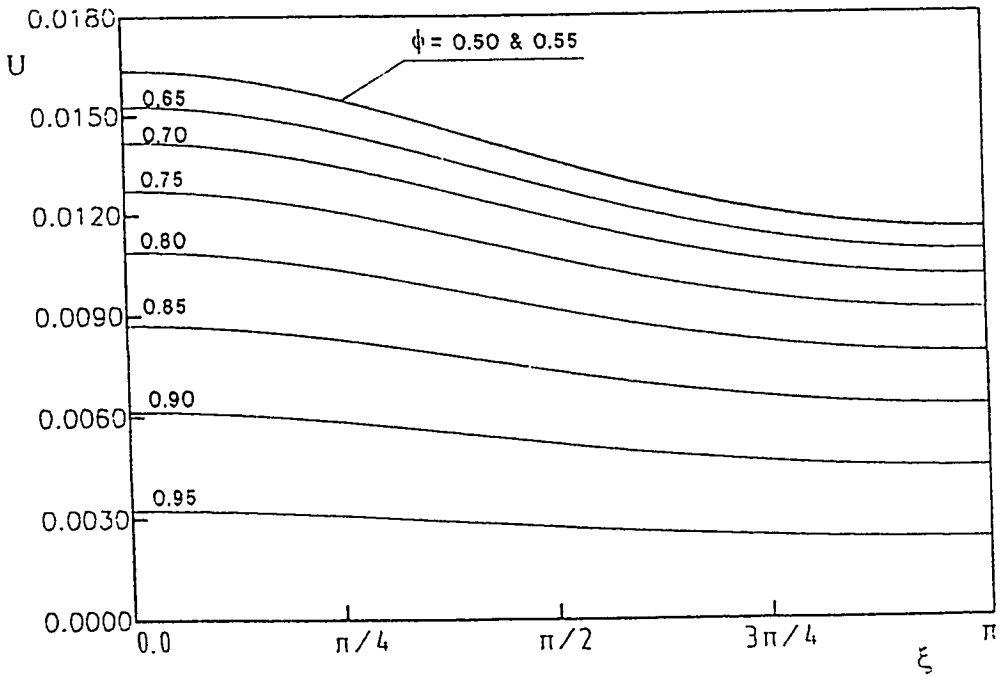


Fig. 6.5(b) : Variation of fully developed axial velocity with ξ at different values of ϕ ranges between 0.5 to 0.95, Case I.I., E = 0.1

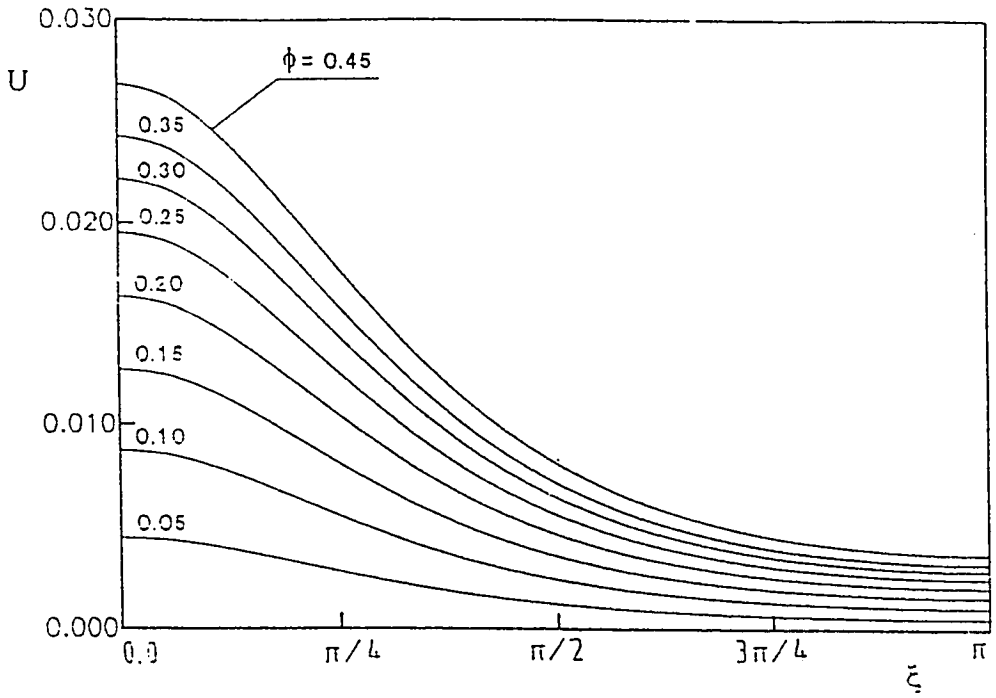


Fig. 6.5(c) : Variation of fully developed axial velocity with ξ at different values of ϕ ranges between 0.05 to 0.45, Case I.I., E = 0.5

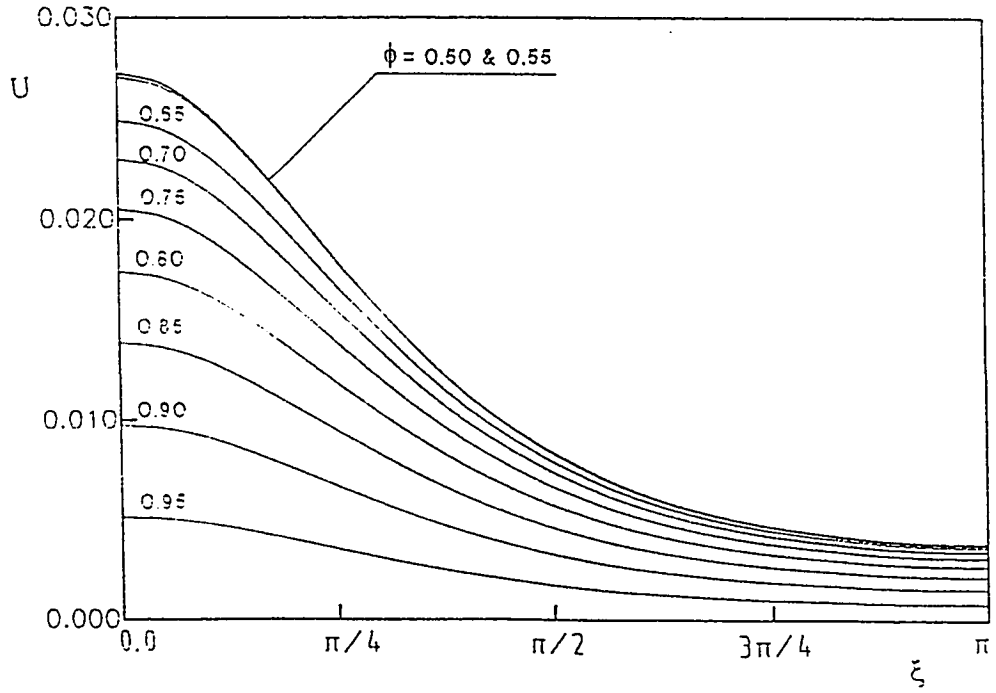


Fig. 6.5(d) : Variation of fully developed axial velocity with ξ at different values of ϕ ranges between 0.5 to 0.95, Case I.I., E = 0.5

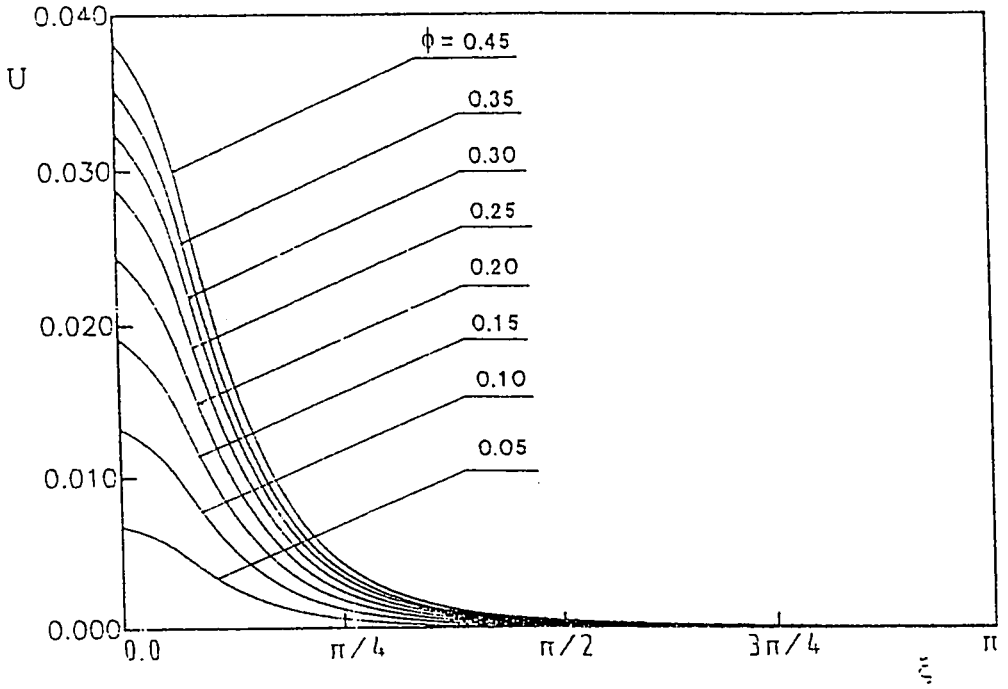


Fig. 6.5(e) : Variation of fully developed axial velocity with ξ at different values of ϕ ranges between 0.05 to 0.45, Case I.I., E = 0.9

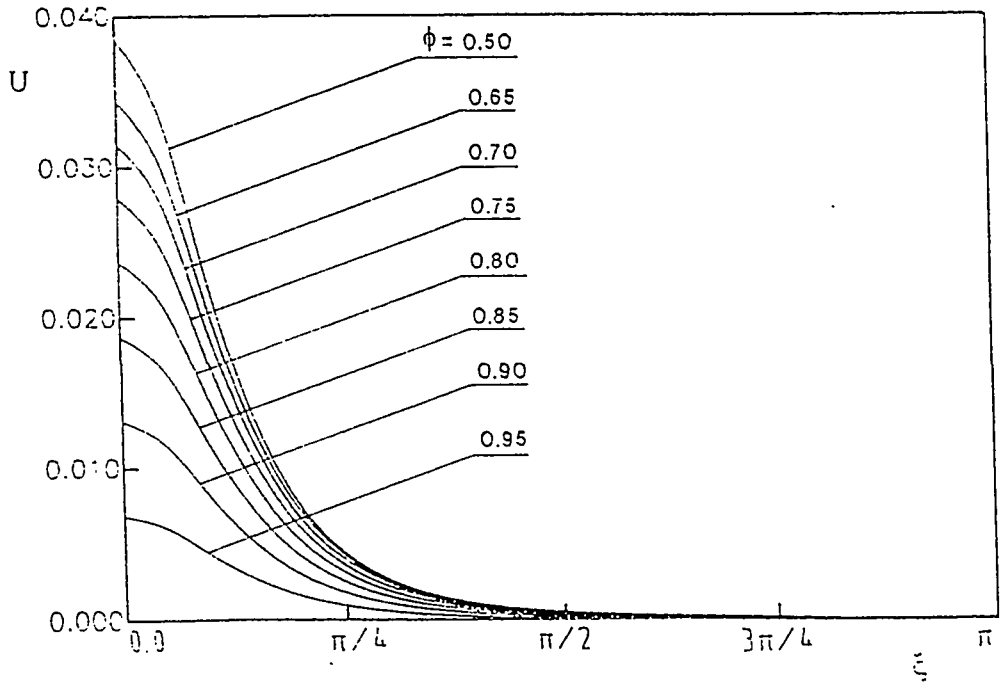


Fig. 6.5(f) : Variation of fully developed axial velocity with ξ at different values of ϕ ranges between 0.5 to 0.95, Case I.I., E = 0.9

Similarly, Figs. 6.5(e) and 6.5(f) give the U-$\xi$ variation in a very eccentric annulus having E = 0.9. Figures 6.6(a-f) present the corresponding results for case 1.O. For a given eccentricity E, velocity profiles similar to those presented in Figs. 6.2(a-f) and 6.3(a-f) could be obtained by cross plotting in Figs. 6.5(a-f) or Figs. 6.6(a-f). The phenomenon of asymmetric axial-velocity profiles is attributed to the increase/decrease in the resistance to flow in the narrow/wide side of the annular gap as a result of eccentricity. The resistance to flow in the narrowest gap will always be larger than that in the widest gap because of higher velocity gradients in the former than the latter. Thus increasing the eccentricity (E) increases/decreases the values of U in the widest/narrowest side of the gap. However, a net result will be an increase in the average value $\bar{U}$ as will be shown later.

For a given eccentricity (E), the effect of having the heated boundary on either the inner or the outer wall of the annulus can be clarified by comparing the velocity profiles corresponding to cases 1.I. and 1.O. This comparison is shown in Figs. 6.7(a) and 6.7(b). Figure 6.7(a) shows for a slight eccentric annulus (E = 0.1) a comparison between the computed velocity profiles as one rotates around the annulus from its widest gap side ( $\psi = \xi/\pi = 0$ ) to its narrowest gap side ( $\psi = 1$, i.e., $\xi = \pi$ ). Moreover, Figure 6.7(b) shows velocity profiles corresponding to cases 1.I and 1.O for two values of eccentricity, namely E = 0.1 and E = 0.5, in the widest and narrowest sides of the annulus. As can be seen from Figs. 6.7 (a-b), in either case 1.I or 1.O, the heating of a boundary causes the velocity profiles to be skewed towards this boundary (i.e., shifts the

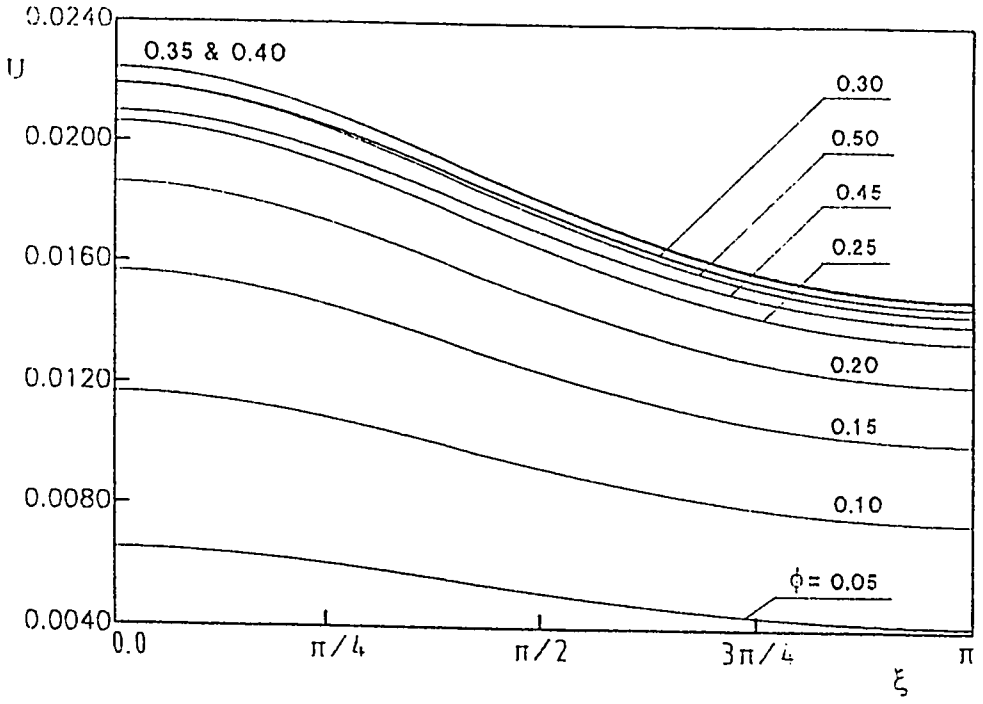


Fig. 6.6(a) : Variation of fully developed axial velocity with ξ at different values of ϕ ranges between 0.05 to 0.5, Case 1.O., E = 0.1

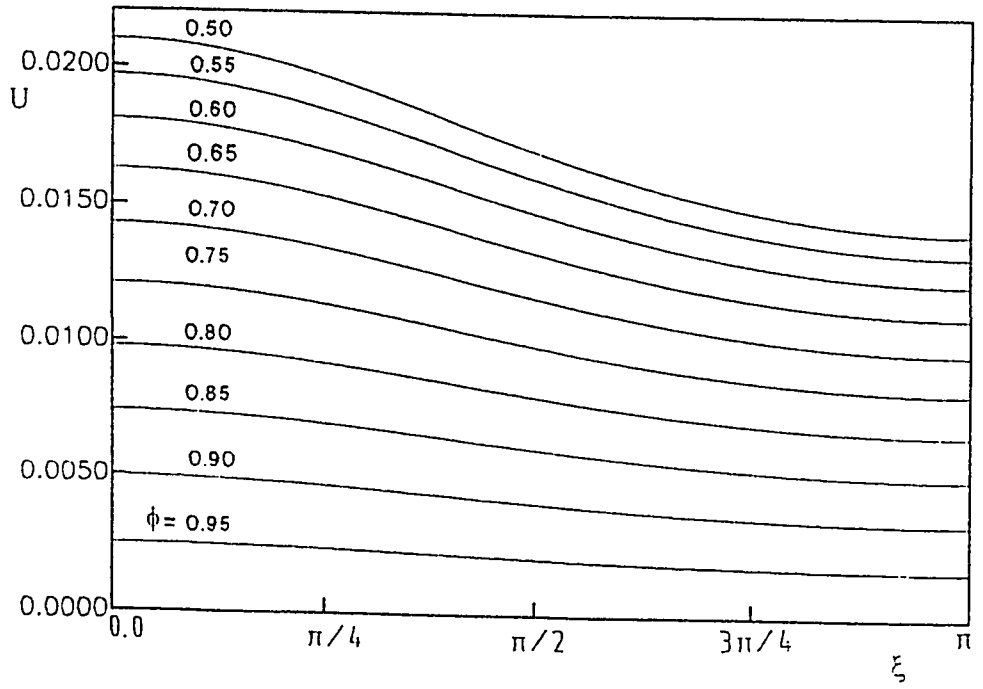


Fig. 6.6(b) : Variation of fully developed axial velocity with ξ at different values of ϕ ranges between 0.5 to 0.95, Case 1.O., E = 0.1

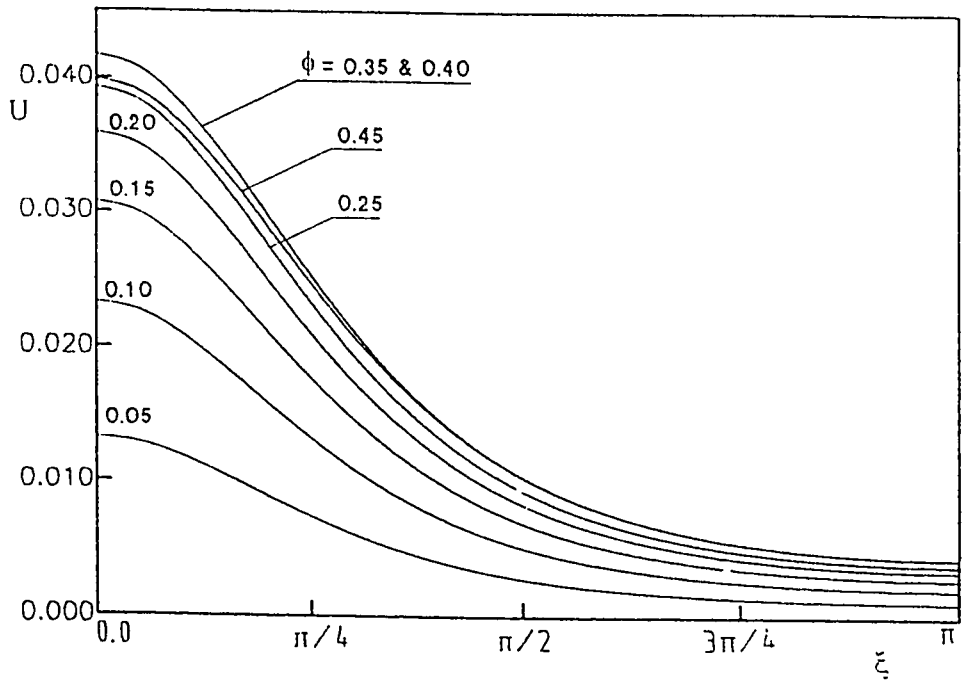


Fig. 6.6(c) : Variation of fully developed axial velocity with ξ at different values of ϕ ranges between 0.05 to 0.45, Case 1.O., E = 0.5

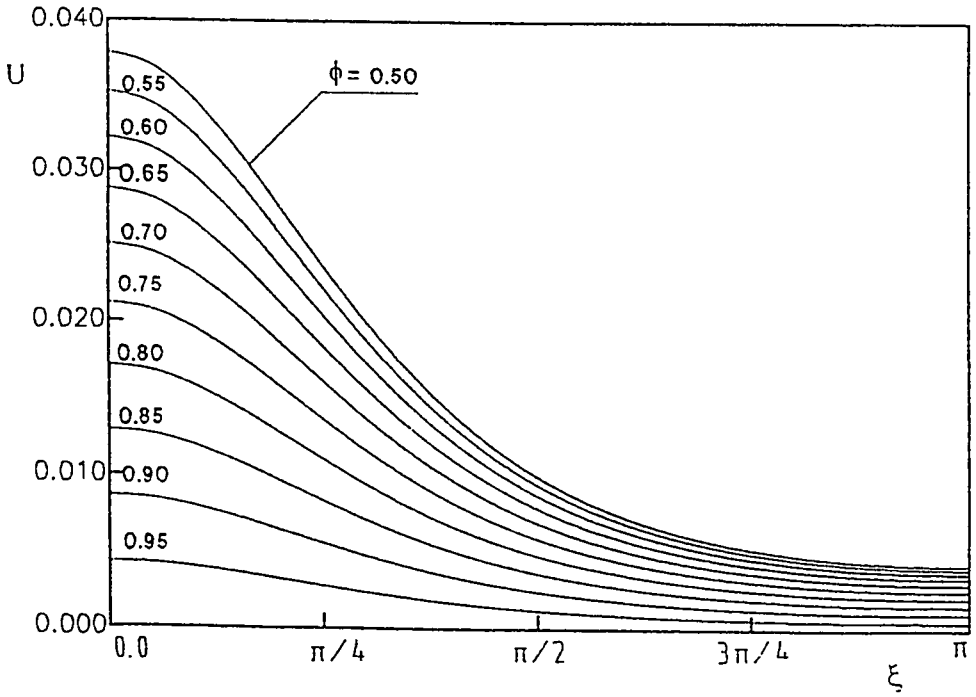


Fig. 6.6(d) : Variation of fully developed axial velocity with ξ at different values of ϕ ranges between 0.5 to 0.95, Case 1.O., E = 0.5

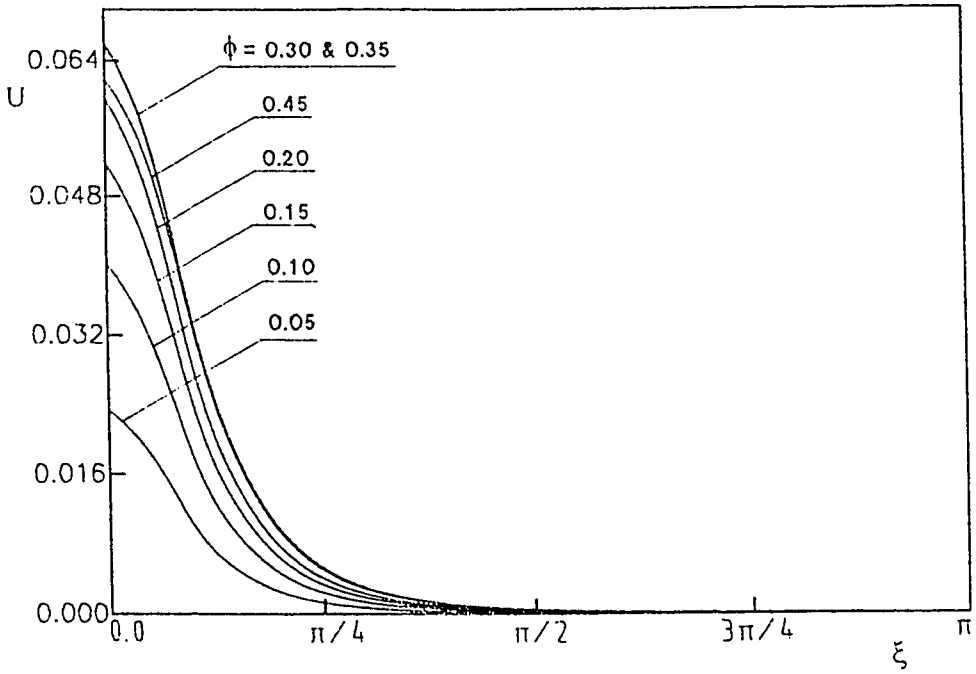


Fig. 6.6(e) : Variation of fully developed axial velocity with ξ at different values of ϕ ranges between 0.05 to 0.45, Case I.O., E = 0.9

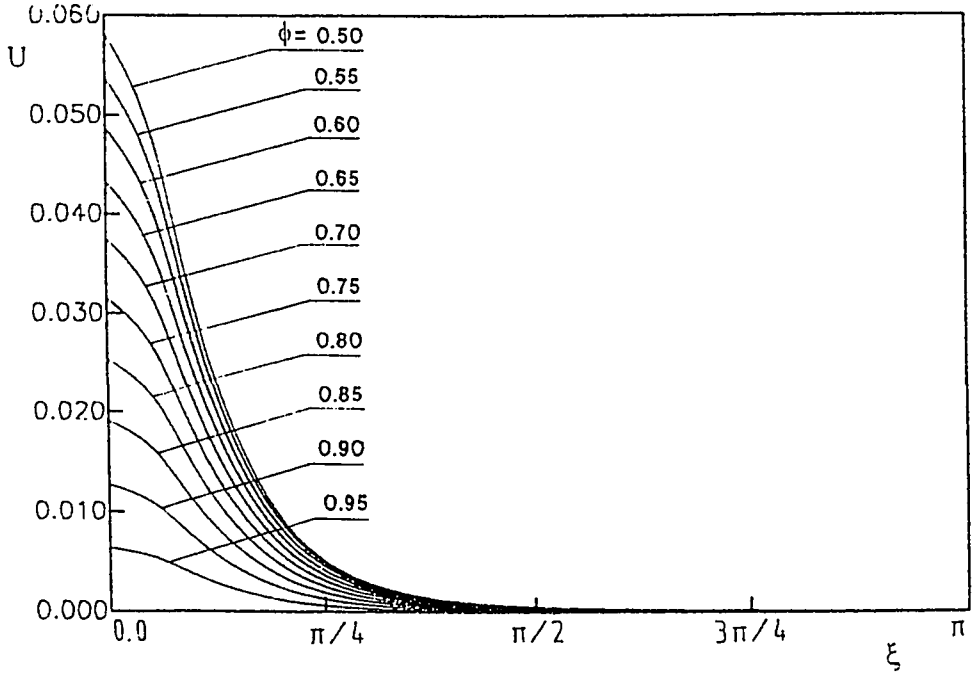


Fig. 6.6(f) : Variation of fully developed axial velocity with ξ at different values of ϕ ranges between 0.5 to 0.95, Case I.O., E = 0.9

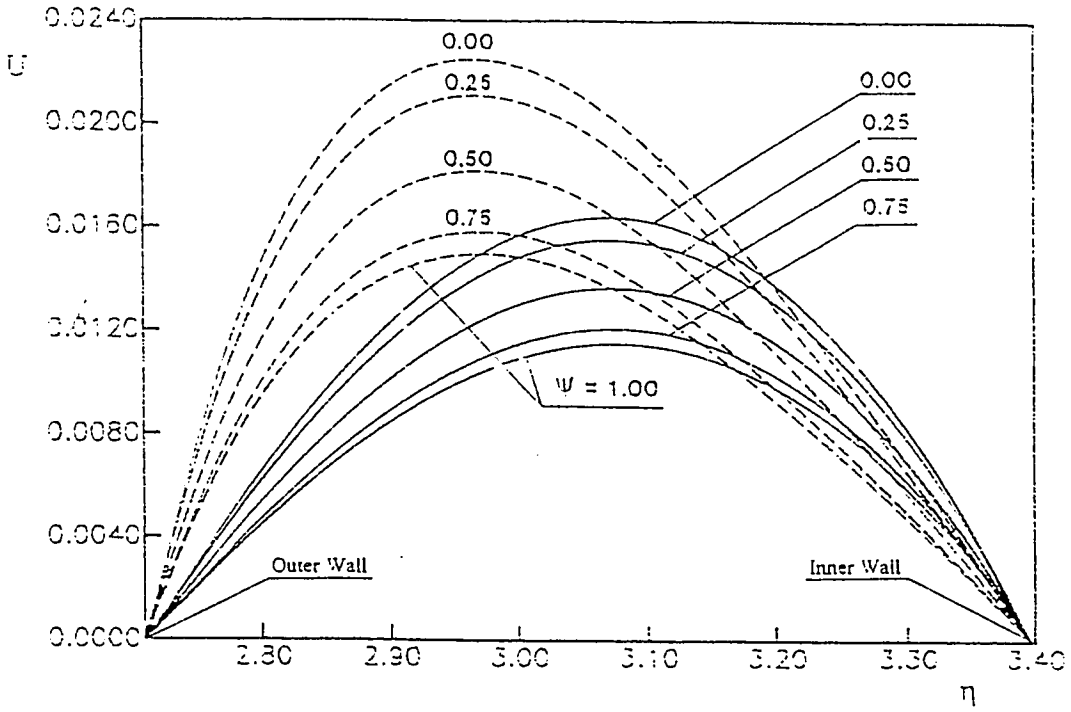


Fig. 6.7(a) : Comparison of the fully-developed velocity profiles, ------ case 1.O, —— case 1.I.

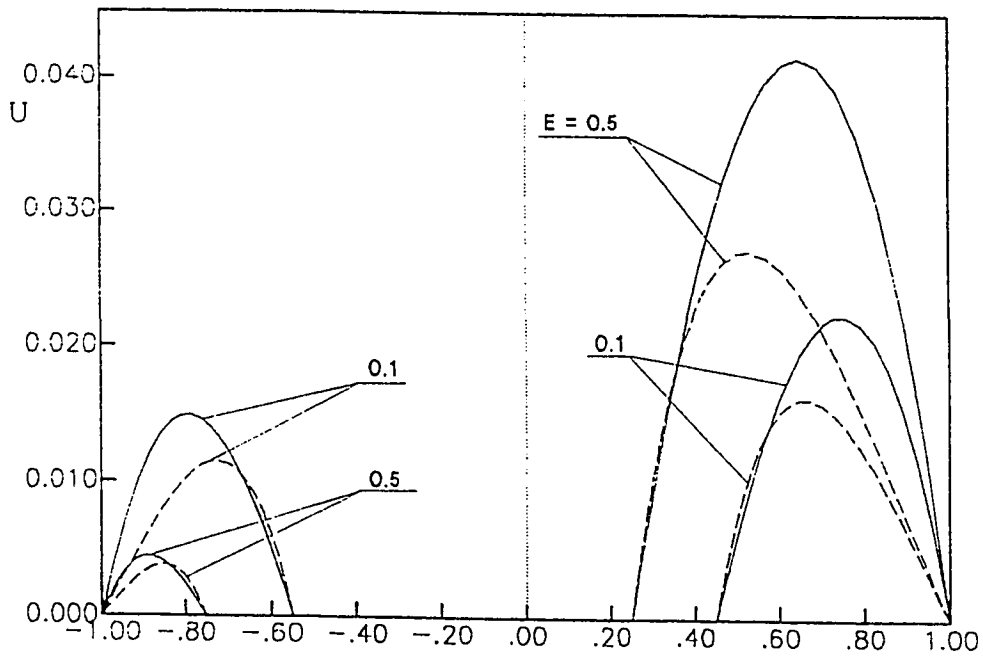


Fig. 6.7(b) : Comparison between velocity profiles at the line of symmetry for different values of eccentricity, —— Case 1.O, ------ Case 1.I.

point of maximum velocity from its location in the case of no heating towards the heated boundary, thus themaximum velocity point becomes remarkably closer to the inner wall in case 1.I. Moreover, these figures also show that, for a given E, the velocity profile has larger values in case 1.O than that in case 1.I. Thus larger induced volumetric flow rates are anticipated in case 1.O. This is attributed to the larger heating surface area in case 1.O when compared to that in case 1.I.

For some selected values of the dimensionless eccentricity (E), the circumferential variations in the local Nusselt number on the inner and outer walls of the annulus are presented for case 1.I in Fig. 6.8(a) and in Fig. 6.8(b) for case 1.O. These figures show that, in general, the highest Nusselt number occurs at the narrowest side of the annular gap and the greatest thermal resistance (hence the lowest Nusselt number) occurs across the widest side of the gap. This can also be attributed to the fact that, since the thickness of the fluid (i.e. the annular gap width) across which the heat passes from the heated boundary (at $T_w$, i.e. $\theta = 1$) to the opposite cooled boundary ( at $T_o$, i.e. $\theta = 0$) is smaller on the narrowest side of the annular gap than that on its widest side, the temperature gradient is always steeper in the former than the latter. Moreover, the increase in the value of the temperature gradient in the narrowest gap over that in the widest gap becomes more and more pronounced, and hence circumferential variation in local Nusselt number becomes more and more noticeable, as the value of the eccentricity E increases. For a given eccentricity E, Fig. 6.8(a) shows that, for case 1.I, the local Nusselt number on the inner wall is larger than that on the outer wall at any value of $\xi$.

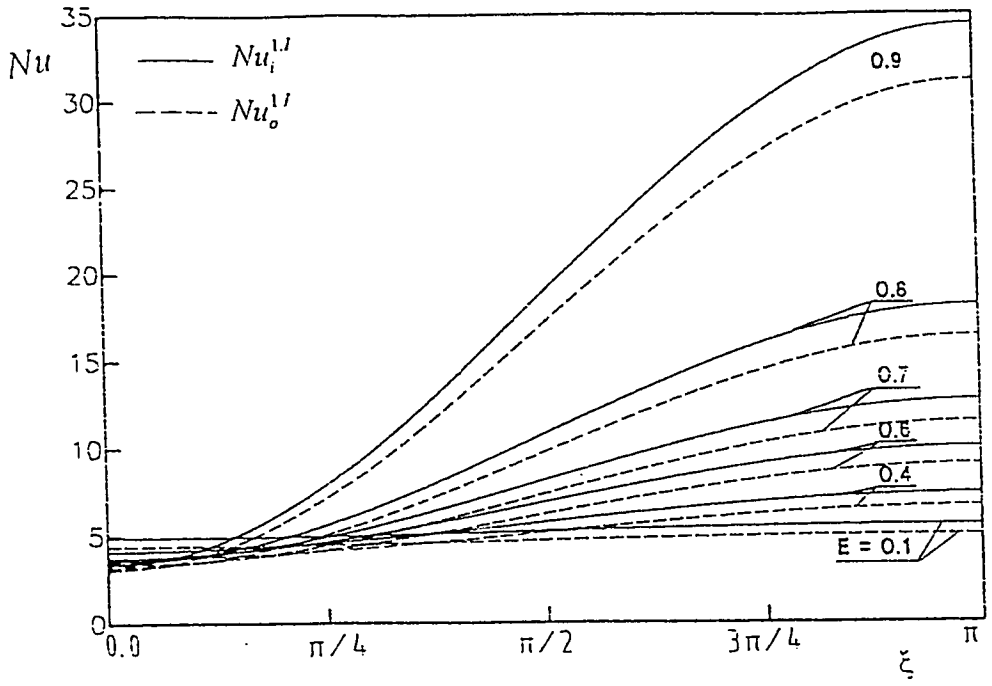


Fig. 6.8(a) : Variation of local Nusselt number around the circular arcs of the inner and outer walls in case 1.1.

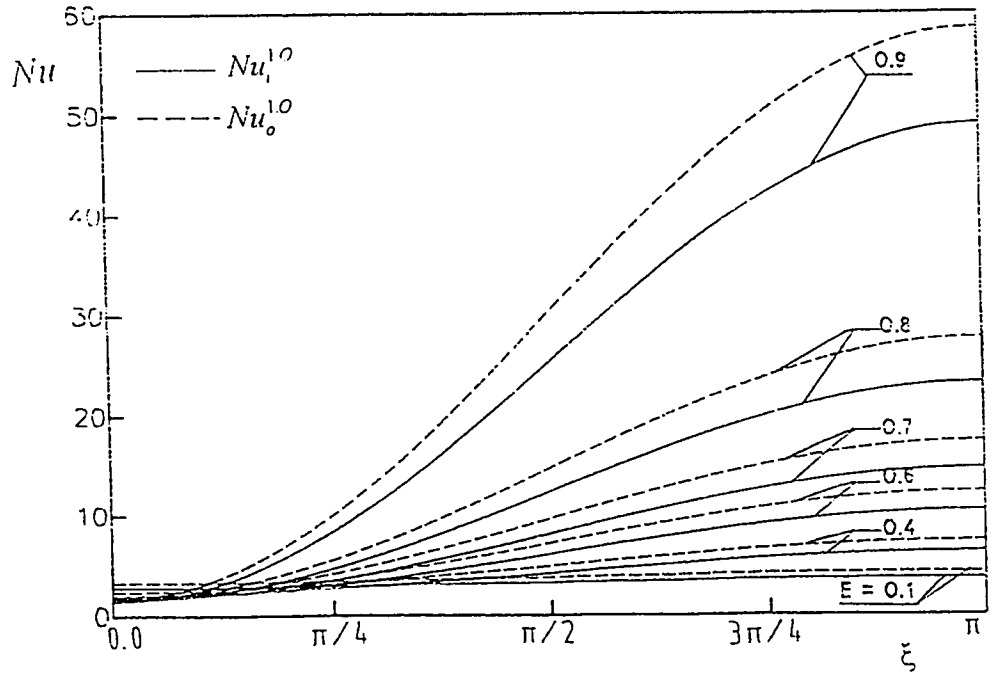


Fig. 6.8 (b) : Variation of local Nusselt number around the circular arcs of the inner and outer walls in case 1.0.

The opposite is true in case 1.O as can be seen from Fig. 6.8(b). This phenomenon is related to the higher/lower fluid velocities near the heated/cooled boundary in each case.

The circumferentially averaged Nusselt number on the inner and outer walls of the annulus is presented in Fig. 6.9 against the eccentricity E for both cases 1.I and 1.O. As expected, the average Nusselt number increases with eccentricity. On the other hand, for a given eccentricity the Nusselt number on the inner wall, in either case 1.I or case 1.O, is larger than that on the outer wall. This is due to the larger thickness of the hydrodynamic boundary-layer which has developed on the outer boundary of the annulus than that which has developed on the inner boundary of the annulus; recall that the outer boundary has a larger surface area and a larger radius of curvature and that the hydrodynamic boundary- layer creates the greatest resistance to heat transfer. Moreover, the magnitudes of the average Nusselt number, for a given eccentricity, are such that $\overline{Nu}_i^{1.I} > \overline{Nu}_i^{1.O} > \overline{Nu}_o^{1.O} > \overline{Nu}_o^{1.I}$. Such a descending order of magnitudes can be explained as follows. In adiabatic flows in annular channels, the point of maximum velocity is known to be nearer to the inner boundary. Now, heat transfer in case 1.I makes the flow faster /slower near the inner/outer wall of the annulus. Consequently, the velocity profile will be more skewed inward with the maximum velocity closer to the inner wall. On the other hand, heat transfer in case 1.O tries to move the point of maximum velocity towards the outer wall, hence reduces the velocity near the inner wall than in case 1.I. In other words, the hydrodynamic boundary-layer on the inner wall is thicker in case 1.O than that in case 1.I. In addition, the nature of an annular flow

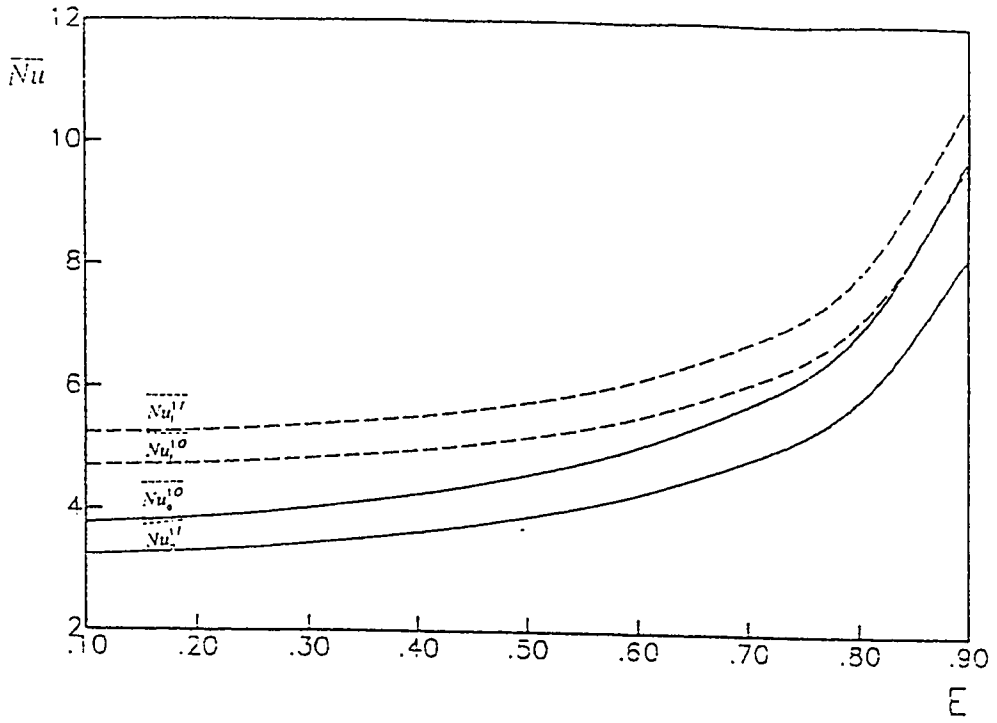


Fig. 6.9 : Nusselt number averaged around the complete circular arcs of the inner and outer walls for case 1.I and 1.O, ------ on inner wall, —— on outer wall

requires the hydrodynamic boundary -layer on the inner boundary to be thinner than that on the outer boundary. The combination of these effects together clarifies the aforementioned sequence of magnitudes.

Engineers are not frequently concerned with the details of the velocity and temperature fields but only with the induced flow rate and the maximum (in case of heating or minimum in case of cooling) bulk temperature which the fluid attains as it passes through the channel and reaches its exit cross-section ( $\bar{T}_m$ ). The latter can be used to calculate the heat gained or lost by the fluid from entrance up to the annulus exit ( $\bar{q}$ ). These two important engineering parameters ( F and $\bar{Q}$ ) are given in Figs. 6.10(a) and 6.10(b). Figure 6.10(a) gives the dimensionless volumetric flow rate ( F ) against the eccentricity E. For a given E, this flow rate is the maximum possible which the present vertical channel can engender under thermal boundary conditions of the first kind. In other words, since fully-developed flow conditions have already been achieved, a further increase in the channel height would not produce any additional flow rate. As shown in Fig. 6.10(a), increasing the eccentricity E causes an increase in F in both cases 1.I and 1.O. This agrees with the trend of previously reported forced flow results in the literature. Moreover, flow rate in case 1.O is larger, for a given E, than the corresponding value in case 1.I. This is a result of the larger heating surface in the former case than the latter.

Under thermal conditions of the first kind, the fully developed $\theta$ and hence $\theta_m$ do not vary with axial distance Z. The bulk temperature $\theta_m$ does not change with further

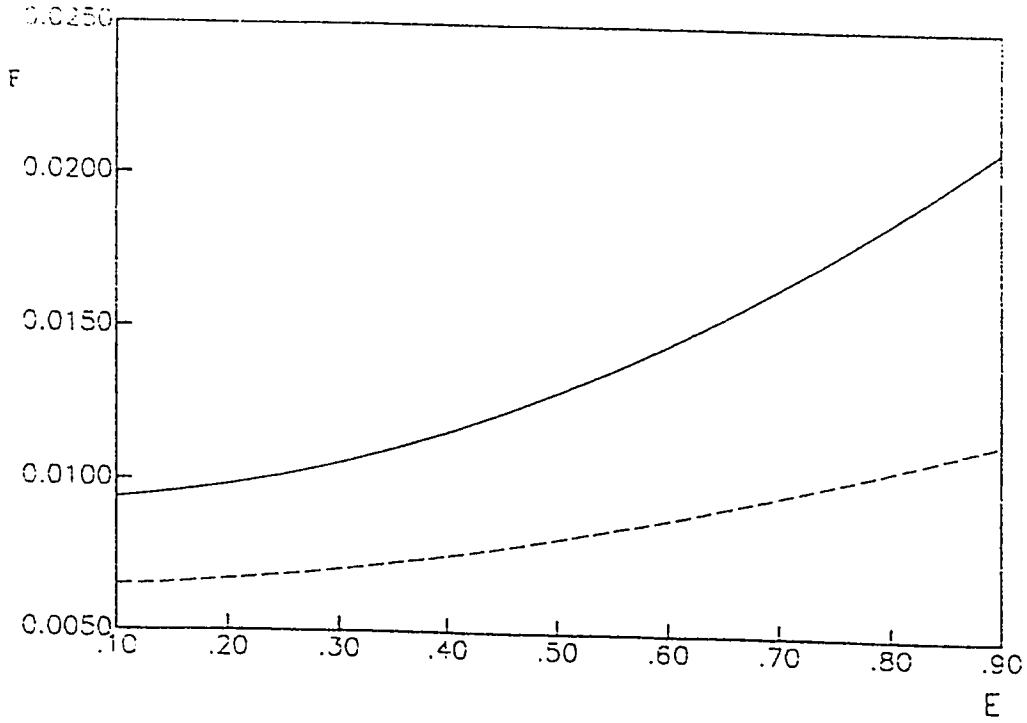


Fig. 6.10(a) : Induced volumetric flow rate versus eccentricity, ----- case 1.I,

—— case 1.O.

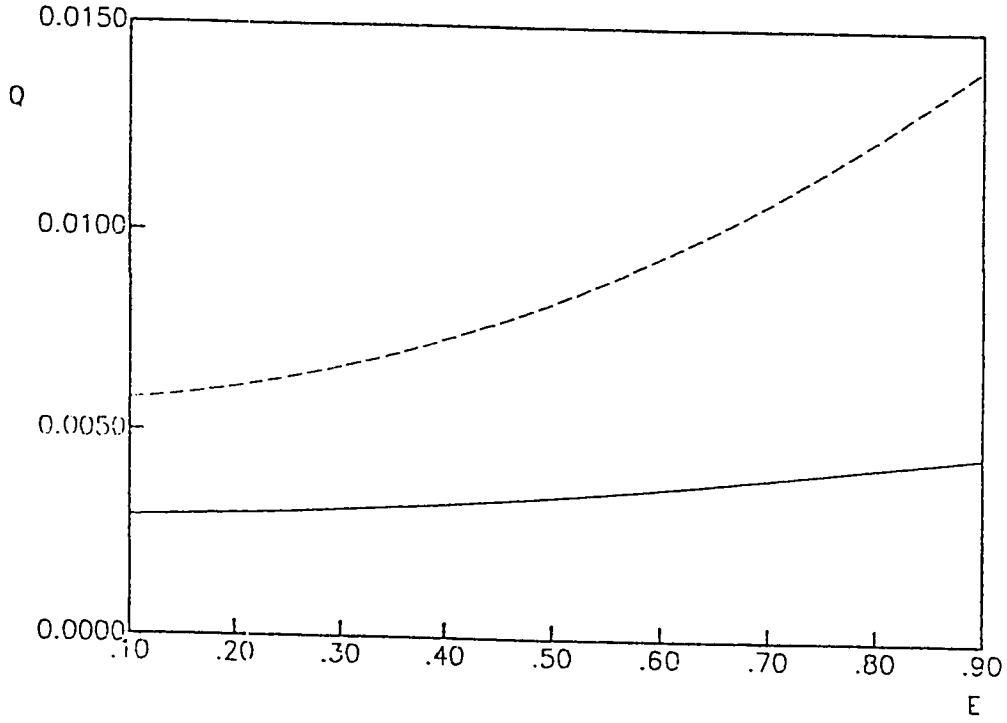


Fig.6.10(b) : Total heat absorbed by fluid versus eccentricity, ----- case 1.O.

—— case 1.I.

increase in the channel height since, under fully-developed flow conditions, the heat passes through the fluid from one wall to the other in such a manner as if the fluid were stationary, i.e. by pure conduction through laminar fluid layers. Thus, for a given E, the computed fully-developed value of $\theta_m$ corresponds also to the fluid bulk temperature at the channel exit $\bar{\theta}_m$ ( i.e. $\theta_m = \bar{\theta}_m$ ). The computed values of $\bar{\theta}_m$ and F are used to obtain $\bar{Q}$ ( $= F\bar{\theta}_m$ ) which is presented in Fig. 6.10(b). Thus the total heat gained or lost by the fluid from entrance up to the channel exit, including the developing length, is obtained without need to integrate the Nusselt numbers over the channel height. However, it is simple to derive an expression for the average Nusselt number over the entire annulus height in terms of Rayleigh number ($Ra^*$) and $\bar{Q}$ (El-Shaarawi and Al-Nimr [14] ).

## 6.3 Fundamental Solution of the Third Kind

Since the wall opposite to the heat transfer surface is perfectly insulated, the fluid temperature in the annulus becomes ultimately uniform at the same temperature as the heated surface ($\theta = 1$ everywhere in the fully-developed region). Therefore, fully-developed free-convection flow under thermal conditions of the third kind is an isothermal flow having a temperature equals that of the heat transfer boundary. Consequently, we have, in both cases 3.I and 3.O, $P = 0$, $\theta = 1$ and $\partial\theta/\partial\eta = \partial\theta/\partial\xi = \partial^2\theta/\partial\eta^2 = \partial^2\theta/\partial\xi^2 = 0$ everywhere (i.e., there is no need to solve the energy equation

(3.29) since it will vanish automatically for this type of boundary conditions). It can be seen also that $Nu_i^{3.I} = Nu_o^{3.I} = Nu_i^{3.O} = Nu_o^{3.O} = 0$. Thus, the physics of the problem of fully-developed free convection does not distinguish between case I and case O under thermal boundary conditions of the third kind and we simply have only one fully-developed solution of the third kind. The derivation of the governing equation of this problem and its method of solution are given in sections 3.3.4 and 4.4.2, respectively.

Figure 6.11 gives examples of the velocity profiles obtained by the application of eq. (4.4) along with the pertinent constants given by eqs. (4.21 a-e) in an annulus of N = 0.5 for the shown selected values of the eccentricity E. It is worth mentioning that the number of terms of the series in eq. (4.4) has a noticeable effect on the solution to be obtained; the higher the value of the eccentricity E the larger the number of terms needed. However, it has been found in the present study that 20 terms give acceptable accuracy with E = 0.9. Therefore, the results presented here are all obtained using 20 terms of the series.

Finally, the induced volumetric flow rate (F), which is of engineering importance, is presented in Figs. 6.12(a) and 6.12(b) against the eccentricity (E) for a wide range of annulus radius ratio ( N = 0.1-0.75). These two figures are self-explanatory.

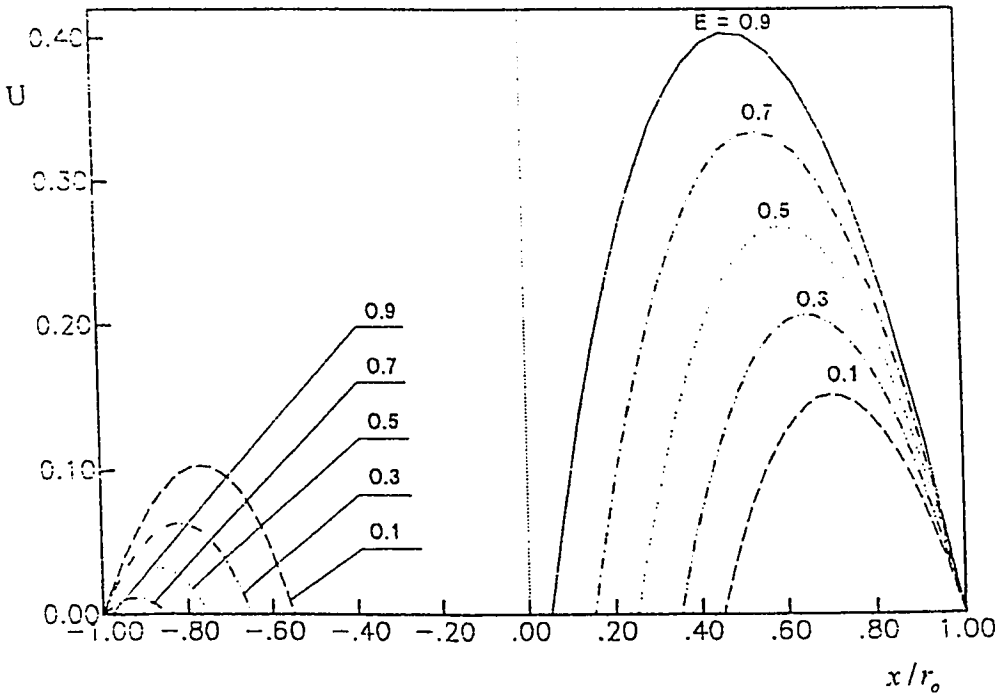


Fig. 6.11 : Velocity profiles in the widest and narrowest gaps under thermal conditions of third kind.

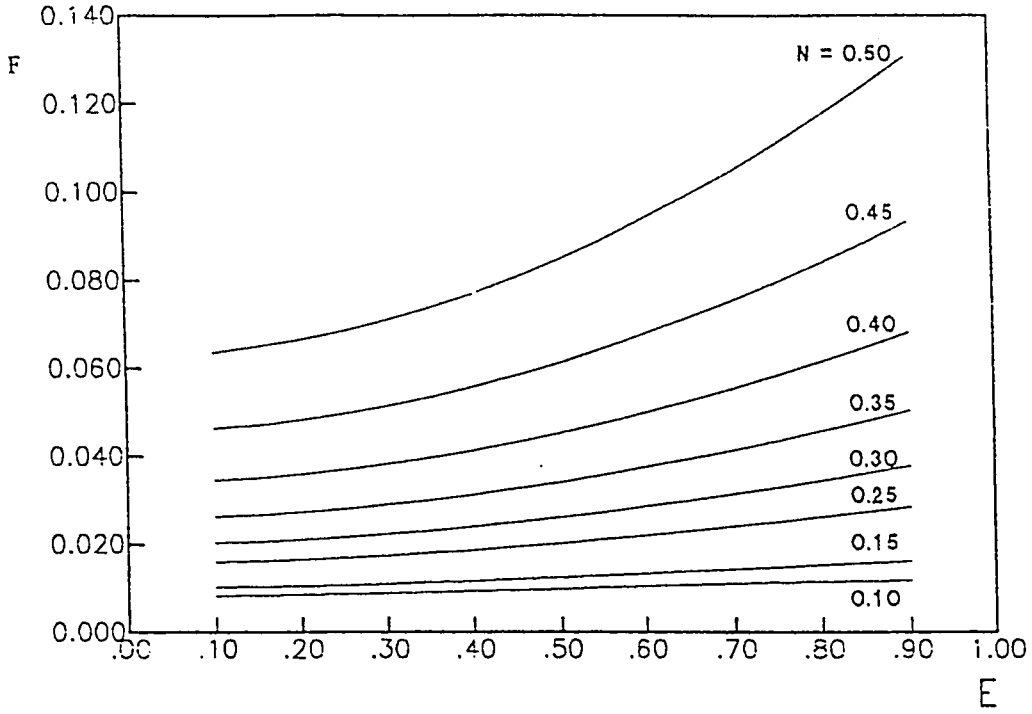


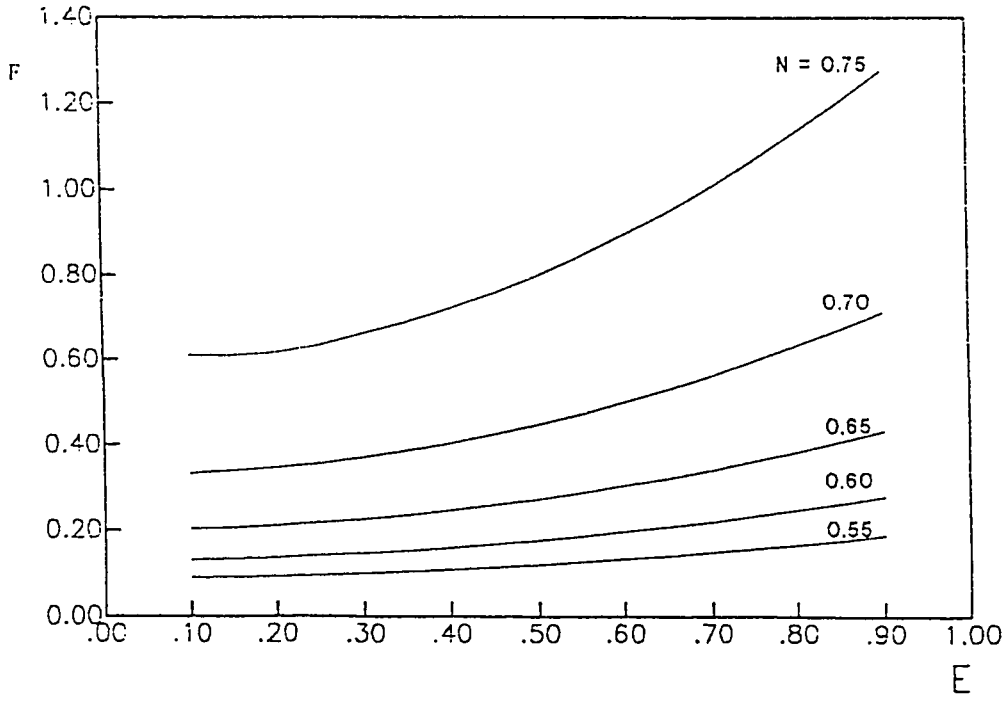


Fig. 6.12(a-b) : Induced volumetric flow rate versus eccentricity for various values of annulus radius ratio, case 3.

## 6.4. Fundamental Solution of the Fourth Kind

In this case, since one of the boundaries is isothermal, the governing equations will be (eq.(3.29)) and (eq.(3.30)) subject to the thermal boundary conditions (eq.(3.19)) tabulated before for case 4.I. and 4.O in addition to the symmetry conditions (eq.(3.17)) and the hydrodynamic boundary conditions (eq.(3.31)). A closed form analytical solution for the energy equation (eq.(3.29)) has been obtained as a special case from the general solution of the steady state conduction equation (eq.(3.20)) by neglecting the internal heat generation (i.e., $C^* = 0.0$) . Hence, the solution of eq.(3.29) subject to the aforesaid boundary conditions is the reduced form of eq.(4.4) which can be written as;

$$\theta = A^*\eta + B + \sum_{n=1}^{\infty}\left(Ce^{n\eta} + De^{-n\eta}\right)Cos(n\xi) \tag{6.23}$$

Where:

**for case 4.I;**

$$A^* = \frac{0.5N}{1-N}$$

$$B = -A^*\,\eta_o$$

$$C = \frac{N}{n(e^{2n\eta_i} + e^{2n\eta_o})(1-N)}$$

$$D = \frac{e^{2n\eta_o}}{n(e^{2n\eta_i} + e^{2n\eta_o})(1-N)}$$

**for case 4.O;**

$$A^* = -\frac{0.5}{1-N}$$

$$B = -A^{*}\,\eta_i$$

$$C = \frac{1}{n(e^{2n\eta_i} + e^{2n\eta_o})(1-N)}$$

$$D = \frac{e^{2n\eta_i}}{n(e^{2n\eta_i} + e^{2n\eta_o})(1-N)}$$

The temperature profiles in the widest and narrowest sides of the annular gap for case 4.I and 4.O and selected values of the eccentricity (E) are shown in Figs. 6.13(a) and 6.13(b), respectively. These two figures show that the temperature level in the wide side is higher than that in the narrow side. The deviation between the temperature levels in the widest and narrowest sides of the annulus increases with the increase of eccentricity. This is attributed to the fact that increasing the eccentricity increases the thickness of the fluid layer in the wide side as compared to that in the narrow side. This results in decreasing the thermal resistance in the wide side compared to that in the narrow side.

To best clarify the effect of the eccentricity on the temperature distribution, the variation of the temperature along the heat transfer wall has been plotted in Fig. 6.13(c). This figure shows that the temperature along the heat transfer wall is not uniform. This was expected since the thermal resistance decreases as one rotates through the annulus from its widest side ($\psi = \xi / \pi = 0$) to its narrowest side ($\psi = 1$) since the thickness of the fluid layer decreases in the same direction. The reduction in the thermal resistance should result in a reduction in the temperature difference between that on the heat transfer wall and that on the isothermal wall as the one moves from the widest to the

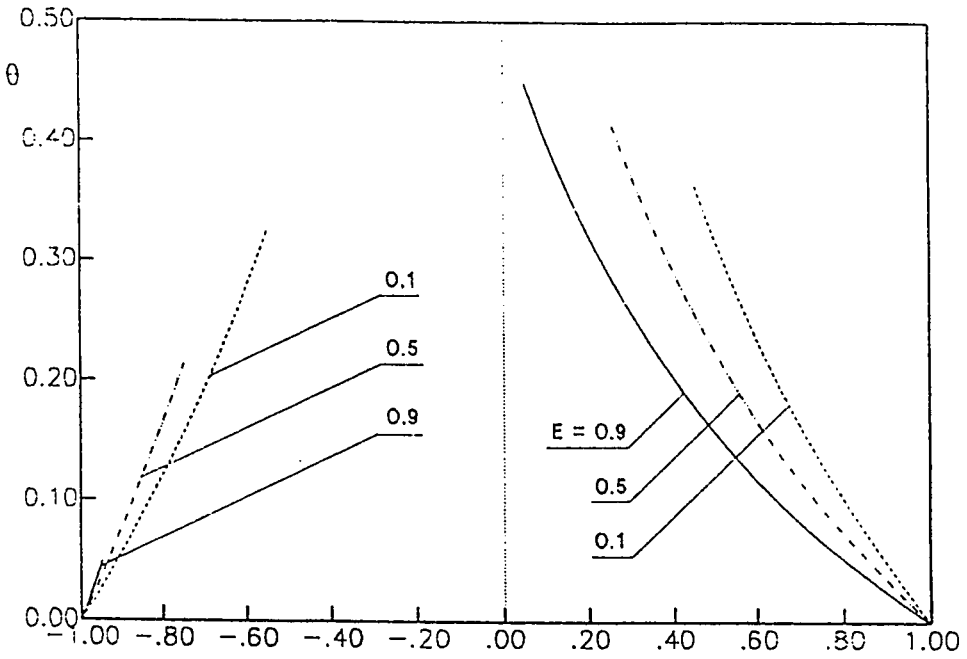


Fig. 6.13(a) : Fully-developed temperature profiles in the widest and narrowest sides of the gap in case 4.I.

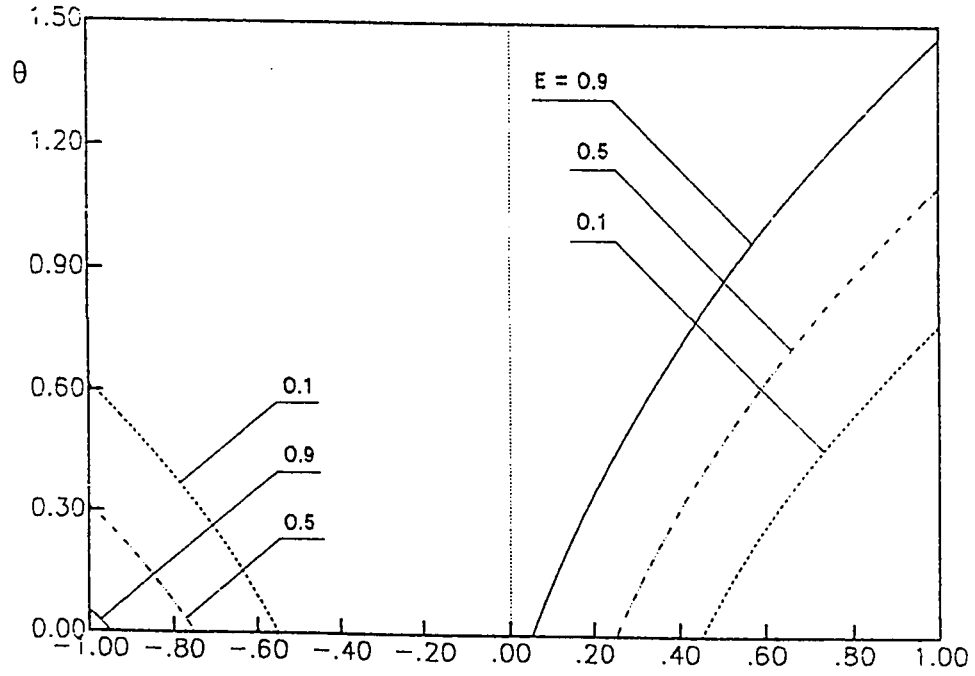


Fig. 6.13(b) : Fully-developed temperature profiles in the widest and narrowest sides of the gap in case 4.O.

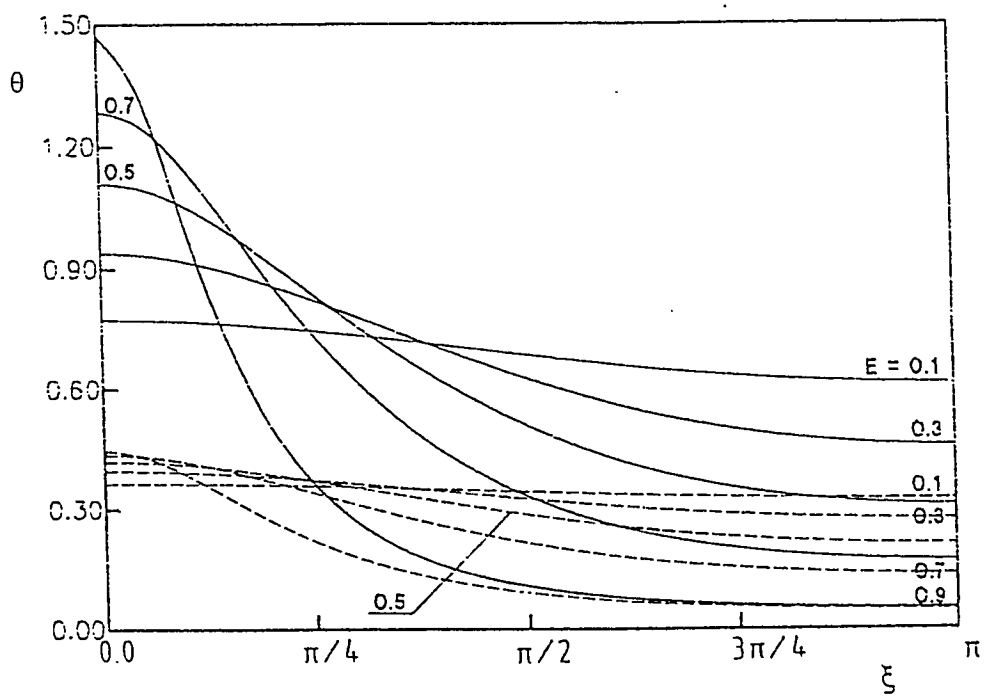


Fig. 6.13(c) : Comaprison between the fully developed temperature variation on the heated wall for selected values of eccentricity, ----- case 4.I, —— case 4.O.

narrowest side of the annulus, since the heat transfer wall has a uniform heat flux while the thermal resistance decreases in the aforementioned direction. Figure 6.13(c) shows also that the nonuniformity of the temperature along the heat transfer wall increases with the increase in the eccentricity for the two cases 4.I and 4.O.

Figures 6.14(a-f) and 6.15 (a-f) show the velocity profiles as one rotates around the annulus from its widest gap side ( $\psi = \xi/\pi = 0$ ) to its narrowest gap side ( $\psi = 1$, i.e., $\xi = \pi$ ). The velocity profiles in the widest and narrowest sides of the annular gap for cases 4.I and 4.O are presented in Figs. 6.16(a) and 6.16(b), respectively. These two figures show clearly the effect of eccentricity on the velocity profiles. Inspecting these two figures show that the slight eccentric annulus (E = 0.1) has velocity profiles which deviate slightly from the axial symmetric profiles existing for the concentric annulus. The deviation from the axial symmetric profiles increases with the increase in the eccentricity (E). This leads to a general increase in the value of the velocity in the wide side and a general decrease of its values in the narrow side (i.e., the maximum velocity always exist in the widest side and precisely at the line of symmetry ( $\psi = \xi / \pi = 0$ )). These figures show also that the maximum velocity (more generally, the velocity in the wide side) increases with the increase in eccentricity. A series of plots that give the variation of U with $\xi$ has been presented in Figs. 6.17(a-f) for case 4.I and Figs. 6.18(a-f) for case 4.O for three selected values of eccentricity (E = 0.1, 0.5 and 0.9). The set of figures 6.14 (a-f) and 6.15 (a-f) and the corresponding set of results presented in Figs. 6.17 (a-f) and 6.18 (a-f) for the same eccentricity complete each other since it gives a complete view of the velocity through out the annulus. Moreover, for a given

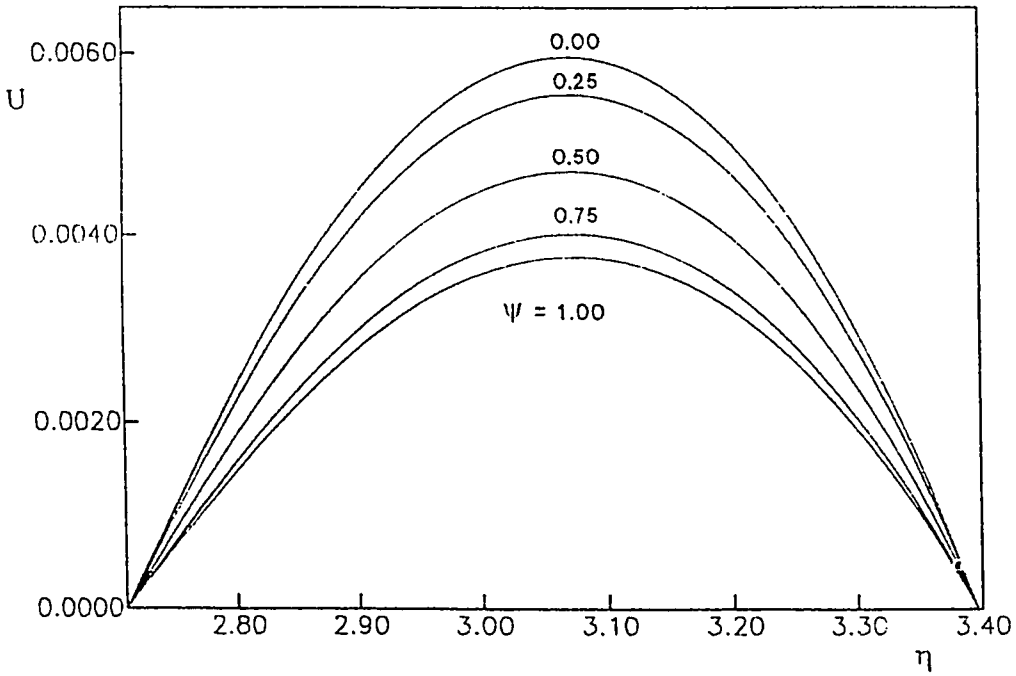


Fig. 6.14(a) : Variation of the fully developed axial velocity, U with η at different values of ψ ranges between 0.0 to 1.0, Case 4.I., E = 0.1

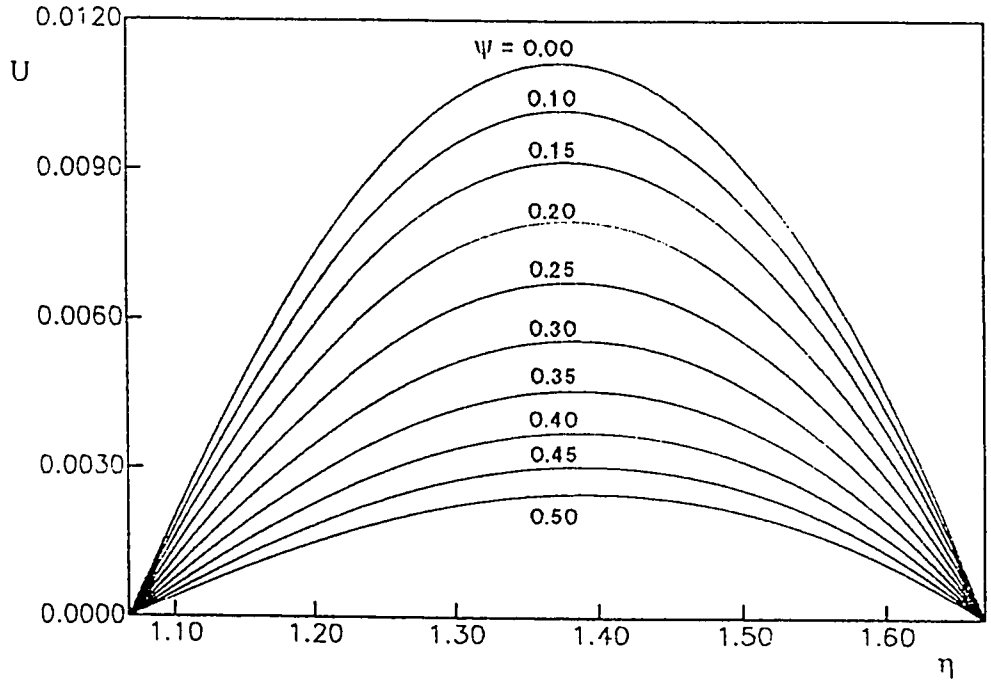


Fig. 6.14(b) : Variation of the fully developed axial velocity, U with η at different values of ψ ranges between 0.0 to 0.5, Case 4.I., E = 0.5

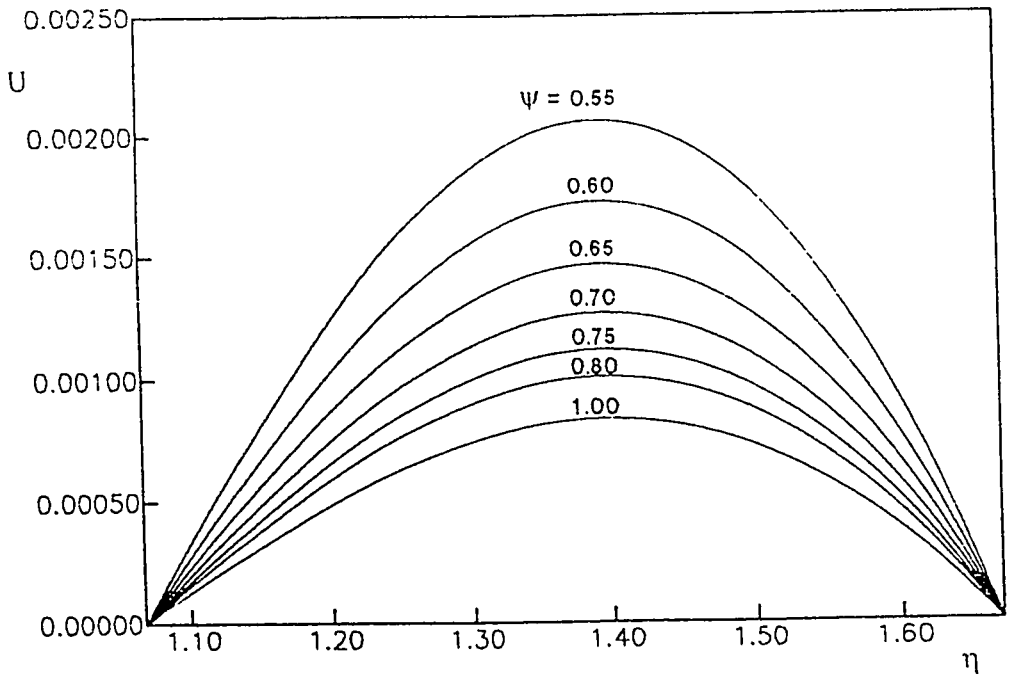


Fig. 6.14(c) : Variation of the fully developed axial velocity, U with η at different values of ψ ranges between 0.55 to 1.0, Case 4.I., E = 0.5

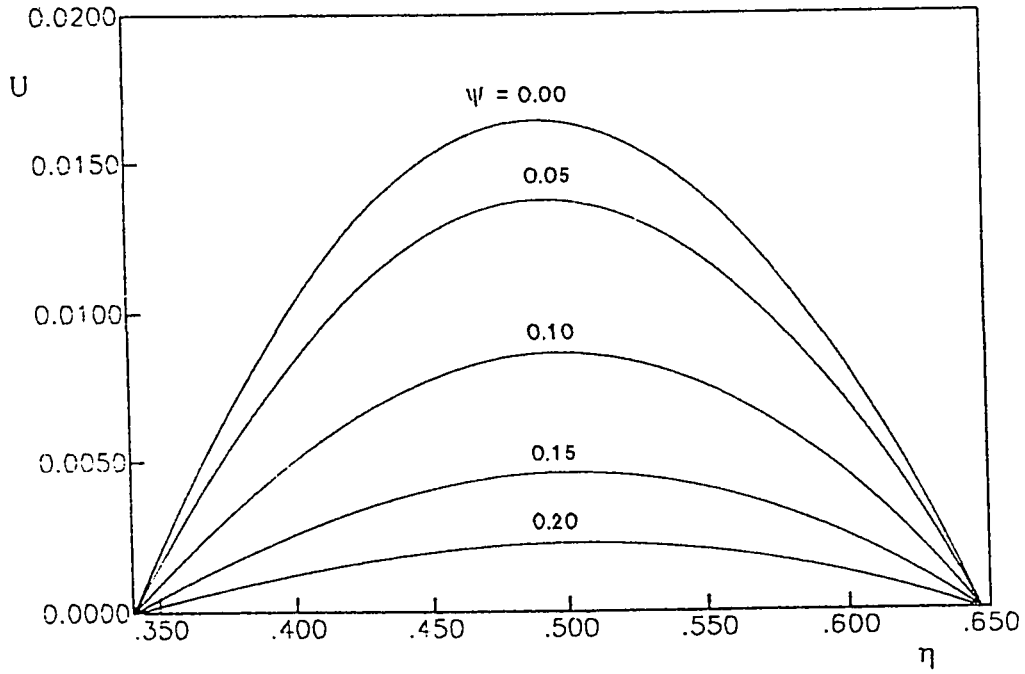


Fig. 6.14(d) : Variation of the fully developed axial velocity, U with η at different values of ψ ranges between 0.0 to 0.2, Case 4.I., E = 0.9

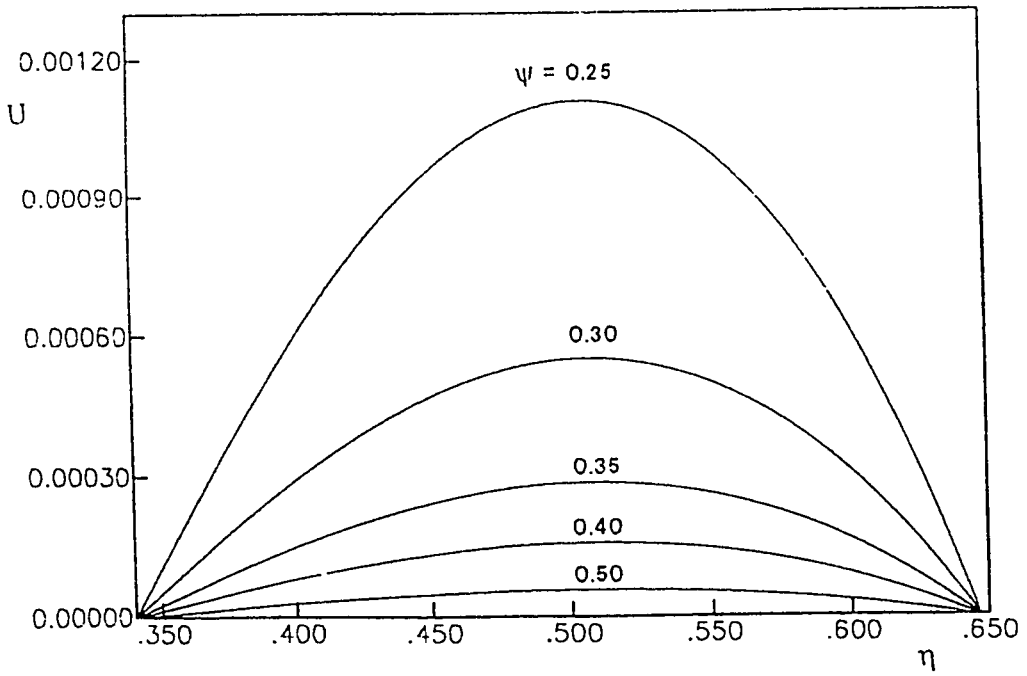


Fig. 6.14(e) : Variation of the fully developed axial velocity, U with η at different values of ψ ranges between 0.25 to 0.5, Case 4.I., E = 0.9

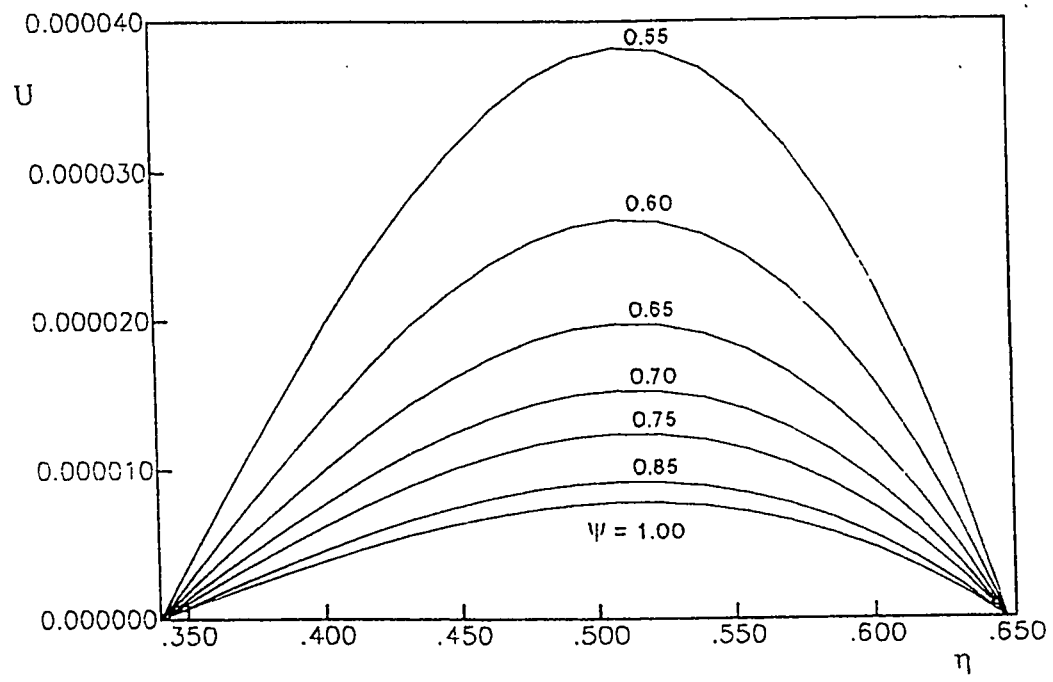


Fig. 6.14(f) : Variation of the fully developed axial velocity, U with η at different values of ψ ranges between 0.55 to 1.0, Case 4.I., E = 0.9

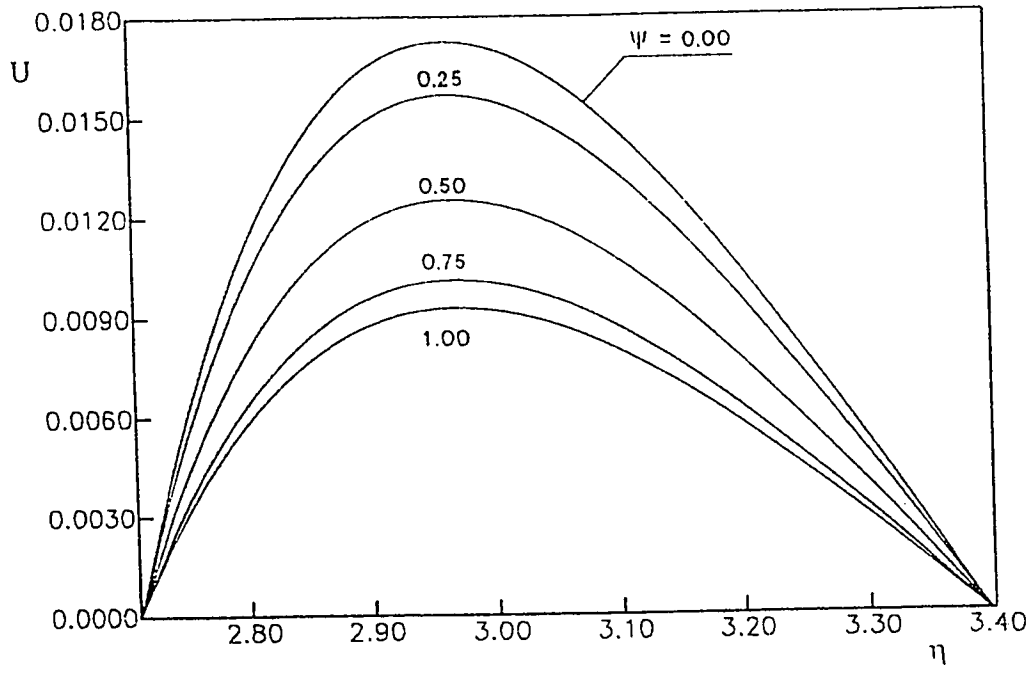


Fig. 6.15(a) : Variation of the fully developed axial velocity, U with η at different values of ψ ranges between 0.0 to 1.0, Case 4.O., E = 0.1

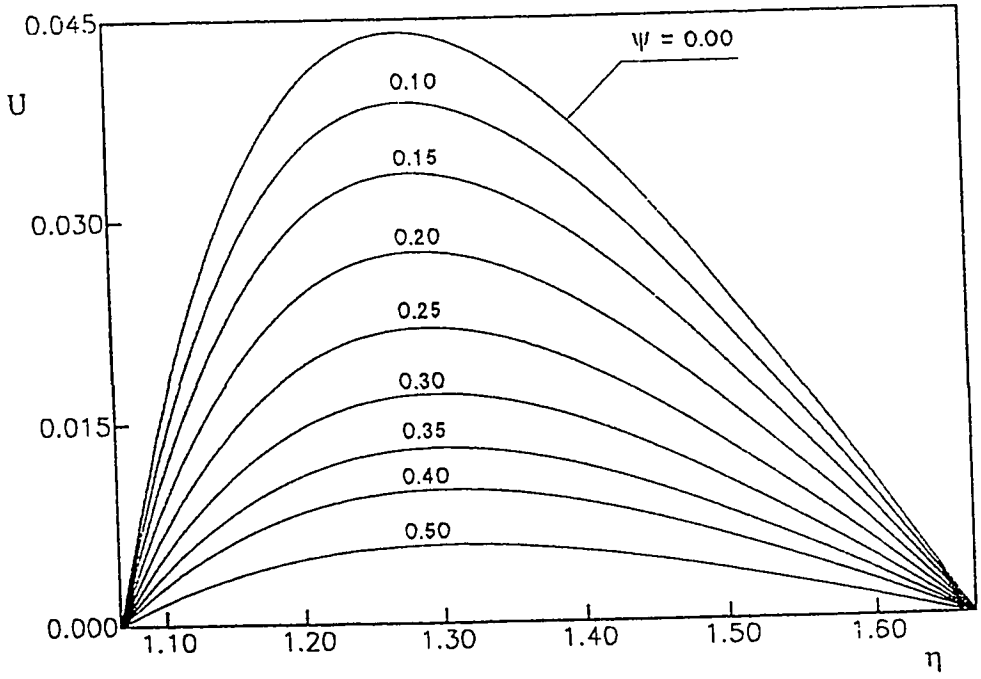


Fig. 6.15(b) : Variation of the fully developed axial velocity, U with η at different values of ψ ranges between 0.0 to 0.5, Case 4.O., E = 0.5

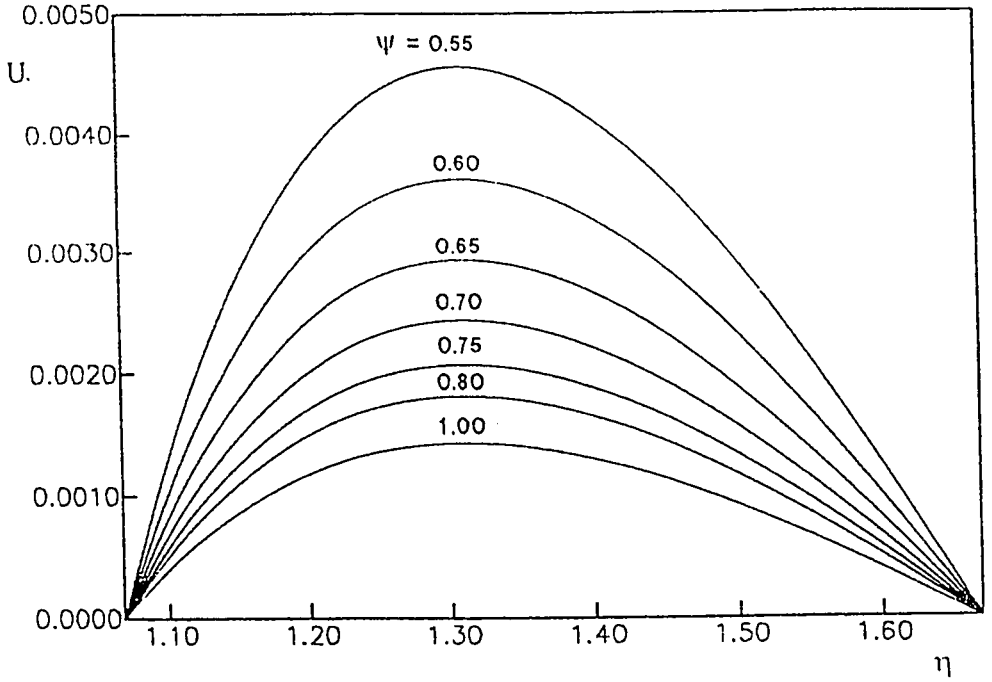


Fig. 6.15(c) : Variation of the fully developed axial velocity, U with η at different values of ψ ranges between 0.55 to 1.0, Case 4.O., E = 0.5

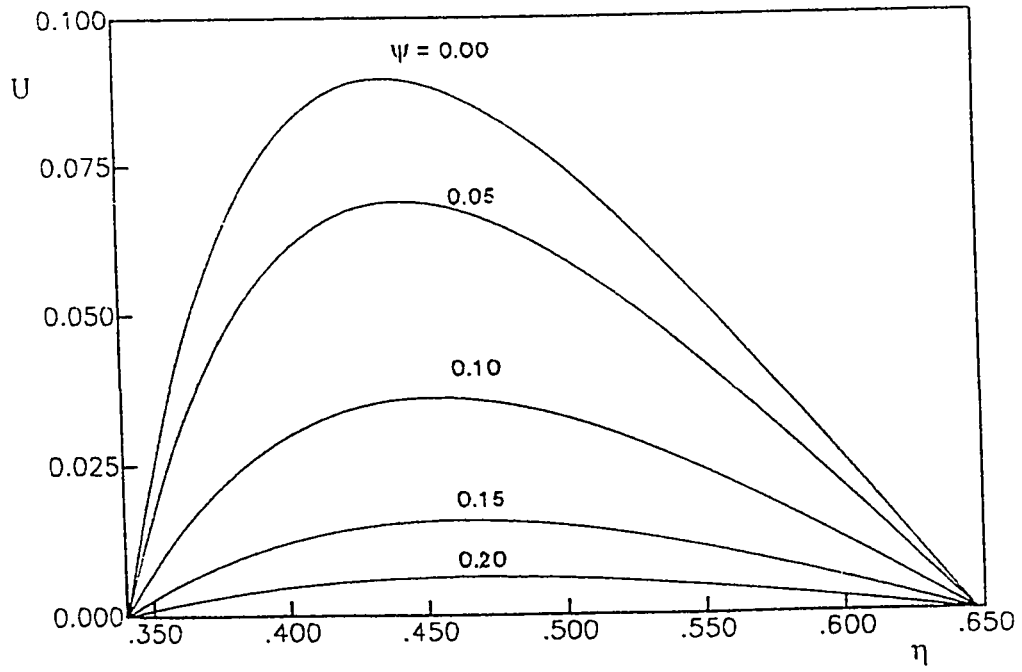


Fig. 6.15(d) : Variation of the fully developed axial velocity, U with η at different values of ψ ranges between 0.0 to 0.2, Case 4.O., E = 0.9

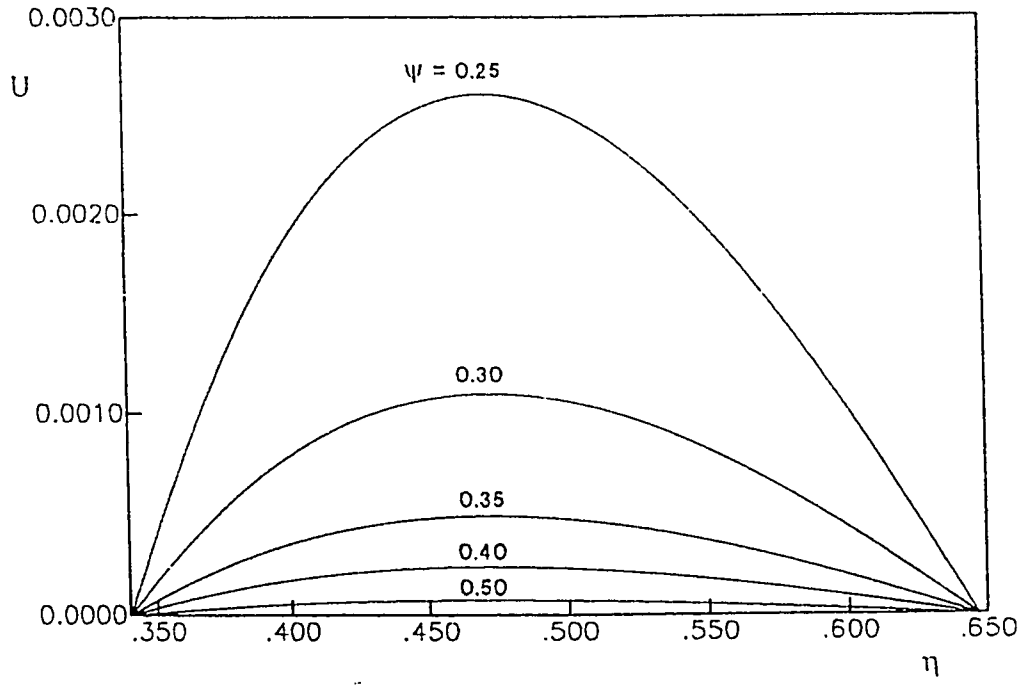


Fig. 6.15(e) : Variation of the fully developed axial velocity, U with η at different values of ψ ranges between 0.25 to 0.5, Case 4.O., E = 0.9

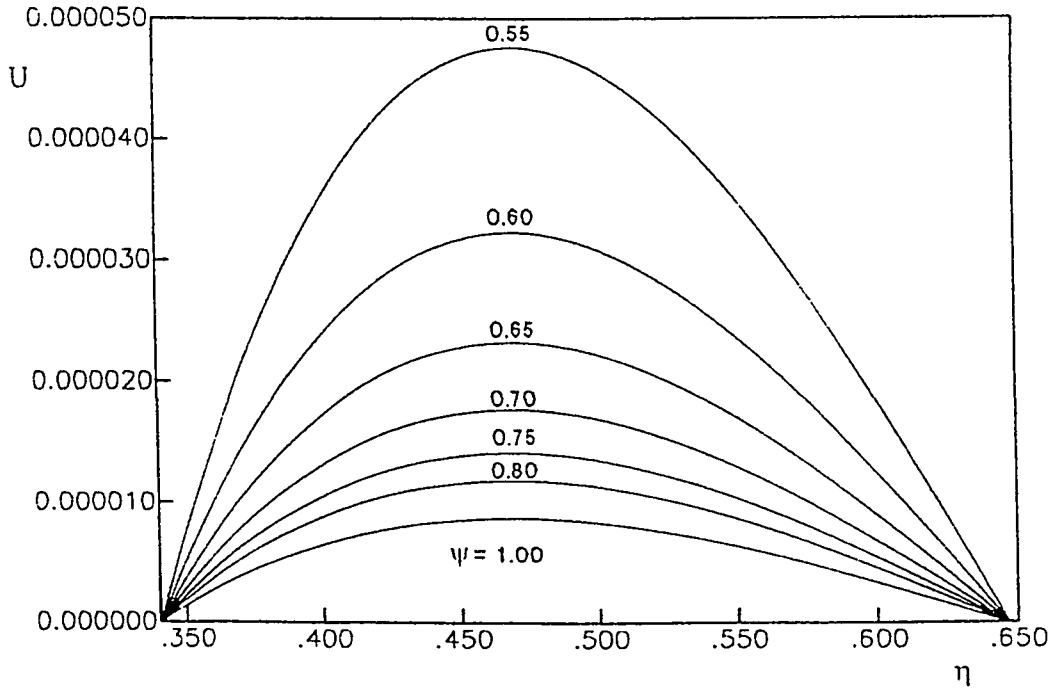


Fig. 6.15(f) : Variation of the fully developed axial velocity, U with η at different values of ψ ranges between 0.55 to 1.0, Case 4.O., E = 0.9

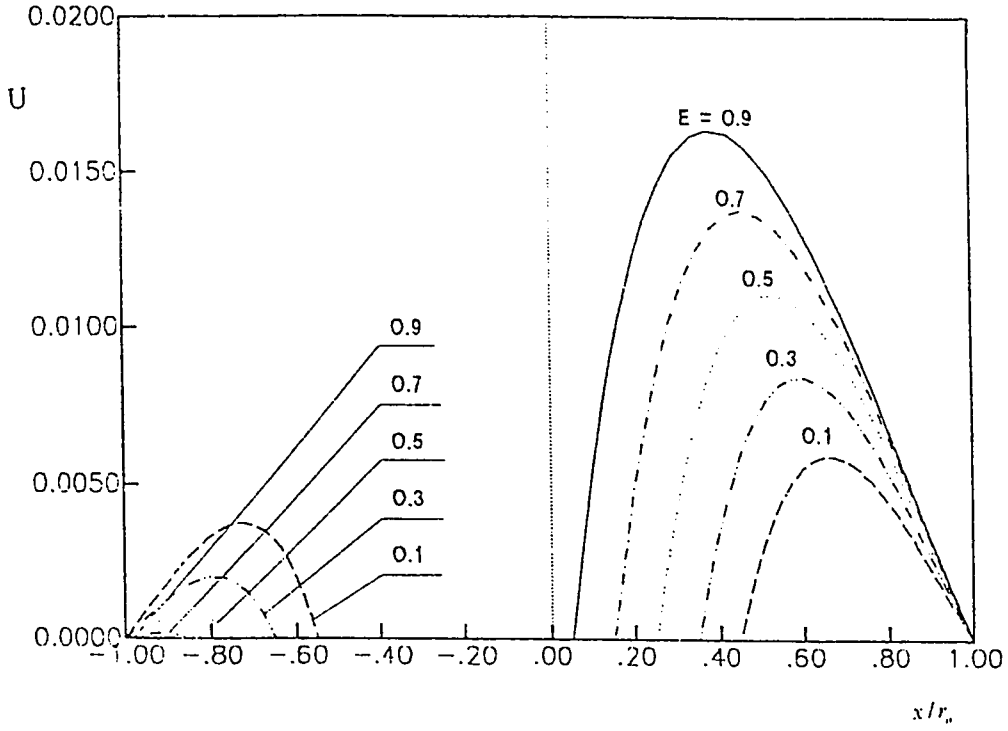


Fig. 6.16(a) : Fully-developed velocity profiles in the widest and narrowest sides of the gap in case 4.1.

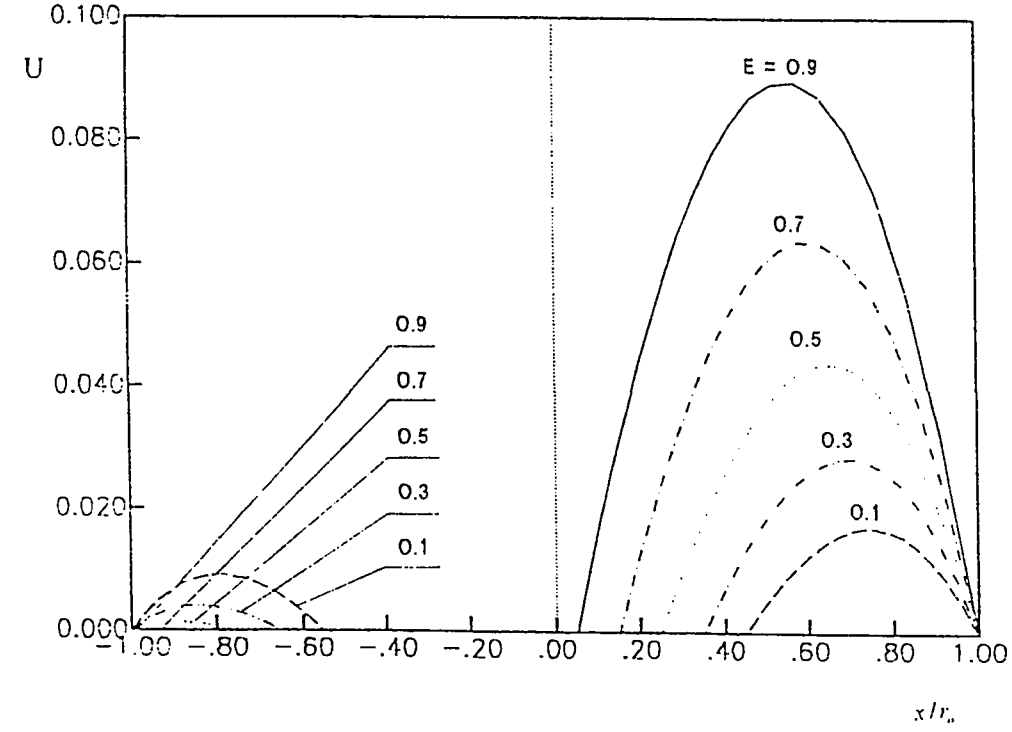


Fig. 6.16(b) : Fully-developed velocity profiles in the widest and narrowest sides of the gap in case 4.O.

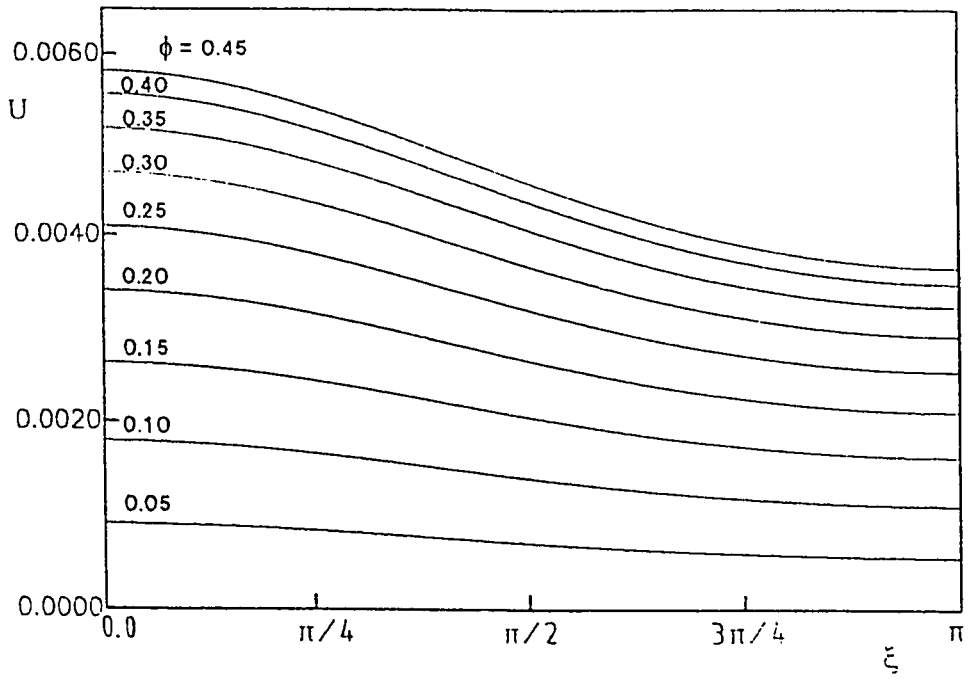


Fig. 6.17(a) : Variation of fully developed axial velocity with ξ at different values of ϕ ranges between 0.05 to 0.45, Case 4.I., E = 0.1

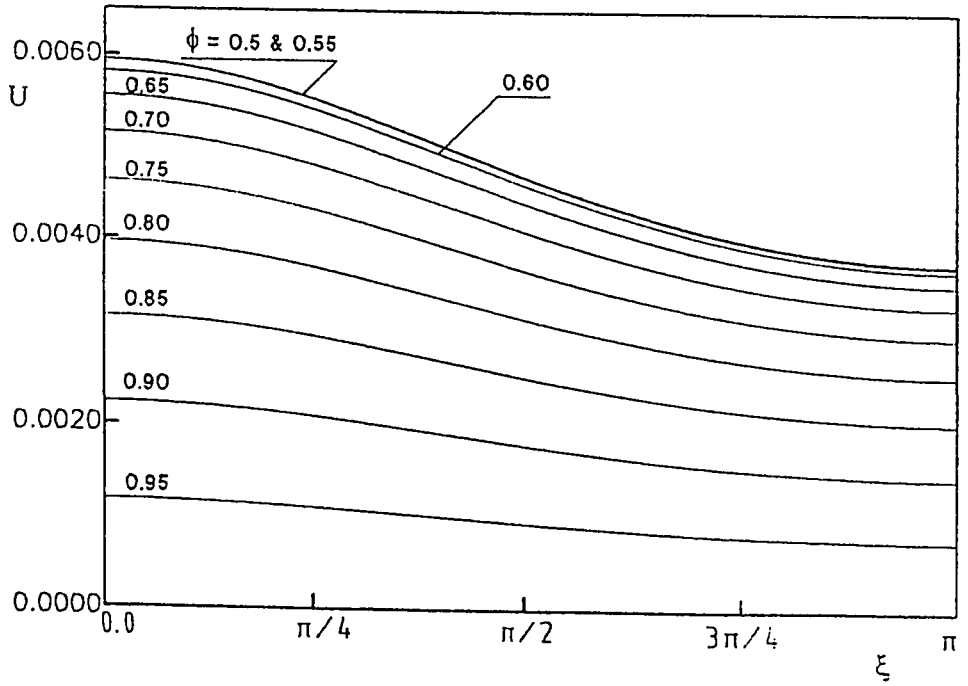


Fig. 6.17(b) : Variation of fully developed axial velocity with ξ at different values of ϕ ranges between 0.5 to 0.95, Case 4.I., E = 0.1

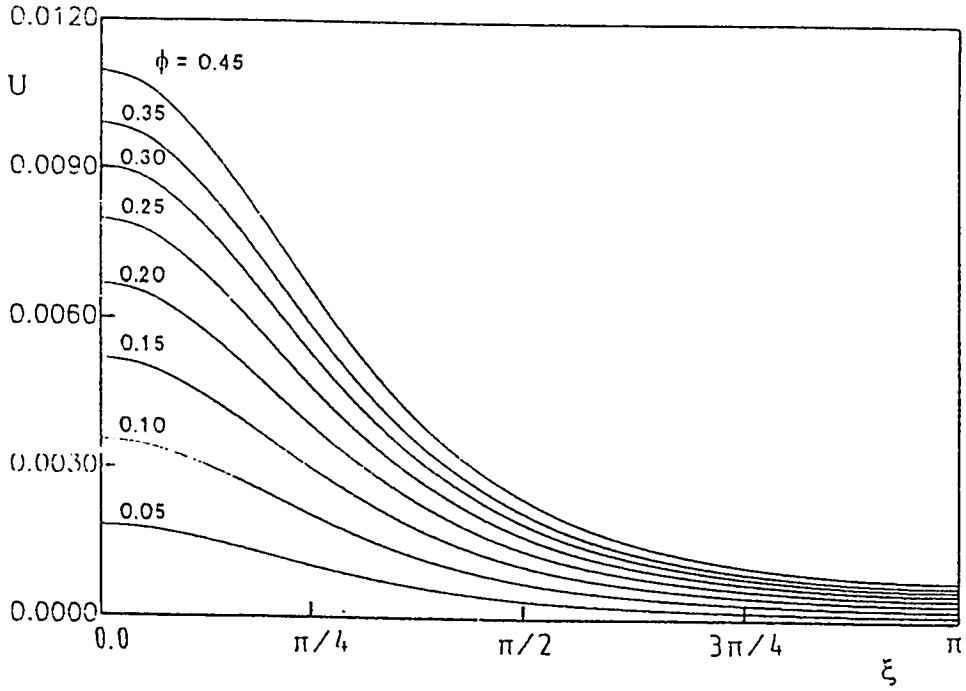


Fig. 6.17(c) : Variation of fully developed axial velocity with ξ at different values of ϕ ranges between 0.05 to 0.45, Case 4.I., E = 0.5

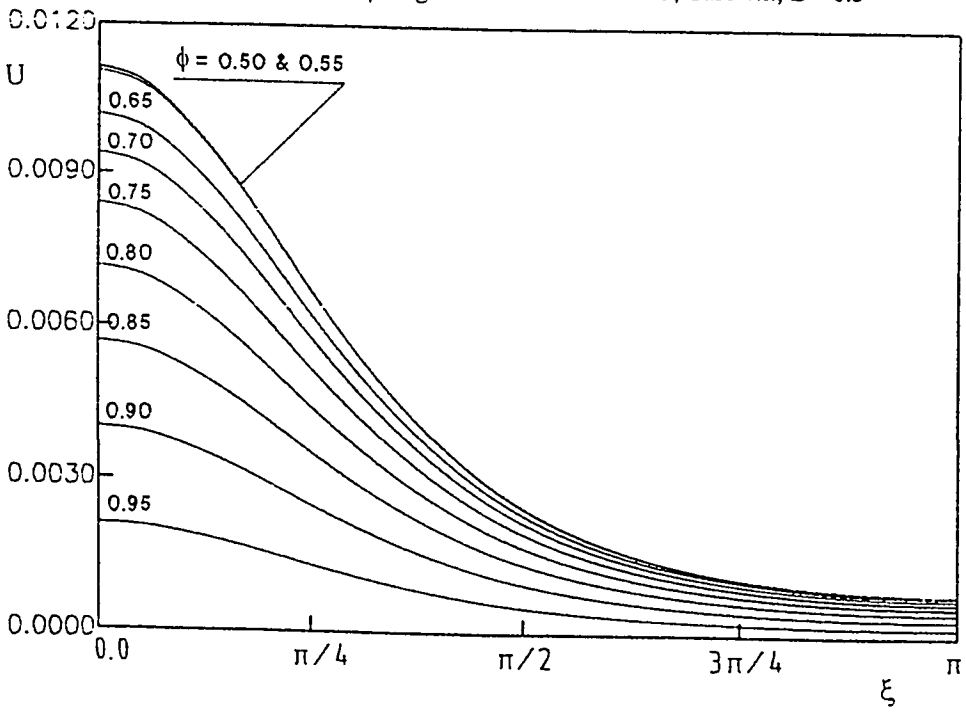


Fig. 6.17(d) : Variation of fully developed axial velocity with ξ at different values of ϕ ranges between 0.5 to 0.95, Case 4.I., E = 0.5

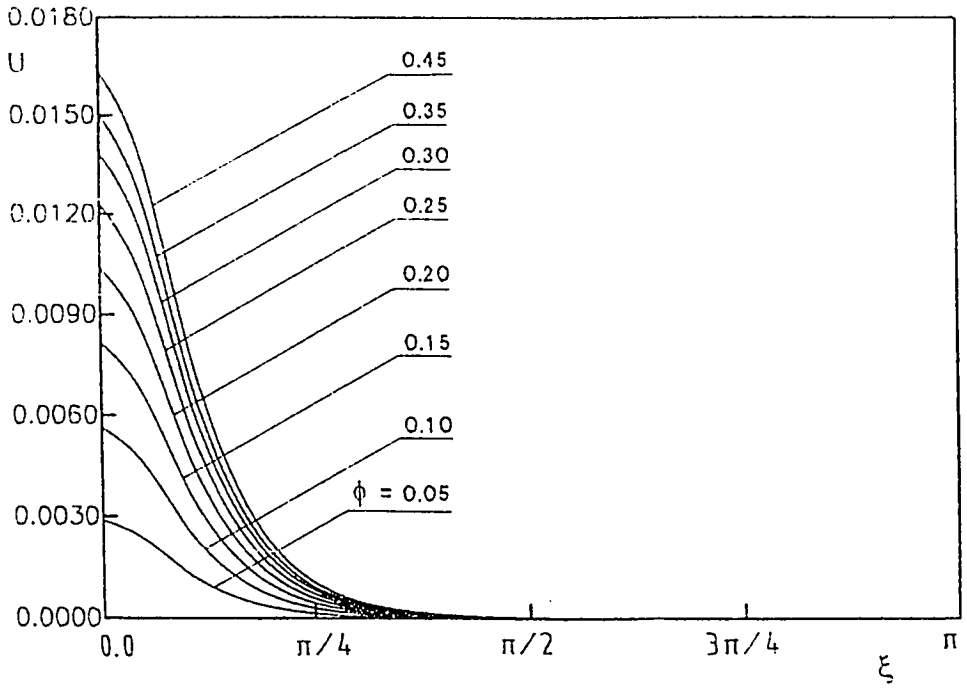


Fig. 6.17(e) : Variation of fully developed axial velocity with ξ at different values of ϕ ranges between 0.05 to 0.45, Case 4.I., E = 0.9

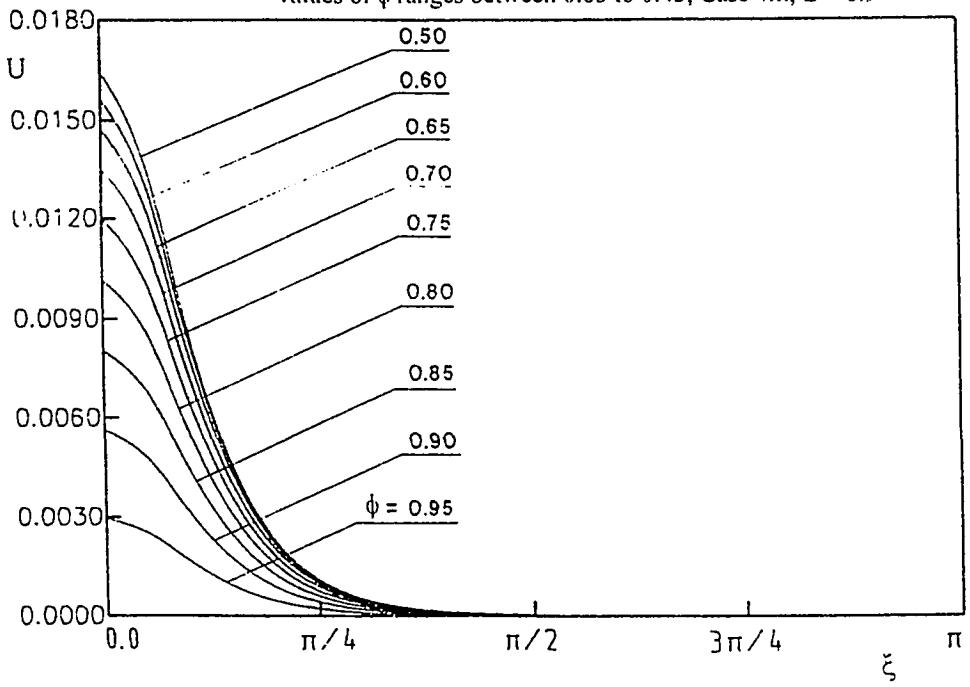


Fig. 6.17(f) : Variation of fully developed axial velocity with ξ at different values of ϕ ranges between 0.5 to 0.95, Case 4.I., E = 0.9

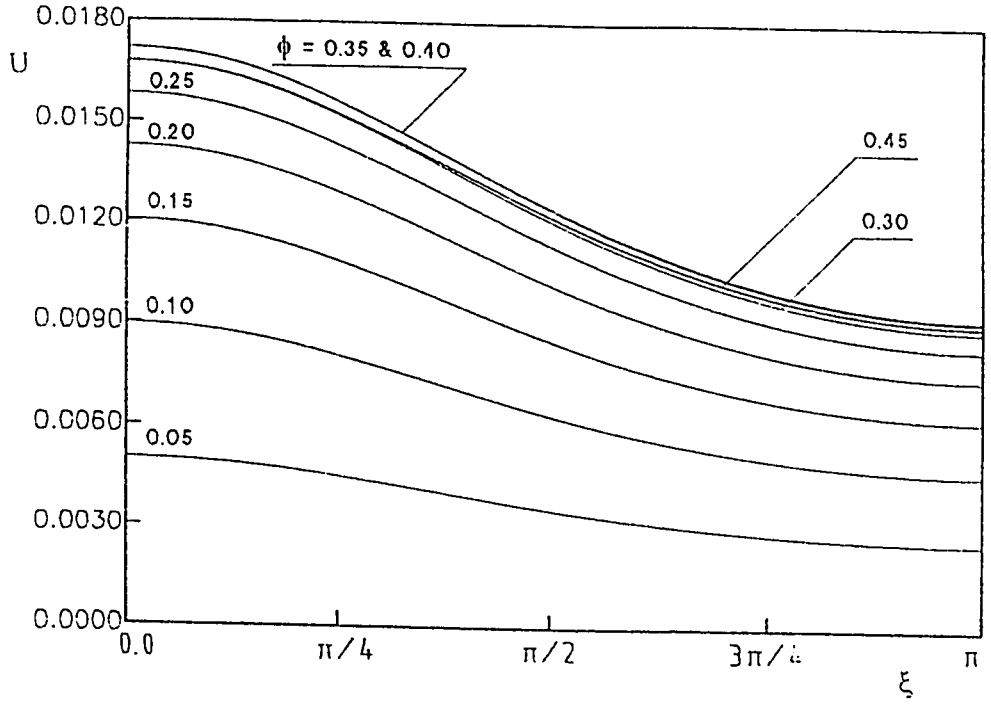


Fig. 6.18(a) : Variation of fully developed axial velocity with ξ at different values of ϕ ranges between 0.05 to 0.5, Case 4.O., E = 0.1

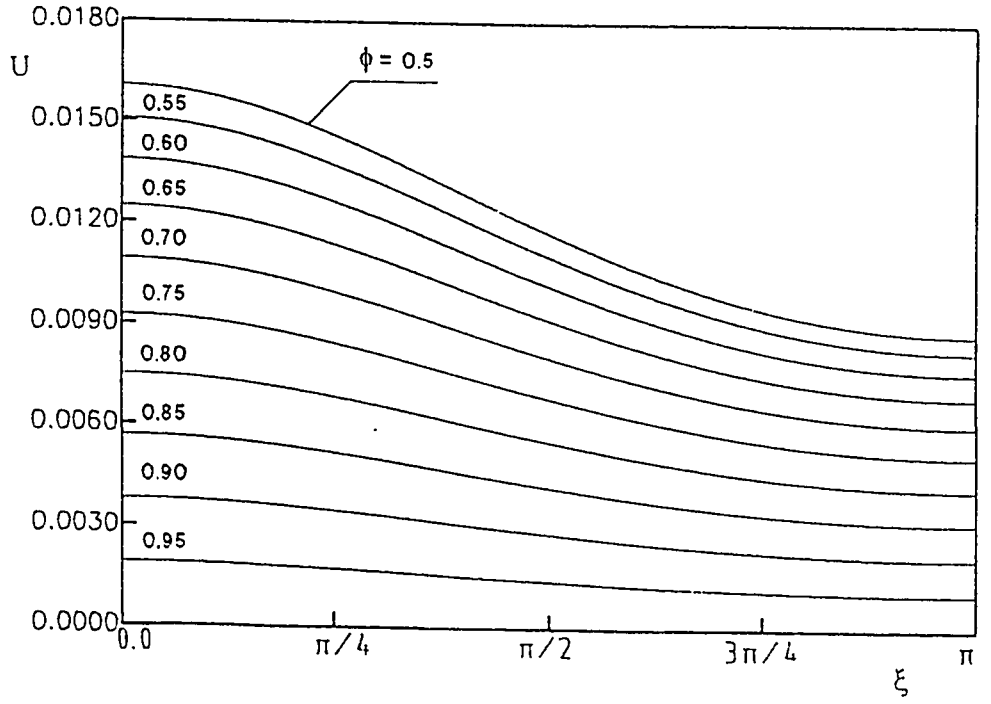


Fig. 6.18(b) : Variation of fully developed axial velocity with ξ at different values of ϕ ranges between 0.5 to 0.95, Case 4.O., E = 0.1

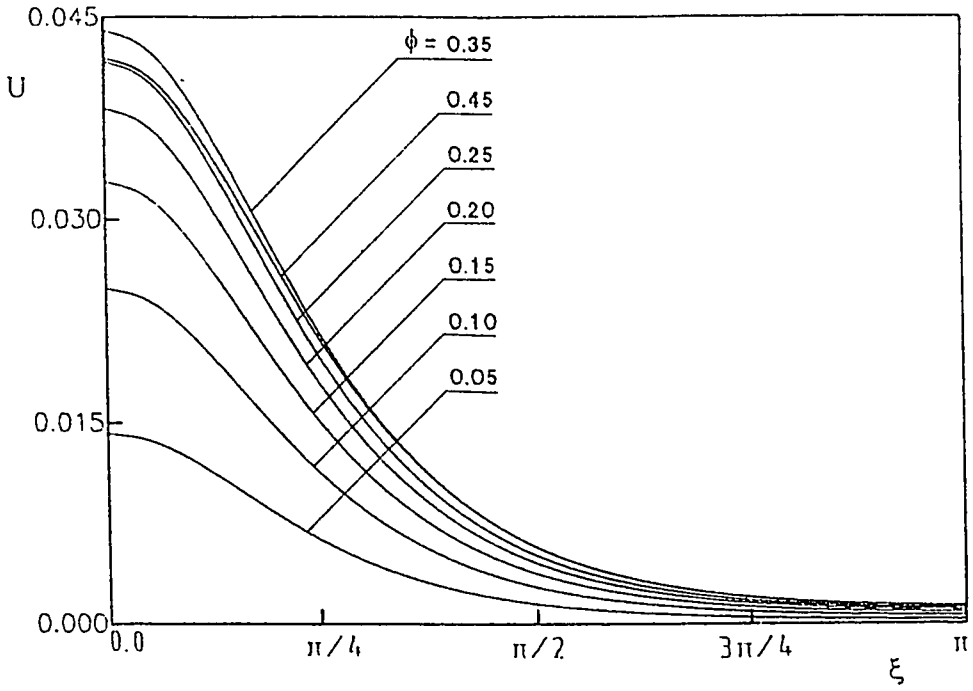


Fig. 6.18(c) : Variation of fully developed axial velocity with ξ at different values of ϕ ranges between 0.05 to 0.45, Case 4.O., E = 0.5

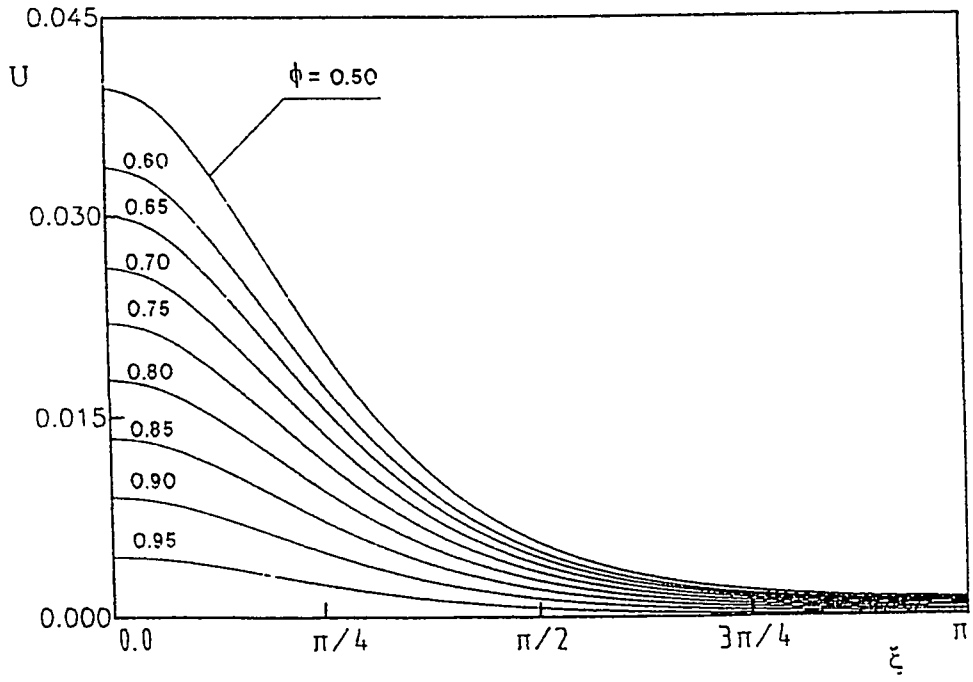


Fig. 6.18(d) : Variation of fully developed axial velocity with ξ at different values of ϕ ranges between 0.5 to 0.95, Case 4.O., E = 0.5

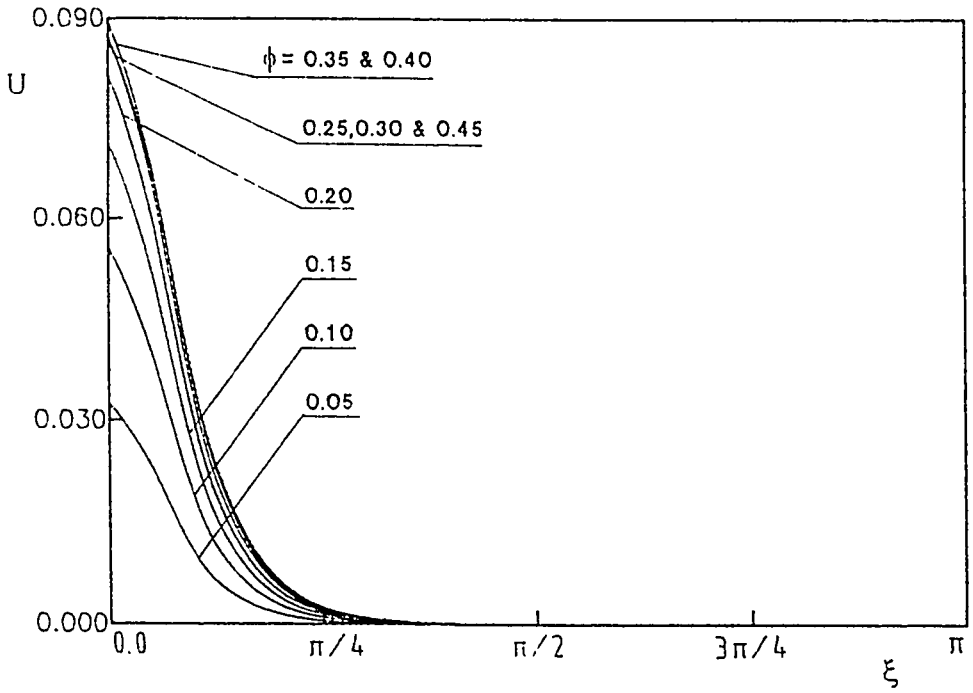


Fig. 6.18(e) : Variation of fully developed axial velocity with ξ at different values of ϕ ranges between 0.05 to 0.45, Case 4.O., E = 0.9

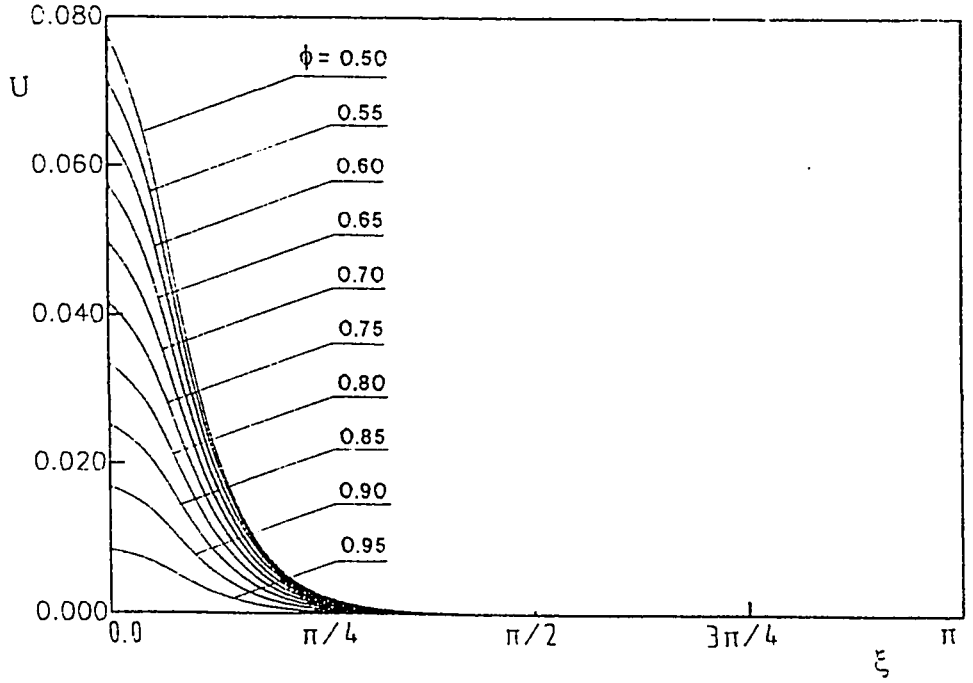


Fig. 6.18(f) : Variation of fully developed axial velocity with ξ at different values of ϕ ranges between 0.5 to 0.95, Case 4.O., E = 0.9

eccentricity (E), velocity profiles presented in Figs. 6.14 (a-f) and 6.15 (a-f) can be obtained by cross-plotting in Figs. 6.17 (a-f) and 6.18 (a-f), respectively.

As indicated before for case 1, the phenomenon of asymmetric axial-velocity profiles is attributed to the increase/decrease in the resistance to flow in the narrow/wide side of the annular gap as a result of eccentricity. The resistance to flow in the narrowest gap will always be larger than that in the widest gap because of higher velocity gradients in the former than the latter. Thus increasing the eccentricity (E) increases/decreases the values of U in the widest/narrowest side of the gap. However, a net result will be an increase in the average value $\bar{U}$ as will be shown later.

A comparison among the velocity profiles corresponding to case 4.I and 4.O is shown in Figs. 6.19(a) and 6.19(b). Figure 6.19(a) shows for a slight eccentric annulus (E = 0.1) this comparison as one rotates around the annulus from its widest gap side ( $\psi = \xi/\pi = 0$ ) to its narrowest gap side ( $\psi = 1$, i.e., $\xi = \pi$ ). To have more insight on the effect of the boundary conditions on the velocity profiles, Fig. 6.19(b) shows a comparison among the velocity profiles for case 4.I and 4.O with two values of eccentricity, namely E = 0.1 and E = 0.5, in the widest and narrowest sides of the annulus. As can be seen from Figs. 6.19 (a-b), in either case 4.I or 4.O, the heating of a boundary causes the velocity profiles to be skewed towards this boundary (i.e., shifts the point of maximum velocity from its location in the case of no heating towards the heated boundary, thus the maximum velocity point becomes remarkably closer to the inner wall in case 4.I). Moreover, these figures also show that, for a given E, the velocity profile

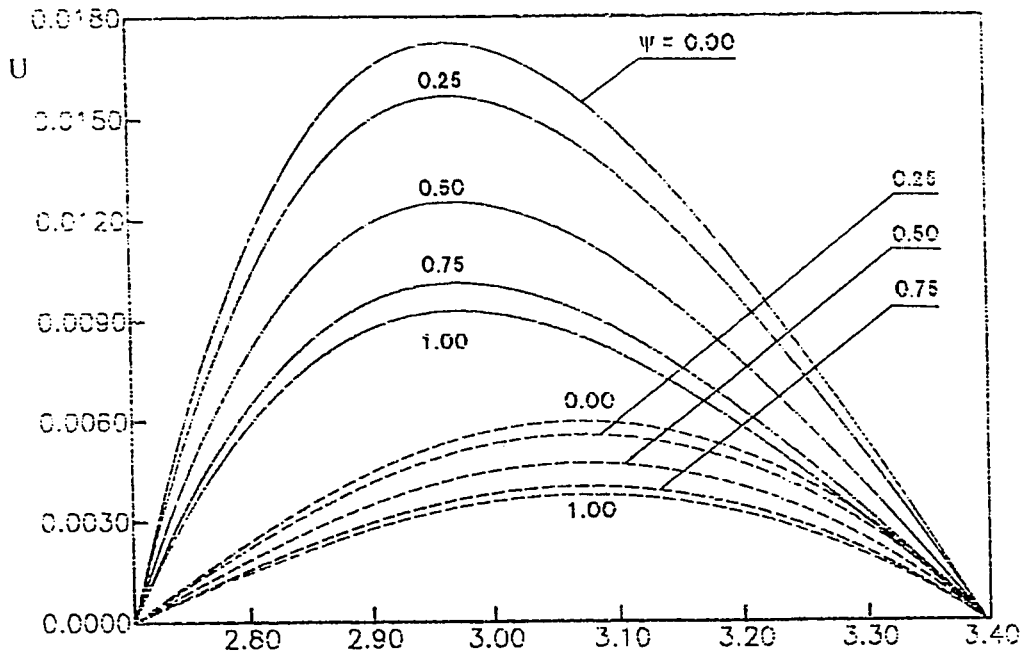


Fig. 6.19(a) : Comparison of the fully-developed velocity profiles, ------ case 4.O, —— case 4.I.

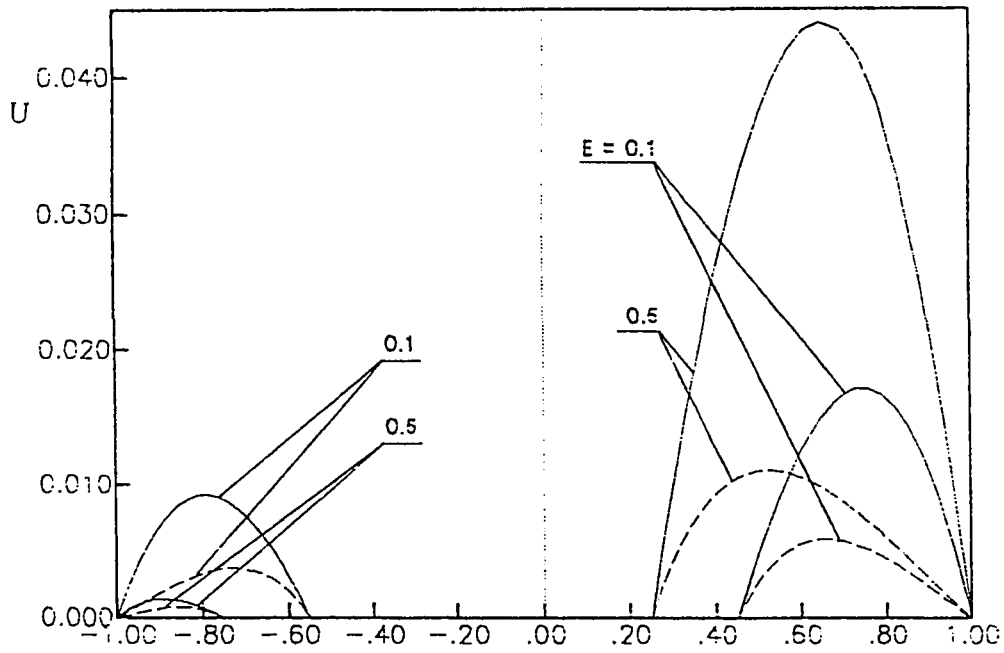


Fig. 6.19(b) : Comparison between velocity profiles at the line of symmetry for different values of eccentricity, —— Case 4.O, ------ Case 4.I.

has larger values in case 4.O than that in case 4.I. Thus larger induced volumetric flow rates are anticipated in case 4.O. This is attributed to the larger heating surface area in case 4.O when compared to that in case 4.I. Figures 6.19(a-b) and Figs. 6.7(a-b) show that for a given eccentricity (E), the effect of having the heated boundary on either the inner or the outer wall of the annulus is more pronounced for case 4 than that for case 1.

For some selected values of the dimensionless eccentricity (E), the circumferential variations of the local Nusselt number on the inner and outer walls of the annulus are presented for case 4.I in Fig. 6.20(a) and for case 4.O in Fig. 6.20(b). These figures show that, in general, the Nusselt number on the heat transfer wall is larger than that on the isothermal wall. Moreover, these two figures show that for large eccentricities the variation of the local Nusselt number with $\xi$ on the heat transfer wall has discontinuity. This discontinuity may be attributed to the nonuniform temperature distribution on the heat transfer wall, Fig. 6.13(c).

Due to this discontinuity of the variation of the Nusselt number along the heat transfer wall, a special formula has been used to evaluate the circumferentially-averaged Nusselt number on the heat transfer wall with a constant heat flux other than that used to evaluate the circumferentially-averaged Nusselt number on the isothermal wall. For the isothermal wall (either the outer wall in case 4.I or the inner wall in case 4.O) the circumferentially-averaged Nusselt number has been calculated by integrating the local Nusselt number along the pertinent wall from the following two equations;

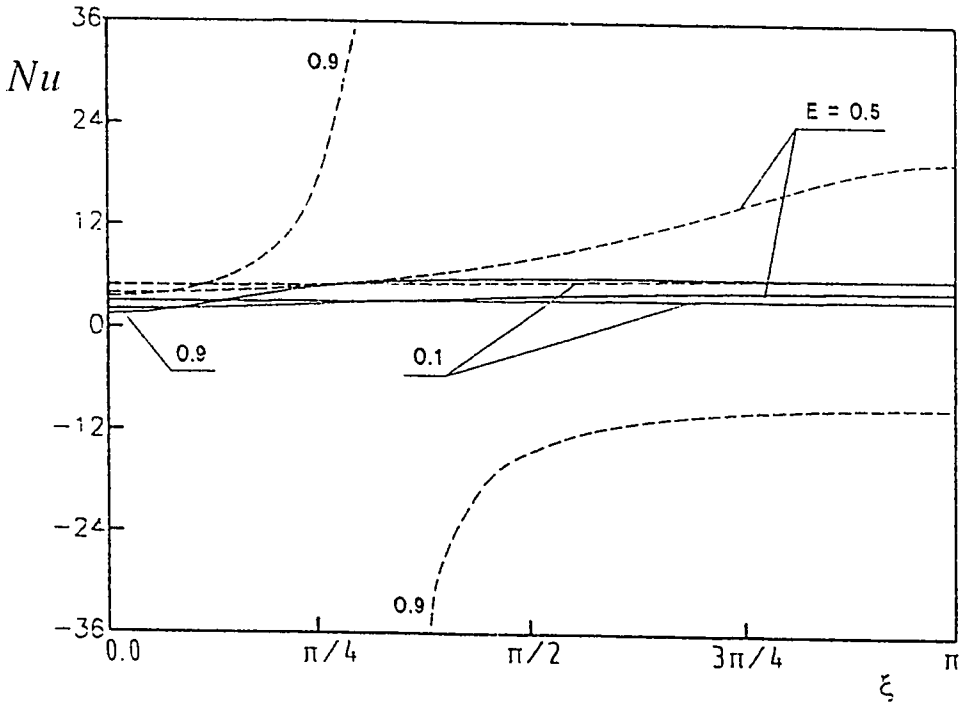


Fig. 6.20(a) : Variation of local Nusselt number around the circular arcs of the inner and outer walls in case 4.I, ------ inner wall, —— outer wall.

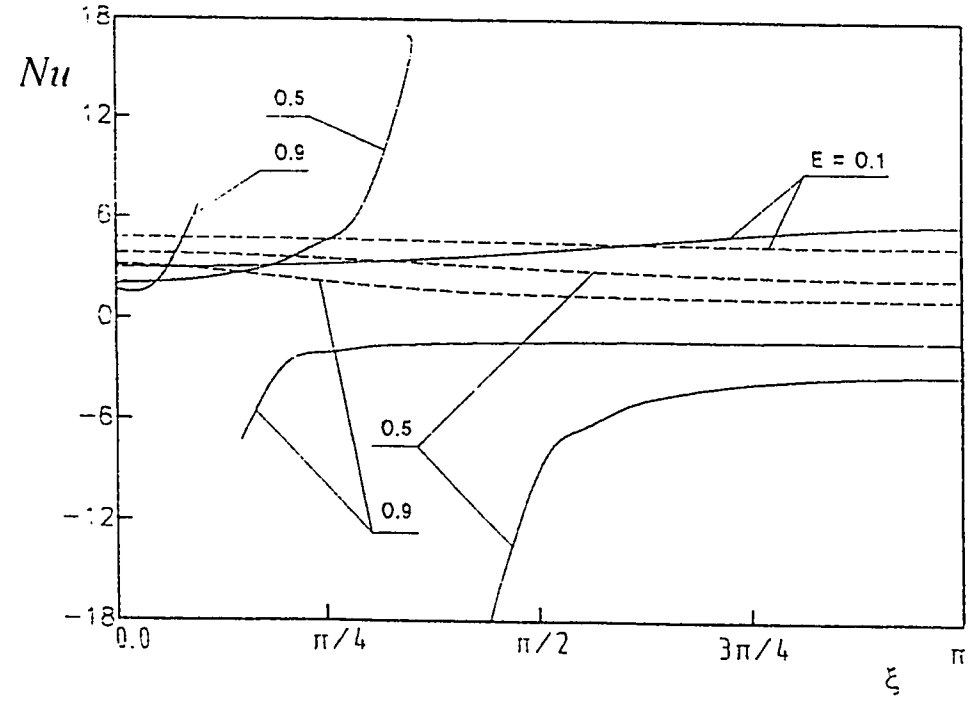


Fig. 6.20 (b) : Variation of local Nusselt number around the circular arcs of the inner and outer walls in case 4.O, ------ inner wall, —— outer wall.

**1 - On the inner wall**

$$\overline{Nu_y^{x.I}} = \frac{2(1-N)}{N\pi}\int_0^{\pi} (Nu_y^{x.I})H(\eta_i,\xi)d\xi \tag{6.9}$$

**2 - On the outer wall**

$$\overline{Nu_y^{x.O}} = \frac{2(1-N)}{\pi}\int_0^{\pi} (Nu_y^{x.O})H(\eta_i,\xi)d\xi \tag{6.10}$$

For the uniform heat flux wall the following equations have been used to calculate the circumfrentially-averaged Nusselt number;

**1 - On the inner wall**

$$\overline{Nu_i^{4.I}} = \frac{1}{\overline{(\theta_{iw})_c} - \theta_m} \tag{6.24}$$

**2 - On the outer wall**

$$\overline{Nu_o^{4.O}} = \frac{1}{\overline{(\theta_{ow})_c} - \theta_m} \tag{6.25}$$

These formulae (6.24 and 6.25) are based on the energy balance used by Trombetta [23]. This energy balance uses the temperature difference between the circumferential averaged wall temperature on the heat transfer wall and the fluid mean bulk temperature rather than the local temperature difference in the calculations of the heat transfer coefficient (Nusselt number). The circumferentially averaged temperature on the heat transfer wall has been calculated using the following two equations;

**1 - On the inner wall :**

$$\overline{(\theta_{iw})}_c = \frac{2(1-N)}{N\pi} \int_0^{\pi} \theta\,(\eta_i,\xi)\, H(\eta_i,\xi)\, d\xi \qquad (6.26)$$

**2 - On the outer wall :**

$$\overline{(\theta_{ow})}_c = \frac{2(1-N)}{\pi} \int_0^{\pi} \theta\,(\eta_o,\xi)\, H(\eta_o,\xi)\, d\xi \qquad (6.27)$$

The trapezoidal rule has been used to evaluate the above integrals. the variations of the circumferentially averaged Nusselt number with eccentricity (E) on the inner and outer walls have been plotted in Figs. 6.21(a) and 6.21(b) for case 4.I and 4.O, respectively. As can be seen from these two figures the circumferentially averaged Nusselt number on the heat transfer wall increases with the increase in eccentricity while that on the isothermal wall slightly decreases. These two figures show also that, through out the studied range of eccentricity (E = 0.1 - 0.9) the circumferentially averaged Nusselt number on the heat transfer wall is larger than that on the isothermal wall with only one exception for case 4.O and E = 0.1 where the opposite is true. This behavior of the circumferentially averaged Nusselt number on both of the inner and outer walls of the annulus can be attributed to the nature of the annular flow and the heat transfer (thermal boundary conditions) effects on both walls.

The annular flow requires the hydrodynamic boundary -layer on the inner boundary to be thinner than that on the outer boundary. However the heat transfer makes the flow faster /slower near the heat transfer/isothermal wall of the annulus. Consequently, the velocity profile will be more skewed inward with the maximum velocity closer to the inner wall in case 4.I and outwards with the maximum velocity

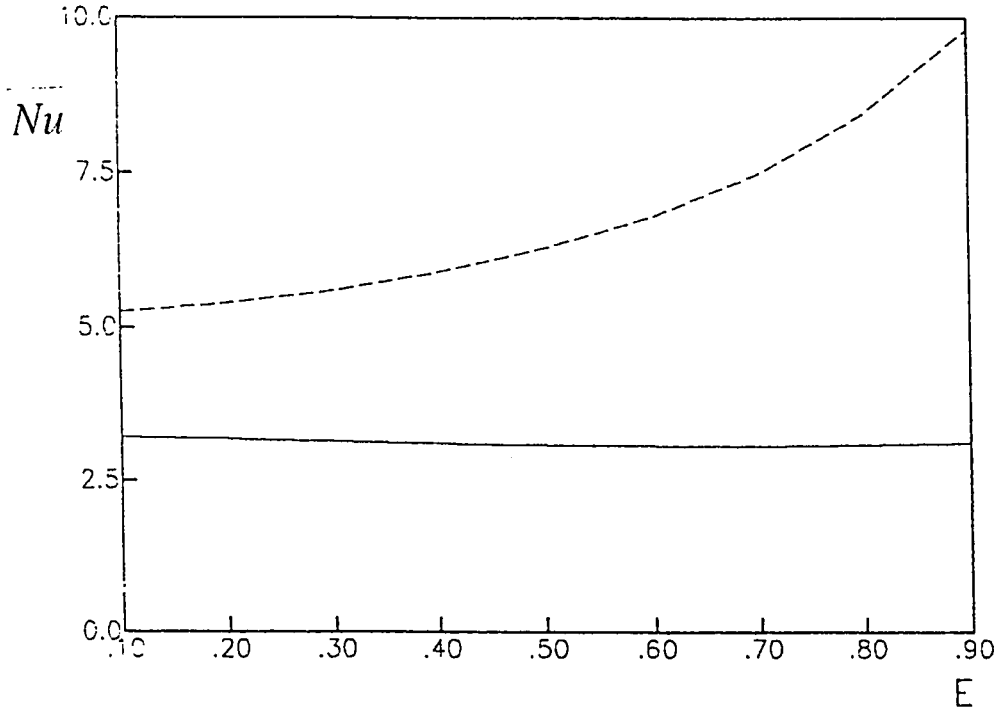


Fig.6.21(a) : Nusselt number averaged around the complete circular arcs of the inner and outer walls for case 4.I, ------ on inner wall, —— on outer wall

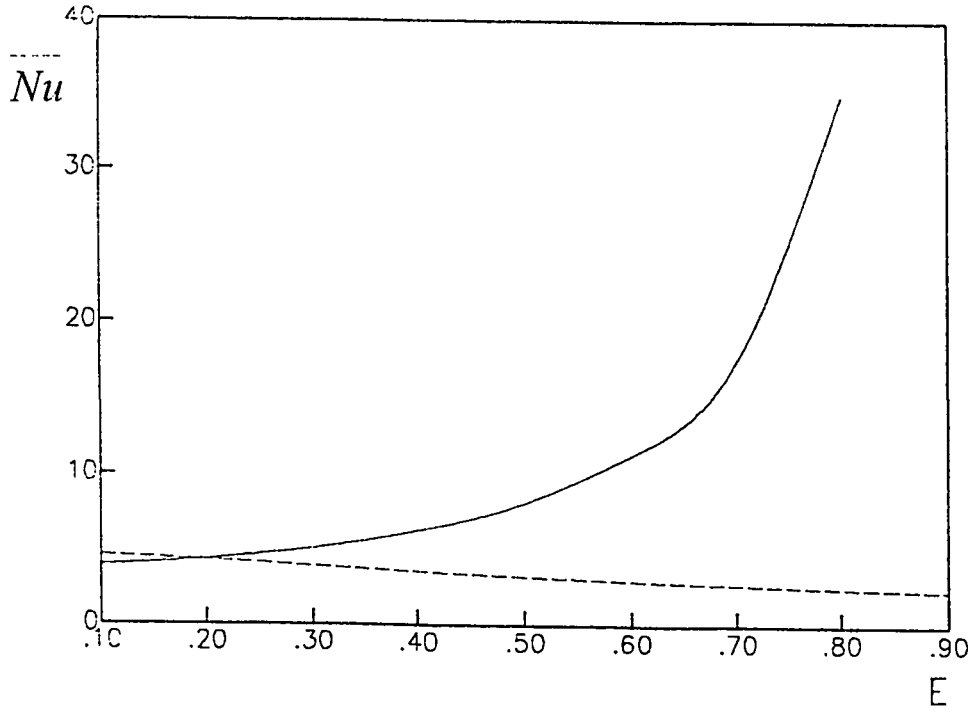


Fig. 6.21(b): Nusselt number averaged around the complete circular arcs of the inner and outer walls for case 4.O, ------ on inner wall, —— on outer wall

closer to the outer wall in case 4.O. Hence, in case 4.I (in which the heat transfer wall is the inner wall), the heat transfer and the nature of the annular flow work together make the hydrodynamic boundary-layer on the inner wall much thinner than that on the outer wall which results in having a larger Nusselt number on the inner wall compared to that on the outer wall. In case 4.O (in which the outer wall is the heat transfer wall), the heat transfer effect opposes that of the annular flow requirements. The latter makes the boundary-layer on the inner wall thinner than that on the outer wall which would result in having larger Nusselt number on the inner wall compared to that in outer wall. However, the former makes the flow faster/slower near the outer/inner wall of the annulus and hence makes the velocity profiles skewed outwards with the maximum velocity closer to the outer wall (i.e., thickening the hydrodynamic boundary layer developed on the inner wall) which results in a larger Nusselt on the outer wall than that on the inner wall. For low eccentricities the effect of the annular flow overcomes that of the heat transfer and the circumferentially averaged Nusselt number will be larger on the inner isothermal wall compared to that on the outer heat transfer wall for $E < 0.2$. However, for larger eccentricities the heat transfer will be dominant and the circumferentially averaged Nusselt number will be larger on the outer heat transfer wall than that on the inner isothermal wall. Again the increase in eccentricity increases/decreases the hydrodynamic resistance to the induced flow in the narrow/wide sides of the annulus since the velocity gradient is much steeper on the narrow side compared to that on the wide side. Hence, increasing the eccentricity increases the induced flow rate with the fact that the heat transfer makes the flow faster/slower near the heat transfer/isothermal wall which makes

the circumferentially averaged Nusselt number increases/decreases on the heat transfer/isothermal wall for both cases 4.I and 4.O.

As mentioned before, engineers are not frequently concerned with the details of the velocity and temperature fields but only with the induced flow rate and the maximum (in case of heating or minimum in case of cooling) bulk temperature which the fluid attains as it passes through the channel and reaches its exit cross-section ( $\bar{T}_m$ ). The latter can be used to calculate the heat gained or lost by the fluid from entrance up to the annulus exit ( $\bar{q}$ ). These two important engineering parameters ( F and $\bar{Q}$ ) are given in Figs. 6.22(a) and 6.22(b). Figure 6.22(a) gives the dimensionless volumetric flow rate ( F ) against the eccentricity E. For a given E, this flow rate is the maximum possible which the present vertical channel can engender under thermal boundary conditions of the fourth kind. In other words, since fully-developed flow conditions have already been achieved, a further increase in the channel height would not produce any additional flow rate. As shown in Fig. 6.22(a), increasing the eccentricity E causes a pronounced increase in F in case 4.O and a slight increase in case 4.I. Moreover, flow rate in case 4.O is larger, for a given E, than the corresponding value in case 4.I. This is a result of the larger heating surface in the former case than the latter.

Under thermal conditions of the fourth kind, the fully developed $\theta$ and hence $\theta_m$ do not vary with axial distance Z. The bulk temperature $\theta_m$ does not change with further increase in the channel height since, under fully-developed flow conditions, the heat

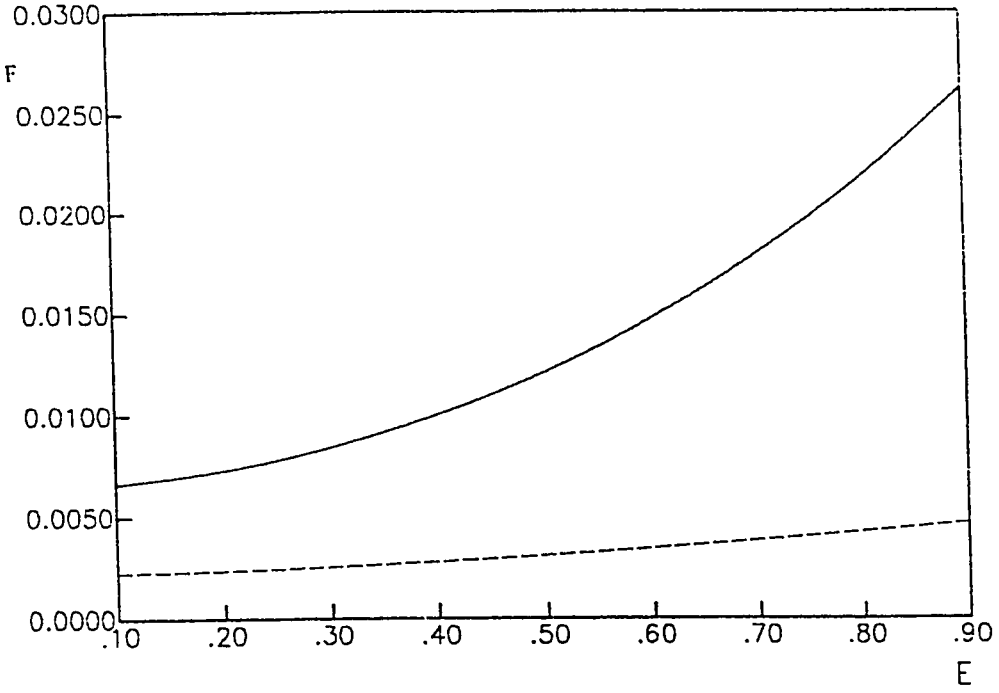


Fig. 6.22(a) : Induced volumetric flow rate versus eccentricity, ----- case 4.I,

—— case 4.O.

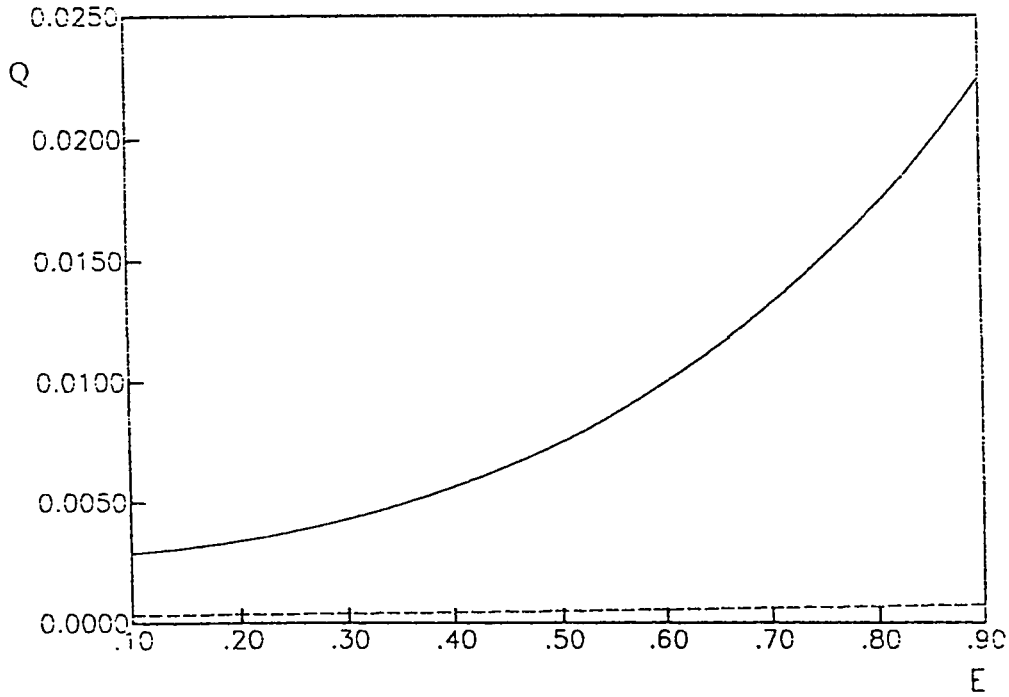


Fig.6.22(b) : Total heat absorbed by fluid versus eccentricity, ----- case 4.I,

—— case 4.O.

passes through the fluid from one wall to the other in such a manner as if the fluid were stationary, i.e. by pure conduction through laminar fluid layers. Thus, for a given E, the computed fully-developed value of $\theta_m$ corresponds also to the fluid bulk temperature at the channel exit $\bar{\theta}_m$ ( i.e. $\theta_m = \bar{\theta}_m$ ). The computed values of $\bar{\theta}_m$ and F are used to obtain $\bar{Q}$ ( = $F\,\bar{\theta}_m$ ) which is presented in Fig. 6.22(b). Thus the total heat gained or lost by the fluid from entrance up to the channel exit, including the neglected developing length, is obtained without need to integrate the Nusselt numbers over the channel height.

# Chapter 7

# RESULTS AND DISCUSSION FOR DEVELOPING LAMINAR FORCED CONVECTION IN ECCENTRIC ANNULI

## 7.1 Introduction

Forced convection heat transfer in eccentric annular channels occur in many situations in the electric, nuclear, solar and other fields. In the electric field, cooling of the underground electric transmission cables is affected by the position of the cable within its outer housing ( Abdulhadi and Chato [1] ). In the nuclear field and double-pipe heat exchangers the interest in eccentricity arises because of the misalignment which might occur during the assembly process or due to manufacturing tolerances. In parabolic-cylindrical solar collectors, the eccentricity between the circular receiver tube and its glass envelop, which are supposed to be situated along the focal line of the parabolic reflector, would indeed affect the heat transfer in this system. In the

aforementioned and many other practical situations, the manufacturing tolerances and operating conditions can introduce eccentricities in nominally concentric annuli.

The developing laminar flow and heat transfer in the limiting case of concentric annular passages have been investigated by many investigators as summarized in Chapter 2. On the other hand, a thorough search of the literature has revealed that only two papers by Feldman et al. [6,7] have dealt with the problem of forced convection in the entry-region of eccentric annuli with simultaneously developing hydrodynamic and thermal boundary layers. In these two papers, the order of magnitude analysis used to derive their boundary-layer models has caused a reduced form of the axial (streamwise) momentum equation to remain while the other two transverse momentum equations drop. Thus their hydrodynamic boundary-layer model comprised only two equations, namely, the aforesaid reduced axial momentum equation and the continuity equation. However, since there are three unknown components of the velocity in addition to the pressure, their 2-equation boundary-layer model do not form a complete mathematical model. Consequently, additional assumptions regarding the transverse flows in the entry-region of the eccentric annular duct were used to facilitate a complete mathematical model and then a numerical solution. These assumptions depend on a relation between the two transverse velocity components in which a constant has to be arbitrarily chosen.

The present work presented in Chapter 3 a mathematically self-independent model for the problem under consideration, i.e. a model capable of describing the forced flow and convection heat transfer in the entry-region of eccentric annuli without need of assumptions dependent on prior knowledge of the mechanism of transverse flows in

such a region. The numerical algorithm which has been developed to solve the obtained model was presented in Chapter 4. In this chapter, numerical results will be presented for the developing velocity profiles, axial variation of pressure, and heat transfer parameters under one thermal boundary condition; namely, case 1.I in which the inner wall is isothermally heated while the outer wall is maintained at inlet fluid temperature ($T_o$). The main objective of these results is the validation of the present model and computer code which will be used in the next chapter to solve the free convection problem.

For a fluid of a given Pr flowing in an annulus of given N and E, numerical solution of the finite-difference equations (4.22 - 4.25) is obtained by first calculating the corresponding values of $\eta_i$ and $\eta_o$ by means of the pertinent relations given in Chapter 4 (eqs. (4.14) and (4.15)) . By selecting the numbers of increments in $\eta$ and $\xi$ directions ( n and m, respectively) the values of $\Delta\eta$ and $\Delta\xi$ can be computed, respectively. For a given axial location (cross-section), the linearized finite-difference equation (4.23) and the integral continuity equation (4.26) are two equations in the two unknowns U and P. These two equations can be solved at the first axial step next to the entrance cross-section as follows. Applying eq. (4.26) throughout the second cross-section, applying eq. (4.23) at each interior node of the numerical grid (i.e., with $i = 2, 3, \ldots, n-1, n$ and $j = 1, 2, 3, \ldots, m, m+1$ ) and taking into consideration the boundary conditions (i.e., $U_{1,j} = U_{n+1,j} = 0$, $W_{i,0} = - W_{i,2}$ and $W_{i,m+2} = - W_{i,m}$ ), one obtains [ $(n-1) \times (m+1) + 1$ ] simultaneous linear algebraic equations in the same number of unknowns ( $U_{2,1}$, $U_{3,1}, \ldots, U_{n,1}, U_{2,2}, U_{3,2}, \ldots, U_{n,2}, U_{2,3}, U_{3,3}, \ldots, U_{n,3}, \ldots, U_{2,m+1}, U_{3,m+1}, \ldots$,

$U_{n,m+1}$ and P). Solving these equations by means of any matrix inversion technique, one gets the unknown values of Us and P at all points of the second cross section; in the present work a special form of Gauss-Jordan elimination scheme ( El-Shaarawi [74] ) was used. Now, the linearized finite-difference eq. (4.24) is applied at each interior node to give *(n-1) x (m+1)* simultaneous linear algebraic equations which when solved give the unknown values of $W$ at this second cross section ; Gauss-Seidel iteration scheme ( Carnahan et al. [77] ) has been used in the present work. Now, eq. (4.22) can be used to obtain the unknown values of $V$ at all interior nodes then the application of eq. (4.25) results in the unknown values of $\theta$ at this second cross-section. Repeating this procedure, one can advance axially downstream along the annulus until the flow becomes fully developed.

All the results to be presented in this chapter have been obtained using a grid of 20 segments in the $\eta$-direction and 20 segments in the $\xi$-direction. Thus, for each axial step, 400 (19x21 + 1 = 399 +1) equations have to be solved to obtain the values of U and P then 399 equations have to be solved for each of W and $\theta$, consecutively. This required about 35 CPU seconds per one axial step on a main frame computer of WF 77 sys D type. On the other hand, for the entrance region flow, the boundary-layer equations (3.33-3.36) become asymptotically exact (i.e. identical to the original Navier-Stokes equations of motion (3.9-3.13)) as the flow moves away from the entrance. This is because (1) as the flow moves away from the entrance, it approaches full development and , hence, the diffusion of momentum and heat in the flow direction ( which have been neglected by boundary-layer assumptions ) becomes vanishingly small, and (2) the

inertia terms gradually vanish. Thus, as a result of this second reason, it is expected that the adverse effect of linearization of the inertia terms and the convection terms on the left hand sides of eqs. (4.23-4.25) will be reduced as the flow moves away from the entrance. Therefore, the results to be presented in this chapter have been obtained by using very small axial steps near the entrance ( $\Delta Z = 10^{-7}$ and $10^{-10}$ for N = 0.5 and 0.9, respectively) then the axial step was increased several times as the flow moves downstream to reach a value no more than $\Delta Z = 10^{-3}$.

## 7.2 Results and Discussion

Due to the neglect of the axial diffusion of momentum, the Reynolds number is inherent in the dimensionless formulation of the problem and thus it is not explicitly needed for the solution. However, three other similarity parameters are explicitly required to solve the problem under consideration. These are the annulus radius ratio (N), the dimensionless eccentricity (E), and the Prandtl number (Pr). Computations were carried out for a fluid of Pr = 0.7 in annuli of N = 0.5 and 0.9. The radius ratio 0.5 was chosen since it represents a typical annular geometry with its value of N far enough from unity (N = 1 ) which represents the case of parallel plate channel. Moreover, some of the heat transfer results presented by Feldman et al. [7] are for this particular radius ratio (N=0.5). These results provide a means of verification of the present computer code and can also be used to compare the present model with the 2-equation boundary-layer model of Feldman et al. [6,7].

Figure 7.1(a) shows examples of the developing axial velocity profiles in the widest and narrowest sides of the gap of an annulus of N = 0.5 and E = 0.5. Each of Figs. 7.1(b) through 7.1(f) gives the developing axial velocity distribution (U versus Z) for a given value of $\xi$ as one rotates around this annulus from its widest side ( $\psi = \xi = 0$ ) to its narrowest side ($\psi = 1$, i.e., $\xi = \pi$ ). It can be seen from Fig. 7.1(a) that, since the eccentricity increases/ decreases the resistance to flow on the narrowest / widest gap side of the annulus, the initially uniform axial velocity profile at the annulus entrance develops with increasing / decreasing values on the widest / narrowest gap side of the annulus as the flow moves away from the entrance. Such a development continues until *U* reaches its invariant fully-developed axial-velocity profile. Velocity profiles similar to those presented in Fig. 7.1(a) could be obtained, for any axial location (*Z*) and a specified value of $\xi$, by cross plotting in Figs. 7.1(b-f). In each of these latter figures, at least eight curves corresponding to some selected values of the normalized $\eta$- coordinate ($\phi$) are drawn. These figures (7.1(b) through 7.1(f)) focus on the entry region before the flow reaches full development. The profiles shown in Fig. 7.1(a) or the distributions given in Figs 7.1(b-f), show that at the early stages of the axial velocity development (small values of *Z*) fluid adjacent to the annulus two walls ( e.g. $\phi$ = 0.05 and 0.95) decelerates due to the formation of the two hydrodynamic boundary-layers on these two boundaries. Consequently, as a result of continuity principle, fluid outside these two boundary-layers ( e.g. $\phi$ = 0.4 or 0.5 ) accelerates. However, due to the increased resistance to flow in the narrow side of the annulus ( as a result of eccentricity ) the fluid on this narrow gap side moves in a tangentially-like direction ( in $\xi$-direction with a

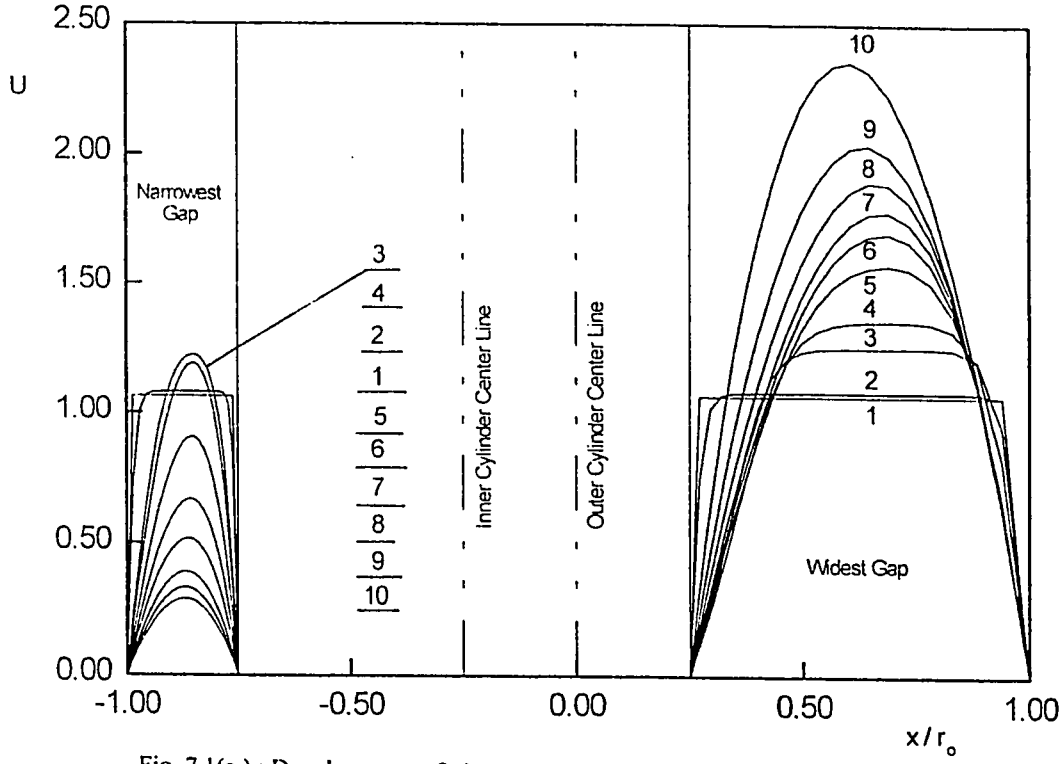


Fig. 7.1(a ) : Development of the axial velocity profiles, N = E = 0.5. The numbers on the profiles indicate the following values of $Z \times 10^4$: (1) $10^{-3}$, (2) 0.6, (3)12, (4)17, (5) 67, (6)117, (7) 167, (8) 267, (9) 467, (10) 2167 (fully developed).

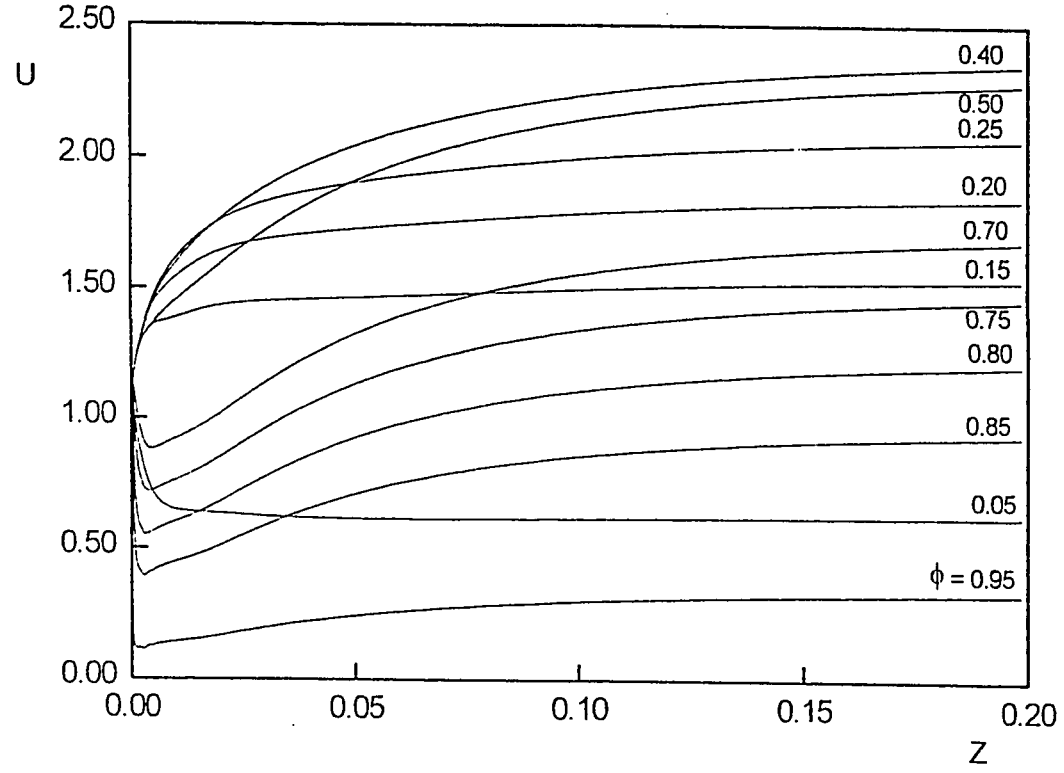


Fig.7.1(b) : Axial velocity development at $\psi = 0.0$ (widest gap). N = E =0.5 .

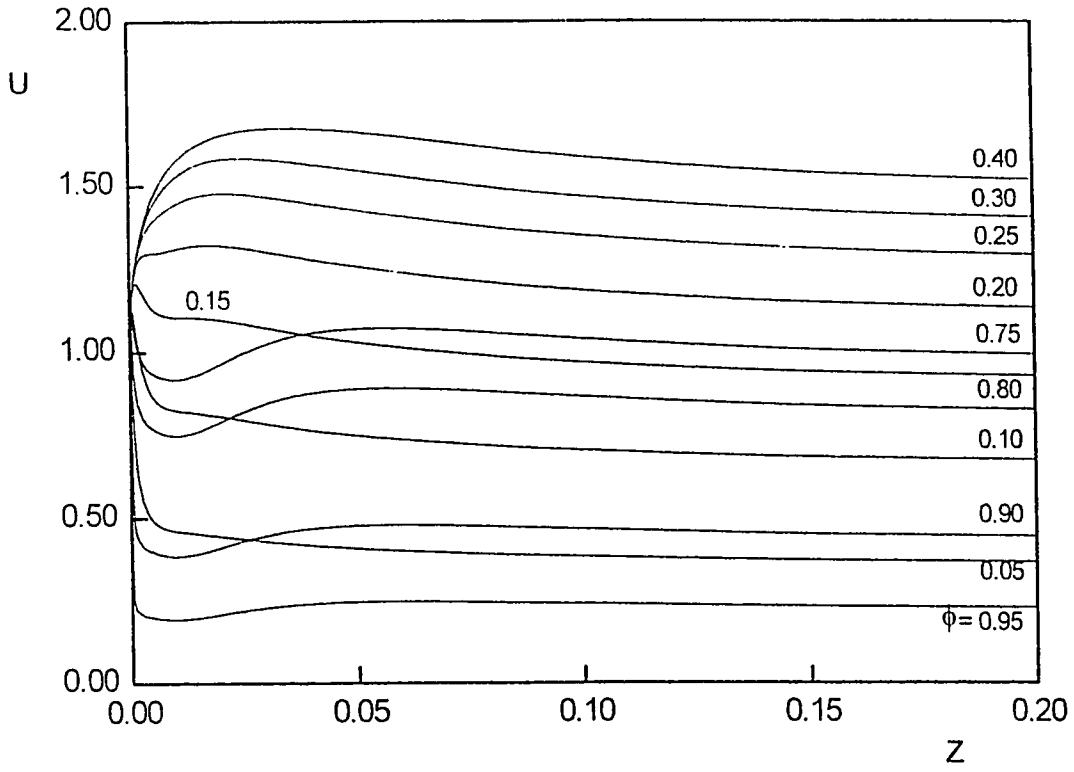


Fig. 7.1(c) : Axial velocity development at $\psi = 0.25$, N = E =0.5 .

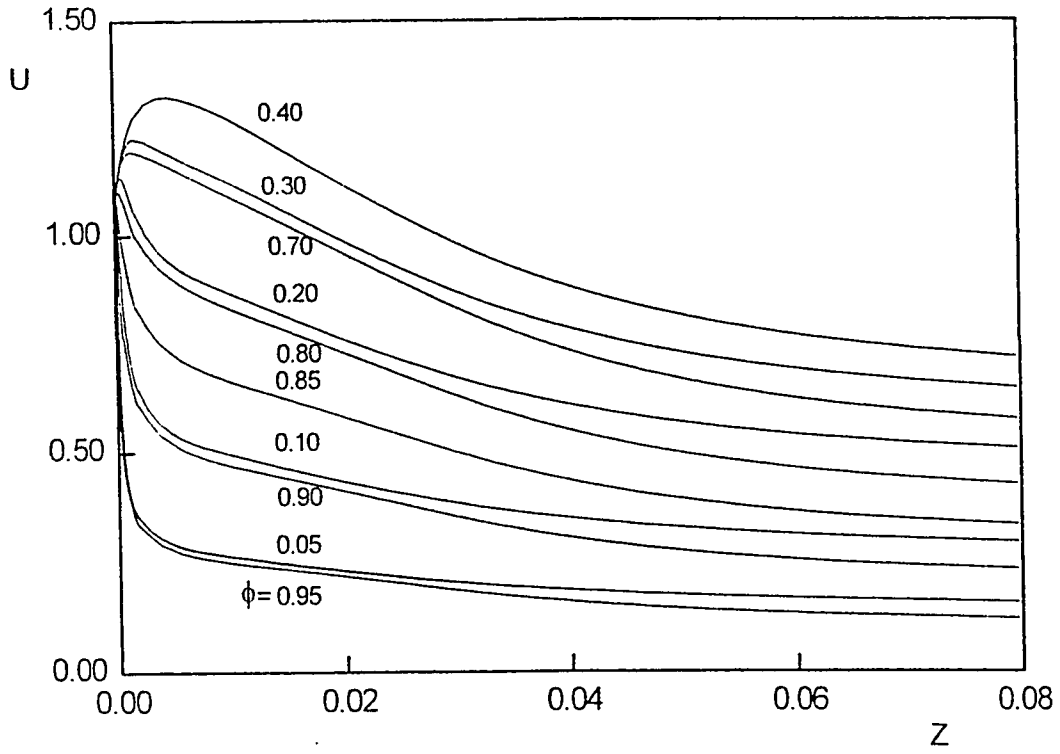


Fig. 7.1(d) : Axial velocity development at $\psi = 0.50$, N = E =0.5 .

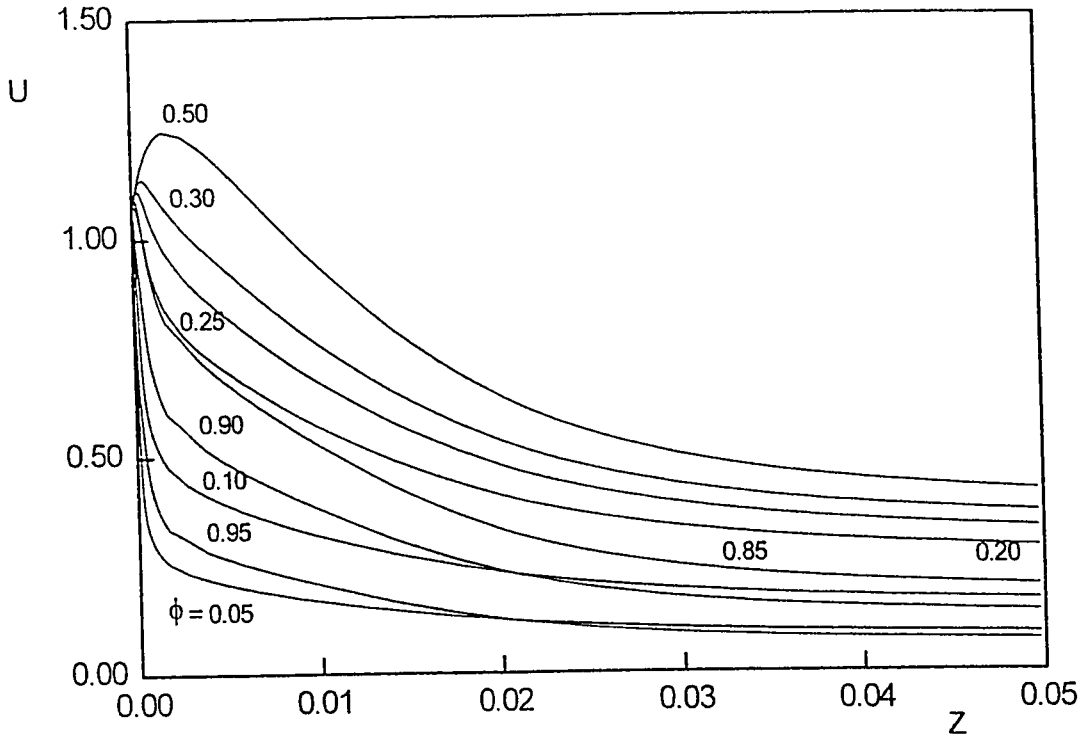


Fig. 7.1(e) : Axial velocity development at $\psi = 0.75$, N = E =0.5 .

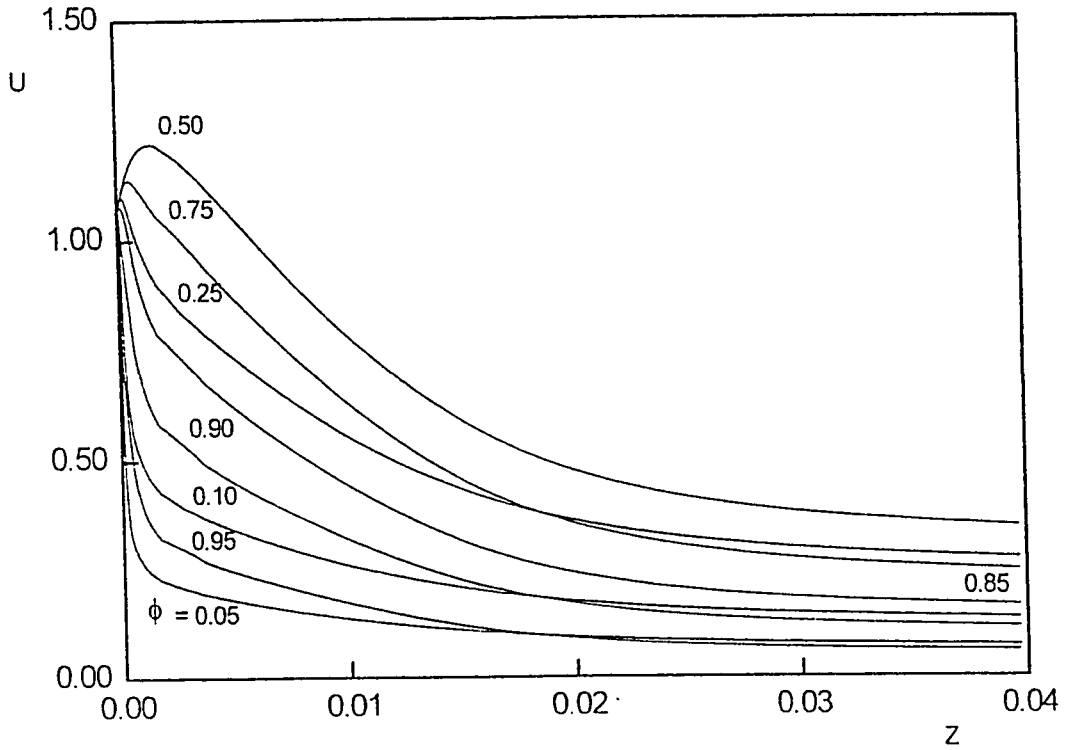


Fig. 7.1(f) : Axial velocity development at $\psi = 1.0$ (narrowest gap), N = E =0.5.

velocity component $W$ ) to the wide gap side of the annulus. Such a tangentially-like fluid transportation from the narrow gap side to the wide gap side increases as the flow moves away from the entrance ( Z increases ) and thus causes a reduction in the values of the axial velocity profile on the narrow gap side and vice versa on the wide gap side. However, far enough from the entrance such a tangential-like transportation decays as the flow approaches hydrodynamic full-development with V = W = 0.

Thus, the acceleration of fluid outside the developing boundary layers on the widest gap side of the annulus is created by (1) transportation of fluid from inside these two boundary layers by means of the V-component of velocity and (2) transportation of fluid from the narrowest gap side of the annulus by means of the W-component of velocity. On the other hand, the fluid outside the two developing hydrodynamic boundary layers on the narrowest gap side of the annulus undergoes two counteracting actions, namely, acceleration due to fluid transportation from inside these two boundary layers by means of the V-component of velocity and deceleration engendered by transportation of fluid from the narrowest gap side to the widest gap side by means of W-component of velocity. The latter action overcomes the first as the flow moves downstream the entrance cross-section and hence the resultant effect creates decreasing values of the axial velocity component on the narrowest gap side of the annulus. However, both actions gradually decay with further increases in the axial distance Z and finally vanish when the flow becomes hydrodynamically fully developed.

The axial velocity distributions given in Figs. 7.1(b) through 7.1(f) indicate also how the eccentricity makes the profile asymmetric; other unpresented results show that

the velocity profiles become more asymmetric as the eccentricity increases. Differences in the velocity at different angular locations ($\psi$), and over the cross section at any angular location, become more pronounced with increasing eccentricity. Such asymmetry will be reflected on the other two velocity components ( V and W). Examples of the widest-gap profiles of the $\eta$-velocity component corresponding to some selected values of the eccentricity E are shown in Figs. 7.2(a) and 7.2(b) for values of $Z = 0.6 \times 10^{-4}$ and $Z = 7 \times 10^{-4}$ in annuli of radius ratio N = 0.5 and 0.9, respectively. These figures clarify the effect of the eccentricity E on the V-profiles. Values of $\phi = 1.0$ and 0.0 represent the inner and outer walls of the annulus, respectively. However, the value of $\phi = 0.5$ does not represent the mid gap in the physical plane. Negative values of V mean in the opposite direction of increasing $\eta$, i.e., from the inner cylinder to the outer cylinder and vice versa.

It is worthy of note that E = 0.0 can not be used for calculations in bipolar coordinates as it represents a singularity for the transformation equations from the Cartesian to bipolar coordinates. However, the results obtained by the present computation for $E = 10^{-6}$ in an annulus of N = 0.9 were found to be in excellent agreement with those of the concentric case ( E = 0.0 ) given by Coney and El-Shaarawi [61]. This provided a check on the adequacy of the present algorithm and computer code.

Examples of the developing tangential-like velocity component (W) near the widest-gap side of the annulus ( $\psi = 0.05$ ) are presented in Figs. 7.3(a) and 7.3(b) for N = 0.5 and 0.9, respectively. Figure 7.3(a) is for a value of the eccentricity E = 0.5 and

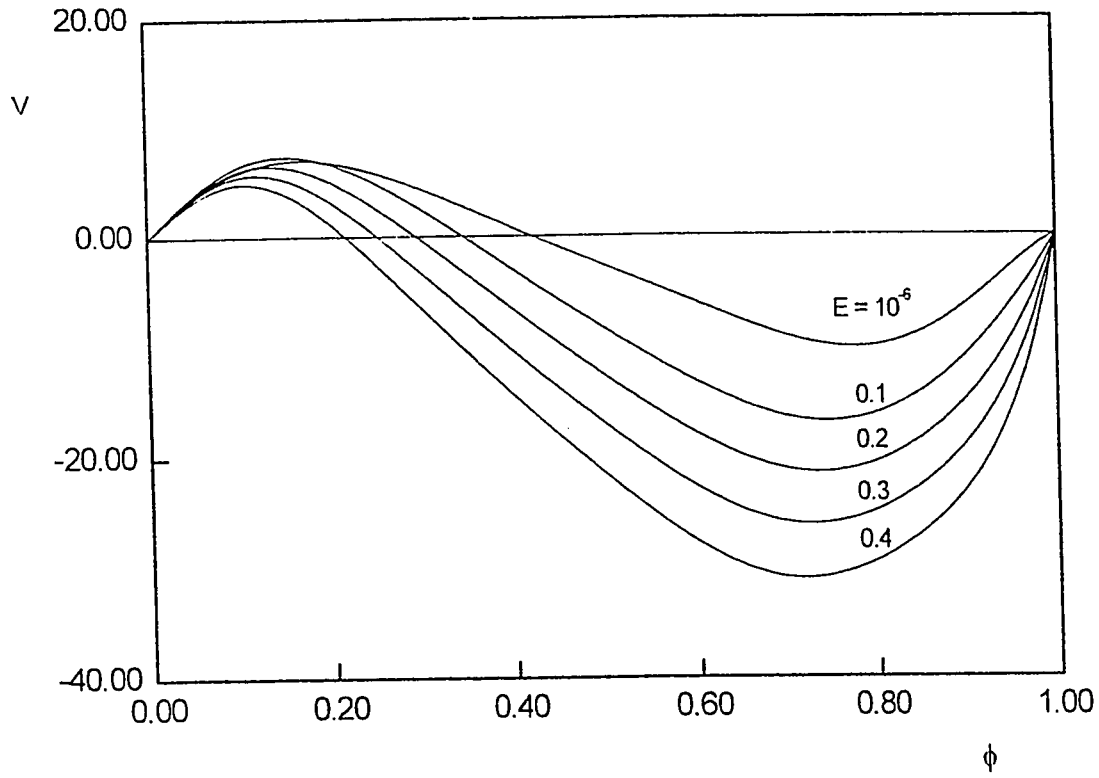


Fig. 7.2(a) : Radial-like velocity profiles in the widest gap ($\psi$ = 0.0 ) at Z = 6.58 x $10^{-8}$ for various values of the eccentricity (E) in an annulus of N = 0.9.

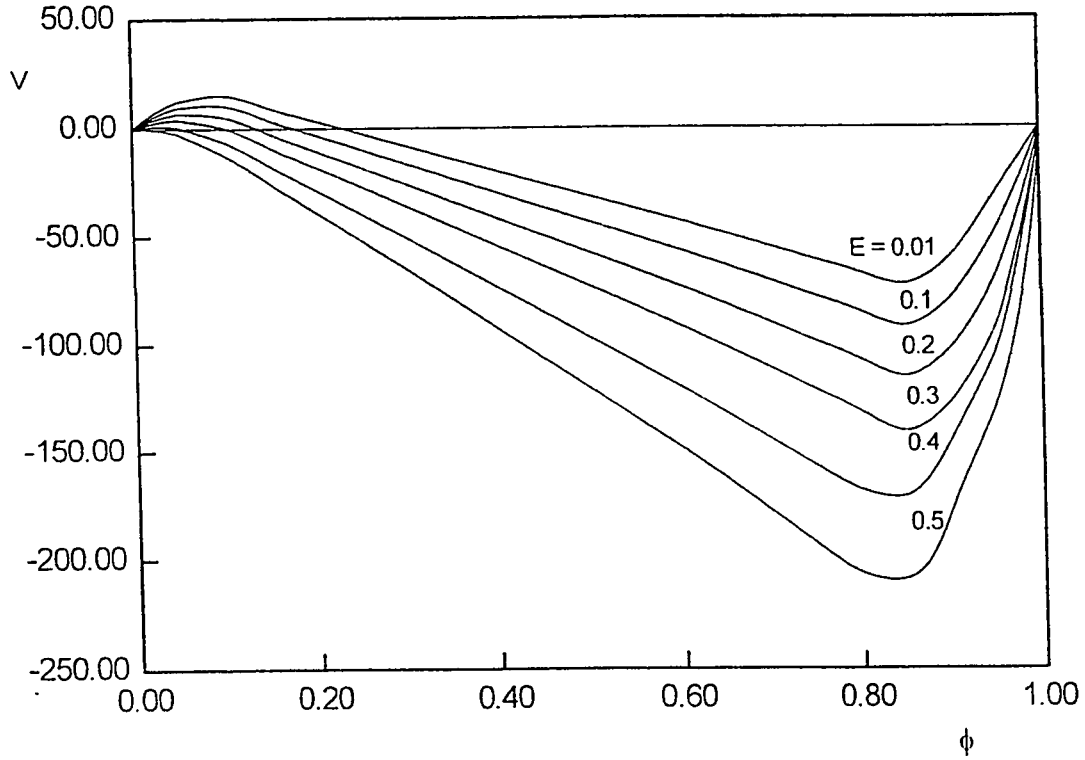


Fig. 7.2(b) : Radial-like velocity profiles in the widest gap ($\psi$ = 0.0 ) at Z =0.58 x $10^{-4}$ for various values of the eccentricity (E) in an annulus of N = 0.5.

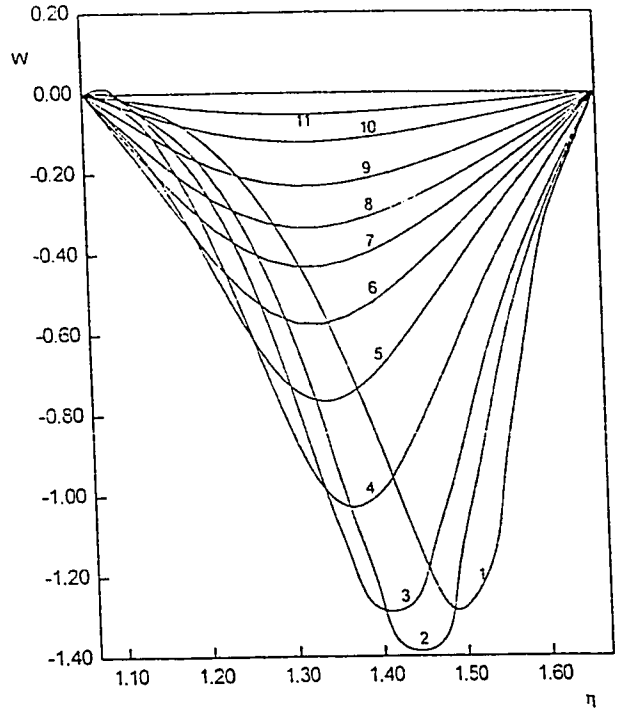


Fig.7.3(a) : Development of the tangential-like velocity profiles near the widest gap ($\psi = 0.05$), N = E = 0.5. The numbers on the profiles indicate the following values of $Z \times 10^4$ : (1) 4, (2) 12, (3) 17, (4) 67, (5) 167, (6) 317, (7) 517, (8) 717, (9) 917, (10) 1417, (11) 2017.

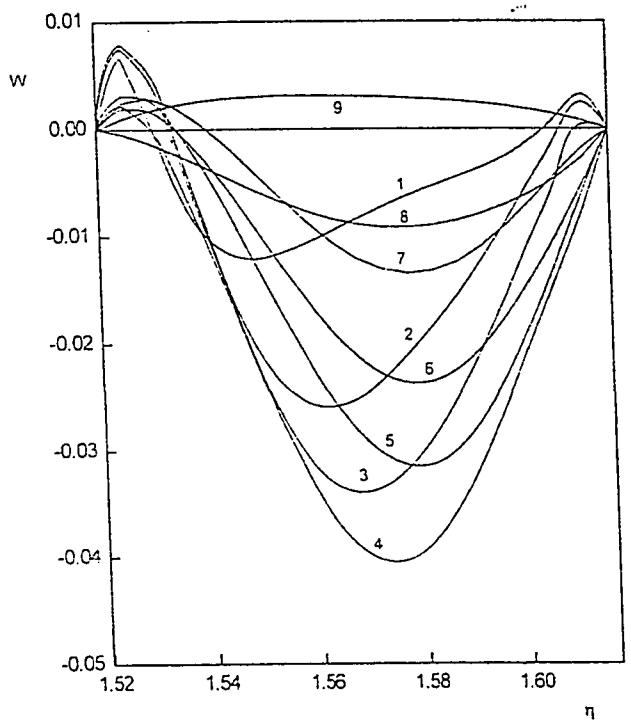


Fig. 7.3(b) : Development of the tangential-like velocity profiles near the widest gap ($\psi = 0.05$), N = 0.9, E = 0.4. The numbers on the profiles indicate the following values of $Z \times 10^4$ : (1) 0.08, (2) 0.6, (3) 1.1, (4) 1.6, (5) 4.1, (6) 6.6, (7) 12, (8) 17, (9) 67, (10) 117.

Fig. 7.3(b) is for E = 0.4. To the author's knowledge, this is the first time that the development of such a velocity component has been presented for the case of entrance-region flows in eccentric annuli. An appreciation of this development leads to a better understanding of the mechanism of development in the entry region. It is worth mentioning that at the lines of symmetry (i.e., $\psi$ = 0.0 and $\pi$), the W-component of velocity has a zero value. On the other hand, at $\psi$ = 0.05, Figs. 7.3(a) and 7.3(b) show how the tangential-like velocity component develops as the flow moves away from the annulus entrance. As can be seen from these two figures, such a tangential-like flow is from the narrowest-side of the annulus towards its widest side (i.e., in the opposite direction of $\xi$ with negative values of W). In all cases, the W-velocity component starts from zero at the annulus entrance, where the velocity profile is uniform, and ends again at zero at the position where the flow reaches the fully developed state.

Engineers are not frequently concerned with the details of the fluid velocities but only with pressure drop. When the flow becomes hydrodynamically fully developed (far away from the annulus entrance cross-section), the pressure drop is due to only the viscous shear action. In this case the pressure drop can be obtained by means of eq. (3.22) which shows that the fully-developed dimensionless pressure is a linear function of Z. Under the assumption of whole channel fully developed flow (i.e., if the flow were fully developed right from the annulus entrance) eqs. (3.37) and (4.4) with their pertinent constants (eqs. 4.21(a-e)) can be used to find $(dP/dZ)_{fd}$ and hence the linear variation of $P_{fd}$ with Z according to eq. (3.22). For a developing flow in the entry region the pressure drop is due to both inertia and viscous actions. Consequently the dimensionless pressure

P in the entry region is a non-linear function of Z. However, if the annulus is sufficiently long, the developing local dimensionless pressure (P) should finally (at large values of Z) follow a linear relationship with Z having the slope as that given by eq. (3.22) for the fully-developed dimensionless pressure, $(dP/dZ)_{fd}$. The difference between P and $P_{fd}$, for a given Z, will be referred to as the pressure drop increment ($\nabla$). This pressure drop increment is due to the inertia forces in the developing region. For an annulus of given radius ratio (N) and eccentricity (E), the pressure drop increment must asymptotically approach a constant value which will be referred to as the fully-developed pressure drop increment ($\nabla_{fd}$).

Figures 7.4(a) and 7.4(b) give the variation of the dimensionless pressure P with Z for some of the selected values of the eccentricity E in annuli of radius ratios 0.5 and 0.9, respectively. The largest value of Z in each of these figures is chosen so as the figure focuses on the developing region in which P varies non-linearly with Z. However, in each of these two figures, the curve corresponding to the largest selected value of E shows clearly how the P-Z variation becomes, at large values of Z, linear and parallel to the variation of $P_{fd}$ with Z. Moreover, these figures show that the pressure drop, for a given Z in a given annulus (N), decreases with increasing the eccentricity (E). Therefore, for a given pressure drop along an annulus, increasing the eccentricity causes an increase in the flow rate through the annular channel. The variation of the ratio between the coefficient of friction ( $f$ ) and the fully developed coefficient of friction ( $f_{fd}$ ) ($\lambda$, as defined by El-Shaarawi [74] ) with Z is presented in Fig. 7.4(c) for a channel of radius ratio N = 0.5 and selected values of eccentricity. The corresponding development of the pressure gradient is presented in Fig. 7.4(d). Moreover, for the sake of comparison, Fig.

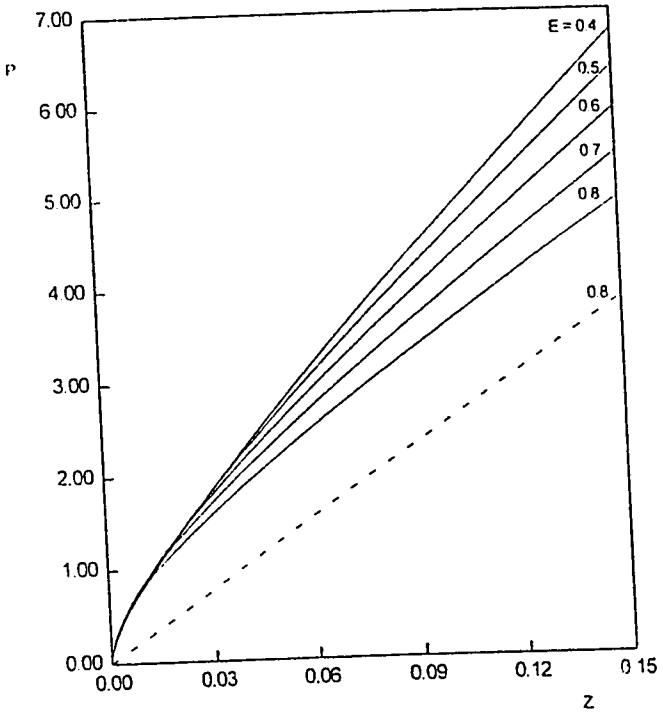


Fig. 7.4(a) : Dimensionless pressure against dimensionless axial coordinate for various values of E in an annulus of N = 0.5, the dotted line represents a case with fully developed flow right from the entrance.

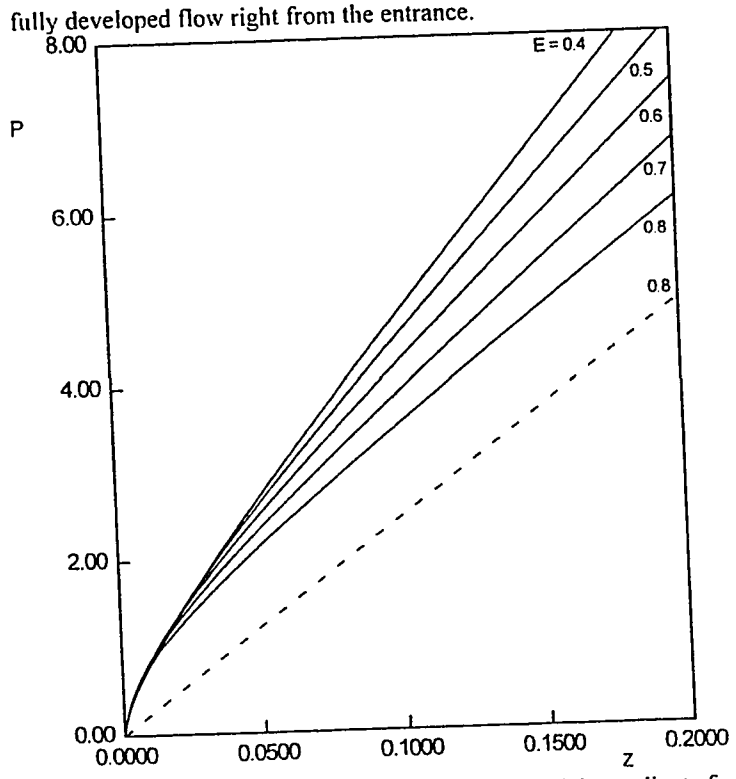


Fig. 7.4(b) : Dimensionless pressure against dimensionless axial coordinate for various values of E in an annulus of N = 0.9, the dotted line represents a case with fully developed flow right from the entrance.

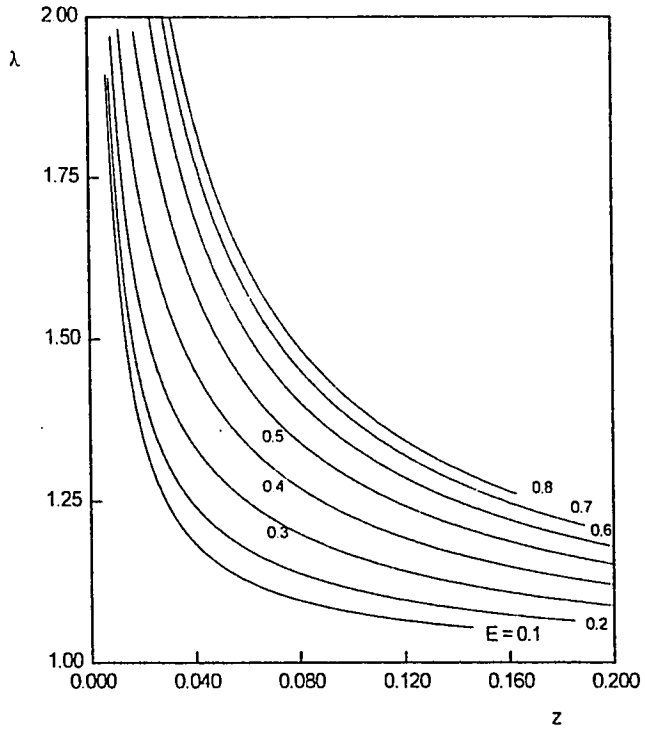


Fig. 7.4(c) : Development of the friction coefficient with Z, for different eceentricities,

N = 0.5

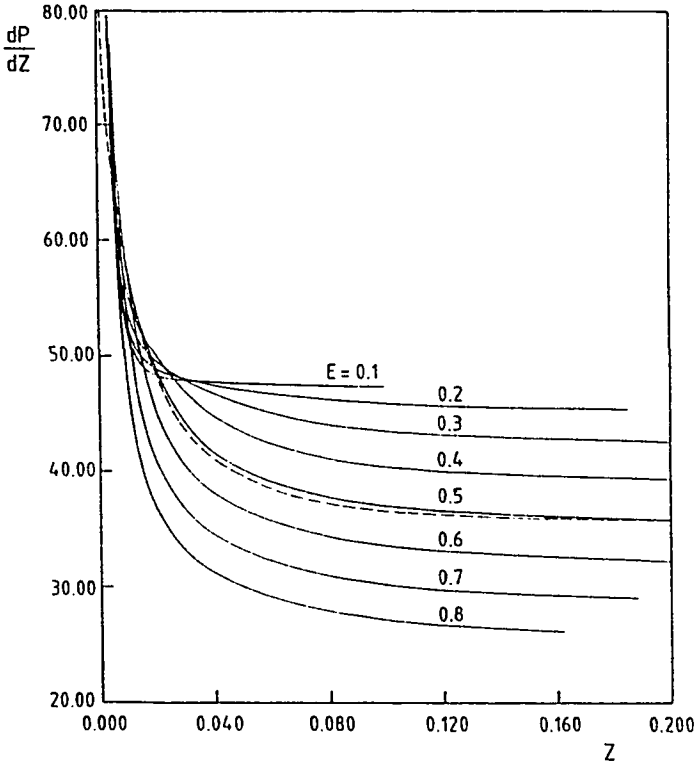


Fig. 7.4(d) : Development of the pressure gradient with Z, for different eccentricities,

N = 0.5, ------ E = 0.5 (Feldman et al. [6]).

7.4(d) includes the results that have previously been reported by Feldman [6] for eccentricity E = 0.5.

Table 7.1 gives the computed values of the fully-developed pressure drop increment ($\nabla_{fd}$ ) in the two annuli under investigation ( N = 0.5 and 0.9) for various values of the eccentricity E. Figures 7.4(a) and 7.4(b) together with Table 7.1 indicate that the assumption of whole channel fully-developed flow would lead to a considerable error in the estimation of the pressure drop in the entry region; this assumption gives considerable underestimated values for the pressure drop. It is worth mentioning that in all the computer runs the obtained numerical results for the developing axial velocity profiles U approached asymptotically (at large values of Z) the fully developed velocity profile given by eq. (4.4) along with its pertinent constants (eqs. 4.21(a-e)). Moreover, validation of the present computer code and its numerical results have also been checked by the trend of other results at large values of Z; the dimensionless pressure (P), the pressure drop increment ($\nabla$)and the pressure gradient $\partial P/\partial Z$ for given N and E, were found to follow the aforesaid linear relationship, has a constant value ($\nabla_{fd}$) and approaches the fully developed analytical value $(dP/dZ)_{fd}$, respectively.

Another important engineering parameter is the hydrodynamic development length ($Z_{fd}$). In both the present work and that of Feldman et al. [6], this length is arbitrarily defined as the distance required for the maximum of the axial velocity profile ( $U_{max,fd}$) to approach within 1 % of its fully developed value. This hydrodynamic development length is given in Table 1 for various values of E. It is worth mentioning that Feldman [78] used ten series-terms in eq. (4.4) when computing the fully

Table 7.1 Values of $\nabla_{fd}$, $Z_{fd}$, $U_{max.fd}$ and $(-dP/dZ)_{fd}$ for different annular geometries.

| E | $\nabla_{fd}$ | | $Z_{fd}$ | | $U_{max.fd}$ | | $-(dP/dZ)_{fd}$ | | | | | |
|---|---|---|---|---|---|---|---|---|---|---|---|---|
| | N = 0.5 | N = 0.9 | N = 0.5 | N = 0.9 | N = 0.5 | N = 0.9 | N = 0.5 | | | N = 0.9 | | |
| | | | | | | | Analytical | Numerical | Tiedt* | Analytical | Numerical | Tiedt* |
| 0.1 | 0.37525 | 0.57572 | 0.146 | 0.102 | 1.78713 | 1.76178 | 47.1381 | 47.2193 | 46.962 | 45.2964 | 47.5808 | 47.284 |
| 0.2 | 0.54370 | 0.94046 | 0.185 | 0.188 | 2.01820 | 2.02849 | 45.2434 | 45.3949 | 45.082 | 44.8168 | 45.5380 | 45.278 |
| 0.3 | 0.75370 | 0.84310 | 0.204 | 0.265 | 2.19275 | 2.23086 | 42.4360 | 42.6407 | 42.278 | 42.1640 | 42.5180 | 42.290 |
| 0.4 | 0.94820 | 1.01910 | 0.216 | 0.340 | 2.31356 | 2.37268 | 39.0702 | 39.2628 | 38.916 | 38.7796 | 38.9100 | 38.716 |
| 0.5 | 1.08601<br>1.0715** | 1.17190 | 0.217<br>0.254** | 0.401 | 2.38109<br>2.372** | 2.45643 | 35.4916<br>35.33** | 35.7084 | 35.342 | 35.0092 | 35.0876 | 34.920 |
| 0.6 | 1.24395 | 1.20680 | 0.208 | 0.455 | 2.40494 | 2.49495 | 31.9629 | 32.2533 | 31.818 | 31.2728 | 31.3396 | 31.186 |
| 0.7 | 1.14876 | 1.28770 | 0.189 | 0.501 | 2.39610 | 2.49876 | 28.6525 | 29.0170 | 28.512 | 27.7584 | 27.8068 | 27.686 |
| 0.8 | 1.01915 | 1.25340 | 0.163 | 0.532 | 2.36449 | 2.47875 | 25.6476 | 26.0630 | 25.510 | 24.5780 | 24.6156 | 24.516 |

* Results of Tiedt [79] as presented by Shah and London [80]

** Results of Feldman et al. [6].

developed axial velocity profile (and hence the value of $U_{max,fd}$). In the present work ten, fifteen and twenty series-terms have been used for E = 0.1, $0.2 \leq E \leq 0.4$ and $E \geq 0.5$, respectively. The corresponding values of $U_{max,fd}$, as obtained from the analytical solution (4.4). are given in Table 7.1.

The pressure gradient at full development $(dP/dZ)_{fd}$ is given also in Table 7.1 for all the annuli investigated. For each value of E, both the analytical value, which has been obtained by eqs. (3.37) and (4.4), and the computed numerical value are given. The agreement between these two sets of results provided another means of validation of the present model and computer code. On the other hand, Table 1 compares also all the present results for $(dP/dZ)_{fd}$ with those of Tiedt [79] and some of the present results for $\nabla_{fd}$ , $Z_{fd}$, $U_{max,fd}$ and $(dP/dZ)_{fd}$ with the corresponding results of Feldman et al. [7] for the case of N = 0.5 and E = 0.5. As can be seen from this table, there is a good agreement between the present results for $(dP/dZ)_{fd}$ and those of Tiedt [79]. Moreover, the agreement between the present results and those of Feldman et al. [6] for $\nabla_{fd}$ , $U_{max,fd}$ and $(dP/dZ)_{fd}$ is excellent ( the difference between the two sets of results is less than 1 % for any of $\nabla_{fd}$ , $U_{max,fd}$ and $(dP/dZ)_{fd}$ ). However, the present hydrodynamic development length is 14.6 % shorter than that obtained by Feldman et al. [6]. This difference might be due to Feldman's use of only ten series-terms in calculating $U_{max,fd}$ (upon which is based the criterion for determining $Z_{fd}$) while twenty terms were used in the present work. However, the comparison for the variation of $\partial P/\partial Z$ with Z, presented in Fig. 7.4(d) has shown an excellent agreement with the corresponding results of Feldman et al. [6].

For fluids having Prandtl number less than unity, the hydrodynamic development length is larger than the thermal entrance length. Consequently, a hydrodynamically fully developed forced flow of a fluid of Pr ≤ 1 is also thermally fully developed. Under such full-development conditions $\partial \theta / \partial Z = 0$, $V = W = 0$ and hence eq. (3.25) reduces to

$$\frac{\partial^2 \theta_{fd}}{\partial \eta^2} + \frac{\partial^2 \theta_{fd}}{\partial \xi^2} = 0 \tag{7.1}$$

Equation (7.1) subject to the boundary conditions (3.19), i.e., case (1.I), has the following closed-form solution ( El-Saden [5] ).

$$\theta_{fd} = (\eta - \eta_o) / (\eta_i - \eta_o) \tag{7.2}$$

This linear relationship between $\theta_{fd}$ and $\eta$ provided an anlytical check on the numerical solution of the energy equation (3.25). At sufficiently large values of Z, the obtained numerical solutions of eq. (3.25) were found to converge to the above $\theta_{fd}$-solution. Such a fully developed solution ($\theta_{fd}$) occurs when the heat transfer through the inner wall of the annulus is equal and opposite to that through its outer wall. The corresponding fully developed mixed-mean temperatures ($\theta_{m,fd}$) as obtained from the present numerical work for the developing flow at large values of Z are given Table 7.2.

As another means of verification, a special computer run has been made with Pr = 1 and the obtained results for the mixed-mean temperature ($\theta_m$) in an annulus of N = E = 0.5 are compared in Fig. 7.5 with the corresponding graphical data of Feldman et al. [7]. Good agreement between the two sets of results can be seen from this figure. The mixed-mean temperature ($\theta_m$) at any cross-section is an important engineering parameter for the calculation of the rate of heat transfer over any length measured from the

Tabl 7.2 Values of $\theta_{m,fd}$ , $\overline{Nu_{i,fd}}$ and $\overline{Nu_{o,fd}}$ for different annular geometries.

| E | $\theta_{m,fd}$ | | $\overline{Nu_{i,fd}}$ | | | | $\overline{Nu_{o,fd}}$ | | | |
|---|---|---|---|---|---|---|---|---|---|---|
| | N = 0.5 | N = 0.9 | N = 0.5 | | N = 0.9 | | N = 0.5 | | N = 0.9 | |
| | | | Present | Trombetta* | Present | Trombetta* | Present | Trombetta* | Present | Trombetta* |
| 0.1 | 0.40844 | 0.47311 | 4.9223 | - | 4.22316 | - | 3.5299 | - | 3.82742 | - |
| 0.2 | 0.40570 | 0.48349 | 4.9593 | 4.945 | 4.20384 | 4.181 | 3.6184 | 3.633 | 3.97103 | 3.993 |
| 0.3 | 0.40050 | 0.48425 | 5.0412 | - | 4.29745 | - | 3.7643 | - | 4.09842 | - |
| 0.4 | 0.39346 | 0.48355 | 5.1794 | 5.166 | 4.45965 | 4.452 | 3.9819 | 3.998 | 4.27886 | 4.287 |
| 0.5 | 0.38465 | 0.48241 | 5.3980 | - | 4.70704 | - | 4.2962 | - | 4.54092 | - |
| 0.6 | 0.37400 | 0.48110 | 5.7432 | 5.746 | 5.08193 | 5.075 | 4.7607 | 4.754 | 4.92933 | 4.936 |
| 0.7 | 0.36043 | 0.47971 | 6.2885 | - | 5.67726 | - | 5.4992 | - | 5.53770 | - |
| 0.8 | 0.34167 | 0.47815 | 7.2773 | 7.420 | 6.73708 | 6.732 | 6.8441 | 6.596 | 6.61175 | 6.617 |

* Results of Trombetta as presented by Shah and London [80].

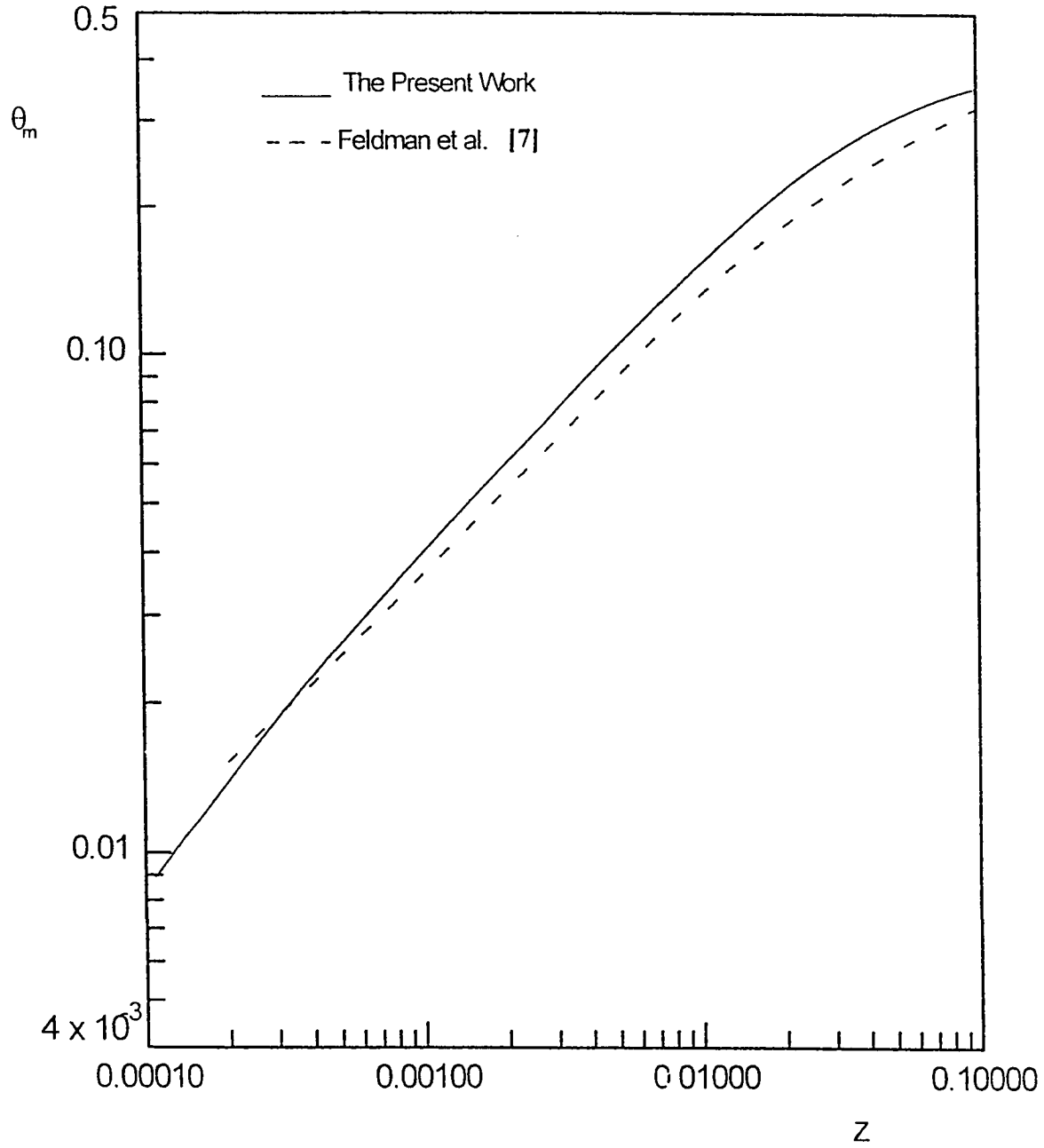


Fig. 7.5 : Comparison between the present results and those of Feldman et al. [7] for the mixed-mean temperature against Z.

entrance. For N = 0.5 and 0.9, Figs. 7.6(a) and 7.6(b), respectively, give the variation of the dimensionless mixed-mean temperature ($\theta_m$) with the dimensionless axial distance (Z) corresponding to various values of the dimensionless eccentricity (E) for a fluid of Pr = 0.7. These two figures show that, for a given Z, $\theta_m$ decreases as the eccentricity E increases. This is attributed to the increase in the mass flow rate as the eccentricity increases. Hence, the heat input through the same length (Z) of the heated boundary produces smaller values of $\theta_m$ as E increases.

For various values of the eccentricity E, Figs. 7.7(a) and 7.7(b) give the axial variation of the circumferentially averaged Nusselt number on the inner heated boundary ( $\overline{Nu_i}$) for the two annuli under invesitigation while Figs. 7.8(a) and 7.8(b) give such axial variations for the circumferentially averaged Nusselt number on the outer cooled boundary ( $\overline{Nu_o}$). As can be seen from these four figures, for given N and Z, the eccentricity increases the circumferentially averaged Nusselt number on both the inner and outer walls of the annulus. This is attributed to the increase in the flow rate through the annular gap as a result of eccentricity. Consequently, the average velocity of flow through the annulus increases with eccentricity, this in turn reduces the resistance to heat transfer and higher circumferentially-averaged Nusselt numbers are obtained on both walls. On the other hand, for given N and E, the Nusselt number generally decreases as the flow moves away from the entrance due to the thickening of the hydrodynamic boundary layer which develops on the inner wall. However, Figs. 7.7(a) and 7.7(b) show the same trend found by Marner and McMillan [81] and El-Shaarawi and Sarhan [63] concerning the unusual increase of Nu with increasing axial distance

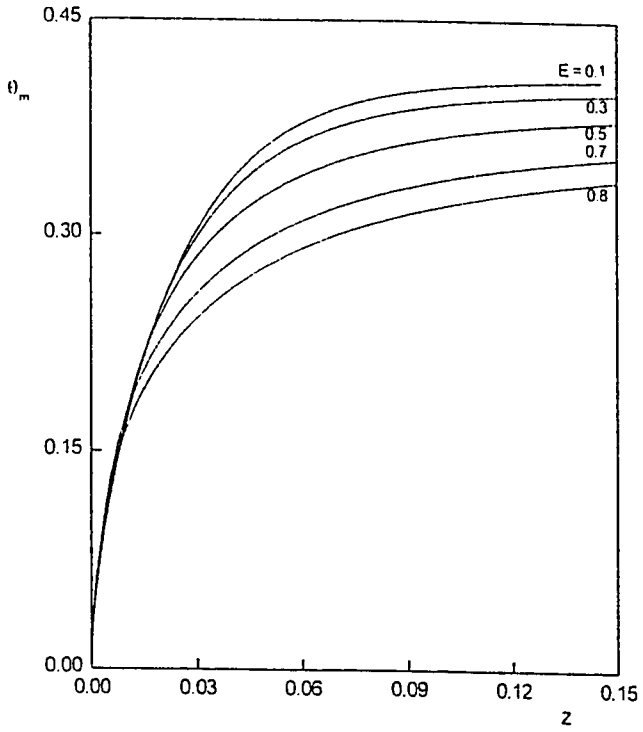


Fig. 7.6(a): Mixed-mean (mean bulk ) temperature against Z for various values of E in an annulus of N = 0.5.

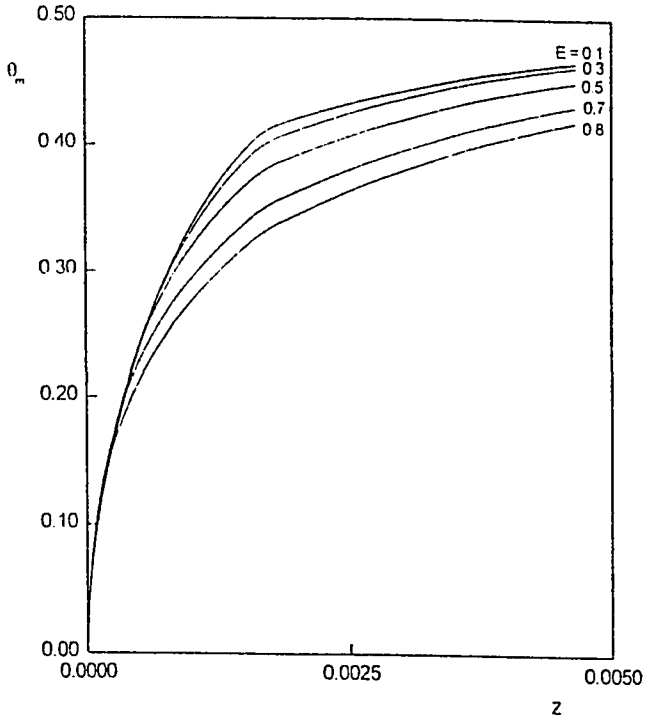


Fig.7.6(b): Mixed-mean (mean bulk ) temperature against Z for various values of E in an annulus of N = 0.5.

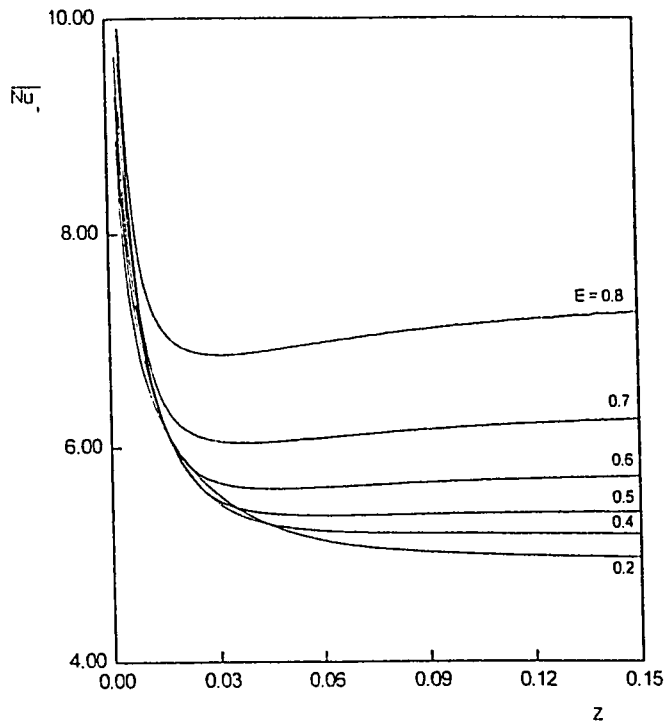


Fig. 7.7(a) : Circumferentially-averaged Nusselt number on the inner wall against Z for various values of E in an annulus of N = 0.5

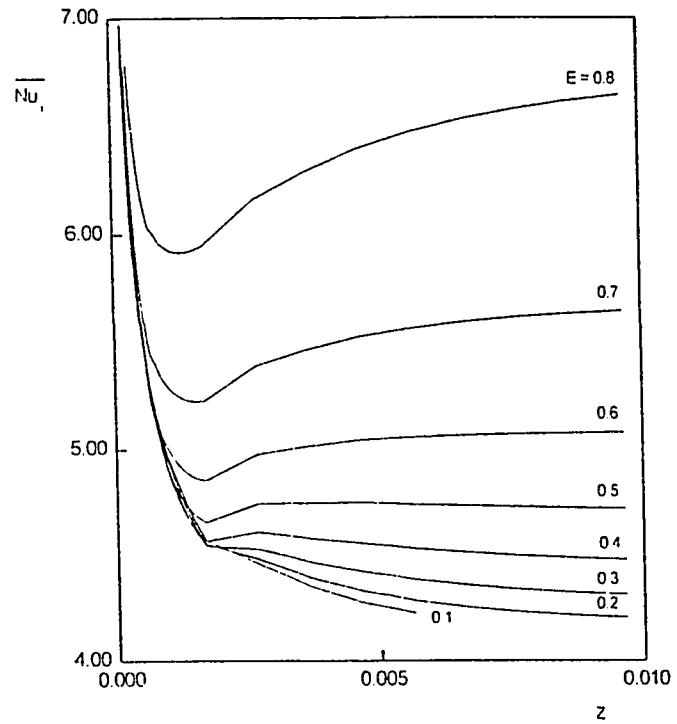


Fig. 7.7(b) : Circumferentially-averaged Nusselt number on the inner wall against Z for various values of E in an annulus of N = 0.9

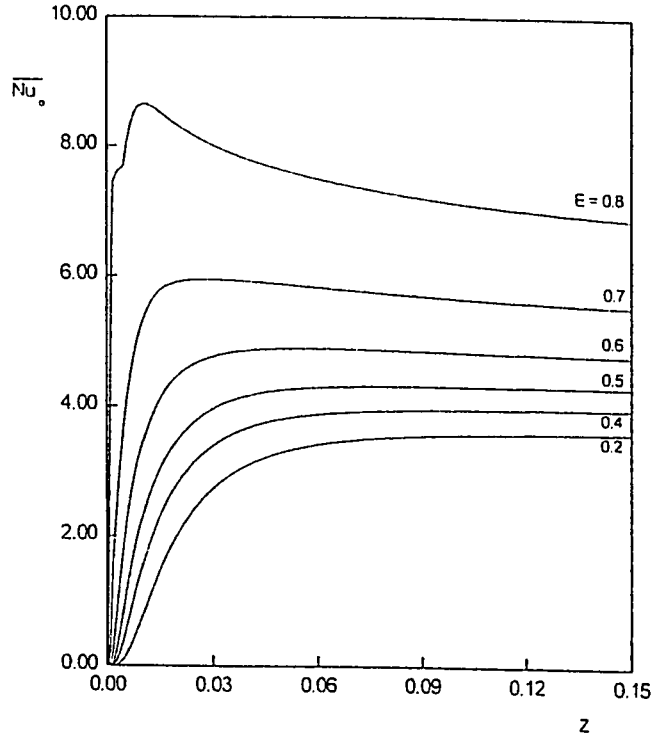


Fig. 7.8(a) : Circumferentially-averaged Nusselt number on the outer wall against Z for various values of E in an annulus of N = 0.5

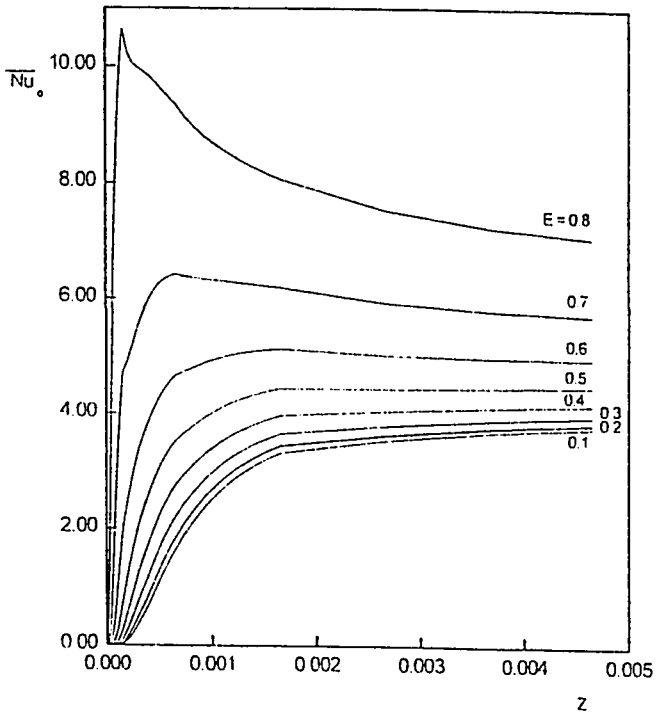


Fig. 7.8(b) : Circumferentially-averaged Nusselt number on the outer wall against Z for various values of E in an annulus of N = 0.9

especially with large values of E. A similar trend might also be observed in Fig. 9 of Feldman et al. [7]. Figures 7.8(a) and 7.8(b) show that, for a given N, the variation of the circumferentially-averaged Nusselt number on the outer cooled wall has a relative maximum; a similar trend has been found by Feldman et al. [7]. All curves for various values of E in these two figures start from zero as both the inlet fluid and the outer wall temperatures equal the ambient temperature; hence local heat flux $q''$ at the outer wall is zero at Z = 0. Near the entrance cross-section pronounced transverse flows are generated and create an increasing transfer of heat through the outer wall. However, further downstream such transverse flows decay and are overcome by the effect of the thickening of the hydrodynamic boundary layer which develops on the outer wall, hence the Nusselt number ($\overline{Nu_o}$) decreases until it reaches its fully-developed value.

Table 7.2 gives the fully-develped values of $\overline{Nu_i}$ and $\overline{Nu_o}$ which have been obtained from the present numerical work for the developing flow at large values of Z for all the annular geometries investigated. Moreover, the table gives some corresponding values as obtained by Trombetta [23] who solved the Graetez problem.

Engineers are concerned with the Nusselt number averaged over the entire surface area of a wall from the inlet to any particular axial location Z ($\overline{\overline{Nu_y}}$). This can be obtained by integrating the local distributions of the circumferentially-averaged Nusselt number given in Figs. 7.7(a) through 7.8(b) from Z = 0 to any paricular value of Z and divide the result by the corresponding value of Z. For N = 0.5 and 0.9, Figs. 7.9(a) and 7.9(b), respectively, give the variation of such a global Nusselt number with Z on the

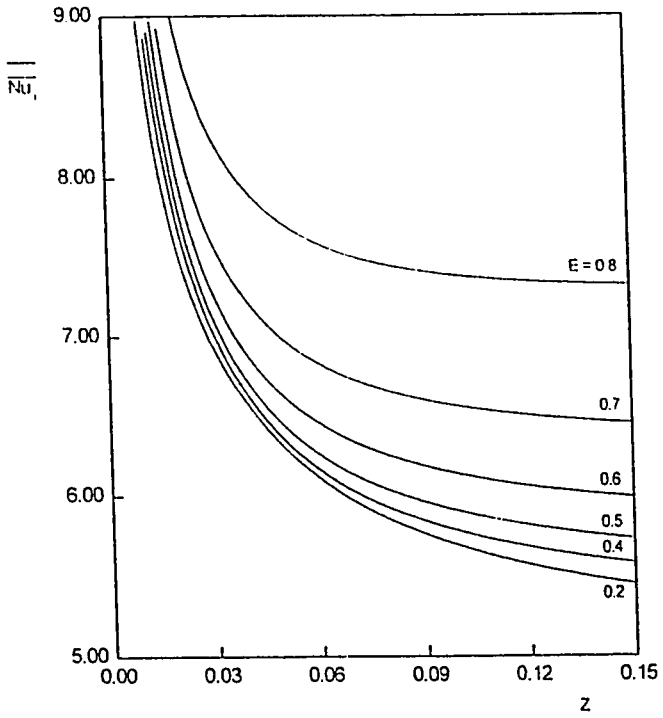


Fig. 7.9(a) : Nusselt number averaged over the entire area of the inner wall versus Z for various values of E, N = 0.5

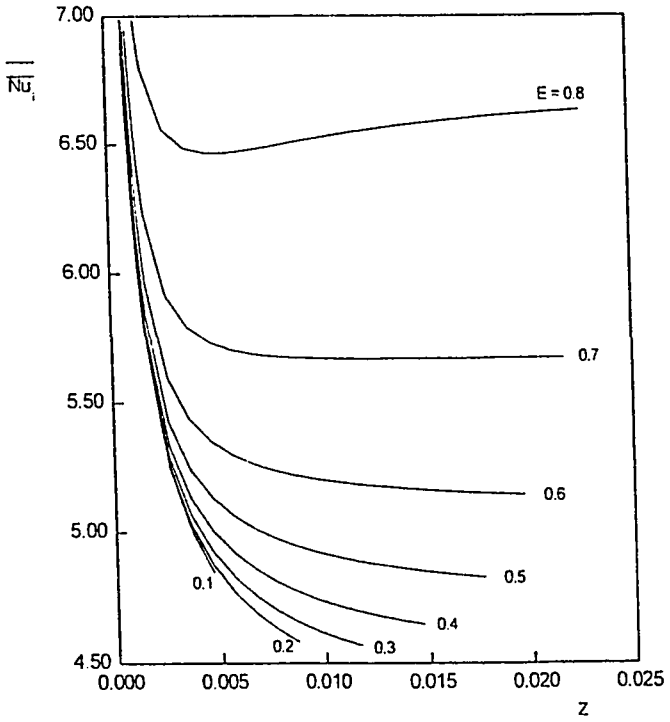


Fig. 7.9(b) : Nusselt number averaged over the entire area of the inner wall versus Z for various values of E, N = 0.9

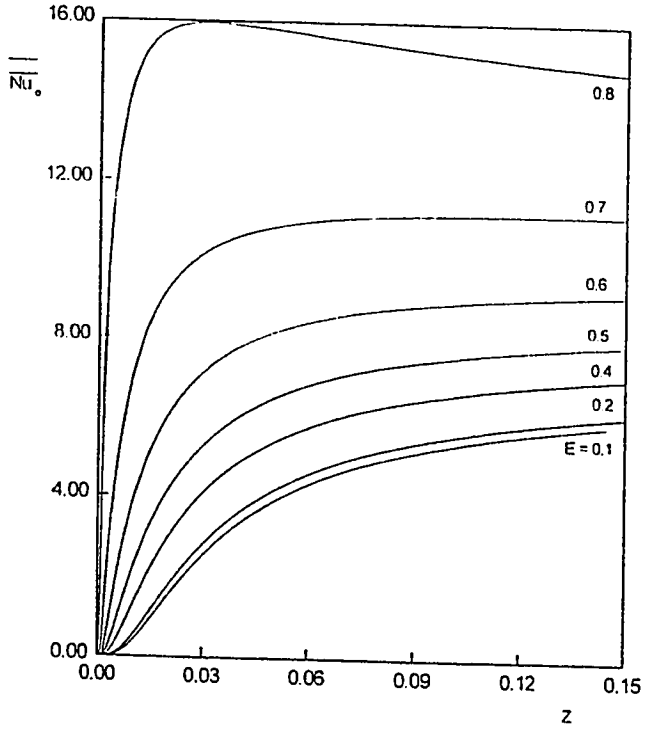


Fig. 7.10(a) : Nusselt number averaged over the entire area of the outer wall versus Z for various values of E, N = 0.5

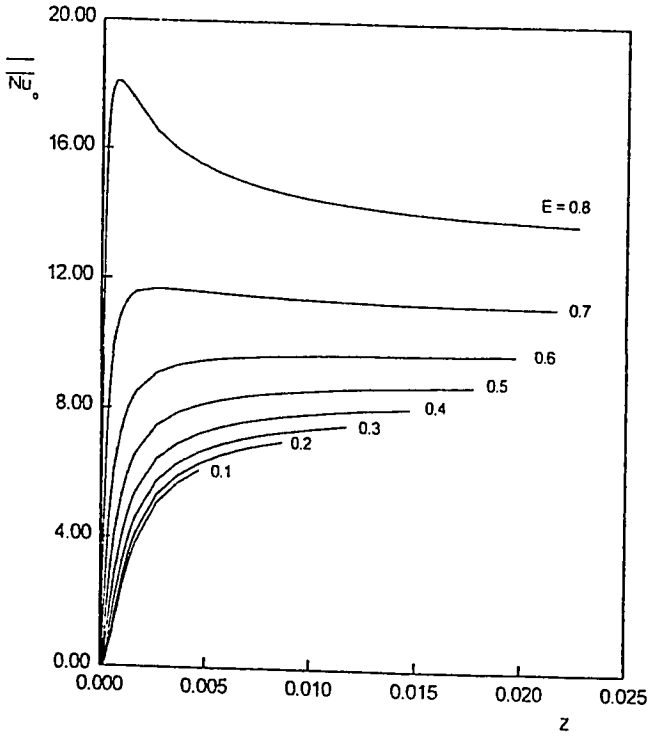


Fig. 7.10(b) : Nusselt number averaged over the entire area of the outer wall versus Z for various values of E, N = 0.9

inner wall while Figs. 7.10(a) and 7.10(b) present the similar variation but on the outer wall.

It is worth mentioning here that for all cases investigated, a correction for the entrance uniform velocity $U_o$ has been taken to make $U_o$ sligtly higher than 1.0 ( the average velocity $\bar{U}$ = 1.0 at any cross section ). This correction has been taken to compensate the loss in accuracy resulted from the numerical approximation ( trapezoidal rule ) used to calculate the average velocity at the entrance cross-section or at any cross section downstream. Similar action has been taken by Feldman [78]. It was noticed that the value by which the entrance uniform velocity $U_o$ should be greater than unity to remedy this loss of accuracy depends on the eccentricity E, radius ratio N and the mesh size ($n$ x $m$ in $\eta$- and $\xi$-direction, respectively). This value has been estimated for all the investigated cases for a ( 20 x 20 ) mesh. The following table summarizes the different values of and the equation developed to get this value for different eccentricities;

| Eccentricity, E | Entrance velocity, $U_o$ | Equation used |
|---|---|---|
| 0.1 | 1.061042 | $U_o = (\bar{U} + 1.7 \times 10^{-7}) / 0.94247$ |
| 0.2 | 1.061548 | $U_o = (\bar{U} + 3.1 \times 10^{-7}) / 0.94202$ |
| 0.3 | 1.062395 | $U_o = (\bar{U} + 3.7 \times 10^{-7}) / 0.94127$ |
| 0.4 | 1.063593 | $U_o = (\bar{U} + 4.1 \times 10^{-7}) / 0.94021$ |
| 0.5 | 1.065156 | $U_o = (\bar{U} + 3.4 \times 10^{-7}) / 0.93383$ |
| 0.6 | 1.067099 | $U_o = (\bar{U} + 4.1 \times 10^{-7}) / 0.93712$ |
| 0.7 | 1.069451 | $U_o = (\bar{U} + 4 \times 10^{-7}) / 0.93506$ |
| 0.8 | 1.072237 | $U_o = (\bar{U} + 3.6 \times 10^{-7}) / 0.93263$ |

The mesh size (20 x 20) has been chosen based on numerical experimentations. In these prelimnary numerical experimentations, different mesh sizes (10 x10 , 15 x 15, 20 x 20 and 30 x 22) mesh sizes have been tested. The impact of the mesh size on the numerically obtained fully-developed pressure gradient and the developing length has been analyzed. For a (10 x 10) mesh the difference between the numerically obtained fully-developed pressure gradient $( dP / dZ )_{f.d}$ and the corresponding analytical value was 4.5 % while it was 0.9 % for (20 x 20) and (30 x 22) meshes. Taking the developing length obtained using a (30 x 22) mesh as a reference, the difference in this parameter for a (15 x 15) mesh was 20.21 % while it was 1.038 % for a (20 x 20) mesh. It was obvious from this prelimnary study that there is no difference in the value of the numerically obtained fully-developed pressure gradient for the (20 x 20) and the (30 x 22) meshes while there is a negligble difference in the value of the developing length between the two cases. However, the execution CPU time increases dramatically with the increase in the number of the grid points used (e.g., the CPU time for a grid of (20 x 20) was about 30-35 secs per axial step and that for a (30 x 22) grid was 60-80 secs. Hence, it was decided to use the (20 x 20) mesh size in all cases investigated since it saves the CPU time and gives a reasonable accuracy.

# Chapter 8

# RESULTS AND DISCUSSION FOR FREE CONVECTION IN VERTICAL OPEN-ENDED ECCENTRIC ANNULI

## 8.1 Introduction

Laminar free convection with simultaneously developing hydrodynamic and thermal boundary layers in vertical eccentric annuli is encountered in many practical applications. In atomic reactors, for example, the heat generated by atomic reactions is transferred to the coolant flowing through the annular gap between the fuel element and the coolant channel wall. In vertical electric motors and generators, the heat generated by irreversible electrical and mechanical processes is transferred through the air gap between the rotor and the stator. The transfer of heat by free convection is always a factor in the cooling of such machines and may be the sole means of cooling of small types of these

devices. Knowledge of the fluid motion is needed to predict the operating temperatures which must be less than the maximum permitted value.

The developing laminar free convection in concentric annular ducts has been investigated by El-Shaarawi et al. [62-65] and others as summarized in Chapter 2. However, a thorough research of the literature has revealed that there is no work dealt with the problem of free convection in vertical open-ended eccentric annuli with simultaneously developing hydrodynamic and thermal boundary layers.

The mathematical model describing this problem of free convection in vertical eccentric annuli has been presented in Chapter 3. This model is capable of describing the natural flow and heat transfer in the entry-region of vertical open-ended eccentric annuli without need of assumptions dependent on prior knowledge of the mechanism of transverse flows in such a region. The numerical algorithm to solve this model has been presented in Chapter 4. Numerical results will be presented for the developing velocity profiles, axial variation of pressure, heights required to suck specified flow rates, and heat transfer parameters under four pairs of fundamental thermal boundary conditions.

In practice, for confined free convection flows the dimensions of the channel (*l and D)* and both the wall and ambient temperatures are normally known (i.e., $L$ is given) while the volumetric flow rate $f$ (and hence $F$ ) is unknown. However, the present model and the method of solution are handling the problem in a reversed manner, i.e., obtaining an unknown dimensionless channel height ($L$) for a given dimensionless volumetric flow rate ($F$). Therefore, the condition $P = 0$ at $Z = L$ is not explicitly imposed on the solution, but continually checked for satisfaction as will be indicated

hereunder. Hence, taking into consideration that its satisfaction establishes the unknown channel height, this condition could be regarded as being implicitly imposed.

For an annulus of given $N$ and $E$ immersed in a fluid of $Pr = 0.7$ and for a selected value of $U_o$ ( and hence the dimensionless volumetric flow rate $F$) , numerical solution of the finite-difference governing equations is obtained by first calculating the corresponding values of $\eta_i$ and $\eta_o$ using the pertinent relations given in Chapter 4 (eqs. (4.14) and (4.15)) . By selecting the numbers of increments in $\eta$ and $\xi$ directions ( n and m, respectively) the values of $\Delta\eta$ and $\Delta\xi$ can be computed, respectively. For a given axial location (cross-section), the finite-difference energy equation (4.25) is linearized by taking the values of the coefficient of the convective terms (i.e., $U^*$, $V^*$ *and* $W^*$) from the preceding axial step. This equation (4.25) is applied at each grid point in the cross-section next to the entrance cross-section (i.e., with $i = 1, 2, 3, \ldots\ldots, n, n+1$, and $j = 1, 2, 3, \ldots\ldots, m, m+1$) taking into consideration the selected thermal-boundary conditions. This results in $[(n+1)(m+1)]$ simultaneous linear algebraic equations in the number of unknowns ( $\theta_{i,j}$ ). Solving this set of equations by any matrix technique(Gauss-Seidel iteration scheme [77] has been used in the present work), one gets the unknown values of $\theta$'*s* at all points of the second cross-section. The obtained values of $\theta$'*s* are used in the solution of the linearized finite-difference axial momentum equation (4.23). This equation together with the integral continuity equation (4.26) represent two equations in the two unknowns $U$ and $P$ and can be solved at the first axial step next to the entrance cross-section as follows. Equation (4.26) is applied throughout the second cross-section while eq. (4.23) is applied at each interior node of the numerical grid and the solution is

obtained in the same manner described for forced convection in Chapter 7. Now, the linearized finite-difference eq. (4.24) is applied at each interior node to give *(n-1) x (m+1)* simultaneous linear algebraic equations which when solved give the unknown values of *W* at this second cross section ; Gauss-Seidel iteration scheme [77] has been used in the present work. Finally, eq. (4.22) can be used to obtain the unknown values of *V* at all interior nodes, then the flow and heat transfer parameter such as *U*, $\theta_m$, and $\overline{\overline{Nu}}_y^{k.x}$ (where; *k* represnts the type of the thermal-boundary conditions and takes the value of 1, 2, 3, or 4 while *x* indicates the heat transfer wall, hence it will be I/O if the heat transfer wall is the inner/outer wall. Moreover, *y* indicates the wall on which the Nusselt number is calculated and it will be either *i* or *o* ) can be calculated by applying the pertinent equations presented in Chapter 5. Repeating this procedure, one can advance axially downstream along the annulus until the pressure becomes zero. One more heat transfer parameter that has not been presented in Chapter 5 is the totally averaged Nusselt number $\overline{\overline{\overline{Nu}}}_y^{M.x}$ (this parameter has been calculated for the developing forced convection, Chapter 7, for thermal-boundary conditions 1.I) where;

$$\overline{\overline{\overline{Nu}}}_y^{M.x} = \frac{1}{L}\int_0^L \overline{\overline{Nu}}_y^{M.x}\, dZ \tag{8.1}$$

All results to be presented in this chapter have been obtained using a grid of 20 segments in the $\eta$-direction and 20 segments in the $\xi$-direction. Thus, for each axial step, 400 (19x21 + 1 = 399 +1) equations have to be solved to obtain the values of U and P then 399 equations have to be solved for W and 399, 430 or 431 equations for $\theta$,

according to the thermal boundary conditions considered. This required 30 to 35 CPU seconds per one axial step on a main frame computer of WF 77 sys D type. Moreover, similar to the case of forced convection, the results to be presented here have been obtained by using very small axial steps near the entrance ( $\Delta Z = 10^{-10}$ for all the cases considered) then the axial step was increased several times as the flow moves downstream to reach a value no more than $\Delta Z = 10^{-3}$.

## 8.2 Results and Discussion

Due to the neglect of the axial diffusion of momentum and the variation of pressure with the two transverse directions, the Reynolds number or the Grashof number is inherent in the dimensionless formulation of the problem and thus neither of these two numbers is explicitly needed for the solution. However, four other similarity parameters are explicitly required to solve the problem under consideration. These are the annulus radius ratio (N), the dimensionless eccentricity (E), the dimensionless flow rate F (or effectively $U_o = F / (1 - N^2)$) and the Prandtl number (Pr). Computations were carried out for a fluid of Pr = 0.7 in an annulus of N = 0.5. The radius ratio 0.5 was chosen since it represents a typical annular geometry with its value of N far enough from unity (N = 1 ) which represents the case of parallel plate channel. Moreover, the heat transfer results presented by El-Shaarawi and Sarhan [62] are for this particular radius ratio (N=0.5). These results provide a means of verification of the present model and the computer code through special runs for very small eccentricity ( $E = 10^{-6}$ ).

Because of the nature of the problem under consideration, a huge amount of results have been generated (e.g., results are generated for a specific eccentricty with different flow rates to predict the pertinent channel heights and other flow and heat transfer parameters under a given boundary condition then the work is repeated for different eccentricities and then for the other 7 thermal boundary conditions). Only a representative sample of the results corresponding to a selected set of eccentricties will be presented. These results are divided into two groups, one group is related to the flow and heat transfer parameters to explain the physics of the problem and the other group includes the engineering parameters.

### 8.2.1 Physical Parameters

The most imprtant flow and heat transfer parameters that can explain the physics of the developing free convection are the velocity and temperature profiles. Figure 8.1(a) shows examples of the developing axial velocity profiles in the widest and narrowest sides of the gap under thermal boundary condition 1.O in an annulus of N = 0.5 and E = 0.5 with an induced flow rate of uniform inlet velocity corresponding very nearly to the fully developed flow rate (F = 0.01365 and $F_{fd}$ = 0.013806). It can be seen from Fig. 8.1(a) that, since the buoyancy force causes the fluid to be induced up in the heated channel, the flow will be accelerated faster near the heated wall. The velocity profiles in the narrowest gap have slightly higher values than those in the widest gap near the entrance where the temperature level in the narrowest gap is higher than that in the widest gap early near the entrance. However, since the eccentricity increases / decreases

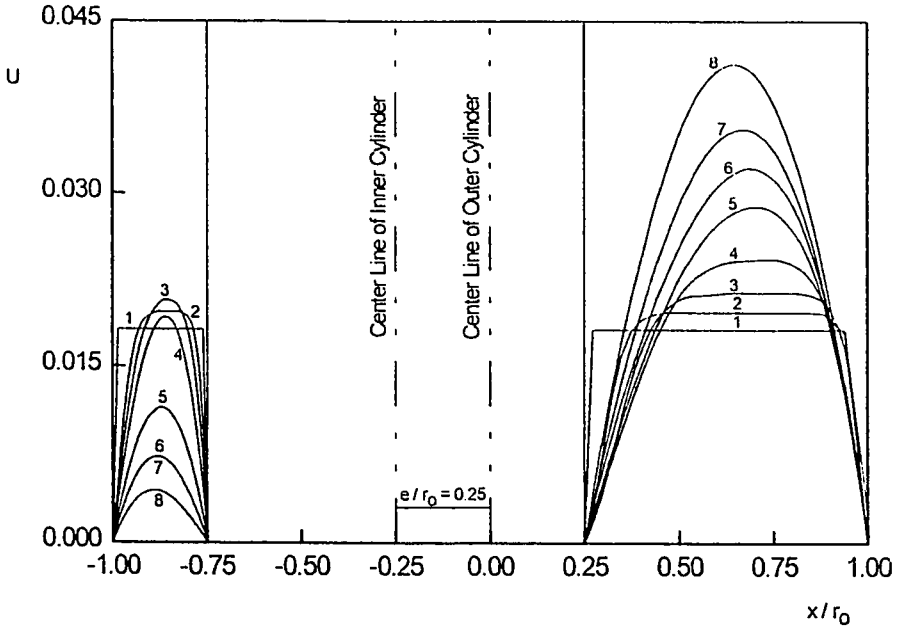


Fig. 8.1(a) : Development of the axial velocity profiles, N = E = 0.5. The numbers on the profiles indicate the following values of $Z \times 10^7$: (1) $10^{-3}$, (2) 71.8, (3)212, (4)712, (5) 3110, (6)8110, (7) 18100, (8) 128.11 x $10^4$(and above, until fully development), case 1.O, N = E = 0.5, $U_o \times 10^3 = 18.2$.

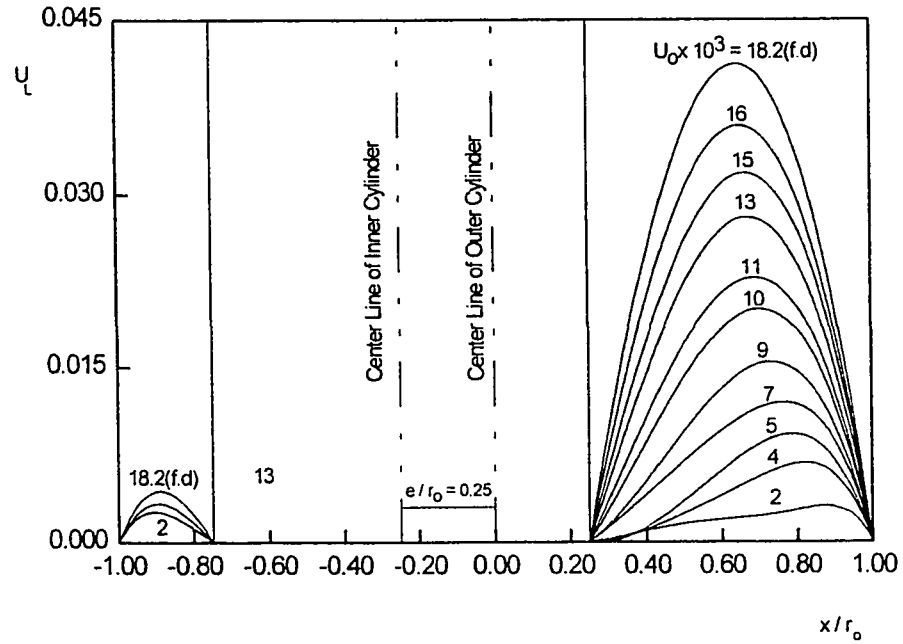


Fig. 8.1(b) : Axial velocity profiles at the channel exit for different flow rates (i.e., different channel heights), case 1.O, N = E = 0.5.

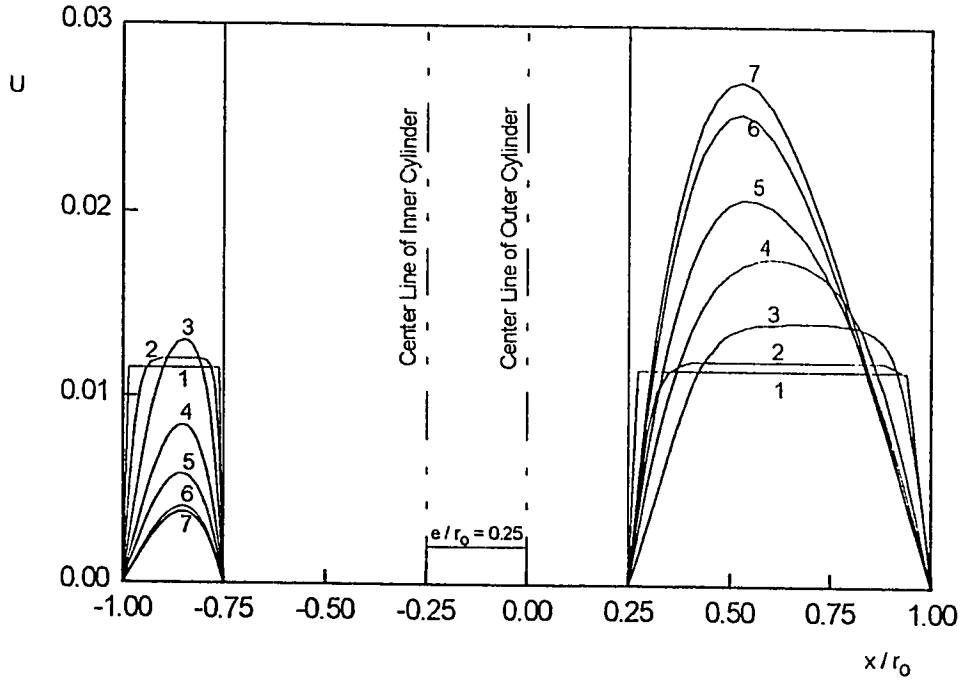


Fig. 8.1(c) : Development of the axial velocity profiles, N = E = 0.5. The numbers on the profiles indicate the following values of $Z \times 10^6$: (1) $10^{-4}$, (2) 2.183, (3)21.183, (4)121.183, (5) 311.183, (6)1311.183, (7) 128211, case 1.I, $N = E = 0.5$, $U_o \times 10^3 = 11$.

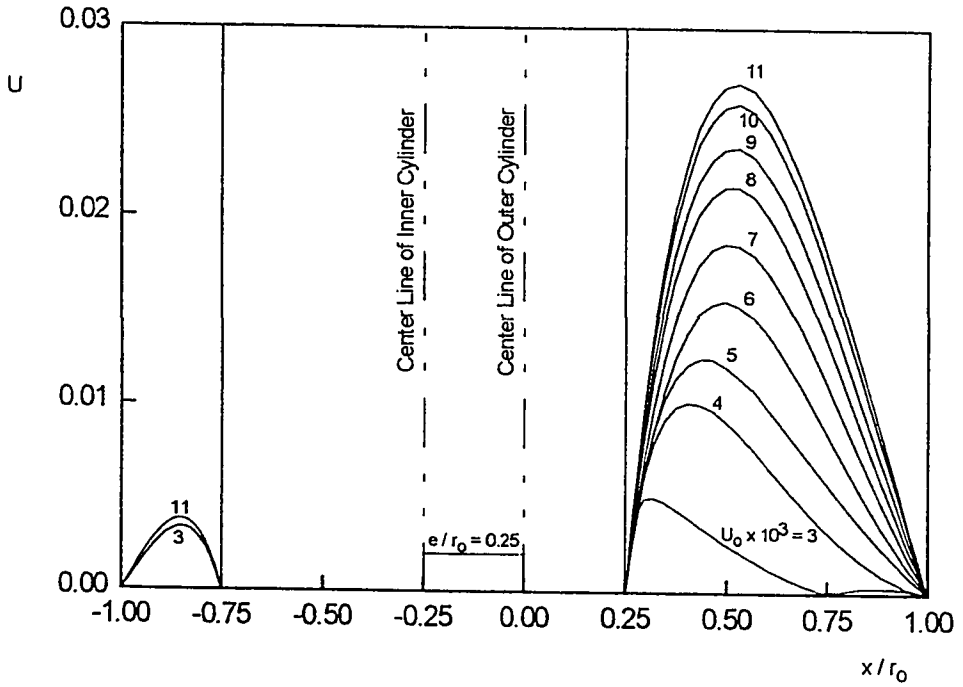


Fig. 8.1(d) : Axial velocity profiles at the channel exit for different flow rates (i.e., different channel heights), case 1.I, N = E = 0.5.

the resistance to flow on the narrowest / widest gap side of the annulus, the axial velocity profile develops with increasing / decreasing values on the widest / narrowest gap side of the annulus as the flow moves away from the entrance. Such a development continues until $U$ reaches its invariant fully-developed axial-velocity profile if the channel is high enough.

Figure 8.1(b) shows the velocity profiles at the channel exit for different induced flow rates (i.e., different channel heights) under boundary conditions 1.O. The developing axial velocity profiles in the widest and narrowest sides of the gap under thermal boundary condition 1.I in an annulus of $N = 0.5$ and $E = 0.5$ for an induced flow rate of uniform inlet velocity corresponding very nearly to the fully developed flow rate ($F = 0.00825$ and $F_{fd} = 0.008682$) are shown in Figure 8.1(c). The velocity profiles at the channel exit for different induced flow rates (i.e., different channel heights) under boundary conditions 1.I are presented in Fig. 8.1(d). The fully-developed velocity profiles obtained via solution of the developing flow in the entry region are in excellent agreement with those obtained by solving the pertinent governing equations for the corresponding fully-developed free convection in vertical eccentric annuli which have been presented in Chapter 5.

Each of Figs. 8.2(a) through 8.2(e) gives the developing axial velocity distribution (U versus Z) for a given value of $\xi$ as one rotates around this annulus($N = E = 0.5$, $F = 0.00825$, case 1.I) from its widest side ( $\psi = \xi = 0$ ) to its narrowest side ($\psi = 1$,i.e., $\xi = \pi$ ). Velocity profiles similar to those presented in Fig. 8.1(a) and 8.1(c) could be obtained, for any axial location ($Z$) and a specified value of $\xi$, by cross plotting in

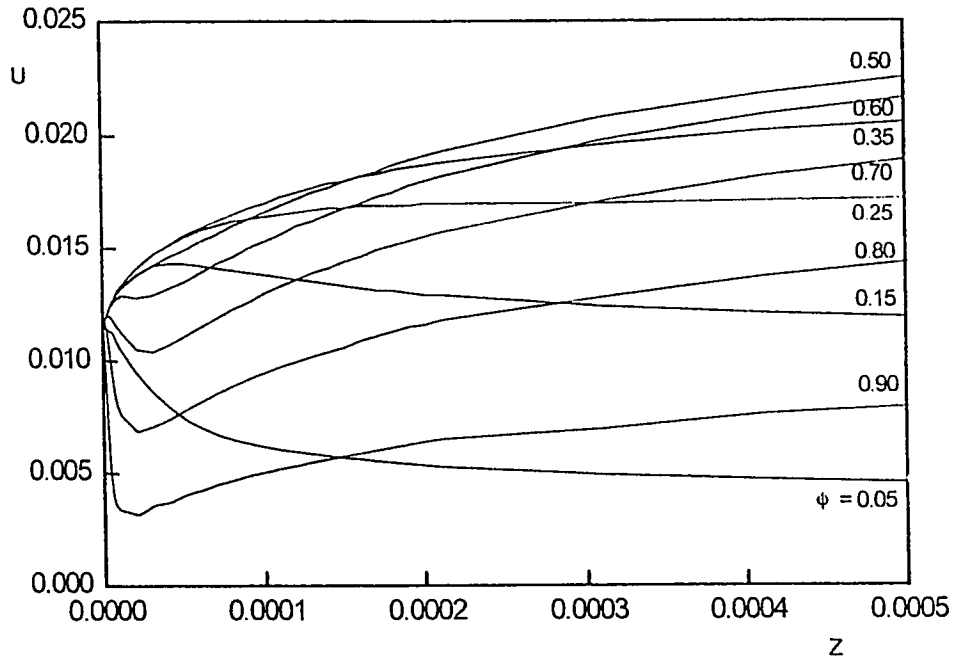


Fig. 8.2(a) : Development of the axial velocity component at different values of $\phi$, $\psi = 0.0$ (widest gap), case 1.I, N = E =0.5.

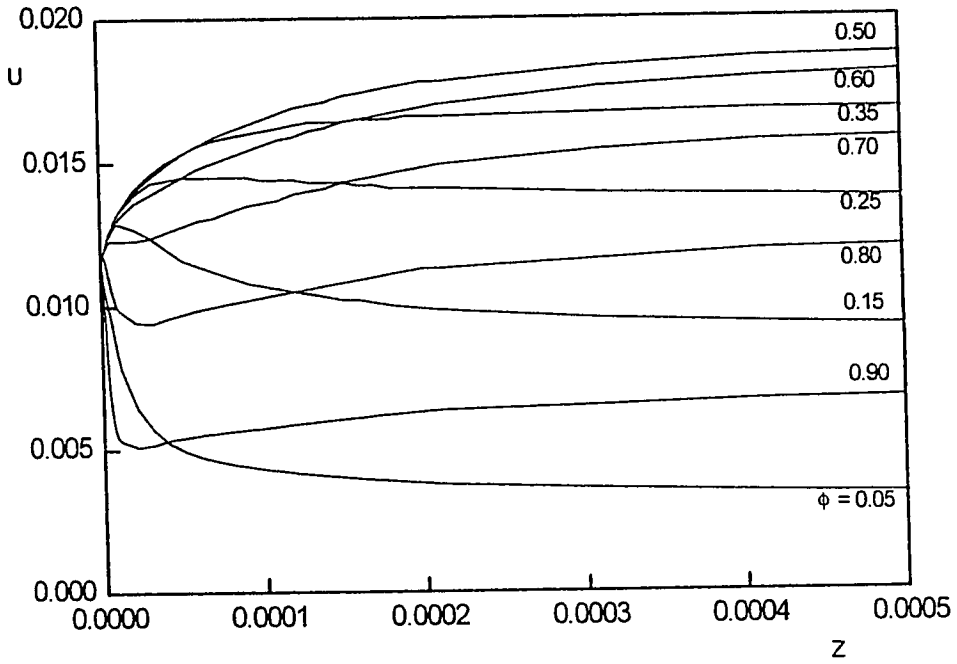


Fig. 8.2(b) : Development of the axial velocity component at different values of $\phi$, $\psi = 0.25$, case 1.I, N = E =0.5.

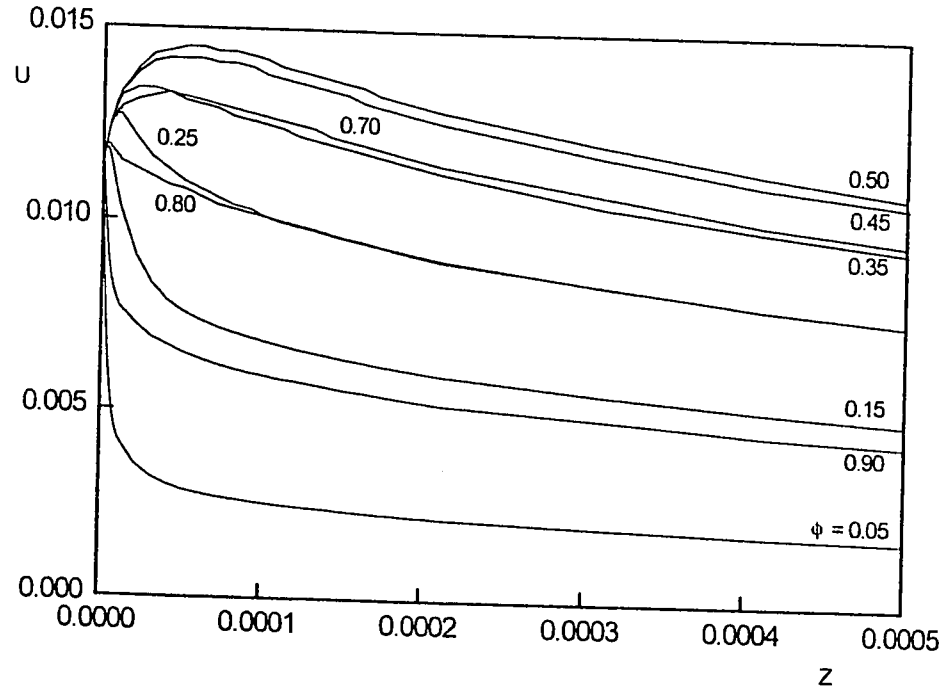


Fig. 8.2(c) : Development of the axial velocity component at different values of $\phi$, $\psi = 0.50$, case 1.I, $N = E = 0.5$.

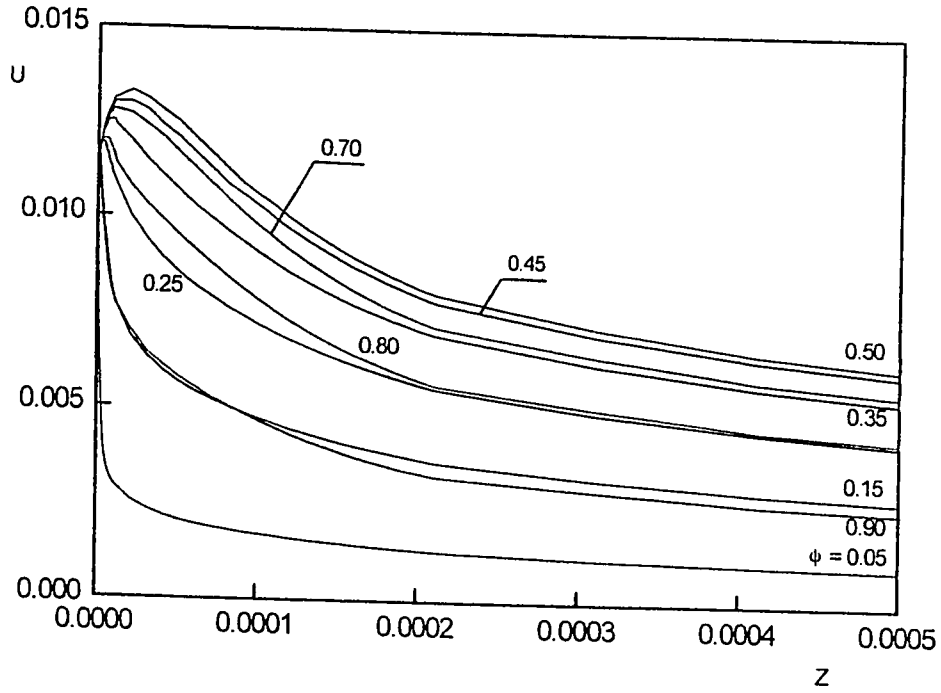


Fig. 8.2(d) : Development of the axial velocity component at different values of $\phi$, $\psi = 0.75$, case 1.I, $N = E = 0.5$.

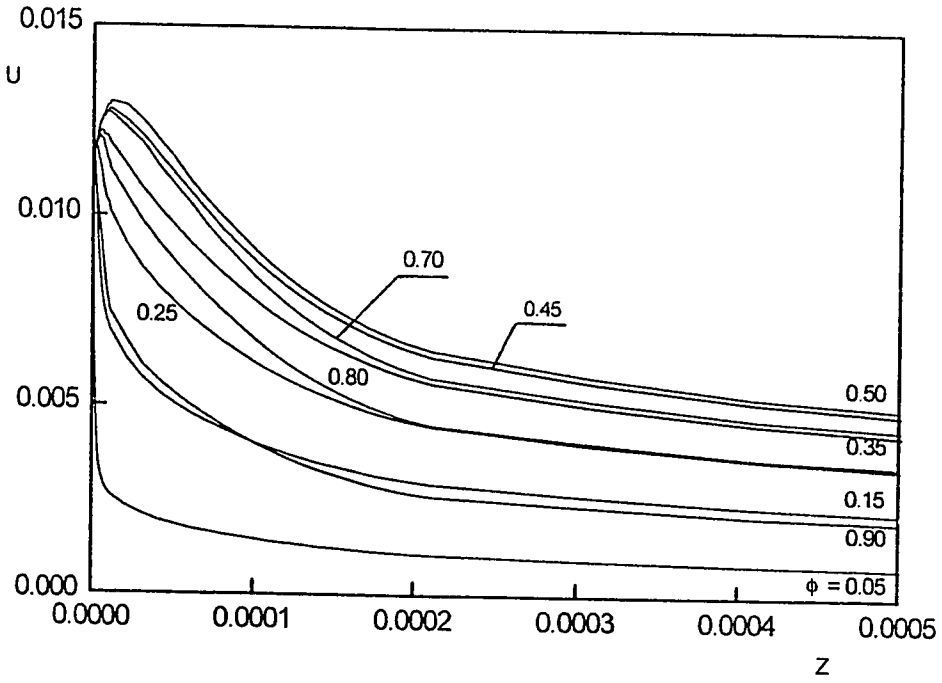


Fig. 8.2(e) : Development of the axial velocity component at different values of $\phi$, $\psi = 1.0$ (narrowest gap), case 1.I, N = E =0.5.

Figs. 8.2(a-e). In each of these latter figures, nine curves corresponding to some selected values of the normalized $\eta$- coordinate ($\phi$) are drawn. These figures (8.2(a) through 8.2(e)) focus on the entry region before the flow reaches full development. The profiles shown in Fig. 8.1(a) or the distributions given in Figs. 8.2(a-e), show similar trends as the profiles in forced convection which were presented in Chapter 7. At the early stages of the axial velocity development (small values of $Z$) fluid adjacent to the annulus two walls ( e.g. $\phi = 0.05$ and 0.95) decelerates due to the formation of the two hydrodynamic boundary-layers on these two boundaries. Consequently, as a result of continuity principle, fluid outside these two boundary-layers ( e.g. $\phi$ = 0.45 to 0.6 ) accelerates. However, due to the increased resistance to flow in the narrow side of the annulus ( as a result of eccentricity ) the fluid on this narrow gap side moves in a tangentially-like direction ( in $\xi$-direction with a velocity component $W$ ) to the wide gap side of the annulus. Such a tangentially-like fluid transportation from the narrow gap side to the wide gap side increases as the flow moves away from the entrance ( Z increases ) and thus causes a reduction in the values of the axial velocity profile on the narrow gap side and vice versa on the wide gap side. However, far enough from the entrance such a tangential-like transportation decays as the flow approaches hydrodynamic full-development with $V=W = 0$. Again, the acceleration of fluid outside the developing boundary layers on the widest gap side of the annulus is thus created by (1) transportation of fluid from inside these two boundary layers by means of the V-component of velocity and (2) transportation of fluid from the narrowest gap side of the annulus by means of the W-component of velocity. On the other hand, the fluid outside

the two developing hydrodynamic boundary layers on the narrowest gap side of the annulus undergoes two counteracting actions, namely, acceleration due to fluid transportation from inside these two boundary layers by means of the V-component of velocity and deceleration engendered by transportation of fluid from the narrowest gap side to the widest gap side by means of W-component of velocity. The latter action overcomes the first as the flow moves downstream the entrance cross-section and hence the resultant effect creates decreasing values of the axial velocity component on the narrowest gap side of the annulus. However, both actions gradually decay with further increases in the axial distance Z and finally vanish when the flow becomes hydrodynamically fully developed.

The development of the temperature profiles on the heat transfer wall in cases with uniform wall heat flux is one of the important heat transfer parameters that can explain the physical behaviour of the Nusselt number on such walls. Figures 8.2 (f) through 8.3(g) present the development of the temperature profiles on the inner heated wall for case 2.I in an annulus of N = 0.5 and eceentricity E = 0.5 for a flow rate F = 0.06. The corresponding development of the temperature profiles on the outer insulated wall under the same boundary conditions are given in Figs. 8.2(i, j and k). Figure 8.2(*l*) presents the development of the temperature profiles on the heat transfer (inner) wall for case 4.I in an annulus of N = 0.5 and eccentricity E = 0.5 for a flow rate F = 0.00326.

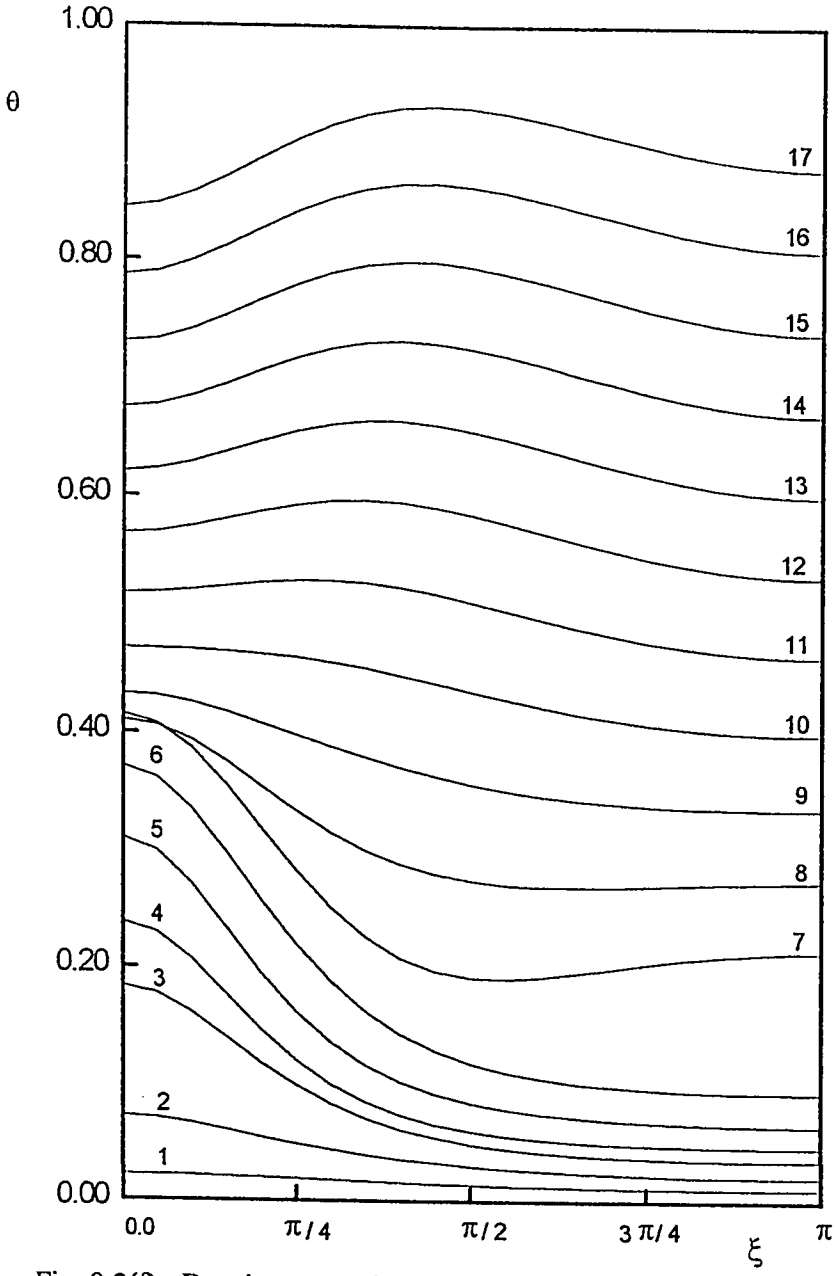


| curve # | distance x10³ |
|---|---|
| 1 | 4 x 10⁻³ |
| 2 | 2.12 |
| 3 | 7.12 |
| 4 | 12.12 |
| 5 | 31.12 |
| 6 | 81.12 |
| 7 | 321.12 |
| 8 | 821.12 |
| 9 | 1321.12 |
| 10 | 1821.12 |
| 11 | 2321.12 |
| 12 | 2821.12 |
| 13 | 3321.12 |
| 14 | 3821.12 |
| 15 | 4321.12 |
| 16 | 4821.12 |
| 17 | 5321.12 |
| 18 | 5821.12 |
| 19 | 6821.12 |
| 20 | 7821.12 |
| 21 | 8821.12 |
| 22 | 9821.12 |
| 23 | 10821.12 |
| 24 | 11821.12 |
| 25 | 12821.12 |
| 26 | 13821.12 |
| 27 | 14321.12 |
| 28 | 15321.12 |
| 29 | 16321.12 |
| 30 | 17321.12 |
| 31 | 18321.12 |
| 32 | 19321.12 |
| 33 | 20321.12 |
| 34 | 21321.12 |
| 35 | 21821.12 |
| 36 | 23321.12 |
| 37 | 24821.12 |
| 38 | 26321.12 |
| 39 | 27821.12 |
| 40 | 29321.12 |
| 41 | 30821.12 |
| 42 | 32321.12 |
| 43 | 33821.12 |
| 44 | 35321.12 |
| 45 | 36821.12 |
| 46 | 38321.12 |
| 47 | 39321.12 |
| 48 | 41321.12 |

Fig. 8.2(f) : Development of the temperature profiles on the inner heated wall, case 2.I, N = Ξ = 0.5.

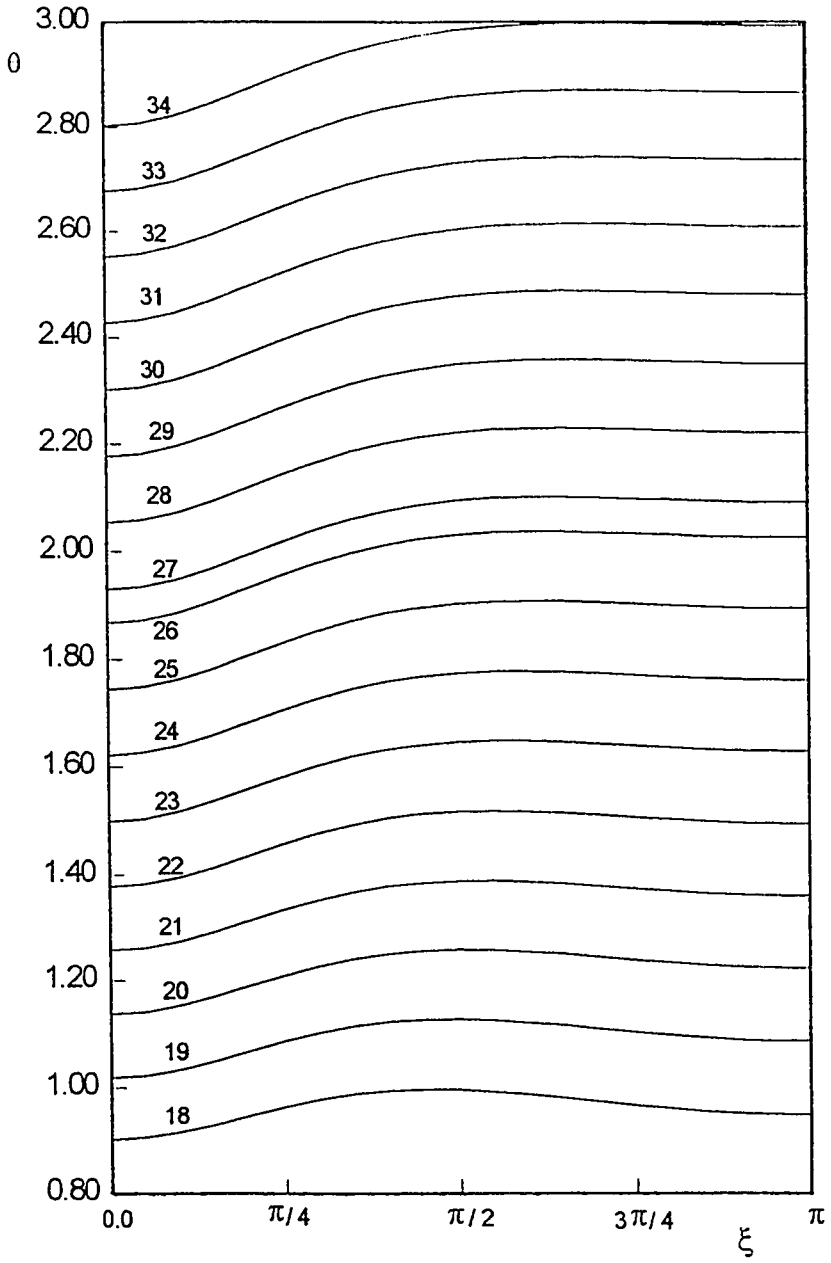


Fig. 8.2(g) : Development of the temperature profiles on the inner heated wall, case 2.I, N = E = 0.5, (previous figure continue)

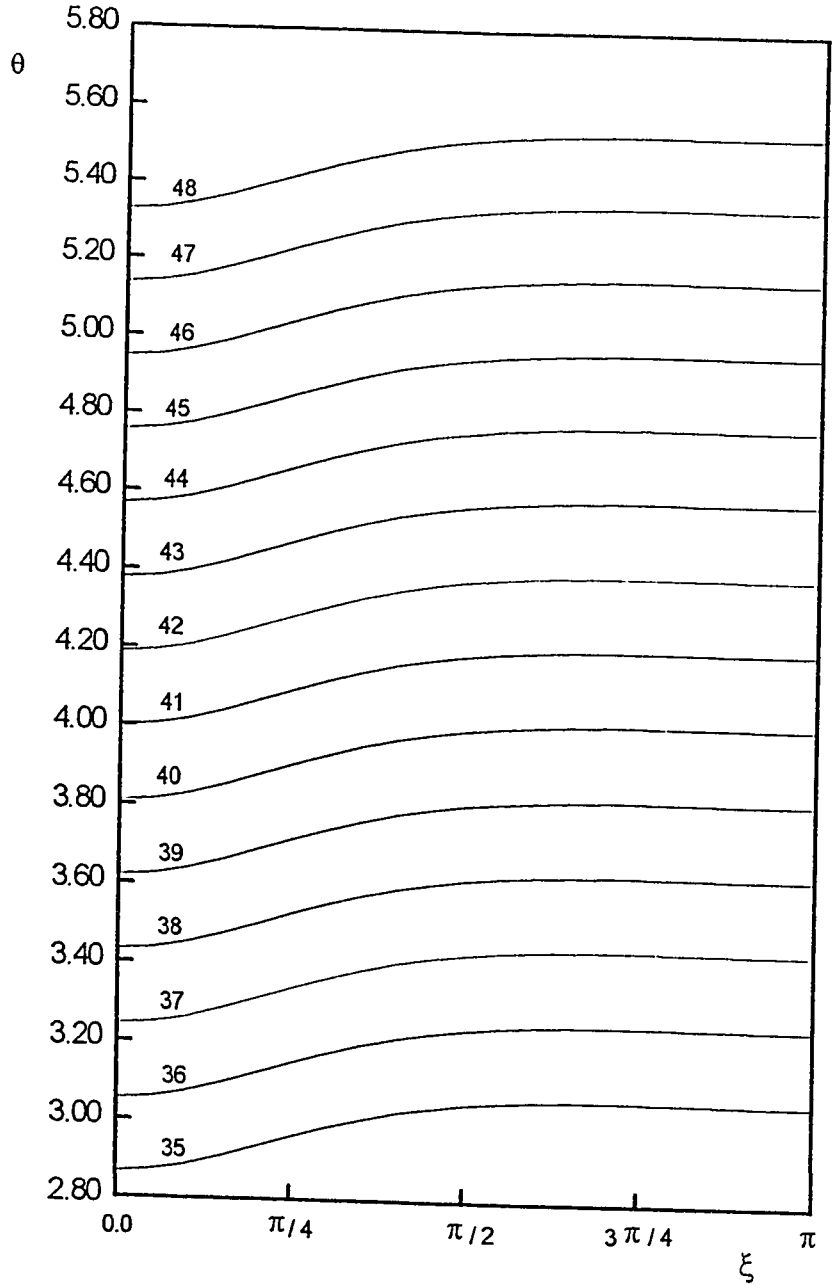


Fig. 8.2(h) : Development of the temperature profiles on the inner heated wall, case 2.I, N = E = 0.5, (previous figure continue).

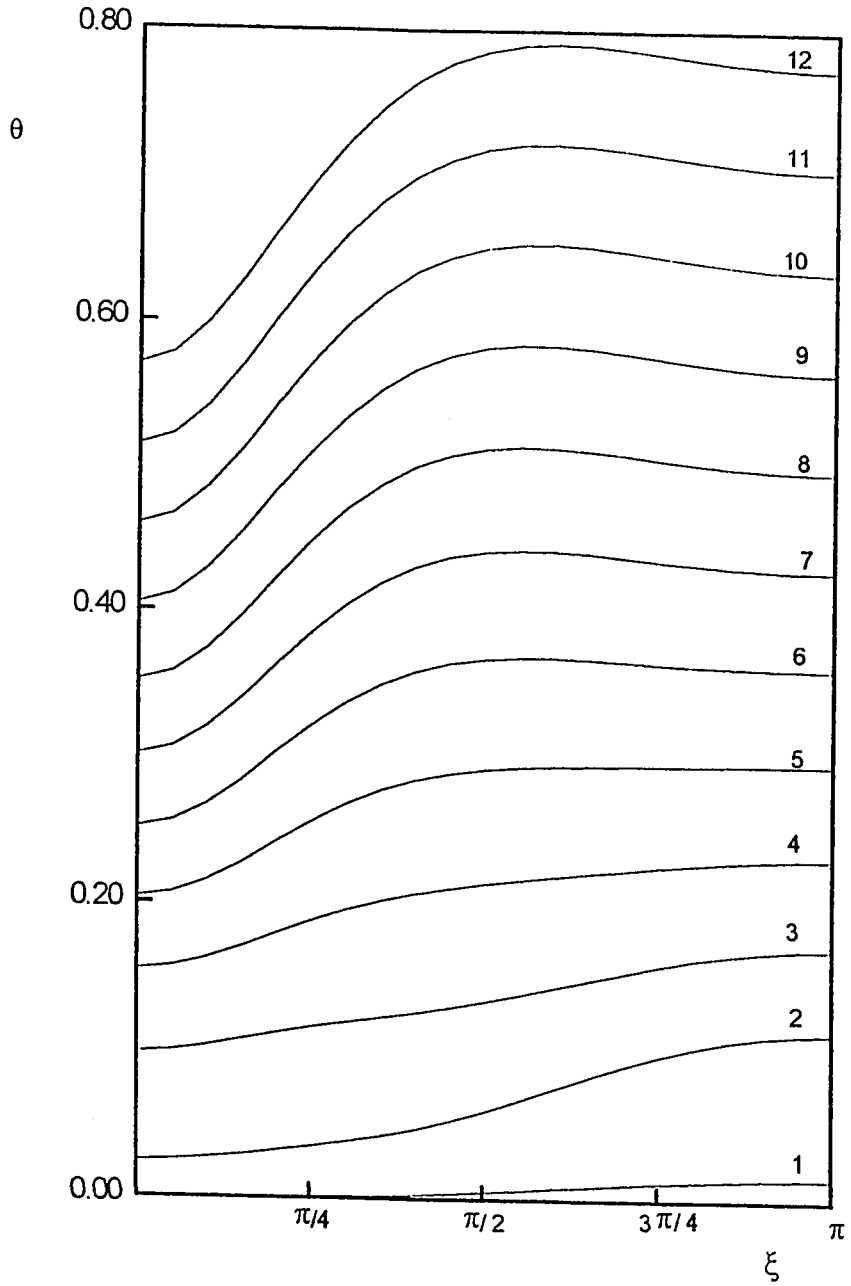


| curve # | distance x10⁴ |
|---|---|
| 1 | 81.12 |
| 2 | 321.12 |
| 3 | 821.12 |
| 4 | 1321.12 |
| 5 | 1821.12 |
| 6 | 2321.12 |
| 7 | 2821.12 |
| 8 | 3321.12 |
| 9 | 3821.12 |
| 10 | 4321.12 |
| 11 | 4821.12 |
| 12 | 5321.12 |
| 13 | 5821.12 |
| 14 | 6821.12 |
| 15 | 7821.12 |
| 16 | 8821.12 |
| 17 | 9821.12 |
| 18 | 10821.12 |
| 19 | 11821.12 |
| 20 | 12821.12 |
| 21 | 13821.12 |
| 22 | 14321.12 |
| 23 | 15321.12 |
| 24 | 16321.12 |
| 25 | 17321.12 |
| 26 | 18321.12 |
| 27 | 19321.12 |
| 28 | 20321.12 |
| 29 | 21321.12 |
| 30 | 21821.12 |
| 31 | 23321.12 |
| 32 | 24821.12 |
| 33 | 26321.12 |
| 34 | 27821.12 |
| 35 | 29321.12 |
| 36 | 30821.12 |
| 37 | 32321.12 |
| 38 | 33821.12 |
| 39 | 35321.12 |
| 40 | 36821.12 |
| 41 | 38321.12 |
| 42 | 39321.12 |
| 43 | 41321.12 |

Fig. 8.2(i) : Development of the temperature profiles on the outer insulated wall, case 2.I, N = E = 0.5.

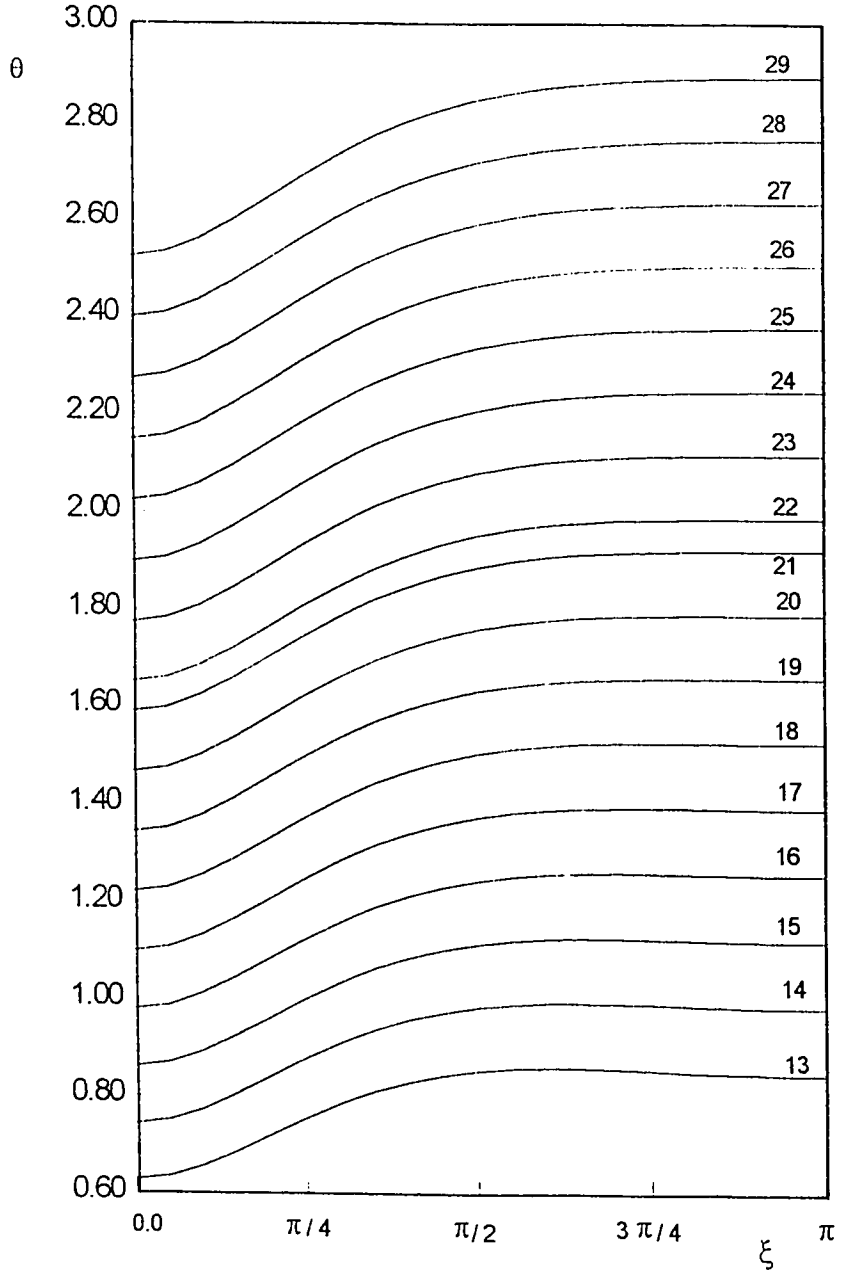


Fig. 8.2(j) : Development of the temperature profiles on the outer insulated wall, case 2.I, N = E = 0.5, (previous figure continue)

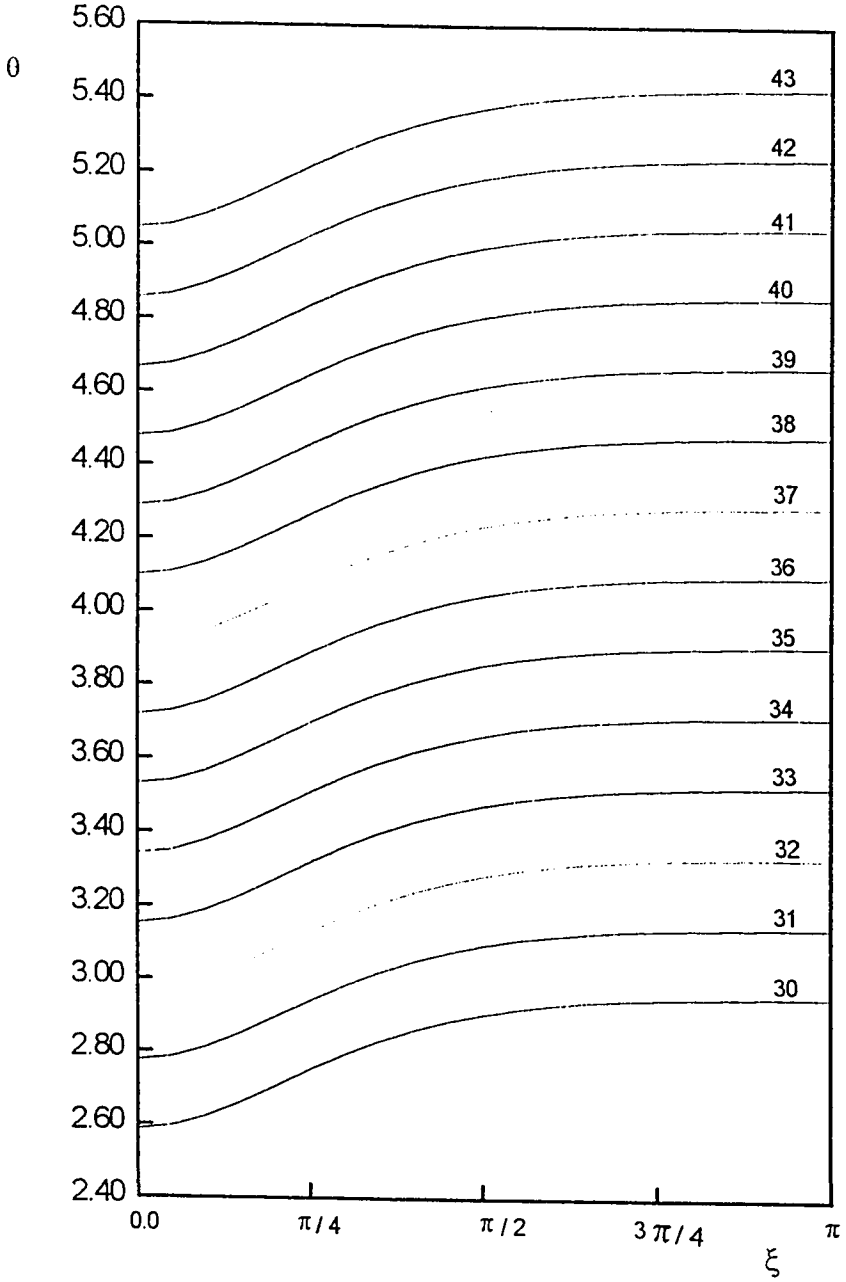


Fig. 8.2(k) : Development of the temperature profiles on the outer insulated wall, case 2.I, N = E = 0.5, (previous figure continue).

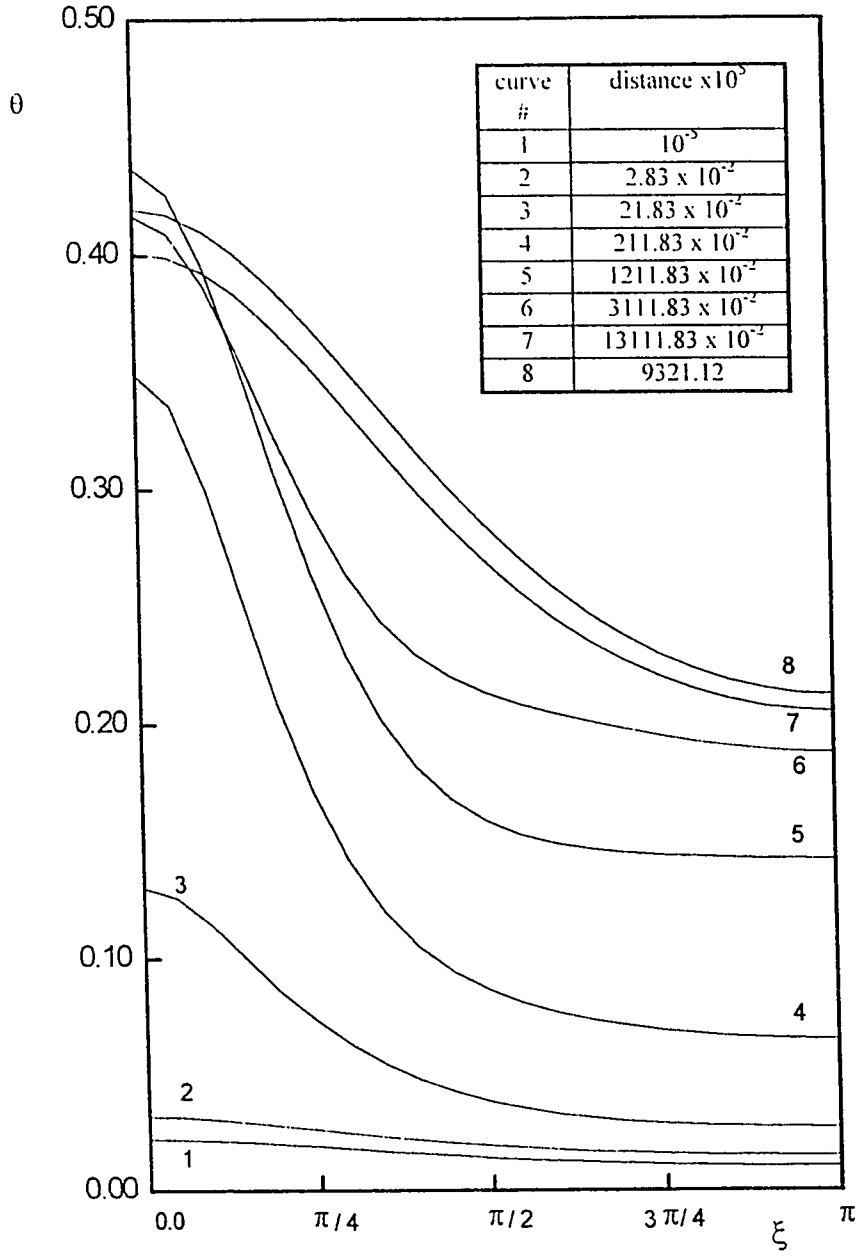


Fig. 8.2(*l*) : Development of the temperature profiles on the inner heated wall, case 4.1, N = E = 0.5.

### 8.2.2 Engineering Parameters

For given N and E, one of the most imprtant engineering parameters is the channel height required to naturally induce a specific flow rate under specific thermal boundary conditions. This channel height can be predicted by monitoring the development of the dimensionless pressure from the entrance of the channel till its exit. The channel exit(channel height) is determined for a specific flow rate when the dimensionless pressure becomes zero. Therefore, the development of the pressure with axial distance has been plotted for all cases considered. The axial development of pressure for cases 1.I and 1.O in an annulus of N = 0.5 and E = 0.1 are presented in Figs. 8.3(a) and (b), respectively. Results for cases 1.I and 1.O with E = 0.5 are presented in Figs. 8.3(c) and (d) while Figs. 8.3(e,f) and 8.3(g,h,i) summarize the results for cases 1.I and 1.O for an annulus of E = 0.7. Figures 8.4(a) through 8.4(f) present the results for cases 2.I and 2.O in annuli of E = 0.1, 0.5 and 0.7. Results for case 3.I in an approximately concentric annulus ( E = $10^{-6}$) are presented in Figs. 8.5(a-c). The development of the pressure with Z for cases 3.I and 3.O with an eccentricity of 0.5 are presented in Figs. 8.5(d) and 8.5(e), respectively. Figures 8.6(a) through 8.6(f) present results for cases 4.I and 4.O with E = 0.1, 0.5 and 0.7. Each of these figures gives the development of the pressure for different flow rates at the same eccentricity and the same thermal boundary conditions. These figures show that the inlet negative pressure will decrease due to friction as the flow moves up in the annulus. The negative pressure gradient will decrease until it reaches a zero value then starts to increase (i.e., it becomes

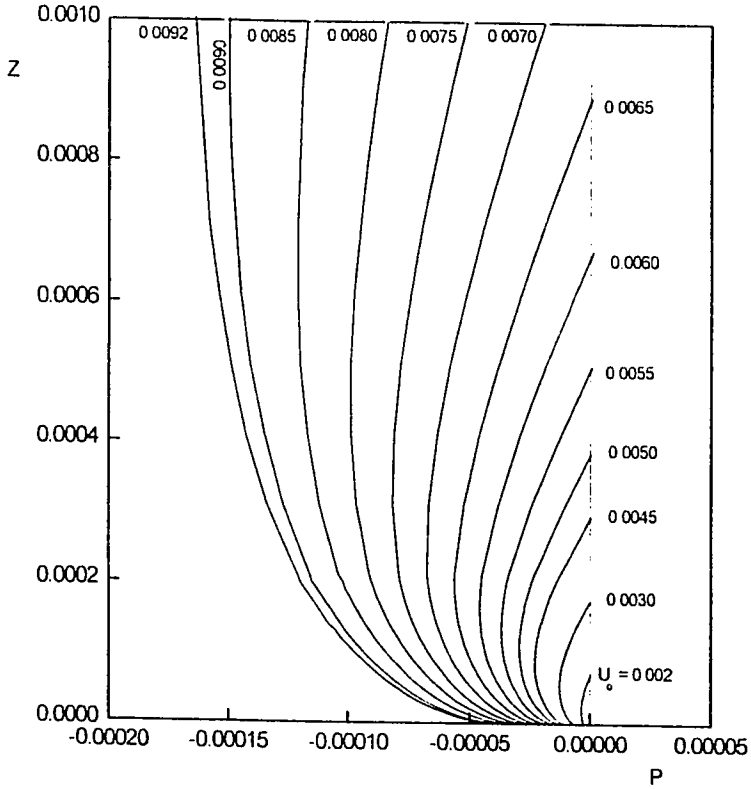


Fig. 8.3(a) : Development of the pressure with Z for different values of the induced volumetric flow rate (i.e., different channel heights), case 1.1, N = 0.5, E = 0.1.

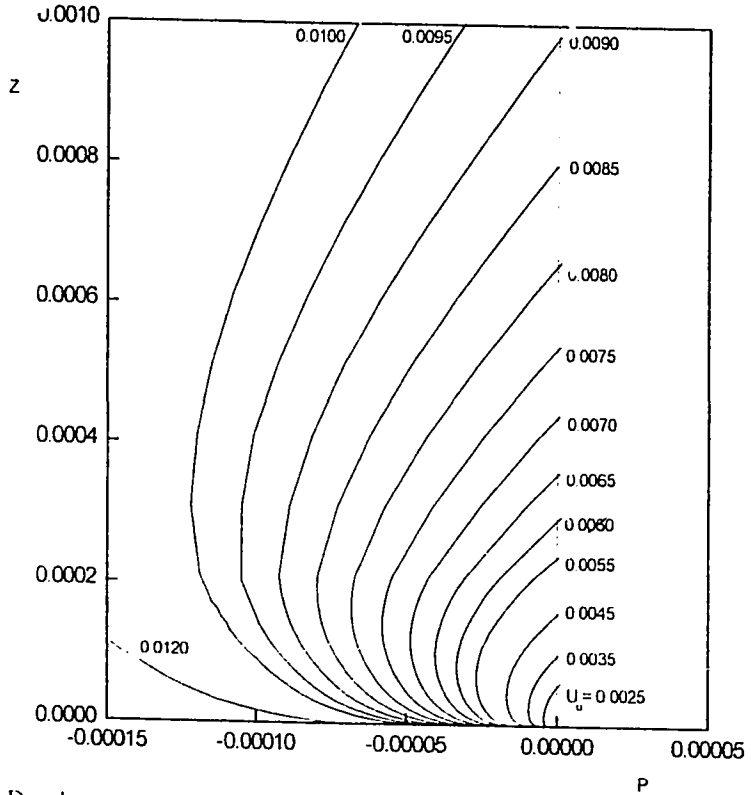


Fig. 8.3(b) : Development of the pressure with Z for different values of the induced volumetric flow rate (i.e., different channel heights), case 1.O, N = 0.5, E = 0.1.

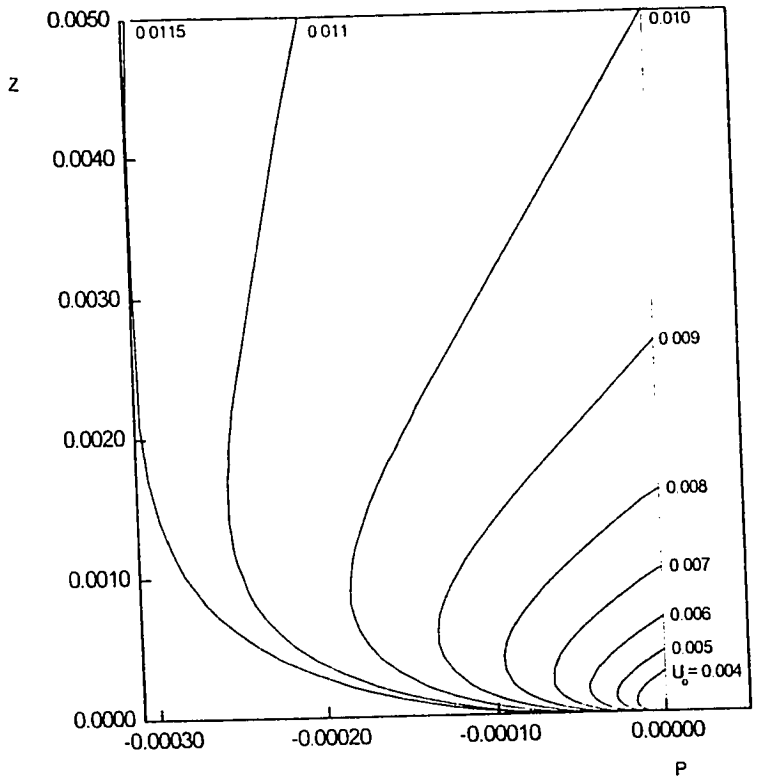


Fig. 8.3(c) : Development of the pressure with Z for different values of the induced volumetric flow rate (i.e., different channel heights), case 1.1, N = 0.5, E = 0.5.

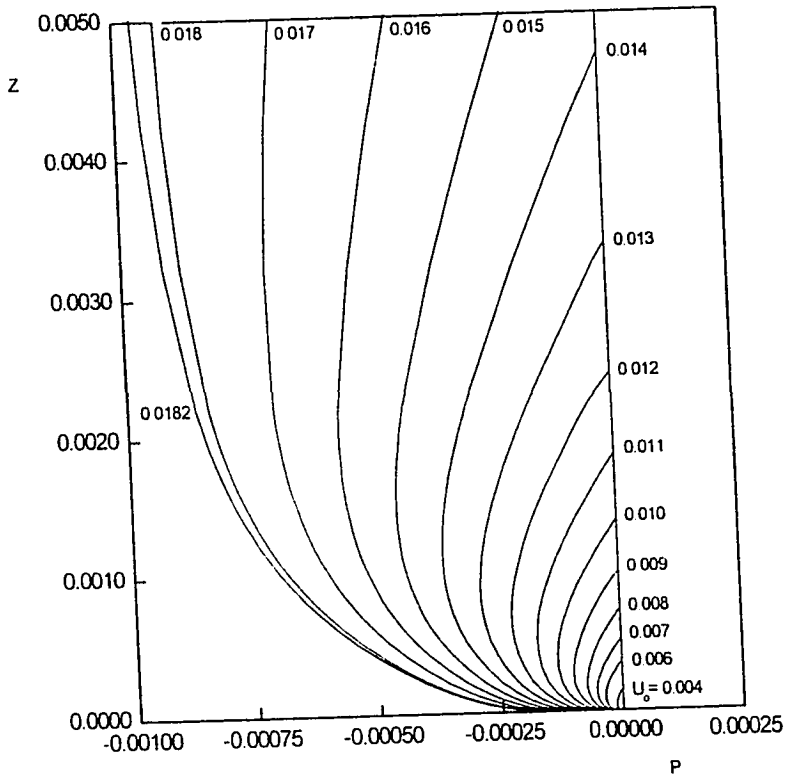


Fig. 8.3(d) : Development of the pressure with Z for different values of the induced volumetric flow rate (i.e., different channel heights), case 1.0, N = 0.5, E = 0.5.

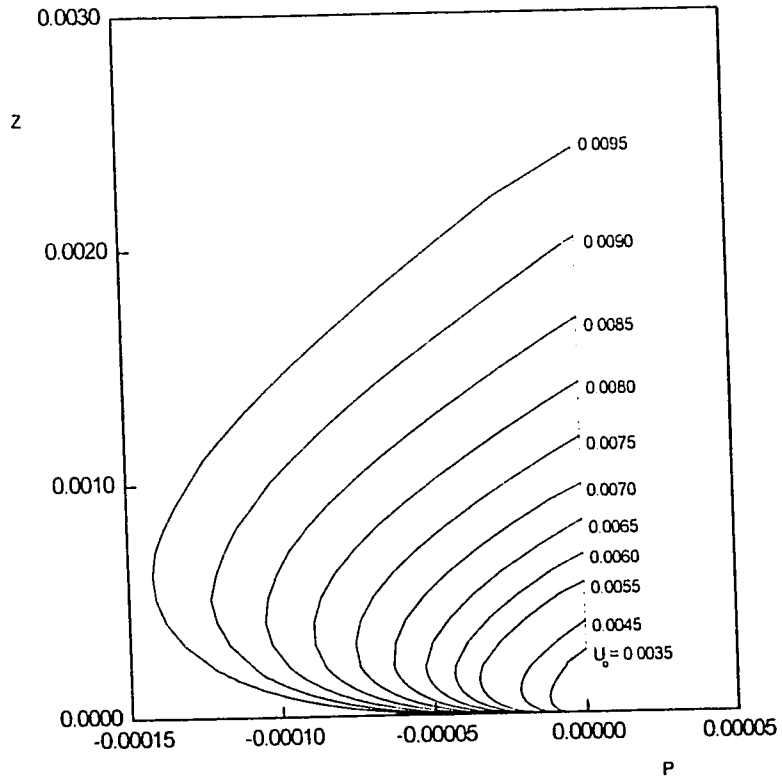


Fig. 8.3(e) : Development of the pressure with Z for different values of the induced volumetric flow rate (i.e., different channel heights), case 1.1, N = 0.5, E = 0.7.

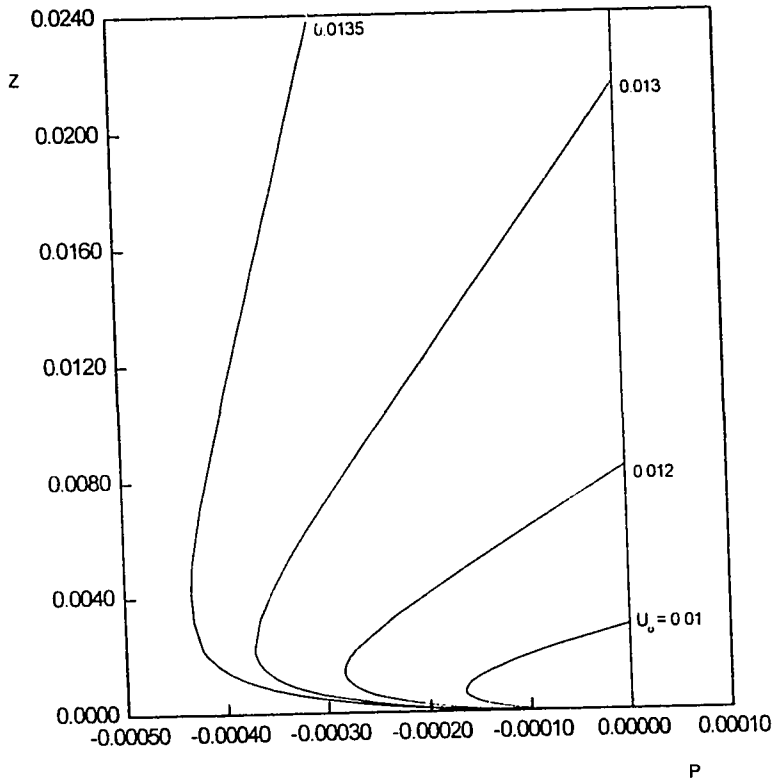


Fig. 8.3(f) : Development of the pressure with Z for different values of the induced volumetric flow rate (i.e., different channel heights), case 1.1, N = 0.5, E = 0.7, (previous figure continue).

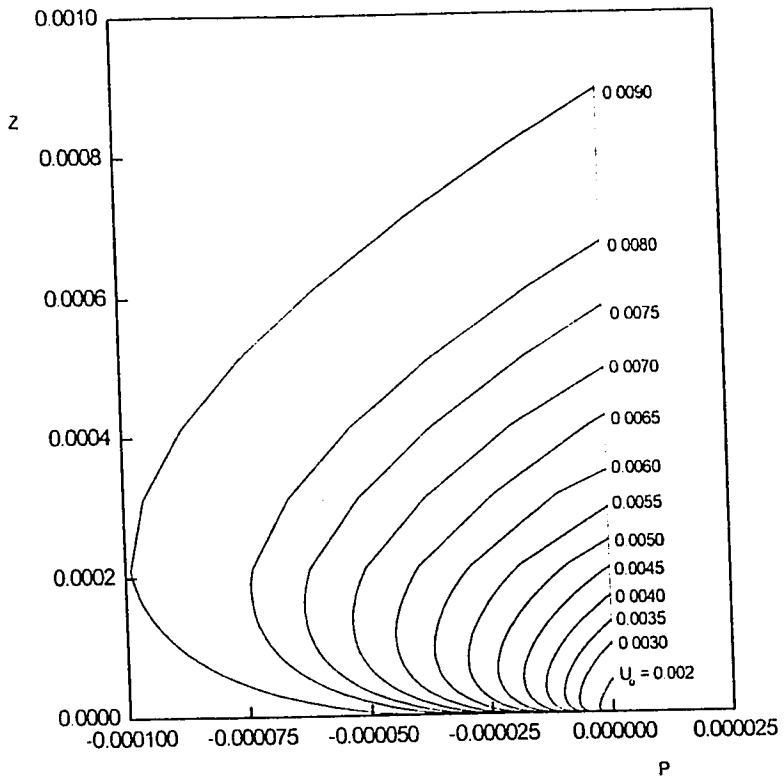


Fig. 8.3(g) : Development of the pressure with Z for different values of the induced volumetric flow rate (i.e., different channel heights), case 1.O, N = 0.5, E = 0.7.

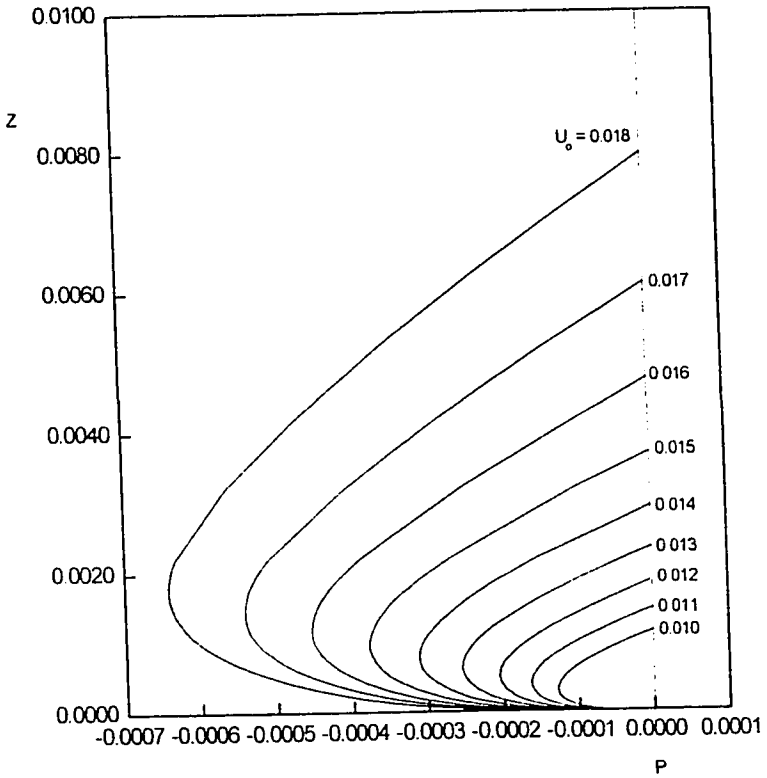


Fig. 8.3(h) : Development of the pressure with Z for different values of the induced volumetric flow rate (i.e., different channel heights), case 1.O, N = 0.5, E = 0.7, (previous figure continue).

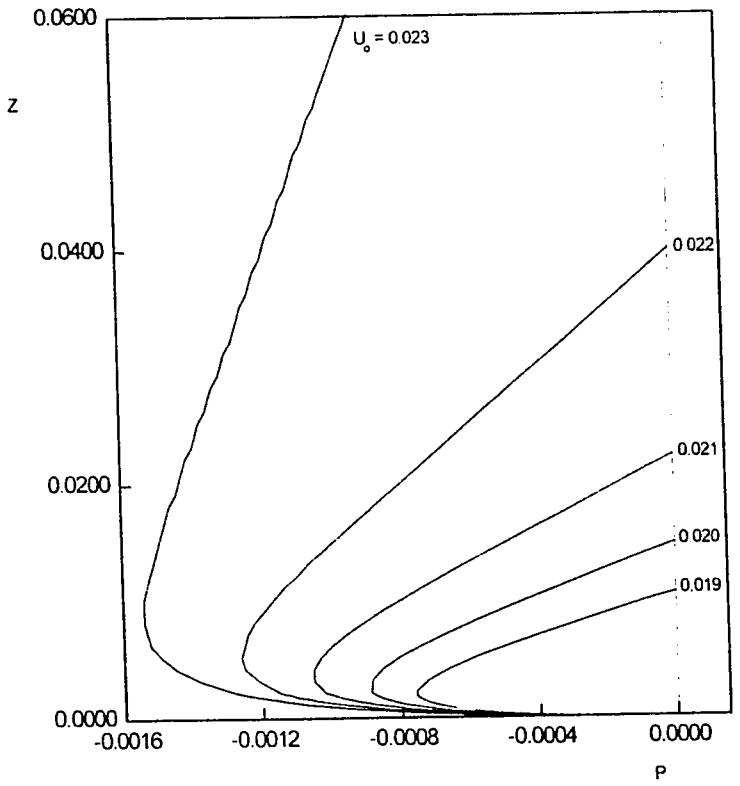


Fig. 8.3(i) : Development of the pressure with Z for different values of the induced volumetric flow rate (i.e., different channel heights), case 1.O, N = 0.5, E = 0.7, (previous figure continue).

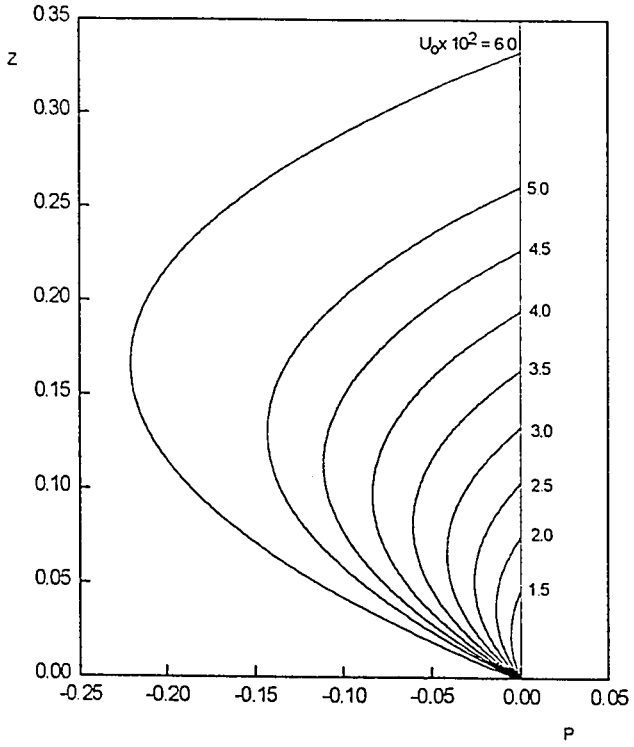


Fig. 8.4(a) : Development of the pressure with Z for different values of the induced volumetric flow rate (i.e., different channel heights), case 2.I, N =0.5, E = 0.1.

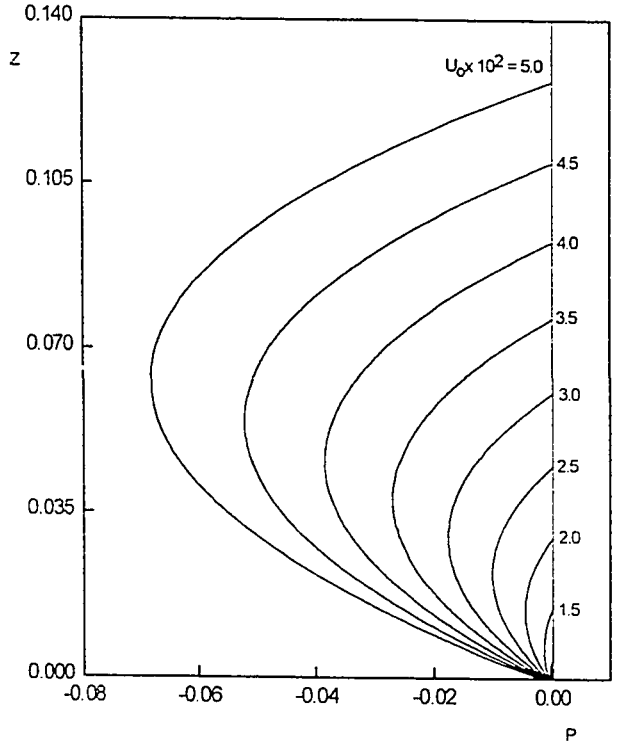


Fig. 8.4(b) : Development of the pressure with Z for different values of the induced volumetric flow rate (i.e., different channel heights), case 2.O, N =0.5, E = 0.1.

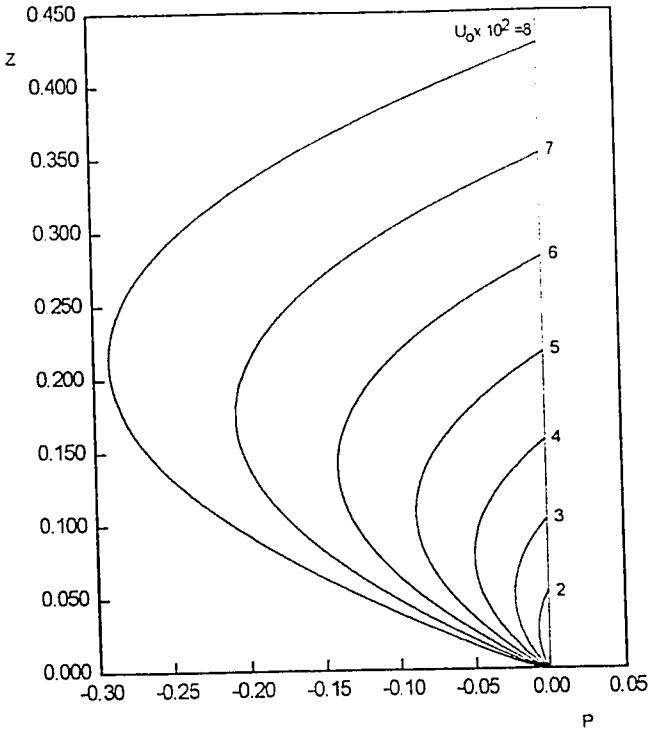


Fig. 8.4(c) : Development of the pressure with Z for different values of the induced volumetric flow rate (i.e., different channel heights), case 2.I, N =0.5, E = 0.5.

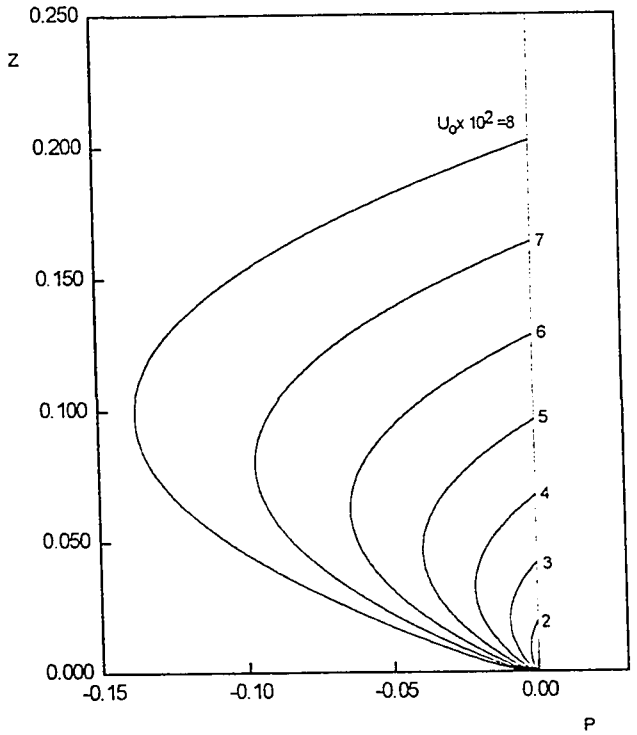


Fig. 8.4(d) : Development of the pressure with Z for different values of the induced volumetric flow rate (i.e., different channel heights), case 2.O, N =0.5, E = 0.5.

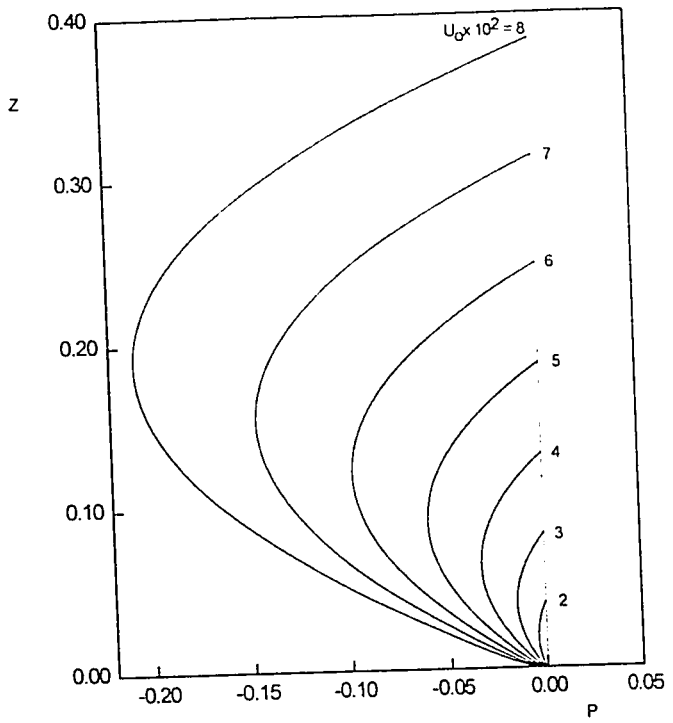


Fig. 8.4(e) : Development of the pressure with Z for different values of the induced volumetric flow rate (i.e., different channel heights), case 2.I, N =0.5, E = 0.7.

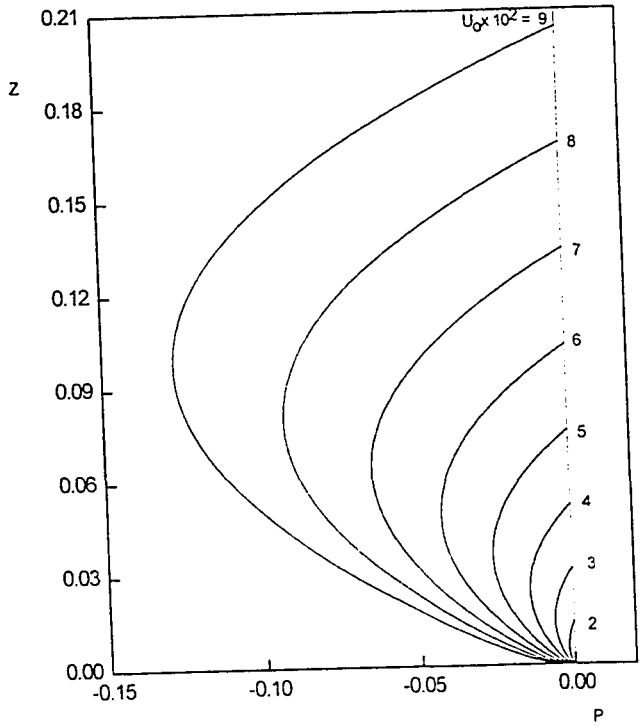


Fig. 8.4(f) : Development of the pressure with Z for different values of the induced volumetric flow rate (i.e., different channel heights), case 2.O, N =0.5, E = 0.7.

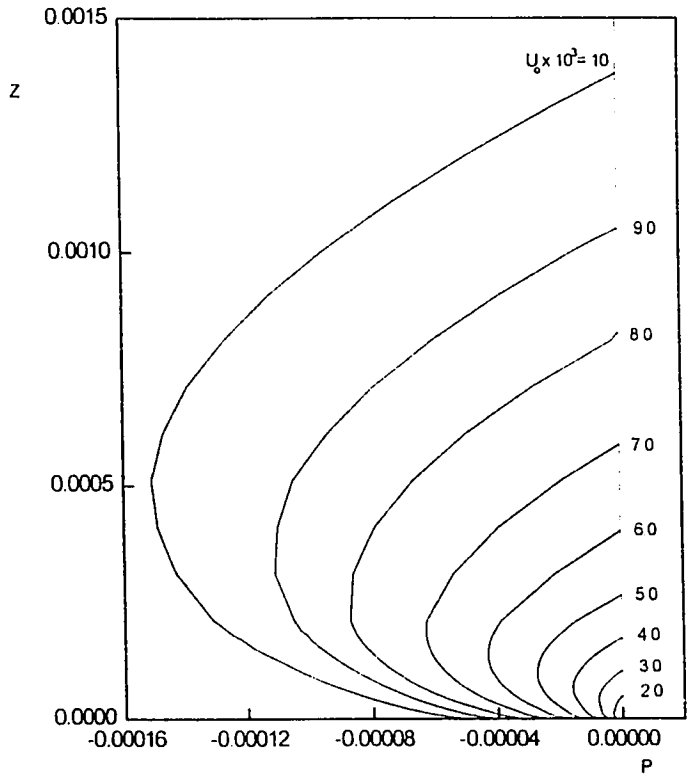


Fig. 8.5(a) : Development of the pressure with Z for different values of the induced volumetric flow rate (i.e., different channel heights), case 3.I, N = 0.5, E = $10^{-6}$.

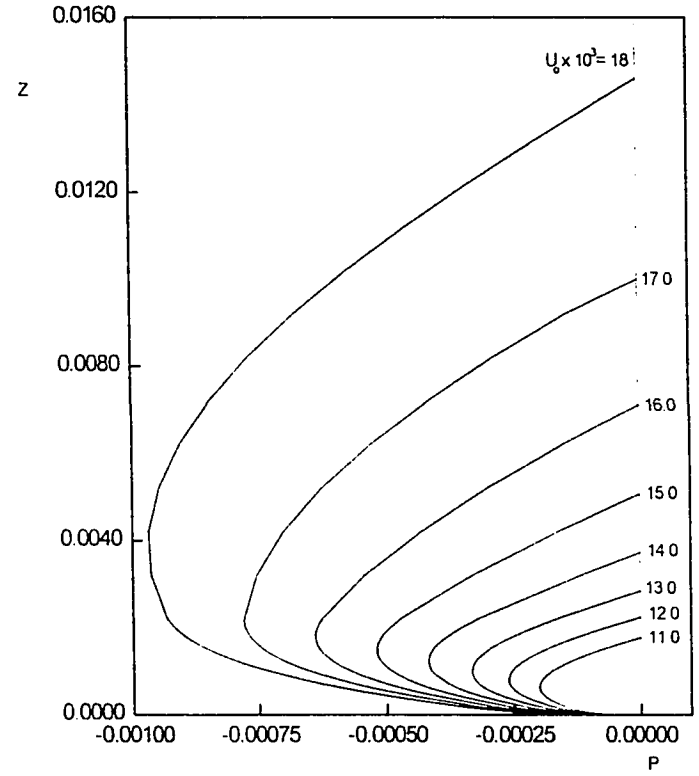


Fig. 8.5(b) : Development of the pressure with Z for different values of the induced volumetric flow rate (i.e., different channel heights), case 3.I, N = 0.5, E = $10^{-6}$, (previous figure continue).

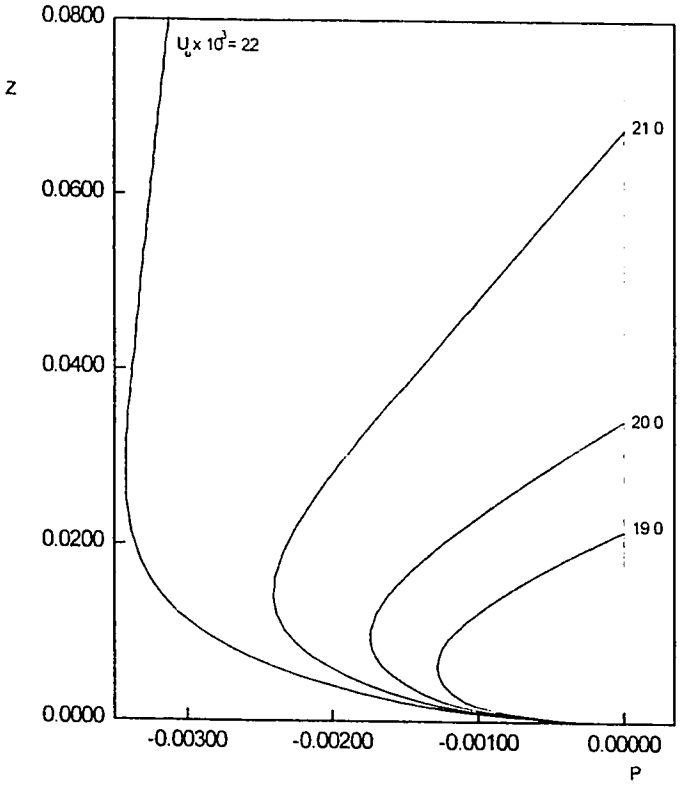


Fig. 8.5(c) : Development of the pressure with Z for different values of the induced volumetric flow rate (i.e., different channel heights), case 3.1, N = 0.5, E = $10^{-6}$, (previous figure continue).

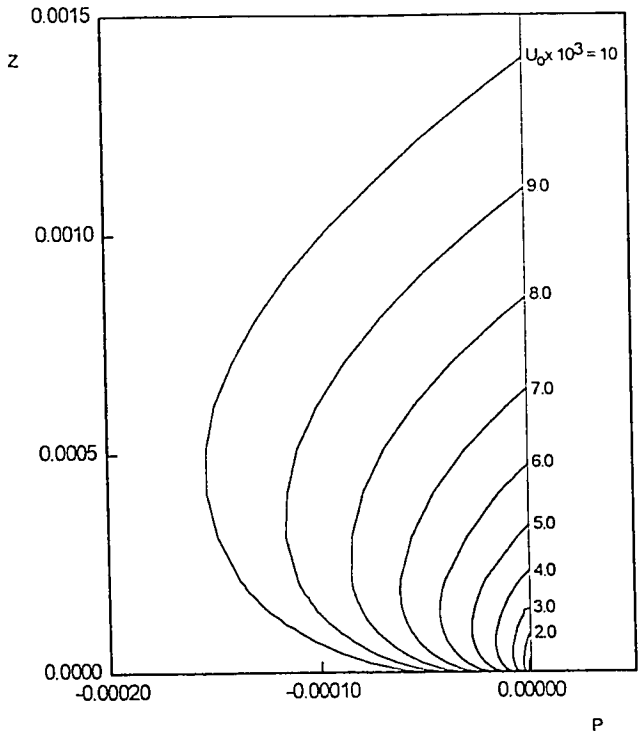


Fig. 8.5(d) : Development of the pressure with Z for different values of the induced volumetric flow rate (i.e., different channel heights), case 3.I, N =0.5, E =0.5.

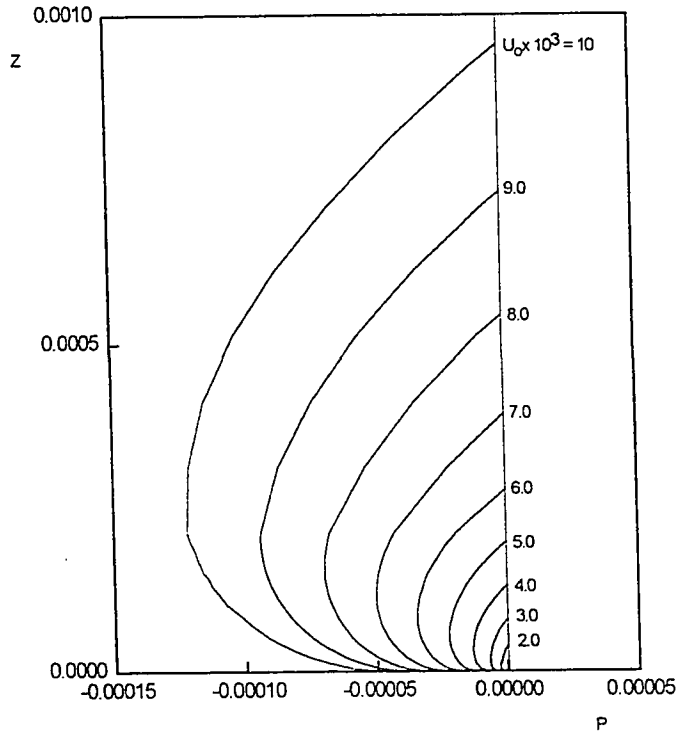


Fig. 8.5(e) : Development of the pressure with Z for different values of the induced volumetric flow rate (i.e., different channel heights), case 3.O, N =0.5, E = 0.5.

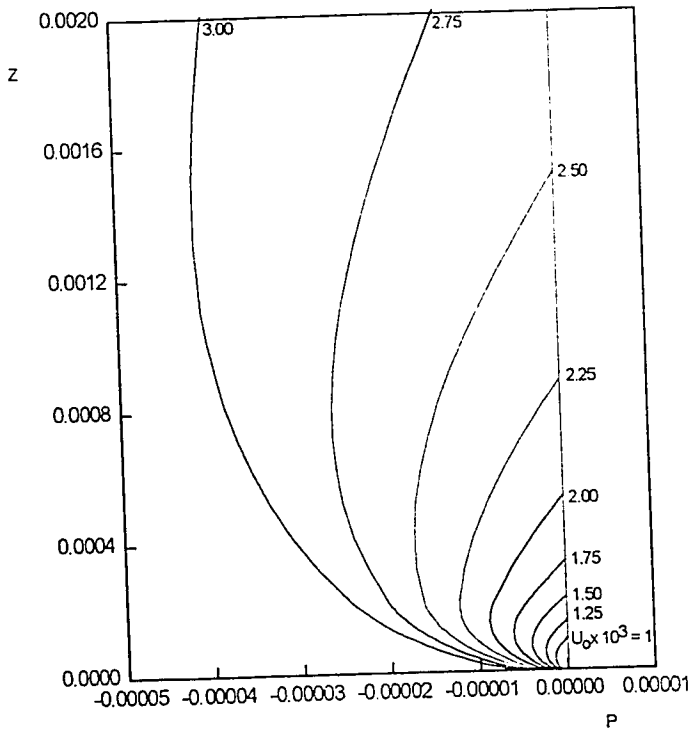


Fig. 8.6(a) : Development of the pressure with Z for different values of the induced volumetric flow rate (i.e., different channel heights), case 4.I, N =0.5, E =0.1.

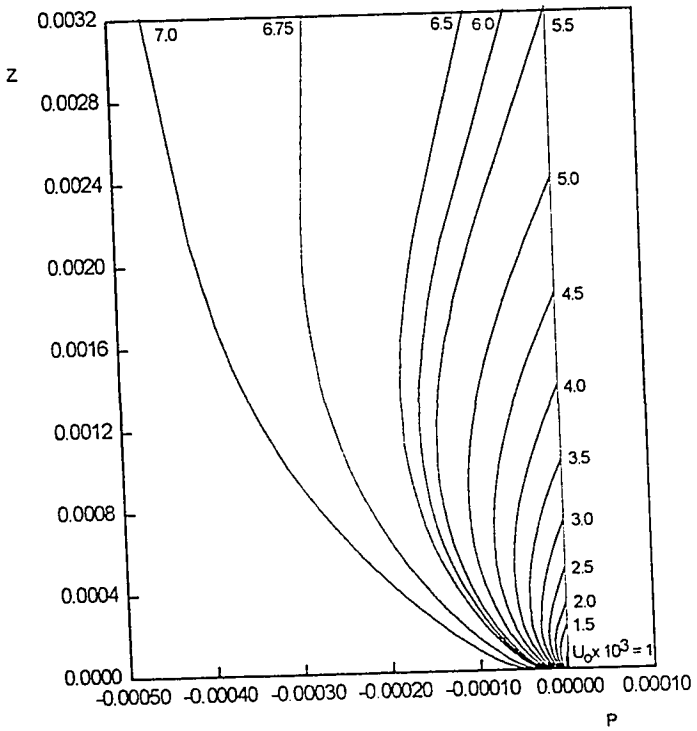


Fig. 8.6(b) : Development of the pressure with Z for different values of the induced volumetric flow rate (i.e., different channel heights), case 4.O, N =0.5, E = 0.1.

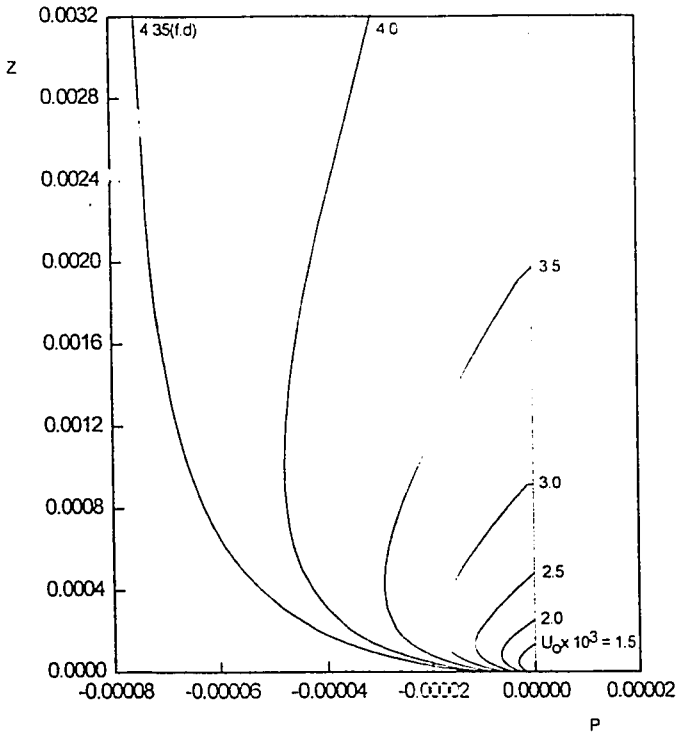


Fig. 8.6(c) : Development of the pressure with Z for different values of the induced volumetric flow rate (i.e., different channel heights), case 4.I, N =0.5, E =0.5.

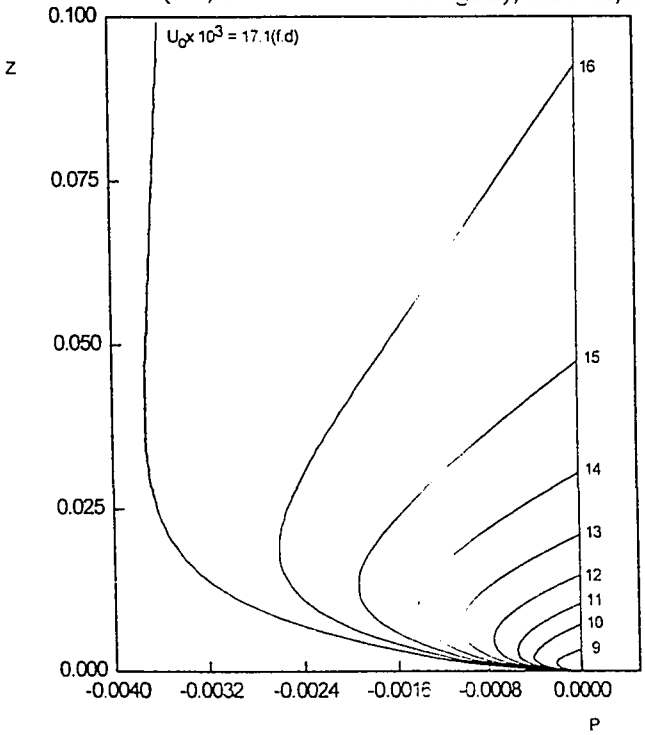


Fig. 8.6(d) : Development of the pressure with Z for different values of the induced volumetric flow rate (i.e., different channel heights), case 4.O, N =0.5, E = 0.5.

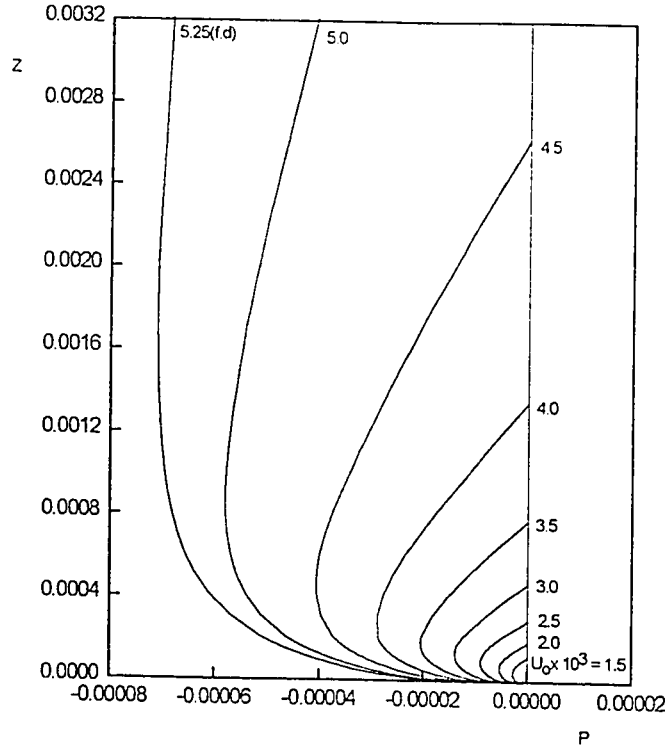


Fig.8.6(e) : Development of the pressure with Z for different values of the induced volumetric flow rate (i.e., different channel heights), case 4.I, N =0.5, E =0.7.

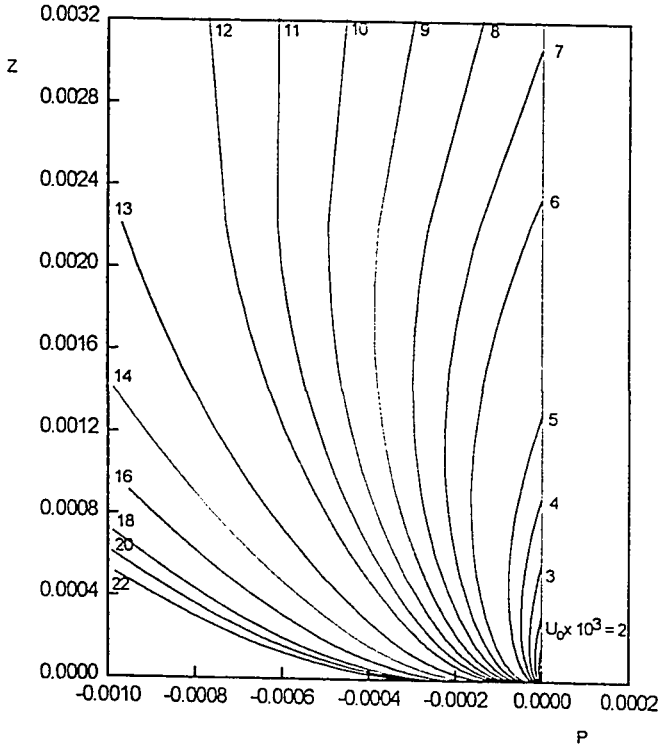


Fig. 8.6(f) : Development of the pressure with Z for different values of the induced volumetric flow rate (i.e., different channel heights), case 4.O, N =0.5, E = 0.7.

a positive pressure gradient) due to the buoyancy force resulted from the heating effect. Increase in the pressure will continue until it reaches zero at the channel exit.

The point at which the pressure becomes zero determines the channel height which is of engineering importance. Hence, the dimensionless channel height required to induce the fluid at a specific dimensionless flow rate can be determined with the aid of this set of figures. As can be seen from this set of figures the channel height increases as the required induced flow rate increases. In other words, one can say that the induced flow rate increases as the channel height increases. However, for cases with isothermal boundary there is a specific channel height beyond which there will be no more increase in the induced flow rate regardless of the channel height. This height is called the fully-developed channel height at which the fluid becomes thermally and hydrodynamically fully developed. It is also clear from these figures that the required channel height to suck up a specific dimensionless flow rate is higher for case I than that for case O in all cases considered. The variation of the induced flow rate with the channel height for all cases considered is shown in Figs. 8.7(a) and 8.7(b) for cases 1.I and 1.O, respectively, for three values of E (0.1, 0.5 and 0.7). Results for cases 2.I and 2.O are given in Figs. 8.8(a) and 8.8(b), respectively, for E = 0.1, 0.5 and 0.7. Figure 8.9 (a) shows the results of cases 3.I and 3.O for E = 0.5. A comaprison between the present results for a nearly concentric annulus($E = 10^{-6}$) and those of El-Shaarawi et al. [63] (concentric annulus) is presented in Fig. 8.9(b). Results for cases 4.I and 4.O are presented in Figs. 8.10(a) and 8.10(b), respectively, for the three eccentricities considered(E = 0.1, 0.5 and 0.7).

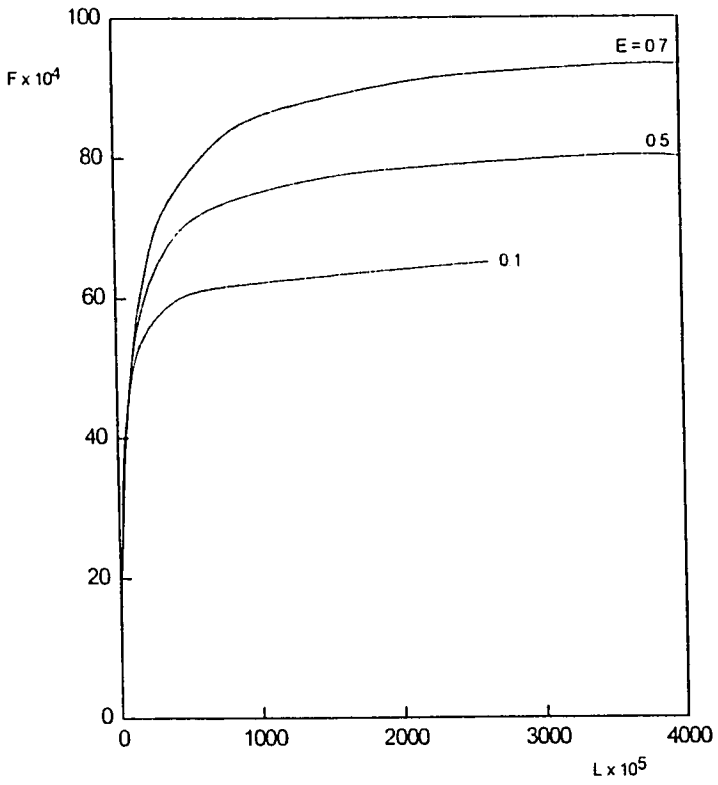


Fig. 8.7(a) : Relation between the induced volumetric flow rate and the channel height, case 1.I, N = 0.5.

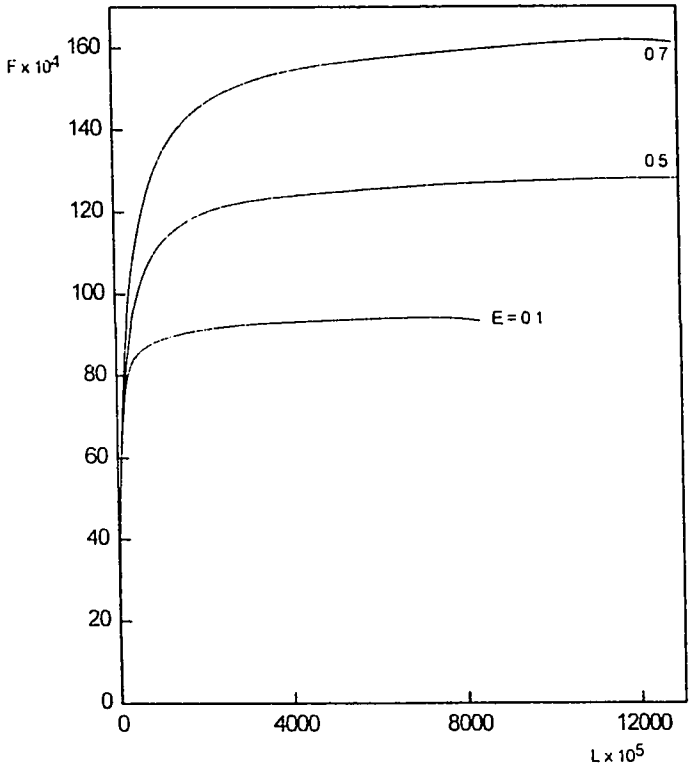


Fig. 8.7(b) : Relation between the induced volumetric flow rate and the channel height, case 1.O, N = 0.5.

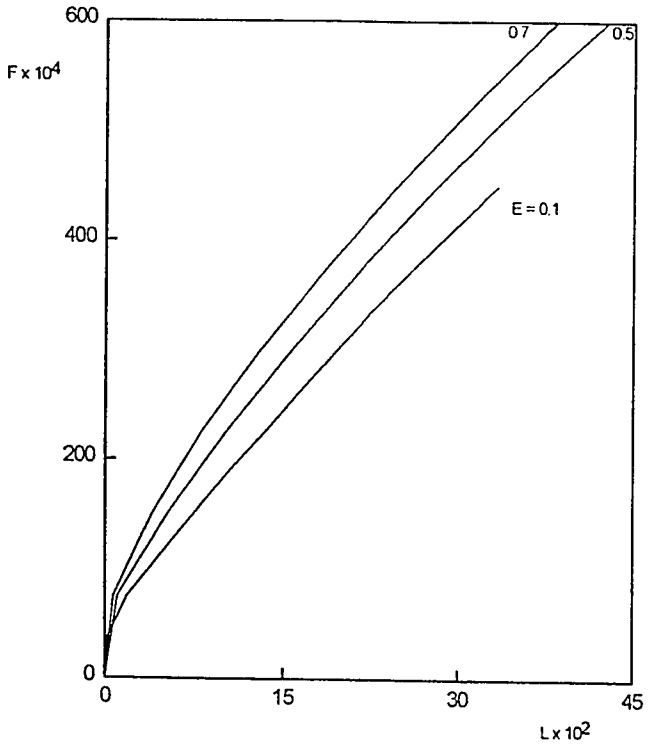


Fig. 8.8(a) : Relation between the induced volumetric flow rate and the channel height, case 2.I, N = 0.5.

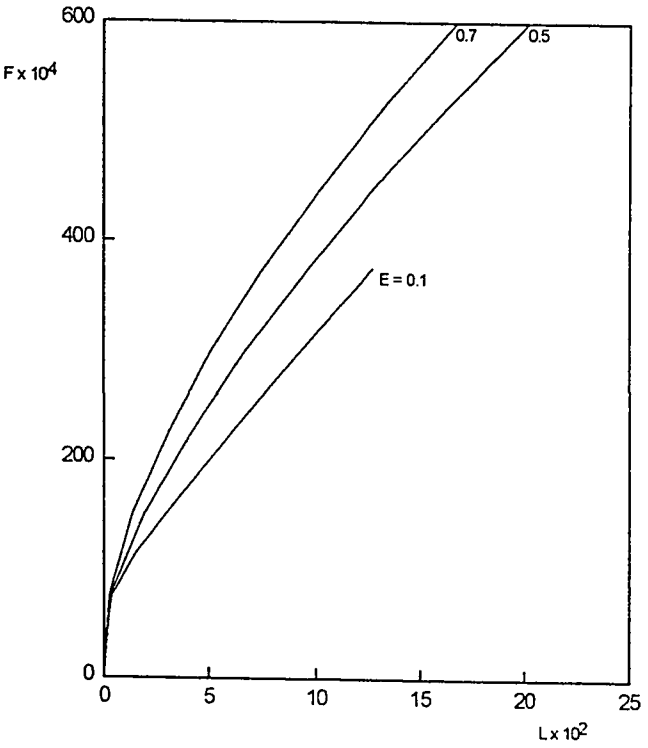


Fig. 8.8(b) : Relation between the induced volumetric flow rate and the channel height, case 2.O, N = 0.5.

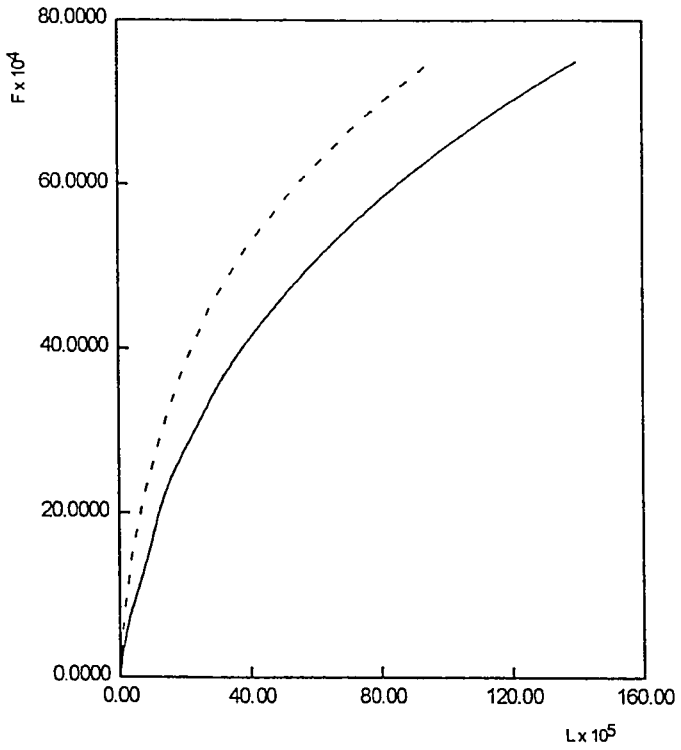


Fig. 8.9(a) : Relation between the induced volumetric flow rate and the channel height, ----- case 3.O, —— case 3.I., N = E = 0.5.

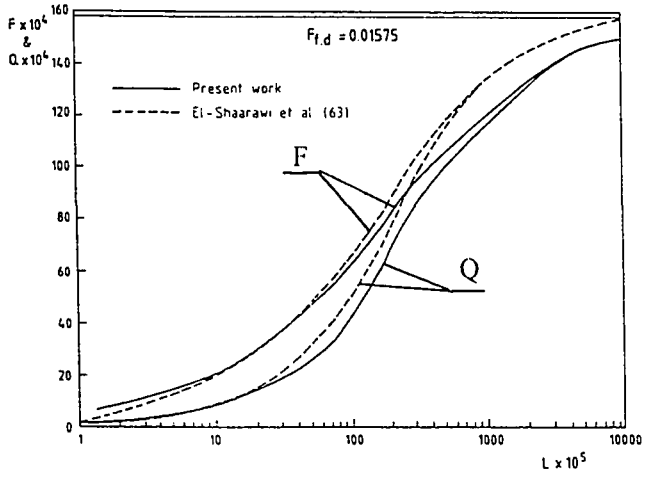


Fig. 8.9(b) : Relation between the induced volumetric flow rate(F), the heat transferred (Q), and the channel height(L), case 3.I, N = 0.5, E = $10^{-6}$.

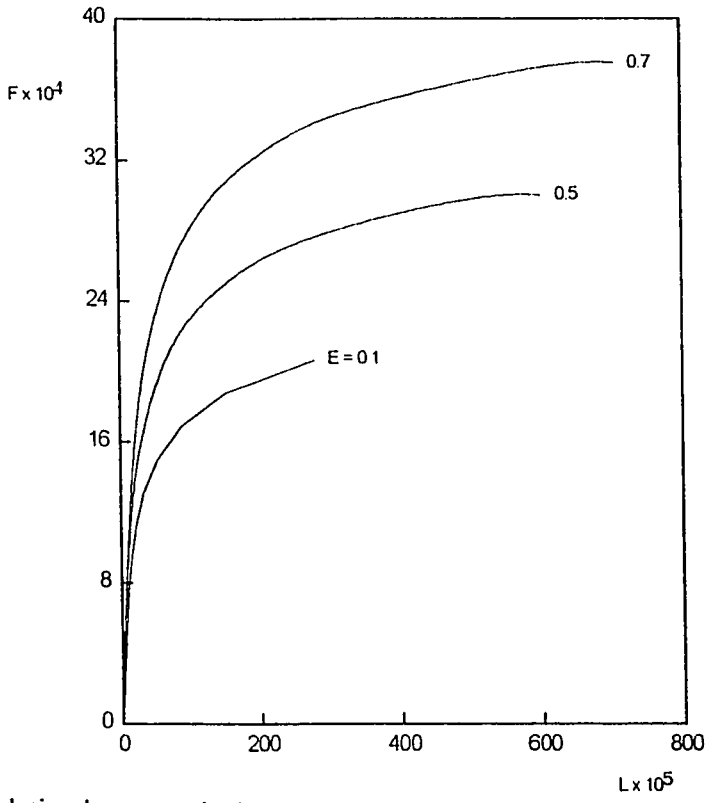


Fig. 8.10(a) : Relation between the induced volumetric flow rate and the channel height, case 4.I, N = 0.5.

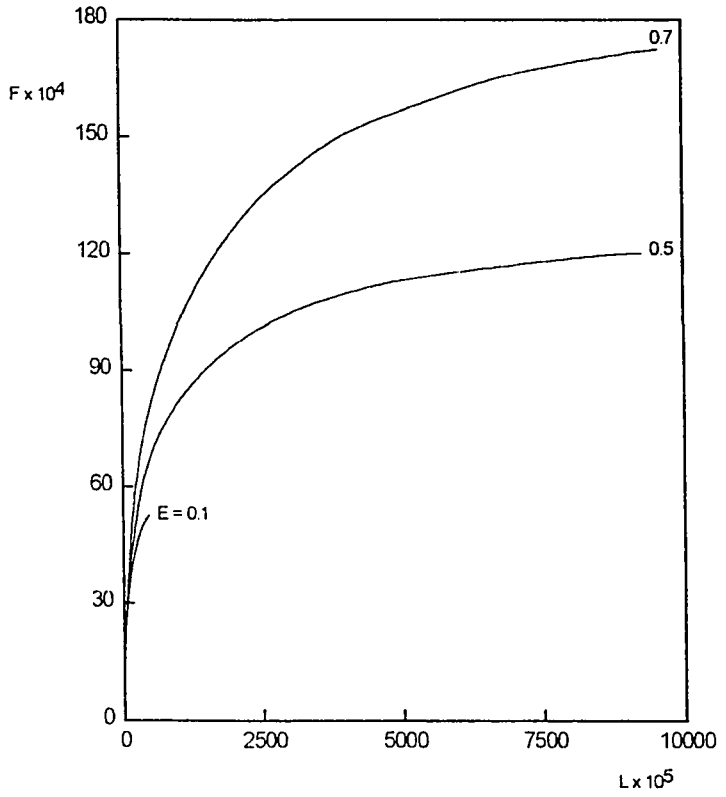


Fig. 8.10(b) : Relation between the induced volumetric flow rate and the channel height, case 4.O, N = 0.5.

The amount of heat absorbed by the fluid as its moves through the channel for boundary conditions 1.I and 1.O is presented in Figs. 8.11(a) and 8.11(b), respectively, for different flow rates at a given eccentricity of E = 0.1. Figures 8.11(c,d) and (e,f) give similar results for cases 1.I and 1.O but for E = 0.5 and 0.7, respectively. The Q-Z results for cases 2.I and 2.O with E = 0.1, 0.5 and 0.7 are given in Figs. 8.12(a-f) while Fig. 8.13(a) shows the results for case 3.I with E = $10^{-6}$. Similar results for cases 3.I and 3.O in an annulus of N = 0.5 and E = 0.5 are presented in Figs. 8.13(b) and 8.13(c), respectively. The results for cases 4.I and 4.O are presented in Figs. 8.14(a-f) with E = 0.1, 0.5 and 0.7.

The variation of the amount of heat carried out with the fluid as it exits from the channel ( $\bar{Q}$ ) with the channel height for all cases considered are given in Figs. 8.15(a) through 8.19(b). The variation of the dimensionless volumetric flow rate $F$ and the thermal energy carried by the fluid at the channel exit ( $\bar{Q}$ ) are tabulated against the channel height for all cases under consideration in the set of tables presented in Appendix F. The variation of the maximum temperature with Z on the inner/outer heated wall for case 2.I/2.O in an annulus of N = 0.5 and E = 0.1 is presented in Figs. 8.20(a) and 8.20(b), respectively. The corresponding development of the temperature on the outer/inner insulated wall in these two cases(2.I and 2.O) is presented in Figs. 8.20(C) and 8.20(d). The development of the mean bulk temperature for boundary conditions 2.I and 2.O with E = 0.5 are presented in Figs. 8.21(a) and 8.21(b).

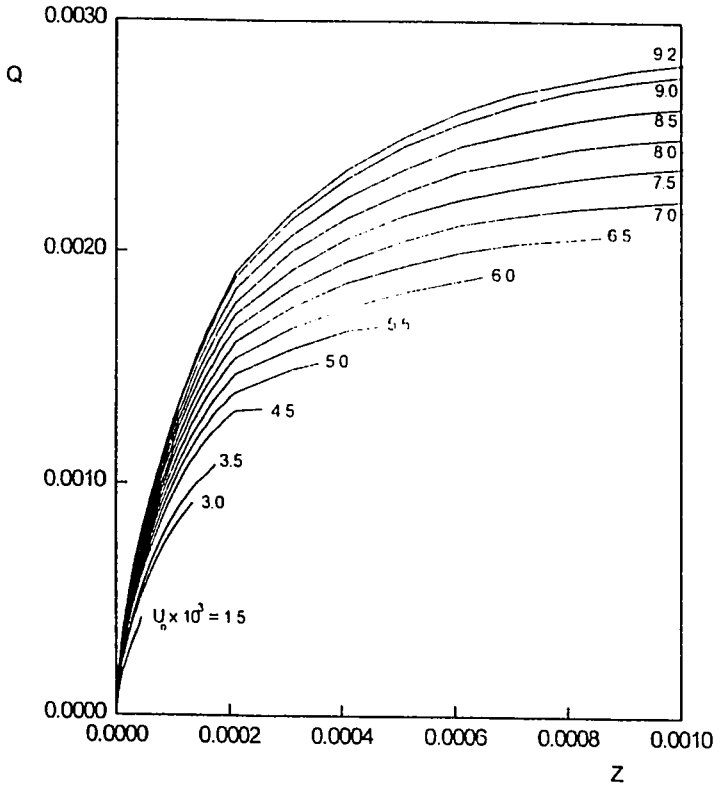


Fig. 8.11(a) : Variation of the heat absorbed by the fluid as it moves up in the channel, for different flow rates (i.e., different channel heights), case 1.1, N = 0.5, E = 0.1.

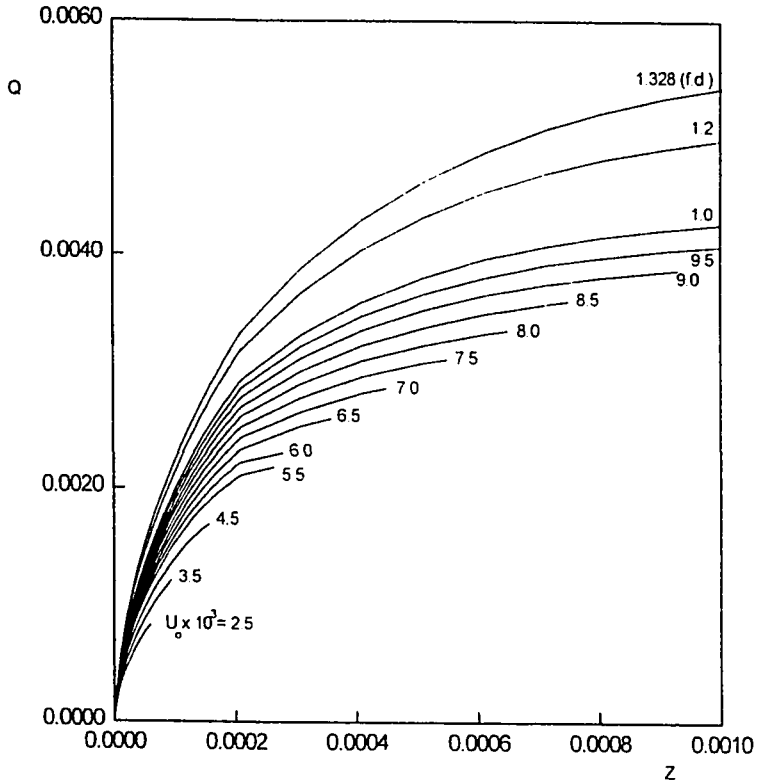


Fig. 8.11(b) : Variation of the heat absorbed by the fluid as it moves up in the channel, for different flow rates(i.e., different channel heights), case 1.0, N = 0.5, E = 0.1.

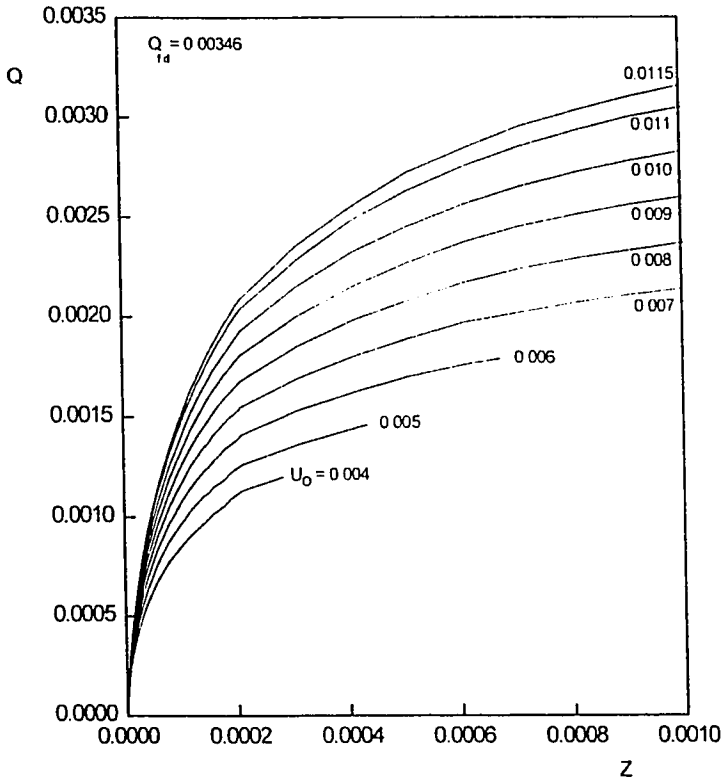


Fig. 8.11(c) : Variation of the heat absorbed by the fluid as it moves up in the channel, for different flow rates (i.e., different channel heights), case 1.1, N = 0.5, E = 0.5.

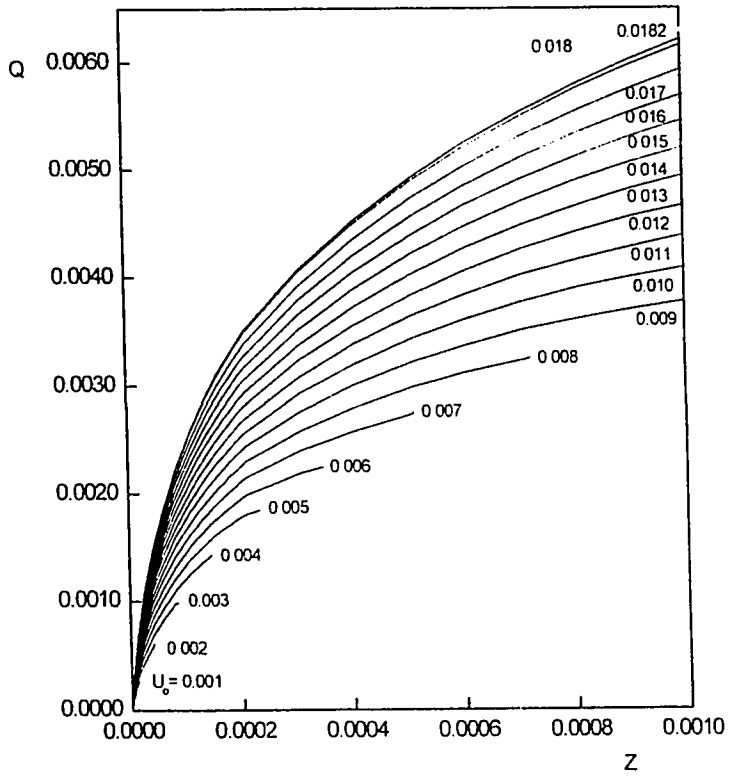


Fig. 8.11(d) : Variation of the heat absorbed by the fluid as it moves up in the channel, for different flow rates (i.e., different channel heights), case 1.0, N = 0.5, E = 0.5.

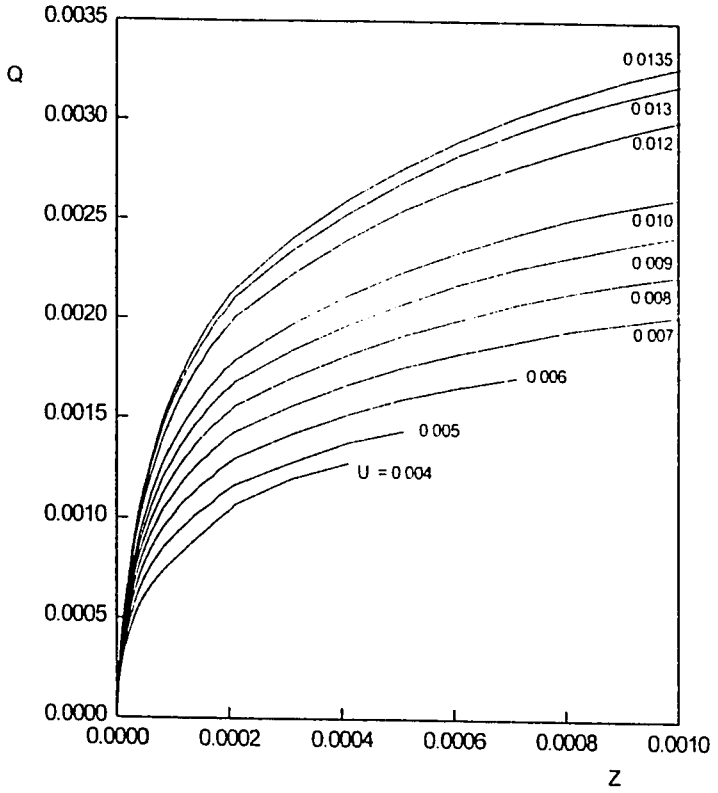


Fig. 8.11(e) : Variation of the heat absorbed by the fluid as it moves up in the channel, for different flow rates (i.e., different channel heights), case 1.I, N = 0.5, E = 0.7.

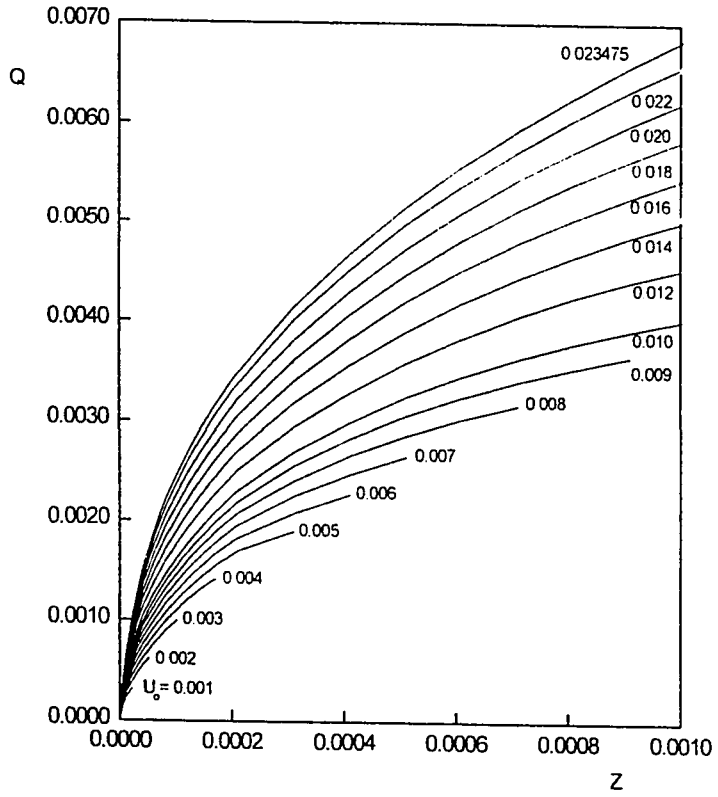


Fig. 8.11(f) : Variation of the heat absorbed by the fluid as it moves up in the channel, for different flow rates (i.e., different channel heights), case 1.O, N = 0.5, E = 0.7.

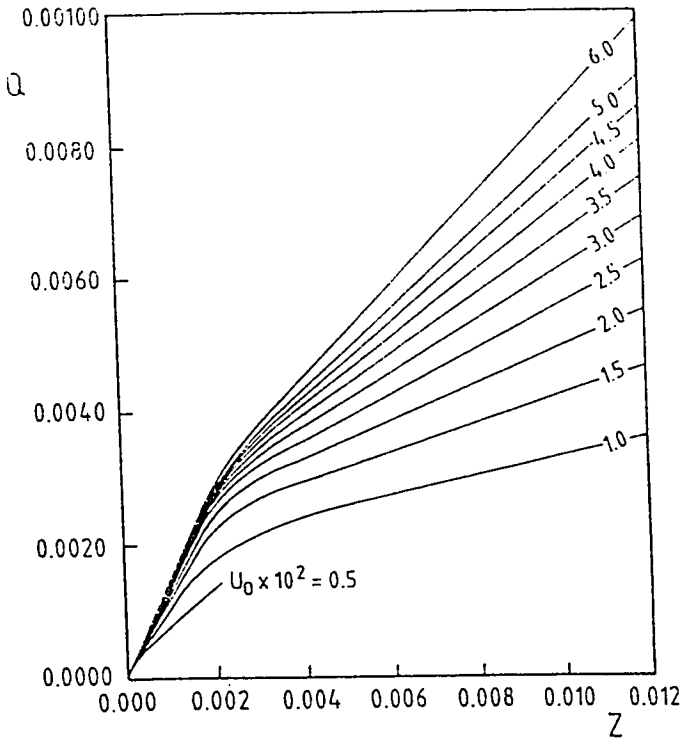


Fig. 8.12(a) : Variation of the heat absorbed by the fluid as it moves up in the channel, for different flow rates(i.e., different channel heights), case 2.I, N = 0.5, E = 0.1.

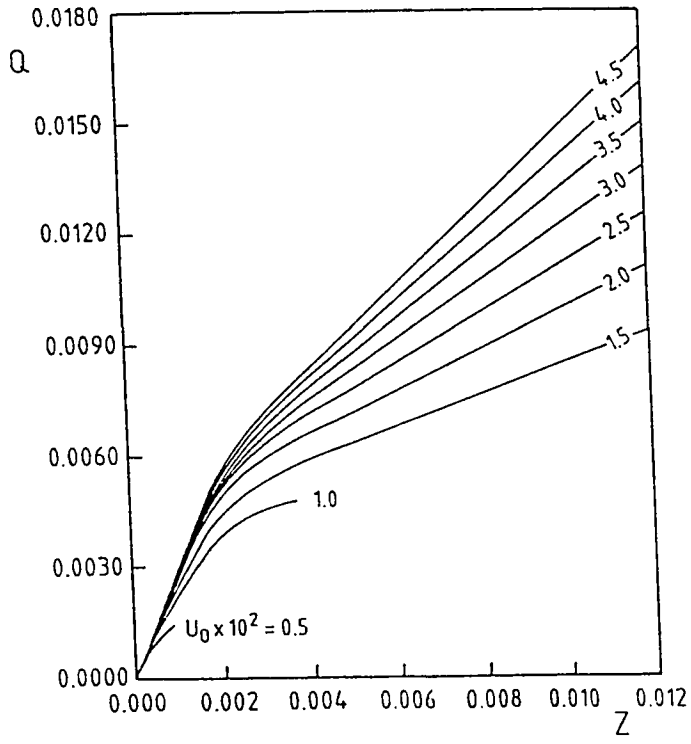


Fig. 8.12(b) : Variation of the heat absorbed by the fluid as it moves up in the channel, for different flow rates(i.e., different channel heights), case 2.O, N = 0.5, E = 0.1.

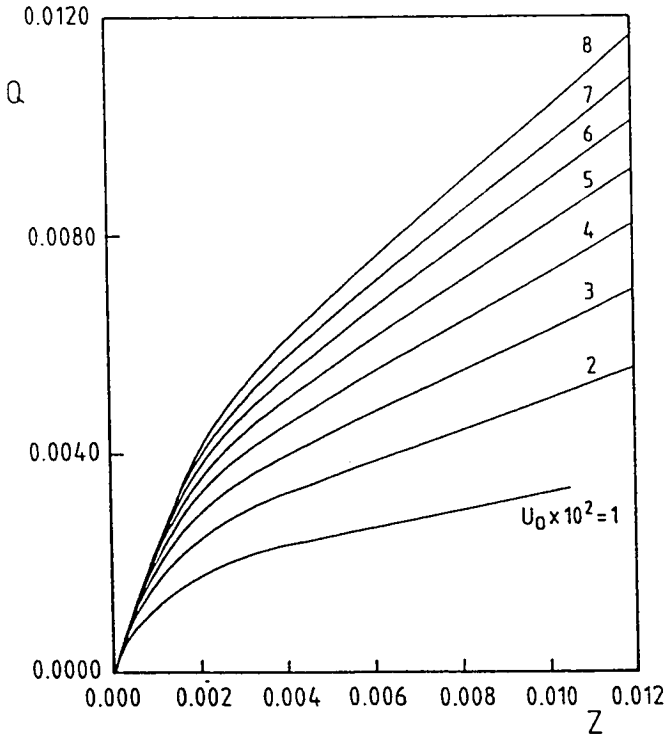


Fig. 8.12(c) : Variation of the heat absorbed by the fluid as it moves up in the channel, for different flow rates(i.e., different channel heights), case 2.I, N = 0.5, E = 0.5.

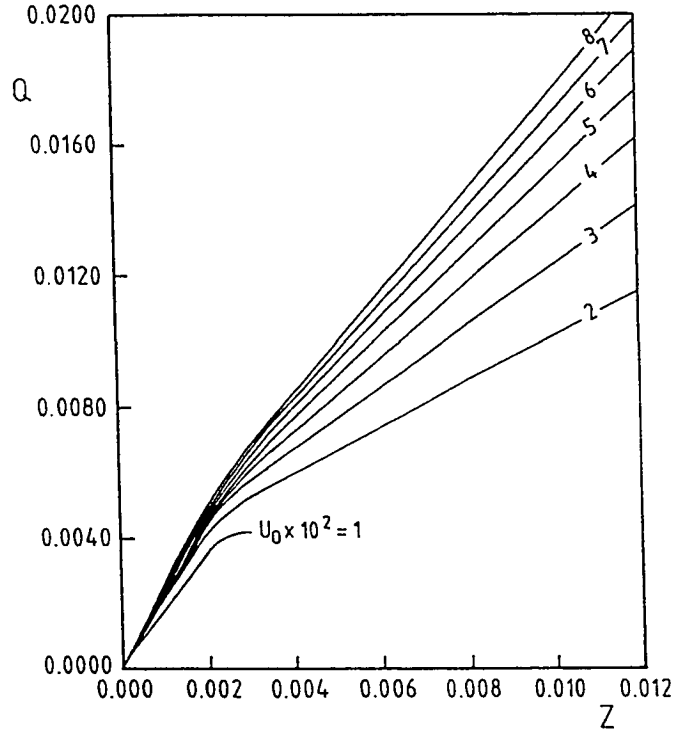


Fig. 8.12(d) : Variation of the heat absorbed by the fluid as it moves up in the channel, for different flow rates(i.e., different channel heights), case 2.O, N = 0.5, E = 0.5.

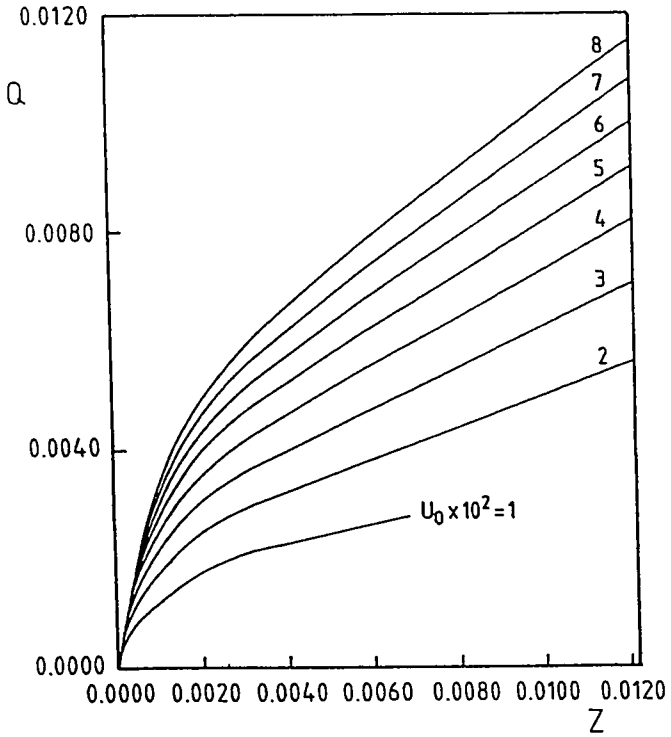


Fig. 8.12(e) : Variation of the heat absorbed by the fluid as it moves up in the channel, for different flow rates(i.e., different channel heights), case 2.I, N = 0.5, E = 0.7.

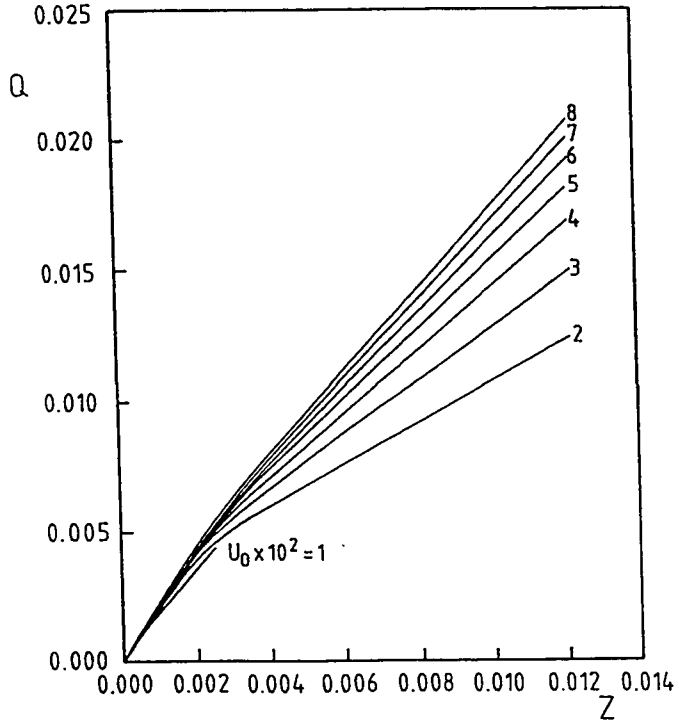


Fig. 8.12(f) : Variation of the heat absorbed by the fluid as it moves up in the channel, for different flow rates(i.e., different channel heights), case 2.O, N = 0.5, E = 0.7.

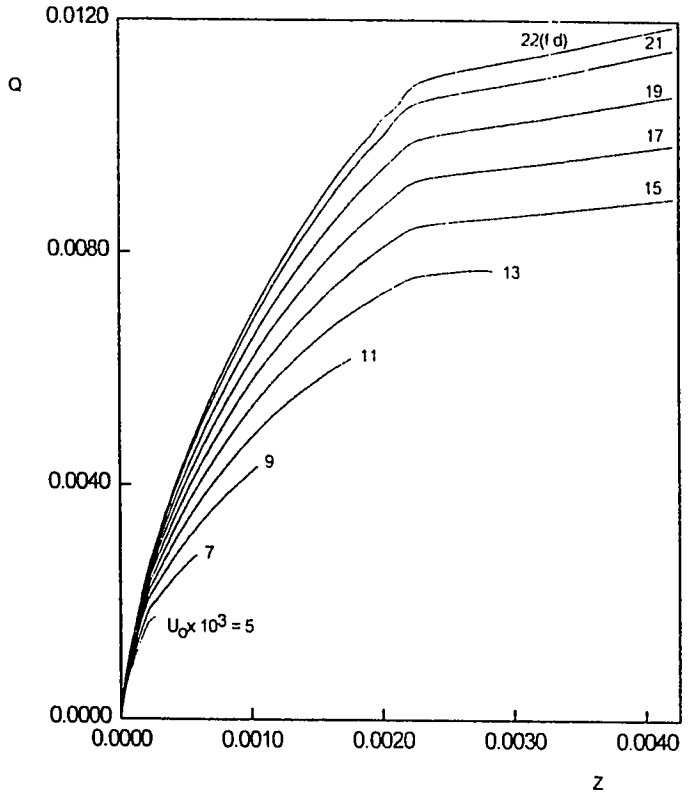


Fig. 8.13(a) : Variation of the heat absorbed by the fluid as it moves up in the channel, for different flow rates(i.e., different channel heights), case 3.I, N = 0.5, E = $10^{-6}$.

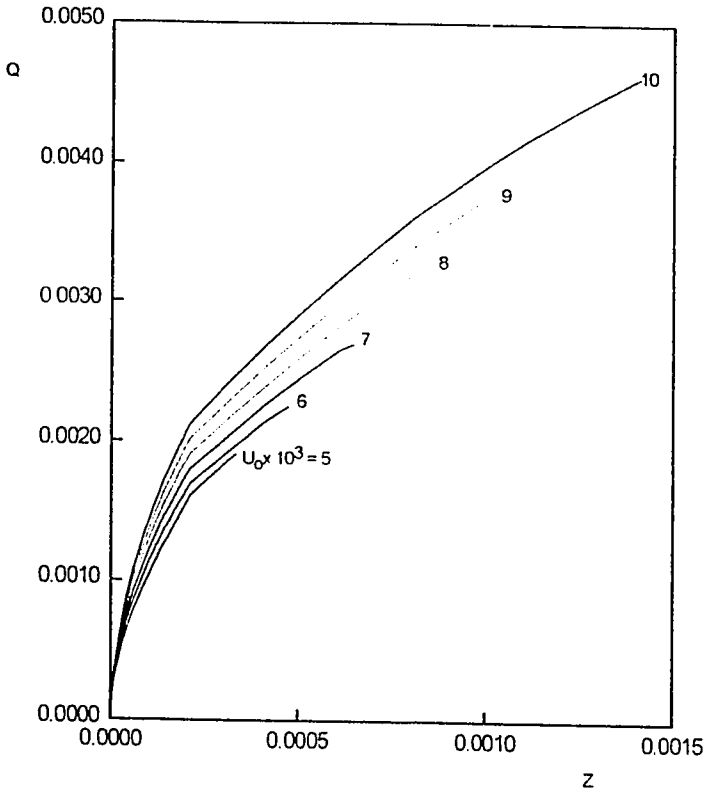


Fig. 8.13(b) : Variation of the heat absorbed by the fluid as it moves up in the channel, for different flow rates(i.e., different channel heights), case 3.I, N = 0.5, E = 0.5.

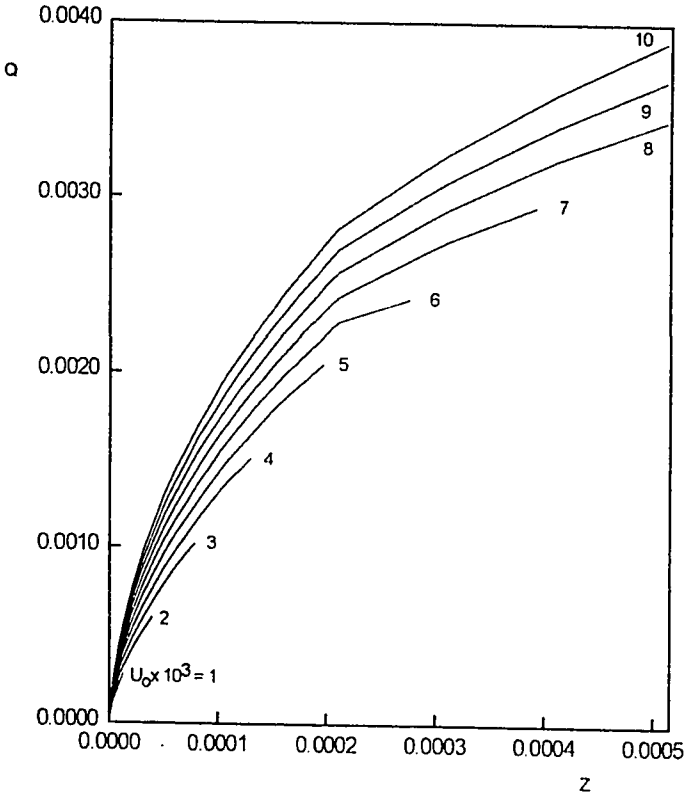


Fig. 8.13(c) : Variation of the heat absorbed by the fluid as it moves up in the channel, for different flow rates(i.e., different channel heights), case 3.O, N = 0.5, E = 0.5.

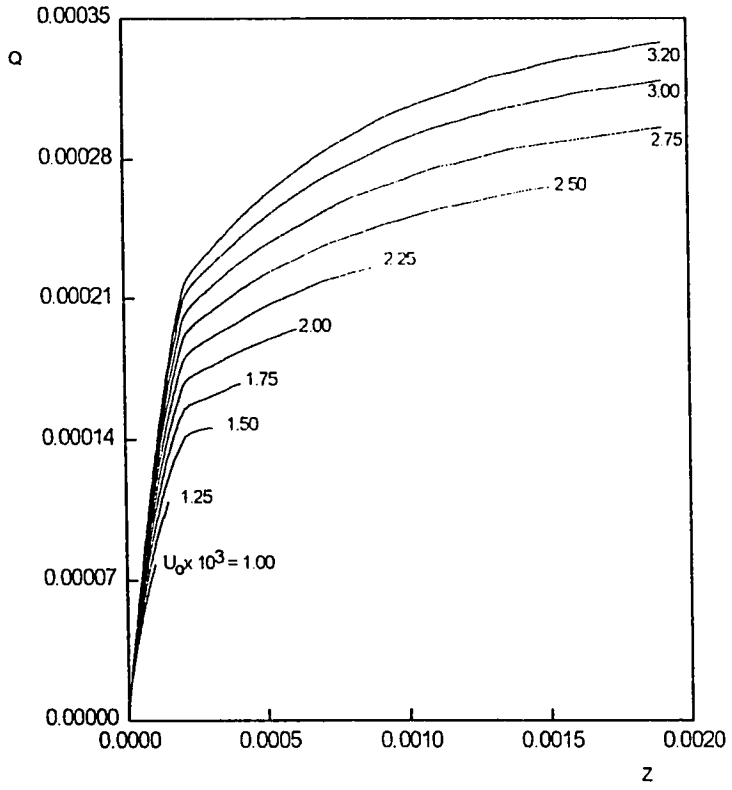


Fig. 8.14(a) : Variation of the heat absorbed by the fluid as it moves up in the channel, for different flow rates(i.e., different channel heights), case 4.I, N = 0.5, E = 0.1.

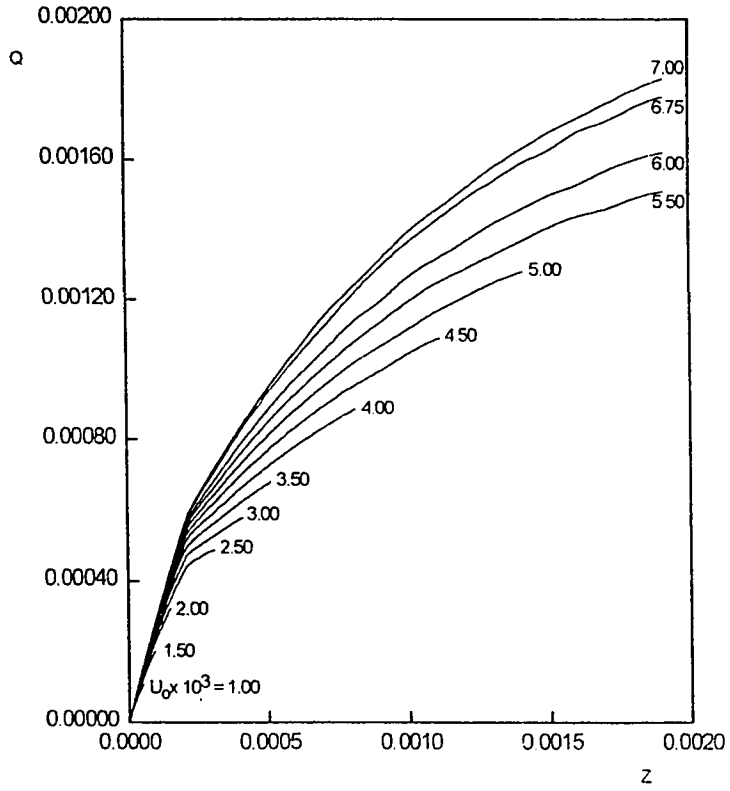


Fig. 8.14(b) : Variation of the heat absorbed by the fluid as it moves up in the channel, for different flow rates(i.e., different channel heights), case 4.O, N = 0.5, E = 0.1.

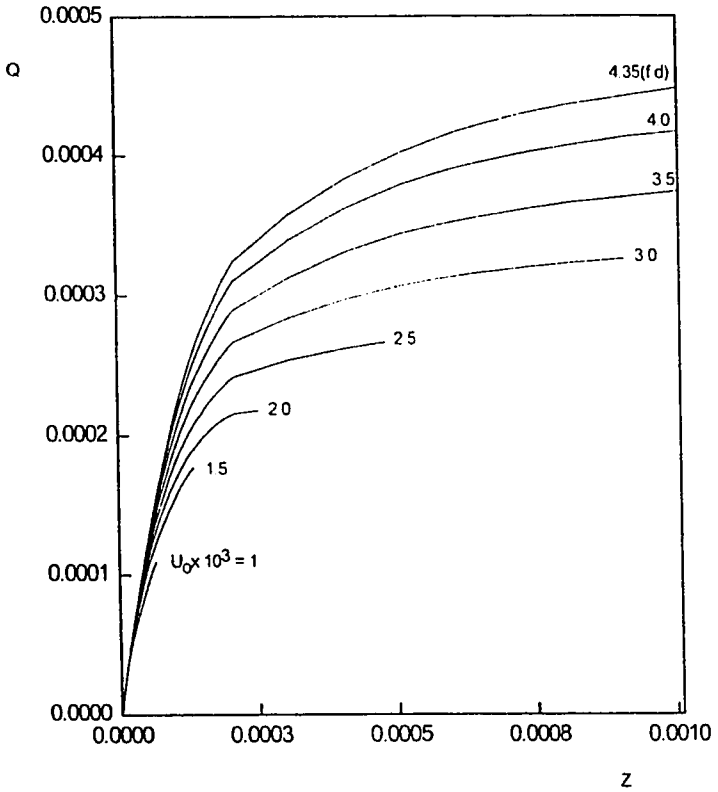


Fig. 8.14(c) : Variation of the heat absorbed by the fluid as it moves up in the channel, for different flow rates(i.e., different channel heights), case 4.I, N = 0.5, E = 0.5.

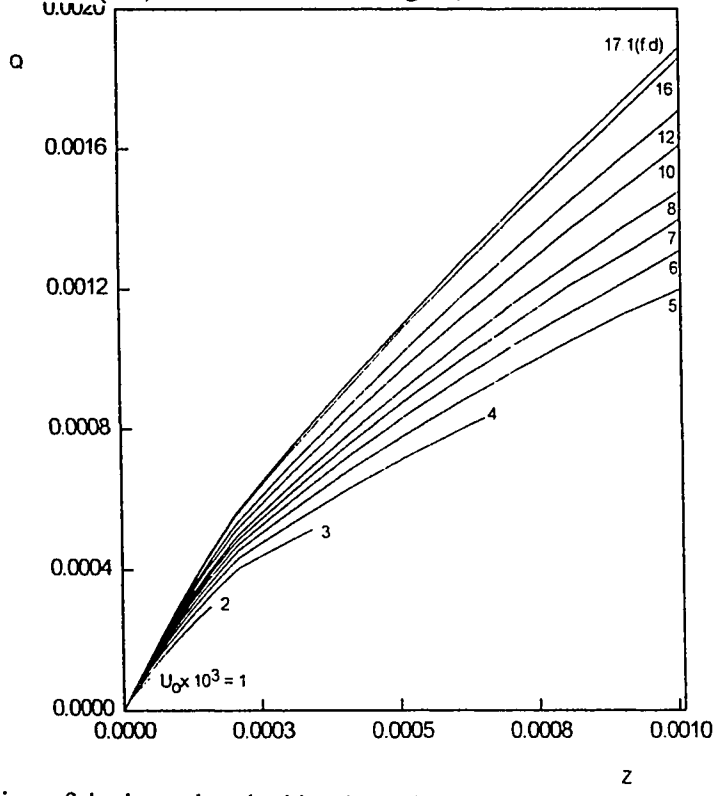


Fig. 8.14(d) : Variation of the heat absorbed by the fluid as it moves up in the channel, for different flow rates(i.e., different channel heights), case 4.O, N = 0.5, E = 0.5.

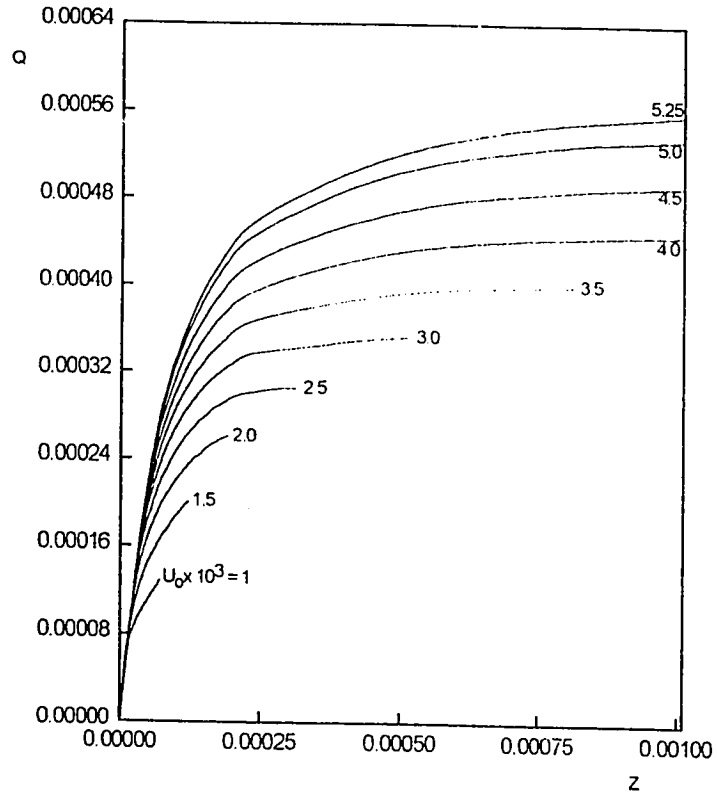


Fig. 8.14(e) : Variation of the heat absorbed by the fluid as it moves up in the channel, for different flow rates(i.e., different channel heights), case 4.I, N = 0.5, E = 0.7.

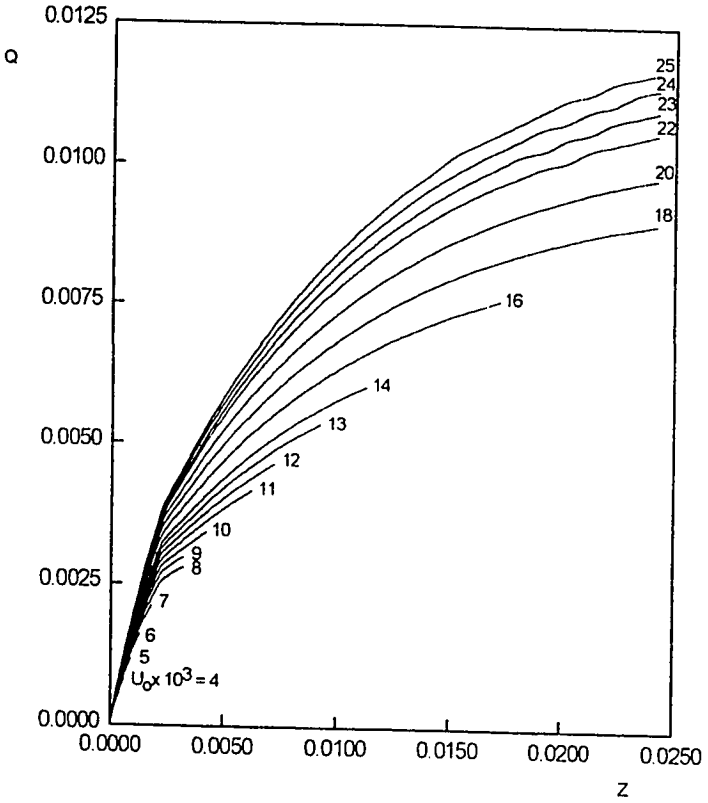


Fif. 8.14(f) : Variation of the heat absorbed by the fluid as it moves up in the channel, for different flow rates(i.e., different channel heights), case 4.O, N = 0.5, E = 0.7.

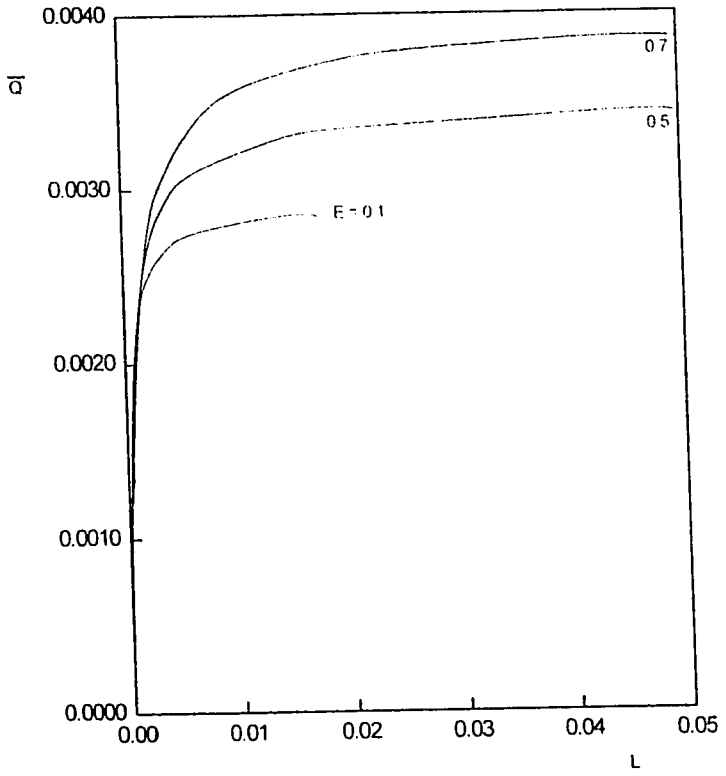


Fig. 8.15(a) : Relation between the heat absorbed by the fluid at exit and the channel height, case 1.I, N = 0.5.

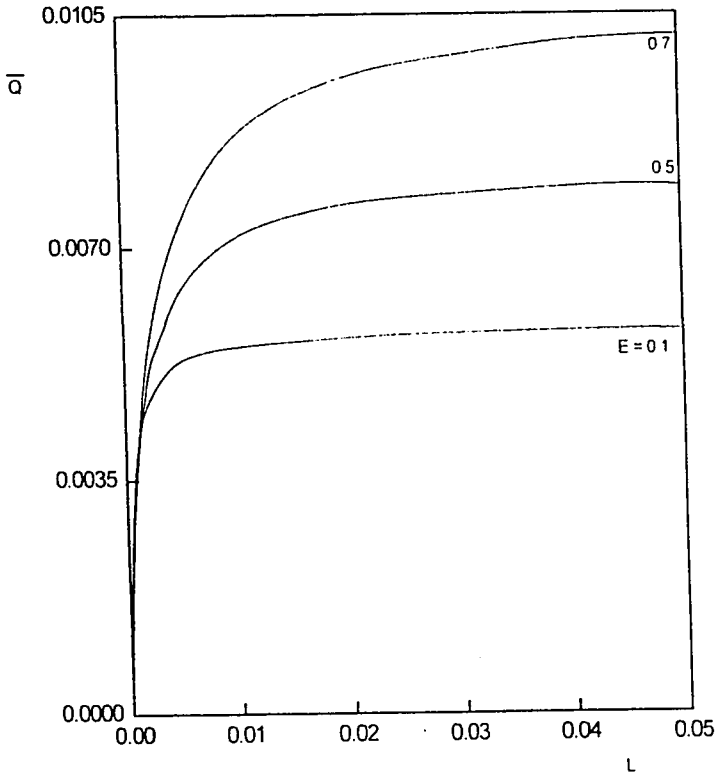


Fig. 8.15(b) : Relation between the heat absorbed by the fluid at exit and the channel height, case 1.O, N = 0.5.

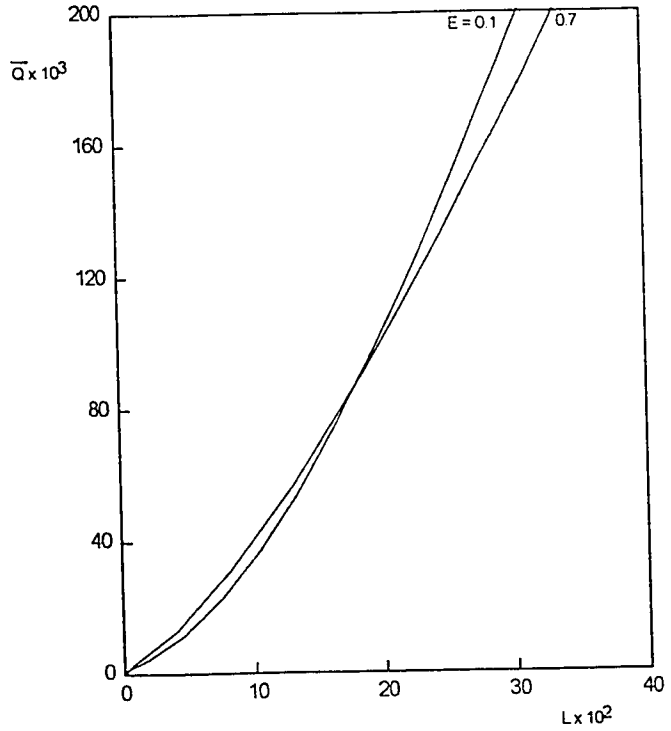


Fig. 8.16(a) : Relation between the heat absorbed by the fluid at exit and the channel height, case 2.I, N = 0.5.

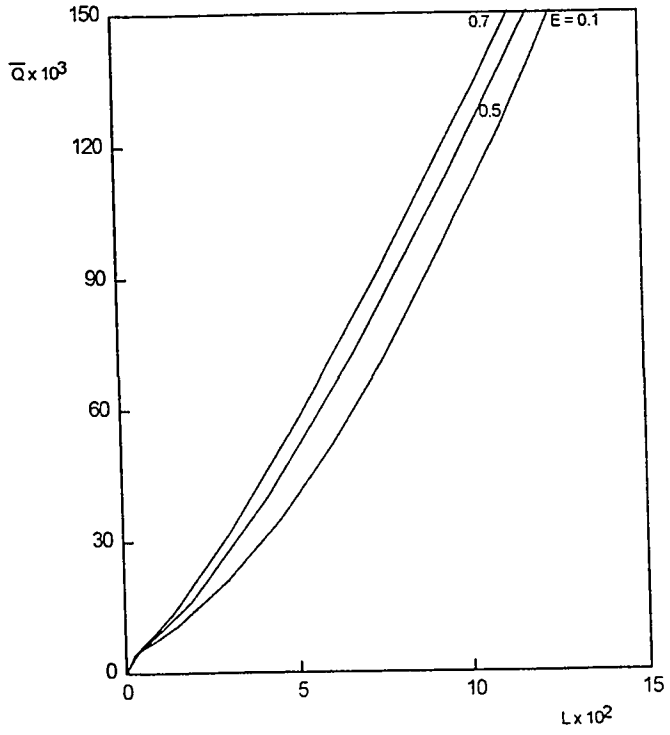


fig. 8.16(b) : Relation between the heat absorbed by the fluid at exit and the channel height, case 2.O, N = 0.5.

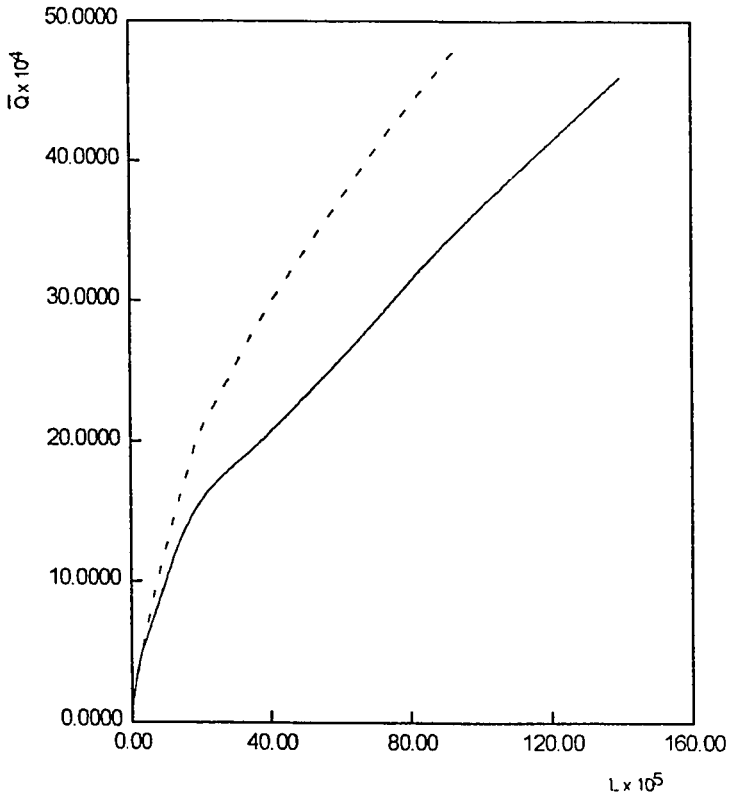


Fig. 8.17 : Relation between the heat absorbed by the fluid at exit and the channel height, ----- case 3.O, —— case 3.I., N = E = 0.5.

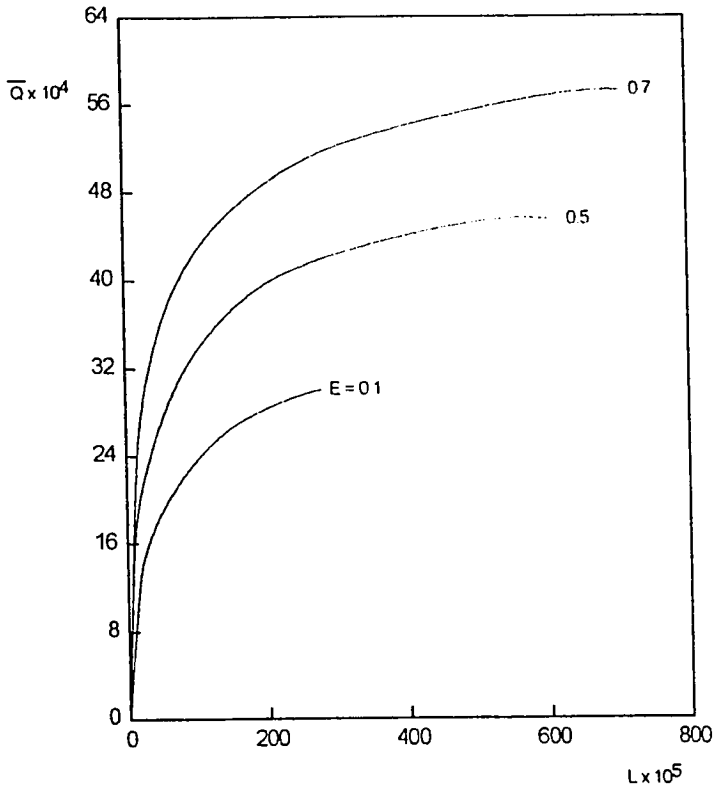


Fig. 8.18(a) : Relation between the heat absorbed by the fluid at exit and the channel height, case 4.I, N = 0.5.

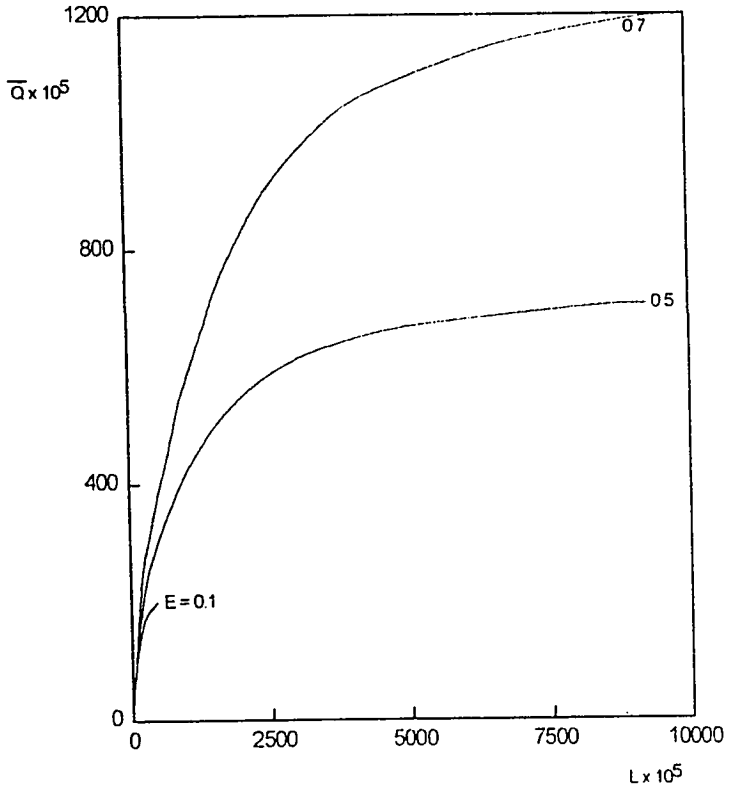


Fig. 8.18(b) : Relation between the heat absorbed by the fluid at exit and the channel height, case 4.O, N = 0.5.

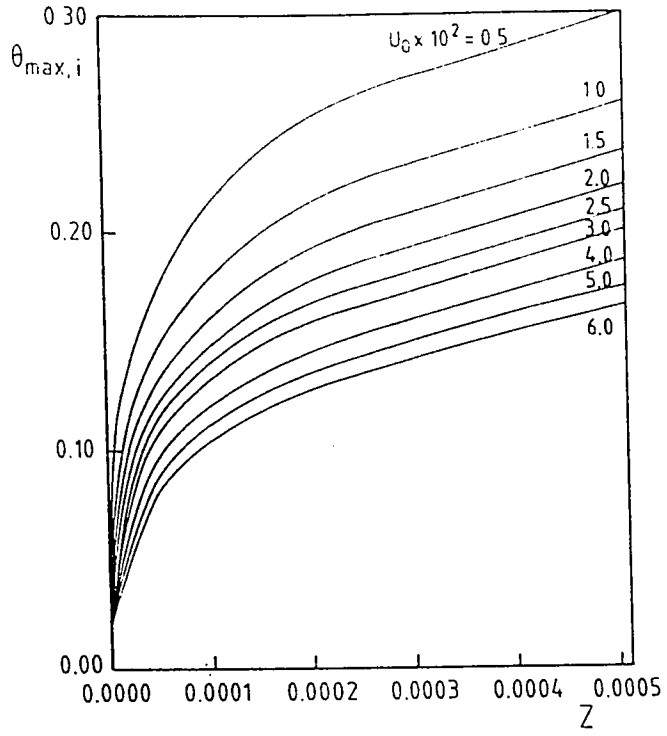


Fig. 8.19(a) : Development of the maximum temperature($\theta_{max}$) at the inner heated wall, case 2.I, N = 0.5, E = 0.1.

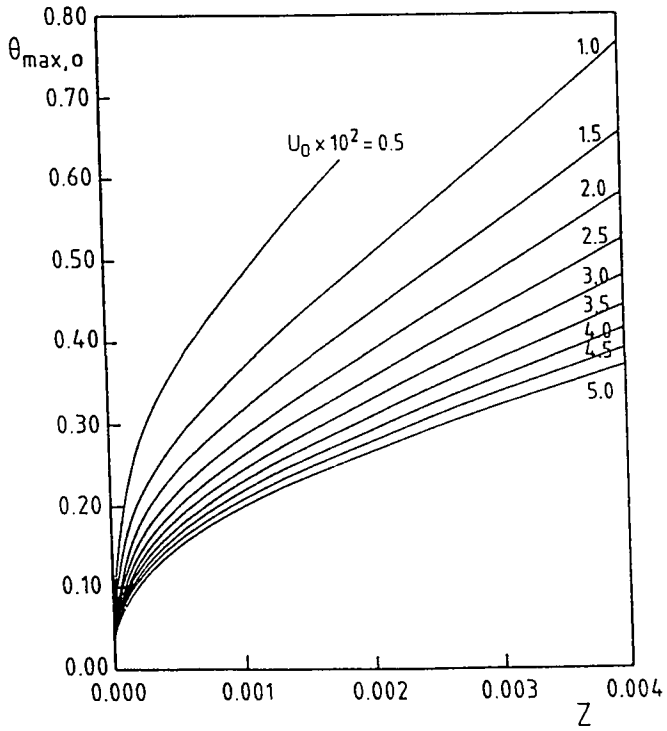


Fig. 8.19(b) : Development of the maximum temperature ($\theta_{max}$) at the outer heated wall, case 2.O, N = 0.5, E = 0.1.

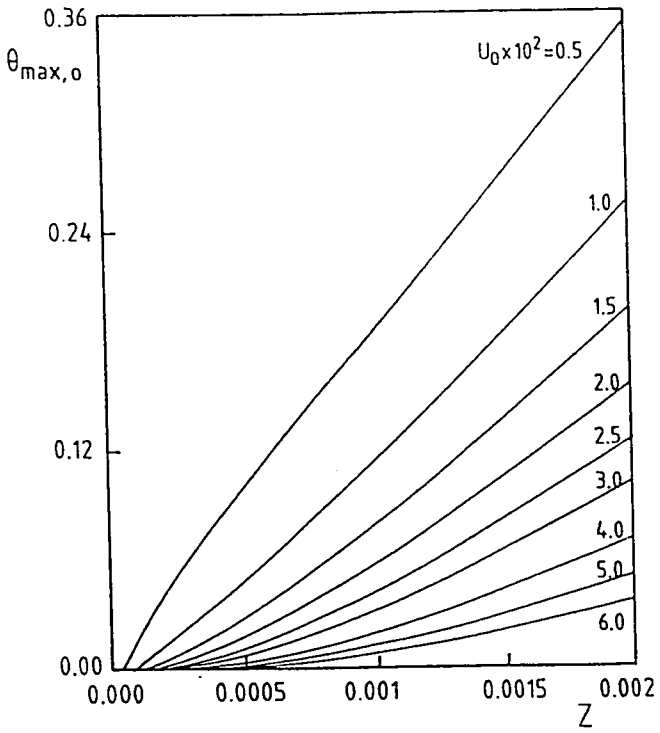


Fig. 8.19(c) : Development of the maximum temperature($\theta_{max}$) at the outer insulated wall, case 2.I, N = 0.5, E = 0.1.

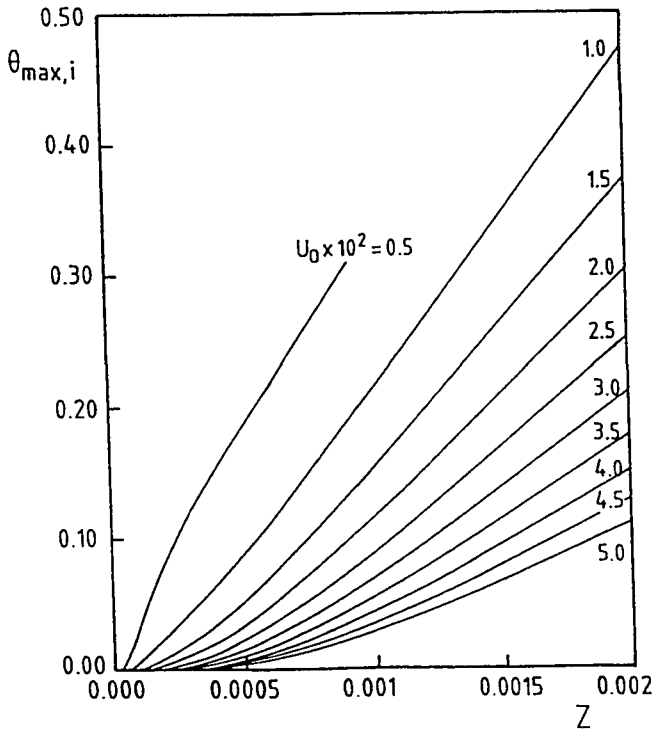


Fig. 8.19(d) : Development of the maximum temperature($\theta_{max}$) at the inner insulated wall, case 2.O, N = 0.5, E = 0.1.

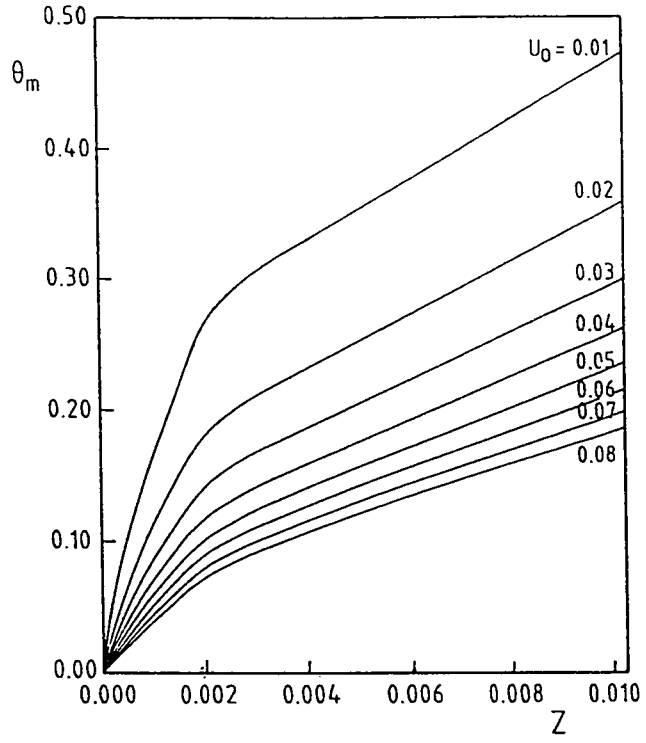


Fig. 8.20(a) : Development of the mean bulk temperature($\theta_m$), case 2.I, N = 0.5, E = 0.5, F = 0.06

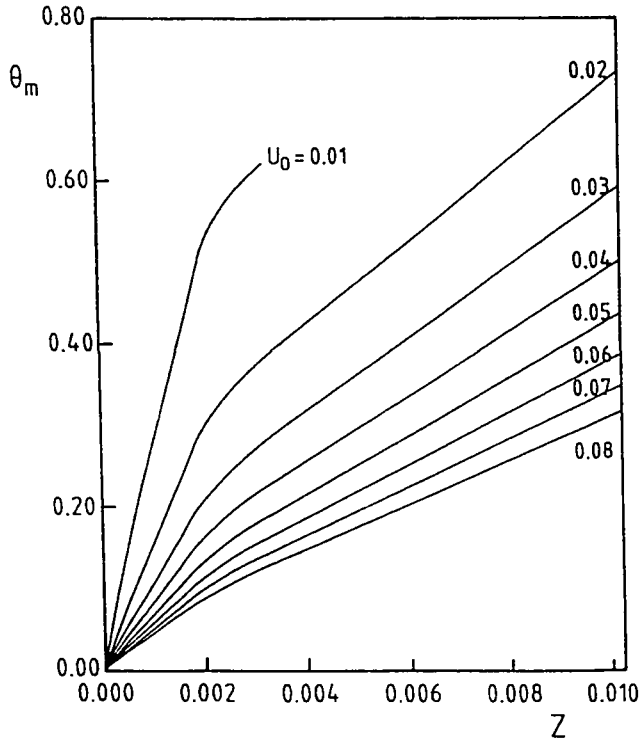


Fig. 8.20(b) : Development of the mean bulk temperature($\theta_m$), case 2.O, N = 0.5, E = 0.5, F = 0.06

# Chapter 9

# CONCLUSIONS AND RECOMMENDATIONS

Heat transfer through eccentric annuli has been studied. This study included transient conduction with uniform internal heat generation in eccentric hollow cylinders, the fully developed free convection in open-ended vertical eccentric annuli, the developing forced convection in eccentric annuli and the developing free convection in open-ended vertical eccentric annuli. Four pairs of thermal boundary conditions have been investigated.

The transient conduction with uniform internal heat generation in eccentric annuli of radius ratio N = 0.5 has been numerically investigated under the four pairs of the fundamental boundary conditions. Analytical solutions have been provided for the steady -state conduction with internal heat generation. This study has shown that two

controlling parameters, namely, the dimensionless eccentricity ($E$) and the dimensionless heat generation $Q$ (or heat ratio in the cases with uniform heat flux at the heat transfer wall) have pronounced effects on the heat transfer process.

The fully developed free convection in open-ended vertical eccentric annuli has been investigated numerically using a finite-difference technique for the momentum equation and an analytical solution for the pertinent energy equation under thermal boundary conditions of the first and fourth kind. Numerical results are presented for a fluid of Pr = 0.7 in a typical annular geometry of radius ratio 0.5 over a wide range of the dimensionless eccentricity ( E = 0.1 - 0.9 ). These results present the fully-developed velocity profiles, the local and circumfrentially-averaged Nusselt numbers on the inner and outer walls of the annulus, the induced volumetric flow rate, and the total heat absorbed by the fluid. For an annulus of a given eccentricity, the presented fully-developed flow rate and total heat absorbed by the fluid are of engineering importance as they represent the maximum possible limiting values which can be physically obtained.

Closed-form analytical solutions are presented for the fully-developed natural convection in vertical eccentric annuli subject to thermal conditions of the third kind. Using this closed-form equations, the variation of the induced volumetric flow rate with the dimensionless eccentricity has been obtained for a wide range of annulus radius ratio ( N = 0.1 - 0.75 ).

A model has been presented for the laminar forced convection heat transfer in the entry region of eccentric annuli and the developing laminar free convection in open-ended vertical eccentric annuli. This model is obtained by assuming the pressure to be a

function of the axial coordinate only, neglecting the axial diffusions of momentum and energy and considering the radial-like component of velocity to be much smaller than the axial and tangential-like components. Compared with the two-equation classical-boundary-layer model of **Feldman et al. [6,7]** the solution of the present model does not need assumptions dependent on prior knowledge of the transverse flows.

A linearized finite-difference algorithm has been developed to numerically solve the equations comprising the model, viz., the tangential-like-momentum, axial-momentum and energy parabolic-equations and the continuity equation. The thermal-boundary conditions of an isothermally heated inner wall while the outer is kept at the inlet fluid temperature have been considered for the case of forced convection. Moreover, the free convection problem has been investigated under the four pairs of the thermal boundary conditions.

The conclusions drawn from the present study will be presented hereunder followed by the recommendations for the future work.

## 9.1 Conclusions

The study of the transient conduction with internal heat generation in eccentric hollow cylinders for the investigated ranges of the dimensionless eccentricity ($E$ = 0.1 - 0.7) and the dimensionless heat generation / heat ratio ($Q$ = 0 -5 ), reveals the following;

- The eccentricity is the dominant factor on the heat transfer parameters. The time needed to reach the steady-state conditions ($t_s$) is very much influenced by the

eccentricity value. Increasing the eccentricity $E$ increases the steady-state time $t_s$ for a given value of $Q$.

- Within the investigated range of $0 \leq Q \leq 5$, the steady-state time $t_s$ is slightly influenced by the value of the dimensionless heat generation / heat ratio $Q$. Increasing $Q$ results in reduction in $t_s$.
- Introducing eccentricity in the nominally concentric annulus results in asymmetry in the temperature distribution within the annulus (for all cases with internal heat generation and the cases with uniform heat flux at the heat transfer wall with or without internal heat generation). This asymmetry increases with the increase in eccentricity.
- The maximum attainable temperature within the annulus material increases with the increase in eccentricity. This may put an upper limit of the eccentricity according to the material requirements.
- Specification of the boundary conditions affects the temperature level within the annulus(i.e., higher temperatures are attainable if the heat transfer wall is the outer wall, case O, compared to those obtained when the heat transfer wall is the inner wall, case I). This is attributed to the area of heat transfer in each case.

The analysis of the fully developed free convection in open-ended vertical eccentric annuli for thermal boundary conditions of the first, third and fourth kinds show that the eccentricity and the boundary conditions are the dominant factors on the flow and heat transfer parameters;

- Introducing eccentricity in the nominally concentric annulus results in asymmetry in the velocity and temperature profiles within the annulus. This asymmetry increases with the increase in eccentricity.
- Increasing the eccentricity results in increasing the asymmetry in the local Nusselt number on the annulus walls.
- The circumfrentially-averaged Nusselt number on both walls increases with the increase in eccentricity (i.e., the eccentricity enhances the heat transfer)
- The induced flow rate F, the mean bulk temperature $\theta_m$ and consequently the heat absorbed by the fluid $Q$ increase with the increase in eccentricity E.

The obtained numerical results for the developing laminar forced convection in eccentric annuli under boundary condition 1. I show that, for a given annulus radius ratio ( N = 0.5 or 0.9);

- Increasing the eccentricity causes reductions in the pressure drop and the mixed-mean temperature.
- On the other hand, increasing the eccentricity causes increases in (1) the local ( at a given dimensionless axial location, Z) circumferentially averaged Nusselt numbers on the inner and outer walls of a given annulus, and (2) the global ( averaged over the entire surface area of the wall from the entrance up to any dimensionless axial location) Nusselt numbers.

Under all the investigated thermal boundary conditions, the numerical results obtained for the developing laminar free convection in open-ended vertical eccentric annuli show that

- The naturally induced flow rate increases with the increase in the channel height for a channel of a given eccentricity under specific boundary conditions. However, for cases with isothermal walls (boundary conditions of the first, third and fourth kinds) there is a channel height beyond which the induced flow rate will be fixed at a specific maximum constant value(depends on the eccentricity E and the kind of the boundary conditions). This channel height is called the fully developed length.
- Increasing the eccentricity increases The induced flow rate F, the mean bulk temperature $\theta_m$ and consequently the heat absorbed by the fluid $Q$ for a specific channel height under the same boundary conditions.
- Having the outer wall as the heat transfer wall results in larger values of the induced flow rate F, the mean bulk temperature $\theta_m$ and consequently the heat absorbed by the fluid $Q$ compared to those for cases with the inner wall is the heat transfer wall.

## 9.2 Recommendations

The following can be recommended as extensions to the present work

- Experimental work is suggested to validate the presently obtained results for the four cases investigated.
- The presently developed mathematical model describing the developing forced convection in eccentric annuli and the developing free convection in open-ended

vertical eccentric annuli could be easily modified to study the problem of mixed convection in vertical eccentric annuli.

- The present model can be used with very minor modifications to solve the forced/free convection problems in the entry region of eccentric annuli with rotating boundaries.
- The present model my be modified to study the transient developing forced/free convection in eccentric annuli with fixed or rotating boundaries.
- the present model can be used to study the developing laminar forced convection in the eccentric annuli for pulsating flow conditions at the entrance.
- The problem of forced/free convection in eccentric annuli can be studied using the present model under oscillating thermal boundary conditions.
- The present model may be modified to solve for different geometries other than the eccentric annuli.

# Appendix A

# BIPOLAR COORDINATE SYSTEM

## A.1 Introduction

The first step in an analytical, or numerical, solution of fluid and heat flow problem is to choose an orthogonal coordinate system such that its coordinate surfaces coincide with the boundary surfaces of the region under consideration. For example the rectangular coordinate system is useful for rectangular regions, the cylindrical coordinate systems are used for regions having boundaries with cylindrical shapes, while the spherical coordinate system is used for bodies having a spherical boundaries and so on.

The most powerful orthogonal curvilinear coordinate system which could be used to express the partial differential equations describing the flow through eccentric

annuli is the bi-polar coordinate system. The bi-polar coordinate system is nothing but a set of orthogonal eccentric cylinders. so that the boundary surfaces of an cccentric annulus may be taken as one of the coordinates and the other coordinate will be the set of the eccentric cylinders which orthogonally intersect the boudoirs of the annulus.

## A.2 Transformation Procedure

To consider the transformation procedure from the cartesian coordinates to the bipolar coordinates system, some useful relations will be listed first. Such relations are;

$$\sin x = \frac{i}{2}(e^{-ix} - e^{ix}) \tag{A.1}$$

$$\cos x = \frac{1}{2}(e^{-ix} + e^{ix}) \tag{A.2}$$

$$\tan x = \frac{\sin x}{\cos x} = \frac{i(1-e^{2ix})}{1+e^{2ix}} \tag{A.3}$$

Replacing $x$ by $ix$ we will obtain the corresponding hyperbolic functions

$$\sin(ix) = \frac{i}{2}(e^{x} - e^{-x}) = i\sinh x \tag{A.4}$$

$$cos(ix) = \frac{1}{2}(e^{x} + e^{-x}) = cosh\, x \tag{A.5}$$

$$tan\,(ix)=\frac{i(e^{2x}-1)}{(e^{2x}+1)}=i\,tan\;\;x \tag{A.6}$$

also we will need the inverse circular function;

$$tan^{-1}\,x=u$$

Since; $tan^{-1}\,x=u$ , it follows from 3.A that;

$$tan\,u=\frac{i(1-e^{2iu})}{(1+e^{2iu})}=x,\quad hence;\; x(1+e^{2iu})=i(1-e^{2iu})$$
$$x+xe^{2iu}=i-ie^{2iu},\; hence;\; e^{2iu}(i+x)=(i-x)$$

hence;

$$e^{2iu}=\frac{(i-x)}{(i+x)} \tag{A.7}$$

$$2iu=ln(\frac{(i-x)}{(i+x)}) \tag{A.8}$$

$$u=tan^{-1}\,x=\frac{1}{2i}ln(\frac{(i-x)}{(i+x)})=-\frac{i}{2}ln(\frac{(i-x)}{(i+x)})=\frac{i}{2}ln(\frac{(i+x)}{(i-x)}) \tag{A.9}$$

Now considering the following geometry, one can define;

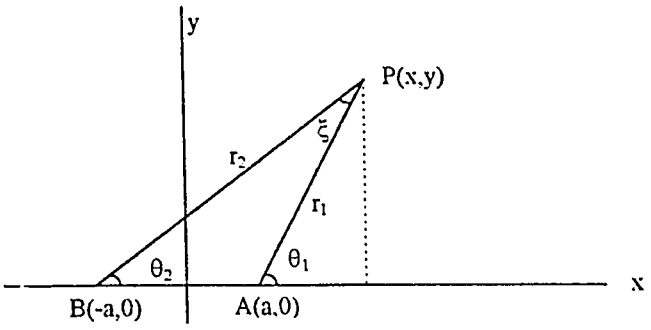


**Figure A1.1**

$$\xi = \theta_1 - \theta_2 \tag{A.10}$$

$$\eta = ln\frac{r_2}{r_1} \tag{A.11}$$

$$\frac{r_2}{r_1} = e^{\eta} \tag{A.12}$$

$$\rho = x + iy \tag{A.13}$$

$$\rho^* = x - iy \tag{A.14}$$

From the geometry we have,

$$x - a = r_1 \cos(\theta_1) \tag{A.15}$$

$$x + a = r_2 \cos(\theta_2) \tag{A.16}$$

using A.14 and A.16,

$$x-a=r_1 Cos\theta_1,\ \ hence,\ \ x=a+r_1 Cos\theta_1$$
$$\because \rho = x+iy,\ \therefore \rho = a+r_1 Cos\theta_1 + iy = a+r_1 Cos\theta_1 + ir_1 Sin\theta_1$$
$$\therefore \rho = a+r_1\ (Cos\theta_1 + iSin\theta_1) = a+e^{i\theta_1}$$

and also we have;

$$x+a=r_2 Cos\theta_2,\ \ hence,\ x=-a+r_2 Cos\theta_2$$
$$\because \rho = x+iy,\ \therefore \rho = -a+r_2 Cos\theta_2 + iy = a+r_2 Cos\theta_2 + ir_2 Sin\theta_2$$
$$\therefore \rho = -a+r_2\ (Cos\theta_2 + iSin\theta_2) = -a+e^{i\theta_2}$$

So that one can write;

$$\rho - a = r_1 e^{i\theta_1} \qquad \text{(A.17)}$$

$$\rho + a = r_2 e^{i\theta_2} \qquad \text{(A.18)}$$

$$\frac{\rho+a}{\rho-a} = \frac{r_2}{r_1} e^{i(\theta_2-\theta_1)} = e^{\eta}\, e^{-i\xi} = e^{-i(\xi+i\eta)} \qquad \text{(A.19)}$$

$$\text{Let} \quad X = \xi + i\eta \qquad \text{(A.20)}$$

$$\frac{\rho+a}{\rho-a} = e^{-iX} \qquad \text{(A.21)}$$

$$\frac{\frac{\rho}{a}+1}{\frac{\rho}{a}-1}=e^{-iX} \tag{A.22}$$

$$\frac{\rho}{a}+1=e^{-iX}\left(\frac{\rho}{a}-1\right) \tag{A.23}$$

$$\frac{\rho}{a}\left(1-e^{-iX}\right)=-\left(e^{-iX}+1\right) \tag{A.24}$$

$$\frac{\rho}{a}=\frac{e^{-iX}+1}{e^{-iX}-1} \tag{A.25}$$

By definition we have; $x=\rho^{*}+iy$

and $x-a=r_1 Cos\theta_1$, hence

$$\rho^{*}+iy-a=r_1 Cos\theta_1 \tag{A.26}$$

$$\rho^{*}-a=r_1 Cos\theta_1-iy=r_1 Cos\theta_1-i\ r_1\ Sin\theta_1=r_1\left(Cos\theta_1-i\ Sin\theta_1\right)$$
$$=r_1\left(Cos(-\theta_1)+i\ Sin(-\theta_1)\right)=r_1 e^{-i\theta_1}$$

Hence,

$$\rho^{*}-a=r_1 e^{-i\theta_1} \tag{A.27}$$

We have also

$x+a=r_2 Cos\theta_2$, hence

$$\rho^{*}+iy+a=r_2 Cos\theta_2 \tag{A.28}$$

$$\rho^{*}+a=r_2 Cos\theta_2-iy=r_2 Cos\theta_2-i\ r_2\ Sin\theta_2=r_2\left(Cos\theta_2-i\ Sin\theta_2\right)$$
$$=r_2\left(Cos(-\theta_2)+i\ Sin(-\theta_2)\right)=r_2 e^{-i\theta_2}$$

hence;

$$\rho^{*}+a=r_2 e^{-i\theta_2} \tag{A.29}$$

hence;

$$\frac{\rho^{*}+a}{\rho^{*}-a}=\frac{r_2}{r_1}e^{i(\theta_1-\theta_2)}=e^{\eta}\,e^{i\xi}=e^{i(\xi-i\eta)}$$

let : $Y=\xi-i\eta$ (A.30)

hence;

$$\frac{\rho^{*}+a}{\rho^{*}-a}=e^{iY} \tag{A.31}$$

$$\frac{\frac{\rho^{*}}{a}+1}{\frac{\rho^{*}}{a}-1}=e^{iY} \tag{A.32}$$

$$\frac{\rho^{*}}{a}+1=e^{iY}\left(\frac{\rho^{*}}{a}-1\right) \tag{A.33}$$

$$\frac{\rho^{*}}{a}(1-e^{iY})=-(e^{iY}+1) \tag{A.34}$$

$$\frac{\rho^{*}}{a}=\frac{e^{iY}+1}{e^{iY}-1} \tag{A.35}$$

since

$$\rho=x+iy \tag{A.36}$$

and by definition;

$$\rho^{*}=x-iy \tag{A.37}$$

using A.25, A.35, A.36 and A.37, one can write

$$x=\frac{\rho+\rho^{*}}{2} \tag{A.38}$$

$$x=\frac{a}{2}\left[\frac{e^{-iX}+1}{e^{-iX}-1}+\frac{e^{iY}+1}{e^{iY}-1}\right]$$

$$x=\frac{a}{2}\left[\frac{(e^{-iX}+1)(e^{iY}-1)+(e^{iY}+1)(e^{-iX}-1)}{(e^{-iX}-1)(e^{iY}-1)}\right]$$

$$=\frac{a}{2}\,\frac{e^{-iX+iY}+e^{iY}-e^{-iX}+e^{-iX+iY}+e^{-iX}-e^{iY}-1}{e^{-iX+iY}-e^{iY}-e^{-iX}+1}=\frac{a}{2}\,\frac{2(e^{-i(X-Y)}-1)}{e^{-i(X-Y)}-e^{iY}-e^{-iX}+1} \tag{A.39}$$

Now substituting for X and Y in terms of $\eta$ and $\xi$ in the above equation using 20 and 30, one get;

$$x=a\,\frac{e^{i(-\xi-i\eta+\xi-i\eta)}-1}{e^{i(-\xi-i\eta-\xi-i\eta)}-e^{i(\xi-i\eta)}-e^{-i(\xi+i\eta)}+1} \tag{A.40}$$

$$x=a\,\frac{e^{2\eta}-1}{e^{2\eta}-e^{\eta}(e^{i\xi}+e^{-i\xi})+1}\,, \qquad \textit{devide by}\quad e^{\eta}$$

$$=a\,\frac{e^{\eta}-e^{-\eta}}{e^{\eta}-(e^{i\xi}+e^{-i\xi})+e^{-\eta}}\,, \qquad \textit{devide by}\quad 2\ \textit{and rearrange}$$

$$=a\,\frac{\frac{e^{\eta}-e^{-\eta}}{2}}{\frac{e^{\eta}+e^{-\eta}}{2}-\frac{e^{i\xi}+e^{-i\xi}}{2}}=a\,\frac{Sinh(\eta)}{Cosh(\eta)-Cos(\xi)}$$

$$x = a\frac{Sinh(\eta)}{Cosh(\eta) - Cos(\xi)} \tag{A.41}$$

Remembering that;

$\rho = x + iy$ and $\rho^* = x - iy$, subtracting gives us;

$$\rho - \rho^* = 2i\,y, hence,\ y = \frac{i}{2}(\rho^* - \rho) \tag{A.42}$$

Substituting from A.25, A.35,A.36 and A.37 into A.42, one gets

$$y = \frac{i}{2}\left[ a\frac{e^{iY}+1}{e^{iY}-1} - a\frac{e^{-iX}+1}{e^{-iX}-1} \right]$$

$$y = \frac{a}{2}i\left[ \frac{(e^{iY}+1)(e^{-iX}-1) - (e^{-iX}+1)(e^{iY}-1)}{(e^{-iX}-1)(e^{iY}-1)} \right]$$

$$= \frac{a}{2}i\,\frac{e^{-iX+iY} - e^{iY} + e^{-iX} - 1 - e^{-iX+iY} + e^{-iX} - e^{iY} + 1}{e^{-iX+iY} - e^{iY} - e^{-iX} + 1} = \frac{a}{2}i\,\frac{2(e^{-iX} - e^{iY})}{e^{i(Y-X)} - e^{iY} - e^{-iX} + 1}$$

Now substituting for X and Y in terms of $\eta$ and $\xi$ in the above equation using A.20 and A.30, one gets;

$$y = ai\frac{e^{-i(\xi+i\eta)} - e^{i(\xi-i\eta)}}{e^{i(\xi-i\eta-\xi-i\eta)} - e^{i(\xi-i\eta)} - e^{-i(\xi+i\eta)} + 1}$$

$$y = a\,i\frac{e^{\eta}(e^{-i\xi}-e^{i\xi})}{e^{2\eta}-e^{\eta}(e^{i\xi}+e^{-i\xi})+1}, \qquad \textit{devide by} \quad e^{\eta}$$

$$= a\,i\frac{e^{-i\xi}-e^{i\xi}}{e^{\eta}-(e^{i\xi}+e^{-i\xi})+e^{-\eta}}, \qquad \textit{devide by} \quad 2i \textit{ and rearrange}$$

$$= -\frac{a}{i}\frac{\frac{e^{-i\xi}-e^{i\xi}}{2}}{\frac{e^{\eta}+e^{-\eta}}{2}-\frac{e^{i\xi}+e^{-i\xi}}{2}} = a\frac{\frac{e^{i\xi}-e^{-i\xi}}{2i}}{\frac{e^{\eta}+e^{-\eta}}{2}-\frac{e^{i\xi}+e^{-i\xi}}{2}} = a\frac{Sin(\xi)}{Cosh(\eta)-Cos(\xi)}$$

$$y = a\frac{Sin(\xi)}{Cosh(\eta)-Cos(\xi)} \tag{A.43}$$

Obtaining the relations between ($\eta$ and $\xi$) and ($x$ and $y$), we will be able to transform any partial differential equation written in the Cartesian coordinates ($x$, $y$ and $z$) into the bipolar coordinates ($\eta$, $\xi$ and $z$) using the scale factor method or other transformation procedures which may found in details in [68,69]. Now we want to express $\eta$ and $\xi$ in terms of $x$ and $y$. From definition we have;

$$\xi = \theta_1 - \theta_2 = tan^{-1}\left(\frac{y}{x-a}\right) - tan^{-1}\left(\frac{y}{x+a}\right).$$

using A.9, one can write;

$$=\frac{i}{2}ln\left(\frac{i+\dfrac{y}{x-a}}{i-\dfrac{y}{x-a}}\right)-\frac{i}{2}ln\left(\frac{i+\dfrac{y}{x+a}}{i-\dfrac{y}{x+a}}\right)=\frac{i}{2}\left[ln\left(\frac{ix-ia+y}{ix-ia-y}\right)-ln\left(\frac{ix+ia+y}{ix+ia-y}\right)\right]$$

$$=\frac{i}{2}ln\left(\frac{(ix-ia+y)(ix+ia-y)}{(ix-ia-y)(ix+ia+y)}\right)=\frac{i}{2}ln\left(\frac{(i(x-a)+y)(ix+ia-y)}{(i(x-a)-y)(ix+ia+y)}\right)$$

$$=\frac{i}{2}ln\left(\frac{-(x-a)(x+a)+iy(x+a)-iy(x-a)-y^2}{-(x-a)(x+a)-iy(x+a)+iy(x-a)-y^2}\right)$$

$$=\frac{i}{2}ln\left(\frac{-(x^2-a^2)+iyx+iya-iyx+iya-y^2}{-(x^2-a^2)-iyx-iya+iyx-iya-y^2}\right)=\frac{i}{2}ln\left(\frac{-(x^2-a^2)+2iya-y^2}{-(x^2-a^2)-2iya-y^2}\right)$$

Rearranging;

$$2i\xi=-ln\left(\frac{-(x^2-a^2)+2iya-y^2}{-(x^2-a^2)-2iya-y^2}\right)=ln\left(\frac{-(x^2-a^2)-2iya-y^2}{-(x^2-a^2)+2iya-y^2}\right)$$

$$e^{2i\xi}=\frac{-x^2+a^2-2iya-y^2}{-x^2+a^2+2iya-y^2}=\frac{x^2+y^2-a^2+2iya}{x^2+y^2-a^2-2iya}$$

Let; $A=x^2+y^2-a^2$ *and* $B=2iya$

hence, $e^{2i\xi}=\dfrac{A+B}{A-B}$, i.e., $A+B=Ae^{2i\xi}-Be^{2i\xi}$, hence;

$$A\,(1-e^{2i\xi})=-B(1+e^{2i\xi}),\quad hence\ A+B\frac{1+e^{2i\xi}}{1-e^{2i\xi}}=0$$

$$hence;\ x^2+y^2-a^2+2iya\frac{e^{i\xi}(e^{-i\xi}+e^{i\xi})}{e^{i\xi}(e^{-i\xi}-e^{i\xi})}=x^2+y^2-a^2+2ya\frac{\frac{(e^{-i\xi}+e^{i\xi})}{2}}{\frac{(e^{-i\xi}-e^{i\xi})}{2i}}=0$$

$$\therefore x^2+y^2-a^2-2ya\frac{\frac{(e^{i\xi}+e^{-i\xi})}{2}}{\frac{(e^{i\xi}-e^{-i\xi})}{2i}}=x^2+y^2-a^2-2ya\frac{Cos(\xi)}{Sin(\xi)}=x^2+y^2-a^2-2ya\,Cot(\xi)=0$$

add and subtract the value of $(a\,Cot(\xi))^2$ to the above equation, one can get;

$$x^2+y^2-2a\,y\,Cot(\xi)+a^2\,Cot^2(\xi)=a^2\,(1+Cot^2(\xi))$$

*hence;*

$$x^2+(y-a\,y\,Cot(\xi))^2=a^2\,Csc^2(\xi)$$

This is an equation of a circle of radius $a\,Csc(\xi)$ and center at $(x=0, y=a\,Cot(\xi))$

Now let's consider an expression for $\eta$ in terms of $x$ and $y$. From definition we have;

$$\eta=ln\frac{r_2}{r_1},\ hence$$

$$e^{\eta}=\frac{r_2}{r_1}\ \ squaring\ both\ sides\ and\ reffering\ to\ fig.1.,\ gives$$

$$e^{2\eta}=\frac{r_2^2}{r_1^2}=\frac{(x+a)^2+y^2}{(x-a)^2+y^2}=\frac{x^2+2ax+a^2+y^2}{x^2-2ax+a^2+y^2}$$

*let;* $A = x^2 + y^2 + a^2$, *and* $B = 2ax$, *hence,* $e^{2\eta} = \dfrac{A+B}{A-B}$

*hence;* $A\left(e^{2\eta} - 1\right) = B\left(e^{2\eta} + 1\right)$,

*rearrange;*

$$A - B\frac{e^{2\eta}+1}{e^{2\eta}-1} = A - B\frac{e^{\eta}\left(e^{\eta}+e^{-\eta}\right)}{e^{\eta}\left(e^{\eta}-e^{-\eta}\right)} = A - B\frac{\dfrac{e^{\eta}+e^{-\eta}}{2}}{\dfrac{e^{\eta}-e^{-\eta}}{2}} = 0$$

$$\textit{hence; } A - B\frac{Cosh(\eta)}{Sinh(\eta)} = 0, \textit{i.e., } x^2 + y^2 + a^2 - 2ax\ Coth(\eta) = 0$$

add and subtract the value of $\left(a\ Coth(\eta)\right)^2$ to the above equation, on can get;

$$x^2 - 2ax\,Coth(\eta) + a^2\,Coth^2(\eta) + y^2 + a^2 - a^2\,Coth^2(\eta) = 0$$

$$\left(x - a\,Coth(\eta)\right)^2 + y^2 = a^2\left(Coth^2(\eta) - 1\right)$$

$$\textit{hence; } \left(x - a\,Coth(\eta)\right)^2 + y^2 = a^2\,Csch^2(\eta)$$

This is an equation of a circle of radius ***a Csch*** $(\eta)$ and center at ***( x = a Coth*** $(\eta)$***, y = 0 )***

# Appendix B

# RELATIONS BETWEEN THE GEOMETRY PARAMETERS AND BIPOLAR COORDINATES

We have learned from the previous appendix that the bipolar coordinates is nothing but a set of eccentric circles orthogonal to another set of eccentric circles. So that the boundaries of the eccentric annuli will coincide with one of this coordinates, while the other coordinate will be orthogonal to it. In this study, we make the coordinate $\eta$ to be coincide with the boundaries of our cylinders. We will give the subscript o to represent the outer cylinder while the subscript i to represent the inner cylinder.

If the location of the positive pole of the bipolar coordinate is at a in the Cartesian coordinate then, we have the η coordinate is a set of eccentric circle of radius *( c Csch η)* and its center at *( x = c Coth η)*. So that for our geometry:

| **Boundary** | **Radius** | **Center** |
|---|---|---|
| **Outer cylinder** | $r_o = c\ Csch(\eta_o) = \frac{c}{Sinh(\eta_o)}$ | $c\ Coth(\eta_o)$ |
| **Inner cylinder** | $r_i = c\ Csch(\eta_i) = \frac{c}{Sinh(\eta_i)}$ | $c\ Coth(\eta_i)$ |

Now we can express the important geometrical parameters of the eccentric annuli in a dimensionless form as;

$$Radius\ Ratio\ \ N = \frac{r_i}{r_o} = \frac{c\ Csch(\eta_i)}{c\ Csch(\eta_o)} = \frac{Sinh(\eta_o)}{Sinh(\eta_i)}$$

$$i.e.\ Sinh(\eta_i) = \frac{1}{N} Sinh(\eta_o)$$

Knowing that eccentricity is the distance between the two cylinder centers, one can define the relative eccentricity $E$ as; $E = \frac{x_o - x_i}{r_o - r_i}$

$$\therefore E = \frac{a\ Coth(\eta_o) - a\ Coth(\eta_i)}{\frac{a}{Sinh(\eta_o)} - \frac{a}{Sinh(\eta_i)}} = \frac{\frac{Cosh(\eta_o)}{Sinh(\eta_o)} - \frac{Cosh(\eta_i)}{Sinh(\eta_i)}}{\frac{1}{Sinh(\eta_o)} - \frac{1}{Sinh(\eta_i)}} = \frac{Cosh(\eta_o)\,Sinh(\eta_i) - Cosh(\eta_i)\,Sinh(\eta_o)}{Sinh(\eta_i) - Sinh(\eta_o)}$$

$$E = \frac{Cosh(\eta_o)\left(\frac{1}{N} Sinh(\eta_o)\right) - Cosh(\eta_i)\,Sinh(\eta_o)}{\frac{1}{N} Sinh(\eta_o) - Sinh(\eta_o)} = \frac{\frac{Cosh(\eta_o)}{N} - Cosh(\eta_i)}{\frac{1}{N} - 1} = \frac{Cosh(\eta_o) - N\,Cosh(\eta_i)}{1 - N}$$

Knowing the identity;

$$Cosh^2(\eta_i)-Sinh^2(\eta_i)=1,\ \therefore Cosh(\eta_i)=\left(Sinh^2(\eta_i)+1\right)^{1/2}$$

Using the above identity , we can write; $E=\dfrac{Cosh(\eta_o)-N\left(Sinh^2(\eta_i)+1\right)^{1/2}}{1-N}$

$$E(1-N)=Cosh(\eta_o)-N\left(1+\frac{1}{N^2}\,Sinh^2(\eta_o)\right)^{1/2}=Cosh(\eta_o)-N\frac{\left(N^2+\,Sinh^2(\eta_o)\right)^{1/2}}{N}$$

$$E(1-N)=Cosh(\eta_o)-\left(N^2+\,Sinh^2(\eta_o)\right)^{1/2},\ \therefore\ \left(N^2+\,Sinh^2(\eta_o)\right)^{1/2}=Cosh(\eta_o)-E(1-N)$$

*Squaring both sides*

$$N^2+\,Sinh^2(\eta_o)=Cosh^2(\eta_o)-2Cosh(\eta_o)E(1-N)+\left(E(1-N)\right)^2$$

$$N^2+Cosh^2(\eta_o)-1=Cosh^2(\eta_o)-2Cosh(\eta_o)E(1-N)+\left(E(1-N)\right)^2$$

$$N^2-1=-2Cosh(\eta_o)E(1-N)+\left(E(1-N)\right)^2,$$

$$\therefore 2Cosh(\eta_o)=\frac{\left(E(1-N)\right)^2-N^2+1}{E(1-N)}=\frac{E^2(1-N)+(1+N)}{E}$$

$$\therefore 2\frac{e^{\eta_o}+e^{-\eta_o}}{2}=\frac{E^2(1-N)+(1+N)}{E},\ \therefore e^{-\eta_o}\left(e^{2\eta_o}+1\right)=\frac{E^2(1-N)+(1+N)}{E},$$

$$\therefore e^{2\eta_o}+1=e^{\eta_o}\left(\frac{E^2(1-N)+(1+N)}{E}\right),\ \therefore e^{2\eta_o}-e^{\eta_o}\left(\frac{E^2(1-N)+(1+N)}{E}\right)+1=0,$$

$$Let:\ e^{\eta_o}=X,\quad \left(\frac{E^2(1-N)+(1+N)}{E}\right)=b$$

$$\therefore X^2-bX+1=0,\ \therefore X=\frac{b+\sqrt{b^2-4}}{2}=\frac{b}{2}+\sqrt{\left(\frac{b}{2}\right)^2-1}$$

$$\therefore X=\left(\frac{E^2(1-N)+(1+N)}{2E}\right)+\sqrt{\left(\frac{E^2(1-N)+(1+N)}{2E}\right)^2-1}$$

$$\therefore e^{\eta_o}=\left(\frac{N(1-E^2)+(1+E^2)}{2E}\right)+\sqrt{\left(\frac{N(1-E^2)+(1+E^2)}{2E}\right)^2-1},$$

$$\therefore X = \left(\frac{E^2(1-N)+(1+N)}{2E}\right)+\sqrt{\left(\frac{E^2(1-N)+(1+N)}{2E}\right)^2-1}$$

$$\therefore e^{\eta_o} = \left(\frac{N(1-E^2)+(1+E^2)}{2E}\right)+\sqrt{\left(\frac{N(1-E^2)+(1+E^2)}{2E}\right)^2-1},$$

*taking Ln for both sides, one gets*

$$\eta_o = Ln\left[\left(\frac{N(1-E^2)+(1+E^2)}{2E}\right)+\sqrt{\left(\frac{N(1-E^2)+(1+E^2)}{2E}\right)^2-1}\right]$$

Now to Express $\eta_i$ we will substitute for $Sinh(\eta_o)$ in terms of $Sinh(\eta_i)$

$$E=\frac{Cosh(\eta_o)Sinh(\eta_i)-Cosh(\eta_i)Sinh(\eta_o)}{Sinh(\eta_i)-Sinh(\eta_o)} = \frac{Cosh(\eta_o)Sinh(\eta_i)-N\,Cosh(\eta_i)Sinh(\eta_i)}{Sinh(\eta_i)-N\,Sinh(\eta_i)}$$

$$=\frac{Cosh(\eta_o)-N\,Cosh(\eta_i)}{1-N}$$

$$E=\frac{\left(N^2\,Sinh^2(\eta_i)+1\right)^{1/2}-NCosh(\eta_i)}{1-N},\ \therefore E(1-N)=\left(1+N^2\,Sinh^2(\eta_i)\right)^{1/2}-N\,Cosh(\eta_i)$$

$$E(1-N)+N\,Cosh(\eta_i)=\left(1+N^2\,Sinh^2(\eta_i)\right)^{1/2},\ \ Squaring\ \ both\ \ sides$$

$$E^2(1-E)^2+2E(1-N)N\,Cosh(\eta_i)+N^2\,Cosh^2(\eta_i)=1+N^2\,Sinh^2(\eta_i)=1+N^2\left(Cosh^2(\eta_i)-1\right)$$

Rearranging

$$\therefore 2Cosh(\eta_i)=\frac{\left(-E(1-N)\right)^2-N^2+1}{E(1-N)N}=\frac{-E^2(1-N)+(1+N)}{E}$$

$$2\frac{e^{\eta_i}+e^{-\eta_i}}{2}=\frac{-E^2(1-N)+(1+N)}{EN},\ \therefore e^{-\eta_i}\left(e^{2\eta_i}+1\right)=\frac{-E^2(1-N)+(1+N)}{EN}$$

$$\therefore e^{2\eta_i}+1=e^{\eta_i}\left(\frac{-E^2(1-N)+(1+N)}{EN}\right),\ \therefore e^{2\eta_i}-e^{\eta_i}\left(\frac{-E^2(1-N)+(1+N)}{EN}\right)+1=0$$

$$Let:\ e^{\eta_i}=X,\quad \left(\frac{-E^2(1-N)+(1+N)}{EN}\right)=b,\ \therefore X^2-bX+1=0$$

$$\therefore X=\frac{b+\sqrt{b^2-4}}{2}=\frac{b}{2}+\sqrt{\left(\frac{b}{2}\right)^2-1}=\left(\frac{-E^2(1-N)+(1+N)}{2EN}\right)+\sqrt{\left(\frac{-E^2(1-N)+(1+N)}{2EN}\right)^2-1}$$

$$\therefore e^{\eta_i}=\left(\frac{N(1+E^2)+(1-E^2)}{2EN}\right)+\sqrt{\left(\frac{N(1+E^2)+(1-E^2)}{2EN}\right)^2-1}$$

*Taking Ln for both sides;*

$$\eta_i=Ln\left[\left(\frac{N(1+E^2)+(1-E^2)}{2EN}\right)+\sqrt{\left(\frac{N(1+E^2)+(1-E^2)}{2EN}\right)^2-1}\right]$$

# Appendix C

# NAVIER-STOKES EQUATIONS

# IN BI-POLAR COORDINATES

Navier stokes equations can be written in a vectorial form as;

$$\rho \frac{DV}{Dt} = F - \nabla P + \mu \nabla^2 V$$

To write the above equation in a general orthogonal curvilinear coordinate system, one should expand the laplacian operator for the vector V in the proper way, [68].

$$\nabla^2 V = \nabla(\nabla.V) - \nabla x(\nabla x V)$$
$$= \text{grad}(\text{div}(V)) - \text{Curl Curl}(V)$$

Referring to reference [68], one can write for any vector E the Laplacian operator in any general curvilinear coordinate system as;

$$\nabla^2 E = a_1 \left\{ \frac{1}{(g_{11})^{1/2}} \frac{\partial \gamma}{\partial U_1} + \left( \frac{g_{11}}{g} \right)^{1/2} \left[ \frac{\partial \Gamma_2}{\partial U_3} - \frac{\partial \Gamma_3}{\partial U_2} \right] \right\}$$

$$+ a_2 \left\{ \frac{1}{(g_{22})^{1/2}} \frac{\partial \gamma}{\partial U_2} + \left( \frac{g_{22}}{g} \right)^{1/2} \left[ \frac{\partial \Gamma_3}{\partial U_1} - \frac{\partial \Gamma_1}{\partial U_3} \right] \right\}$$

$$+ a_3 \left\{ \frac{1}{(g_{33})^{1/2}} \frac{\partial \gamma}{\partial U_3} + \left( \frac{g_{33}}{g} \right)^{1/2} \left[ \frac{\partial \Gamma_1}{\partial U_2} - \frac{\partial \Gamma_2}{\partial U_1} \right] \right\}$$

Where;

*$U_i$ s , I = 1, 2, 3 are the general curvilinear orthogonal coordinates, $a_i$ is unit vector in each direction and $g_{ii}$ s are the transformation factors.*

$$\gamma = g^{-1/2} \left\{ \frac{\partial}{\partial U_1} \left[ \left( \frac{g}{g_{11}} \right)^{1/2} E_1 \right] + \frac{\partial}{\partial U_2} \left[ \left( \frac{g}{g_{22}} \right)^{1/2} E_2 \right] + \frac{\partial}{\partial U_3} \left[ \left( \frac{g}{g_{33}} \right)^{1/2} E_3 \right] \right\}$$

$$\Gamma_1 = \frac{g_{11}}{g^{1/2}} \left\{ \frac{\partial}{\partial U_2} \left[ (g_{33})^{1/2} E_3 \right] - \frac{\partial}{\partial U_3} \left[ (g_{22})^{1/2} E_2 \right] \right\}$$

$$\Gamma_2 = \frac{g_{22}}{g^{1/2}} \left\{ \frac{\partial}{\partial U_3} \left[ (g_{11})^{1/2} E_1 \right] - \frac{\partial}{\partial U_1} \left[ (g_{33})^{1/2} E_3 \right] \right\}$$

$$\Gamma_3 = \frac{g_{33}}{g^{1/2}} \left\{ \frac{\partial}{\partial U_1} \left[ (g_{22})^{1/2} E_2 \right] - \frac{\partial}{\partial U_2} \left[ (g_{11})^{1/2} E_1 \right] \right\}$$

and we have also;

$$div(E) = g^{-1/2} \left\{ \frac{\partial}{\partial U_1} \left[ \left( \frac{g}{g_{11}} \right)^{1/2} E_1 \right] + \frac{\partial}{\partial U_2} \left[ \left( \frac{g}{g_{22}} \right)^{1/2} E_2 \right] + \frac{\partial}{\partial U_3} \left[ \left( \frac{g}{g_{33}} \right)^{1/2} E_3 \right] \right\}$$

= 0.0 for incompressible flows, if $E$ represents the velocity vector.

Looking at the expansion of the Laplacian operator of $V$, putting $V$ instead of $E$, one can conclude that $\gamma = 0.0$, for incompressible flow.

**For bi-polar Coordinates:**

$g_{11}=h^2, g_{22}=h^2, g_{33}=1$

*and*; $g=g_{11}.g_{22}.g_{33}=h^2.h^2.1$

*hence*; $g^{1/2}=h^2$

and;

$U_1=\xi$
$U_2=\eta$
$U_3=Z$

So that we will let;

$E_1$ represents the velocity in ξ- direction, w

$E_2$ represents the velocity in η- direction, v

$E_3$ represents the velocity in Z- direction, u

Now writing the expansion of the Laplacian operator of the vector E in $U_1$ direction, we get;

$$\nabla^2 E=a_1\left\{0+\left(\frac{g_{11}}{g}\right)^{1/2}\left[\begin{array}{l}\dfrac{\partial}{\partial U_3}\left[\dfrac{g_{22}}{g^{1/2}}\left\{\dfrac{\partial}{\partial U_3}\left[(g_{11})^{1/2}E_1\right]-\dfrac{\partial}{\partial U_1}\left[(g_{33})^{1/2}E_3\right]\right\}\right] \\ -\dfrac{\partial}{\partial U_2}\left[\dfrac{g_{33}}{g^{1/2}}\left\{\dfrac{\partial}{\partial U_1}\left[(g_{22})^{1/2}E_2\right]-\dfrac{\partial}{\partial U_2}\left[(g_{11})^{1/2}E_1\right]\right\}\right]\end{array}\right]\right\}$$

Now for ξ- direction;

$$(\nabla^2 V)_\xi=\left(\frac{h^2}{h^4}\right)^{1/2}\left[\begin{array}{l}\dfrac{\partial}{\partial Z}\left[\dfrac{h^2}{h^2}\left\{\dfrac{\partial}{\partial Z}\left[(h^2)^{1/2}w\right]-\dfrac{\partial}{\partial \xi}\left[(1)^{1/2}u\right]\right\}\right] \\ -\dfrac{\partial}{\partial \eta}\left[\left(\dfrac{1}{h^4}\right)^{1/2}\left\{\dfrac{\partial}{\partial \xi}\left[(h^2)^{1/2}v\right]-\dfrac{\partial}{\partial \eta}\left[(h^2)^{1/2}w\right]\right\}\right]\end{array}\right]$$

$$(\nabla^2 V)_\xi = \frac{1}{h}\left[\frac{\partial}{\partial Z}\left[\left\{\frac{\partial}{\partial Z}[hw]-\frac{\partial u}{\partial \xi}\right\}\right]-\frac{\partial}{\partial \eta}\left[\frac{1}{h^2}\left\{\frac{\partial}{\partial \xi}[hv]-\frac{\partial}{\partial \eta}[hw]\right\}\right]\right]$$

$$(\nabla^2 V)_\xi = \frac{1}{h}\left[\frac{\partial^2}{\partial Z^2}(hw)-\frac{\partial}{\partial Z}\left(\frac{\partial u}{\partial \xi}\right)-\frac{\partial}{\partial \eta}\left(\frac{1}{h^2}\frac{\partial (hv)}{\partial \xi}\right)+\frac{\partial}{\partial \eta}\left(\frac{1}{h^2}\frac{\partial (hw)}{\partial \eta}\right)\right]$$

$$(\nabla^2 V)_\xi = \frac{1}{h}\left[\begin{array}{l}\dfrac{\partial^2}{\partial Z^2}(hw)-\dfrac{\partial}{\partial Z}\left(\dfrac{\partial u}{\partial \xi}\right)-\dfrac{1}{h^2}\dfrac{\partial}{\partial \eta}\left(\dfrac{\partial (hv)}{\partial \xi}\right)+\dfrac{2}{h^3}\dfrac{\partial h}{\partial \eta}\dfrac{\partial (hv)}{\partial \xi} \\ +\dfrac{1}{h^2}\dfrac{\partial^2 (hw)}{\partial \eta^2}-\dfrac{2}{h^3}\dfrac{\partial h}{\partial \eta}\dfrac{\partial (hw)}{\partial \eta}\end{array}\right]$$

rearranging;

$$(\nabla^2 V)_\xi = \frac{1}{h}\left[\begin{array}{l}\dfrac{\partial^2}{\partial Z^2}(hw)+\dfrac{1}{h^2}\dfrac{\partial^2 (hw)}{\partial \eta^2}-\dfrac{1}{h^2}\left[h^2\dfrac{\partial}{\partial Z}\left(\dfrac{\partial u}{\partial \xi}\right)+\dfrac{\partial}{\partial \eta}\left(\dfrac{\partial (hv)}{\partial \xi}\right)\right] \\ +\dfrac{2}{h^3}\dfrac{\partial h}{\partial \eta}\left[\dfrac{\partial (hv)}{\partial \xi}-\dfrac{\partial (hw)}{\partial \eta}\right]\end{array}\right]$$

$$(\nabla^2 V)_\xi = \frac{1}{h}\left[\begin{array}{l}\dfrac{\partial^2}{\partial Z^2}(hw)+\dfrac{1}{h^2}\dfrac{\partial^2 (hw)}{\partial \eta^2}-\dfrac{1}{h^2}\left[\dfrac{\partial}{\partial Z}\left(h^2\dfrac{\partial u}{\partial \xi}\right)+\dfrac{\partial}{\partial \eta}\left(\dfrac{\partial (hv)}{\partial \xi}\right)\right] \\ +\dfrac{2}{h^3}\dfrac{\partial h}{\partial \eta}\left[\dfrac{\partial (hv)}{\partial \xi}-\dfrac{\partial (hw)}{\partial \eta}\right]\end{array}\right]$$

hint;

$$\frac{\partial}{\partial \xi}(h^2 u)=h^2\frac{\partial u}{\partial \xi}+2uh\frac{\partial h}{\partial \xi}$$

differentiating both sides w.r.t Z, one can get;

$$\frac{\partial}{\partial Z}\left(\frac{\partial}{\partial \xi}(h^2 u)\right)=\frac{\partial}{\partial Z}\left(h^2\frac{\partial u}{\partial \xi}+2uh\frac{\partial h}{\partial \xi}\right)$$

Invert the differentiation index on the L.H.S. and carry out the differentiation in the R.H.S.;

$$\frac{\partial}{\partial \xi}\left(\frac{\partial}{\partial Z}(h^2 u)\right)=\frac{\partial}{\partial Z}\left(h^2\frac{\partial u}{\partial \xi}\right)+\frac{\partial}{\partial Z}\left(2uh\frac{\partial h}{\partial \xi}\right)$$

$$\frac{\partial}{\partial \xi}\left(\frac{\partial}{\partial Z}(h^2 u)\right)=\frac{\partial}{\partial Z}\left(h^2\frac{\partial u}{\partial \xi}\right)+2uh\frac{\partial}{\partial Z}\left(\frac{\partial h}{\partial \xi}\right)+\frac{\partial h}{\partial \xi}\frac{\partial (2uh)}{\partial Z}$$

Noticing that , h, is not a function of Z, hence the second term in the R.H.S. is zero, and one can write;

$$\frac{\partial}{\partial \xi}\left(\frac{\partial}{\partial Z}(h^2 u)\right)=\frac{\partial}{\partial Z}\left(h^2\frac{\partial u}{\partial \xi}\right)+2\frac{\partial h}{\partial \xi}\frac{\partial (uh)}{\partial Z}$$

hence, from the above equation, one can write;

$$\frac{\partial}{\partial Z}\left(h^2\frac{\partial u}{\partial \xi}\right)=\frac{\partial}{\partial \xi}\left(\frac{\partial}{\partial Z}(h^2 u)\right)-2\frac{\partial h}{\partial \xi}\frac{\partial (uh)}{\partial Z}$$

taking the above identity and substituting into the last equation;

$$\left(\nabla^2 V\right)_\xi=\frac{1}{h}\left[\begin{array}{l}\dfrac{\partial^2}{\partial Z^2}(hw)+\dfrac{1}{h^2}\dfrac{\partial^2 (hw)}{\partial \eta^2}-\dfrac{1}{h^2}\left[\dfrac{\partial}{\partial \xi}\left(\dfrac{\partial (h^2 u)}{\partial Z}\right)-2\dfrac{\partial h}{\partial \xi}\dfrac{\partial (hu)}{\partial Z}+\dfrac{\partial}{\partial \eta}\left(\dfrac{\partial (hv)}{\partial \xi}\right)\right] \\ +\dfrac{2}{h^3}\dfrac{\partial h}{\partial \eta}\left[\dfrac{\partial (hv)}{\partial \xi}-\dfrac{\partial (hw)}{\partial \eta}\right]\end{array}\right]$$

rearranging;

$$(\nabla^2 V)_\xi = \frac{1}{h}\left[\begin{array}{l} \dfrac{\partial^2}{\partial Z^2}(hw)+\dfrac{1}{h^2}\dfrac{\partial^2(hw)}{\partial \eta^2}-\dfrac{1}{h^2}\left[\dfrac{\partial}{\partial \xi}\left(\dfrac{\partial(h^2u)}{\partial Z}+\dfrac{\partial(hv)}{\partial \eta}\right)\right] \\ +\dfrac{2}{h^2}\dfrac{\partial h}{\partial \xi}\dfrac{\partial(hu)}{\partial Z}+\dfrac{2}{h^3}\dfrac{\partial h}{\partial \eta}\left[\dfrac{\partial(hv)}{\partial \xi}-\dfrac{\partial(hw)}{\partial \eta}\right] \end{array}\right]$$

From the continuity equation, we have;

$$\frac{\partial(h^2U)}{\partial Z}+\frac{\partial(hv)}{\partial \eta}=-\frac{\partial(hw)}{\partial \xi}$$

hence, substituting with this into the last equation;

$$(\nabla^2 V)_\xi = \frac{1}{h}\left[\begin{array}{l} \dfrac{\partial^2}{\partial Z^2}(hw)+\dfrac{1}{h^2}\dfrac{\partial^2(hw)}{\partial \eta^2}-\dfrac{1}{h^2}\left[\dfrac{\partial}{\partial \xi}\left(-\dfrac{\partial(hw)}{\partial \xi}\right)\right] \\ +\dfrac{2}{h^2}\dfrac{\partial h}{\partial \xi}\dfrac{\partial(hu)}{\partial Z}+\dfrac{2}{h^3}\dfrac{\partial h}{\partial \eta}\left[\dfrac{\partial(hv)}{\partial \xi}-\dfrac{\partial(hw)}{\partial \eta}\right] \end{array}\right]$$

so that we can write finally,

$$(\nabla^2 V)_\xi = \frac{1}{h}\left[\begin{array}{l} \dfrac{\partial^2}{\partial Z^2}(hw)+\dfrac{1}{h^2}\dfrac{\partial^2(hw)}{\partial \eta^2}+\dfrac{1}{h^2}\dfrac{\partial^2(hw)}{\partial \xi^2} \\ +\dfrac{2}{h^2}\dfrac{\partial h}{\partial \xi}\dfrac{\partial(hu)}{\partial Z}+\dfrac{2}{h^3}\dfrac{\partial h}{\partial \eta}\left[\dfrac{\partial(hv)}{\partial \xi}-\dfrac{\partial(hw)}{\partial \eta}\right] \end{array}\right]$$

**Gradient of Scalar**

According to reference [69], the gradient of a scalar quantity in general curvilinear coordinate system can be written as;

$$(\nabla P)_i = \frac{1}{h_i}\frac{\partial P}{\partial U_i}$$

**Material derivative**

According to the same reference [69], the material derivative for a vector can be written as;

$$\frac{DV_1}{Dt}=\frac{\partial V_1}{\partial t}+\frac{V_1}{X_1}\frac{\partial V_1}{\partial X_1}+\frac{V_2}{X_2}\frac{\partial V_1}{\partial X_2}+\frac{V_3}{X_3}\frac{\partial V_1}{\partial X_3}$$
$$-V_2\left(\frac{V_2}{h_2 h_1}\frac{\partial h_2}{\partial X_1}-\frac{V_1}{h_1 h_2}\frac{\partial h_1}{\partial X_2}\right)+V_3\left(\frac{V_1}{h_1 h_3}\frac{\partial h_1}{\partial X_3}-\frac{V_3}{h_3 h_1}\frac{\partial h_3}{\partial X_1}\right)$$

In bi-polar Coordinates;

$h_1=h_2=h$ *and* $h_3=1.$

$X_1=\xi,\quad X_2=\eta,\quad X_3=Z$

So that the last term in the R.H.S. will be zero.

Remembering that;

$V_1=w,\ V_2=v,\ V_3=u$

Now writing the material derivative of the velocity in bipolar coordinates in ξ-direction for steady state;

$$\frac{Dw}{Dt}=\frac{w}{h}\frac{\partial w}{\partial \xi}+\frac{v}{h}\frac{\partial w}{\partial \eta}+u\frac{\partial w}{\partial Z}-\frac{v^2}{h^2}\frac{\partial h}{\partial \xi}+\frac{vw}{h^2}\frac{\partial h}{\partial \eta}$$

Combining the second and the last term in the R.H.S., one can write;

$$\frac{Dw}{Dt}=\frac{w}{h}\frac{\partial w}{\partial \xi}+\frac{v}{h^2}\frac{\partial (hw)}{\partial \eta}+u\frac{\partial w}{\partial Z}-\frac{v^2}{h^2}\frac{\partial h}{\partial \xi}$$

Now one can write the Navier Stokes equations for incompressible flow with constant properties except for the density in the body force term in bipolar coordinate as;

**1 - in ξ- direction**

$$\rho\left(\frac{w}{h}\frac{\partial w}{\partial \xi}+\frac{v}{h^2}\frac{\partial w}{\partial \eta}+u\frac{\partial w}{\partial Z}-\frac{v^2}{h^2}\frac{\partial h}{\partial \xi}\right)=F_\xi-\frac{1}{h}\frac{\partial P}{\partial \xi}+\frac{\mu}{h}\left\{\begin{array}{l}\frac{\partial^2}{\partial Z^2}(hw)+\frac{1}{h^2}\frac{\partial^2(hw)}{\partial \eta^2}+\frac{1}{h^2}\frac{\partial^2(hw)}{\partial \xi^2}\\ +\frac{2}{h^3}\left(\frac{\partial(hv)}{\partial \xi}-\frac{\partial(hw)}{\partial \eta}\right)\frac{\partial h}{\partial \eta}+\frac{2}{h^2}\frac{\partial h}{\partial \xi}\frac{\partial(hu)}{\partial Z}\end{array}\right\}$$

Now one can follow the same analysis to write the Navier Stokes equations in the other two direction;

**2. In η- direction**

$$\rho\left(\frac{w}{h^2}\frac{\partial(hv)}{\partial\xi}+\frac{v}{h}\frac{\partial v}{\partial\eta}+u\frac{\partial v}{\partial Z}-\frac{w^2}{h^2}\frac{\partial h}{\partial\eta}\right)=F_\eta-\frac{1}{h}\frac{\partial P}{\partial\eta}+\frac{\mu}{h}\left\{\begin{array}{l}\frac{\partial^2}{\partial Z^2}(hv)+\frac{1}{h^2}\frac{\partial^2(hv)}{\partial\eta^2}+\frac{1}{h^2}\frac{\partial^2(hv)}{\partial\xi^2}\\ -\frac{2}{h^3}\left(\frac{\partial(hv)}{\partial\xi}-\frac{\partial(hw)}{\partial\eta}\right)\frac{\partial h}{\partial\xi}+\frac{2}{h^2}\frac{\partial h}{\partial\eta}\frac{\partial(hu)}{\partial Z}\end{array}\right\}$$

**3. In Z - direction**

$$\rho\left(\frac{w}{h}\frac{\partial u}{\partial\xi}+\frac{v}{h}\frac{\partial u}{\partial\eta}+u\frac{\partial u}{\partial Z}\right)=F_z-\frac{\partial P}{\partial Z}+\frac{\mu}{h}\left[\frac{\partial^2 u}{\partial\xi^2}+\frac{\partial^2 u}{\partial\eta^2}+h^2\frac{\partial^2 u}{\partial Z^2}\right]$$

**The Steady State Energy Equation in Bipolar Coordinates :**

$$\left(\frac{w}{h}\frac{\partial T}{\partial\xi}+\frac{v}{h}\frac{\partial T}{\partial\eta}+u\frac{\partial T}{\partial Z}\right)=\frac{\alpha}{h^2}\left[\frac{\partial^2 T}{\partial\xi^2}+\frac{\partial^2 T}{\partial\eta^2}+h^2\frac{\partial^2 T}{\partial Z^2}\right]+Q'''+\Phi$$

where;

$Q'''$ is the heat generation per unit mass, and $\Phi$ is the energy dissipated due to viscous effects.

The above equations are the governing equations along with

**The Continuity Equation**

$$\frac{\partial hw}{\partial\xi}+\frac{\partial hv}{\partial\eta}+\frac{\partial h^2u}{\partial Z}=0$$

# Appendix D

# ORDER OF MAGNITUDE ANALYSIS

Knowledge of the relative magnitude of the individual terms of the governing equations will enable us to judge the relative importance of each term. The values of the terms vary throughout the entrance region and cannot be known on a local basis unless the solution of the equations is known. We can, however, determine in a global sense relative magnitudes of the terms such that the values thus obtained represent averages taken over the entire entrance region. If we assume that the global magnitude of a term is a measure of its impact on the solution, then we can asses the degree of approximation in dropping that term.

The order of magnitude of a quantity, f, will be designated by $o(f)$. The order of magnitude of a first derivative is the order of magnitude of the ratio of the change of the quantity in the numerator to that of the quantity of the denominator. Hence,

$$o\left(\frac{\partial f}{\partial s}\right)=o\left(\frac{\Delta f}{\Delta s}\right)$$

where, $\Delta f$ and $\Delta s$ are the changes in $f$ and $s$, respectively. similarly,

$$o\left(\frac{\partial^2 f}{\partial s^2}\right)=o\left(\frac{\Delta f}{(\Delta s)^2}\right)$$

Before proceeding in carrying out our order of magnitude analysis, we want to introduce some definitions and comments on some variables that will be involved in the governing equations.

$l$ : is the developing length which is larger than any other length in the geometry under study.

$b$ : is the difference between the outer and inner radii, i.e., $b = r_o - r_i$

$\delta$ : is the boundary layer thickness and its value is much less than $l$. Its maximum value can be equal to $b$. Its dimensionless form is $\delta^* = \delta / l$

$h\Delta\eta$ : is a small segment in an arc length along a curve of constant $\xi$. The global magnitude of $h\Delta\eta$ can be generally approximated by $b$. In order to prevent loss of generality we will consider any small dimensional length, compared to $l$, to be of the order $\delta$, i.e.,$b = o(\delta)$.Its dimensionless form is $H\Delta\eta = h\Delta\eta / l = o(\delta^*)$

$h\Delta\xi$ : is a small segment in an arc length along a curve of constant $\eta$. The global magnitude of $h\Delta\xi$, therefore is a length of a semicircular arc along a curve of constant $\eta$ between $\xi = 0$ and $\xi = \pi$. This length is generally greater than $b$. In order to prevent loss of generality we will consider it to be of the same order as $b$, i.e. of the same order as $\delta$. Its dimensionless form is $H\Delta\xi = h\Delta\xi / l = o(\delta^*)$

The first step in the traditional procedure for carrying out an order of magnitude analysis, is to put the governing equations into a dimensionless form, by referring all the variables to reference variables. For example; the reference length may be taken as the developing length, $l$, which much is larger than any other length in the geometry considered. Also the reference velocity may be considered as the uniform inlet velocity, $U_o$ . After putting all the variables in a dimensionless form, one substitute for the dimensional variables in terms of the nondimensional variables into the governing equations. Having the governing equations written in a dimensionless form, one can judge the order of magnitude of each term with respect to the other terms.

Now consider the continuity equation divided by $h^2$,

$$\frac{1}{h^2}\frac{\partial (hw)}{\partial \xi}+\frac{1}{h^2}\frac{\partial (hv)}{\partial \eta}+\frac{\partial u}{\partial z}=0$$

which can be written approximately as

$$\approx\frac{\Delta w}{h\Delta \xi}+\frac{\Delta v}{h\Delta \eta}+\frac{\Delta u}{\Delta z}=0$$

Now looking at the different terms of the continuity equations, we can conclude the following remarks. $o\,(\,\Delta u/\Delta z\,)$ can be represented by the magnitude of the overall, or global change in $u$ divided by the overall or global magnitude of $\Delta z$. This overall change in $u$ can be represented by $u$ itself, whose maximum value is $U_o$ . So that the global change in $u$, on dimensionless basis, is of order 1. Similarly $\Delta z$ can be represented by the global value of $z$ itself which is $l$. i,e., also on dimensionless basis, the global change in $z$ is of order 1. Also, $\Delta V$ and $\Delta W$ can be represented by $V$ and $W$

respectively. So putting the continuity equation in a dimensionless form, and writing the order of magnitude of each term underneath, we get the following form;

$$\frac{\Delta W}{H\Delta\xi}+\frac{\Delta V}{H\Delta\eta}+\frac{\Delta U}{\Delta Z}=0$$
$$\approx\frac{W}{H\Delta\xi}+\frac{V}{H\Delta\eta}+\frac{U}{Z}=0$$
$$o\left(\frac{?}{\delta^*}\right)\quad o\left(\frac{?}{\delta^*}\right)\quad o\left(\frac{1}{1}\right)$$

From the above equation, one can see that the last term is of order 1. So that to keep consistency in the continuity equation the other two terms should be of order 1 also. Hence, both $W$ and $V$ should be of order $\delta^*$. Based on these information we will treat the rest of the governing equations. Now consider the axial momentum equation.

**Z - ( Axial ) Momentum Equation**

$$\rho\left(\frac{w}{h}\frac{\partial u}{\partial\xi}+\frac{v}{h\partial\eta}\frac{\partial u}{\partial\eta}+u\frac{\partial u}{\partial z}\right)=F_z-\frac{\partial P}{\partial z}+\frac{\mu}{h^2}\left(h^2\frac{\partial^2 u}{\partial z^2}+\frac{\partial^2 u}{\partial\eta^2}+\frac{\partial^2 u}{\partial\xi^2}\right)$$

Putting in a dimensionless form and writing the order of magnitude, we will get.

$$W\frac{\Delta U}{H\Delta\xi}+V\frac{\Delta U}{H\Delta\eta}+U\frac{\Delta U}{\Delta Z}=-\frac{\Delta P}{\Delta Z}+\frac{Gr}{Re^2}\Delta\theta+\frac{1}{Re}\left(\frac{\Delta U}{(H\Delta\xi)^2}+\frac{\Delta U}{(H\Delta\eta)^2}+\frac{\Delta U}{(\Delta Z)^2}\right)$$

$$\delta^*\frac{1}{\delta^*}\qquad\delta^*\frac{1}{\delta^*}\quad 1\frac{1}{1}\qquad\frac{?}{1}\qquad\frac{?}{?}\;1\qquad\frac{1}{?}\left(\frac{1}{(\delta^*)^2}\qquad\frac{1}{(\delta^*)^2}\quad\frac{1}{1}\right)$$

Looking at the above equation, we can see that the L.H.S. is of order 1, so that the R.H.S. should be of order 1 also. This gives us a tool to asses the order of the values

in the places of the question mark. For example from the first term in the R.H.S., we can see that $\Delta P$ should be of order 1, while the second term shows us that *Gr* number should be of the same order as that of $Re^2$. The first two terms between the bracket are of a very large magnitude since it is the inverse of a very small value, $\delta^*$. So that to have them within the order of 1, the order of magnitude of *Re* number ( the question mark outside the bracket), should be of order $1 / (\delta^*)^2$ . Knowing this information we can proceed to the other two transverse momentum equations with the body forces in the transverse directions omitted since we are treating the flow in a vertical annulus.

**ξ - Momentum Equation**

$$\rho\left(\frac{w}{h}\frac{\partial w}{\partial \xi}+\frac{v}{h^2}\frac{\partial hw}{\partial \eta}+u\frac{\partial w}{\partial z}-\frac{v^2}{h^2}\frac{\partial h}{\partial \xi}\right)$$

$$=-\frac{1}{h}\frac{\partial p}{\partial \xi}+\frac{\mu}{h}\left(\begin{array}{l}\dfrac{\partial^2(hw)}{\partial z^2}+\dfrac{1}{h^2}\dfrac{\partial^2(hw)}{\partial \eta^2}+\dfrac{1}{h^2}\dfrac{\partial^2(hw)}{\partial \xi^2} \\ +\dfrac{2}{h^3}\left(\dfrac{\partial(hv)}{\partial \xi}-\dfrac{\partial(hw)}{\partial \eta}\right)\dfrac{\partial h}{\partial \eta}+\dfrac{2}{h^2}\dfrac{\partial h}{\partial \xi}\dfrac{\partial hu}{\partial z}\end{array}\right)$$

Putting in a dimensionless form and writing the order of magnitude, we will get

$$W\frac{\Delta W}{H\Delta\xi}+V\frac{\Delta W}{H\Delta\eta}+U\frac{\Delta W}{\Delta Z}-\frac{V^2}{H\Delta\xi}=-\frac{\Delta P}{H\Delta\xi}+\frac{1}{Re}\left(\frac{\Delta W}{(\Delta Z)^2}+\frac{\Delta W}{(H\Delta\eta)^2}+\frac{\Delta W}{(H\Delta\xi)^2}\right)$$

$$\delta^*\frac{\delta^*}{\delta^*}\quad\delta^*\frac{\delta^*}{\delta^*}\quad 1\frac{\delta^*}{1}\quad\frac{(\delta^*)^2}{\delta^*}\quad\frac{1}{\delta^*}\quad\frac{1}{\frac{1}{(\delta^*)^2}}\left(\frac{\delta^*}{1}\quad\frac{\delta^*}{(\delta^*)^2}\quad\frac{\delta^*}{(\delta^*)^2}\right)$$

$$\delta^*\quad\delta^*\quad\delta^*\quad\delta^*\quad\frac{1}{\delta^*}\quad(\delta^*)^3\quad\delta^*\quad\delta^*$$

$$+\frac{1}{Re}\left(\left(\frac{\Delta V}{H\Delta\xi}-\frac{\Delta W}{H\Delta\eta}\right)\frac{1}{H\Delta\eta}+\frac{1}{H\Delta\xi}\frac{\Delta U}{\Delta Z}\right)$$

$$\frac{1}{\frac{1}{(\delta^*)^2}}\left(\left(\frac{\delta^*}{\delta^*}\quad\frac{\delta^*}{\delta^*}\right)\frac{1}{\delta^*}\quad\frac{1}{\delta^*}\quad\frac{1}{1}\right)$$

$$(\delta^*)^2\left(\frac{1}{\delta^*}\quad\frac{1}{\delta^*}\quad\frac{1}{\delta^*}\right)$$

$$\delta^*\quad\delta^*\quad\delta^*$$

**η - Momentum Equation**

$$\rho\left(\frac{w}{h^2}\frac{\partial hv}{\partial\xi}+\frac{v}{h}\frac{\partial v}{\partial\eta}+u\frac{\partial v}{\partial z}-\frac{w^2}{h^2}\frac{\partial h}{\partial\eta}\right)$$

$$=-\frac{1}{h}\frac{\partial p}{\partial\eta}+\frac{\mu}{h}\left(\begin{array}{l}\dfrac{\partial^2(hv)}{\partial z^2}+\dfrac{1}{h^2}\dfrac{\partial^2(hv)}{\partial\eta^2}+\dfrac{1}{h^2}\dfrac{\partial^2(hv)}{\partial\xi^2}\\ -\dfrac{2}{h^3}\left(\dfrac{\partial(hv)}{\partial\xi}-\dfrac{\partial(hw)}{\partial\eta}\right)\dfrac{\partial h}{\partial\xi}+\dfrac{2}{h^2}\dfrac{\partial h}{\partial\eta}\dfrac{\partial hu}{\partial z}\end{array}\right)$$

Putting in a dimensionless form and writing the order of magnitude, we will get

$$W\frac{\Delta V}{H\Delta\xi}+V\frac{\Delta V}{H\Delta\eta}+U\frac{\Delta V}{\Delta Z}-\frac{W^2}{H\Delta\eta}=-\frac{\Delta P}{H\Delta\eta}+\frac{1}{\mathrm{Re}}\left(\frac{\Delta V}{(\Delta Z)^2}+\frac{\Delta V}{(H\Delta\eta)^2}+\frac{\Delta V}{(H\Delta\xi)^2}\right)$$

$$\delta^*\frac{\delta^*}{\delta^*}\quad\delta^*\frac{\delta^*}{\delta^*}\quad 1\frac{\delta^*}{1}\quad\frac{(\delta^*)^2}{\delta^*}\quad\frac{1}{\delta^*}\quad\frac{1}{\frac{1}{(\delta^*)^2}}\left(\frac{\delta^*}{1}\quad\frac{\delta^*}{(\delta^*)^2}\quad\frac{\delta^*}{(\delta^*)^2}\right)$$

$$\delta^*\quad\delta^*\quad\delta^*\quad\delta^*\quad\frac{1}{\delta^*}\quad(\delta^*)^3\quad\delta^*\quad\delta^*$$

$$+\frac{1}{\mathrm{Re}}\left(-\left(\frac{\Delta V}{H\Delta\xi}-\frac{\Delta W}{H\Delta\eta}\right)\frac{1}{H\Delta\xi}+\frac{1}{H\Delta\eta}\frac{\Delta U}{\Delta Z}\right)$$

$$\frac{1}{\frac{1}{(\delta^*)^2}}\left(\left(\frac{\delta^*}{\delta^*}\quad\frac{\delta^*}{\delta^*}\right)\frac{1}{\delta^*}\quad\frac{1}{\delta^*}\quad\frac{1}{1}\right)$$

$$(\delta^*)^2\left(\frac{1}{\delta^*}\quad\frac{1}{\delta^*}\quad\frac{1}{\delta^*}\right)$$

$$\delta^*\quad\delta^*\quad\delta^*$$

**Energy Equation**

$$\rho\,C_p\left(\frac{w}{h}\frac{\partial T}{\partial\xi}+\frac{v}{h}\frac{\partial T}{\partial\eta}+u\frac{\partial T}{\partial z}\right)=\frac{K}{h^2}\left(h^2\frac{\partial^2 T}{\partial z^2}+\frac{\partial^2 T}{\partial\eta^2}+\frac{\partial^2 T}{\partial\xi^2}\right)$$

Knowing that the change in the temperature on a dimensionless basis is of order 1, and substituting for the other variables in terms of their dimensionless forms with the

knowledge of their order of magnitude, we can write the energy equation in a dimensionless form along with the order of magnitude as follows

$$W\frac{\Delta\theta}{H\Delta\xi}+V\frac{\Delta\theta}{H\Delta\eta}+U\frac{\Delta\theta}{\Delta Z}=\frac{1}{Re.Pr}\left(\frac{\Delta\theta}{(\Delta Z)^2}+\frac{\Delta\theta}{(H\Delta\xi)^2}+\frac{\Delta\theta}{(H\Delta\eta)^2}\right)$$

$$\delta^*\frac{1}{\delta^*}\quad\delta^*\frac{1}{\delta^*}\quad 1\,\frac{1}{1}\quad\frac{1}{\frac{1}{(\delta^*)^2}.1}\left(\frac{1}{1}\quad\frac{1}{(\delta^*)^2}\quad\frac{1}{(\delta^*)^2}\right)$$

$$1\qquad 1\qquad 1\qquad (\delta^*)^2\qquad 1\qquad 1$$

Notice that we take $Pr$ = o( 1 ) .

Using the dimensionless groups mentioned in the nomenclature one can write the governing equations after carrying out the order of magnitude analysis as;

**1 - ξ- Momentum Equation**

$$\frac{W}{H}\frac{\partial W}{\partial\xi}+\frac{V}{H^2}\frac{\partial HW}{\partial\eta}+4(1-N)^2U\frac{\partial W}{\partial Z}-\frac{V^2}{H^2}\frac{\partial H}{\partial\xi}=-\frac{Gr^2}{H}\frac{\partial P}{\partial\xi}+\frac{1}{H^3}\left(\frac{\partial^2 HW}{\partial\eta^2}+\frac{\partial^2 HW}{\partial\xi^2}\right)$$
$$-\frac{2}{H^4}\left(\frac{\partial HW}{\partial\eta}-\frac{\partial HV}{\partial\xi}\right)\frac{\partial H}{\partial\eta}+\frac{8(1-N)^2}{H^2}\frac{\partial H}{\partial\xi}\frac{\partial U}{\partial Z}$$

**2 - η- Momentum Equation**

$$\frac{W}{H^2}\frac{\partial HV}{\partial\xi}+\frac{V}{H}\frac{\partial V}{\partial\eta}+4(1-N)^2U\frac{\partial V}{\partial Z}-\frac{W^2}{H^2}\frac{\partial H}{\partial\eta}=-\frac{Gr^2}{H}\frac{\partial P}{\partial\eta}+\frac{1}{H^3}\left(\frac{\partial^2 HV}{\partial\eta^2}+\frac{\partial^2 HV}{\partial\xi^2}\right)$$
$$+\frac{2}{H^4}\left(\frac{\partial HW}{\partial\eta}-\frac{\partial HV}{\partial\xi}\right)\frac{\partial H}{\partial\xi}+\frac{8(1-N)^2}{H^2}\frac{\partial H}{\partial\eta}\frac{\partial U}{\partial Z}$$

**3 - Z- Momentum Equation**

$$\frac{W}{H}\frac{\partial U}{\partial\xi}+\frac{V}{H}\frac{\partial U}{\partial\eta}+U\frac{\partial U}{\partial Z}=-\frac{1}{4(1-N)^2}\frac{\partial P}{\partial Z}+\frac{\theta}{4(1-N)^2}+\frac{1}{H^2}\left[\frac{\partial^2 U}{\partial\xi^2}+\frac{\partial^2 U}{\partial\eta^2}\right]$$

**4. Continuity Equation**

$$\frac{\partial HW}{\partial \xi}+\frac{\partial HV}{\partial \eta}+4(1-N)^2\frac{\partial H^2U}{\partial Z}=0$$

**5. Energy Equation**

$$\frac{W}{H}\frac{\partial \theta}{\partial \xi}+\frac{V}{H}\frac{\partial \theta}{\partial \eta}+4(1-N)^2U\frac{\partial \theta}{\partial Z}=\frac{1}{\mathrm{Pr}.H^2}\left(\frac{\partial^2\theta}{\partial \xi^2}+\frac{\partial^2\theta}{\partial \eta^2}\right)$$

# Appendix E

# EXPANSION OF $\dfrac{Cosh(\eta)}{Cosh(\eta)-Cos(\xi)}$

## Procedure

Find Fourier expansion of $\dfrac{1}{Cosh(\eta)-Cos(\xi)}$ in terms of Cos ($\xi$)

**Notes :**

1 - This is an even function, so that it is suitable to find the Fourier -cosine expansion.

$$\frac{1}{Cosh(\eta)-Cos(\xi)}=\frac{a_o}{2}+\sum_{n=1}^{\infty}a_n\,Cos(n\xi)$$

where;

$$a_n=\frac{1}{\pi}\int_{-\pi}^{\pi}\frac{Cos(n\xi)}{Cosh(\eta)-Cos(\xi)}d\xi$$

and

$$a_o=\frac{1}{\pi}\int_{-\pi}^{\pi}\frac{1}{Cosh(\eta)-Cos(\xi)}d\xi$$

Hint; $a_o$ can be evaluated from the general expression an by putting n = 0

## Evaluation of $a_n$

Knowing that ; $\int_{-\pi}^{\pi} \frac{\mathrm{Sin}(n\xi)}{\mathrm{Cosh}(\eta)-\mathrm{Cos}(\xi)} d\xi = 0$, one can write ;

$$a_n = \frac{1}{\pi} \int_{-\pi}^{\pi} \frac{\mathrm{Cos}(n\xi)+i\mathrm{Sin}(n\xi)}{\mathrm{Cosh}(\eta)-\mathrm{Cos}(\xi)} d\xi$$

Now, putting, $Cos(n\xi)+iSin(n\xi)=e^{in\xi}$, so that

$$a_n = \frac{1}{\pi} \int_{-\pi}^{\pi} \frac{e^{in\xi}}{\mathrm{Cosh}(\eta)-\mathrm{Cos}(\xi)} d\xi$$

$$= \frac{1}{\pi} \int_{-\pi}^{\pi} \frac{\left(e^{i\xi}\right)^n}{\mathrm{Cosh}(\eta)-\mathrm{Cos}(\xi)} d\xi$$

This integration can be easily evaluated by changing the variable $e^{i\xi}$ *to* $Z$ and using contour integration.

### Changing the variables;

$Z = e^{i\xi}$, $\therefore dZ = ie^{i\xi} d\xi = iZ d\xi$

$$\therefore d\xi = \frac{dZ}{iZ}$$

*and* ; $Cos(\xi) = \frac{e^{i\xi}+e^{-i\xi}}{2} = \frac{Z+Z^{-1}}{2}$

*also putting*, $Cosh(\eta) = \frac{e^{\eta}+e^{-\eta}}{2}$

Now one can write;

$$a_n = \frac{1}{\pi}\int_{-\pi}^{\pi}\frac{\left(e^{i\xi}\right)^n}{\mathrm{Cosh}(\eta)-\mathrm{Cos}(\xi)}d\xi=\frac{1}{\pi}\int_{-\pi}^{\pi}\frac{Z^n}{\frac{e^{\eta}+e^{-\eta}}{2}+\frac{Z+Z^{-1}}{2}}\frac{dZ}{iZ}$$

$$=\frac{1}{\pi}\frac{1}{i}\int_{-\pi}^{\pi}\frac{Z^n}{\frac{1}{2}\left(e^{\eta}+e^{-\eta}-Z-Z^{-1}\right)Z}dZ=\frac{1}{\pi}\frac{2}{i}\int_{-\pi}^{\pi}\frac{Z^n}{\left(-Z^2+Z\left(e^{\eta}+e^{-\eta}\right)-1\right)}dZ$$

$$=-\frac{1}{\pi}\frac{2}{i}\int_{-\pi}^{\pi}\frac{Z^n}{\left(Z^2-Z\left(e^{\eta}+e^{-\eta}\right)+1\right)}dZ$$

Factoring the dominator, one can write;

$$Z^2-\left(e^{\eta}+e^{-\eta}\right)Z+1=(Z-Z_1)(Z-Z_2)$$

*where;*

$$Z_{1.2}=\frac{e^{\eta}+e^{-\eta}\pm\sqrt{e^{2\eta}+2e^{\eta}e^{-\eta}+e^{-2\eta}-4}}{2}$$

$$=\frac{e^{\eta}+e^{-\eta}\pm\sqrt{e^{2\eta}+2e^{\eta}e^{-\eta}+e^{-2\eta}-4e^{\eta}e^{-\eta}}}{2}$$

$$=\frac{e^{\eta}+e^{-\eta}\pm\sqrt{e^{2\eta}-2e^{\eta}e^{-\eta}+e^{-2\eta}}}{2}=\frac{e^{\eta}+e^{-\eta}\pm\sqrt{\left(e^{\eta}-e^{-\eta}\right)^2}}{2}=\frac{e^{\eta}+e^{-\eta}\pm\left(e^{\eta}-e^{-\eta}\right)}{2}$$

*Hence;*

$Z_1=e^{\eta}$, *and* $Z_2=e^{-\eta}$

*So that one can write;*

$$Z^2-\left(e^{\eta}+e^{-\eta}\right)Z+1=\left(Z-e^{\eta}\right)\left(Z-e^{-\eta}\right)$$

*and this leads to;*

$$-\frac{2}{i}\int_{-\pi}^{\pi}\frac{Z^n}{\left(Z-e^{\eta}\right)\left(Z-e^{-\eta}\right)}dZ=-\frac{2}{i}\oint_C\frac{Z^n}{\left(Z-e^{\eta}\right)\left(Z-e^{-\eta}\right)}dZ$$

where the contour C is a circle of unit radius about the origin. The integrand has one simple pole at ( $Z=e^{-\eta}$), since $\eta$ is assumed to be positive and real, see the definition of $\eta$. Using Cauchy theorem of contour integration, one can write;

$$\oint_c \frac{f(Z)}{Z-b} dZ = 2\pi i f(b)$$

*Letting* $f(Z) = \frac{Z^n}{(Z-e^{\eta})}$ *, and* $b = e^{-\eta}$*, one can write;*

$$\oint_c \frac{Z^n}{(Z-e^{\eta})(Z-e^{-\eta})} dZ = 2\pi i \left( \frac{(e^{-\eta})^n}{e^{-\eta} - e^{\eta}} \right) (-1)$$

So that;

$$a_n = \frac{1}{\pi}\left(-\frac{2}{i}\right) 2\pi i \frac{\left(e^{-\eta}\right)^n}{e^{\eta} - e^{-\eta}} (-1) = 2 \frac{\left(e^{-\eta}\right)^n}{\frac{e^{\eta} - e^{-\eta}}{2}}$$

$$a_n = 2 \frac{\left(e^{-\eta}\right)^n}{\mathrm{Sinh}(\eta)}$$

putting n=0, gives;

$$a_o = 2 \frac{1}{\mathrm{Sinh}(\eta)}$$

So that one can write;

$$\frac{1}{Cosh(\eta) - Cos(\xi)} = \frac{a_o}{2} + \sum_{n=1}^{\infty} a_n Cos(n\xi) = \frac{1}{Sinh(\eta)} + \frac{2}{Sinh(\eta)} \sum_{n=1}^{\infty} e^{-n\eta} Cos(n\xi)$$

*Hence;*

$$\frac{Cosh(\eta)}{Cosh(\eta) - Cos(\xi)} = Cosh(\eta) \left( \frac{1}{Sinh(\eta)} + \frac{2}{Sinh(\eta)} \sum_{n=1}^{\infty} e^{-n\eta} Cos(n\xi) \right)$$

$$\frac{Cosh(\eta)}{Cosh(\eta) - Cos(\xi)} = Coth(\eta) \left( 1 + 2 \sum_{n=1}^{\infty} e^{-n\eta} Cos(n\xi) \right)$$

# Appendix F

# FLOW AND HEAT TRANSFER PARAMATERS FOR DEVELOPING FREE CONVECTION

The flow and heat transfer parameters for all the cases investigated for the developing free convection in vertical open-ended eccentric annuli are summarised in the following set of tables.

Table F.1 Flow and heat transfer parameters, for Case 1.I, E = 0.1

| $U_0 \times 10^3$ | Induced Flow Rate $F \times 10^4$ | Channel Height $L \times 10^5$ | Heat absorbed $Q \times 10^4$ | $\overline{Nu}_{i,e}^{1.I}$ | $\overline{Nu}_{o,e}^{1.I}$ | $\overline{\overline{Nu}}_{i,e}^{1.I}$ | $\overline{\overline{Nu}}_{o,e}^{1.I}$ |
|---|---|---|---|---|---|---|---|
| 1.0 | 7.50 | 2.5 | 3.00 | 10.99 | 0.78365 | 10.99 | 0.843 |
| 1.5 | 11.25 | 4.5 | 4.20 | 8.77 | 1.22209 | 9.242 | 1.266 |
| 2.0 | 15.00 | 6.5 | 5.60 | 8.030 | 1.61044 | 8.606 | 1.654 |
| 2.5 | 18.75 | 9.5 | 7.35 | 7.6612 | 2.04075 | 8.133 | 2.176 |
| 3.0 | 22.50 | 13.5 | 9.15 | 7.08686 | 2.3587 | 7.697 | 2.697 |
| 3.5 | 26.25 | 17.5 | 10.80 | 6.44226 | 2.52587 | 7.342 | 3.042 |
| 4.0 | 30.00 | 24.0 | 12.60 | 6.12708 | 2.64127 | 7.098 | 3.291 |
| 4.5 | 33.75 | 26.0 | 13.20 | 6.08258 | 2.61429 | 7.013 | 3.121 |
| 5.0 | 37.5 | 36.0 | 15.20 | 5.95278 | 2.72283 | 6.749 | 3.753 |
| 5.5 | 41.25 | 47.0 | 16.80 | 5.81633 | 2.83603 | 6.538 | 4.124 |
| 6.0 | 45.00 | 65.0 | 19.00 | 5.62494 | 2.98279 | 6.265 | 4.639 |
| 6.5 | 48.75 | 86.0 | 20.70 | 5.50247 | 3.06605 | 6.091 | 4.498 |
| 7.0 | 52.50 | 116.0 | 22.50 | 5.40027 | 3.13310 | 5.916 | 5.262 |
| 7.5 | 56.25 | 165.0 | 24.10 | 5.32957 | 3.18013 | 5.739 | 5.576 |
| 8.0 | 60.00 | 260 | 25.50 | 5.39579 | 3.20440 | 5.617 | 5.573 |
| 8.5 | 63.75 | 460 | 27.00 | 5.27128 | 3.2264 | 5.449 | 6.101 |

Table F.2 Flow and heat transfer parameters, for Case 1.O, E = 0.1

| $U_o \times 10^3$ | Induced Flow Rate $F \times 10^4$ | Channel Height $L \times 10^5$ | Heat absorbed $Q \times 10^4$ | $\overline{Nu}_{i,e}^{1.O}$ | $\overline{Nu}_{o,e}^{1.O}$ | $\overline{\overline{Nu}}_{i,e}^{1.O}$ | $\overline{\overline{Nu}}_{o,e}^{1.O}$ |
|---|---|---|---|---|---|---|---|
| 1.0 | 7.50 | 1.22 | 2.74 | 0.689 | 9.639 | 0.415 | 10.1856 |
| 2.0 | 15.00 | 3.90 | 6.03 | 1.347 | 7.252 | 0.649 | 8.3314 |
| 3.0 | 22.50 | 8.00 | 10.00 | 2.447 | 6.066 | 1.196 | 7.2596 |
| 4.0 | 30.00 | 12.60 | 14.70 | 3.156 | 5.371 | 1.644 | 6.6025 |
| 5.0 | 37.5 | 19.60 | 19.45 | 3.684 | 4.885 | 2.077 | 6.0894 |
| 6.0 | 45.00 | 28.00 | 23.00 | 3.791 | 4.583 | 2.601 | 5.6024 |
| 7.0 | 52.50 | 45.00 | 28.50 | 4.089 | 4.299 | 2.959 | 5.1509 |
| 8.0 | 60.00 | 65.00 | 33.50 | 4.322 | 4.125 | 3.219 | 4.9046 |
| 9.0 | 67.50 | 93.00 | 38.70 | 4.507 | 3.976 | 3.506 | 4.6669 |
| 10.0 | 75.00 | 142.0 | 43.60 | 4.619 | 3.875 | 3.810 | 4.4319 |
| 12.0 | 90.00 | 450.0 | 52.40 | 4.685 | 3.801 | 4.398 | 3.99647 |

Table F.3 Flow and heat transfer parameters,for Case 1.I, E = 0.5

| $U_o \times 10^3$ | Induced Flow Rate $F \times 10^4$ | Channel Height $L \times 10^5$ | Heat absorbed $Q \times 10^4$ | $\overline{Nu}^{1.I}_{i.e}$ | $\overline{Nu}^{1.I}_{o.e}$ | $\frac{\overline{Nu}^{1.I}_{i.e}}{\overline{Nu}^{1.I}_{i.e}}$ | $\frac{\overline{Nu}^{1.I}_{o.e}}{\overline{Nu}^{1.I}_{o.e}}$ |
|---|---|---|---|---|---|---|---|
| 4.0 | 30.00 | 28.50 | 12.00 | 6.982 | 3.575 | 7.2118 | 6.1057 |
| 5.0 | 37.5 | 43.60 | 14.60 | 6.240 | 3.563 | 6.3856 | 6.4766 |
| 6.0 | 45.00 | 67.50 | 17.90 | 6.107 | 3.622 | 6.4294 | 6.6874 |
| 7.0 | 52.50 | 102.0 | 21.40 | 6.045 | 3.669 | 6.2664 | 6.9245 |
| 8.0 | 60.00 | 158.0 | 24.70 | 5.955 | 3.739 | 6.1488 | 7.1117 |
| 9.0 | 67.50 | 265.0 | 27.60 | 5.889 | 3.795 | 6.0054 | 7.3658 |
| 10.0 | 75.00 | 501.0 | 30.30 | 5.835 | 3.8412 | 5.9203 | 7.5175 |

Table F.4 Flow and heat transfer parameters, for Case 1.O, E = 0.5

| $U_o \times 10^3$ | Induced Flow Rate $F \times 10^4$ | Channel Height $L \times 10^5$ | Heat absorbed $Q \times 10^4$ | $\overline{\overline{Nu}}^{1.O}_{i,e}$ | $\overline{\overline{Nu}}^{1.O}_{o,e}$ | $\overline{\overline{Nu}}^{1.O}_{i,c}$ | $\overline{\overline{Nu}}^{1.O}_{o,c}$ |
|---|---|---|---|---|---|---|---|
| 1.0 | 7.50 | 1.32 | 02.65 | 1.483 | 9.589 | 1.3105 | 9.9885 |
| 2.0 | 15.00 | 4.14 | 06.09 | 3.145 | 7.179 | 2.4956 | 7.9652 |
| 3.0 | 22.5 | 8.62 | 09.88 | 4.218 | 6.047 | 3.3821 | 7.0147 |
| 4.0 | 30.00 | 14.80 | 14.30 | 4.864 | 5.396 | 4.0995 | 6.3477 |
| 5.0 | 37.50 | 23.50 | 18.50 | 4.951 | 5.005 | 4.6828 | 5.6497 |
| 6.0 | 45.00 | 35.10 | 22.50 | 5.083 | 4.804 | 4.9155 | 5.3935 |
| 7.0 | 52.50 | 51.20 | 27.50 | 5.164 | 4.682 | 5.1028 | 5.1320 |
| 8.0 | 60.00 | 72.50 | 32.50 | 5.212 | 4.609 | 5.2293 | 4.9724 |
| 9.0 | 67.50 | 100.0 | 37.70 | 5.241 | 4.562 | 5.3209 | 4.8637 |
| 10.0 | 75.00 | 137.0 | 43.00 | 5.213 | 4.799 | 5.3666 | 4.7537 |
| 11.0 | 82.50 | 184.0 | 48.30 | 5.187 | 4.605 | 5.3848 | 4.6832 |
| 12.0 | 90.00 | 242.0 | 53.10 | 5.155 | 4.626 | 5.3352 | 4.6366 |
| 13.0 | 97.50 | 335.0 | 57.10 | 5.162 | 4.612 | 5.3314 | 4.6042 |
| 14.0 | 105.0 | 472.0 | 62.50 | 5.169 | 4.604 | 5.333 | 4.5781 |
| 15.0 | 112.5 | 691.0 | 67.40 | 5.168 | 4.595 | 5.3138 | 4.5649 |
| 16.0 | 120.0 | 1090 | 72.20 | 5.168 | 4.618 | 5.2817 | 4.5649 |
| 17.0 | 127.5 | 2050 | 76.60 | 5.177 | 4.610 | 5.2446 | 4.5729 |

Table F.5 Flow and heat transfer parameters, for Case 1.I, E = 0.7

| $U_o \times 10^3$ | Induced Flow Rate $F \times 10^4$ | Channel Height $L \times 10^5$ | Heat absorbed $Q \times 10^4$ | $\overline{Nu}_{i,e}^{1.I}$ | $\overline{Nu}_{o,e}^{1.I}$ | $\overline{\overline{Nu}}_{i,e}^{1.I}$ | $\overline{\overline{Nu}}_{o,e}^{1.I}$ |
|---|---|---|---|---|---|---|---|
| 3.0 | 22.50 | 16.10 | 11.20 | 12.5128 | 3.5115 | 8.8998 | 8.8539 |
| 3.5 | 26.25 | 24.10 | 11.40 | 9.0083 | 4.0521 | 8.3325 | 8.7525 |
| 4.0 | 30.00 | 32.10 | 12.80 | 8.0924 | 4.2705 | 8.0583 | 8.9549 |
| 4.5 | 33.75 | 39.10 | 13.00 | 7.6251 | 4.5291 | 7.7036 | 9.2178 |
| 5.0 | 37.5 | 46.00 | 14.10 | 7.2976 | 4.5904 | 7.4679 | 9.3468 |
| 5.5 | 41.25 | 56.00 | 15.40 | 7.1426 | 4.6259 | 7.3131 | 9.4532 |
| 6.0 | 45.00 | 68.00 | 16.90 | 7.0683 | 4.6493 | 7.2094 | 9.5392 |
| 6.5 | 48.75 | 82.50 | 18.60 | 7.0908 | 4.6023 | 7.1307 | 9.5670 |
| 7.0 | 52.50 | 98.00 | 20.10 | 7.0450 | 4.6391 | 7.0763 | 9.6364 |
| 7.5 | 56.25 | 118.0 | 21.90 | 7.0434 | 4.6369 | 7.0329 | 9.6631 |
| 8.0 | 60.00 | 141.0 | 23.50 | 7.0479 | 4.6302 | 6.9996 | 9.6679 |
| 8.5 | 63.75 | 169.0 | 25.16 | 7.0139 | 4.6597 | 6.9669 | 9.7081 |
| 9.0 | 67.50 | 203.0 | 26.70 | 7.0004 | 4.6716 | 6.9428 | 9.7116 |
| 9.5 |  | 241.0 | 28.10 | 6.9878 | 4.6870 | 6.9359 | 9.6488 |
| 10.0 | 75.00 | 291.0 | 29.40 | 6.9467 | 4.7252 | 6.9036 | 9.7220 |
| 12.0 | 90.00 | 840.0 | 34.90 | 6.8523 | 4.8118 | 6.8335 | 9.7501 |

Table F.6 Flow and heat transfer parameters, for Case 1.O, E = 0.7

| $U_o \times 10^3$ | Induced Flow Rate $F \times 10^4$ | Channel Height $L \times 10^5$ | Heat absorbed $Q \times 10^4$ | $\overline{Nu}_{i,e}^{1.O}$ | $\overline{Nu}_{o,e}^{1.O}$ | $\overline{\overline{Nu}}_{i,e}^{1.O}$ | $\overline{\overline{Nu}}_{o,e}^{1.O}$ |
|---|---|---|---|---|---|---|---|
| 1.0 | 7.50 | 1.42 | 02.68 | 4.0103 | 8.7063 | 4.7340 | 9.7267 |
| 1.5 | 11.25 | 2.82 | 04.00 | 5.2928 | 7.7787 | 6.1370 | 8.6333 |
| 2.0 | 15.00 | 4.72 | 05.90 | 5.7426 | 7.1708 | 6.9057 | 7.8961 |
| 3.0 | 22.50 | 9.83 | 09.88 | 6.2889 | 6.3870 | 7.8141 | 7.0051 |
| 4.0 | 30.00 | 16.60 | 13.95 | 6.4989 | 5.9598 | 8.1697 | 6.4591 |
| 5.0 | 37.5 | 24.50 | 17.80 | 6.2852 | 5.6173 | 8.6789 | 6.0663 |
| 6.0 | 45.00 | 34.50 | 21.50 | 6.4255 | 5.4414 | 8.0312 | 5.8402 |
| 7.0 | 52.50 | 49.10 | 26.20 | 6.5274 | 5.3262 | 8.1507 | 5.6773 |
| 8.0 | 60.00 | 67.20 | 31.10 | 6.4639 | 5.4397 | 8.007 | 5.5404 |
| 9.0 | 67.50 | 89.00 | 36.60 | 6.4317 | 5.3499 | 7.9445 | 5.4489 |
| 10.0 | 75.00 | 115.00 | 41.60 | 6.3446 | 5.4357 | 7.7845 | 5.3927 |
| 11.0 | 82.5 | 147.00 | 46.90 | 6.2969 | 5.4925 | 7.6925 | 5.3561 |
| 12.0 | 90.00 | 187.00 | 52.40 | 6.2368 | 5.5754 | 7.5603 | 5.3442 |
| 13.0 | 97.50 | 235.00 | 57.40 | 6.1111 | 5.6247 | 7.0894 | 5.3325 |
| 14.0 | 105.0 | 293.00 | 61.90 | 6.1624 | 5.5257 | 7.2106 | 5.3905 |
| 15.0 | 112.5 | 370.00 | 66.80 | 6.1365 | 5.5916 | 7.0440 | 5.4213 |
| 16.0 | 120.0 | 474.00 | 71.80 | 6.1237 | 5.6431 | 6.9417 | 5.4375 |
| 17.0 | 127.5 | 611.00 | 77.10 | 6.1178 | 5.6823 | 6.8791 | 5.4464 |
| 18.0 | 135.0 | 797.00 | 82.30 | 6.0975 | 5.7655 | 6.7437 | 5.4944 |
| 19.0 | 142.5 | 1060.0 | 87.35 | 6.0865 | 5.8209 | 6.6113 | 5.5511 |

Table F.7 Flow and heat transfer parameters, for Case 2.I, E = 0.1

| $U_0 \times 10^2$ | Induced Flow Rate $F \times 10^2$ | Channel Height $L \times 10^2$ | Heat absorbed $Q \times 10^3$ |
|---|---|---|---|
| 0.50 | 37.50 | 0.2123 | 1.43 |
| 1.00 | 75.00 | 1.868 | 4.57 |
| 1.50 | 112.5 | 4.665 | 11.98 |
| 2.00 | 150.0 | 7.495 | 22.81 |
| 2.50 | 187.5 | 10.367 | 36.90 |
| 3.00 | 225.0 | 13.308 | 54.20 |
| 3.50 | 262.5 | 16.341 | 74.40 |
| 4.00 | 300.0 | 19.479 | 98.40 |
| 4.50 | 337.5 | 22.737 | 125.20 |
| 5.00 | 375.0 | 26.121 | 155.17 |
| 6.00 | 450.0 | 33.298 | 224.60 |

Table F.8 Flow and heat transfer parameters, for Case 2.O, E = 0.1

| $U_0 \times 10^2$ | Induced Flow Rate $F \times 10^2$ | Channel Height $L \times 10^2$ | Heat absorbed $Q \times 10^3$ |
|---|---|---|---|
| 0.50 | 37.50 | 0.087 | 1.42 |
| 1.00 | 75.00 | 0.371 | 4.79 |
| 1.50 | 112.5 | 1.462 | 10.50 |
| 2.00 | 150.0 | 2.963 | 21.00 |
| 2.50 | 187.5 | 4.500 | 34.80 |
| 3.00 | 225.0 | 6.057 | 52.00 |
| 3.50 | 262.5 | 7.645 | 72.70 |
| 4.00 | 300.0 | 9.275 | 96.28 |
| 4.50 | 337.5 | 10.96 | 122.86 |
| 5.00 | 375.0 | 12.69 | 153.10 |

Table F.9 Flow and heat transfer parameters, for Case 2.I, E = 0.5

| $U_o \times 10^2$ | Induced Flow Rate $F \times 10^2$ | Channel Height $L \times 10^2$ | Heat absorbed $Q \times 10^3$ |
|---|---|---|---|
| 1.00 | 75.00 | 1.0458 | 3.36 |
| 2.00 | 150.0 | 5.2899 | 16.50 |
| 3.00 | 225.0 | 10.1913 | 39.60 |
| 4.00 | 300.0 | 15.6395 | 72.60 |
| 5.00 | 375.0 | 21.6199 | 115.20 |
| 6.00 | 450.0 | 28.1244 | 168.50 |
| 7.0 | 525.0 | 35.1553 | 230.60 |
| 8.0 | 600.0 | 42.7196 | 302.40 |

Table F.10 Flow and heat transfer parameters, for Case 2.O, E = 0.5

| $U_o \times 10^2$ | Induced Flow Rate $F \times 10^2$ | Channel Height $L \times 10^2$ | Heat absorbed $Q \times 10^3$ |
|---|---|---|---|
| 1.00 | 75.00 | 0.3023 | 4.16 |
| 2.00 | 150.0 | 1.9242 | 16.4 |
| 3.00 | 225.0 | 4.1541 | 40.0 |
| 4.00 | 300.0 | 6.7101 | 72.6 |
| 5.00 | 375.0 | 9.6006 | 114.2 |
| 6.00 | 450.0 | 12.8233 | 166.0 |
| 7.0 | 525.0 | 16.3650 | 227.5 |
| 8.0 | 600.0 | 20.2179 | 298.2 |

Table F.11 Flow and heat transfer parameters, for Case 2.I, E = 0.7

| $U_o \times 10^2$ | Induced Flow Rate $F \times 10^2$ | Channel Height $L \times 10^2$ | Heat absorbed $Q \times 10^3$ |
|---|---|---|---|
| 1.00 | 75.00 | 0.678 | 2.7469 |
| 2.00 | 150.0 | 3.988 | 13.01 |
| 3.00 | 225.0 | 8.186 | 31.20 |
| 4.00 | 300.0 | 13.0692 | 56.99 |
| 5.00 | 375.0 | 18.5789 | 90.73 |
| 6.00 | 450.0 | 24.6634 | 132.48 |
| 7.0 | 525.0 | 31.2759 | 182.27 |
| 8.0 | 600.0 | 38.3866 | 240.08 |

Table F.12 Flow and heat transfer parameters, for Case 2.O, E = 0.7

| $U_o \times 10^2$ | Induced Flow Rate $F \times 10^2$ | Channel Height $L \times 10^2$ | Heat absorbed $Q \times 10^3$ |
|---|---|---|---|
| 1.00 | 75.00 | .2511 | 4.0255 |
| 2.00 | 150.0 | 1.364 | 13.508 |
| 3.00 | 225.0 | 3.067 | 32.128 |
| 4.00 | 300.0 | 5.118 | 58.380 |
| 5.00 | 375.0 | 7.514 | 91.840 |
| 6.00 | 450.0 | 10.254 | 132.827 |
| 7.0 | 525.0 | 13.332 | 183.133 |
| 8.0 | 600.0 | 16.727 | 237.541 |

Table F.13 Flow and heat transfer parameters, for Case 3.I, $E = 10^{-6}$

| $U_o \times 10^3$ | Induced Flow Rate $F \times 10^4$ | Channel Height $L \times 10^5$ | Heat absorbed $Q \times 10^4$ | $\overline{Nu}_{i,e}^{3.I}$ | $\frac{\overline{Nu}_{i,e}^{3.I}}{Nu_{i,e}^{3.I}}$ |
|---|---|---|---|---|---|
| 1 | 7.50 | 1.34 | 02.22 | 8.9580 | 10.1300 |
| 2 | 15.0 | 4.78 | 04.96 | 7.6742 | 8.8975 |
| 3 | 22.5 | 10.31 | 08.84 | 6.9060 | 8.0512 |
| 4 | 30.0 | 17.42 | 13.46 | 6.5120 | 7.5854 |
| 5 | 37.5 | 26.37 | 17.45 | 6.3812 | 7.1448 |
| 6 | 45.0 | 40.19 | 20.17 | 6.2853 | 6.9823 |
| 7 | 52.5 | 58.69 | 28.07 | 6.1729 | 6.7573 |
| 8 | 60.0 | 82.89 | 35.64 | 6.5607 | 6.0739 |
| 9 | 67.5 | 105.3 | 43.17 | 6.0217 | 6.4882 |
| 10 | 75.0 | 138.07 | 52.13 | 5.9728 | 6.3974 |
| 11 | 77.5 | 176.99 | 61.68 | 5.9297 | 6.3093 |
| 12 | 90.0 | 223.60 | 71.15 | 5.8989 | 6.1827 |
| 13 | 97.5 | 283.74 | 76.98 | 6.1846 | 6.0382 |
| 14 | 105.0 | 373.00 | 83.54 | 6.0452 | 6.1597 |
| 15 | 112.5 | 507.91 | 91.31 | 6.0415 | 6.1412 |
| 16 | 120.0 | 710.38 | 100.7 | 6.0327 | 6.1145 |
| 17 | 127.5 | 971.50 | 110.01 | 6.0219 | 6.0898 |
| 18 | 135.0 | 1460.3 | 121.04 | 6.0114 | 6.0657 |
| 19 | 142.5 | 2162.4 | 132.00 | 6.0036 | 6.0467 |
| 20 | 150.0 | 3420.0 | 141.00 | 5.9999 | 6.0288 |

Table F.14 Flow and heat transfer parameters for case 3.I, E = 0.1

| $U_o \times 10^3$ | Induced Flow Rate $F \times 10^4$ | Channel Height $L \times 10^5$ | Heat absorbed $Q \times 10^4$ | $\overline{Nu}_{i.e}^{3.I}$ | $\overline{\overline{Nu}}_{i.e}^{3.I}$ |
|---|---|---|---|---|---|
| 1 | 7.5 | 2.1573 | 2.66 | 23.3564 | 15.2192 |
| 2 | 15.0 | 5.8829 | 5.35 | 8.4385 | 8.71058 |
| 3 | 22.5 | 11.0504 | 9.05 | 7.5779 | 7.97224 |
| 4 | 30.0 | 17.9470 | 13.9 | 6.73903 | 7.43066 |
| 5 | 37.5 | 26.7908 | 17.6 | 6.4523 | 7.0006 |
| 6 | 45.0 | 40.4734 | 21.96 | 6.2749 | 6.81450 |
| 7 | 52.5 | 58.6340 | 27.30 | 6.12116 | 6.60240 |
| 8 | 60.0 | 81.5330 | 35.70 | 5.9944 | 6.42055 |
| 9 | 67.5 | 108.8758 | 43.30 | 5.9264 | 6.34121 |
| 10 | 75 | 141.5574 | 52.37 | 5.82768 | 6.21987 |

Table F.15 Flow and heat transfer parameters for case 3.O, E = 0.1

| $U_o \times 10^3$ | Induced Flow Rate $F \times 10^4$ | Channel Height $L \times 10^5$ | Heat absorbed $Q \times 10^4$ | $\overline{Nu}^{3.O}_{o,e}$ | $\overline{\overline{Nu}}^{3.O}_{o,e}$ |
|---|---|---|---|---|---|
| 1 | 7.5 | 1.304 | 3.46 | 9.53 | 10.13 |
| 2 | 15.0 | 3.7667 | 6.22 | 7.23 | 8.32 |
| 3 | 22.5 | 7.2182 | 10.7 | 6.05 | 7.26 |
| 4 | 30.0 | 11.7683 | 15.1 | 5.50 | 6.72 |
| 5 | 37.5 | 17.7980 | 20.6 | 5.13 | 6.26 |
| 6 | 45.0 | 25.2100 | 26.9 | 4.72 | 5.68 |
| 7 | 52.5 | 36.0158 | 31.7 | 4.58 | 5.46 |
| 8 | 60.0 | 51.1180 | 38.8 | 4.42 | 5.17 |
| 9 | 67.5 | 70.3310 | 44.8 | 4.38 | 5.09 |
| 10 | 75 | 94.0695 | 53.5 | 4.28 | 4.88 |

Table F.16 Flow and heat transfer parameters for case 3.I, E = 0.5

| $U_o \times 10^3$ | Induced Flow Rate $F \times 10^4$ | Channel Height $L \times 10^5$ | Heat absorbed $Q \times 10^4$ | $\overline{Nu}_{i,e}^{3.I}$ | $\overline{\overline{Nu}}_{i,e}^{3.I}$ |
|---|---|---|---|---|---|
| 1 | 7.5 | 3.098 | 5.5269 | 36.55 | 25.66 |
| 2 | 15.0 | 8.810 | 9.1745 | 18.18 | 11.72 |
| 3 | 22.5 | 14.60 | 12.80 | 11.53 | 9.09 |
| 4 | 30.0 | 22.80 | 16.44 | 7.84 | 7.78 |
| 5 | 37.5 | 33.47 | 19.09 | 6.38 | 6.80 |
| 6 | 45.0 | 47.30 | 22.58 | 5.29 | 6.11 |
| 7 | 52.5 | 64.48 | 27.17 | 4.69 | 5.64 |
| 8 | 60.0 | 85.26 | 32.76 | 4.41 | 5.37 |
| 9 | 67.5 | 110.25 | 39.18 | 4.20 | 5.21 |
| 10 | 75 | 139.94 | 46.05 | 3.93 | 4.99 |
| 20 | 150 | 1267.7 | 124.95 | 3.35 | 3.67 |

Table F.17 Flow and heat transfer parameters for case 3.O, E = 0.5

| $U_o \times 10^3$ | Induced Flow Rate $F \times 10^4$ | Channel Height $L \times 10^5$ | Heat absorbed $Q \times 10^4$ | $\overline{Nu}^{3.O}_{o.e}$ | $\overline{\overline{Nu}}^{3.O}_{o.e}$ |
|---|---|---|---|---|---|
| 1 | 7.5 | 1.25 | 2.67 | 9.73 | 10.06 |
| 2 | 15.0 | 3.85 | 5.94 | 7.18 | 8.17 |
| 3 | 22.5 | 7.85 | 10.28 | 6.02 | 7.13 |
| 4 | 30.0 | 12.99 | 15.13 | 5.19 | 6.42 |
| 5 | 37.5 | 19.63 | 20.46 | 4.51 | 5.82 |
| 6 | 45.0 | 27.59 | 24.59 | 4.12 | 5.25 |
| 7 | 52.5 | 39.18 | 29.13 | 3.91 | 4.95 |
| 8 | 60.0 | 54.28 | 35.14 | 3.65 | 4.58 |
| 9 | 67.5 | 73.06 | 41.55 | 3.45 | 4.35 |
| 10 | 75 | 95.38 | 48.27 | 3.29 | 4.18 |
| 20 | 150 | 817.1 | 125.0 | 2.52 | 2.86 |

Table F.18 Flow and heat transfer parameters for case 3.I, E = 0.7

| $U_o \times 10^3$ | Induced Flow Rate $F \times 10^4$ | Channel Height $L \times 10^5$ | Heat absorbed $Q \times 10^4$ | $\overline{Nu}_{i,e}^{3.I}$ | $\overline{\overline{Nu}}_{i,e}^{3.I}$ |
|---|---|---|---|---|---|
| 1 | 7.5 | 3.0115 | 5.12 | 34.2389 | 20.8885 |
| 2 | 15.0 | 9.120 | 8.62 | 14.2195 | 10.2078 |
| 3 | 22.5 | 14.6072 | 12.10 | 9.62259 | 8.32839 |
| 4 | 30.0 | 24.8799 | 17.20 | 6.77609 | 6.98746 |
| 5 | 37.5 | 36.2220 | 19.70 | 5.42916 | 6.09911 |
| 6 | 45.0 | 50.4716 | 22.10 | 4.46956 | 5.44389 |
| 7 | 52.5 | 67.0550 | 26.60 | 3.85678 | 4.91414 |
| 8 | 60.0 | 87.0514 | 31.30 | 3.54282 | 4.59894 |
| 9 | 67.5 | 110.6549 | 36.30 | 3.33003 | 4.39192 |
| 10 | 75 | 138.263 | 42.30 | 3.07936 | 4.15770 |

Table F.19 Flow and heat transfer parameters for case 3.O, E = 0.7

| $U_o \times 10^3$ | Induced Flow Rate $F \times 10^4$ | Channel Height $L \times 10^5$ | Heat absorbed $Q \times 10^4$ | $\overline{Nu}_{o,e}^{3.O}$ | $\frac{\overline{Nu}_{o,e}^{3.O}}{\overline{Nu}_{o,e}^{3.O}}$ |
|---|---|---|---|---|---|
| 1 | 7.5 | 1.28065 | 3.47 | 34.2389 | 20.8885 |
| 2 | 15.0 | 4.13325 | 6.74 | 14.2195 | 10.2078 |
| 3 | 22.5 | 8.54099 | 10.50 | 9.62259 | 8.32839 |
| 4 | 30.0 | 14.0775 | 14.60 | 6.77609 | 6.98746 |
| 5 | 37.5 | 20.9753 | 19.50 | 5.42916 | 6.09911 |
| 6 | 45.0 | 28.9344 | 23.80 | 4.46956 | 5.44389 |
| 7 | 52.5 | 40.0387 | 28.10 | 3.85678 | 4.91414 |
| 8 | 60.0 | 53.7108 | 34.60 | 3.54282 | 4.59894 |
| 9 | 67.5 | 70.2030 | 39.00 | 3.33003 | 4.39192 |
| 10 | 75 | 89.2792 | 45.60 | 3.07936 | 4.15770 |

Table F.20 Flow and heat transfer parameters for case 4.I, E = 0.1

| $U_o \times 10^3$ | Induced Flow Rate $F \times 10^4$ | Channel Height $L \times 10^5$ | Heat absorbed $Q \times 10^5$ | $\overline{Nu}^{4.I}_{o.e}$ | $\frac{\overline{Nu}^{4.I}_{o.e}}{Nu^{4.I}_{o.e}}$ |
|---|---|---|---|---|---|
| 1.00 | 7.5000 | 9.5633 | 7.40 | 2.5028 | 3.7607 |
| 1.25 | 9.3750 | 14.9317 | 10.85 | 2.7046 | 4.1835 |
| 1.50 | 11.250 | 22.0054 | 14.20 | 2.8778 | 4.9229 |
| 1.75 | 13.125 | 33.0310 | 16.40 | 2.9495 | 5.1400 |
| 2.00 | 15.000 | 52.7200 | 19.10 | 3.0123 | 5.4096 |
| 2.25 | 16.875 | 88.0328 | 22.60 | 3.0669 | 5.6361 |
| 2.50 | 18.750 | 150.7929 | 26.58 | 3.1229 | 5.8708 |
| 2.75 | 20.500 | 276.8500 | 30.00 | 3.1633 | 6.1163 |
| 3.00 | 22.500 | 759.802 | 32.80 | 3.1909 | 6.2882 |

Table F.21 Flow and heat transfer parameters for case 4.O, E = 0.1

| $U_o \times 10^3$ | Induced Flow Rate $F \times 10^4$ | Channel Height $L \times 10^5$ | Heat absorbed $Q \times 10^5$ | $\overline{Nu}_{i,e}^{4.0}$ | $\frac{\overline{Nu}_{i,e}^{4.0}}{Nu_{i,e}^{4.0}}$ |
|---|---|---|---|---|---|
| 1 | 7.50 | 4.1254 | 9.160 | 2.5644 | 1.5825 |
| 1.5 | 11.25 | 8.3888 | 19.00 | 3.2500 | 2.062 |
| 2.0 | 15.00 | 14.1720 | 30.80 | 3.6967 | 2.5176 |
| 2.5 | 18.75 | 21.7092 | 45.00 | 3.8128 | 3.1047 |
| 3.0 | 22.50 | 32.4951 | 55.00 | 3.8594 | 3.2086 |
| 3.5 | 26.25 | 49.2850 | 62.70 | 3.9284 | 3.2716 |
| 4.0 | 30.00 | 72.5009 | 85.50 | 4.1203 | 3.5083 |
| 4.5 | 33.75 | 101.864 | 107.0 | 4.2429 | 3.6539 |
| 5.0 | 37.50 | 138.020 | 127.0 | 4.3269 | 3.7582 |
| 5.5 | 41.25 | 182.685 | 150.0 | 4.4054 | 3.8971 |
| 6.0 | 45.00 | 233.716 | 170.0 | 4.4334 | 4.1014 |
| 6.5 | 48.75 | 322.134 | 184.0 | 4.4541 | 4.1796 |
| 7.0 | 52.50 | 458.083 | 199.5 | 4.4736 | 4.2336 |

Table F.22 Flow and heat transfer parameters for case 4.I, E = 0.5

| $U_o \times 10^3$ | Induced Flow Rate $F \times 10^4$ | Channel Height $L \times 10^5$ | Heat absorbed $Q \times 10^5$ | $\overline{Nu}^{4.I}_{o,e}$ | $\frac{\overline{Nu}^{4.I}_{o,e}}{Nu^{4.I}_{o,e}}$ |
|---|---|---|---|---|---|
| 1.0 | 7.50 | 6.57 | 10.95 | 1.4247 | 2.1131 |
| 1.5 | 11.25 | 13.54 | 17.72 | 2.0345 | 2.8749 |
| 2.0 | 15.00 | 25.26 | 21.81 | 2.6373 | 4.1306 |
| 2.5 | 18.75 | 48.23 | 26.63 | 2.7764 | 4.7035 |
| 3.0 | 22.50 | 91.44 | 32.61 | 2.9245 | 5.2306 |
| 3.5 | 26.25 | 196.9 | 39.56 | 3.0199 | 5.6261 |
| 4.0 | 30.00 | 600.8 | 45.48 | 3.0520 | 5.9635 |

Table F.23 Flow and heat transfer parameters for case 4.O, E = 0.5

| $U_o \times 10^3$ | Induced Flow Rate $F \times 10^4$ | Channel Height $L \times 10^5$ | Heat absorbed $Q \times 10^4$ | $\overline{Nu}_{i,e}^{4.0}$ | $\frac{\overline{Nu}_{i,e}^{4.0}}{Nu_{i,e}^{4.0}}$ |
|---|---|---|---|---|---|
| 1.00 | 7.500 | 4.62 | 00.92 | 3.6204 | 3.5267 |
| 2.00 | 15.00 | 16.11 | 02.96 | 4.3493 | 4.2935 |
| 3.00 | 22.50 | 34.32 | 05.14 | 3.9852 | 4.4287 |
| 4.00 | 30.00 | 65.55 | 08.32 | 3.8432 | 4.4360 |
| 5.00 | 37.50 | 108.6 | 12.53 | 3.7325 | 4.3920 |
| 6.00 | 45.00 | 164.1 | 17.29 | 3.6035 | 4.2903 |
| 7.00 | 52.50 | 314.6 | 23.31 | 3.4138 | 3.9615 |
| 8.00 | 60.00 | 343.2 | 25.65 | 3.4108 | 3.9615 |
| 9.00 | 67.50 | 488.5 | 29.98 | 3.4043 | 3.9403 |
| 10.0 | 75.00 | 719.0 | 35.67 | 3.3386 | 3.8461 |
| 11.0 | 82.50 | 1038.2 | 42.18 | 3.2367 | 3.6932 |
| 12.0 | 90.00 | 1478.2 | 49.01 | 3.1976 | 3.6124 |
| 13.0 | 97.50 | 2098.9 | 55.62 | 3.1715 | 3.5278 |
| 14.0 | 105.0 | 3046.1 | 61.53 | 3.1619 | 3.4412 |
| 15.0 | 112.5 | 4753.5 | 66.40 | 3.1708 | 3.3677 |
| 16.0 | 120.0 | 9258.8 | 70.50 | 3.1875 | 3.2940 |

Table F.24 Flow and heat transfer parameters for case 4.I, E = 0.7

| $U_o \times 10^3$ | Induced Flow Rate $F \times 10^4$ | Channel Height $L \times 10^5$ | Heat absorbed $Q \times 10^5$ | $\overline{Nu}_{o,e}^{4.I}$ | $\frac{\overline{Nu}_{o,e}^{4.I}}{Nu_{o,e}^{4.I}}$ |
|---|---|---|---|---|---|
| 1 | 7.50 | 6.35 | 12.3 | 1.4228 | 2.1010 |
| 1.5 | 11.25 | 11.42 | 19.8 | 1.7498 | 2.4415 |
| 2.0 | 15.00 | 18.46 | 26.0 | 2.1826 | 2.9938 |
| 2.5 | 18.75 | 29.05 | 30.5 | 2.4431 | 3.7111 |
| 3.0 | 22.50 | 46.87 | 35.1 | 2.6325 | 4.3144 |
| 3.5 | 26.25 | 77.61 | 40.1 | 2.8095 | 4.7893 |
| 4.0 | 30.00 | 135.26 | 45.2 | 2.9716 | 5.2656 |
| 4.5 | 33.75 | 262.83 | 51.1 | 3.0129 | 4.7893 |
| 5.0 | 37.50 | 707.40 | 57.2 | 3.0367 | 5.7334 |

Table F.25 Flow and heat transfer parameters for case 4.O, E = 0.7

| $U_o \times 10^3$ | Induced Flow Rate $F \times 10^4$ | Channel Height $L \times 10^5$ | Heat absorbed $Q \times 10^5$ | $\overline{Nu}_{i,e}^{4.O}$ | $\frac{\overline{Nu}_{i,e}^{4.O}}{Nu_{i,e}^{4.O}}$ |
|---|---|---|---|---|---|
| 1.00 | 7.500 | 4.76 | 8.830 | 4.3595 | 6.2035 |
| 2.00 | 15.00 | 15.76 | 28.50 | 4.4055 | 6.2516 |
| 3.00 | 22.50 | 31.81 | 53.90 | 3.7086 | 5.4511 |
| 4.00 | 30.00 | 56.65 | 78.60 | 3.6554 | 5.3735 |
| 5.00 | 37.50 | 88.66 | 113.0 | 3.5184 | 5.1571 |
| 6.00 | 45.00 | 128.65 | 159.0 | 3.3891 | 4.9349 |
| 7.00 | 52.50 | 177.26 | 208.5 | 3.2779 | 4.7403 |
| 8.00 | 60.00 | 234.00 | 260.0 | 3.1332 | 4.6725 |
| 9.00 | 67.50 | 307.00 | 291.0 | 3.1165 | 4.3609 |
| 10.0 | 75.00 | 405.62 | 336.0 | 3.0436 | 4.1832 |
| 11.0 | 82.50 | 533.92 | 392.0 | 2.8977 | 3.8836 |
| 12.0 | 90.00 | 692.59 | 451.0 | 2.8777 | 3.8423 |
| 13.0 | 97.50 | 884.54 | 532.0 | 2.8116 | 3.7022 |
| 14.0 | 105.0 | 1111.9 | 600.0 | 2.7719 | 3.6083 |
| 16.0 | 120.0 | 1699.5 | 758.0 | 2.7011 | 3.4002 |
| 18.0 | 135.0 | 2553.4 | 908.0 | 2.6655 | 3.2257 |
| 20.0 | 150.0 | 3927.7 | 1044.0 | 2.6569 | 3.0823 |

# References


1. J. Abdulhadi and J.C. Chato, "Combined Natural and Forced Convective Cooling of Underground Electric Cables.", I.E.E.E. Transactions on Power Apparatus and Systems , Vol. 96,1977, pp. 1-8 .
2. R.S. Notaro and D. J. Webster, " Thermal Analysis of Forced Cooled Cables.", I.E.E.E. Transactions on Power Apparatus and Systems, Vol. 90, 1971, pp. 1225-1231.
3. W.E. Lowry, B.W. Davis and H. Cheung, "The Effect of Annular Air Gabs Surrounding an Emplaced Nuclear Waste Canister in Deep Geologic Storage.", In Heat transfer in Nuclear Waste Disposal(Edited by Kulaki, F.A., and Lyezkowski, R.W.), ASME Winter Annual Meeting HTD, Vol. 11, 1980, pp. 69-76.
4. K. Kyu-Jung, C. Jae-Ou and C. Tae-Yong, " A Performance Simulation for Spark Ignition Wankel Rotary Engine.", Proceedings of the 6 th International Pacific Conference on Automotive Engineering, October 1991, pp. 237-245.

5. M. R. El-Saden, "Heat Conduction in an Eccentrically Hollow, Infinitely long Cylinder with Internal Heat Generation." Journal of Heat Transfer, Transactions of the ASME, Vol.83, No. 4, 1961, pp. 510-511.

6. E.E. Feldman, R.W. Hornbeck and J. F. Osterle, "A Numerical Solution of Laminar Developing Flow in Eccentric Annular Ducts.", International Journal of Heat and Mass Transfer, Vol. 25, No. 2, 1982, pp. 231-241.

7. E.E. Feldman, R.W. Hornbeck and J. F. Osterle, "A Numerical Solution of Temperature for Laminar Developing Flow in Eccentric Annular Ducts.", International Journal of Heat and Mass Transfer, Vol. 25, No. 2, 1982, pp. 243-253.

8. E. R. G. Eckert, and R.M. Drake, Analysis of Heat and Mass Transfer, McGraw Hill, New York (1972), pp.99-106.

9. H. M. Macdonald, " On the Torsional Strength of a Hollow Shaft." , Proc. Cambridge, Philos. Soc., Vol. VIII (8), 1893, pp. 62 - 69.

10. H. H. Bau and S.S. Sadhal, "Heat Losses from a Fluid Flowing in a Buried Pipe," International Journal of Heat and Mass Transfer, Vol. 25, 1982, pp. 1621-1629.

11. R. F. DeFelice and H.H. Bau, "Conductive Heat Transfer between Eccentric Cylinders with Boundary Conditions of the Third Kind.", Journal of Heat Transfer, Transactions of the ASME, Vol. 105, 1983, pp. 678-680.

12. R. Thiyagarajan and M.M. Yovanovich, "Thermal Resistance of a Buried Cylinder with Constant Flux Boundary Condition.", Journal of Heat Transfer, Transactions of the ASME, Vol.96, 1974, pp. 249-250.

13. W. C. Reynolds, R.E. Lundberg and P.A. McCuen, "Heat Transfer in Annular Passages. General Formulation of the Problem for Arbitrarily Prescribed Wall Temperatures or Heat Fluxes.", International Journal of Heat and Mass Transfer, Vol. 6, 1963, pp. 483-493.

14. M. A. I. El-Shaarawi and M.A . Al-Nimr , "Fully Developed Natural Convection in Open-ended Vertical Concentric Annuli.", International Journal of Heat and Mass Transfer, Vol. 33., No. 9., 1990, pp. 1873 - 1884.

15. J. Cladwell ,"The Hydraulic Mean Depth as a Basis for Form Comparison in the Flow of Fluids in Pipes.", J.R. Tech. Coll (Glasgow)2, 1930, pp. 203 - 220.

16. N. A. V. Piercy, M.S. Hooper and H.F. Winny, " Viscous Flow through Pipes with Cores.", London Edinburg Dublin, Philos. Mag. J. Sci, 15, 1933, pp. 647 - 676.

17. J. F. Heyda, " A Green's Function Solution for the Case of Laminar Incompressible Flow between Non-Concentric Cylinders.", J. Franklin Inst., Vol. 267, 1959, pp. 25 - 34.

18. W. T. Snyder, " An Analysis of Slug Flow Heat Transfer in an Eccentric Annulus.", A.I.Ch.E. Journal, Vol. 9, No. 4, Jully 1963, pp. 503 - 506.

19. W. T. Snyder and G. A. Goldstein, " An Analysis of a Fully Developed Laminar Flow in an Eccentric Annulus.", A.I.Ch.E. Journal, Vol. 11, No. 3, May 1965, pp. 462 - 469.

20. P.J. Redberger and M.E. Charles, " Axial Laminar Flow in a Circular Pipe Containing a Fixed Eccentric Core.", The Canadian Journal of Chemical Engineering, August 1962, pp. 148 - 151.

21. K. C. Cheng and G.J. Hwang, " Laminar Forced Convection in Eccentric Annuli.", A.I.Ch.E. Journal, Vol. 14, No. 3, May 1968, pp. 510 - 512.

22. K.C. Cheng and M. Jamil, "Laminar Flow and Heat Transfer in Ducts of Multiply Connected Cross Sections.", ASME Paper, 67 - HT - 6, 1967.

23. M. L. Trombeta, " Laminar Forced Convection in Eccentric Annuli.", International Journal of Heat and Mass Transfer, Vol. 14, 1972, pp. 1161 - 1172.

24. T. L. Guckes, " Laminar Flow of Non-Newtonian Fluids in an Eccentric Annulus.", Journal of Engineering for Industry, Transactions of the ASME, May 1975, pp. 498 - 506.

25. D. V. von Rosenberg, Methods for the Numerical Solution of Partial Differential Equations, Appendix E, pp. 121., American Elsevier Publishing Co., New York, 1969.

26. C. Özgen and I. Tosun, " Application of Geometric Inversion to the Eccentric Annulus System.", A.I.Ch.E. Journal, Vol. 33, No. 11, , November 1987, pp. 1903 - 1907.

27. K. Suzuki, J.S. Szmyd and H. Ohtsuka, " Laminar Forced Convection Heat Transfer in Eccentric Annuli.", *Heat transfer-Japanese Research*, Vol.20, 1990, pp. 169-183.

28. P. Sathymurthy, K.C. Karki and S.V. Patankar, " Laminar Fully Developed Mixed Convection in a Vertical Eccentric Annulus.", Numerical Heat Transfer, Part A., Vol. 22, 1992, pp. 71 - 85.

29. W. Elenbaas, " Heat Dissipation of Parallel Plates by Free Convection.", Physica, Vol. 9, No. 1, 1942, pp. 1- 28.

30. W. Elenbaas, "The Dissipation of Heat by Free Convection (from) the Inner Surface of Vertical Tubes of Different Shapes of Cross section.", Physica, Vol. 9, No. 8, 1942, pp. 865-674.

31. J. R. Bodoia and J.F. Osterle, "The Development of Free Convection between Heated Vertical Plates.", Journal of Heat transfer, Transactions of the ASME, Vol. 84, 1962, pp. 40 - 44.

32. J. R. Dyer and J.H Fowler, "The Development of Natural Convection in a Partially-Heated Vertical Channel Formed by Two Parallel Plates Surfacse.", Mechanical and Chemical engineering Transactions, The Institute of Engineers, Australia, MC2, 1966, pp. 12-16.

33. W. Aung, L.S. Fletcher and V. Sernas, "Developing laminar Free Convection between Vertical Flat Plates with Asymmeteric Heating.", International Journal of Heat and Mass Transfer, Vol. 15, 1972, pp. 2293-2308.

34. O. Miyatake and T. Fujii, "Free Convection Heat Transfer between Vertical Parallel Plates, One plate Isothermally Heated and the Other Isothermally Insulated.", Journal of Heat Transfer , Japanese Research, Vol. 1, No. 3, 1972, pp. 30-38.

35. O. Miyatake and T. Fujii, "Natural Convection Heat Transfer between Vertical parallel Plates at Unequal Uniform Temperatures.", Journal of Heat Transfer , Japanese Research, Vol. 2, No. 4, 1973, pp.79-88.

36. O. Miyatake, T. Fujii, M. Fujii and H. Tanaka, "Natural Convection Heat Transfer between Vertical Parallel Plates, One Plate with a Uniform Heat Flux and the other

Thermally Insulated.", Journal of Heat Transfer , Japanese Research, Vol. 2, No. 1, 1973, pp.25-33.

37. J. Quintiere and W. K. Mueller, "An Analysis of Laminar Free Convection and Forced Convection between Finite Vertical Parallel Plates.", Journal of Heat Transfer, Transactions of the ASME, Vol. 95, 1973, pp. 53-59.

38. B. S. Narang, "Exact Solution for Entrance Region Flow between Parallel Plates.", International Journal of Heat and Fluid Flow, Vol. 4, No. 3, Sebtember 1983, pp. 177-181.

39. B. S. Narang and G. Krishnamoorthy, " Laminar Flow in the Entrance Region of parallel plates.", Journal of Heat Transfer, Transactions of the ASME, March 1976, pp. 186-188.

40. W. Aung and G. Worku, "Developing Flow and Flow Reversal in a Vertical Channel with Asymmetric Wall Temperaturer.", Journal of Heat Transfer, Transactions of the ASME, Vol. 108, May 1980, pp. 299-304.

41. W. Aung and G. Worku, "Theory of Fully Developed Combined Convection Including Flow Reversal.", Journal of Heat Transfer, Transactions of the ASME, Vol. 108, May 1980, pp. 485-488.

42. D. B. Ingham, D.J. Keen and P.J. Heggs, "Flows in Vertical Channels with Asymmetric Wall Temperature and Including Situations where Reverse Flow Occure.", Journal of Heat Transfer, Transactions of the ASME, Vol. 110, November 1988, pp. 910-9170

43. C. H. Cheng, H.S. Kou and W.H. Huang, "Locally Fully Developed Laminar Free Convection within Asymmetrically Heated Vertical Channel.", JSME, International Journal , Series II, Vol. 33, No. 2, 1990, pp. 305-315.

44. A. A. Rostami and S.S. Mortazavi, "Analytical Prediction of Nusselt Number in a Simultaneously Developing Laminar Flow between Parallel Plates.", International Journal of Heat and Fluid Flow, Vol. 11, No. 1, March 1990, pp. 44-47.

45. H.L Langhar, "Steady Flow in the Transition Length of a Straight Tube.", Journal of Applied Mechanics, Vol. 9, Transactions of the ASME, Vol. 64, 1942, pp. A55-A58.

46. T. S. Lundgren E.M. Sparrow and J. B. Starr, "Pressure Drop Due to the Entrance Region in Ducts of Arbitrary Cross section.", Journal of Basic Engineering, Transactions of the ASME, Vol. 86, 1964, pp. 620-626.

47. R. W. Hornbeck, "Laminar Flow in the Entrance Region of a Pipe.", Applied Scientific Research, Section A, Vol. 13, 1964, pp. 224-232.

48. J. R. Bodoia and J.F. Osterle, "Finite Difference Analysis of a plane Poiseuile and Couette Flow Developments.", Applied Scientific Research, Section A, Vol. 10, 1961, pp.265-276.

49. L. S. Han, "Hydrodynamic Entrance Length for Incompressible Flow in Rectangular Ducts.", Journal of Applied Mechanics, Vol. 27, Transactions of the ASME, Vol. 82, Series E, 1960, pp. 403-409.

50. E. M. Sparrow, S. H. Lin and T.S. Lundgren, "Flow Development in the Hydrodynamic Entrance Region of Tubes and Ducts.", Physics of Fluids, Vol. 7, 1964, pp. 338-347.

51. M. Kageyama and R. Izumi, "Natural Heat Convection in a Circular Tube.", Bulletin of JSME, Vol. 13, No. 57, 1970, pp. 382-394.

52. L. P. Davis and J. J. Perona, "Development of Free Convection Flow of a Gas in a Heated Vertical Open Tube.", International Journal of Heat and Mass Transfer, Vol. 14, 1971, pp. 889-903.

53. J. R. Dyer, "The Development of Laminar Natural Convection Flow in a Vertical Uniform Heat Flux Duct.", International Journal of Heat and Mass Transfer, Vol. 18, 1975, pp. 1455-1465.

54. H. S. Takhar, "Entry-Length Flow in a Vertical Cooled Pipe.", Journal of Fluid Mechanics, Vol. 34, 1968, pp. 641-650.

55. R. A. Meric, " An Analytical Study of Natural Convection in a Vertical Open Tube.", International Journal of Heat and Mass Transfer, Vol. 20, 1977, pp. 429-431.

56. G. A. Carlson and R. W. Hornbeck, "A Numerical Solution for Laminar Entrance Flow in a Square Duct.", Journal of Applied Mechanics, Transactions of the ASME, 1973, pp. 25- 30.

57. A. P. Hatton and A. Quarmby, "Heat Transfer in the Thermall Entry Length with Laminar Flow in an Annulus.", International Journal of Heat and Mass Transfer, Vol. 5, 1962, pp. 973-980.

58. H. S. Heaton, W.C. Reynolds and W. M. Kays, "Heat Transfer in Annular Passages. Simultaneous Development of Velocity and Temperature Fields in Laminar Flow.", International Journal of Heat and Mass Transfer, Vol. 5, 1964, pp 763-781.

59. E. M. Sparrow and S. H. Lin, "The Developing Laminar Flow and Pressure Drop in the Entrance Region of Annular Ducts.", Journal of the Basic Engineering, Transactions of the ASME, Vol. 86, 1964, pp. 827-834.

60. J. E. R. Coney and M.A.I. El-Shaarawi, "A Contribution to the Numerical Solution of Developing Laminar Flow in the Entrance Region of Concentric Annuli with Rotating Inner Walls.", Journal of Fluid Engineering, Vol. 96, December 1974, pp. 333-340.

61. J. E. R. Coney and M.A.I. El-Shaarawi, "Finite Difference Analysis for Laminar Flow Heat Transfer in Concentric Annuli with Simultaneously Developing Hydrodynamic and Thermal Boundary Layers.", International Journal for Numerical Methods in Engineering, Vol. 9, 1975, pp. 17-38.

62. M. A. I. El-Shaarawi and A. Sarhan, "Developing Laminar Free Convection in an Open Ended Vertical Annulus with a Rotating Inner Cylinder.", Journal of Heat Transfer, Transactions of the ASME, Vol. 103, August 1981, pp. 552-558.

63. M. A. I. El-Shaarawi and A. Sarhan, "Developing Laminar Free Convection in a Heated Vertical Open Ended Annulus.", Ind. Eng. Chem. Fundam., Vol. 20, 1981, pp. 388-394.

64. M. Al-Arabi, M.A.I. El-Shaarawi and M. Khamis, "Natural Convection in Uniformly Heated Vertical Annuli.", International Journal of Heat and Mass Transfer, Vol.30, No. 7, !987, pp. 1381-1389.

65. M. A. I. El-Shaarawi and Z. Kodah, "Natural Convection in an Annulus with Two Rotating Boundaries.", JSME, International Journal, Series II, Vol. 33, No. 2, 1990, pp. 316-325.

66. B. B. Rogers and L.S. Yao, "Natural Convection in a Heated Annuli.", International Journal of Heat and Mass Transfer, Vol. 36, No. 1, 1993, pp. 35-47.

67. V. D. Vilenskii, Y.V. Mironov and V.P. Smirnov, "Numerical Solution of the Problem of Heat Transfer in an Annular Channel.", High temperature, Vol. 9, 1971, pp. 699-704.

68. P. Moon and D.E. Spencer, Field Theory Handbook, 2nd Eddition, Springer Verlag Berlin, Heidlberg, New York, 1971, pp.1-3.

69. W. F. Hughes and E.W. Gaylord, " Basic Equations of Engineering Science.", Schaum Outlines Ser., 1964, pp. 12 - 13.

70. M. N. Ozisik, Heat Conduction, Wiley, New York, 1980, P. 96.

71. H. Schlichting, Boundary Layer Theory, seventh ed., McGraw Hill, New York, 1987, pp. 127-149.

72. M. A. I., El-Shaarawi, " Derivation of Boundary Layer Equations for Cases with Curved Boundaries.", Int. J. Engineering Fluid Mechanics, Vol. 3, No. 2, 1990, pp. 113-128.

73. P. M. Morse and H. Feshback, Metods of Theoretical physics-II, McGraw Hill, New York, 1953, pp. 1214-1215.

74. M. A. I. El-Shaarawi, Heat Transfer and Hydrodynamics in the Entrance Region of Concentric Annuli with Stationary and Rotating Inner Walls, Ph.D. Dissertation, Leeds University, England, 1974.

75. M. A. I. El-Shaarawi and E. Mokheimer, "Transient Conduction in Eccentrically Hollow Cylinders.", International Journal of Heat and Mass Transfer, Vol. 38, No. 11, July 1995, pp. 2001-2010.

76. M. A. I. El-Shaarawi and I. Mokheimer, "Unsteady Conduction in Eccentric Annuli .", Warme - und Stoffubertragung (Heat and Mass Transfer), Vol. 30, 1995, pp.249-257.

77. B. Carnahan, H. A.Luther, and J. D Wilkes, Applied Numerical methods, *Wiley*, 1969, pp.298-301, 450.

78. E. E. Feldman, " The Numerical Solution of the Combined Thermal and Hydrodynamic Entrance Region of an Eccentric Annulus", Ph.D. Dissertation, Carnegie-Mellon University, Pittsburgh, Pennsylvania, U.S.A, 1974.

79. W. Tiedt, English translation-Transl. Bur. No. 0151, P. 248, Transp. Dev. Agency Libr., Montereal, 1971.

80. R. K. Shah, and A. L. London, Laminar Flow Forced Convection in Ducts, Academic Press, New York, 1978, pp. 326 - 330.

81. W. J. Marner, and H. K. McMillan, " Combined Free and Forced Laminar Forced Convection in a Vertical Tube with Constant Wall Temperature", J. Heat Transfer, Vol. 92, 1970, pp. 559-562

# Vitae

- Esmail Mohamed Ali Mokheimer
- Born in El-Marg, Cairo, Egypt
- Received bachelor's degree in Mechanical Engineering from Faculty of Engineering, Ain Shams University, Cairo, Egypt in June, 1985.
- Received Master's degree in Mechanical Engineering from Faculty of Engineering, Ain Shams University, Cairo, Egypt in December, 1988.
- Completed Doctor of Philosophy degree requirements (in Mechanical Engineering) at King Fahd University of Petroleum and Minerals, Dhahran, Saudi Arabia in November, 1995.